IGNEOUS AND HYDROTHERMAL MINERALS AND TEXTURES IN THE OFFSHORE CANTERBURY BASIN

A thesis submitted in partial fulfilment of the requirements for the

Degree

of Master of Science in Geology

in the University of Canterbury

by R. J. Newman

University of Canterbury

2015

Acknowledgements

The author wishes to thank the University of Canterbury Department of Geological Sciences for the loan of their mineral sample collection, the Engineering Department for the use of and assistance with their scanning electron microscope and NZ Petroleum &Minerals for allowing detailed sampling of Clipper-1 cuttings, and for sending additional material from 790m for geochemical analysis. In addition, special thanks to Kari Basset, Chris Oze, Andy Gize, Jane Newman for help and advice and to Newman Energy Research Ltd for use of their equipment and help with sample preparation. Thanks also to Steve Weaver for his advice on igneous carbonates and Stephen Brown for assisting with XRD and XRF analyses.

Abstract

The Canterbury Basin is located on a passive margin on the east coast of the South Island, developed by the rifting of the New Zealand continental fragment from Antarctica in the Late Cretaceous. Well cuttings produced during petroleum exploration in the offshore Canterbury Basin have been examined for secondary minerals and textures. Minerals and textures have been identified primarily from optical examination in reflected light, with a particular focus on producing high-resolution images. Additional identifications are made using thin sections, SEM, XRD and XRF analysis.

The focus of this study is the Clipper-1 well in the Clipper sub-basin as it contains the most abundant mineralisation and covers the full depth of the Canterbury Basin sedimentary sequence. Examination of cuttings from this well has revealed intrusive igneous carbonates and native metals including iron, aluminium and copper. The trace element concentrations in the igneous carbonates indicates they are derived from crustal material. Textures indicating fluidisation and recrystallisation of sedimentary material are also present.

The proposed mechanism for producing these unusual mineral assemblages is a late Pliocene or younger mafic intrusion into the schist basement of the Canterbury Basin. The igneous carbonates are inferred to be derived from melting of carbonates in the schist. The native metals have been produced from melt due to highly reducing conditions produced by interaction of the intrusion with coal and limestone. The combination of native metals and igneous carbonates with a conspicuous absence of typical silicate igneous rocks is inferred to represent a new type of intrusive environment that has not previously been described in the scientific literature.

Table of contents

List of figures.

List of tables.

1.0 Introduction

The aim of this thesis is to identify the secondary minerals and textures present in the Clipper-1 petroleum exploration well as a result of hydrothermal and igneous activity and propose a mechanism for their formation in the setting of the Canterbury Basin. This includes a particular focus on the production of a high-quality visual record of secondary minerals and textures as seen in reflected light microscopy, with additional SEM and thin section images.

The impetus for this study was the observation of many curious minerals and textures in petroleum well samples during my work with Newman Energy Research Ltd (NER). Although the organic components of the well samples have been studied in detail, the minerals have thus far been largely ignored. Clipper-1 provides an ideal setting for study, as it covers the full sequence of Canterbury Basin sediments down to basement and contains abundant mineralisation. Work on the organic components by NER has previously shown this well to have a complex thermal history.

It is hoped that the visual identification of minerals may become a useful tool in revealing the igneous and hydrothermal histories of sedimentary basins. This is particularly important in the search for petroleum resources, where knowledge of thermal events is a key component in predicting potential petroleum source rocks. Although this study largely focuses on a single well, the results are likely to have relevance to the wider Canterbury Basin and other basins in New Zealand and around the world.

1.1 Tectonic Setting and sedimentary History

1.1.1 Location

The Canterbury Basin is located on a passive margin on the east coast of the South Island, developed by the rifting of the New Zealand continental fragment from Antarctica in the Late Cretaceous (Weaver et al. 1994; Lawver and Gahagan 1994). It covers the Canterbury Plains, areas of coastal Otago and offshore (Fig. 1). The landward margins of the basin are marked by the Otago Peninsula in the south and the edge of the Southern Alps foothills in the west. Banks Peninsula is considered by some to mark the northern edge of the basin, while others consider it to extend to the northern end of Pegasus Bay (Wylie & Haskell 1997; Lu et al 2003; Sykes 2004). The offshore margins of the basin are less well defined, but are approximately marked by the Chatham Rise and Bounty Trough in the north and east. To the south, the Canterbury Basin merges with the Great South Basin. The boundary between the two is marked by the Takapu High, an area of thinner sediments off the coast of the Otago Peninsula (NZP&M 2013a). Neogene sediments thin towards the margins of the basin except in the east, where the thickest sediments can be found near the edge of the continental shelf.

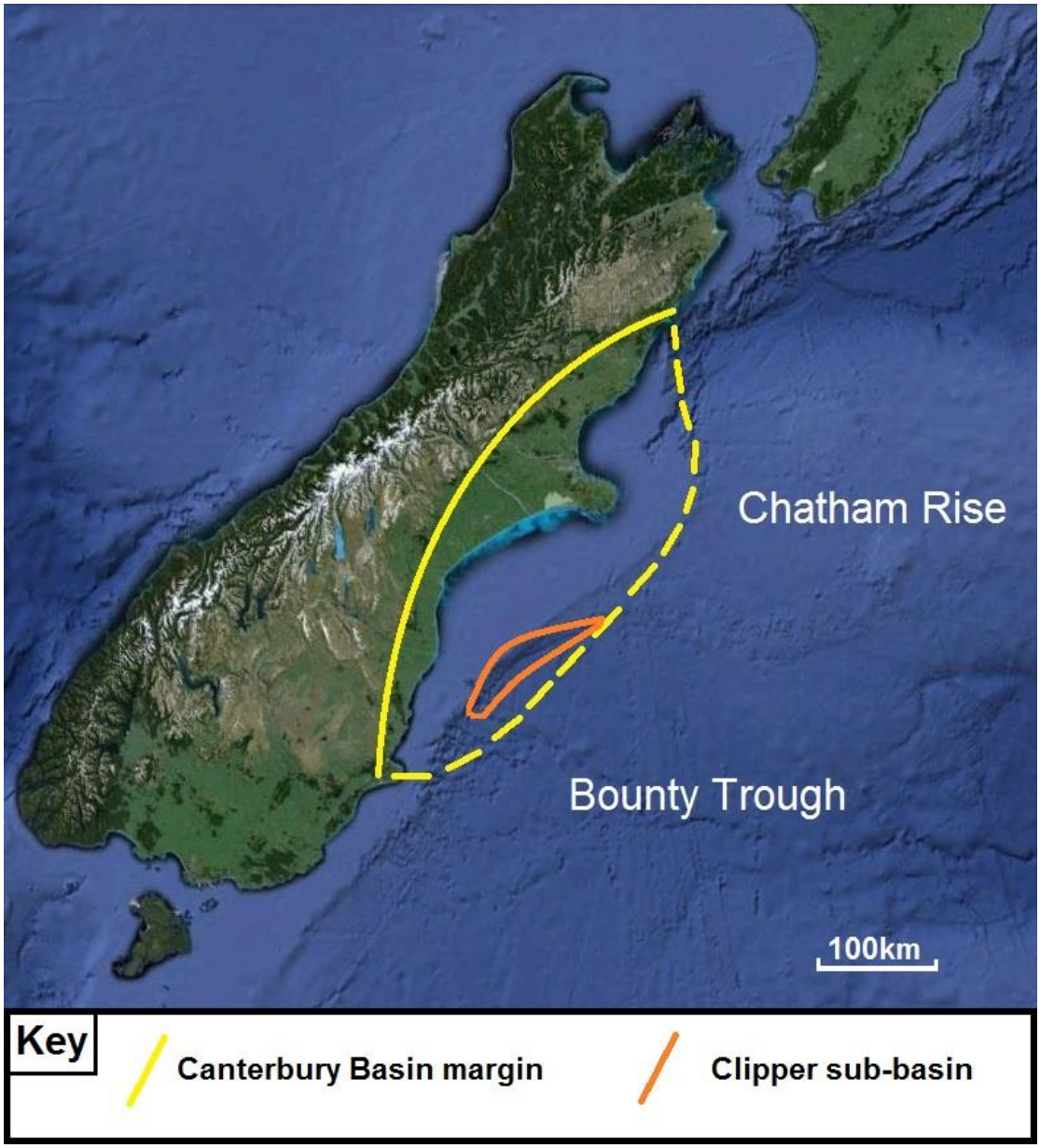

Fig. 1. The Canterbury Basin and Clipper sub-basin. Broken lines indicate an approximate location of the margin.

1.1.2 Basin history

Mid-Cretaceous Rifting

The Clipper sub-basin, located east of Oamaru near the edge of the continental shelf, was one of the first depocentres to form within the wider Canterbury Basin (Field & Browne 1989). Terrestrial sediments accumulated here during the initial phases of rifting between New Zealand and Antarctica. Sedimentation initially began with the deposition of coarse sandstones and conglomerates in alluvial fans, then progressed into finer terrestrial sediments and later carbonaceous mudstones and coal beds deposited in a river delta setting. Extension of the crust resulted in partial melting of the Torlesse terrane basement rocks, producing widespread calc-alkaline volcanism in central Canterbury (Barley 1987).

Late Cretaceous-Oligocene Transgression

As post-rifting transgression progressed during the Late Cretaceous, the wider area experienced subsidence and the Clipper Basin was submerged, reaching bathyal water depths by the end of the Cretaceous (Crux et al. 1984). On the margins of the Clipper Basin and in the wider Canterbury Basin, peat accumulated in a gymnosperm-dominated brackish coastal plain and fluvial sediments were deposited in a flood plain and river delta setting (Sykes 2004). As these areas subsided below sea level, terrestrial sedimentation gave way to marine sandstones, siltstones and mudstones with occasional beds of limestone.

Basaltic tuffs found in the Endeavor-1 well southeast of Oamaru indicate that submarine basaltic volcanism was occurring during the Paleocene (Coombs et al. 1986; Field & Browne 1989). Reactivation of faults formed during rifting caused differential rates of subsidence across the Canterbury Basin (Field & Browne 1989).

As subsidence and erosion reduced the area of land remaining above sea level, sediment supply to offshore basins became restricted, resulting in a transition from mudstone and siltstone deposition to limestone formation during the Late Eocene. Volcanic activity resumed during the late Eocene and progressed into the Oligocene. Surtseyan eruptions on

the continental shelf produced small volcanic cones and pillow lavas, and sills were formed by the intrusion of basalt into shallow, poorly-indurated marine sediments (Coombs et al. 1986; Corcoran & Moore 2008). Volcanic activity in the south of the basin ended by the mid Oligocene, but eruptions of basalt continued further north (Field & Browne 1989).

Deposition of limestone continued into the Oligocene, spreading further towards the edges of the basin as terrestrial sediment supply became more limited during maximum transgression. During the mid-Oligocene, many areas of the Canterbury Basin experienced erosion or an interruption in limestone deposition producing a surface known as the Marshal Paraconformity. This event is thought to be linked to the development of the Antarctic Circumpolar Current, which caused a reduction in marine temperatures in addition to more intense current activity and a fall in sea level due to glaciation in Antarctica (Fulthorpe et al. 1996).

During the Late Oligocene, localised erosion occurred between Banks Peninsula and Oamaru due to the formation of the Endeavour High, a ridge on a NE-SW alignment a short distance east of the present day coastline. The formation of the high is not well understood. Contradictory seismic data suggest either faulting or variations in sediment compaction may be responsible (Field & Browne 1989). Evidence of dissolution in limestones near Dunedin indicates that parts of the high were exposed above sea level (Lewis & Belliss 1984). East of the Endeavour High, deposition of limestone continued through the Oligocene and into the Miocene without interruption.

Miocene-Present Regression and Sedimentation

At the beginning of the Miocene, volcanism began to increase in intensity at both the northern and southern ends of the Canterbury Basin with the eruption of trachyte near Dunedin and rhyolite at what would later become Banks Peninsula. This activity proceeded through to the late Miocene with eruptions of mostly basaltic lava forming the large shield volcanoes at Lyttelton and Akaroa and the Dunedin Volcanic Complex (Stipp & MacDougall 1968; Coombs et al. 1986).

The Endeavour High persisted until the end of the Early Miocene, acting as a barrier restricting sediment supply to the eastern part of the Canterbury Basin (Field & Browne 1989). Sediment supply to the Canterbury Basin increased sharply in the mid-Miocene due to the beginning of uplift along the Alpine Fault, exposing more land above sea level to erosion (Field & Browne 1989). Uplift along the western edge of the basin resulted in the complete removal of accumulated sediments in some areas, exposing the basement rock. Glaciation in the Late Miocene caused a glacioeustatic fall in sea level, resulting in erosion and the formation of unconformities across large areas of the basin (Hodell et al. 1986; Kennett 1986).

Cooling temperatures during the Pliocene resulted in the development of glaciers in the newly-formed Southern Alps (Devereux et al. 1970; Kennet et al. 1971). Along with the continuing uplift on the Alpine Fault, this contributed to the formation of a 'high-resolution' record of depositional conditions in the offshore area of the Canterbury Basin, with sedimentation rates of up to 300 metres per million years (Field & Browne 1989). Ocean currents have had a significant influence on sedimentation patterns. As currents flow northward along the coast, large drifts of sediment are accreted onto the edge of the continental shelf (Fulthorpe & Carter 1991). The western edge of the basin experienced continued uplift and erosion of accumulated sediments. The intensity of uplift decreases sharply away from the basin's western margin, and the offshore sediments appear to have experienced little or no vertical movement (Lu et al 2003).

During the late Pliocene, sheets of basalt were erupted near Timaru and Geraldine (Duggan & Reay 1986). This is the most recent known volcanism in the Canterbury region.

1.2 Canterbury Basin stratigraphy at Clipper-1

The following stratigraphy is based on well logs from Clipper-1 by BP Shell Todd with further refinements by Field & Browne (1989). Clipper-1 is the deepest well in the Canterbury Basin and covers the full stratigraphy down to basement (Fig. 2). It is located within the Clipper sub-basin, the first area to accumulate sediment during rifting in the Cretaceous and the location of the basin's thickest sediments. These factors make it the most complete record of sedimentation in the Canterbury Basin since its formation in the Cretaceous. All depths listed are BRT (below rotary table). Sea level is 26m below 0m BRT.

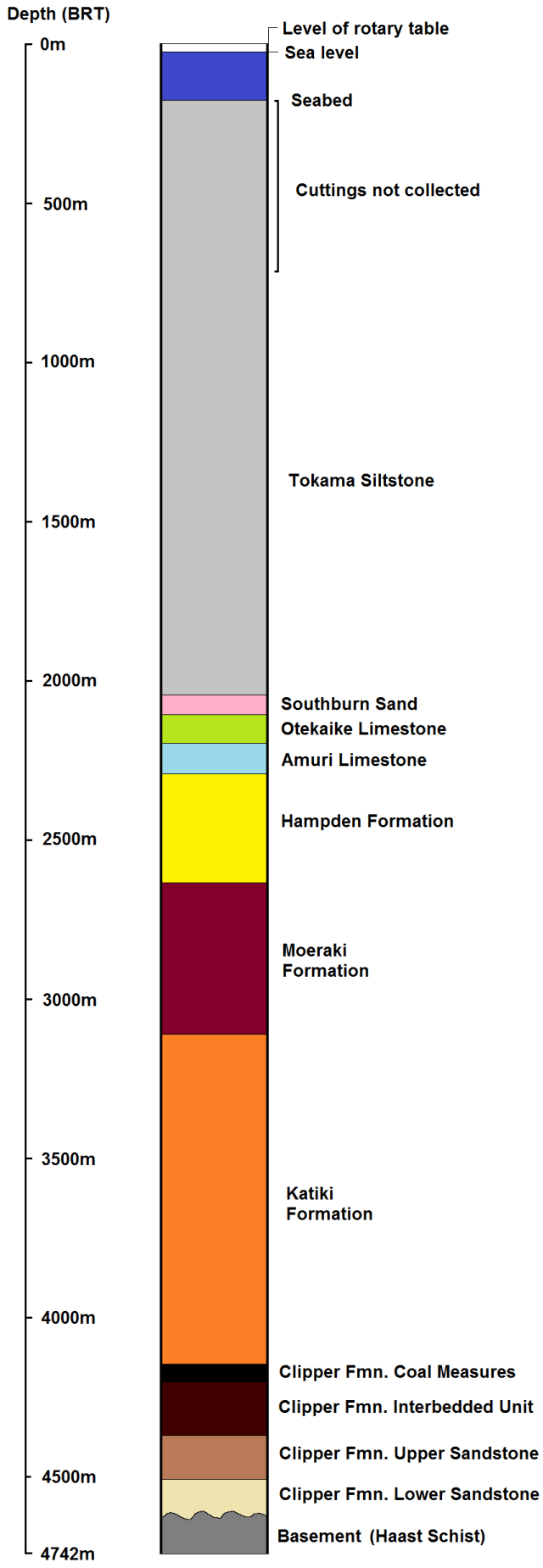

Fig. 2.

Stratigraphic column of Clipper-1 showing thickness of major rock units and water depth.

Basement (4684.5m)

The basement rock at the bottom of Clipper-1 is a low-grade schistose rock correlative of Haast Schist. The major minerals are quartz, albite, muscovite and calcite (Fig. 3). In composition it is similar to schists found in the Kakanui area of North-East Otago (Shell BP Todd 1984). The calcite crystals are undeformed and cut foliation, indicating that they formed after metamorphism. Graphite is also more abundant than in typical Otago schist. These minerals may have been formed during post-metamorphic hydrothermal alteration, similar to schists from eastern Otago (Craw et al. 1982).

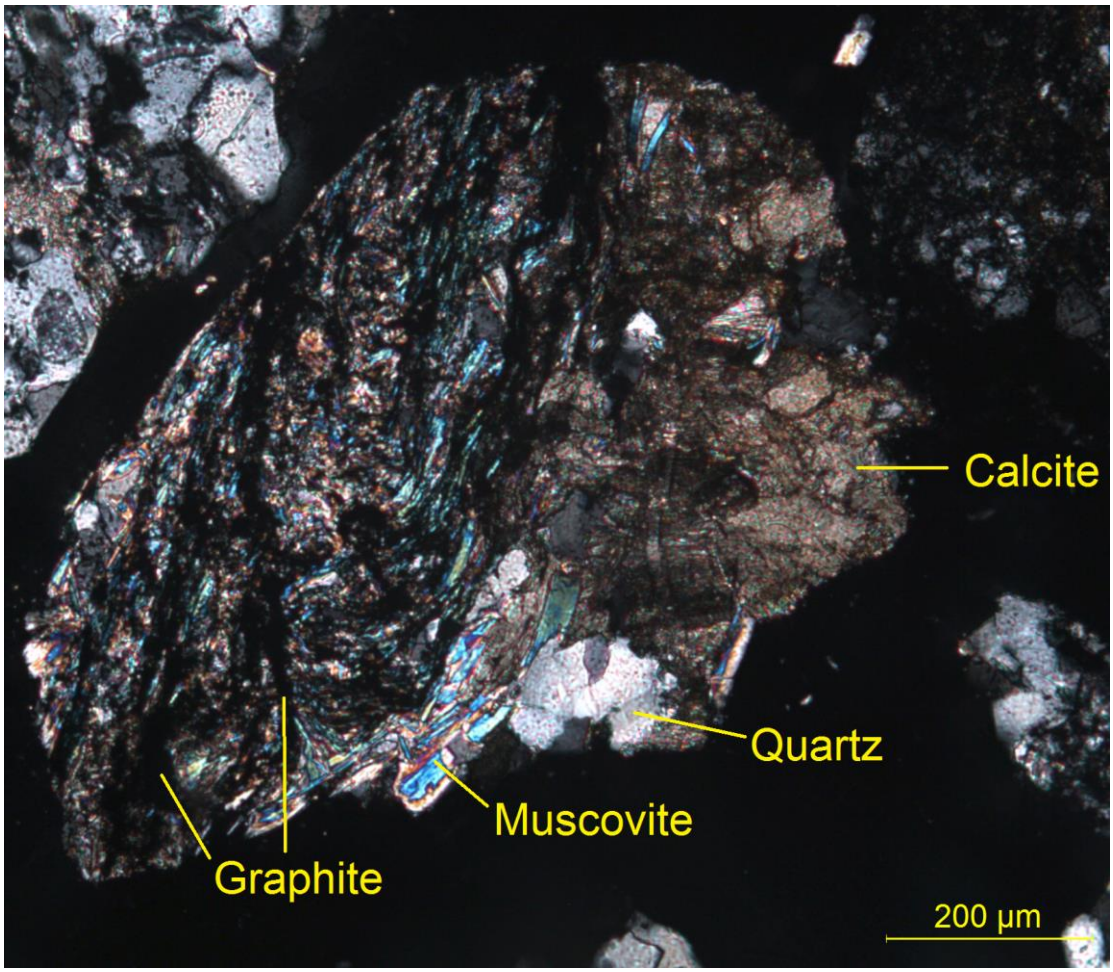

Fig. 3. Cross-polarised light thin section image of schist from the bottom of Clipper-1.

Clipper Formation (4205-4684.5m)

The Upper Cretaceous Clipper Formation is a 480m thickness of fluvial sediments and coal measures deposited onto the eroded surface of the Haast Schist basement rock. It is divided into four units: a lower and upper sandstone unit, an interbedded unit and a unit of coal measures. The sandstones fine upwards, ranging from very coarse sand and conglomerates at the base of the formation to very fine sand near the top. The Clipper-1 well was drilled here as the coal measures were a potential petroleum source. Although gas shows and hydrocarbon fluorescence were present in the interbedded and coal measure units, there was no indication of commercially viable quantities of oil or gas.

Lower Sandstone unit (4566-4684.5m)

118m of interbedded conglomerates, sandstone and mudstone. The sandstones are massive, poorly sorted and coarse to very coarse in grain size with a well-developed silica cement. Derived from eroded Haast Schist, they are primarily quartzose with some schist lithics. The sandstones are interbedded with carbonaceous mudstones.

Upper sandstone unit (4428-4566m)

138m of interbedded sandstone and siltstone. The sandstones are quartzose, fine to coarse sand sized and occasionally carbonaceous with thicker and more well-sorted beds than in the lower sandstone unit.

Interbedded unit (4261.5-4428m)

168m of sandstone, siltstone and mudstone. This unit is primarily mudstone, separated by sandstone interbeds 1-5m thick. The sandstones are quartzose, very fine to fine sand sized and carbonaceous. Type and degree of cementation is variable, with both silica cement and kaolinite matrix present. The mudstones are highly carbonaceous.

Coal measures unit (4205-4261.5m)

55.5m of siltstone, mudstone and coal beds. This unit is primarily mudstone and siltstone, interbedded with vitrinite rich coal. The mudstones and siltstones are carbonaceous and non-calcareous.

Katiki Formation (3167.5m-4205m)

1037.5m of mostly carbonaceous siltstone with occasional thin mudstone, sandstone and limestone beds. Towards the base of the formation, sediments become more calcareous with occasional limestone beds.

Moeraki Formation (2692-2832.5m)

475.5m of carbonaceous, pyritic mudstones grading into siltstone. Occasional interlaminations of limestone. Pyrite and glauconite are most abundant in the lower 300 metres of the formation, along with tuffaceous mudstones.

Hampden Formation (2387-2410m BRT)

342m of carbonaceous, glauconitic mudstone and siltstone. Increasingly calcareous towards the top of the formation.

Amuri Limestone (2290-2387m)

97m of arenaceous limestone with calcareous mudstone at the base.

Otekaike Limestone (2201-2290m)

The bottom 10m of this unit, consisting of very fine-grained calcareous sandstone, may be a correlative of the Kokoamu Greensand. Above that is 89m of limestone, occasionally sandy, with calcareous sandstone at the base.

Southburn Sand (2139.5-2201m)

61.5m of calcareous, quartzose very fine sandstone with occasional beds of sandy limestone. Becomes less glauconitic upsection.

Tokama Siltstone (2139.5-177m)

1962.5m of siltstone with occasional sandstone beds (Fig. 4). Mostly calcareous with common shell debris.

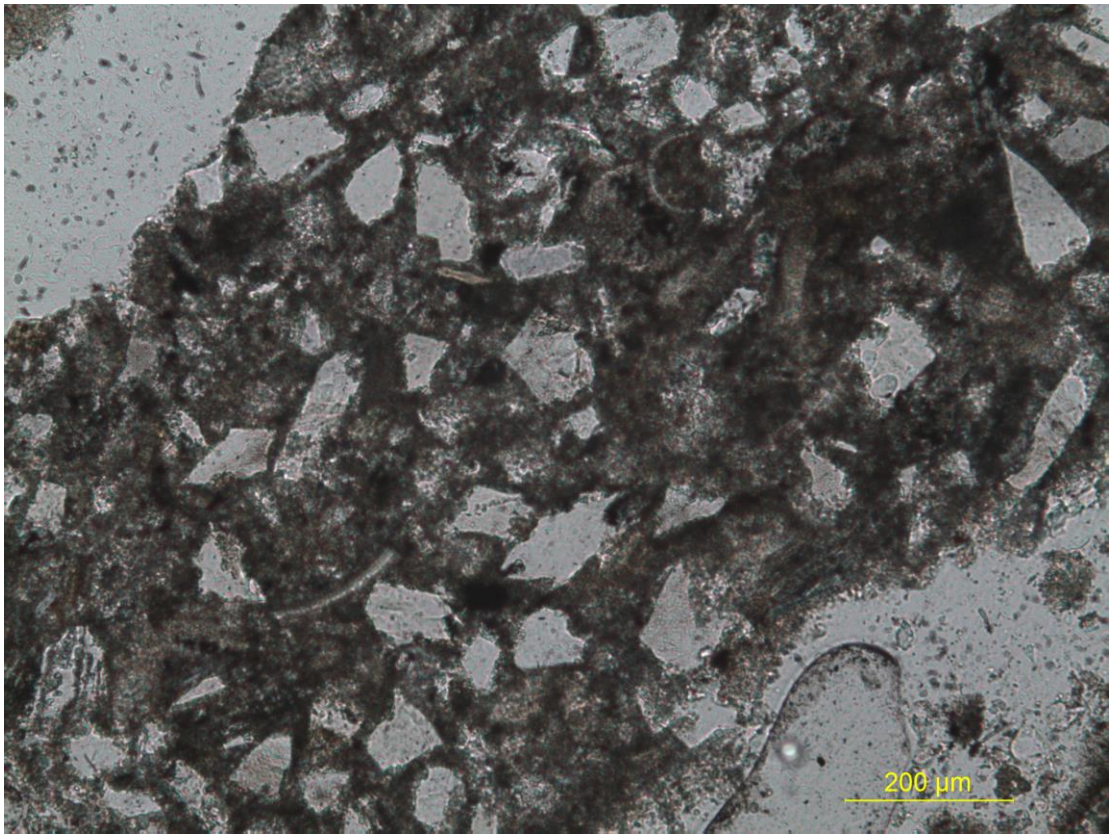

Fig. 4. Thin section of Tokama Siltstone from 780m depth in Clipper-1. Image in plane polarised light.

1.3 Exploration history

Exploration of the Canterbury Basin began onshore in 1914 when a 700m well was drilled northeast of Ashburton. Two more shallow wells were drilled in the early 1960s near Oamaru, followed by two deeper ones later that decade and another in 1978 near Amberley. Exploration recommenced in 2000 with the drilling of two more onshore wells near Rangiora and south west of Ashburton, followed by a final well near Amberley in 2008. None of these wells showed any potential for hydrocarbon extraction (Fig. 5).

The offshore areas of the Canterbury Basin were first investigated with seismic exploration in the 1970s. This was followed by more seismic exploration and five wells drilled from 1970 to 1985. Exploration recommenced in 2006 with the drilling of the Cutter-1 well. Details of the offshore wells are listed below. Unless otherwise stated, the wells were drilled by Shell BP Todd.

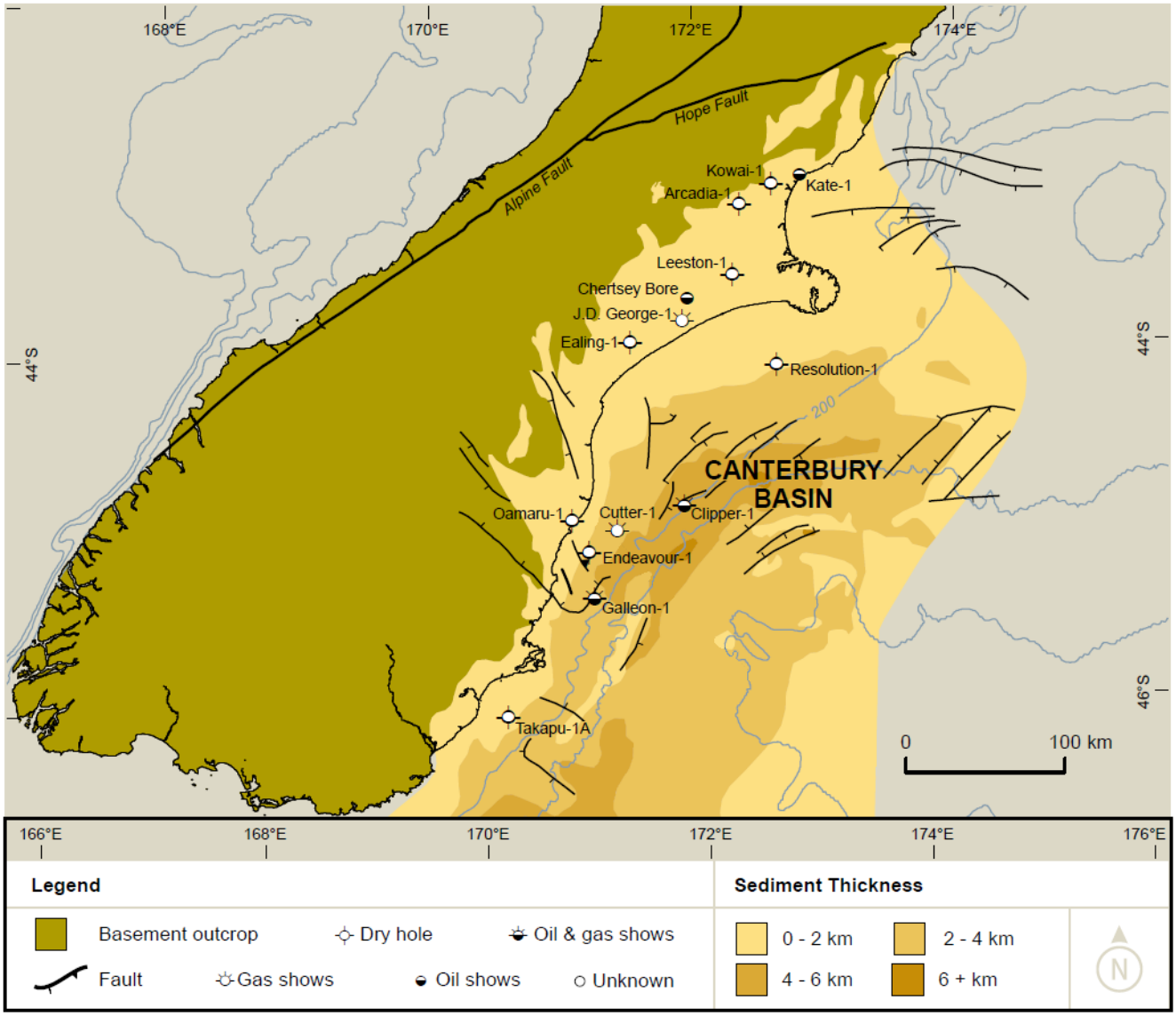

Fig. 5. Location of petroleum exploration wells in the Canterbury Basin (modified from NZP&M 2013b).

Endeavour-1

Endeavour-1 was drilled in 1970, and was the first offshore well to be drilled in the Canterbury Basin. It is located 20 kilometres southeast of Oamaru on the Endeavour High and reached a total depth of 2741m. It did not reach basement, but terminated in the Clipper Formation which lies directly on top of basement. No hydrocarbons were found.

Takapu-1A

Takapu-1A was drilled in 1974 by Hunt International Petroleum. It is located 35 kilometres south of Dunedin, at the southernmost end of the Canterbury Basin. As sediments at the basin margins are thin, the well reached basement at only 890m. No hydrocarbons were found.

Resolution-1

Resolution-1 was drilled in 1975. It is located 40km south of Banks Peninsula and reached a depth of 1963m. The well terminates in Cretaceous sediments intruded by a mafic sill of Miocene age, which may be related to the Miocene volcanism at Banks Peninsula. No hydrocarbons were found.

Clipper-1

Clipper-1 was drilled in 1984. It is located 80 kilometres east of Oamaru and near the basin's thickest sedimentary section (Field & Browne 1989). This location was chosen for drilling due to the presence of an anticline that may have acted as a trap structure for hydrocarbons generated by the Upper Cretaceous coal measures of the Clipper Formation. Sandstones, also in the Clipper Formation, could potentially act as a hydrocarbon reservoir capped by the lower-permeability siltstone of the Katiki Formation. The sandstones proved to be less permeable than expected due to the development of silica cement, illite and kaolinite during diagenesis. Small quantities of hydrocarbons were found in the Clipper, Katiki and Moeraki Formations, but due to their low volume and the poor permeability of the reservoir rocks the well was deemed uneconomic (Shell BP Todd 1984). Clipper-1 is by far the deepest well drilled in the Canterbury Basin, reaching a total depth of 4742m (BRT).

Galleon-1

Galleon-1 was drilled in 1985. It is located 24 km east of Shag Point, approximately halfway between Oamaru and Dunedin. It reached a depth of 3086m and terminated in microgabbro which has been determined by potassium-argon dating to be Paleocene in age (Haskell & Wylie 1997). The Katiki Formation yielded gas and gas condensate in sufficient quantities to warrant further testing, but ultimately the well was deemed uneconomic and abandoned.

Cutter-1

Cutter-1 was drilled in 2006 by Tap Oil, AWE, Beach and ANZON. It is located 36 kilometres east of Oamaru, and reached a depth of 2930m. Gas was encountered in Eocene sediments, but in insufficient quantities for any commercial development.

Scientific drilling

Four offshore boreholes were drilled in 2011 by the Integrated Ocean Drilling Program (IODP) on the edge of the continental shelf near Clipper-1. The purpose of this expedition was to investigate the effect of global sea level change (eustasy) on sedimentation above the Marshal Paraconformity (Fulthorpe et al. 2011). Core from below the paraconformity has been used in the study of stylolites: dissolution surfaces in limestones formed during burial (Vandeginste & John 2013).

Seismic surveys

Much of the research into sedimentation in the Canterbury Basin has been based on seismic surveys. These have mainly focused on the Miocene and later sediments, as the high sedimentation rates caused by the erosion of uplifted rocks along the Alpine Fault provides the best conditions for investigating sedimentary sequences (Fulthorpe 1991). Seismic data has been used to investigate the effect of various factors on sedimentation including eustasy, tectonic activity and ocean currents, and the interaction between them (Fulthorpe 1991; Fulthorpe & Carter 1991; Lu et al. 2005). This research has primarily been based on seismic surveys performed by BP Shell Todd during petroleum exploration in 1974 and 1982. Further surveys of the Clipper sub-basin were completed in 2013 by New Zealand Oil & Gas.

1.4 Burial and thermal history modelling

An important part of predicting the potential of a basin to produce petroleum is reconstructing the burial history of the potential petroleum source. This is required to determine whether the source rock has reached the temperatures required for oil generation (known as the oil generation window) and if so, when this occurred. If a source rock reached oil generating temperatures too far back in its history, any oil or gas produced may have dissipated through the overlying sediments and no longer be recoverable. The degree of heating experienced by the source rock is known as its thermal maturity. Burial by sediments is usually the primary method of heating, but igneous intrusions and fluid flow can also be important factors.

1.4.1 Vitrinite reflectance and VIRF

One of the standard methods of determining the maturity of a source rock is to measure the reflectance of vitrinite, a type of plant-derived organic matter found in coals and carbonaceous sediments (Taylor et al. 1998). Samples of the rock are mounted in pellets of resin and cut to produce a polished cross section. Light is directed at the surface in oil immersion and the percentage that is reflected back is measured. As vitrinite is exposed to higher temperatures, the ratio of carbon to volatile components increases as the volatiles are driven off. This results in a positive correlation between reflectance and source rock maturity.

Vitrinite reflectance (VR) works well in coals, where vitrinite can easily be distinguished from other organic materials, but in sediments with dispersed organic matter this can be impossible. Sediments may also be contaminated with material that has caved from further up the well, or contain older, re-worked organic matter derived from their sediment source. Vitrinite deposited in marine sediments is often perhydrous (hydrogen-rich), producing an anomalously low reflectance material known as suppressed vitrinite that is difficult to distinguish visually from normal (orthohydrous) vitrinite (Taylor et al. 1998). These factors make VR an unreliable method of determining the maturity of marine source rocks.

VIRF (vitrinite-inertinite reflectance & fluoresence) utilises quantitative fluorescence to objectively classify reflectance populations on a bivariate chart (Newman et al. 2000). It allows normal vitrinite to be distinguished from caved, reworked or perhydrous vitrinite, and from other organic constituents such as inertinite. Samples from Clipper-1 have been used in a case study comparing VIRF to VR (Newman et al. 2000). In addition to providing more accurate data on sediment maturity, features suggesting igneous intrusion and hydrothermal activity were noted. These include brecciation and the precipitation of sulfide and carbonate minerals in the lower part of the well. Textures indicative of coking were noted in coals in the Clipper Formation. Coking requires temperatures above 400°C. Present day temperatures in the Clipper Formation are below 200°C (Funnell 2005).

1.4.2 Modelling of the Canterbury Basin

Determining the thermal history of a basin first requires a burial history model, constructed using the age, depth, thickness and rock type of each sedimentary unit. Any compaction of the sediments during burial needs to be taken into account (Funnell 2005). Once a burial history model is established, it can be combined with data on thermal conditions including direct measurements of temperature in wells, any evidence of igneous intrusion and analysis of the organic matter contained within sediments, including coal if present. This allows the development of a maturity model, which defines the thermal history of the source rocks and their production of hydrocarbons through time (Funnell 2005).

In the Canterbury Basin, the potential petroleum source rocks are the coals and carbonaceous sediments deposited early in the basin's history, during and shortly after rifting in the Cretaceous (Field & Browne 1989). Other potential source rocks are Paleocene to Eocene carbonaceous shales including the Katiki, Waipawa and Moeraki Formations, although as these rocks are less deeply buried they are considered unlikely to have reached sufficient maturity to produce hydrocarbons (Sykes & Funnell 2002).

Early modelling of the thermal history of the Canterbury Basin focused on the sedimentary history and present-day temperature readings from the bottom of exploration wells. Funnell & Allis (1996) concluded that the sediments of the Canterbury Basin had

experienced a 20-40°C temperature rise over the past 5 million years due to the deposition of large foresets derived from glacial erosion of the Southern Alps. This model assumes that present-day thermal conditions represent the maximum temperatures experienced by the basin sediments, as they are at their maximum burial depth. This leads to the conclusion that any source rocks that have reached sufficient maturity to produce hydrocarbons have done so only recently.

More recently, a new modelling study was commissioned from GNS by Austal Pacific Energy (NZ) Ltd. (Funnell 2005). This report focused on the Clipper sub-basin and made use of new data to develop a more detailed model of its thermal history. In particular, the VIRF data provided by Newman et al. (2000) showed that the basin sediments had experienced a much more complex thermal history than could be explained solely by basin subsidence. Earlier analysis of Clipper-1 using standard vitrinite reflectance indicated a fairly simple profile for the well, with reflectance increasing gradually with depth down to 3500m followed by a more rapid increase to the bottom of the well (Field & Browne 1989). In contrast, the VIRF data produced by Newman et al. (2000) shows a more complex profile with four distinct segments (Fig. 6).

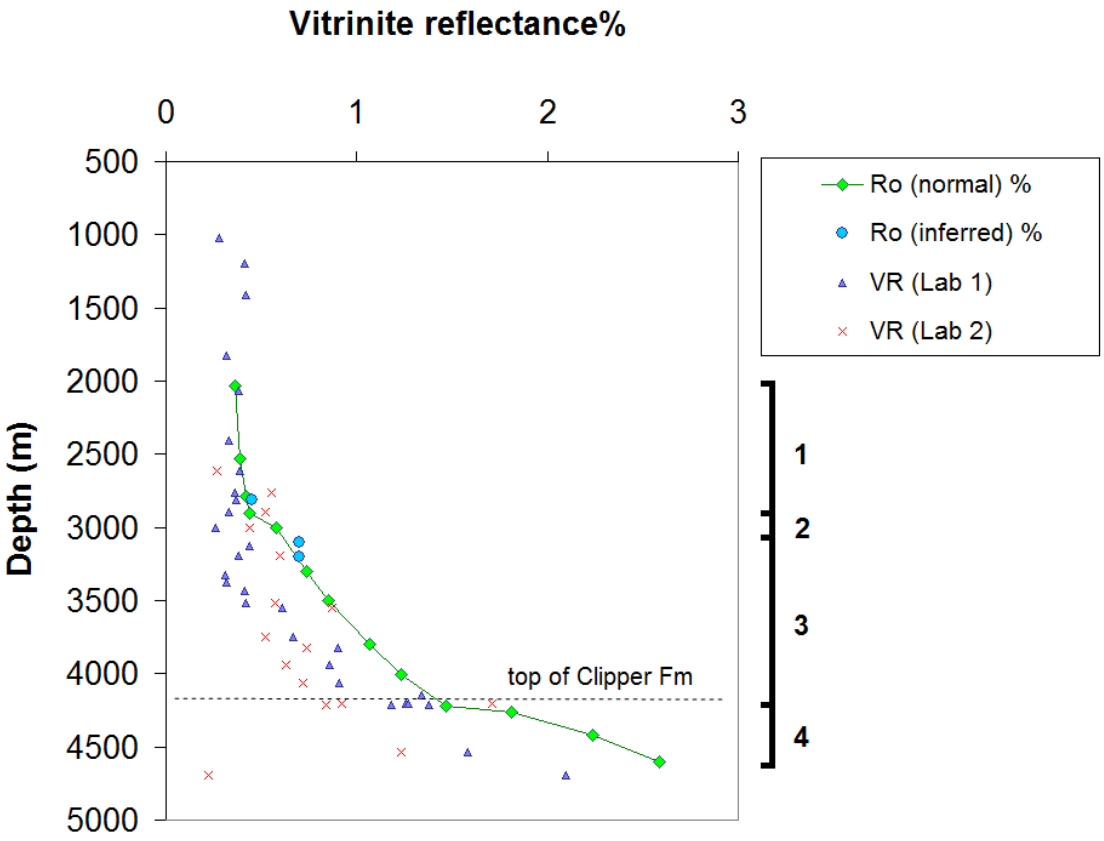

Fig. 6. VIRF (Ro normal %) and VR profiles for Clipper-1. The numbered sections define distinct segments of the profile:

1. A gradual increase in vitrinite reflectance from the uppermost analysed sample (2035m) down to 2905m.

2. A distinct step in vitrinite reflectance from 0.44% to 0.58% between 2905m and 3005m.

3. A steep increase in vitrinite reflectance between 3005m and 4222m.

4. A very steep increase in vitrinite reflectance between 4222m and the base of the sediments.

In order to explain the sharp increase in vitrinite reflectance below 4222m, Funnell (2005) modelled an igneous intrusion below the basement contact, estimated to occur immediately following rifting at 85 Ma. His inferred temperature history is of high heat flow conditions in the Cretaceous followed by a gradual cooling until the late Miocene, when the uplift of the Southern Alps produced a sharp increase in sedimentation and rapid burial of the older sediments.

However, this intrusion could not be the cause of the step in reflectance around 3000m or the rapid increase in the Katiki and lower Moeraki Formations, as with the exception of the lower Katiki Formation these sediments were deposited after the completion of rifting. In order to explain these features of the VIRF profile, Funnell (2005) inferred a late Miocene intrusion at 4000m depth, possibly related to the volcanic activity occurring at that time at Dunedin and Banks Peninsula. This is based entirely on the VIRF profile, as no physical evidence has been found for an intrusion at that level. The step in reflectance around 3000m remains unexplained. Features such as this can be caused by the erosion of a previous sediment covering, but in this case the erosion of around 1000m of sediment would be required (Newman et al. 2000). This event would form a major unconformity in the Moeraki Formation, and as biostratigraphic and seismic data do not indicate the presence of an unconformity here another explanation is more likely. Other possibilities suggested by Funnell (2005) include a facies change or heating by advective fluid flow. Normal faulting could also produce a step in reflectance values by bringing shallower, lower maturity sediments in the hanging wall into contact with the deeper, higher maturity sediments of the footwall (Newman et al. 2000).

1.4.3 Present-day thermal conditions

Temperature readings from the bottom of exploration wells can be used to calculate the surface heat flow in that area of the basin. Surface heat flow across the Canterbury Basin is not uniform, indicating that sediment thickness is not the only factor affecting the present-day thermal conditions of the basin (Funnell & Allis 1996). Onshore wells show a lower heat flow than would be expected for their depth, possibly due to the infiltration of cold groundwater from aquifers beneath the Canterbury Plains. Offshore, heat flow is higher in

the central and southern areas of the basin than in the north. Resolution-1, located 40km south of Banks Peninsula, has a surface heat flow of 63 mW m^{-2}. This is comparable to the heat flow of other New Zealand sedimentary basins including the Great South Basin and parts of the Taranaki Basin (Funnell & Allis 1996). Further south, the heat flow around Galleon-1, Endeavour-1 and Clipper-1 ranges from 71 to 74 mW m^{-2} (Funnell & Allis 1996; Funnell 2005). At the far southern end of the basin, Takapu-1A and shallow onshore wells near Dunedin show a heat flow of 85 mW m^{-2} and higher. This suggests that partial melting of the mantle is occurring at shallow depths in the area around the Otago Peninsula, possibly a remnant of the Miocene volcanic activity which produced the Dunedin Volcanic Field (Funnell & Allis 1996). This is further supported by anomalies in the ratio of ^{3}He to ^{4}He detected in gas seeps near Dunedin and Oamaru (Giggenbach et al. 1993). The lower heat flow in Resolution-1 suggests the Banks Peninsula Volcanic Field, despite being of the same age, does not have any residual activity at depth.

It is uncertain whether the high heat flow in Galleon-1, Endeavour-1 and Clipper-1 is related to the thermal anomaly around Dunedin or due to other factors. This is particularly true of Clipper-1, which is substantially further away from the Dunedin Volcanic Field than the other two wells. Analysis of the oils and condensates in Clipper-1 and Galleon-1 suggests that the sediments at the bottom of those wells have experienced a recent thermal event which may be due to the Dunedin thermal anomaly (Funnell & Allis 1996). Hot connate water from deeper in the basin has been suggested as another possible cause (Gibbons & Fry 1986).

2.0 Methods

Cuttings from Clipper-1 were obtained from Newman Energy Research Ltd and the New Zealand Petroleum and Minerals core store in Featherston. Samples from other offshore Canterbury Basin wells were also obtained from Newman Energy Research Ltd. Clipper-1 was chosen as the main focus as this well covers the full depth of the Canterbury Basin down to the basement rock, and unusual minerals and textures had been noted during previous work by Newman Energy Research Ltd.

2.1 Outcrop sampling

Igneous rocks and associated sediments and secondary minerals were sampled from outcrops in Otago and Lyttelton Harbour in order to look for examples of similar minerals and textures to those found in the offshore Canterbury Basin, as outcrops provides information on intrusive environment and igneous structures that are difficult or impossible to discern from well cuttings. A rock hammer was used to break up the samples and expose unweathered material where available. In the case of porous or poorly indurated sediments, selected pieces were further crushed with a mortar and pestle to allow resin to soak into the material. Hard, low-porosity samples were broken into chips 5-10mm in length with a rock hammer.

2.2 Sample preparation

Samples were dried at 50°C, then mounted in 3cm wide pellets of polyester or epoxy resin. Epoxy was used for samples that had produced sharp-edged fragments during crushing, as polyester resin is more brittle and these can cause it to split during curing. The drying process is needed to avoid moisture in the samples interfering with the resin curing process. Once cured, the pellets were mechanically ground and polished to produce a polished section for reflectance microscope analysis. (Fig. 7).

Fig. 7. Polished sample pellet attached to glass slide for reflected light analysis.

2.3 Mineral identification and photography

Initial mineral identification was based on the visible properties of a polished surface under reflected light (non-polarised, plane and cross polarised) using a Zeiss UMSP50 microscope (Fig. 8). Properties examined included colour, hardness (indicated by scratches produced during polishing), crystal structure, isotropy and internal reflections. Further identifications could be made by measuring the reflectance of a polished mineral surface. Samples of pure magnetite and pyrite were used as calibration standards. In order to produce high-quality photographs, oil immersion was used and large subjects were photographed in multiple frames under high power magnification for the construction of high-resolution photomontages.

Fig. 8. Zeiss UMSP50 microscope used for reflected light analysis.

In order to supplement the visual identification of minerals and determine the composition of metals and glass, selected samples were analysed for elemental composition using a JSM7000F scanning electron microscope with EDS x-ray detector. SEM analysis requires that the sample be coated with a conductive material. As native metals had been identified using reflectance microscopy, carbon was chosen for the coating rather than gold or other metals.

Thin sections of selected samples were prepared in order to identify translucent minerals and textures that are difficult to view using reflectance microscopy. These were examined and photographed in plane and cross polarised light. Resin pellets previously used for reflectance microscopy were re-used as material for thin sectioning.

The sample depths and analyses performed are listed in Table 1. In addition to the samples analysed by light microscope and SEM, loose cuttings from every 50m of Clipper-1 were visually assessed for mineralisation and exposed to a magnet in order to detect ferrous minerals.

Sample depth (m)	Reflected light	Thin section	SEM
780	•	•	
1010	•		
1570	•		
2035	•		•
2055	•		•
2125	•	•	•
2325	•		
2765	•		
2775	•		
2795	•		
2905	•		
2950	•		
3400	•		
3550	•		
3625	•		
3799	•		
3901	•		
4198	•		
4222	•		
4313	•		
4603	•		
4666	•		
4675	•		
4681	•		
4702	•		
4741	•	•	

Table 1. Sample depths and type of microscope analysis performed on samples from Clipper-1.

A pure sample of one type of mineral assemblage was hand-picked and sent to GNS for qualitative X-ray diffraction to determine the mineralogy. This analysis was performed using a Phillips X'Pert Pro instrument using CoKα radiation and the following operating conditions:

Start Position [°2Th.]	2.000
End Position [°2Th.]	80.000
Step Size [°2Th.]	0.050
Scan Step Time [s]	1.00
Generator Settings	40kV, 45mA

In order to determine the origin of a particular mineral assemblage, X-ray fluorescence was used to determine its trace element concentrations. This can indicate whether a rock originated in the crust or the mantle. The analysis was performed simultaneously by CRL Energy Ltd and the University of Canterbury in order to ensure the accuracy of the results.

3.0 Clipper-1 secondary minerals and textures

The majority of the analysed material from the offshore Canterbury Basin comes from the Clipper-1 cuttings, as this well contains the richest and most varied igneous and hydrothermal minerals and textures. Samples were obtained from Newman Energy Research Ltd and the NZ Petroleum & Minerals core store in Featherston.

The data obtained by this study is largely visual. Opaque minerals have been photographed in reflected light under oil immersion in order to obtain the highest possible image quality. Transparent and translucent minerals have also been photographed in thin section. Photomontages, made by joining multiple photographs taken at high magnification in oil immersion, have been made to show structures and textures in high resolution. All photomicrographs are taken in oil immersion and unpolarised light unless otherwise stated.

In order to confirm the mineral identifications made from optical characteristics, the elemental composition of the various minerals has been analysed using a scanning electron microscope with EDS x-ray detector. This also provides information on the composition of glass, which lacks identifying crystal structures, and the alloying elements or impurities present in native metals. Elemental composition is listed here as major elements with quantities in mass % normalised to 100%. A major element is defined as one that occurs at a concentration of at least 1% by mass in at least one sample of the mineral. Due to carbon coating of the samples in preparation for SEM analysis, carbon has been omitted from most analyses. For the complete results from the elemental analysis of Clipper-1 material using SEM with EDS, see Appendix 1.

3.1 Opaque iron oxides

Iron minerals are a common feature in Clipper-1 and they occur as three distinct assemblages. The first is referred to here as "opaque iron oxides" due to their lack of internal reflections. These commonly occur as linear veins, often with small internal voids and sometimes displaying growth bands. They are grey in colour with patches of differing

reflectance, suggesting that they are a mix of several minerals (Fig. 9). When viewed in cross-section, veins may display internal shrinkage cracks resembling columnar jointing. The internal cracks and pore spaces may be partially infilled with pyrite (Fig. 10).

Edges, including both original vein edges and broken surfaces, are commonly altered to hematite, which can be recognised in reflected light by its blue-grey colour with red internal reflections (Fig 11-12). Broken vein fragments are commonly found incorporated into other iron mineral formations, indicating that the opaque oxides were formed earlier than the surrounding minerals (Fig. 13). This material is interpreted to be an early phase of mineralisation, formed by hydrothermal activity in advance of a magmatic intrusion.

The major element composition as measured by SEM with EDS indicates that the majority of the oxides are wüstite (FeO) with small amounts of manganese (Table 2).

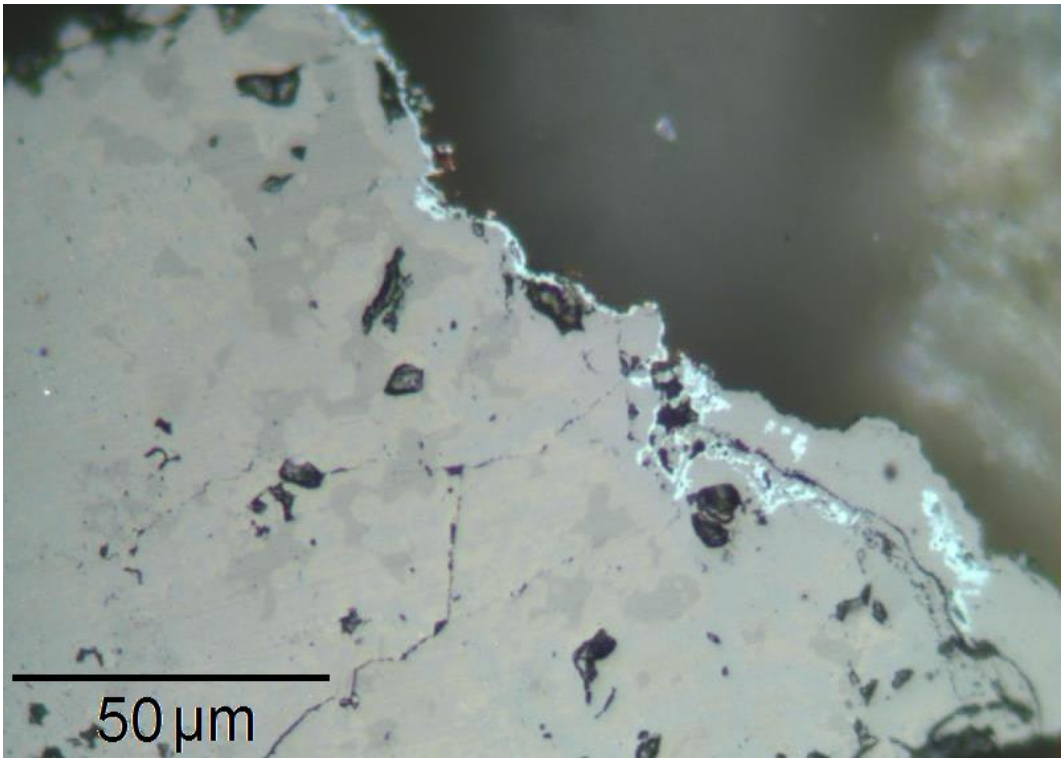

Fig. 9. Iron oxide vein with variable reflectance suggesting that a mix of minerals are present (medium grey shades), with hematite alteration at the edge (light blue-grey). From 2035m depth in Clipper-1, image in reflected light.

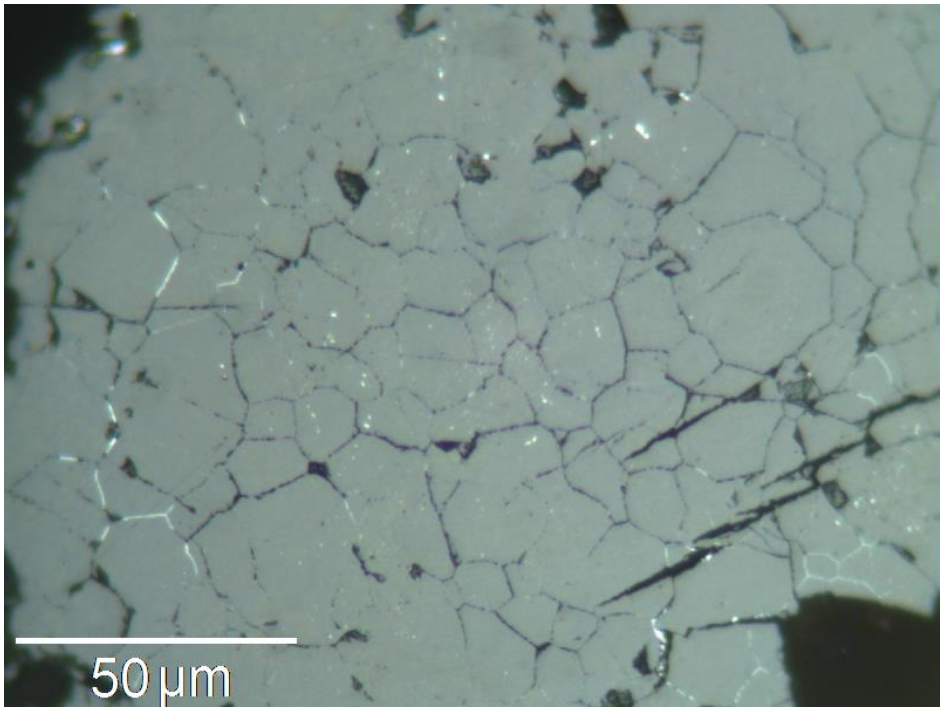

Fig. 10. Cross-section of iron oxide vein (grey) with shrinkage cracks and secondary pyrite (white). From 2035m depth in Clipper-1, image in reflected light.

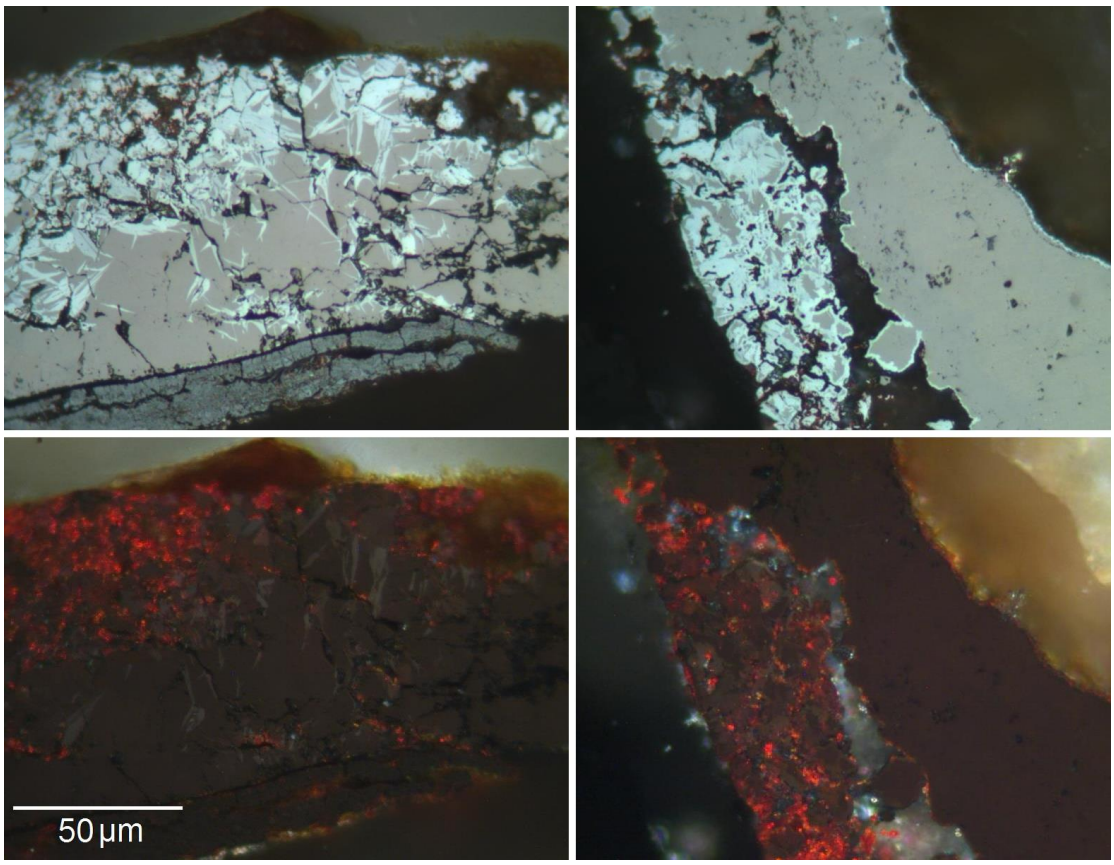

Fig. 11. Plane polarised (top) and cross polarised images of iron oxide vein with hematite alteration. Small, broken fragments show bright red internal reflections in cross polarised light, a distinctive feature of hematite. From 2035m depth in Clipper-1, image in reflected light.

Fig. 12. Photomontage of a large fragment of iron oxide vein. Hematite alteration (blue-white) on vein edges and in pore spaces indicate surfaces exposed to hydrothermal fluids. The surfaces without hematite alteration are fresh breaks produced during sample collection. From 2035m depth in Clipper-1, image in reflected light.

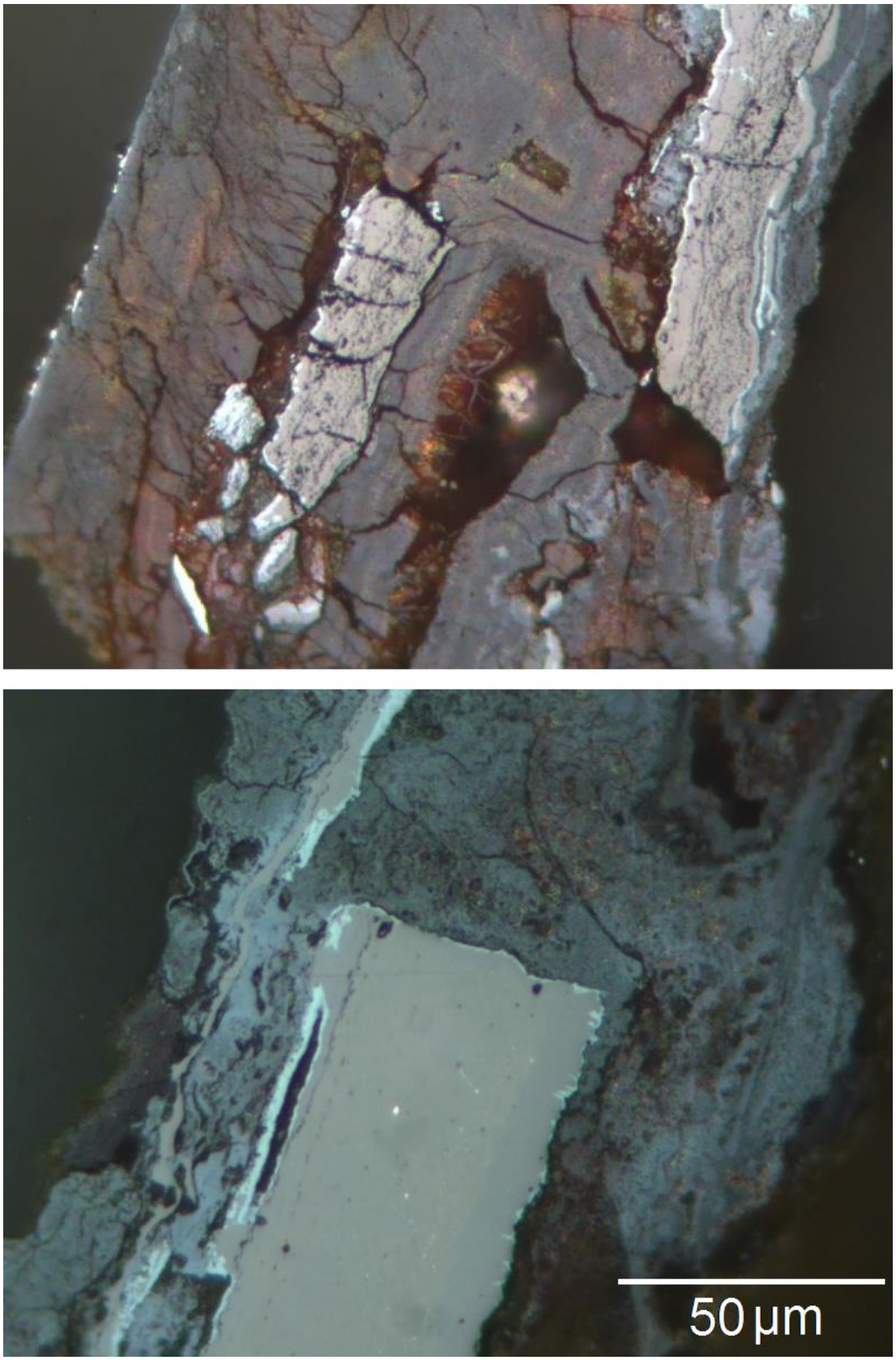

Fig. 13. Broken fragments of iron oxide veins surrounded by later mineral growth. From 2035m depth in Clipper-1, image in reflected light.

Sample	Fe	O	Mn
2035 024	80.4	18.6	1.0
2035 025	77.3	22.0	0.7
2035 026	74.9	24.1	0.9
2035 027	80.7	18.3	1.0
2055 001	72.9	25.7	1.4
2055 002	74.0	24.8	1.2
2055 003	72.5	25.8	1.7
2055 004	72.9	25.4	1.7
2055 005	74.4	24.5	1.0
2055 006	73.9	25.0	1.1
2055 007	74.3	24.6	1.1
2055 008	74.5	24.3	1.2
2055 010	69.3	29.4	1.3
2055 013	74.2	24.9	0.9
2055 014	71.6	26.7	1.6

Table 2. Major element composition of solid iron oxides from Clipper-1 samples at 2035 and 2055m depth. Figures are in mass% (Appendix 1).

3.2 Fissure fillings

Iron-based fissure fillings are a common feature in Clipper-1, with an extremely high concentration in the lower mineralisation band and significant amounts in the upper band (Chapter 3.5). Lower concentrations are found in sediments between the lower band and the bottom of the well. Fissure fillings consist of a lens or tube-shaped intrusion of iron minerals into sediments (Fig 14-15). The edge of the fissure features a sharply-defined boundary between intruded material and the surrounding sediment, which is often cemented with iron oxides (Fig. 16). The interior of the fissure mostly comprises iron oxide and hydroxide minerals, primarily goethite, but may also contain native iron, pearlite, graphite and occasional oil inclusions (Fig. 17). The fissure fillings are usually solid but occasionally contain a central void (Fig. 18).

Due to the cementation of the surrounding sediment, fissure fillings are often found as intact structures that have been separated from the surrounding less-altered sediments during drilling. This allows the full structure of the fissures to be seen even in crushed material. However, it is difficult to determine the true extent of sediment alteration around the fissures as less well-cemented material has usually been broken away.

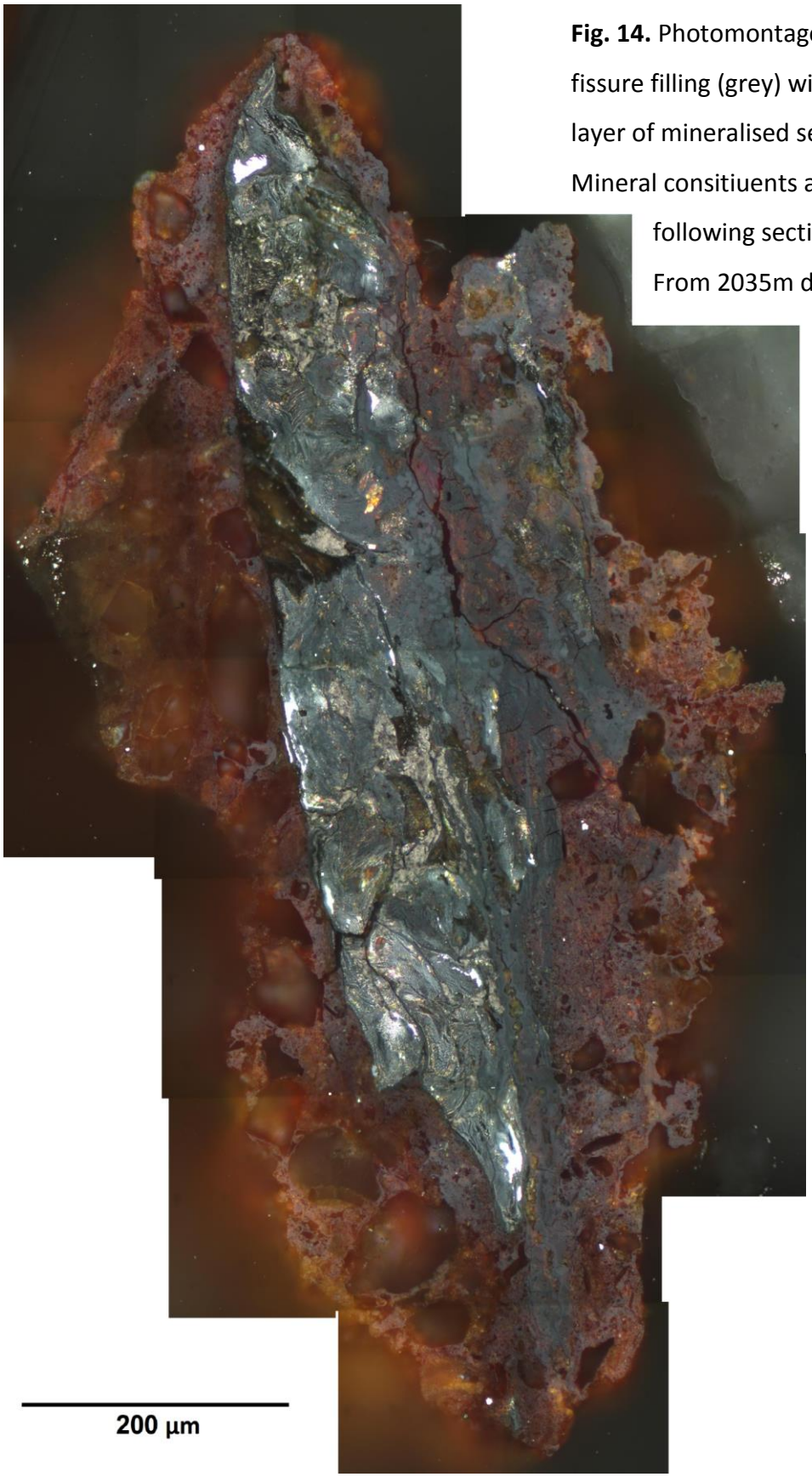

Fig. 14. Photomontage of an intact fissure filling (grey) with surrounding layer of mineralised sediment (orange). Mineral consitiuents are described in the following sections (3.2.1-3.2.4). From 2035m depth in Clipper-1, image in reflected light.

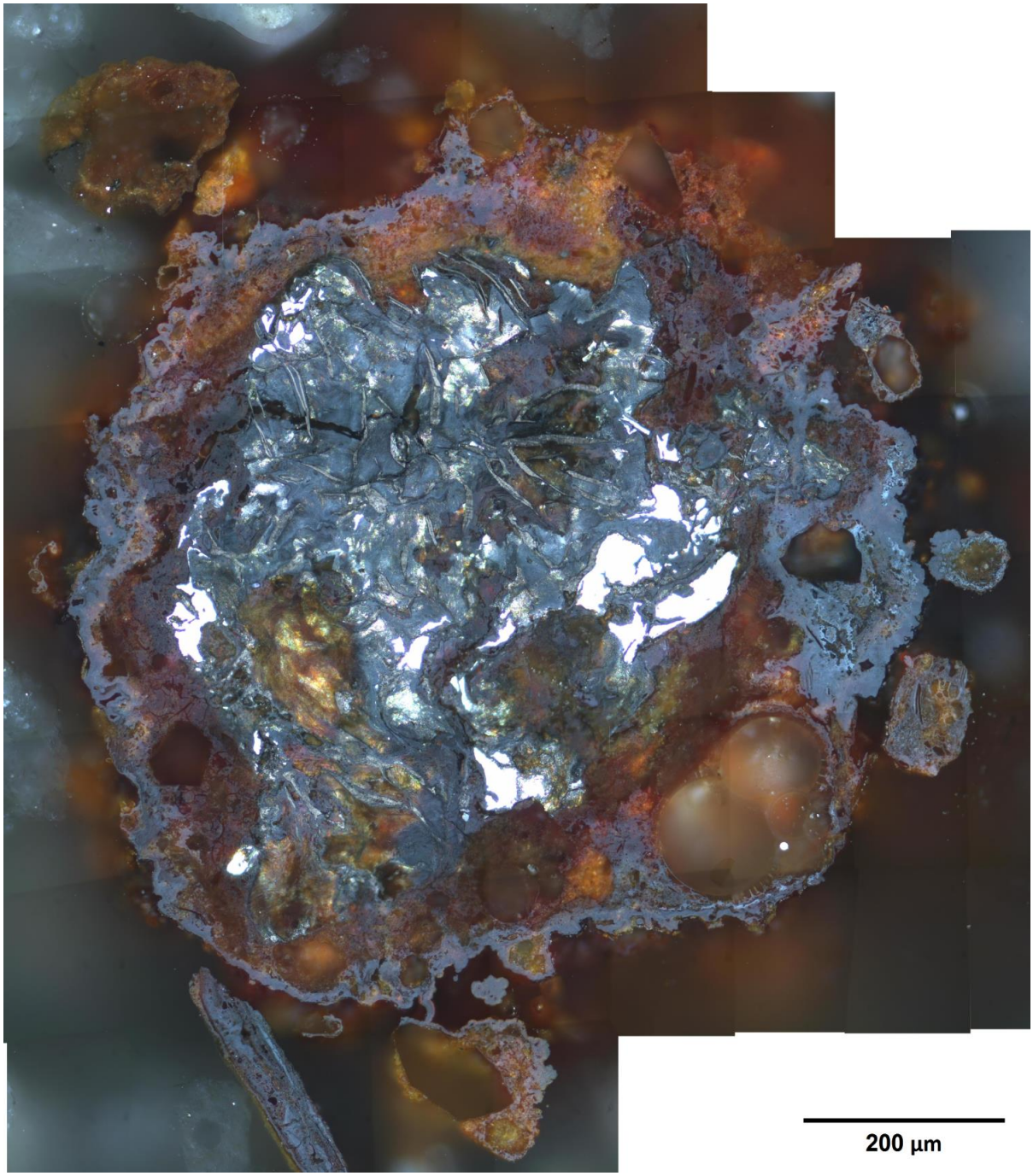

Fig. 15. Photomontage of a cross-section of a tube-shaped fissure filling. The mineralised sediment on the outer edge includes microscopic shells (lower right). From 2035m depth in Clipper-1, image in reflected light.

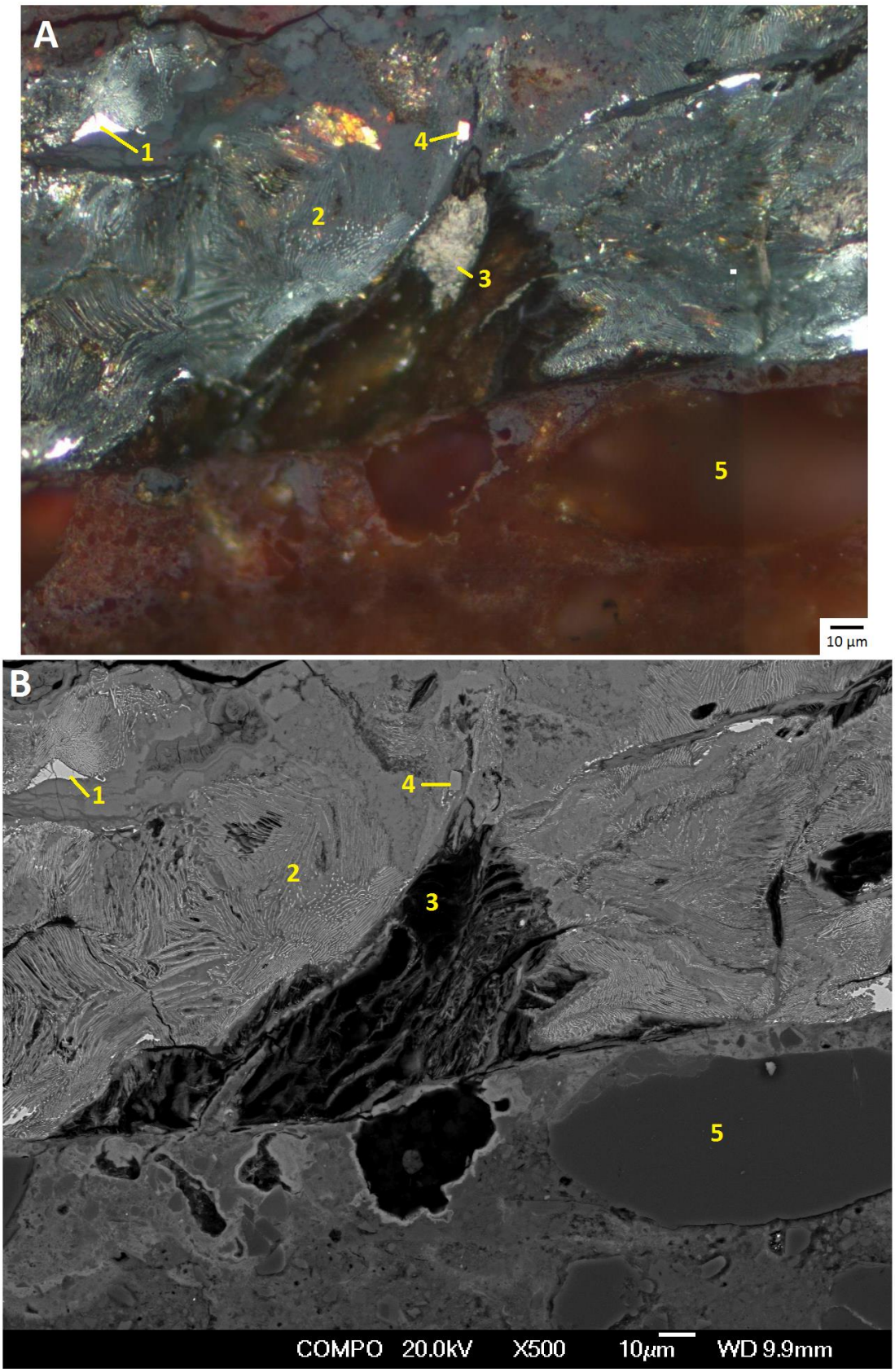

Fig. 16. The sharply-defined edge between a fissure filling and the surrounding iron cemented sediment in reflected light (A) and under SEM (B). (1) Ferrite, (2) Pearlite, (3) Graphite, (4) Titanium, (5) Sediment grains. From 2035m depth in Clipper-1.

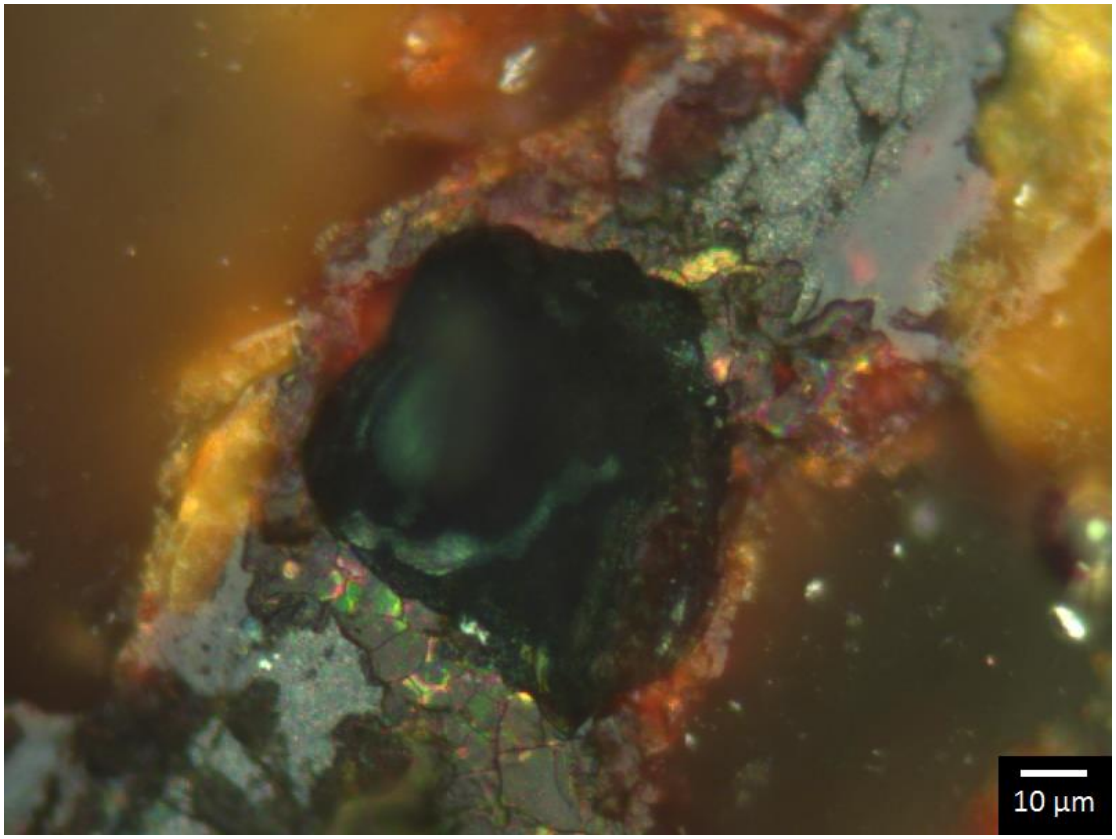

Fig. 17. Oil inclusion in a fissure filling (dark green, centre). From 3550m depth in Clipper-1, image in reflected light.

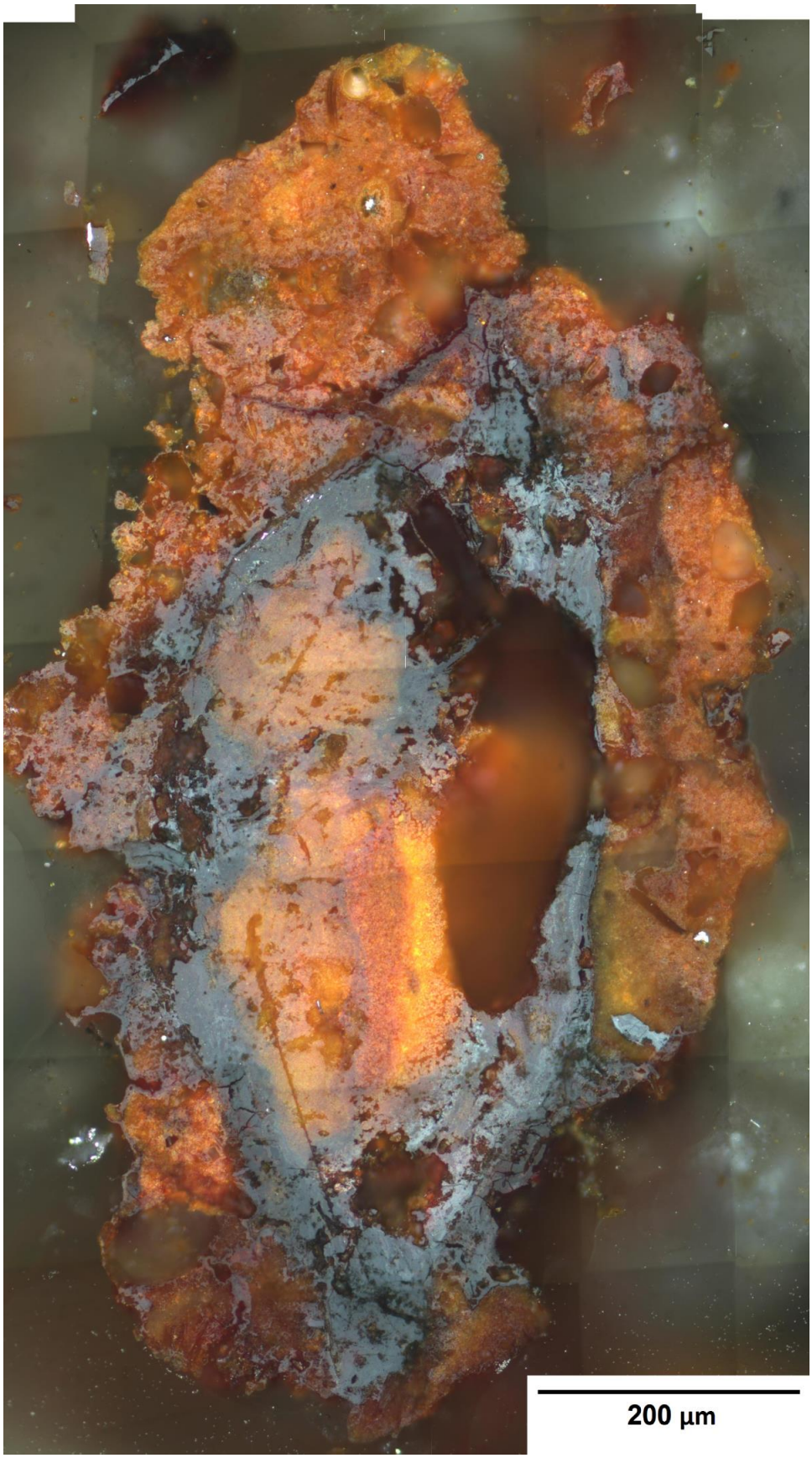

Fig. 18. Photomontage of an intact fissure filling with a central void. Image in reflected light, from 2125m depth in Clipper-1.

3.2.1 Goethite

Goethite (FeO(OH)) is the most abundant component of fissure fillings in Clipper-1. It is also commonly found on the outer edges of opaque oxide veins or surrounding broken fragments, and also occurs in isolation. It is medium grey and partially translucent with strong orange internal reflections. Goethite commonly occurs in acicular or botryoidal crystal shapes, indicating growth into an open void space (Fig 19-20). Analysis of the elemental composition of the major components of fissure fillings in Clipper-1 indicates that the goethite is mixed with smaller concentrations of wüstite, as the concentration of iron is higher than in pure goethite (Table 3).

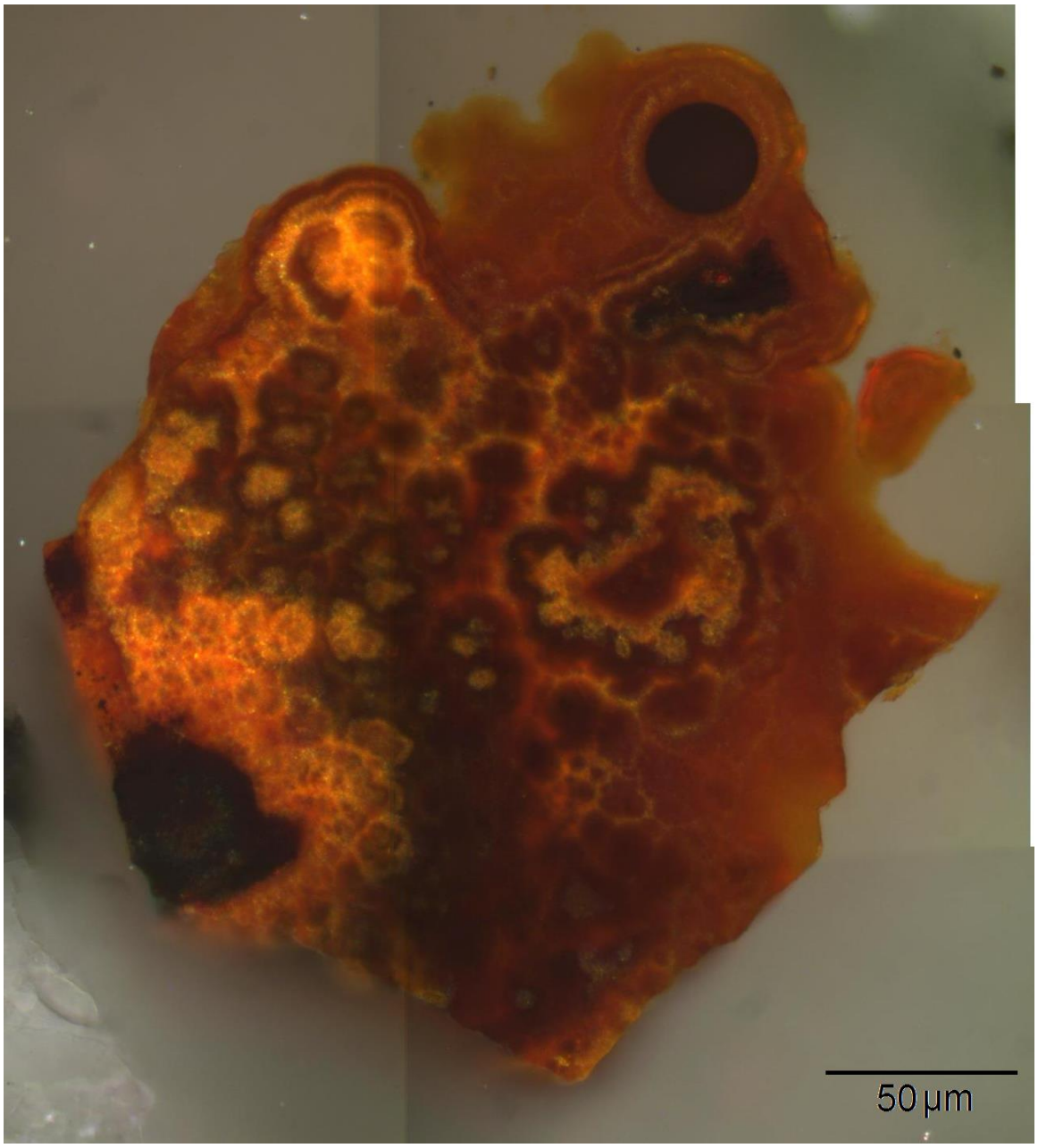

Fig. 19. Photomontage of botryoidal goethite and wüstite (opaque circle, top right) in cross-polarised reflected light. From 2035m depth in Clipper-1.

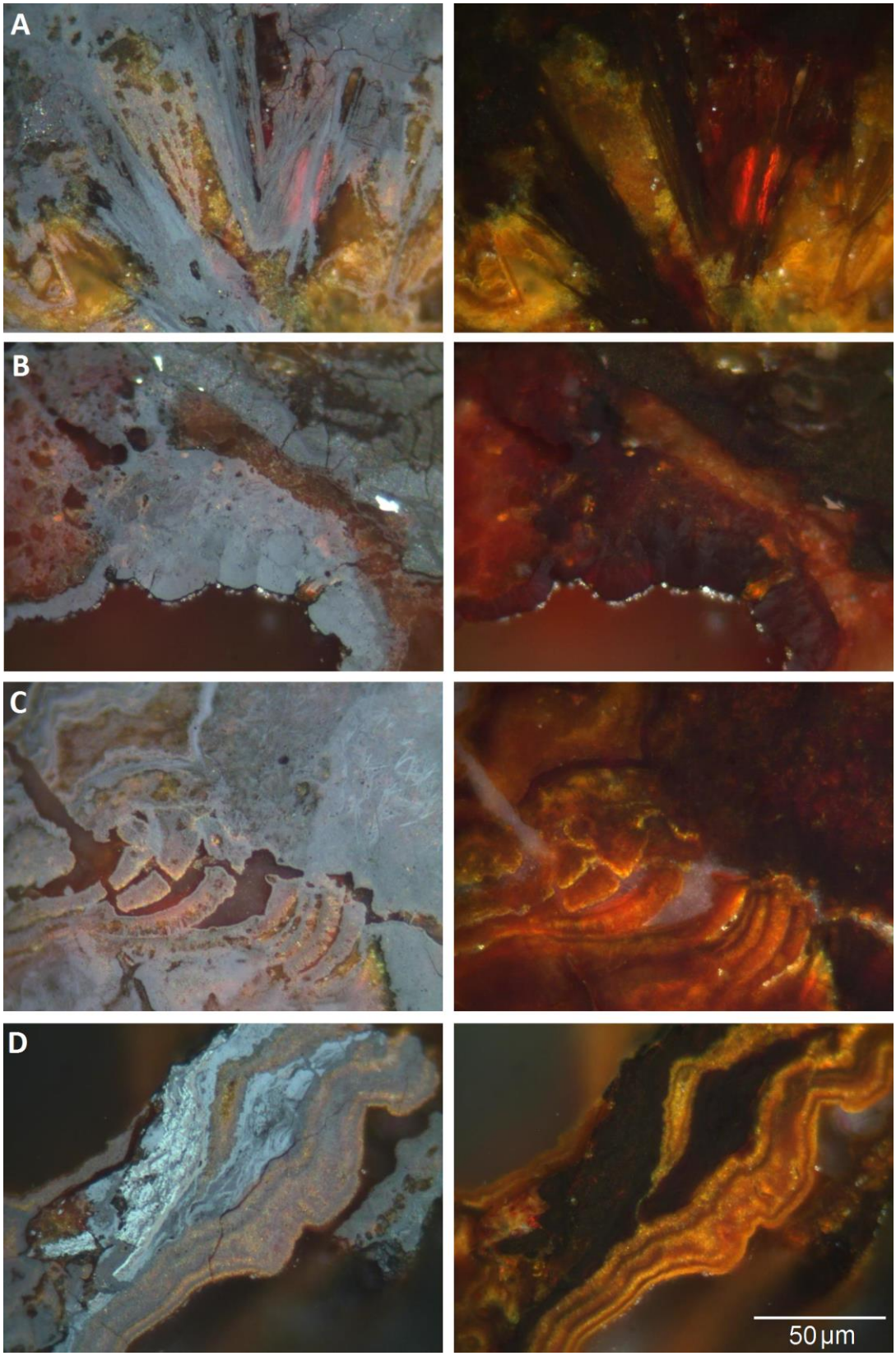

Fig. 20. Plane polarised (left) and cross polarised (right) reflected light images of goethite crystal growths in Clipper-1 indicating the presence of open pore space. (A). Acicular crystals, (B). Botryoidal crystals, (C-D). A mixture of both crystal forms. From 2035m and 2125m depth in Clipper-1.

Sample	Fe	O	Ca	Si	Na	Cl
2055 094	61.3	30.4	4.6	2.0	1.6	-
2055 095	67.6	30.5	0.4	0.6	0.9	-
2055 096	66.7	29.8	2.1	0.8	0.6	-
2055 097	71.2	22.5	-	-	-	6.3
2055 098	60.6	36.1	0.6	0.5	1.7	0.5

Table 3. Elemental composition of goethite in fissure fillings measured by SEM with EDS. Figures are in mass % (Appendix 1).

3.2.2 Ferrite

Ferrite, the pure form of native iron, occurs as solid, amorphous blobs surrounded by iron oxides and hydroxides (Fig. 21). Polished surfaces may display a faint myrmekitic texture (Fig. 22). This becomes more apparent when the surface is corroded by oil inclusions (Fig. 23). Small crystals of impure titanium 5-10 µm in length are occasionally present in the native iron or surrounding iron oxides (Fig. 24). Ferrite frequently occurs as small, irregular-shaped blobs in the interior of fissure fillings, and more rarely as larger, more solid veins. The iron contains silicon and manganese in concentrations of 1-2% by mass (Table 4). Carbon is almost certainly present, but was not able to be measured due to carbon coating of the sample for SEM analysis. One titanium crystal from a depth of 2035m was analysed. It is a titanium-iron alloy with small concentrations of vanadium, chromium and silicon (Table 4).

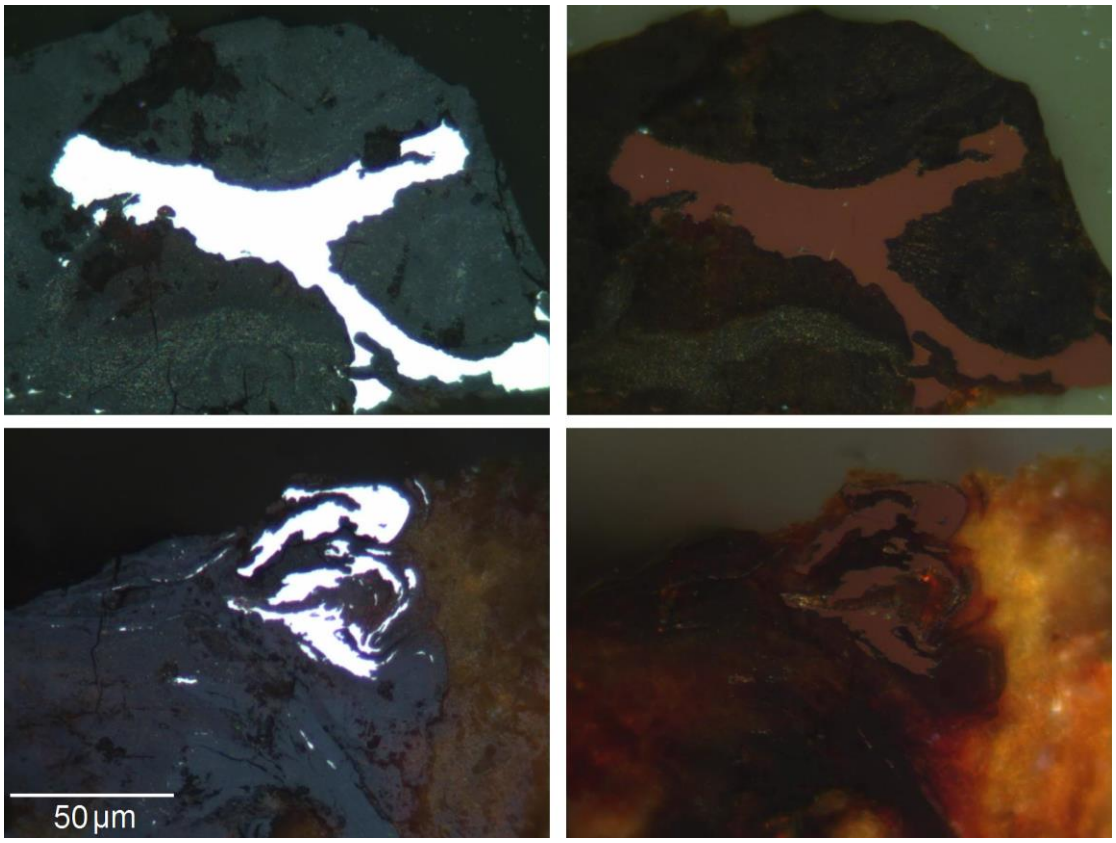

Fig. 21. Photos of polished ferrite in plane polarised reflected light (bright white, left) and cross polarised reflected light (brown, right).

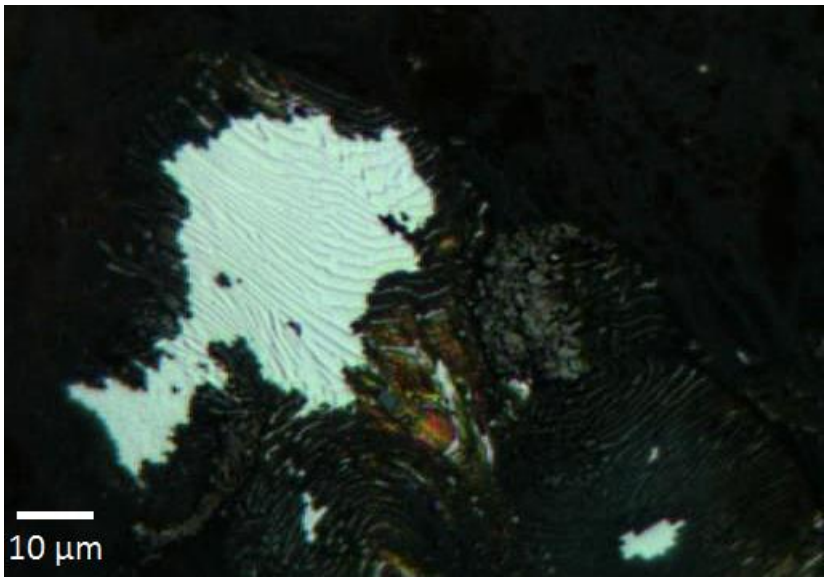

Fig. 22. Ferrite displaying a myrmekitic texture. In Clipper-1 at 2035m, image in reflected light.

Fig. 23. A small oil inclusion in a piece of ferrite has been cut during polishing, allowing the oil to seep out. This has corroded the polished surface of the iron, revealing a myrmekitic texture. From Clipper-1 at 2125m, image in reflected light.

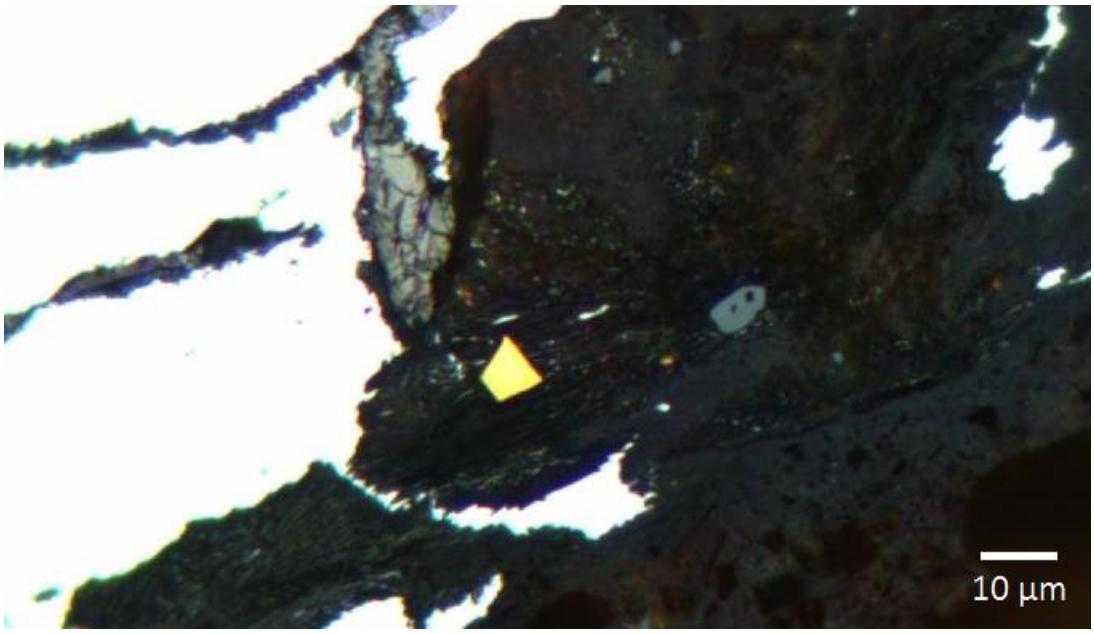

Fig. 24. A small crystal of impure titanium (yellow) contained in the iron oxides surrounding a vein of ferrite (white). From Clipper-1 at 2125m, image in reflected light.

Ferrite

Sample	Fe	Si	Mn
2035 012	97.2	1.8	1.0
2055 099	97.1	1.1	1.8
2055 100	98.4	1.6	-
2055 101	97.3	1.5	1.2
2055 102	98.3	1.7	-
2055 103	97.1	1.7	1.2

Titanium

Sample	Ti	Fe	Cr	V	Si
2035 030	67.0	27.2	2.1	2.0	1.7

Table 4. Elemental composition of ferrite and titanium found in fissure fillings measured by SEM with EDS. Figures are in mass % (Appendix 1).

3.2.3 Pearlite

A material consisting of very fine lamellae of native iron, resembling a myrmekitic texture (Fig. 25). The lamellae can often be observed as a continuous texture crossing from myrmekitic ferrite to pearlite. This texture commonly occurs in industrially-produced cast iron. Analysis of the elemental composition using SEM with EDS indicates that the Clipper-1 pearlite contains a substantial concentration of iron oxides (Table 5). Silicon is present in higher concentrations than in the associated ferrite. Sodium, manganese and chlorine are present in variable concentrations below 3%.

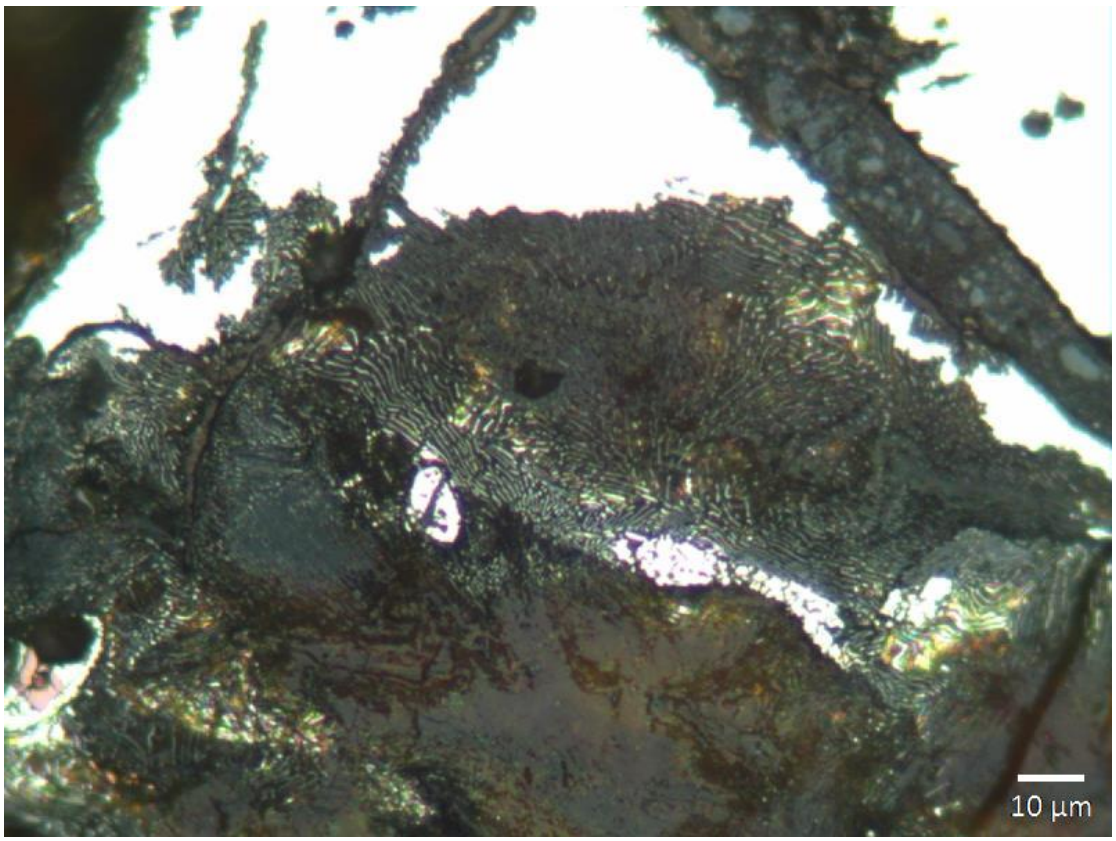

Fig. 25. Pearlite at the edge of ferrite. From Clipper-1 at 2125m, image in reflected light.

Sample	Fe	O	Si	Mn	Na	Cl
2035 016	68.3	21.6	5.8	2.9	1.4	-
2035 017	56.8	34.9	4.3	0.5	1.5	1.9
2035 018	65.7	28.1	4.2	0.8	1.2	-
2035 029	69.0	27.5	3.5	-	-	-
2055 105	63.2	31.4	2.7	-	1.3	1.4

Table 5. Elemental composition of pearlite found in fissure fillings measured by SEM with EDS. Figures are in mass % (Appendix 1).

3.2.4 Graphite

In fissure fillings where pearlite is present, distinctive V-shaped inclusions of graphite may occur (Fig. 26). This is also a feature observed in industrially-produced cast iron. Analysis by SEM with EDS has detected substantial concentrations of iron oxide, and silicon in concentrations of up to 1% (Table 6).

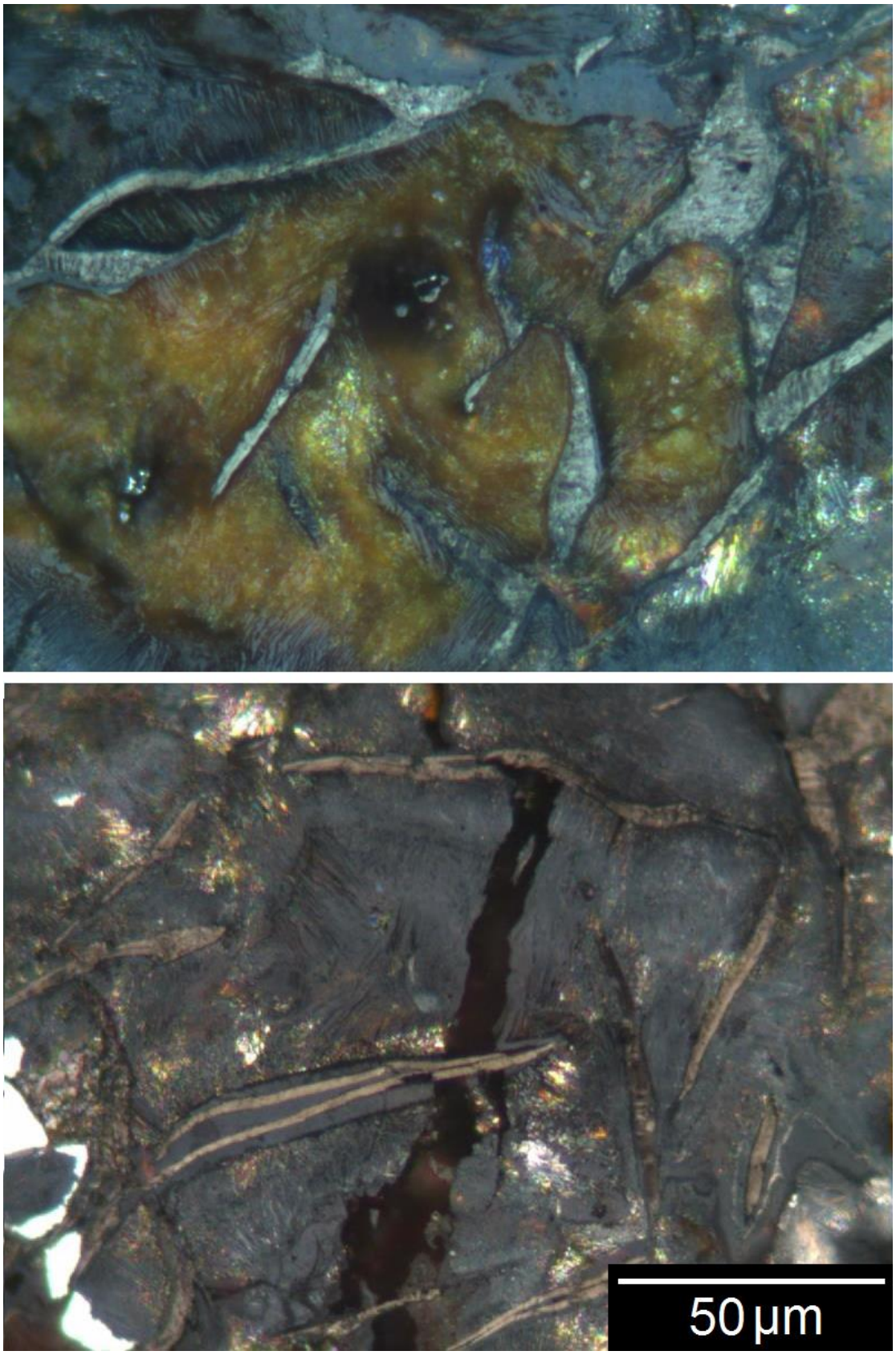

Fig. 26. V-shaped graphite inclusions associated with ferrite, iron oxides and pearlite. Image in reflected light, from 2035m depth in Clipper-1.

Sample	C	O	Fe	Si
2035 013	76.1	16.8	6.3	0.8
2035 014	68.0	16.6	14.6	0.7
2035 015	77.0	11.2	11.5	0.4
2035 028	87.8	7.9	4.0	0.3
2055 104	83.8	10.5	4.7	1.0

Table 6. Elemental composition of graphite found in fissure fillings measured by SEM with EDS. Figures are in mass % (Appendix 1). Although carbon coating of the sample for SEM analysis may affect the readings, carbon was included in the measurements in this instance as it is the most abundant element.

3.3 Aluminium

Native aluminium occurs in Clipper-1 as a very bright white, soft metal with a pitted surface. It is easily distinguished from other metals and metal sulfides by the way scratches and pits generated during grinding and polishing show up as bright marks in cross-polarised light. This material was initially misidentified as electrum, a naturally occurring alloy of gold and silver, based on hardness, colour and reflectance. Native aluminium occurs so rarely in nature that it was not considered as a possibility until elemental composition data was made available by SEM probe.

Native aluminium in Clipper-1 occurs as two distinct morphologies: large, blob-shaped pieces up to 2mm in length and thin, laminated pieces that appear to have experienced deformation (Fig. 27-29). It is always found with a colourless glassy material that may be entirely transparent or partially devitrified. This is identified as glass by the presence of shrinkage cracks and its optical properties in thin section (Fig. 28, 30). Due to the transparency of the glass, it may be very difficult to see in reflected light unless devitrified, which produces a cloudy appearance that makes it more visible in reflected light (Fig. 31-32). In well cuttings, the aluminium appears as hard, dull grey and white flakes up to 10mm in length and approximately 1-2mm thick (Fig. 33).

The native aluminium contains inclusions consisting of a mixture of metals with variable composition. These are usually present as irregular-shaped streaks and blobs, often fragmented, but also occur as euhedral crystals. They may also display graphic or

myrmekitic textures (Fig. 34). The fragmentation of the inclusions indicates that they are less ductile than the aluminium.

Analysis of the elemental composition of the Clipper-1 aluminium assemblage indicates that the native aluminium is 93-94% pure, with the remainder composed of copper, magnesium, silicon and sodium (Table 7). There is some variation in composition between samples at different depths. The inclusions are a highly varied mix of silicates and native metals. All measured inclusions contain aluminium. The other metals found include copper, iron, manganese, magnesium, arsenic and nickel, none of which was found to occur in every measured inclusion. The glass component of the aluminium assemblage contains no silica, but is instead composed primarily of aluminium oxides with smaller concentrations of sodium and chlorine with occasional copper and calcium (Table 7).

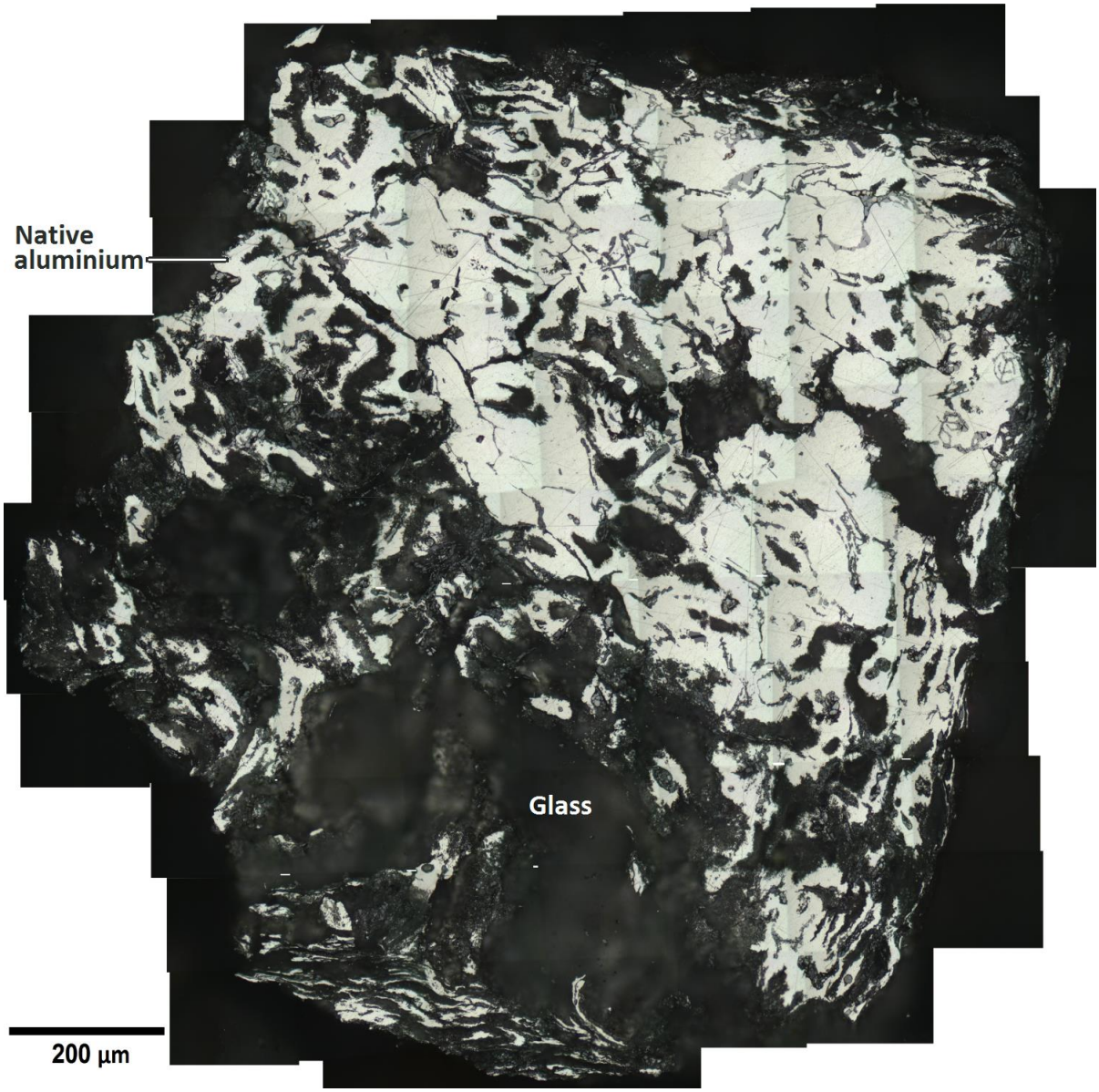

Fig. 27. Photomontage of blob-shaped native aluminium grain in reflected light, showing native aluminium with inclusions of silicates and mixed metals (grey strands within the aluminium) intermingled with glass. Fig. 28 shows the same subject under SEM. Sample from Clipper-1 at 2035m depth.

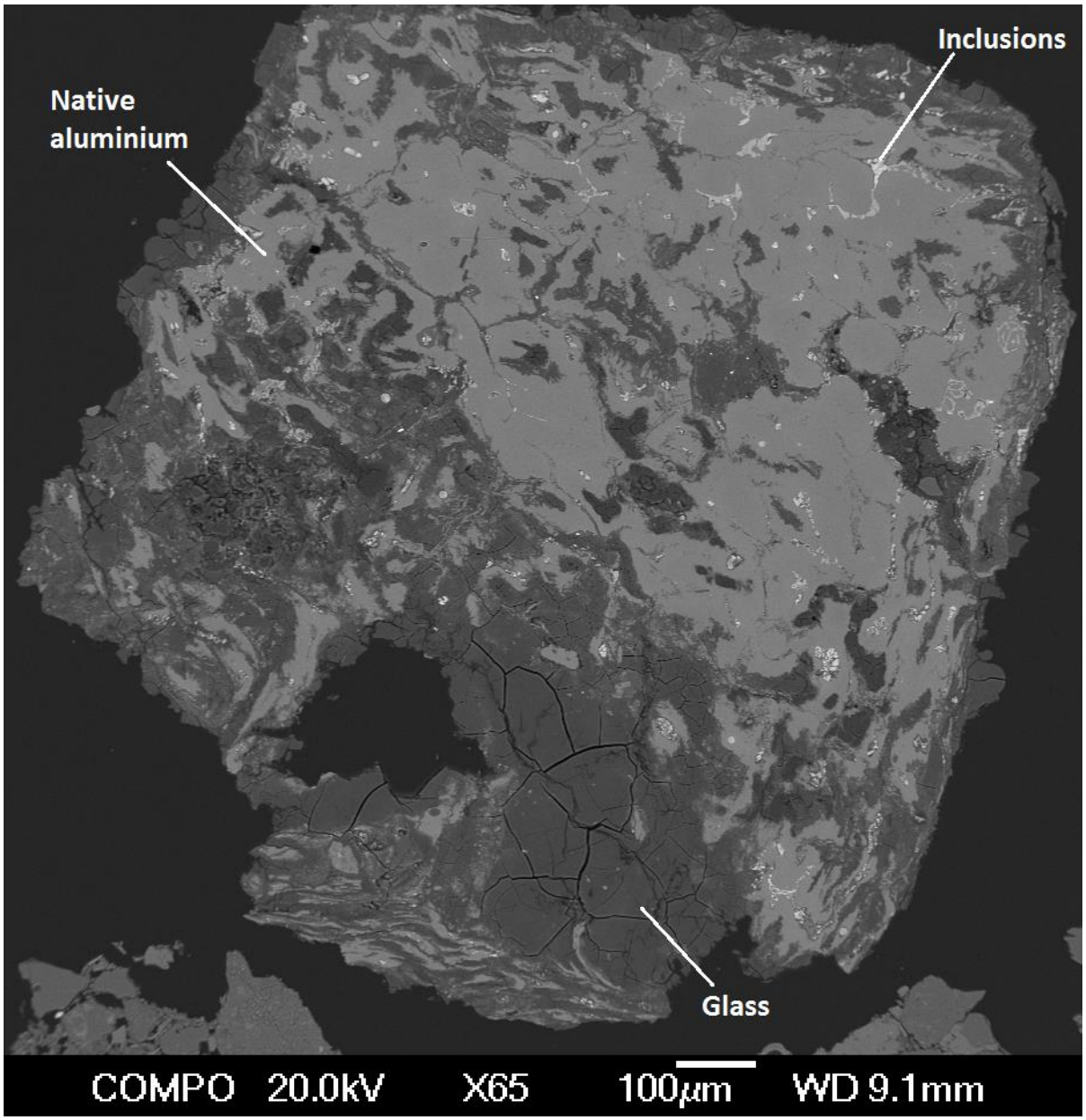

Fig. 28. Sample of native aluminium from Fig. 27 viewed under SEM. Due to the highly transparent nature of the glass, features such as shrinkage cracks are easier to discern under SEM than in reflected light. Sample from Clipper-1 at 2035m depth.

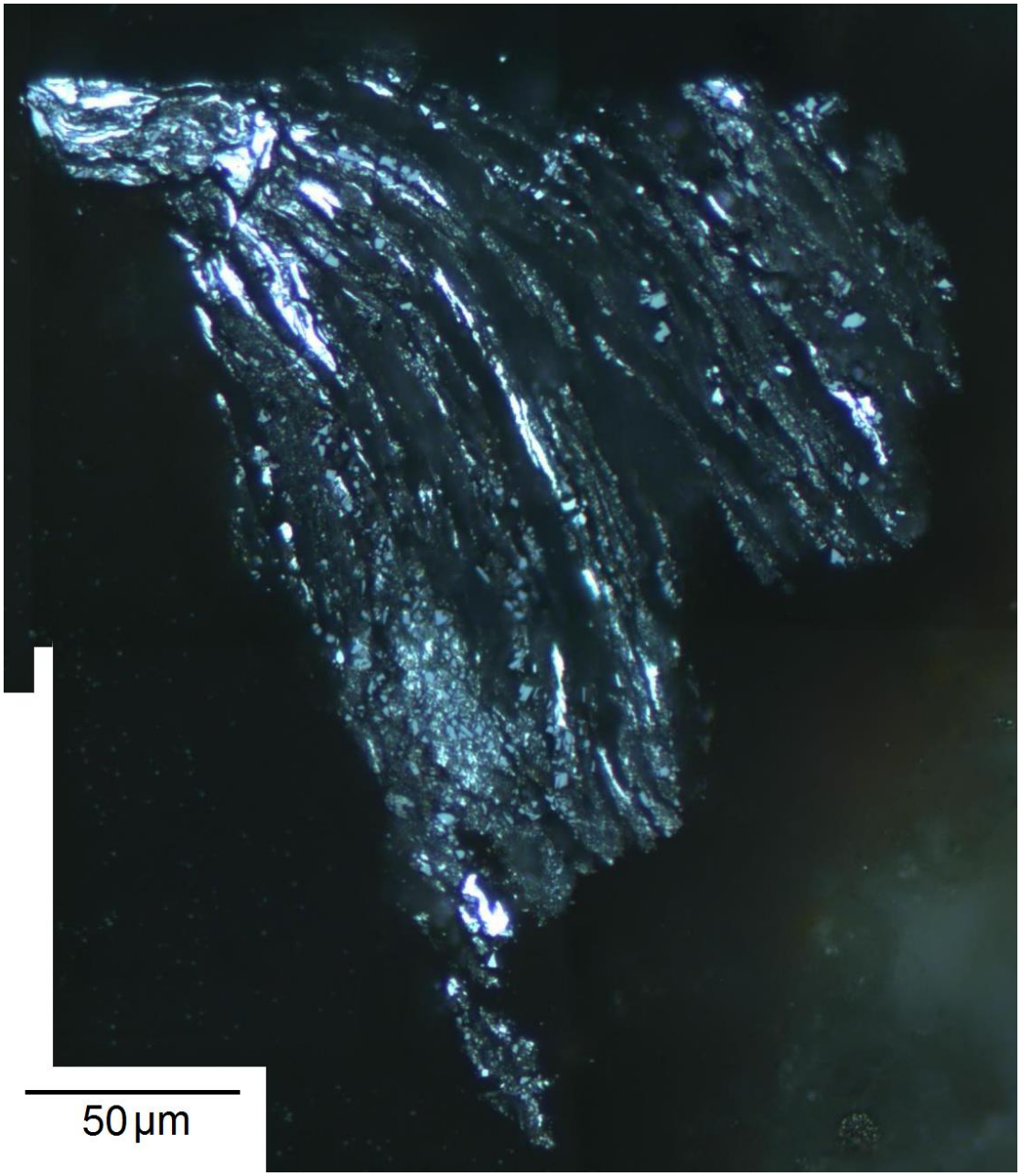

Fig. 29. Photomontage of native aluminium (bright material) flattened into thin lamellae between layers of transparent glass. The inclusions (grey) have become fragmented and separated from the aluminium. Sample from Clipper-1 at 2125m depth, image in reflected light.

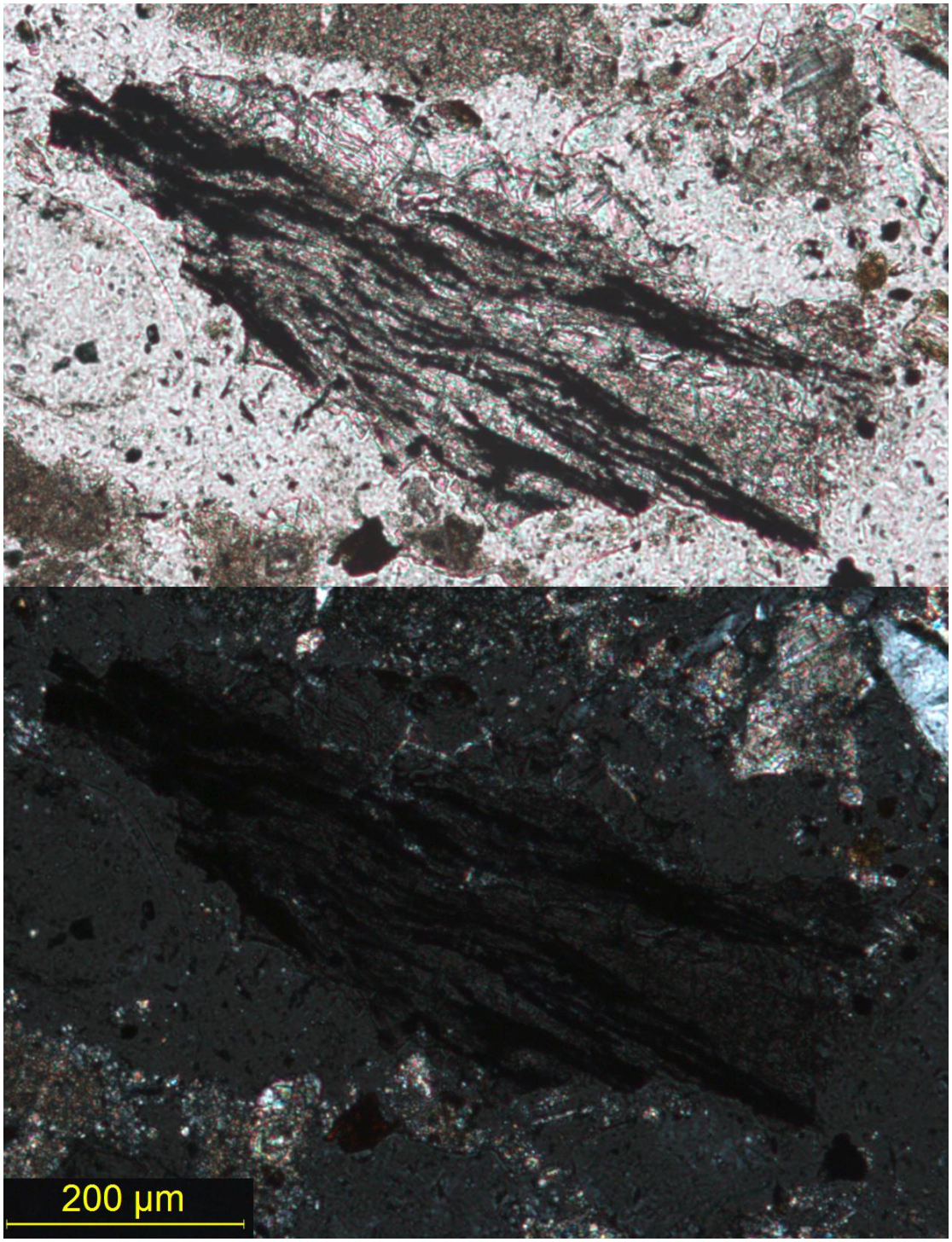

Fig. 30. Native aluminium (black) and associated glass (transparent) in plane and cross-polarised transmitted light (thin section). Shrinkage cracks are visible in the glass. From 2125m depth in Clipper-1.

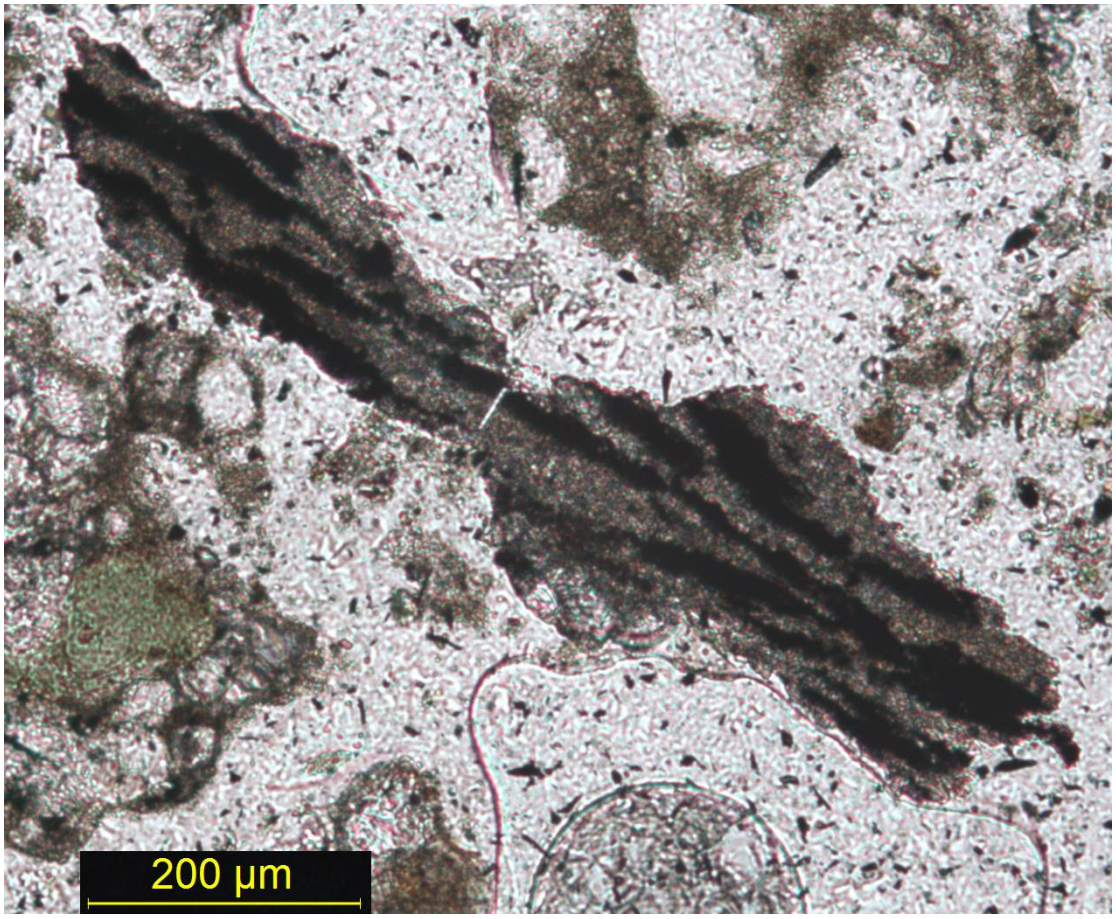

Fig. 31. Native aluminium and partially devitrified glass, viewed in transmitted light (thin section). From 2125m depth in Clipper-1.

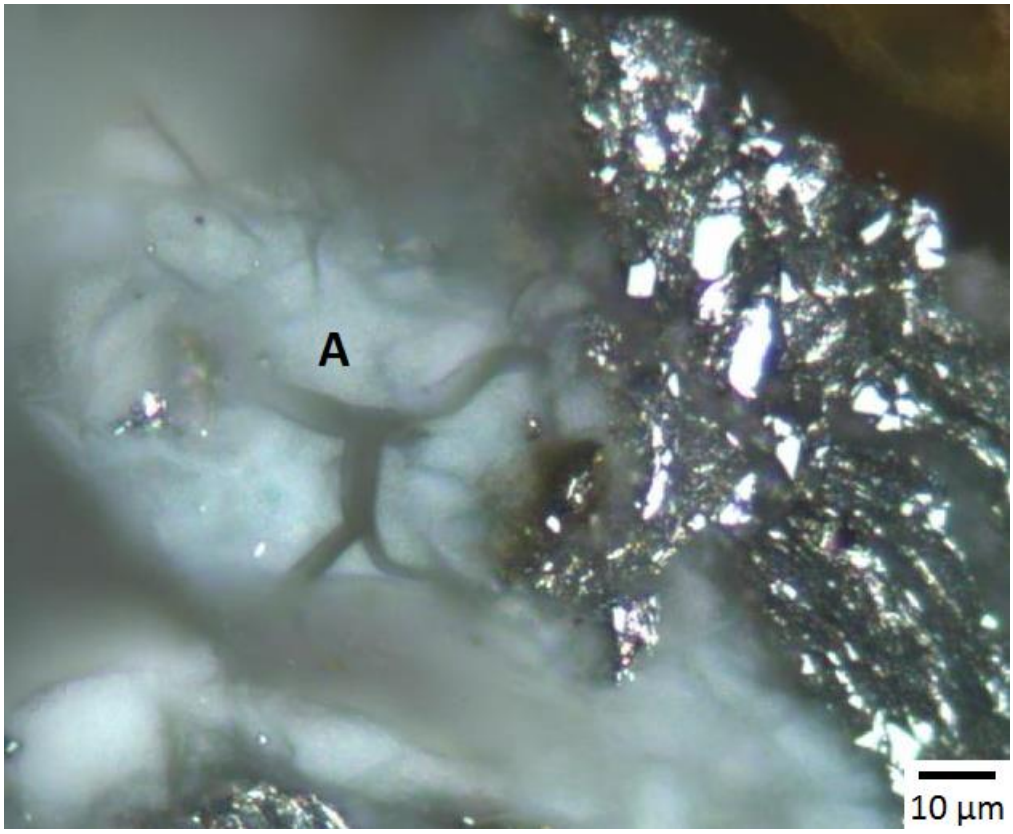

Fig. 32. Devitrified glass with shrinkage cracks (A) in association with native aluminium. From 2055m depth in Clipper-1, image in reflected light.

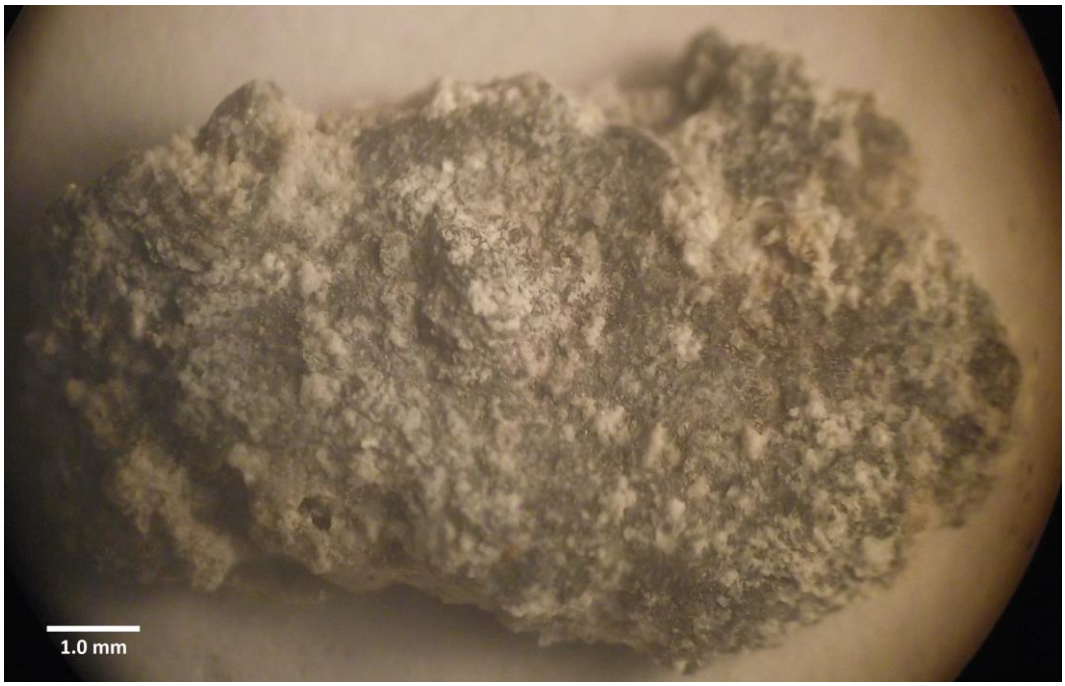

Fig. 33. Unpolished flake of native aluminium (grey) and associated glass (white) from Clipper-1 at 780m depth.

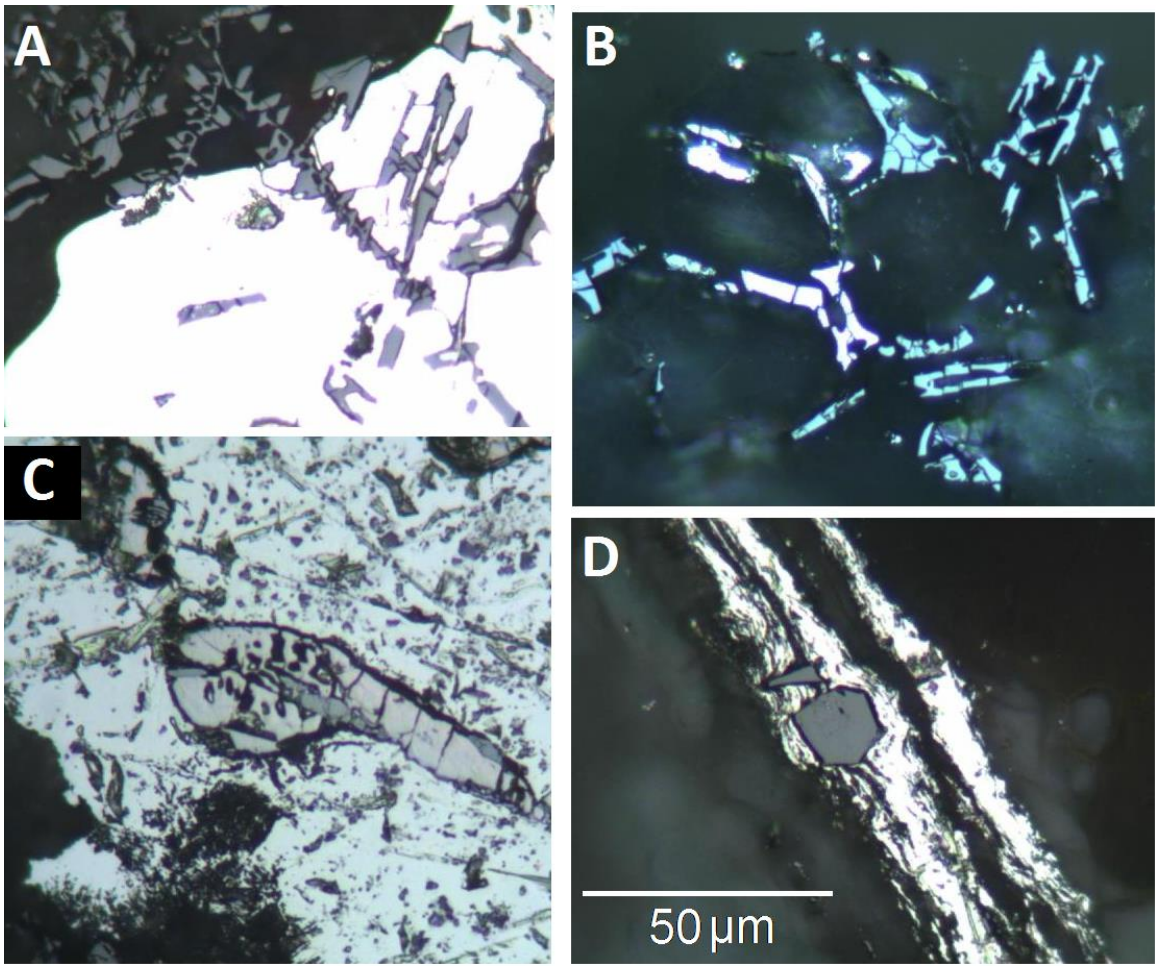

Fig. 34. Mixed metal and silicate inclusions in native aluminium. (A, B) Graphic texture, (C) Myrmekitic texture, (D) Euhedral hexagonal crystal. From 2055m depth in Clipper-1, image in reflected light.

Native aluminium

Sample	Al	Cu	Mg	Si	O	Na
2035 019	94.0	-	-	3.1	1.4	1.4
2055 083	93.2	5.3	1.5	-	-	-
2055 084	93.8	4.8	1.4	-	-	-
2055 085	93.9	4.7	1.4	-	-	-
2055 086	92.8	5.7	1.5	-	-	-
2055 087	93.9	4.6	1.5	-	-	-

Inclusions

Sample	Al	Cu	Fe	O	Si	Mn	Mg	As	Ni
2035 021	60.9	6.2	20.8	-	9.2	2.9	-	-	-
2035 022	39.1	46.5	-	8.3	-	-	-	-	-
2035 023	16.8	-	-	9.3	73.9	-	-	-	-
2055 088	48.1	34.7	10.3	2.3	-	4.6	-	-	-
2055 089	50.4	36.0	-	1.2	-	-	9.4	9.4	3.0
2055 090	36.5	47.4	-	-	-	-	12.4	12.4	3.7
2055 091	55.3	27.4	9.0	3.2	-	5.1	-	-	-
2055 093	55.9	31.2	9.5	-	-	3.4	-	-	-

Glass

Sample	O	Al	Na	Cl	Cu	Ca
2035 020	53.8	32.3	12.4	1.4	-	-
2055 078	58.1	35.6	5.3	1.0	-	-
2055 079	61.7	34.3	1.7	1.1	-	1.2
2055 080	51.3	41.9	2.2	0.9	3.7	-
2055 081	57.0	38.8	2.1	1.0	-	1.0
2055 082	58.5	38.0	2.5	1.0	-	-

Table 7. Elemental composition of the components of the Clipper-1 native aluminium assemblage measured by SEM with EDS. Figures are in mass % (Appendix 1).

3.4 Copper alloy, graphite and lead compounds

This assemblage consists of loosely packed threads and granules of graphite with thin flakes of copper and copper-zinc alloy 1-2µm wide and up to 30µm long, granules of lead compounds and occasional native iron (Fig. 35-36). The graphite occasionally retains the structure of organic matter resembling inertinite, indicating it is derived from coal or carbonaceous sediments rather than forming by inorganic processes (Fig. 37). The lead is a mixture of oxides, sulfides and native metal. This assemblage occurs sparsely at the depths where native iron and/or aluminium are abundant.

Analysis of the elemental composition of this assemblage indicates that the copper varies in purity between 79 and 95 percent (Table 8). In the samples with lower purity, it is alloyed with zinc. One flake of native iron with an identical structure to the copper flakes was measured, and was found to be alloyed with manganese. The shape and size of the flakes made measurement of the elemental composition difficult, as they presented very little surface area on which to measure. This may have affected the accuracy of the readings. The lead component was consistently found to contain sulfur and oxygen, indicating that it is partially composed of galena (PbS) and lead oxide. There is an excess of lead in comparison to these elements, indicating that some of the lead must be in its native state.

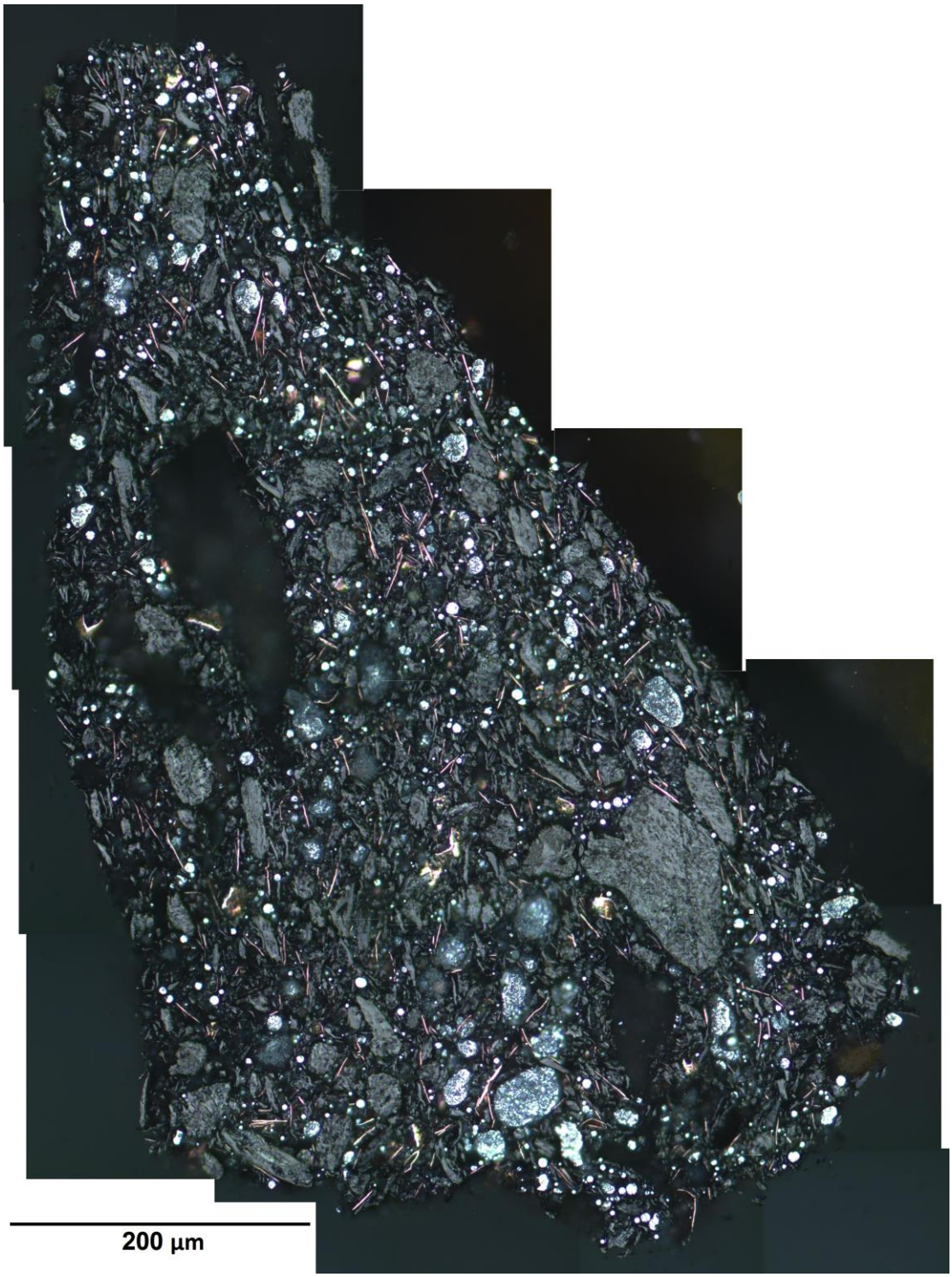

Fig. 35. Photomontage of copper alloy (pink-orange threads), graphite (grey) and lead compounds (white). From 2055m depth in Clipper-1, image in reflected light.

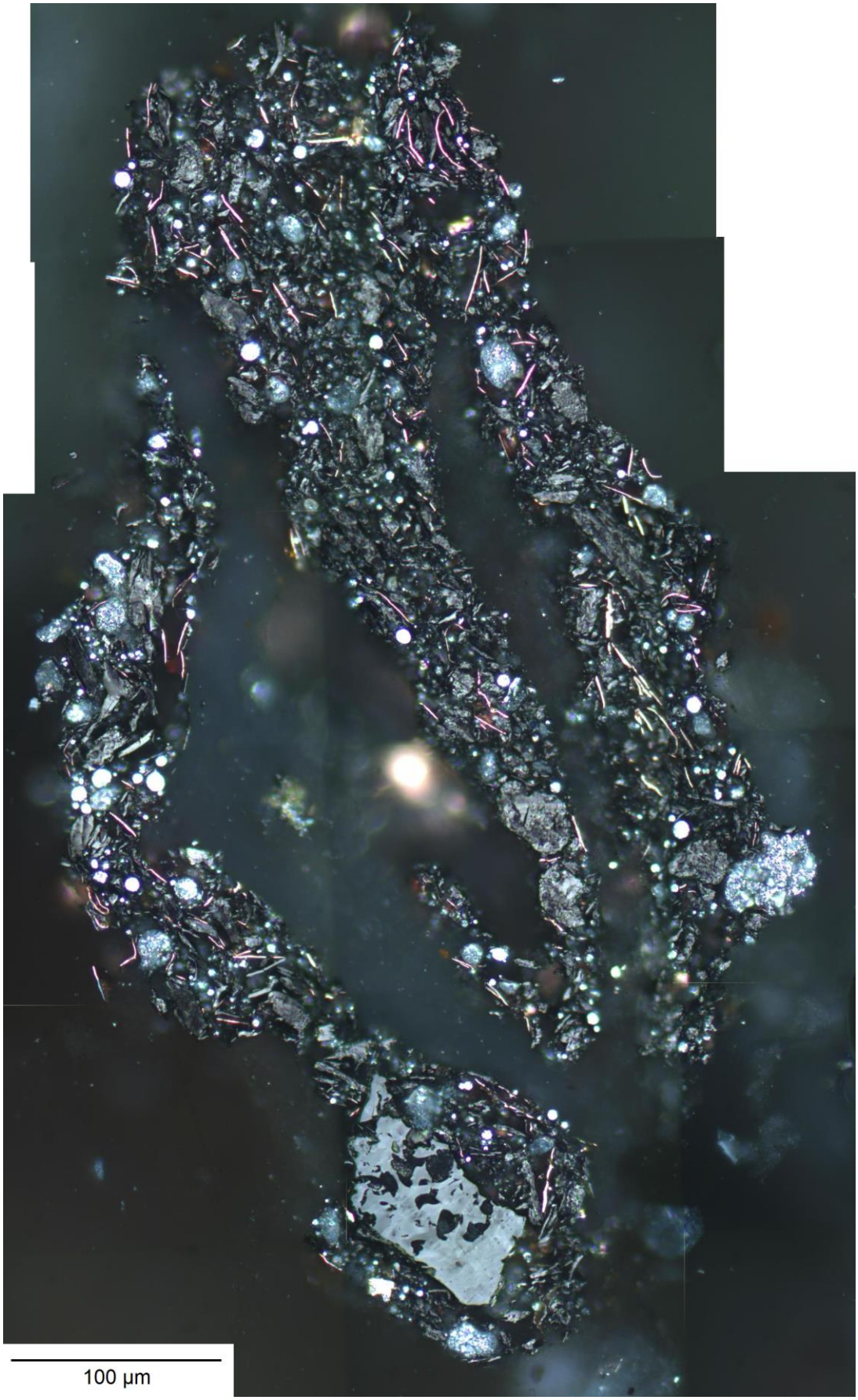

Fig. 36. Photomontage of copper, graphite and lead assemblage. From 2055m depth in Clipper-1, image in reflected light.

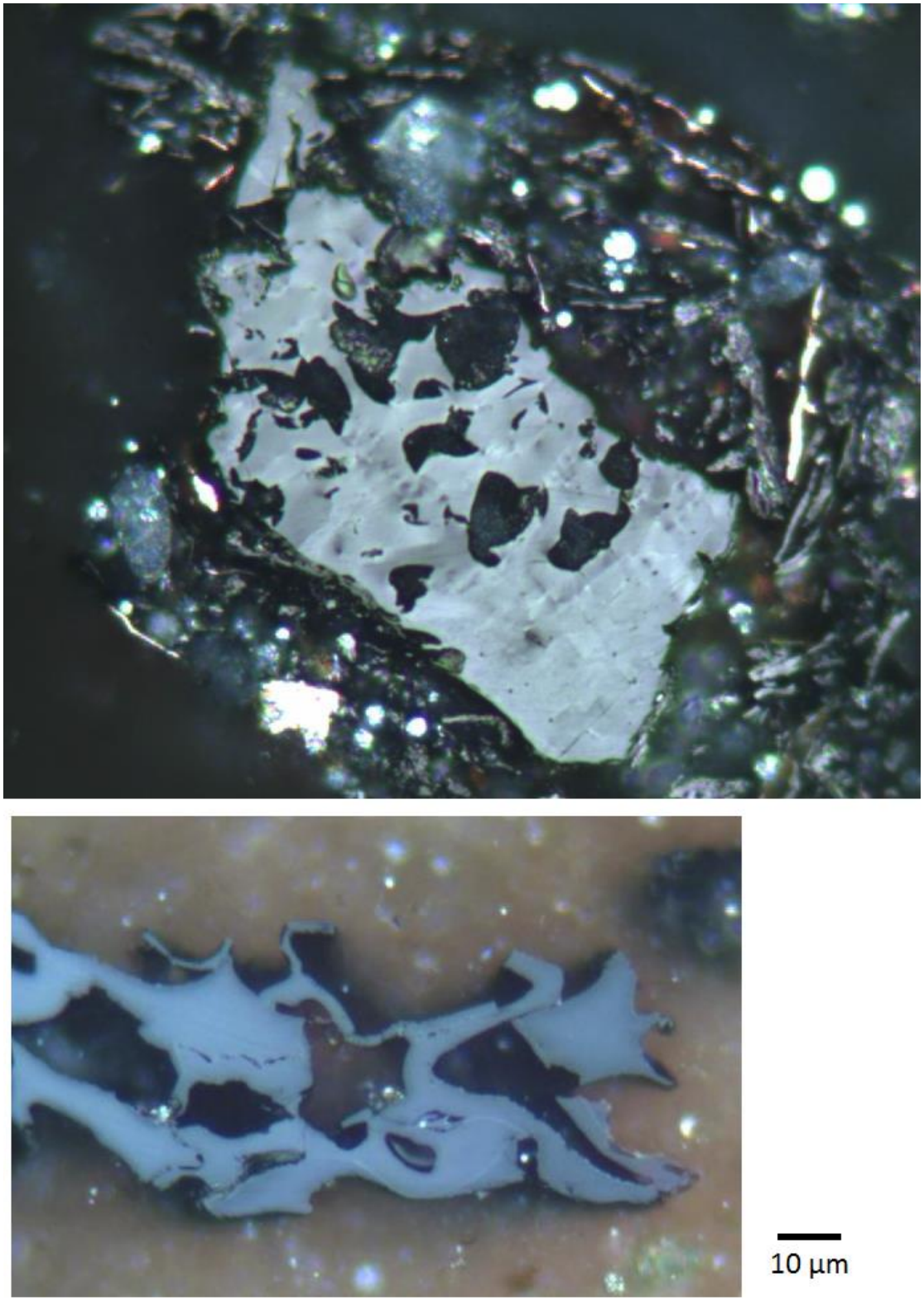

Fig. 37. Baked inertinite in a copper, lead and graphite assemblage (top) in comparison to unaltered inertinite from Clipper-1 sediments (bottom). Graphite from 2055m depth in Clipper-1, image in reflected light.

Copper

Sample	Cu	O	Zn	Pb	Cl
2055 027	95.0	3.3	-	1.7	-
2055 028	86.8	2.1	11.1	-	-
2055 029	79.1	7.7	11.8	-	1.4

Iron

Sample	Fe	Mn	O
2055 026	86.2	12.4	1.4

Lead

Sample	Pb	S	O	Cu
2055 021	70.2	4.7	3.4	21.7
2055 022	92.3	6.1	1.6	-
2055 023	91.8	6.3	1.9	-
2055 024	91.9	6.9	1.2	-
2055 025	91.7	5.9	2.3	-

Table 8. Elemental composition of the components of the Clipper-1 native aluminium assemblage measured by SEM with EDS. Figures are in mass % (Appendix 1).

3.5 Distribution of native metals

Native metals in Clipper-1 are concentrated in two distinct brackets (Fig. 38). The upper bracket at 2050m is centred on the Southburn Sand, extending into the top of the Otekaike Limestone and the base of the Tokama Siltstone in sediments of early to middle Miocene age. The lower bracket at 3550m is located in the middle of the Katiki Formation in carbonaceous siltstone of late Cretaceous age. Native metals are present in small concentrations above the upper and below the lower mineralisation brackets, but entirely absent from the area between the two brackets.

Iron minerals including native iron are extremely abundant in the lower mineralisation bracket and moderately abundant in the upper bracket. They occur sparsely throughout much of the well including into basement rocks. Native aluminium is almost non-existent below the upper mineralisation bracket, and the few pieces seen in deeper samples may be the result of caving. The native copper, lead and graphite assemblage is very sparsely distributed in both the upper and lower mineralisation brackets.

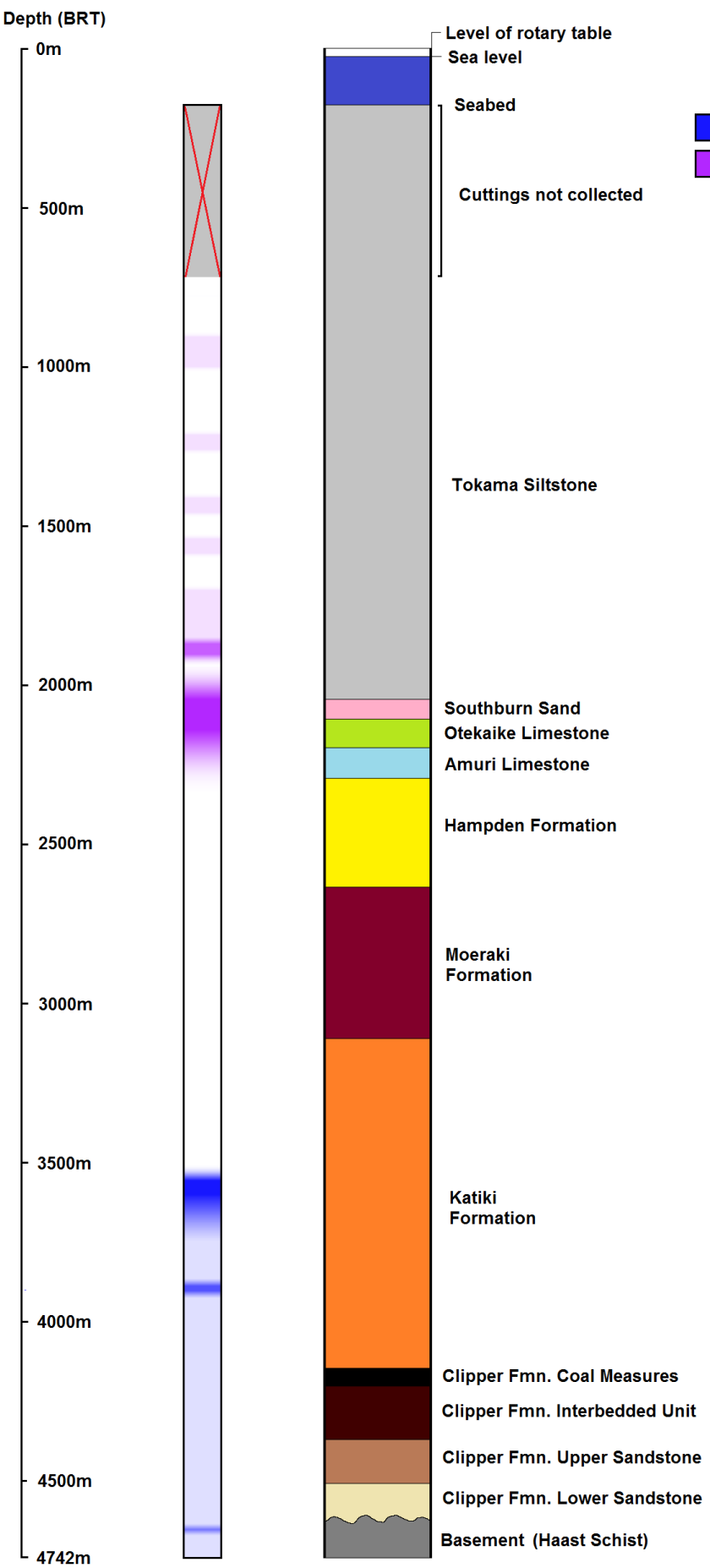

Fig. 38. Native metal distribution in Clipper-1 compared to a stratigraphic column of the well.

3.6 Iron sulfides

Framboidal pyrite is found throughout Clipper-1. It is a common feature of marine sediments. In some cases, framboids have been recrystallised into solid spheres or euhedral pyrite crystals (Fig. 39). In carbonaceous sediments, framboids may be partially altered to iron oxide (Fig. 40). This is attributed to chemical changes during burial, as opposed to alteration during sample storage. Pyrite can be altered during sample storage, particularly under moist conditions, but the product of this alteration is typically gypsum ($CaSO_4 \cdot 2H_2O$) rather than iron oxide.

Pyrite in Clipper-1 also occurs as massive, coarse-grained material containing angular grains of quartz and mica (Fig. 41). This texture may be the result of fluid flow removing finer sediments, leaving open pore space between larger grains that has been infilled with pyrite. Euhedral sulfides are present in the form of marcasite laths and cubic crystals of pyrite (Fig. 42).

Analysis under SEM with EDS reveals calcite in association with pyrite, a difficult feature to see under reflected light due to the transparency of calcite (Fig. 43). Analysis of the elemental composition of these minerals confirms that the sulfides are FeS, corresponding to both pyrite and marcasite, and that the transparent material found in association with the sulfides is calcite (Table 9).

Fig. 39. Framboidal pyrite in various stages of recrystallisation, from unaltered framboids (left) to solid spheres of pyrite (right). From 4222m depth in Clipper-1, image in reflected light.

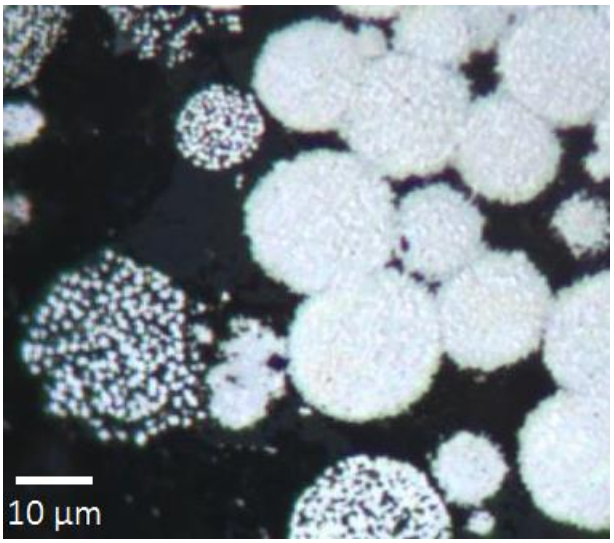

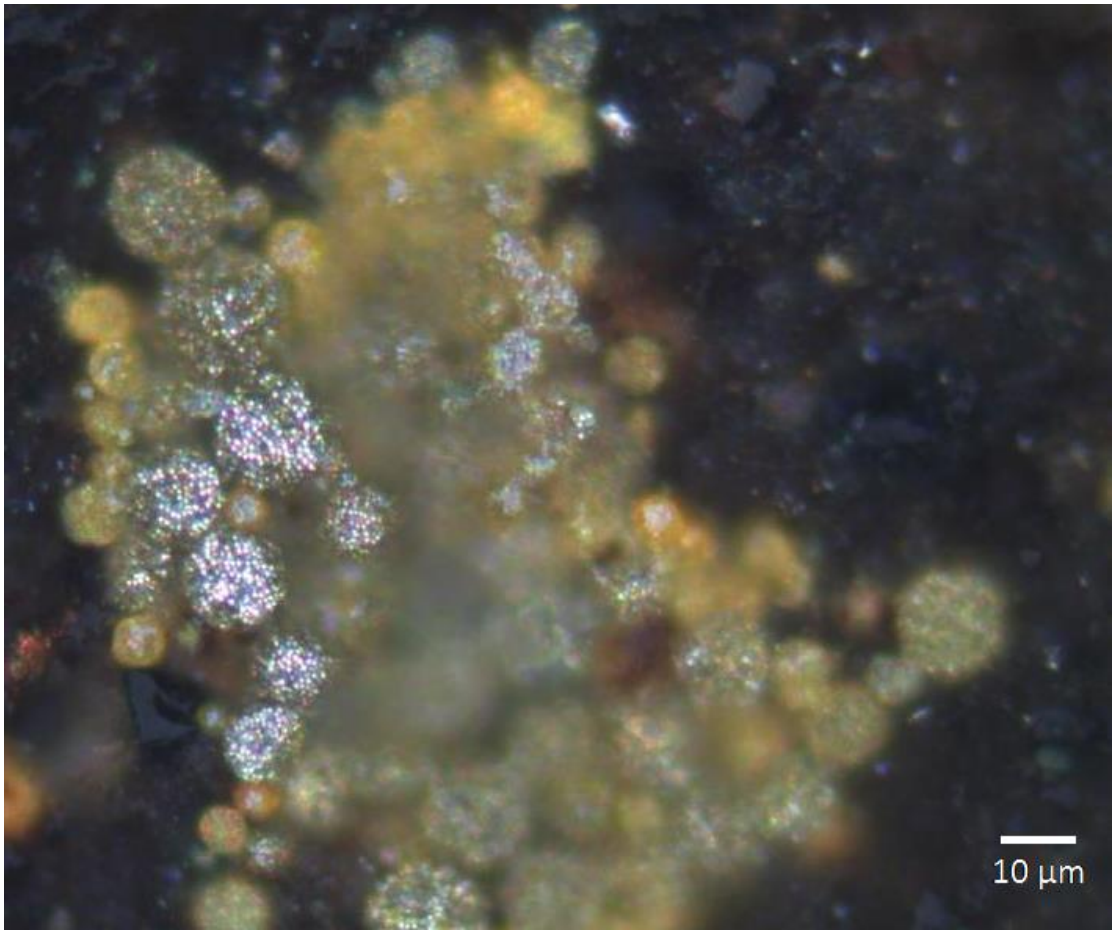

Fig. 40. Framboidal pyrite in carbonaceous sediment. The pyrite is partially altered to iron oxide. From 2775m depth in Clipper-1, image in reflected light.

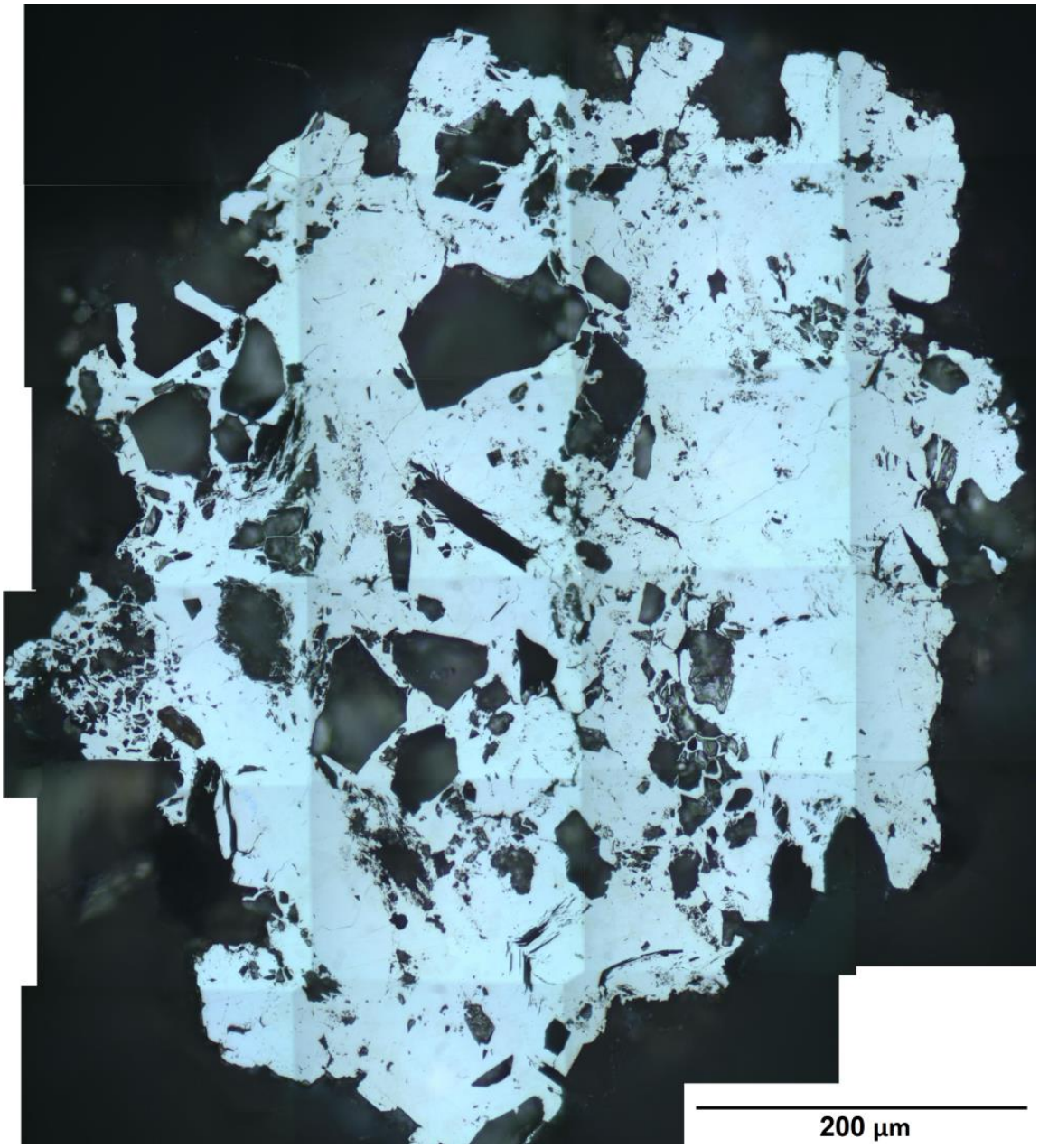

Fig. 41. Photomontage of a pyrite concretion containing silt and very fine sand-sized sediment grains. From 2035m depth in Clipper-1, image in reflected light.

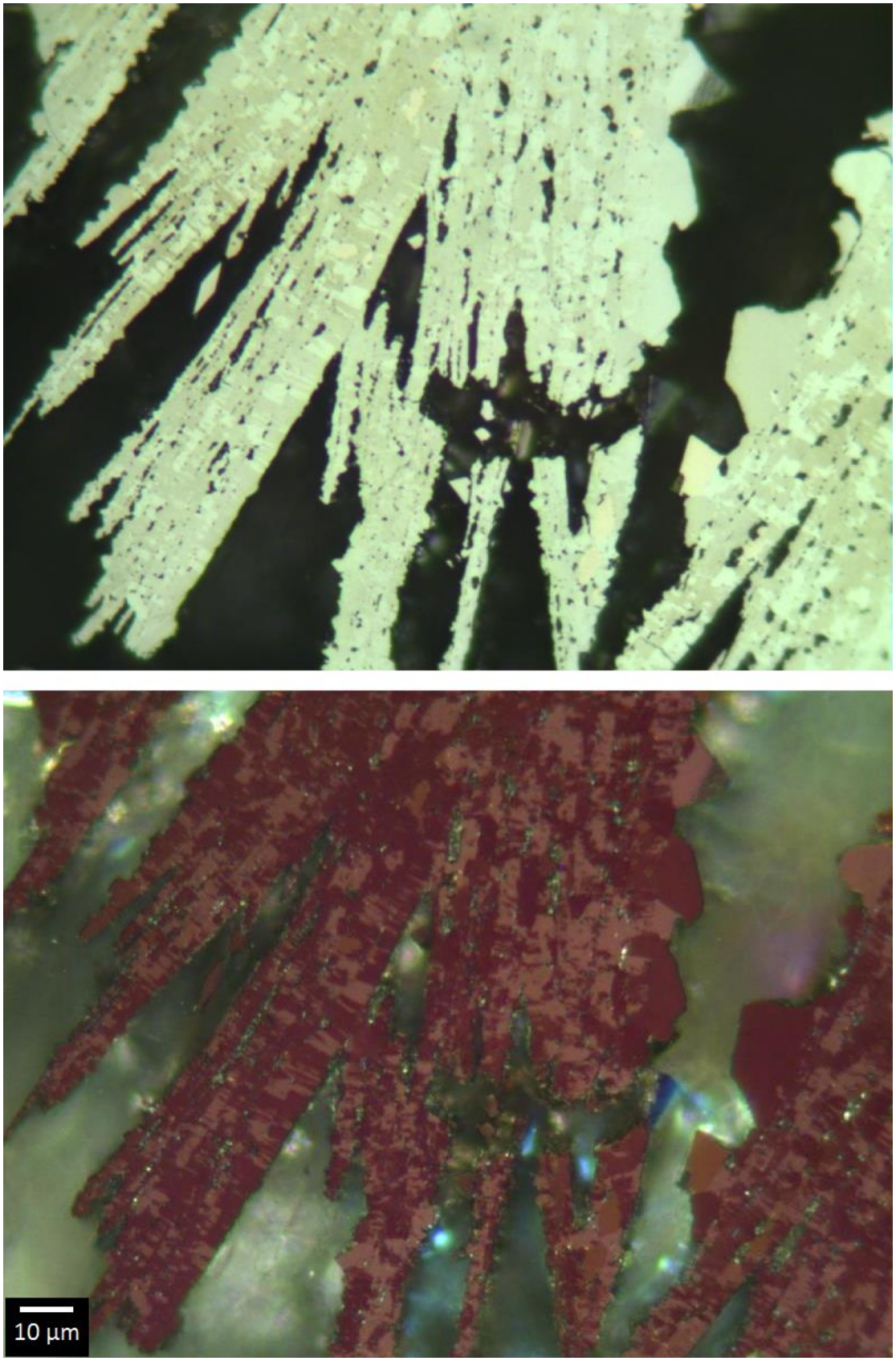

Fig. 42. Acicular pyrite and marcasite crystals in plane polarised light (top) and cross polarised light (bottom). From 4666m depth in Clipper-1, image in reflected light.

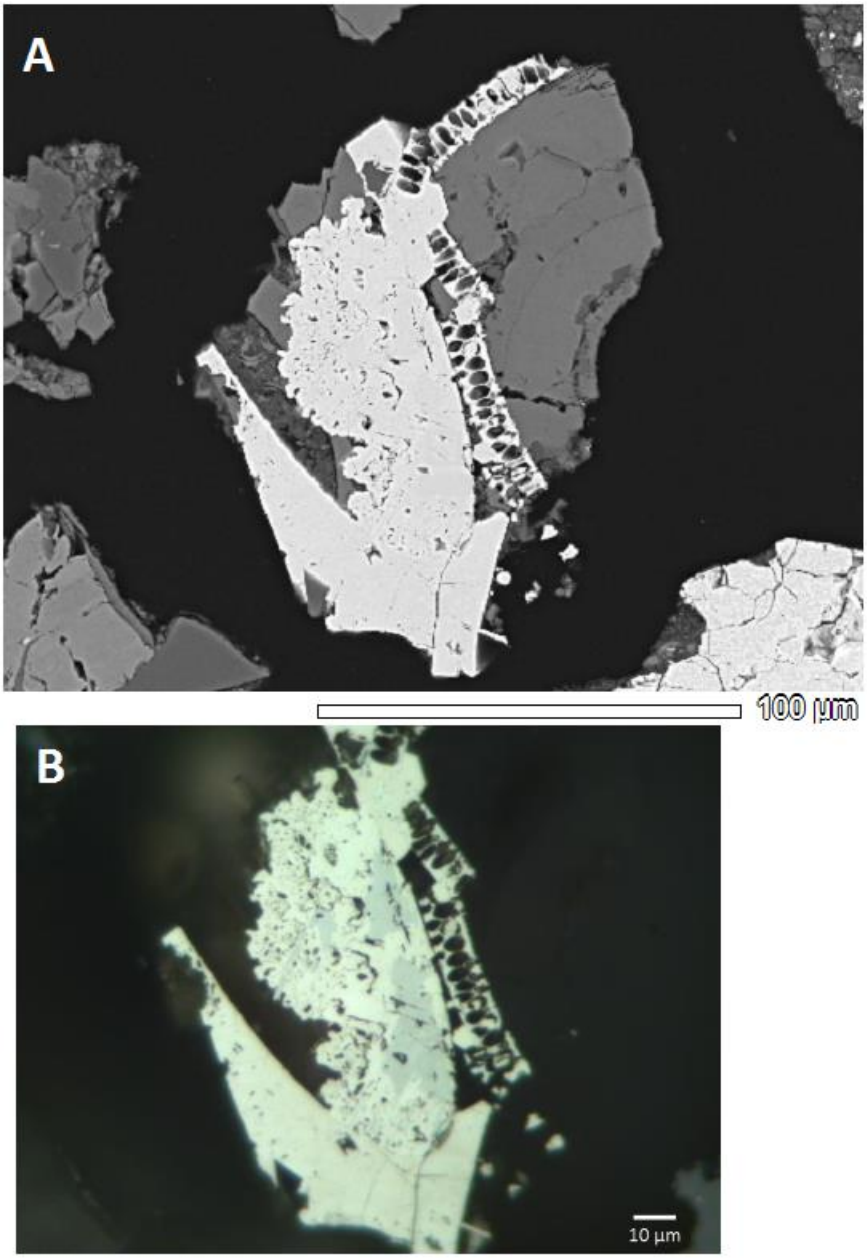

Fig. 43. (A) SEM image of pyrite (white) with calcite (grey), including pyrite replacement of a bioclast. (B) Reflected light image of same grain. The calcite is transparent and very difficult to distinguish from the polyester resin the sample is set in. From Clipper-1, 2035m depth.

Iron sulfide

Sample	S	Fe
2035 009	51.6	48.4
2035 010	51.5	48.5

Calcite

Sample	O	Ca	C
2035 011	41.2	39.4	19.5

Table 9. Major element composition of iron sulfides and associated calcite from Clipper-1. Figures are in mass % (Appendix 1).

3.7 Microfacies VS

A distinctive assemblage consisting of fragments of an aphanitic material, with euhedral phenocrysts and infilled vesicles surrounded by a slightly translucent glassy matrix, contained within a carbonate groundmass (Fig. 44, 50). As this material has not been matched to any named rock type based on appearance or composition, the name "Microfacies VS" has been applied. VS stands for "vesicular", referring to the presence of infilled vesicles. This material usually occurs in a brecciated state (Fig. 45).

When viewed as loose, unpolished granules, Microfacies VS is light grey in colour with the glassy material appearing as black flecks. It is very similar in appearance to Tokama Siltstone, and as a result was not recognised as igneous material during the original analysis of the Clipper-1 well by Shell BP Todd. Granules can be identified as VS by their hardness; compared to siltstone, they require more force to break and do not produce loose silt grains when scratched.

Microfacies VS is found throughout Clipper-1, ranging from basement to the uppermost sample at 790m depth. It is particularly abundant in the top sample and also at 3550m depth. It is present in smaller concentrations throughout the well. It has also been observed in samples from the Galleon-1 well, located 85 kilometres south-west of Clipper-1 (Fig. 46).

When viewed in thin section, Microfacies VS is grey-brown in colour and variably translucent (Fig. 47). Vesicles are present on two different scales. Small vesicles, 5-80 µm in diameter, are contained within glass and filled with carbonate minerals (Fig. 48). Larger

vesicles, 100-400 µm in diameter, are found in the groundmass of brecciated Microfacies VS and are not infilled (Fig. 49).

Analysis of the elemental composition of the components of Microfacies VS reveals that the phenocrysts are primarily quartz containing a variety of metals, including iron, calcium, magnesium, sodium and aluminium (Table 10). Some calcite phenocrysts are also present. The glass is primarily composed of calcium carbonate with substantial concentrations of iron. Silicon is present at far lower concentrations than would be expected for a typical volcanic glass. The vesicles are filled with silica (SiO_2). As the vesicle fillings do not have the optical properties of quartz when viewed in thin section, they are likely to be amorphous silica. The groundmass surrounding brecciated fragments of Microfacies VS has concentrations of silica intermediate between those of the vesicle fillings and the glass.

The mineralogy of the phenocrysts was analysed using qualitative XRD (Fig. 51). This revealed the presence of calcite ($CaCO_3$), pyrrhotite ($Fe_{1-x}S$ where x = 0 to 0.17) and vaterite, a rare form of $CaCO_3$. Quartz has been identified using SEM with EDS, but was not detected by XRD. It may have been obscured by the high concentrations of carbonate minerals in Microfacies VS.

In order to determine whether Microfacies VS is of crustal or mantle origin, trace elements were measured using XRF (Table 11) on a sample of Clipper-1 well cuttings from 780m, where the highest concentration of Microfacies VS is found. The low concentrations of certain trace elements including Nb, Zr, La and Ce indicate that this material did not originate in the mantle. The loss on ignition figure was unusually high for an igneous rock due to the high concentration of carbonates in Microfacies VS. The analysis was performed by two separate laboratories, at CRL and the University of Canterbury, in order to ensure the accuracy of the results.

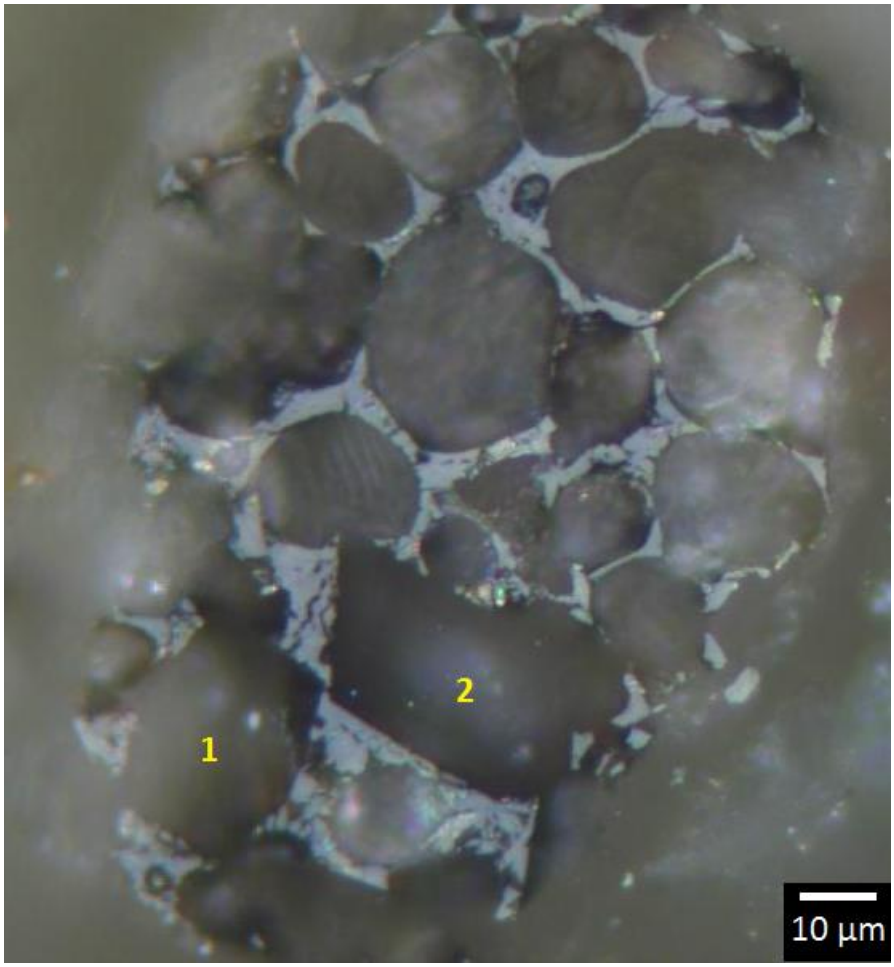

Fig. 44. Intact piece of Microfacies VS with infilled vesicles and euhedral phenocrysts surrounded by a grey, slightly translucent glass. Based on their crystal shapes, the phenocrysts are likely to be (1) hexagonal quartz and (2) rhombohedral calcite. From 2035m depth in Clipper-1, image in reflected light.

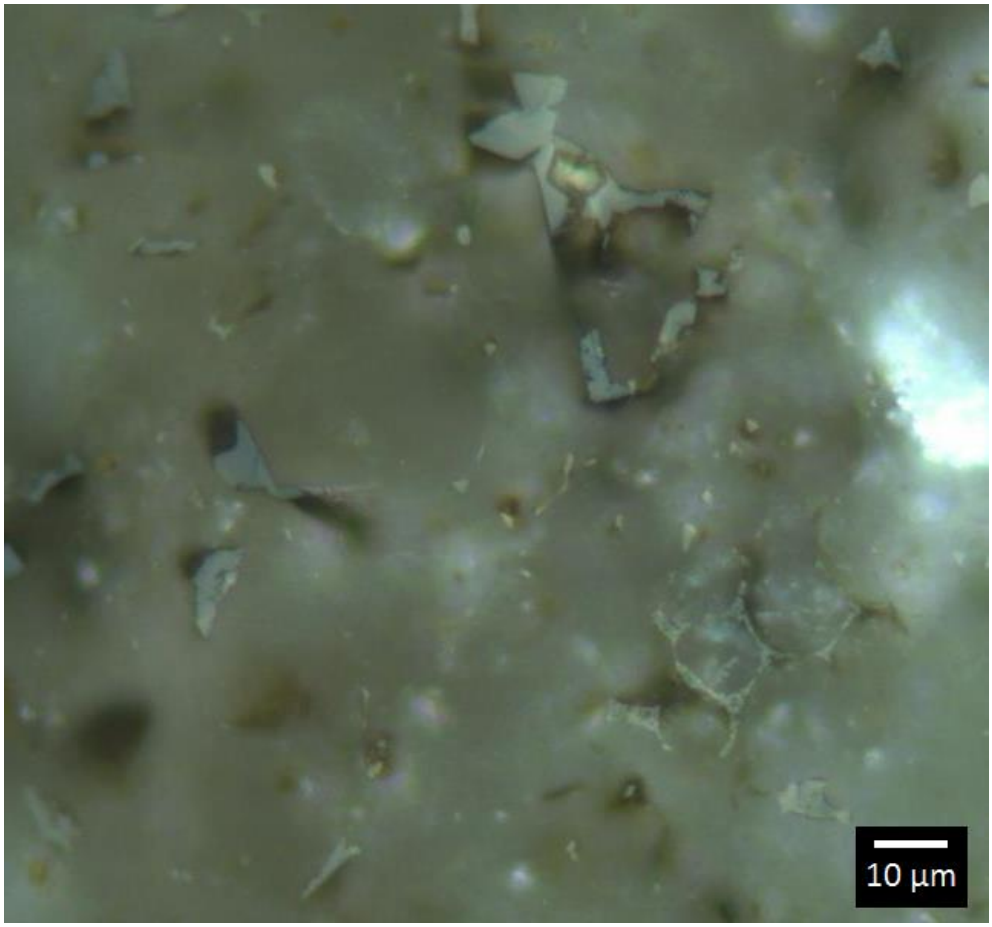

Fig. 45. Brecciated Microfacies VS. From780 m depth in Clipper-1, image in reflected light.

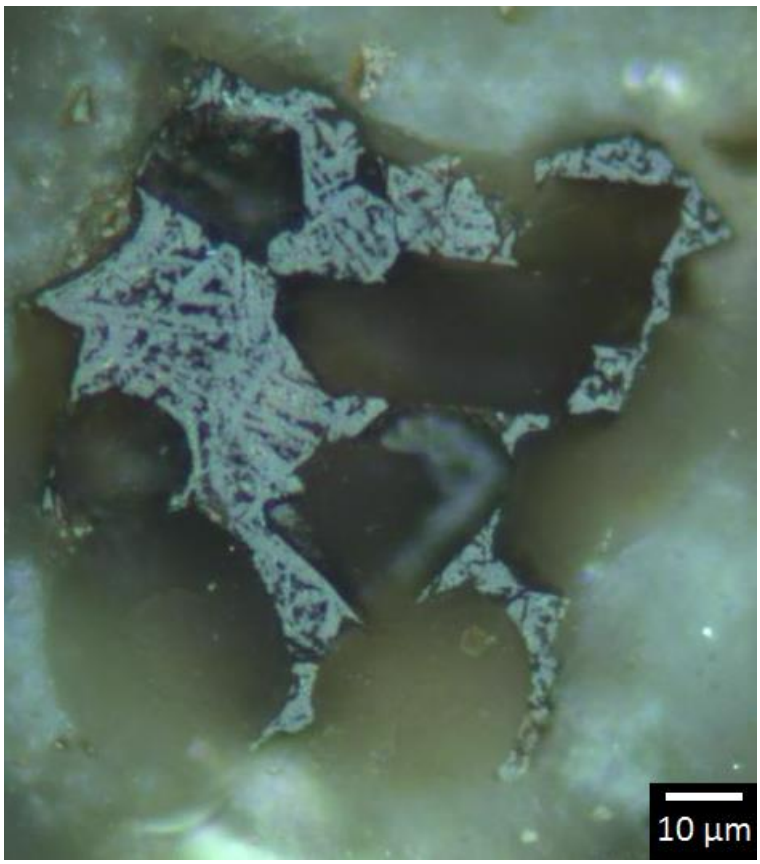

Fig. 46. Microfacies VS from Galleon-1 at 500m depth. Image in reflected light.

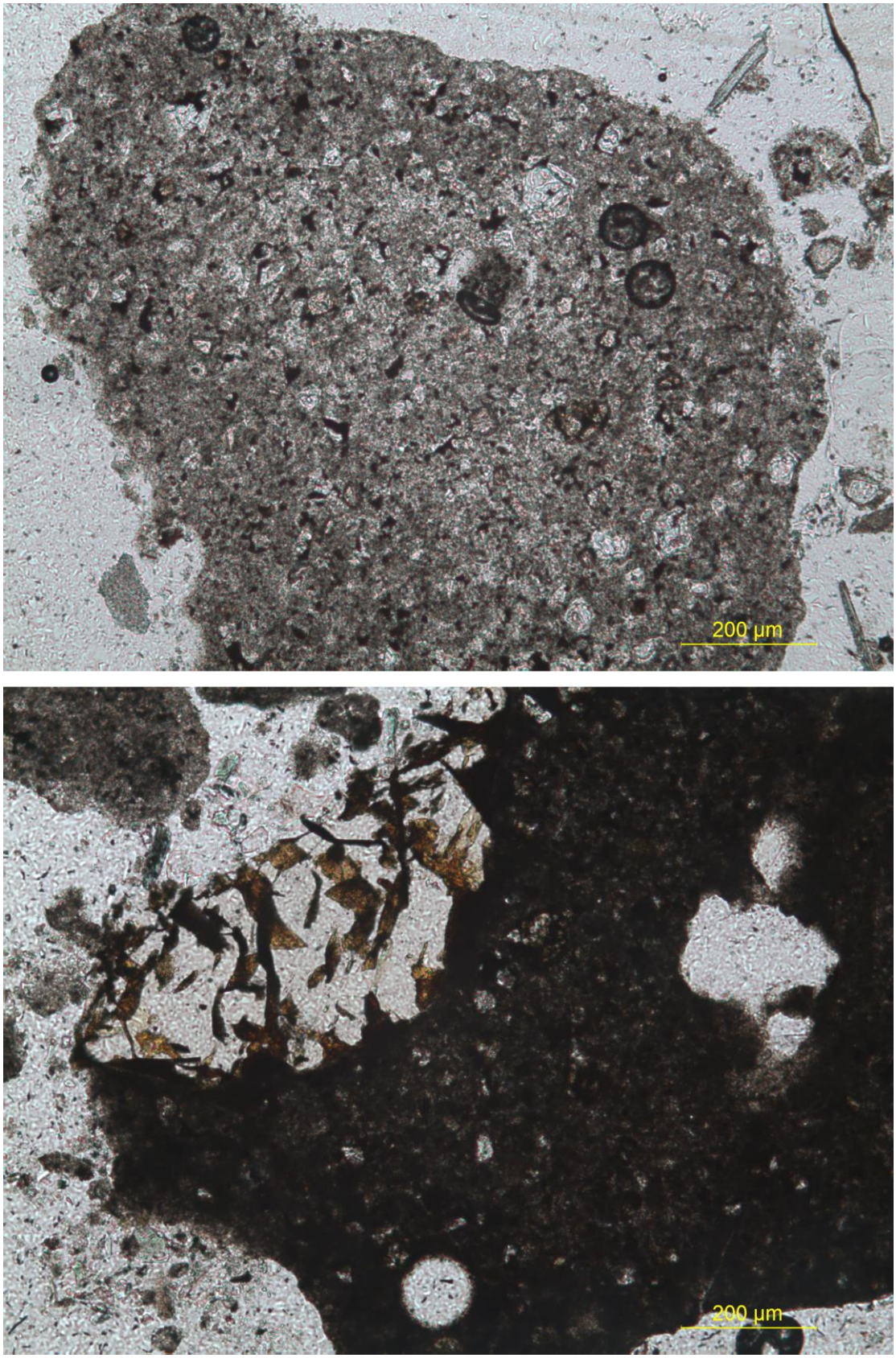

Fig. 47. Microfacies VS grains from Clipper-1 (780m) in transmitted light showing variations in translucency. The lower grain contains part of a large, transparent euhedral phenocryst.

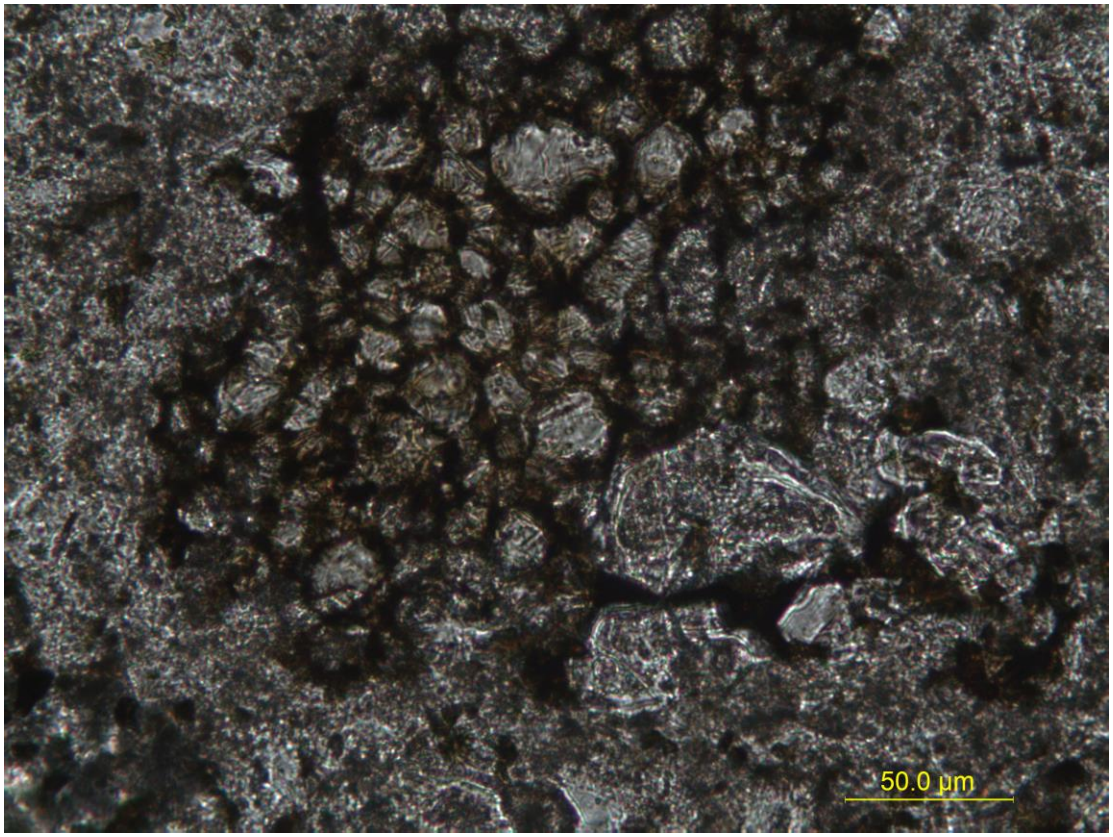

Fig. 48. Small-scale vesicles in Microfacies VS, contained within dark brown glass and filled with transparent carbonate minerals. From 780m depth in Clipper-1, image in transmitted light

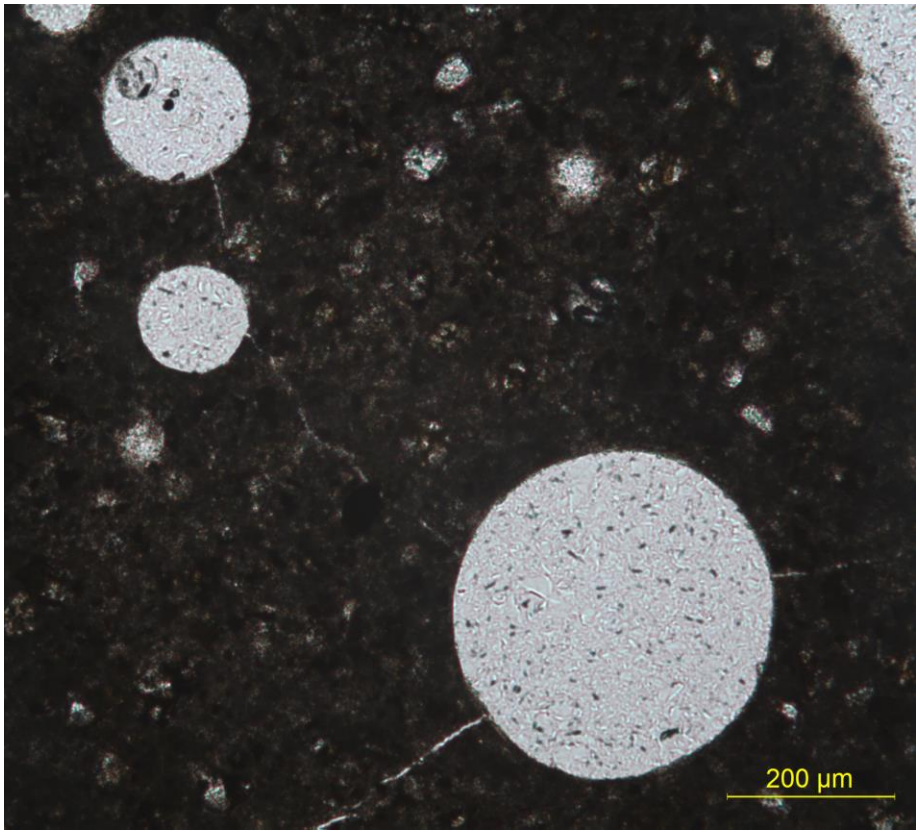

Fig. 49. Larger vesicles in brecciated Microfacies VS. Unlike the small-scale vesicles, these are not contained in glass and contain no mineral fill. The radiating cracks may have been produced during grinding and polishing of the sample. From 780m depth in Clipper-1, image in transmitted light.

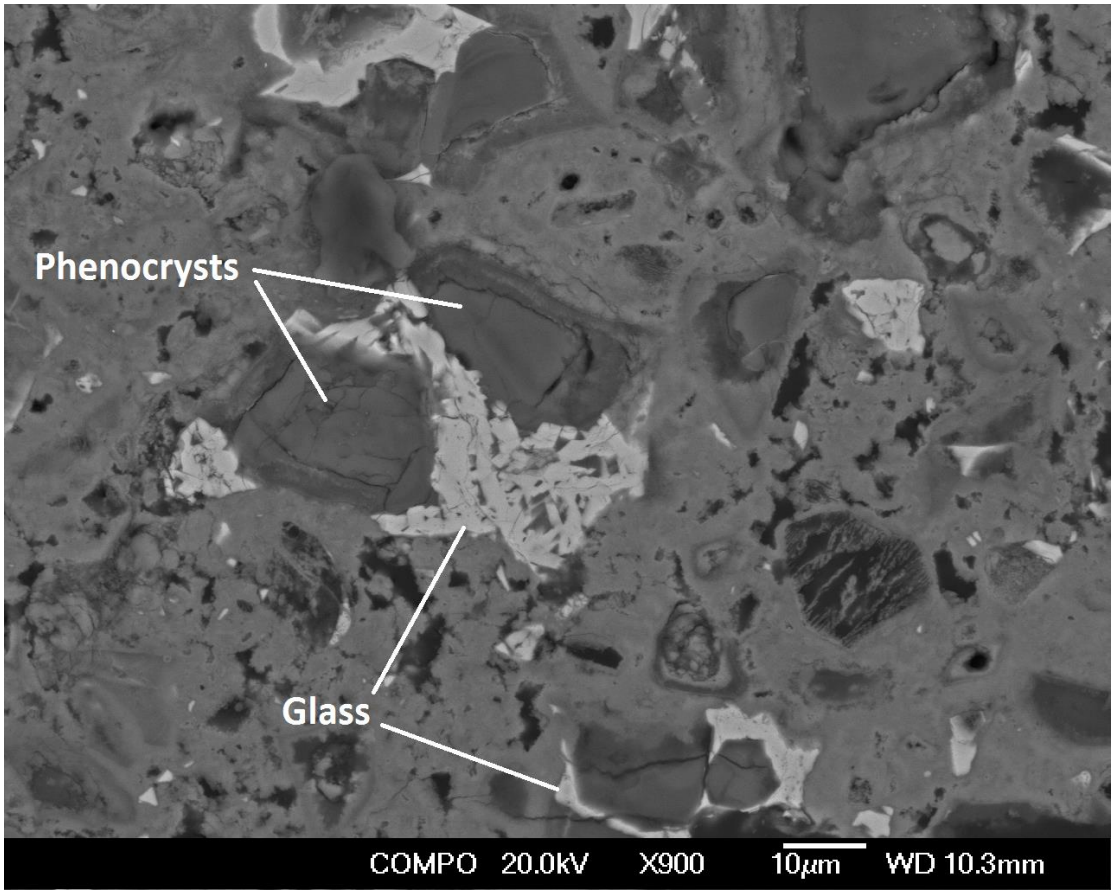

Fig. 50. SEM image of brecciated Microfacies VS showing phenocrysts and glass surrounded by a carbonate groundmass. From Clipper-1, 2125m depth.

Phenocrysts

Sample	Si	O	Fe	Ca	Mg	Na	Al	Cl	S
2125 003	46.4	45.2	2.1	1.8	1.6	1.4	1.2	0.3	-
2125 004	41.2	46.4	2.4	5.0	1.7	1.6	1.3	0.3	-
2055 066	38.6	48.1	3.9	4.8	1.2	-	1.8	1.7	-
2055 068	-	48.9	-	49.4	0.6	-	-	-	1.1
2055 069	35.2	44.2	-	-	-	9.1	11.5		-
2055 070	29.9	47.2	4.2	12.8	0.7	0.8	2.3	2.0	-
2055 072	51.4	47.4	-	1.2	-	-	-	-	-
2055 074	22.9	51.4	-	20.9	0.8	1.1	2.2	0.8	-

Glass

Sample	O	Ca	Fe	Al	Si	Mg	K
2125 001	33.8	32.1	20.9	9.0	2.6	1.6	-
2125 002	33.1	32.9	20.4	10.3	2.1	1.3	-
2055 058	30.4	37.9	16.3	10.2	3.0	1.0	1.1
2055 059	28.6	36.5	23.6	7.5	2.4	1.4	-
2055 060	30.4	36.7	16.8	12.4	2.1	1.0	0.5
2055 061	28.8	36.8	24.3	6.9	1.9	1.3	-
2055 076	29.3	35.2	19.5	12.3	2.3	1.4	-
2055 077	28.8	36.5	23.6	7.6	2.1	1.4	-

Vesicle fillings

Sample	O	Si	Ca	Fe	Cl	Al	Mg
2055 054	47.2	38.2	5.3	3.5	2.7	1.8	1.4
2055 055	47.9	38.1	4.3	3.7	3.1	1.9	0.9
2055 056	47.2	40.3	4.4	3.7	2.5	1.9	-
2055 057	47.5	37.4	5.9	3.9	2.5	2.2	0.5

Groundmass

Sample	O	Ca	Si	Fe	Al	Cl	Na	Mg	Tl
2125 005	52.5	29.9	12.2	2.2	1.4	0.8	0.6	0.4	-
2055 062	40.4	14.7	33.8	-	5.0	3.4	1.5	1.2	-
2055 064	37.2	44.9	11.8	-	1.8	0.9	-	0.3	3.1

Table 10. Major element composition of the components of Microfacies VS from Clipper-1. Figures are in mass % (Appendix 1).

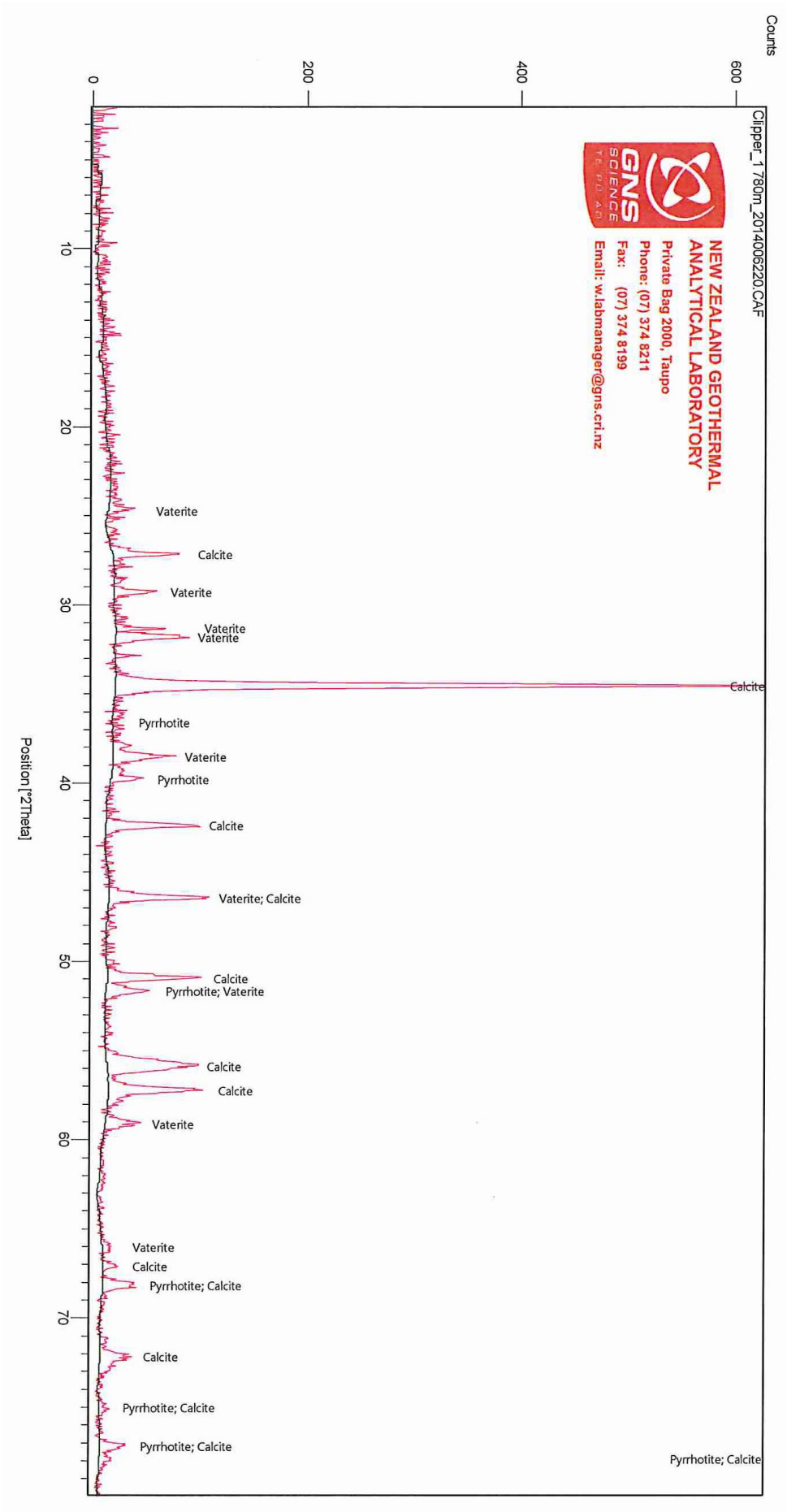

Fig. 51. Qualitative XRD scan showing the mineralogy of a pure sample of Microfacies VS from Clipper-1 at 780m depth.

Major oxides (weight %)

	Fe_2O_3	MnO	TiO_2	CaO	K2O	SO_3	P_2O_5	SiO_2	Al_2O_3	MgO	Na_2O	LOI	Total
CRL	2.87	0.08	0.15	38.76	0.13	1.59	0.06	20.61	3.03	1.36	0.24	30.41	99.30
UC	2.94	0.08	0.19	38.34	0.29	1.59	0.07	21.65	3.38	1.47	0.96	28.63	99.59

Trace elements (ppm)

	As	Ba	Ce	Cr	Cu	Ga	La	Nb	Ni	Pb	Rb	Sc	Sr	Th	U	V	Y	Zn	Zr	Nd
CRL	5	482	35	22	12	4	14	4	12	16	9	6	484	1	2	31	8	24	54	-
UC	-	417	19	31	-	4	15	5	13	16	8	-	471	3	-	34	9	41	63	40

Table 11. XRF analysis of Microfacies VS rich cuttings from Clipper-1 at 780m depth. Analysis performed by CRL and University of Canterbury. LOI = loss on ignition. Null values indicate a trace element that was not included in the analysis.

3.8 Fluidised and mineralised sediment

Fluidisation of sediment is indicated by visibly reduced porosity and the loss of original sedimentary textures. Mica grains are roughly aligned with the direction of fluid flow (Fig. 52). This texture is found down to 1010m in Clipper-1, in the upper part of the Tokarahi Siltstone. In the top sample at 780m, a single grain showing more extreme alteration was found (Fig. 53). This grain contains substantial secondary mineralisation with the formation of euhedral crystals and loss of sedimentary textures.

In deeper sediments, a distinct texture occurs as a result of recrystallisation of silica, carbonate and sulfide minerals, and/or precipitation of newly formed hydrothermal minerals This obscures the original texture of the sediment, resulting in a less translucent material with a crenulated fabric and no visible grain boundaries (Fig. 54). This texture occurs in distinct bands with a sharp boundary between highly recrystallised material and less altered sediments (Fig. 55). This may be a result of the better induration of the deeper sediments where it occurs.

Fluidisation of sediment is also indicated by deformation of pyrite framboids (Fig. 56).

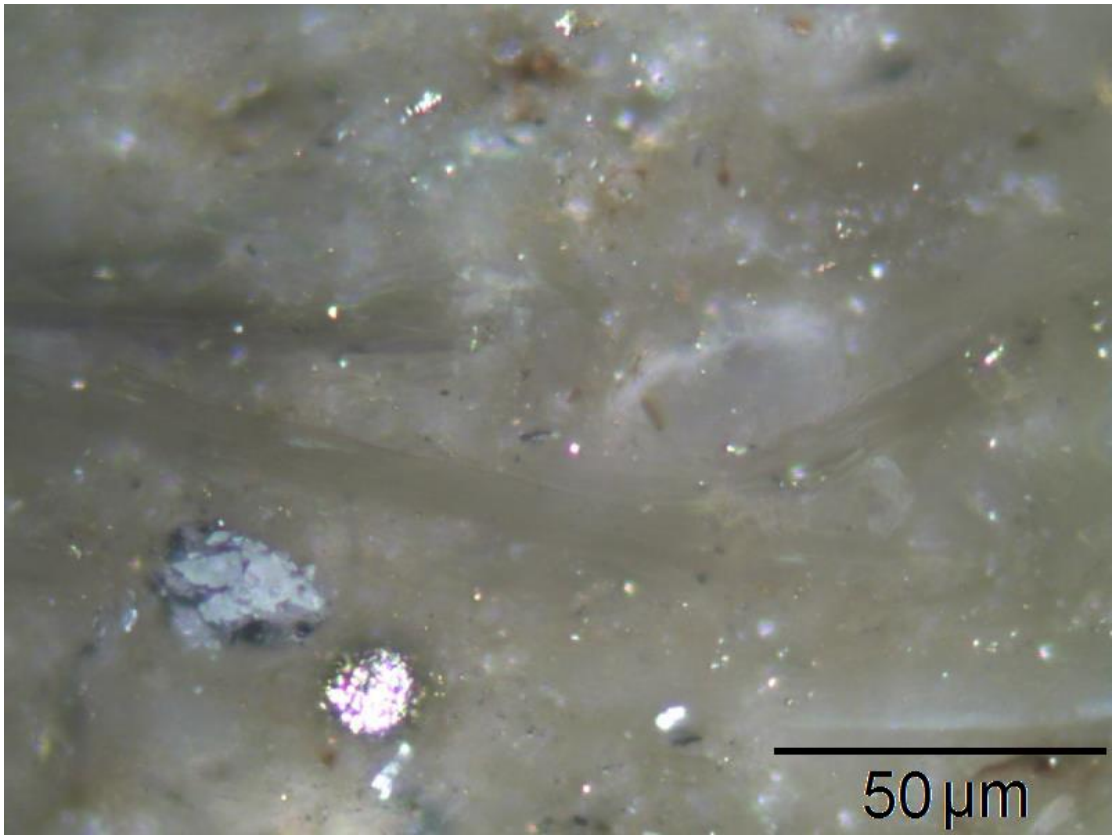

Fig. 52. Fluidised sediment from the middle of the Tokama Siltstone with mica crystals aligned in the direction of flow. From 1010m depth in Clipper-1, image in reflected light.

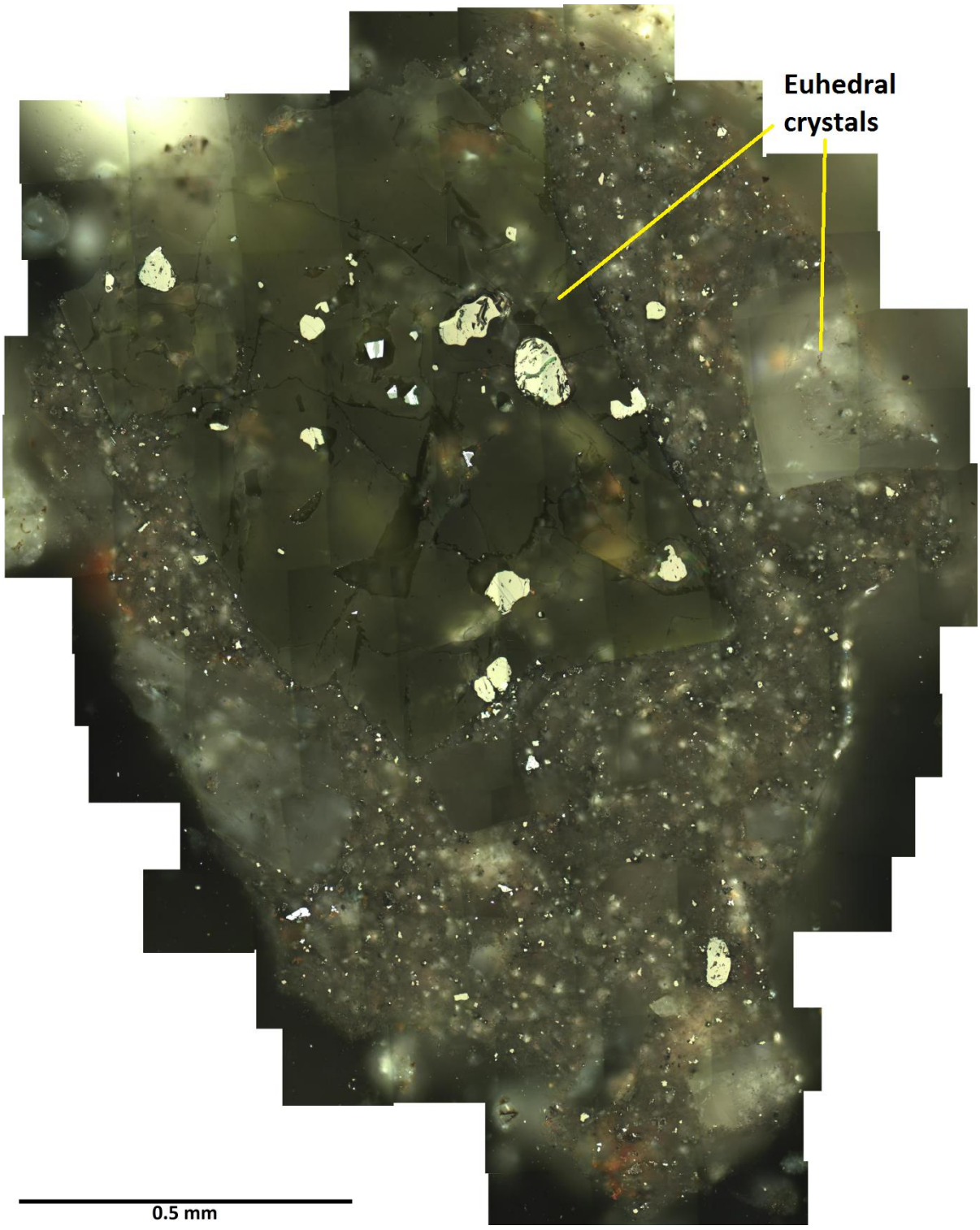

Fig. 53. Photomontage of recrystallised sediment with secondary euhedral crystals. From 780m depth in Clipper-1, image in reflected light. The tesselated pattern visible on parts of the image is due to uneven lighting across each frame of the photomontage.

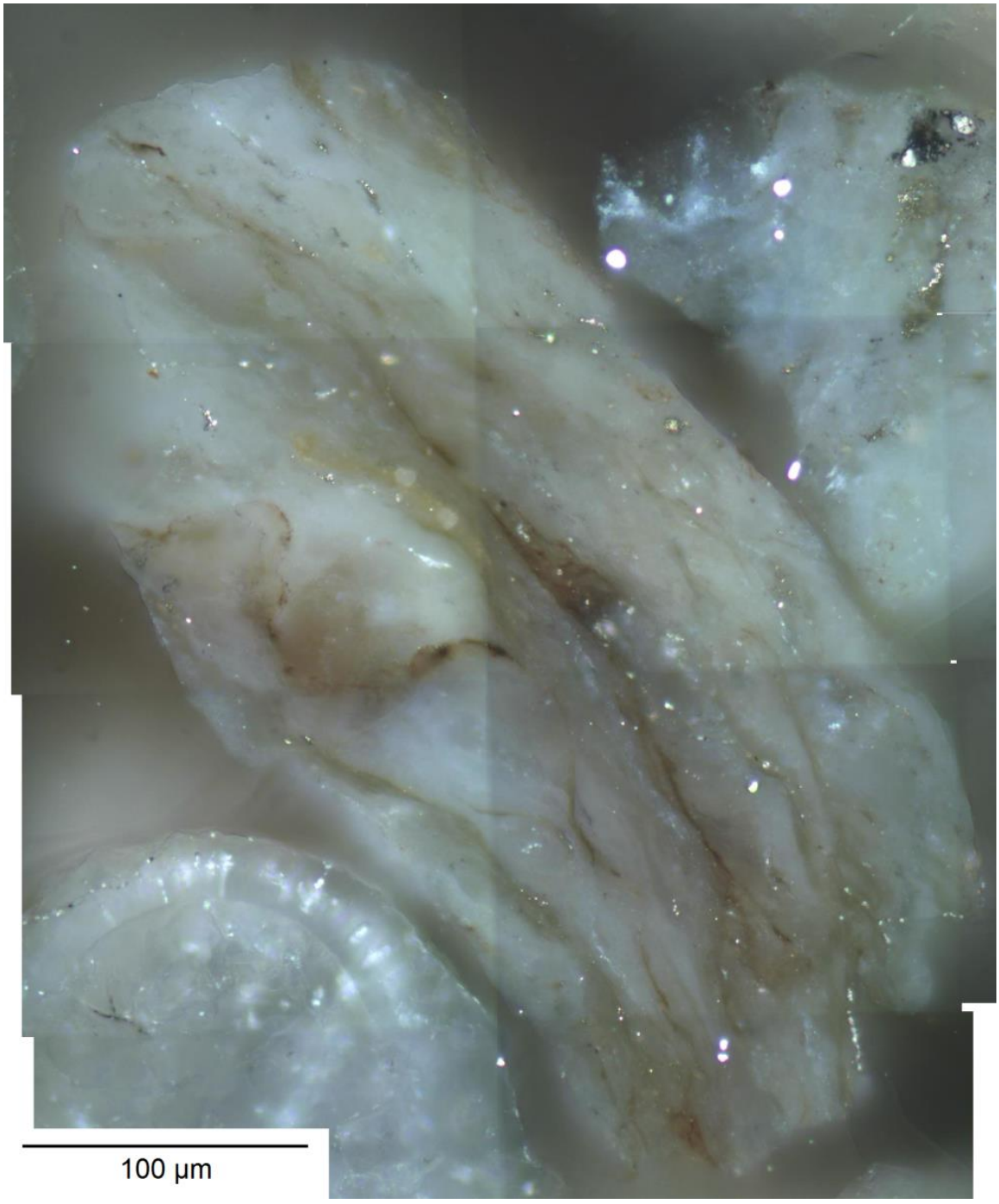

Fig. 54. Photomontage of mineralised sediment with crenulated fabric from the base of the Tokama Siltstone. From 2035m depth in Clipper-1, image in reflected light.

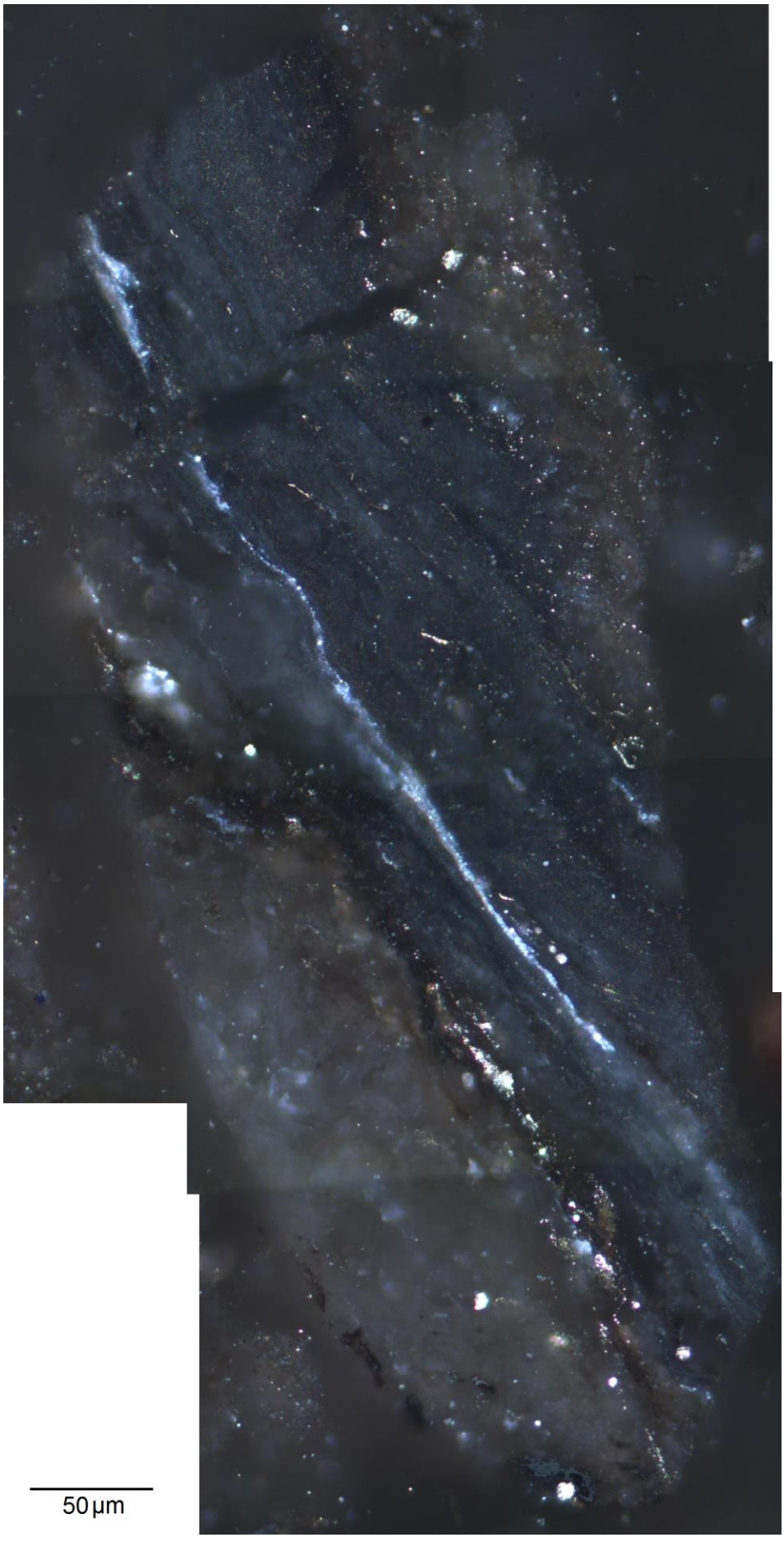

Fig. 55. Photomontage of a band of intense hydrothermal alteration in siltstone. Precipitation of minerals in linear patterns reveals the direction of fluid flow. From 3901m depth in Clipper-1, image in reflected light.

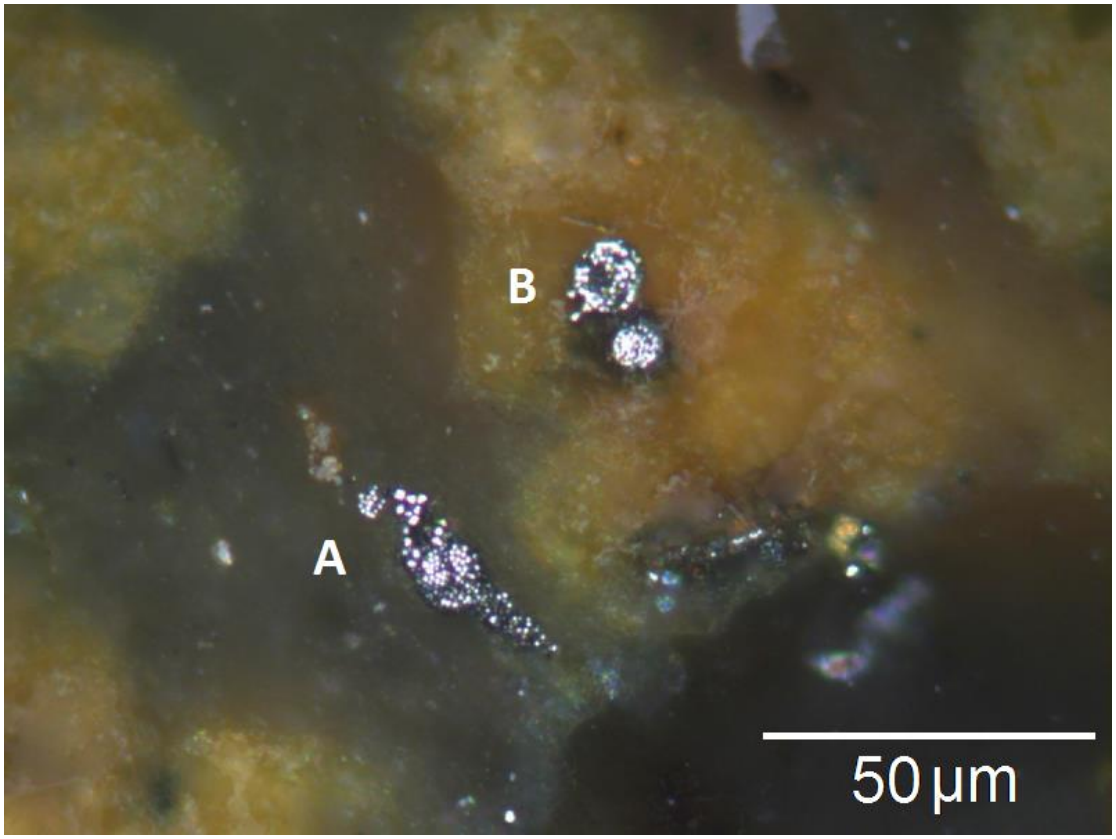

Fig. 56. (A) Framboidal pyrite deformed during fluidisation of sediment.
(B) Undeformed framboids contained within fragments of mineralised sediment (orange) that did not fluidise. From 2795m depth in Clipper-1, image in reflected light.

3.9 Basement rock secondary minerals and textures

The basement rock in the Clipper sub-basement is correlative of Haast Schist. The Clipper-1 well extends 57 metres below the unconformity that marks the top of the basement rock, allowing sampling of relatively fresh, unweathered rock (Fig. 57).

The schist contains abundant calcite crystals that lack deformation and cut across the foliation of the schist, indicating that they are post-metamorphic in origin (Fig. 58). Euhedral pyrite crystals are also present (Fig. 59). The mica-rich layers of the schist are rich in graphite, in some cases in sufficiently high concentration to make the rock opaque in thin section (Fig. 60). Microbrecciation, in some cases associated with crenulated fabric, indicate shearing and fluid flow in the schist (Fig. 61-63).

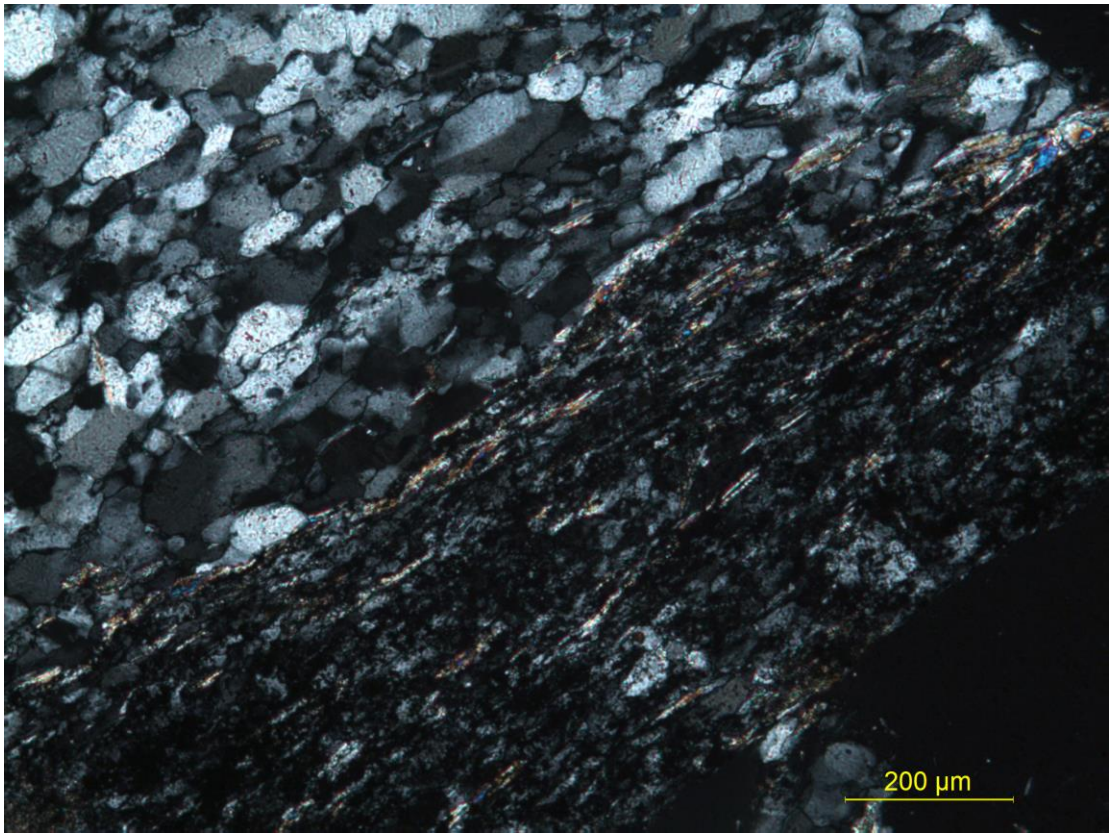

Fig. 57. Typical schist from the base of Clipper-1, showing quartz-rich (top) and mica-rich (bottom) layers. From 4741m depth in Clipper-1, image in cross-polarised transmitted light.

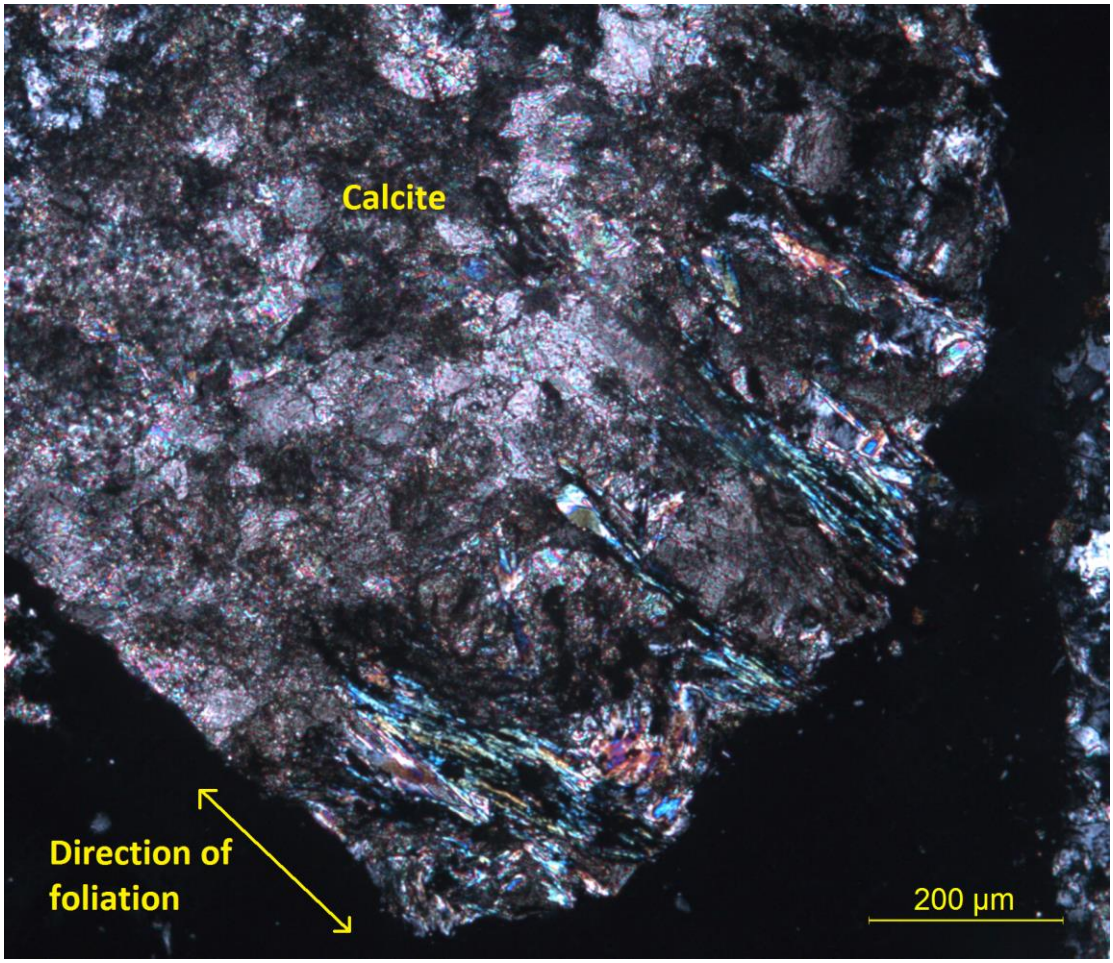

Fig. 58. Schist with calcite crystals cutting across foliation. From 4741m depth in Clipper-1, image in cross-polarised transmitted light.

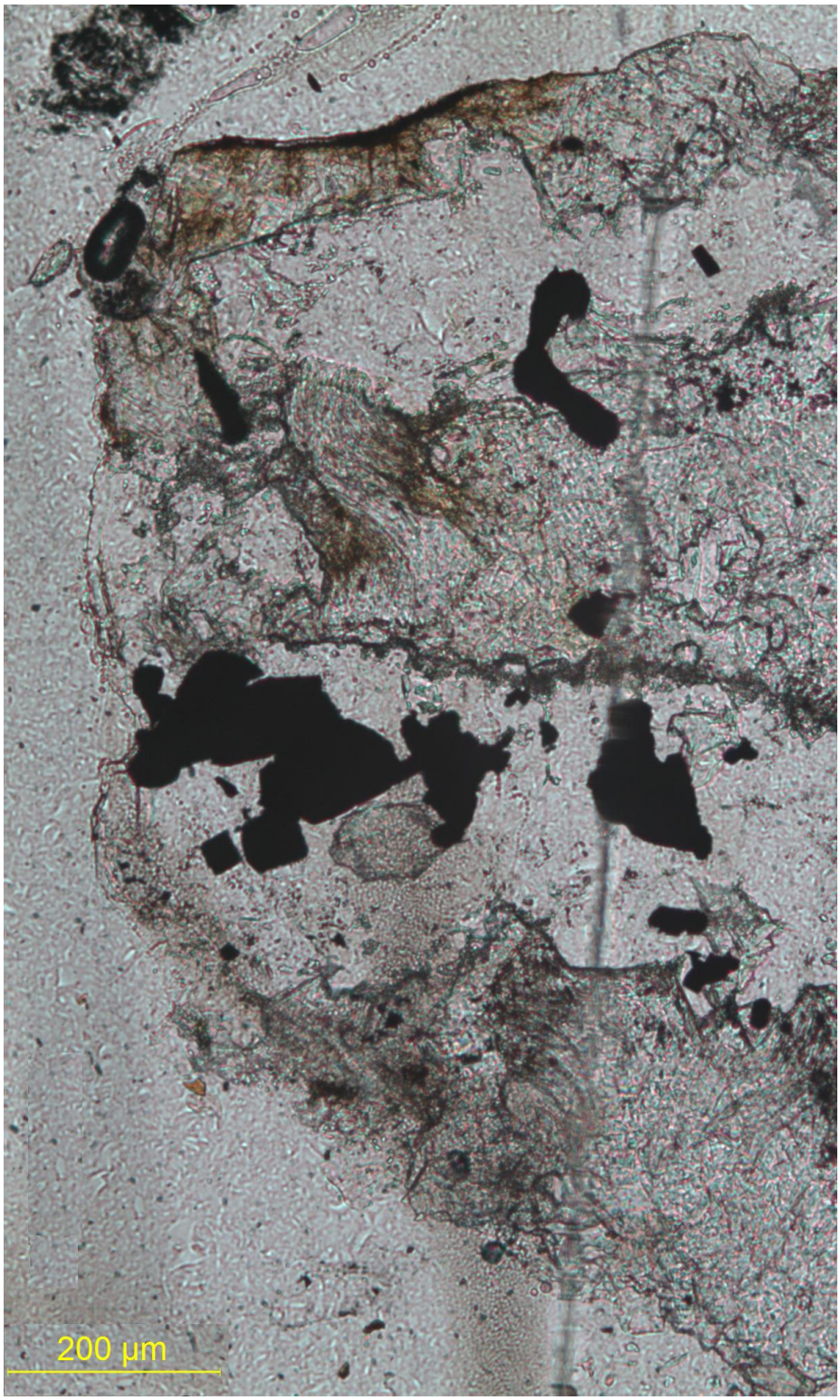

Fig. 59. Euhedral pyrite crystals (opaque) in schist. From 4741m depth in Clipper-1, image in transmitted light.

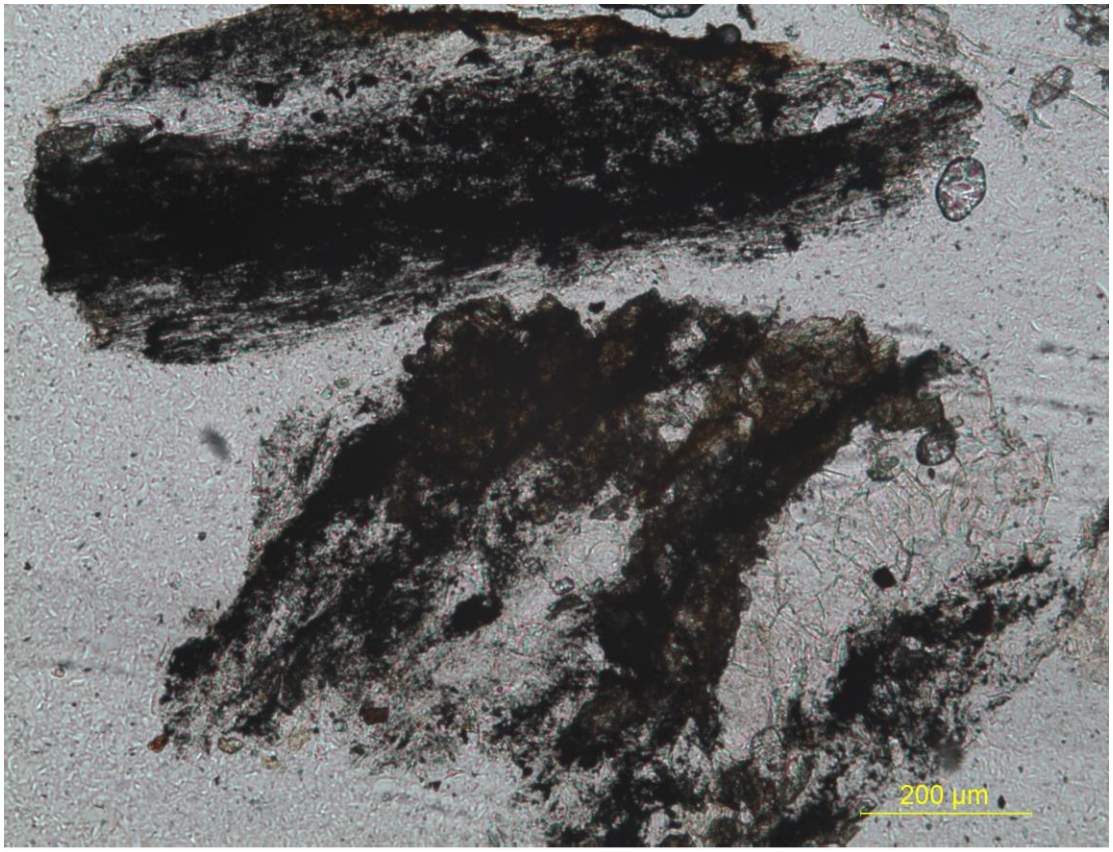

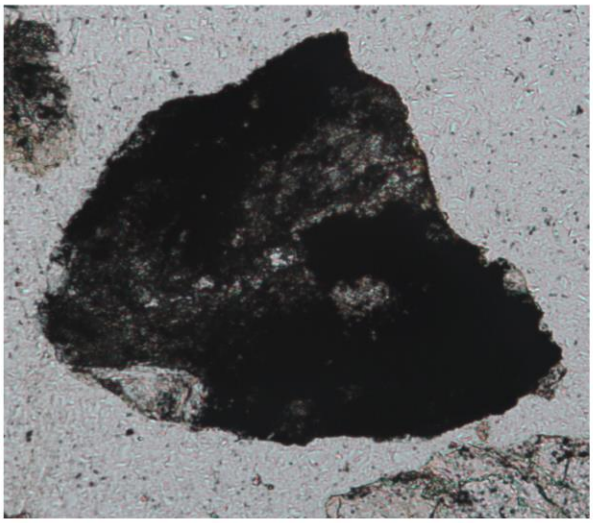

Fig. 60. (Above and left) Schist with abundant graphite (black), which is concentrated in the mica-rich layers of the schist.
From 4741m depth in Clipper-1, image in transmitted light.

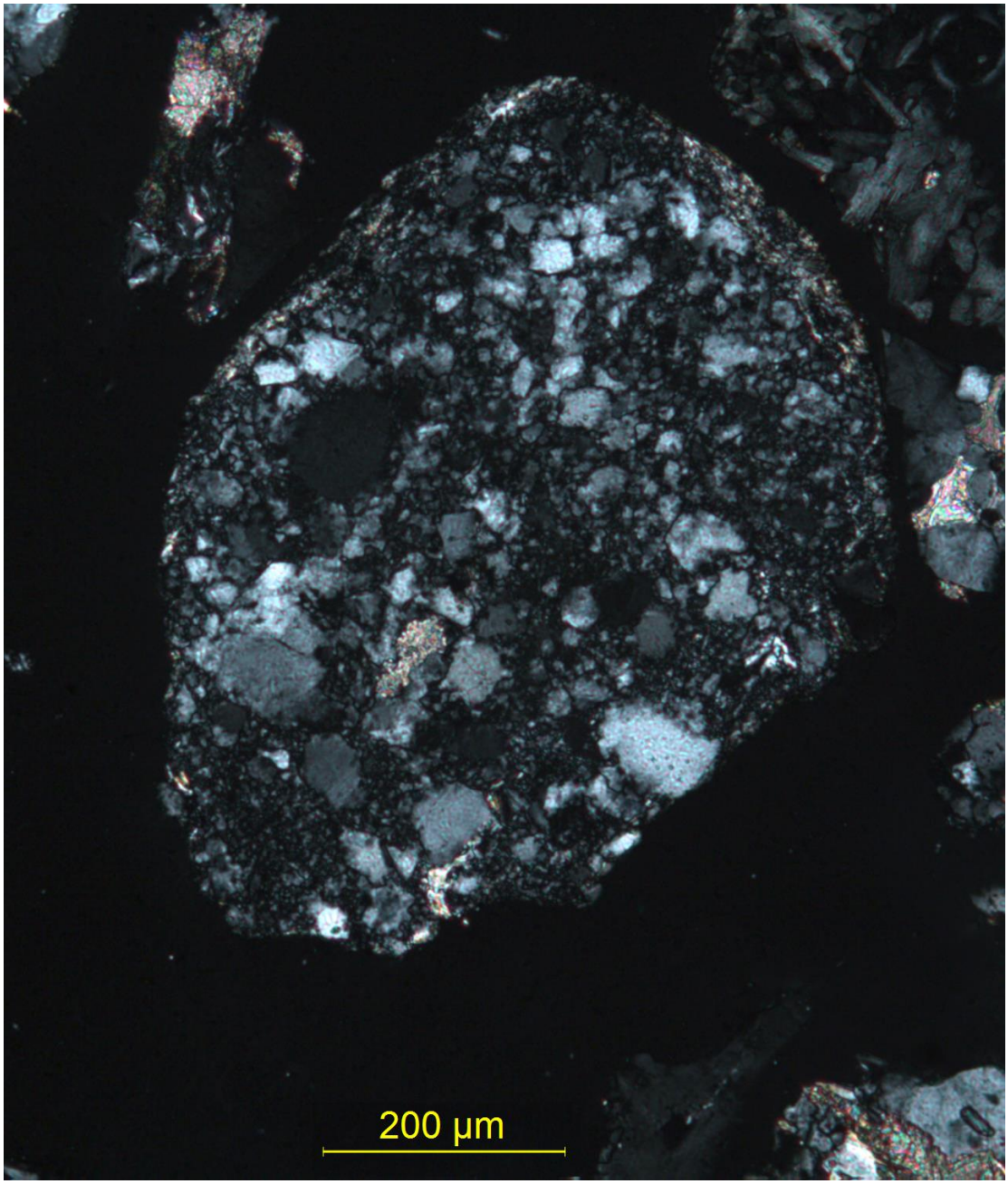

Fig. 61. Schist with micro-brecciated quartz. From 4741m depth in Clipper-1, image in cross-polarised transmitted light.

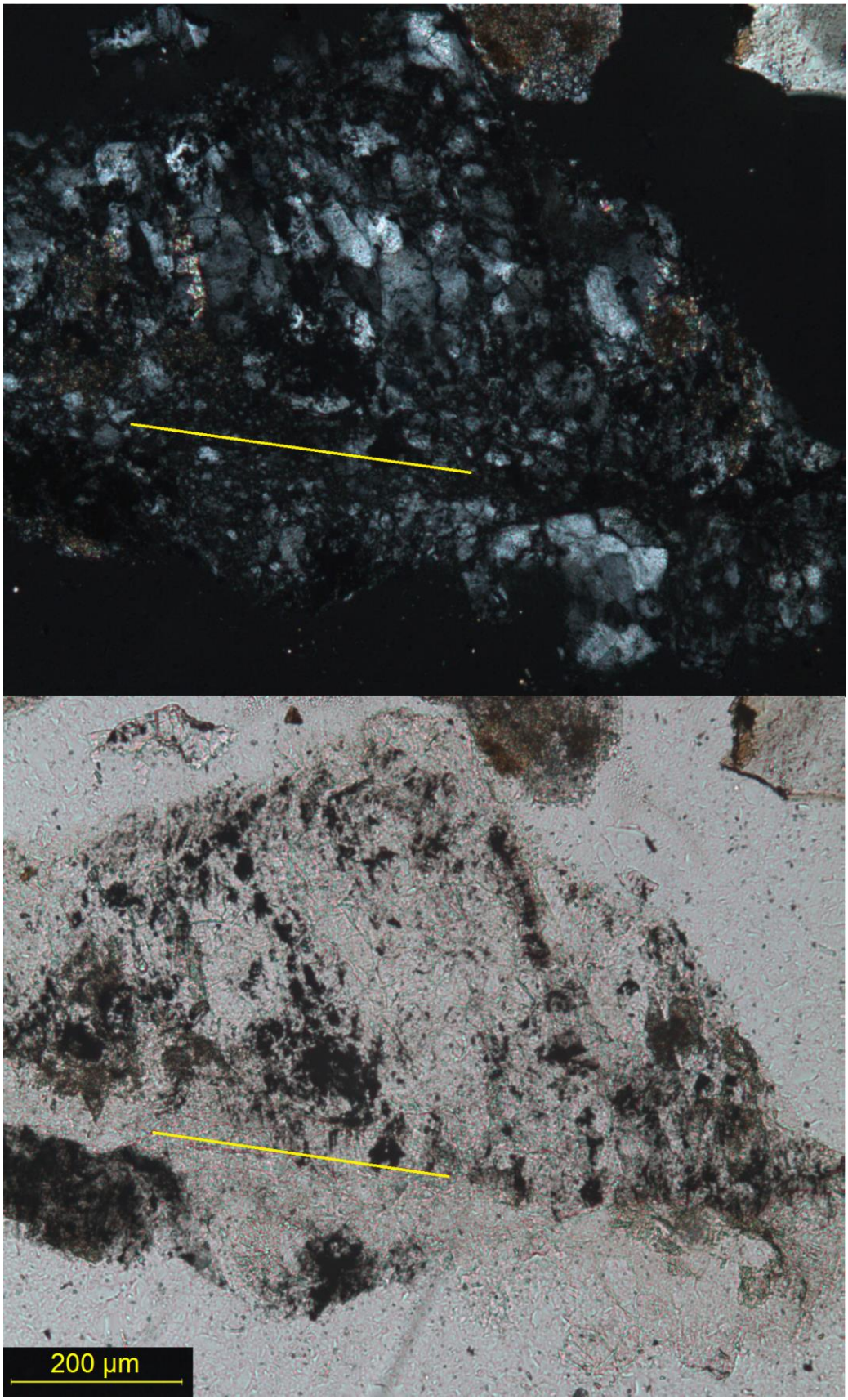

Fig. 62. Schist with micro-brecciated quartz along a linear shear (yellow line). From 4741m depth in Clipper-1, image in cross-polarised (top) and plane polarised transmitted light.

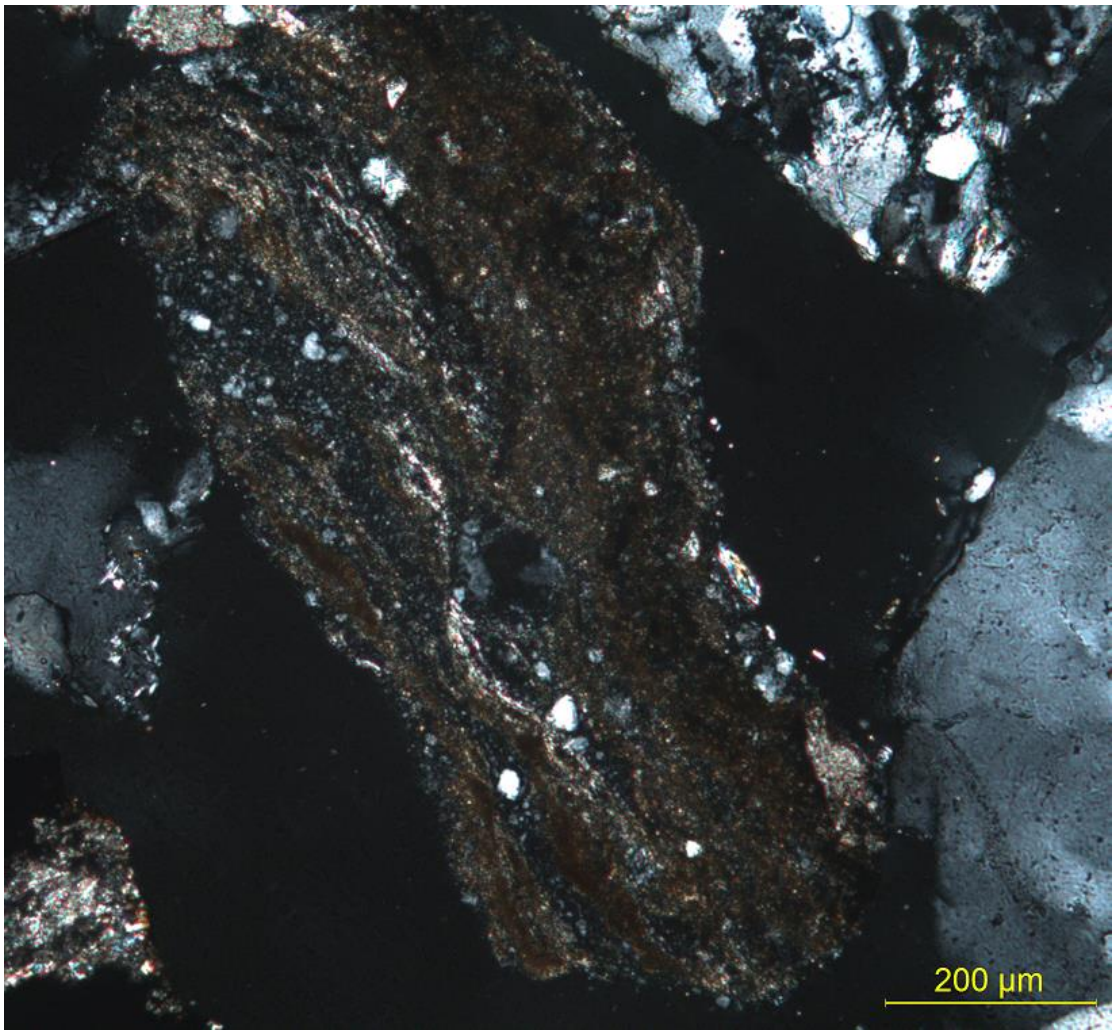

Fig. 63. Micro-brecciated schist with crenulated fabric. The brown colouration is produced by calcite. From 4741m depth in Clipper-1, image in cross-polarised transmitted light.

4.0 Outcrop sampling

When investigating the geological structure and history of offshore sequences, we are limited to the information provided by core, cuttings and seismic surveys. The wider picture provided by onshore rock exposures is not available, making it considerably more difficult to determine the precise conditions under which a rock or mineral formed. In an attempt to find an onshore parallel for the igneous and hydrothermal processes that have affected the Clipper-1 well sediments, samples of a range of volcanic rocks and closely associated sediments were taken from areas of Banks Peninsula and Otago that have experienced volcanism during the history of the Canterbury Basin. If any of these rock samples contained similar minerals and structures to the Clipper-1 sediments, this could help reveal the igneous setting in which they were formed. All photomicrographs are taken in oil immersion and unpolarised light unless otherwise stated.

4.1 Kakanui Mineral Breccia

Along the coast south of Oamaru, several tuff rings have been exposed by coastal erosion (Fig. 64-65). These tuffs are part of the late Eocene to early Oligocene Deborah Volcanic Formation, and are the remnants of small volcanic cones (~ 1km diameter) formed by material ejected during Surtseyan eruptions in a shallow marine environment and subsequently re-worked by mass flow and wave action (Corcoran & Moore 2008).

Fig. 64. Sampling location at Kakanui. The circular outline of the volcanic cone is clearly visible where overlying sediments have been eroded by wave action.

Fig. 65. View from the Kakanui sampling location, facing south.

The tuff in the sampling area south of the Kakanui river mouth is a crystal-vitric lapillistone primarily comprised of palagonite and basalt clasts. The clasts are cemented with calcite and calcite veins are present (Fig. 66). Phenocrysts of hornblende are abundant. Closer to the original vent site, in material deposited inside the crater, a thickly-bedded deposit contains phenocrysts of hornblende up to 8cm long and basalt bombs up to boulder size. This deposit also contains angular clasts of finely laminated siltstone, representing pieces of the original seabed broken up during explosive eruptions and incorporated into the tuff. Some of these sedimentary clasts show evidence of baking, with a red coloured margin surrounding a green-grey centre (Fig. 67).

Rock samples were taken from a range of lapilli tuffs, mineral veins and sedimentary clasts contained within the tuff. This covers several possibilities for mineral formation: crystallisation from magma, precipitation from hydrothermal fluids and alteration of intruded sediments. Samples were dried, crushed and mounted in resin pellets for examination with reflectance microscopy.

The tuff contains abundant iron oxides including hematite (Fig. 68), ilmenite and iron oxide minerals (Fig. 69). Iron oxide staining is present on the edges of phenocrysts and vesicles in the tuff (Fig. 70). Pale yellow devitrified glass is evidence of palagonitization (Fig. 71). The veins primarily consist of calcite with abundant iron minerals including hematite (Fig. 72). Goethite has been precipitated in open pore spaces (Fig. 73). The sediment clast contained within the tuff features iron oxide precipitating in cracks and on the outer edges of sediment grains, indicating that it has been infiltrated by iron-rich hydrothermal fluids (Fig. 74).

Fig. 66. A hard, distinctly pink vein in tuff close to the site of the largest phenocrysts and sedimentary clasts. On the edges of the vein, individual pieces of scoria are separated by vein material suggesting that the tuff clasts were not cemented when the vein formed. Rock hammer for scale.

Fig. 67. Tuff boulder showing calcite cement and baked sedimentary clast. Rock hammer for scale.

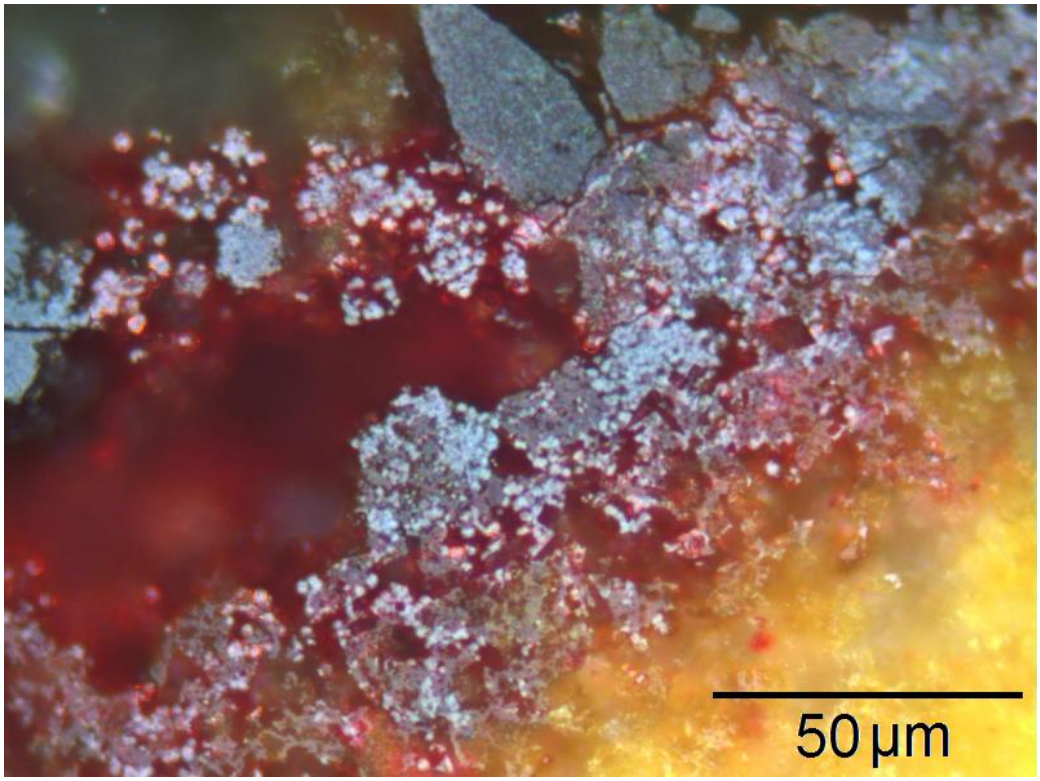

Fig. 68. Hematite in the Kakanui tuff displaying strong red internal reflections. Image in reflected light.

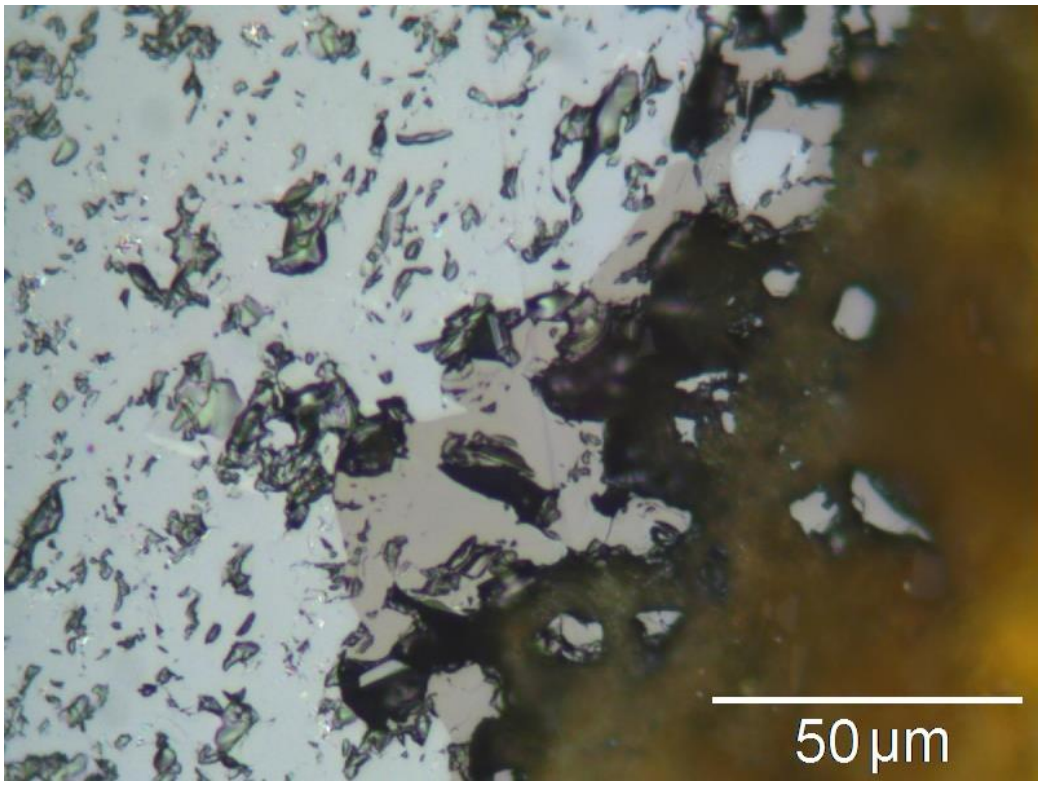

Fig. 69. Opaque iron oxides occur as large, isolated pieces and small phenocrysts in the glassy material of the Kakanui tuff. Differences in reflectance indicate that more than one type of mineral is present. Image in reflected light.

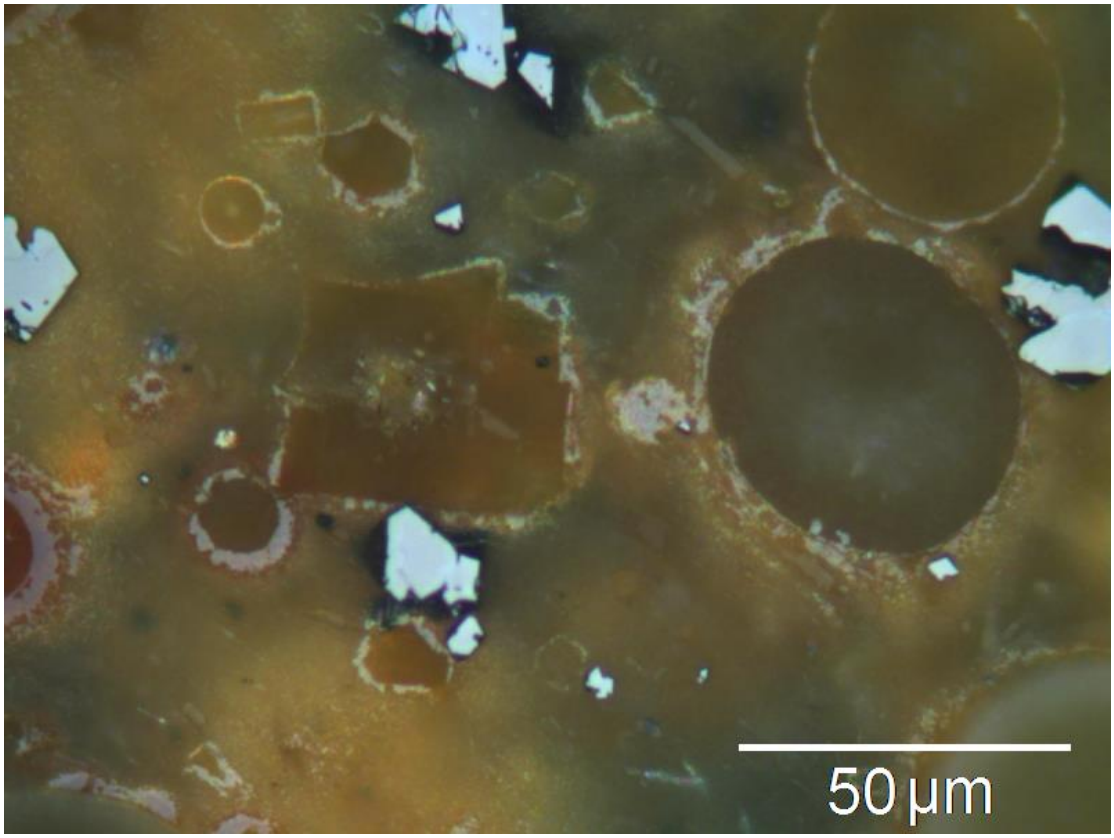

Fig. 70. Transparent glass from the Kakanui tuff showing iron oxide formation at the edges of vesicles and phenocrysts. Image in reflected light.

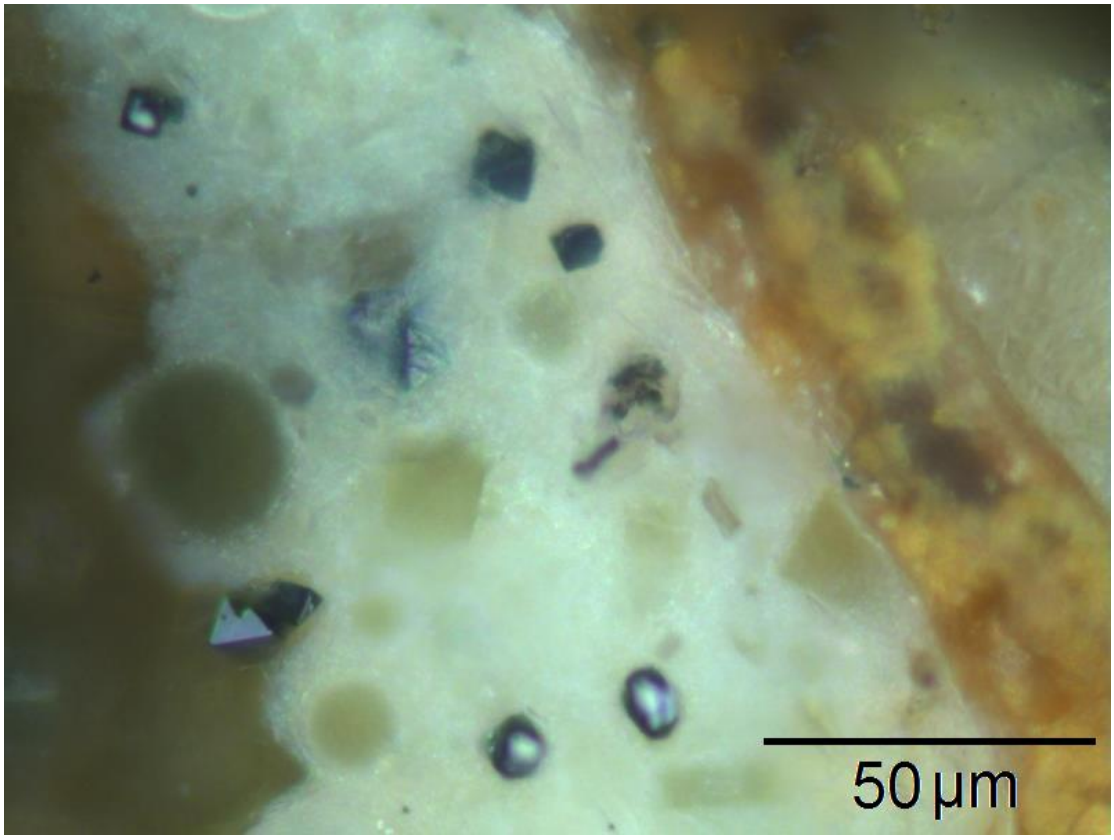

Fig. 71. Devitrified glass from the Kakanui tuff. Image in reflected light.

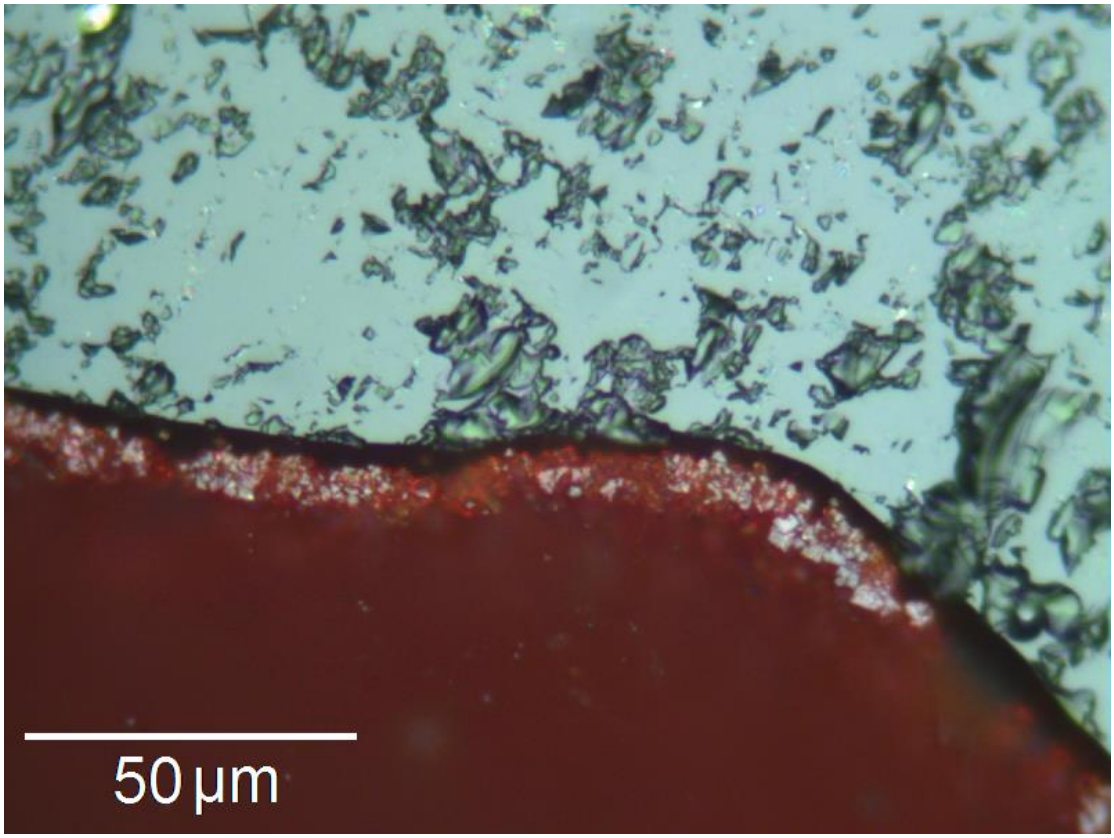

Fig. 72. Hematite crystals (red) in calcite vein. Image in reflected light.

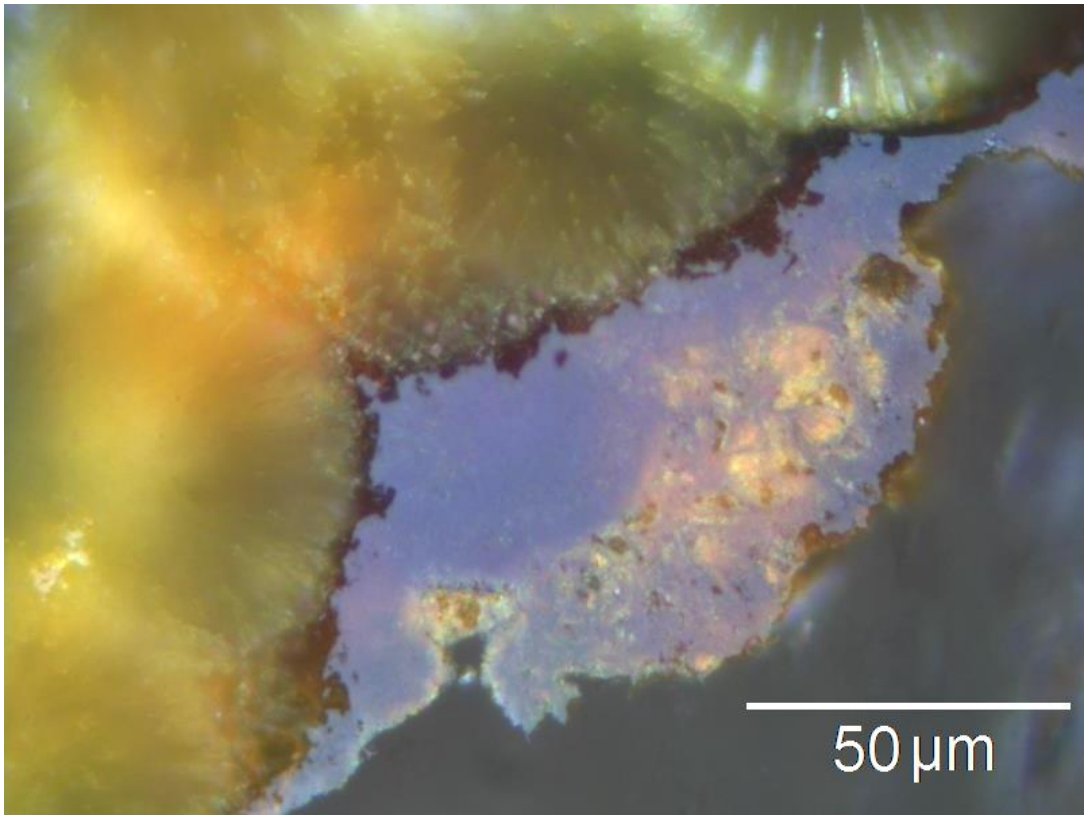

Fig. 73. Goethite (centre) filling open pore spaces in calcite vein. Image in reflected light.

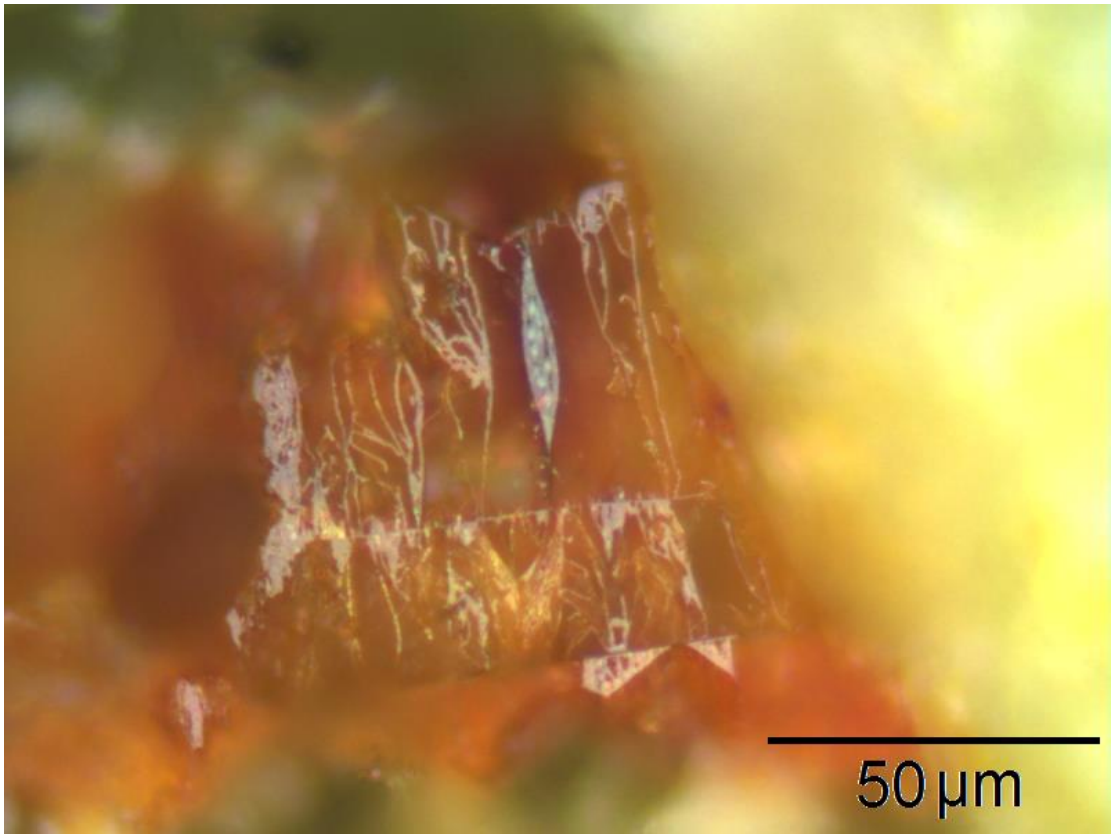

Fig. 74. Sediment grain from Kakanui mineral breccia with secondary iron oxide deposition. Image in reflected light.

4.2 Moeraki Sill

Moeraki Peninsula, on the Otago coastline south of Oamaru, features tuffs and basaltic intrusions that are well exposed in sea cliffs. As with the deposits at Kakanui, these are part of the late Eocene to early Oligocene Deborah Volcanic Formation. The edges of the intrusion are glassy and vesicular, indicating quenching of the magma as it came in contact with the wet sediments. The original composition of the basalt was olivine tholeiite, typical of continental intraplate volcanism. Aqueous fluids circulating through fractures in the basalt have altered the composition, with vesicles infilled and olivine replaced by secondary minerals (Coombs et al. 1986). Much of the glass has been altered to palagonite.

The sampling location at Moeraki is on the north side of the peninsula where a basalt sill has intruded soft, wet marine mud (Fig. 75). Samples were taken of the margins of the sill and the altered mudstone and vein material above the sill.

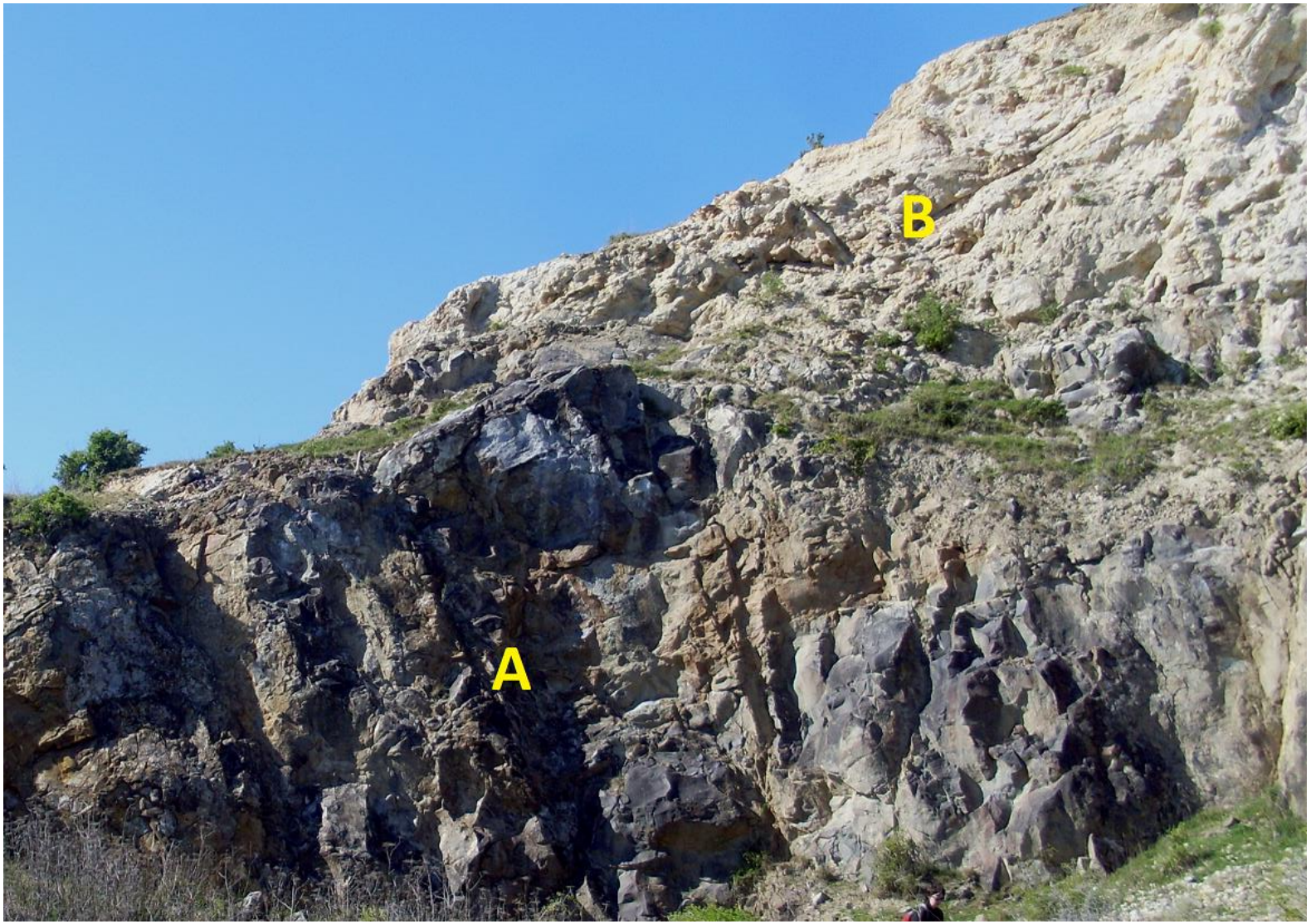

Fig. 75. The Moeraki Sill (A) beneath mudstone baked by the intrusion (b).

Immediately above the sill contact there is a very fine grained, well indurated baked mudstone (Fig. 76). Similar to the sediment clasts in the Kakanui tuffs, these sediments contain iron oxides (Fig. 77).

1-2 metres above the sill contact, a different type of alteration occurs. The mudstone here is filled with spherical voids 1-10mm in diameter, likely formed by boiling of connate water as the magma intruded (Fig. 78). These have later become filled with carbonates and iron oxides (Fig. 79). These sediments also contain carbon, most likely derived from baked organic matter (Fig. 80).

Veins 1-3cm in width are filled with quartz and calcite including euhedral crystals growing into open voids, similar to a geode (Fig. 81). The outer margins of the veins are heavily stained with iron oxide. Other parts of the mudstone feature shrinkage cracks with radiating dendritic crystal growths (Fig. 82-84). The presence of open voids in the mudstone suggests that contact metamorphism has hardened the previously soft, wet mud to the point where open cracks can form.

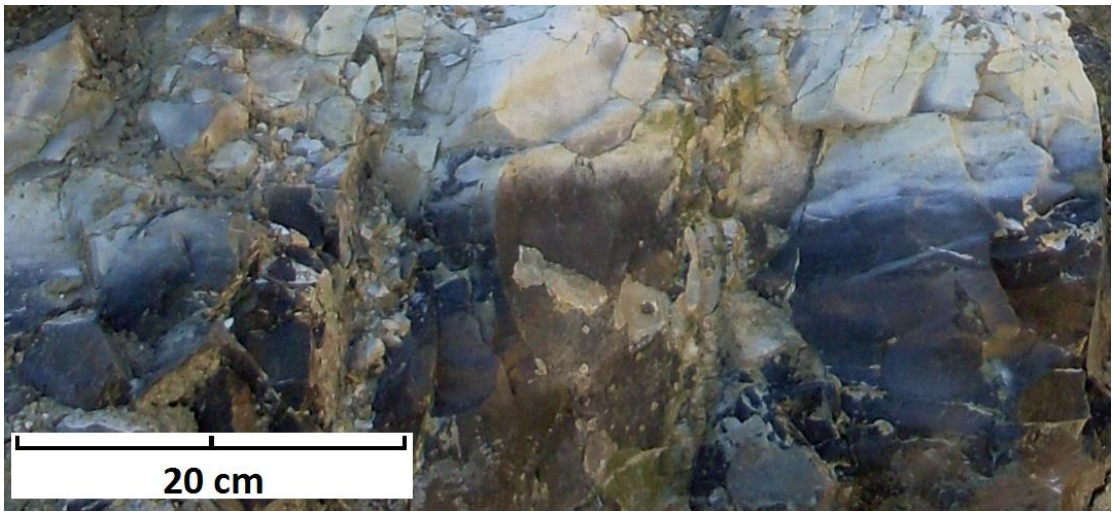

Fig. 76. Baked mudstone immediately above the sill contact. Both the dark and light material is sedimentary.

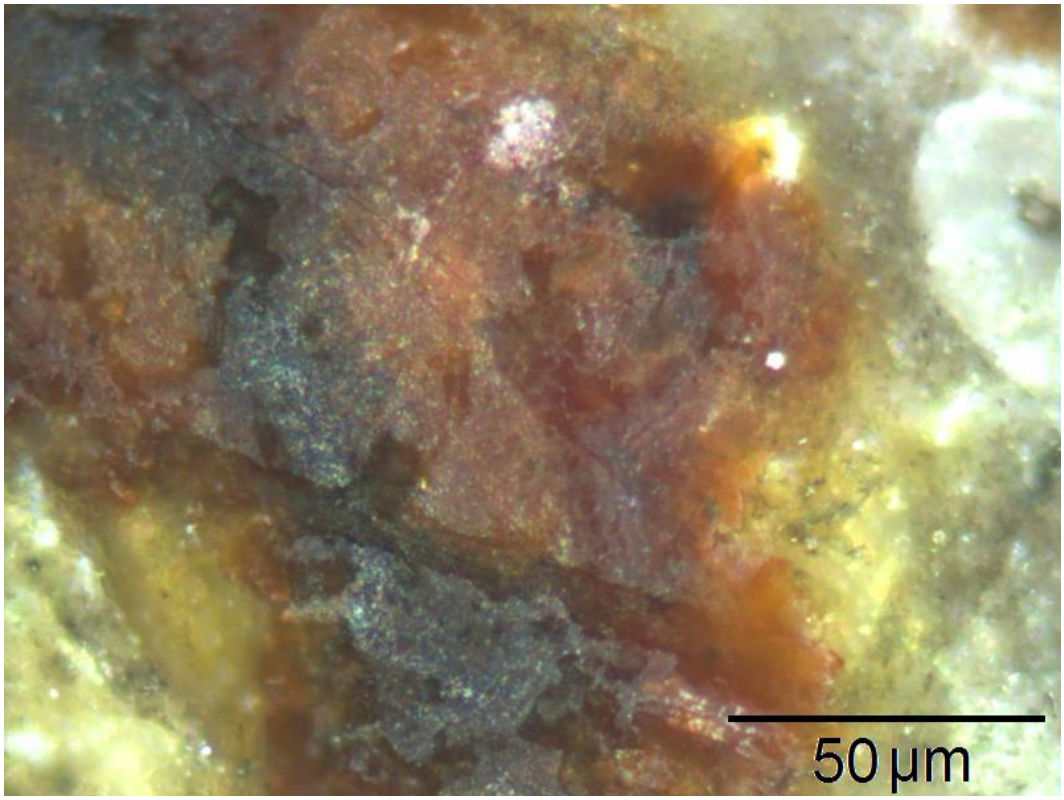

Fig. 77. Secondary iron oxides in the baked sediments immediately above the Moeraki Sill. Image in reflected light.

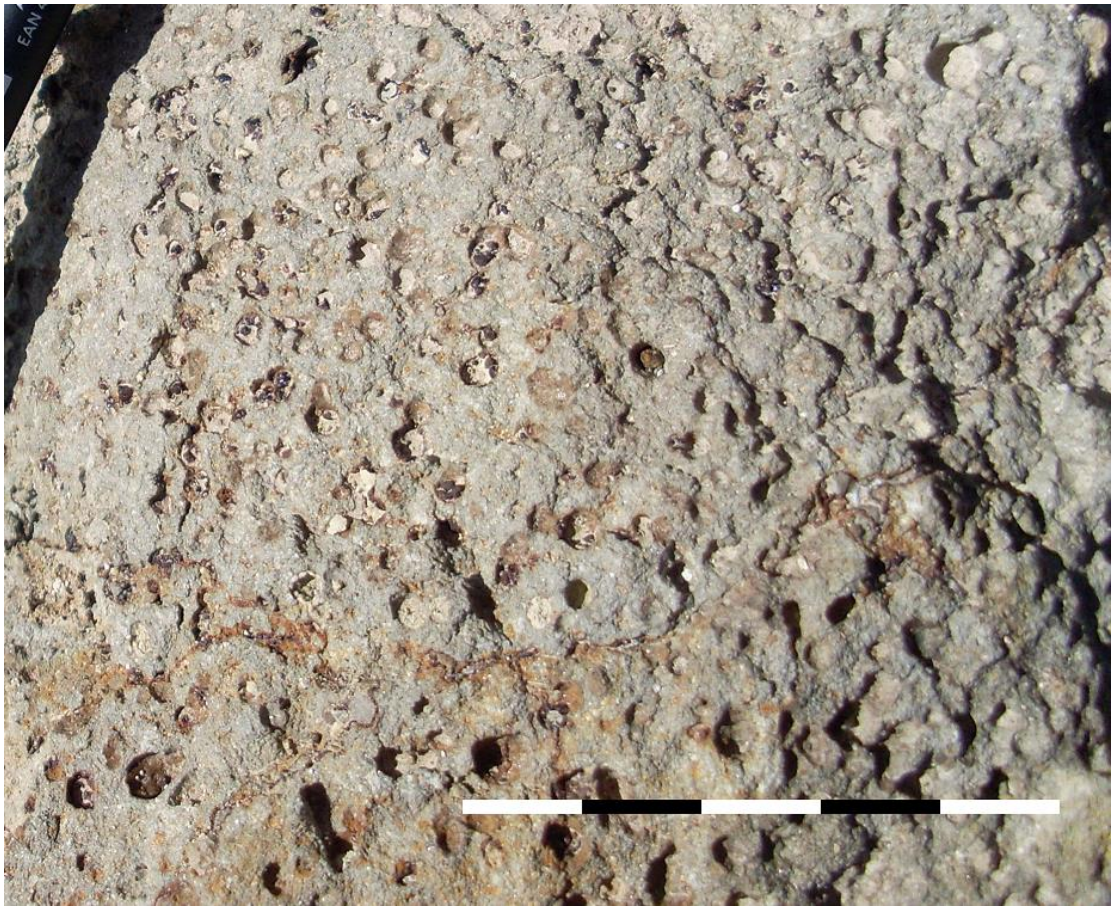

Fig. 78. Spherical voids in baked mudstone above the Moeraki Sill. Scale bar in cm.

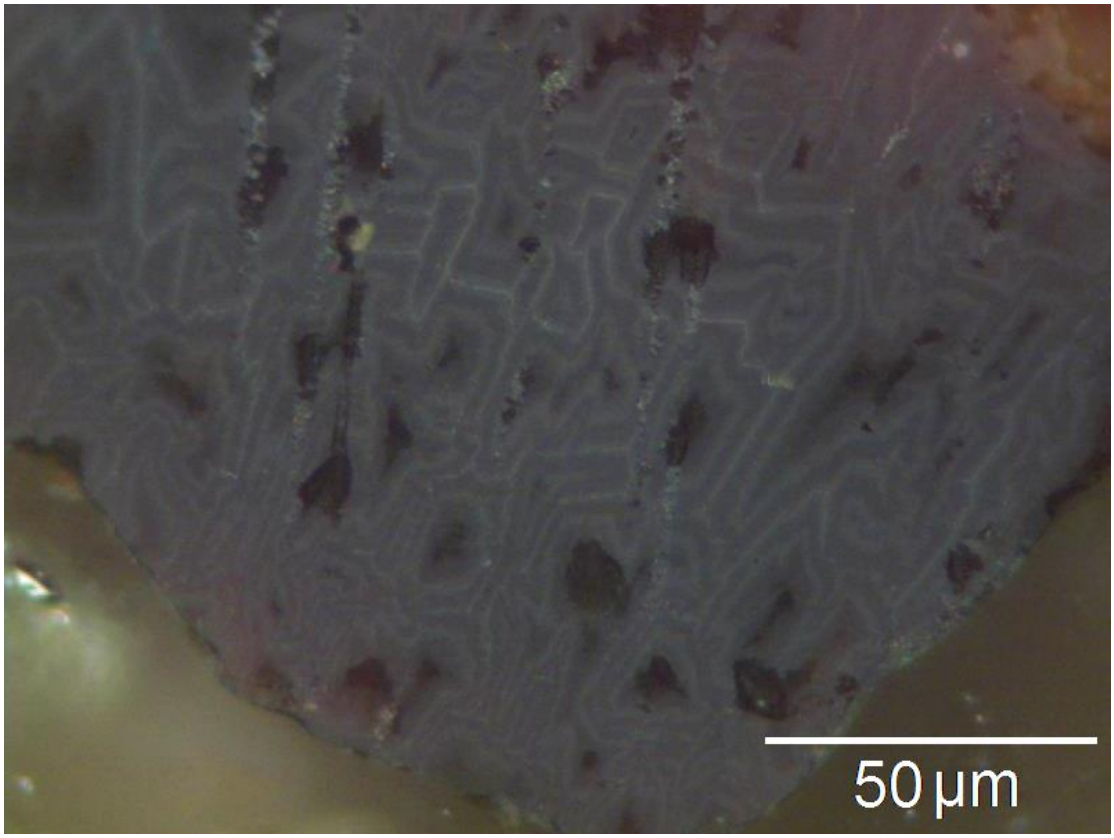

Fig. 79. Polished section of the iron oxide filling spherical voids in the baked mudstone above the Moeraki Sill. Image in reflected light.

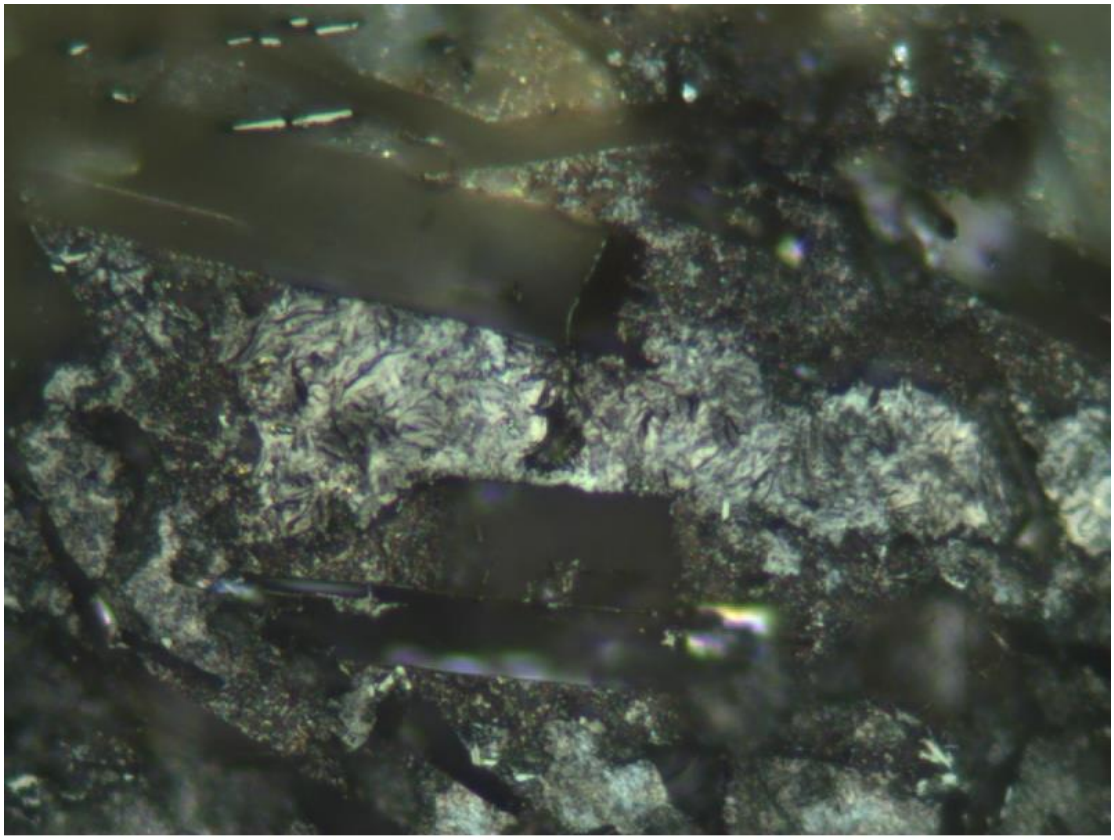

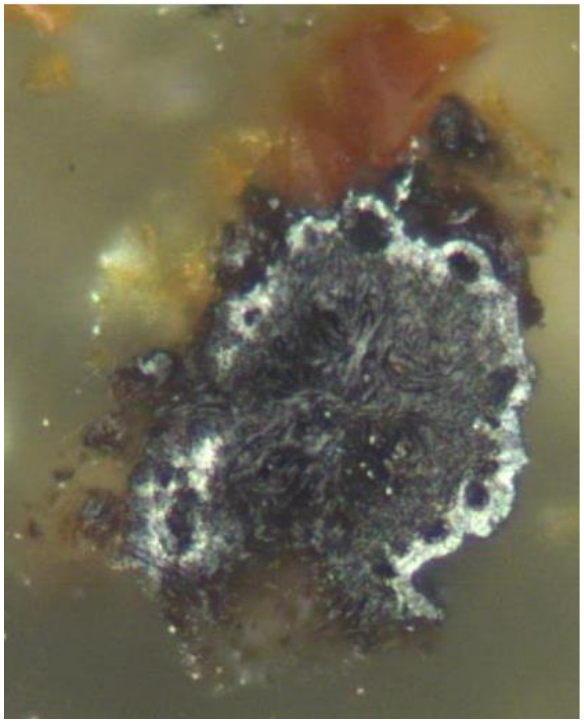

10 µm

Fig. 80. (Above and left) Carbon in the baked mudstone 1-2 metres above the Moeraki Sill. Images in reflected light.

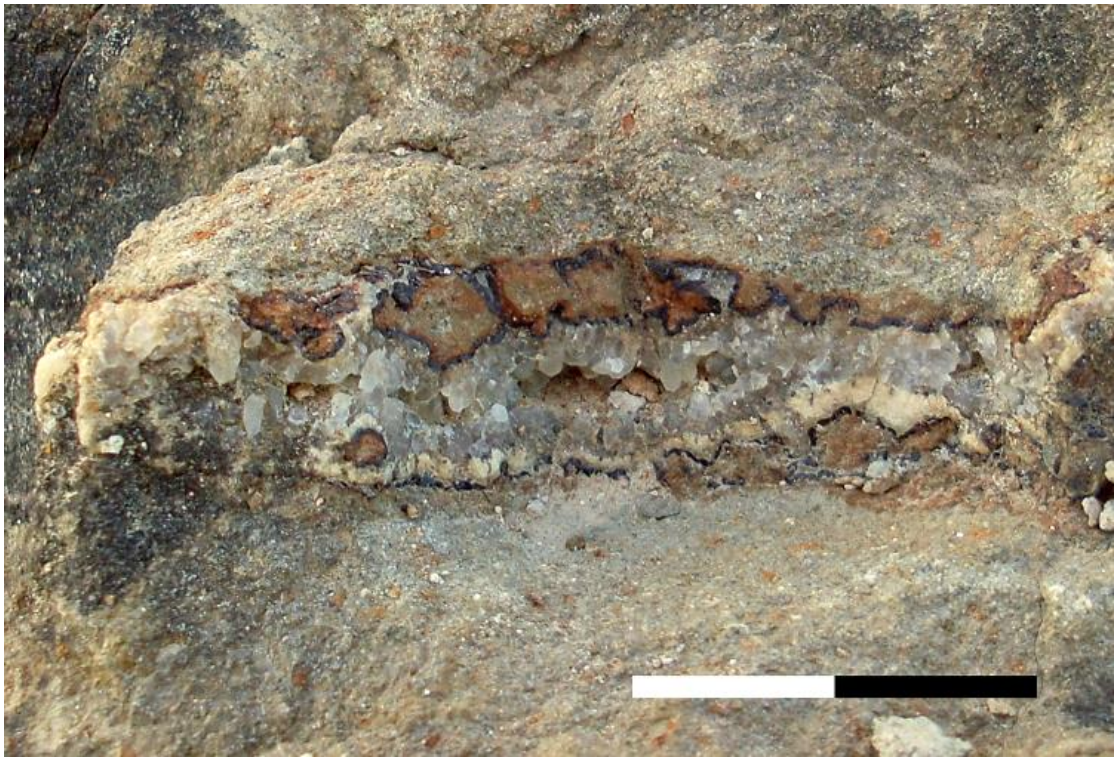

Fig. 81. Quartz vein with central void lined with euhedral quartz crystals. The outer margins of the vein are coated with dark red iron minerals. Scale bar in cm.

Fig. 82. Shrinkage cracks in a vertical face of the mudstone above the Moeraki Sill. Scale bar in cm.

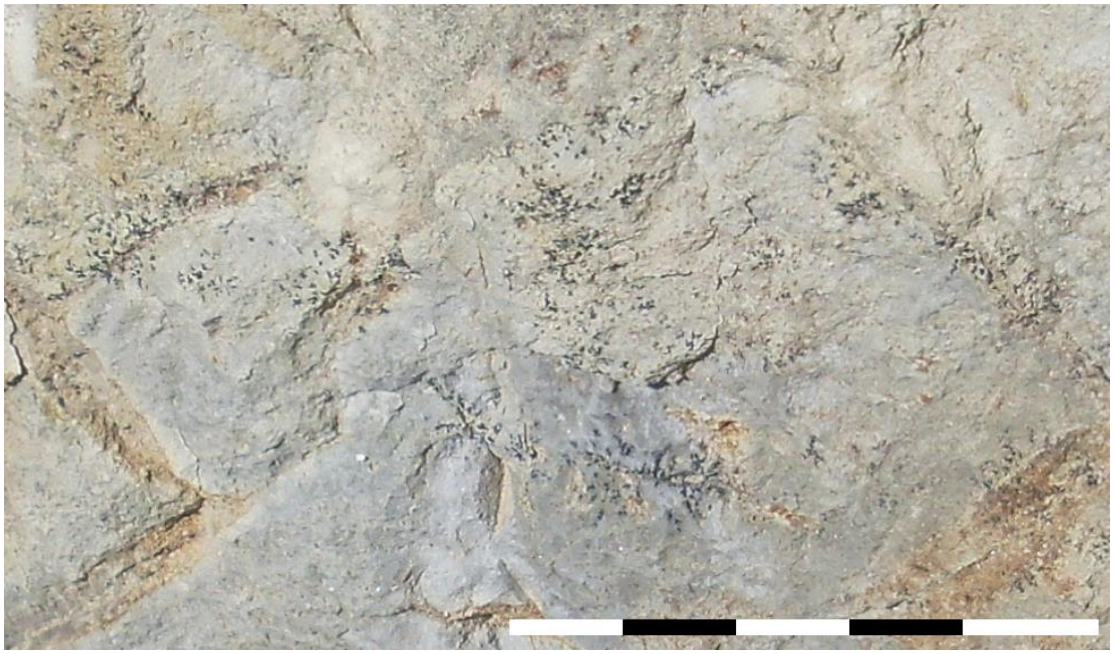

Fig. 83. Dendritic crystal growth radiating outward from shrinkage cracks in the mudstone. Scale bar in cm.

Fig. 84. Dendritic crystals in a hand sample of the Moeraki Sill mudstone.

4.3 Tokarahi Sill

Near Tokarahi in inland Otago, the full thickness of a basaltic sill is exposed in a road cut (Fig. 85). The sill features well-developed columnar jointing and is located in the middle-Eocene Tapui Glauconitic Sandstone. Glassy margins and sediment dikes in parts of the sill suggest it was intruded into wet, unconsolidated sediment (Coombs et al. 1986). The Tokarahi sill was intruded during the same phase of volcanism as the Kakanui and Moeraki tuffs and sills, and has similar chemistry.

The sediment dikes consist of marine sands injected into fractures in the sill from below by boiling fluids. Glassy, vesicular tubes running vertically through the sill appear to be gas escape structures formed by steam rising as the wet sediments beneath the sill were boiled (Fig. 86). The sediment dikes, formed by boiling connate fluids injecting loose sediment into fractures in the cooling sill, contain abundant evidence of sediment fluidisation and recrystallisation such as alignment of mica crystals with the direction of fluid flow and loss of original sediment porosity (Fig. 87-88).

Fig. 85. The Tokarahi Sill exposed in a road cut, showing columnar basalt (A) and baked sediments (B).

Fig. 86. Vertical gas escape structure in Tokarahi Sill columnar basalt. Scale bar in cm.

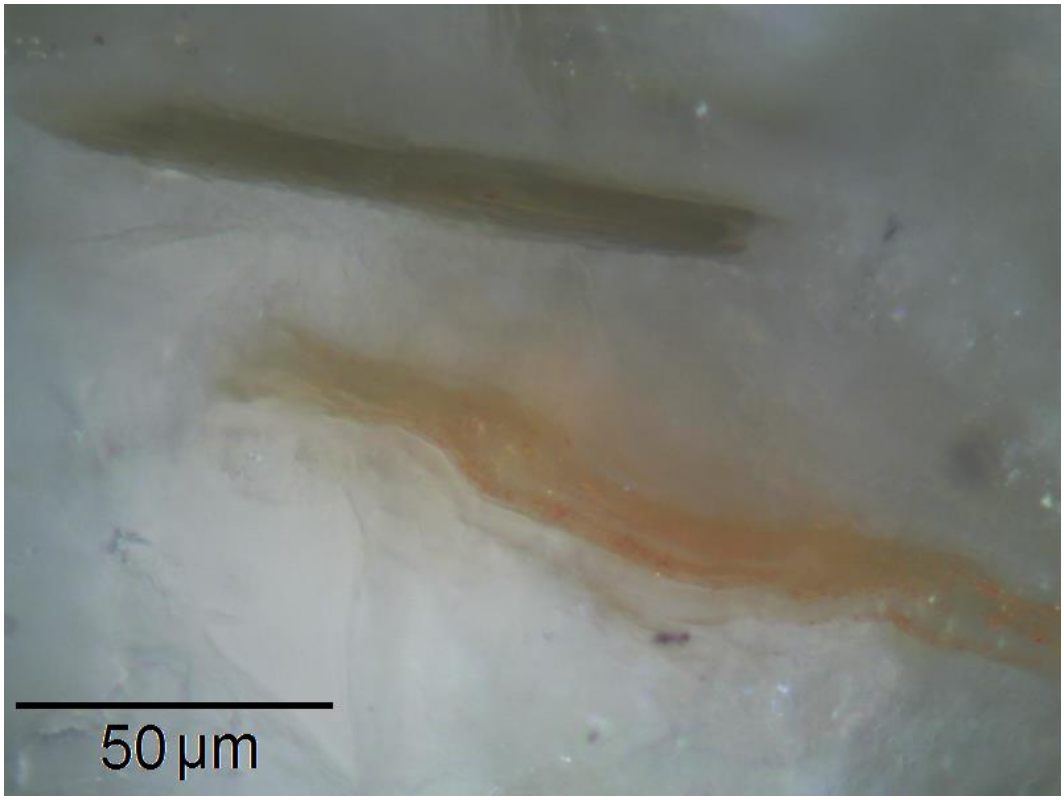

Fig. 87. Fluidised sediment from within the Tokarahi Sill, showing mica crystals aligned with the direction of flow. Image in reflected light.

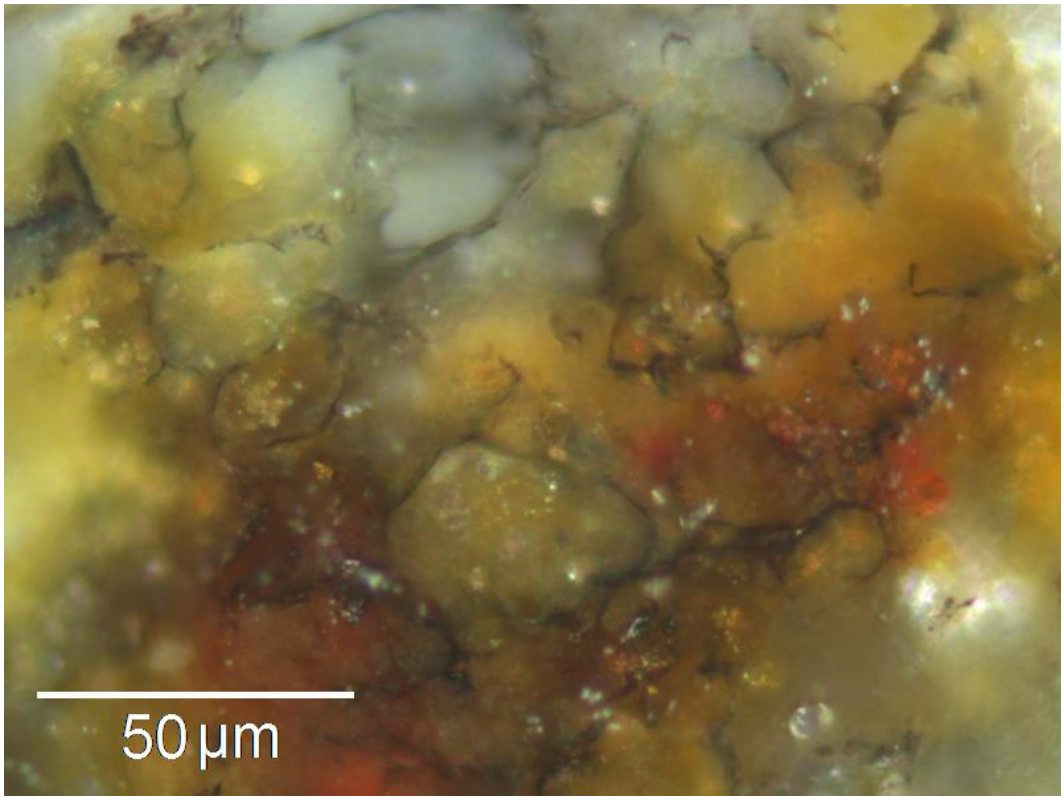

Fig. 88. Recrystallised sediment with iron oxide and reduced porosity from a sediment dike in the Tokarahi Sill. Image in reflected light.

4.4 Lyttelton Harbour

Sampling in Lyttelton Harbour was focused on the sedimentary rocks that pre-date the Miocene volcanism that formed the shield volcanoes of Lyttelton and Akaroa. In the interior of Lyttelton Harbour, erosion has removed the overlying volcanic rocks and exposed the sediments beneath the volcano.

Three sites were sampled: a road cut in Charteris Bay, the Orton Bradley Park quarry and a shoreline site at the Head Of The Bay (Fig. 89).

Fig. 89. Location of Lyttelton Harbour sampling sites.

4.4.1 Charteris Bay road cut

A well known road cut along the Teddington to Purau road in Charteris Bay, illustrated by Sewell et al. (1988), reveals the unconformable contacts between the top of the Marine Drive Formation (Eocene) and the bottom of the Bradley Sandstone (Miocene) (Fig. 90). Both rock units were intruded by the Allandale Rhyolite during the Miocene, and dikes are well exposed in the road cut. The intrusion of the Allandale Rhyolite represents the beginning of the extensive Miocene volcanism at Banks Peninsula. The road cut reveals a section of this early phase of volcanism, allowing sampling of both the rhyolite and the surrounding sediments which have been altered during intrusion producing secondary minerals including goethite and euhedral quartz (Fig. 91). A potential limitation of this site is the highly weathered state of the rocks.

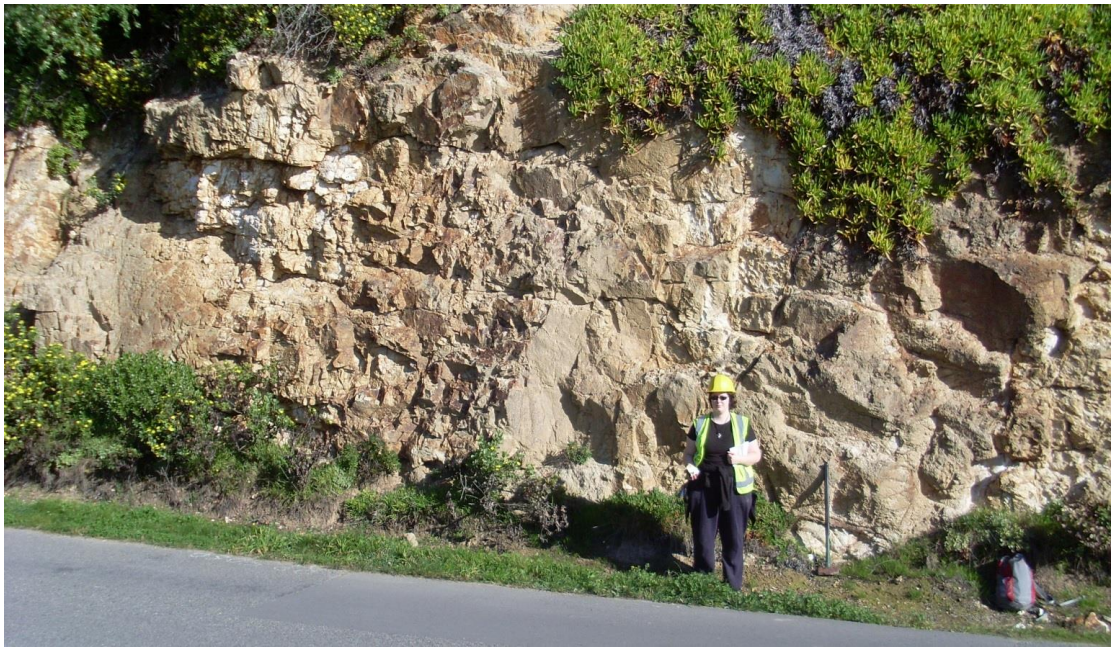

Fig. 90. Bradley Sandstone in the Charteris Bay road cut.

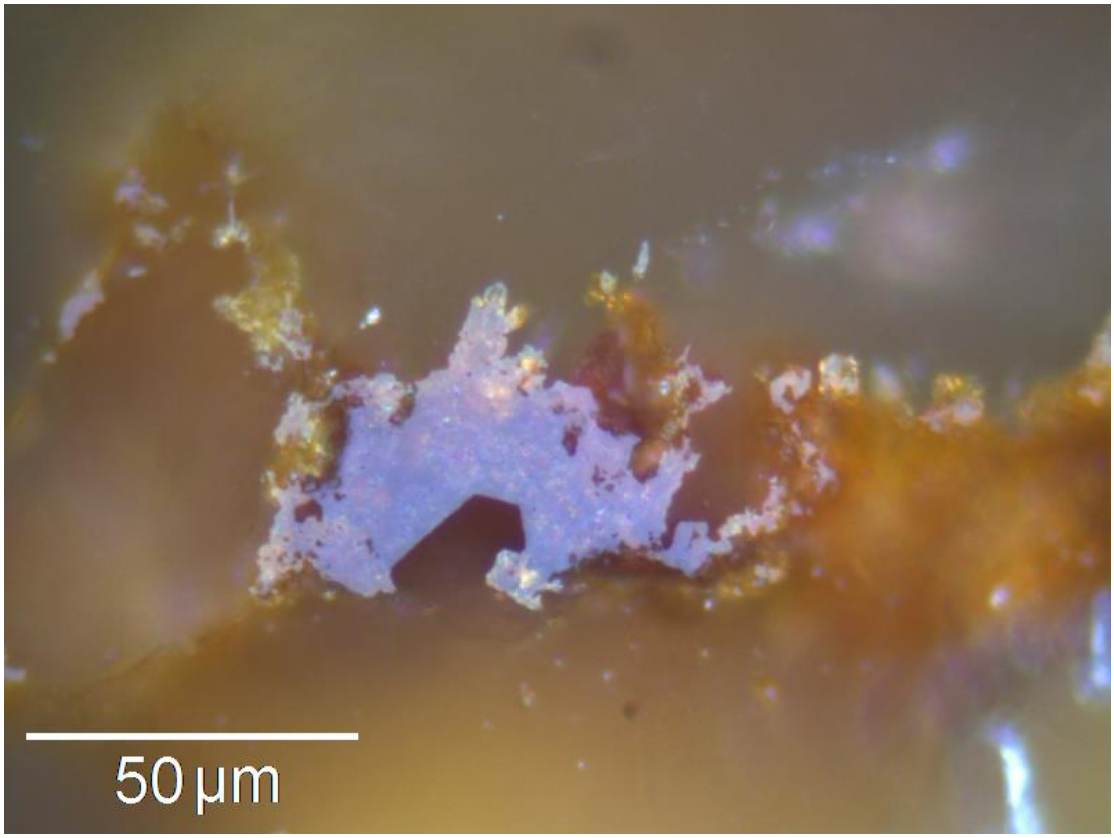

Fig. 91. Goethite and euhedral quartz in Marine Drive Formation from the Charteris Bay road cut outcrop, indicating alteration of the sediments during intrusion. Image in reflected light.

4.4.2 Orton Bradley Park

Orton Bradley Park, also in Charteris Bay, contains a quarry site that allows access to relatively fresh Bradley Sandstone. The sandstone at this site has not been intruded, and so provides a useful comparison to sandstone from the road cut site.

4.4.3 Head Of The Bay

This site is marked on the geological map of Lyttelton as Torlesse greywacke intruded by dikes (Sewell et al. 1988). However, investigation of the outcrop did not reveal any greywacke. The country rock is a quartzose sandstone, moderately well indurated with medium to very fine sand-sized grains. Based on these features, the rock is identified as Charteris Bay Sandstone (Fig. 92). This sandstone is cut by a number of dikes with altered sediments adjacent to the dike margins (Fig. 93, 94, 97, 98). Based on their location, these dikes are most likely to be part of the Miocene-age Allandale Rhyolite.

This location reveals how difficult it can be to distinguish sedimentary and igneous rocks in outcrop or hand specimen when their textures have been altered by contact metamorphism, hydrothermal fluid flow and weathering. The rocks comprising dikes 2 and 3 are visually indistinguishable from siltstone in hand specimen and these structures could be mistaken for sediment dikes or even bedding (Fig. 95, 99). It is necessary to examine the rocks under a microscope to confirm that they are fine-grained igneous rocks (Fig. 96). Similarly, some of the sedimentary rock adjacent to dike 3 is dark in colour and very well indurated, resembling a mafic or intermediate volcanic rock (Fig. 100). Microscopic examination reveals small fragments of organic matter, indicating that it is a sedimentary rock (Fig. 101). The unusual appearance may have been produced by contact metamorphism from the adjacent dike in addition to fluidisation and recrystallisation due to hydrothermal fluid flow.

The paler sandstone adjacent to dike 3 also appears to be Charteris Bay Sandstone, but has an unusual pale green colour not seen in other examples of this rock (Fig. 102). A polished section under reflected light reveals that it contains grains with a similar colour to malachite (Fig. 103). Hydrothermal fluid flow during intrusion of the sediment may have precipitated copper minerals, producing the green colour.

Fig. 92. Hand sample of Charteris Bay Sandstone from the Head of the Bay.

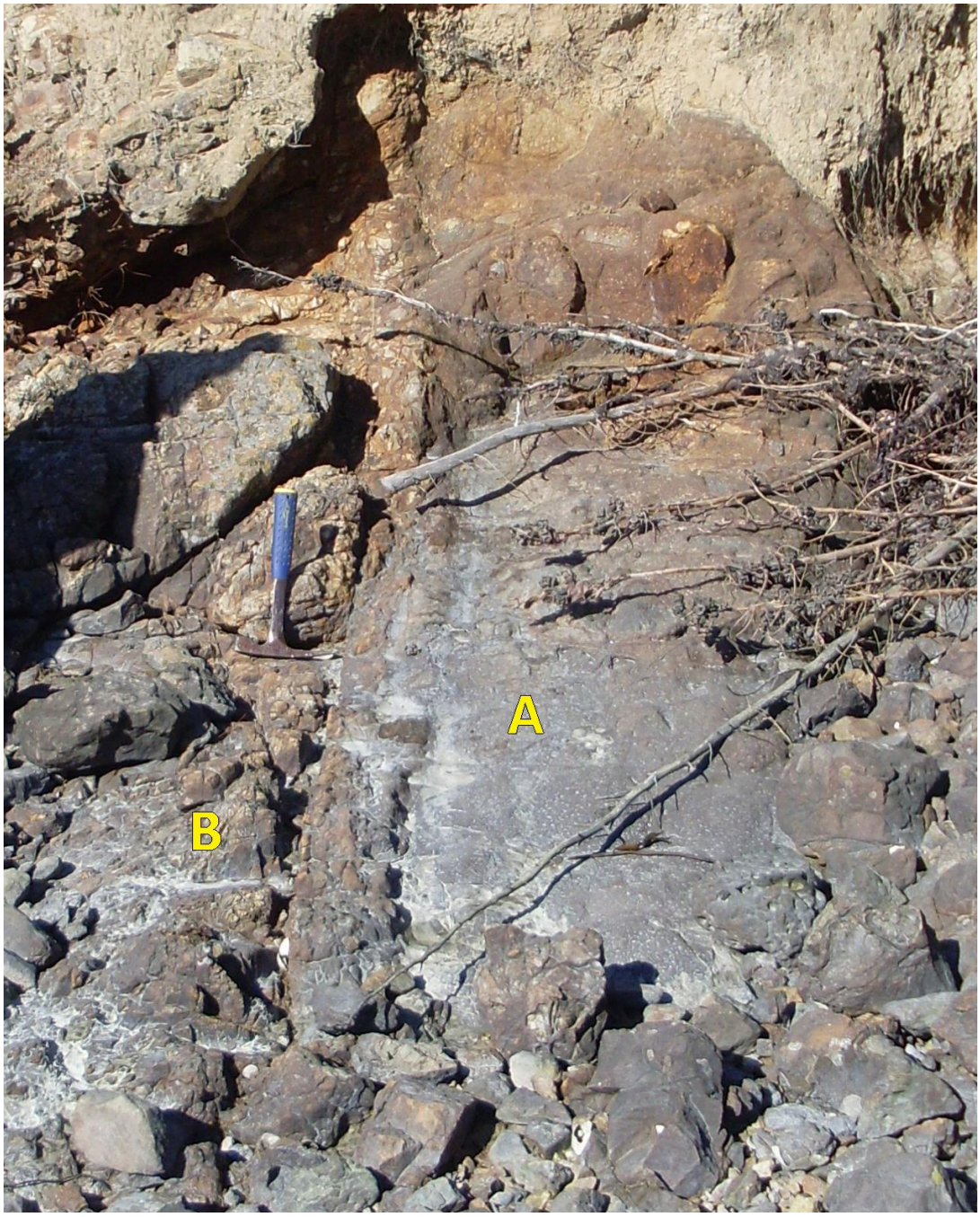

Fig. 93. Dike 1: Fine-grained, medium-grey igneous dike (A) cutting through Charteris Bay Sandstone (B). Rock hammer for scale.

Fig. 94. Dike 2: One of two parallel dikes 2 metres apart, consisting of fine-grained, highly fractured rock.

Fig. 95. Hand sample of dike 2.

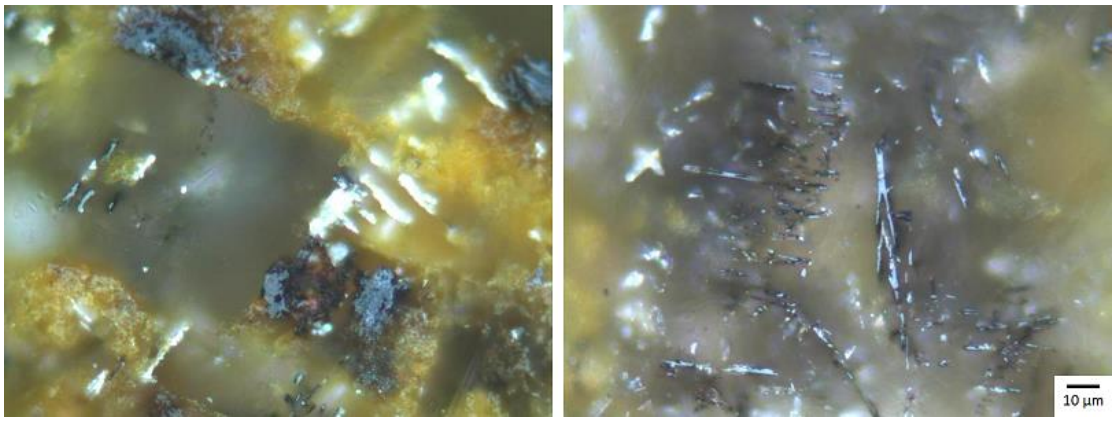

Fig. 96. Polished section of rock sample from dike 2. The rock is a highly weathered, fine-grained igneous rock with abundant secondary iron oxides (orange, left). Plane polarised, reflected light in oil immersion.

Fig. 97. Hand sample of sandstone adjacent to dike 2.

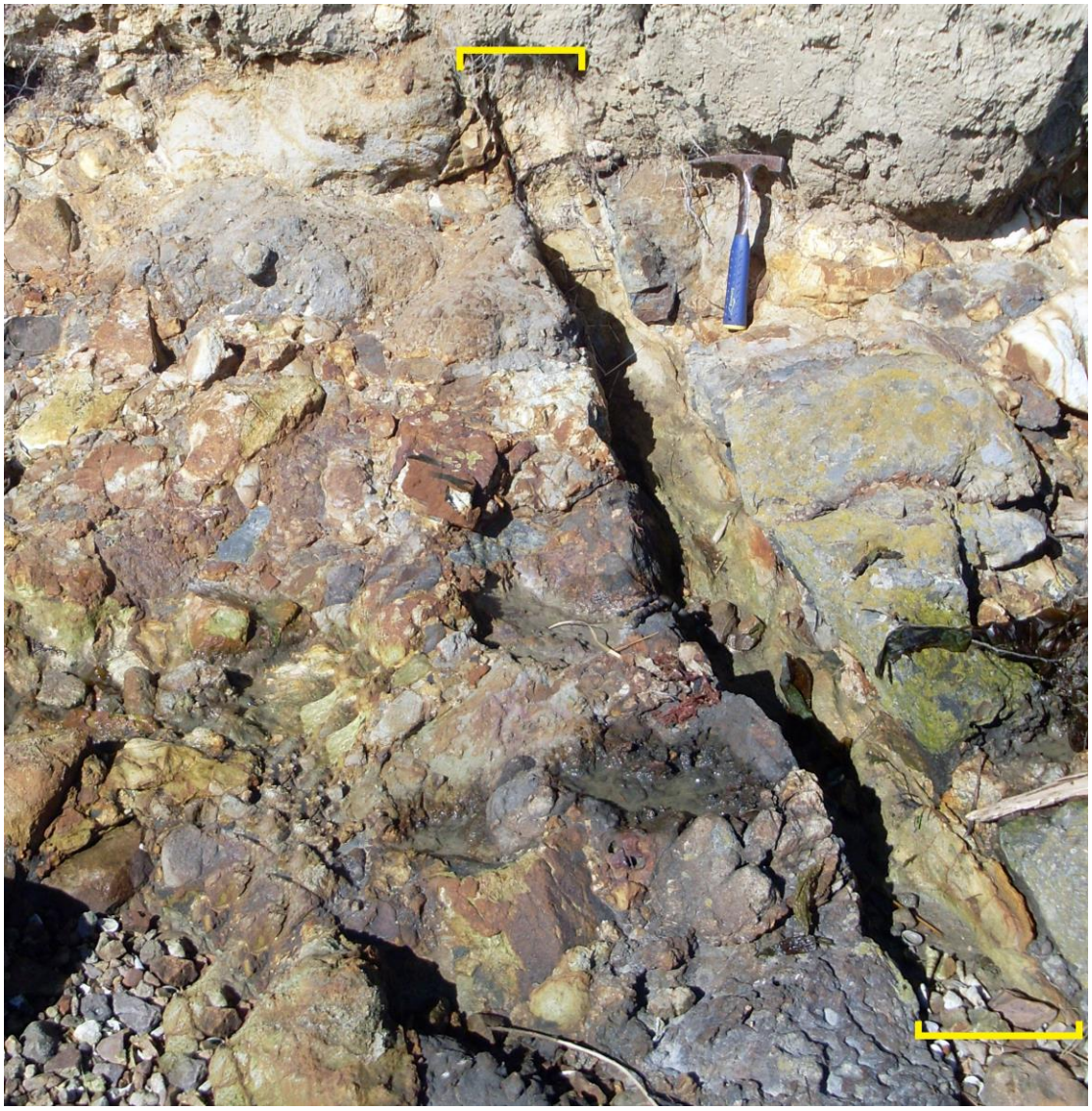

Fig. 98. Dike 3: A very highly weathered narrow dike (between yellow brackets) intruded into a mix of dark grey and pale green sandstones.

Fig. 99. Hand sample from dike 3.

Fig. 100. Hand sample of dark grey, well-indurated sandstone adjacent to dike 3.

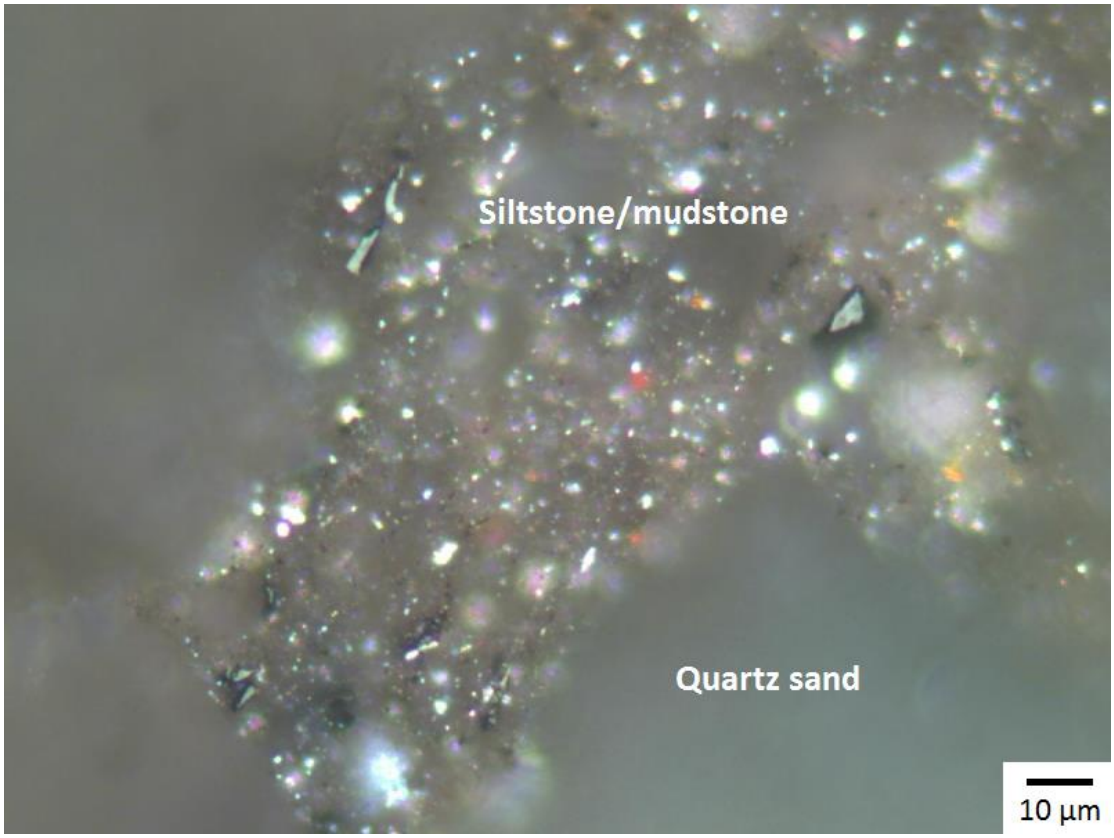

Fig. 101. Polished section of the dark grey sandstone adjacent to dike 3. A mixture of medium to coarse quartz sand grains and fine silt-mud with sparse organic matter. Plane polarised, reflected light in oil immersion.

Fig. 102. Hand sample of pale green quartzose sandstone adjacent to dike 3.

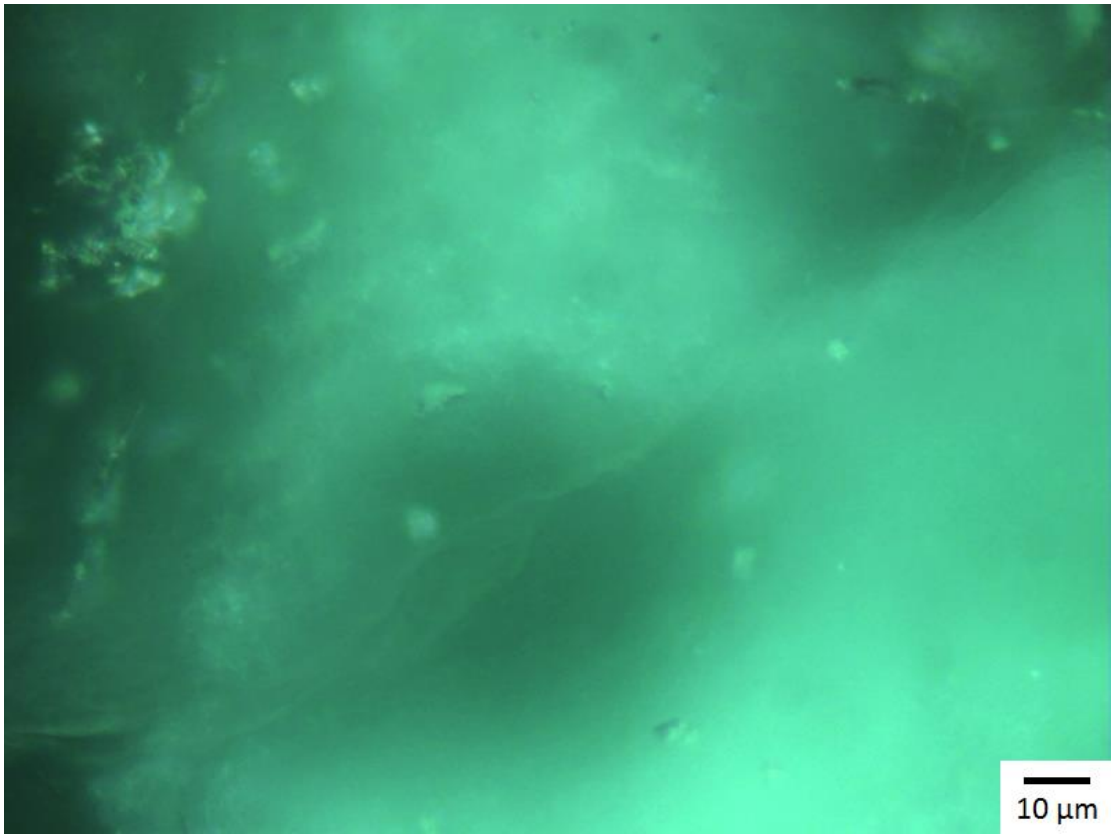

Fig. 103. Polished section of a strongly green coloured clast in the pale green sandstone. The colour may be due to the deposition of copper minerals by infiltrating hydrothermal fluids. Plane polarised, reflected light in oil immersion.

5.0 Discussion and interpretations

Prior to this investigation the evidence for hydrothermal or igneous mineralisation in Clipper-1 was limited to informal and unpublished observations of sulfide and iron oxide minerals seen during analysis of the organic content in order to determine the thermal history of the Canterbury Basin. The initial phase of formal mineral identification undertaken during the present study revealed the unexpected presence of native metals, which had previously been mis-identified as sulfide minerals. The scientific literature on native metals produced from a naturally-occurring melt is largely restricted to large mafic intrusions and areas of active seafloor spreading, and very little precedent exists for native metals forming in passive margin basins such as the Canterbury Basin. Documented occurrences of native aluminium in any type of geological setting are rare. An understanding of how these minerals could occur in Clipper-1 has required a literature search well beyond the initial expected bounds of the research. It has also been necessary to investigate Microfacies VS, an enigmatic lithology that has never been formally described or interpreted.

5.1 Native metals in the literature

5.1.1 Native aluminium

Native aluminium was not accepted as a naturally-occurring mineral by the International Mineralogical Association until 1983, and there is ongoing controversy over the validity of reports of naturally-occurring native aluminium (Clark 1993). It is an amphoteric element, able to act as either an acid or a base in chemical reactions. Due to its highly reactive nature, some researchers consider it doubtful that it could form and persist in Earth's oxygen-rich environment and consider that contamination of samples by man-made aluminium is a much more likely explanation for its presence (Dekov et al. 2009). Unless native aluminium is found intergrown with non-anthropogenic minerals such as alumosilicates, the possibility of contamination must be seriously considered. Despite the unusual conditions required for its formation, native aluminium has been reported from a wide variety of settings, including

oceanic metalliferous sediments (Butuzova et al. 1987; Iyer et al. 2007), igneous rocks (Kovalski & Oleynikov 1985; Bai et al. 2004; Dekov et al. 2009), skarns (Novgorodova et al. 1981) and mud volcanoes (Novgorodova & Mamedov 1996). Although numerous processes have been suggested for the formation of native aluminium, all share the common themes of low oxygen fugacity and a highly reducing environment. This section will cover the settings and mechanisms that have been proposed for the formation of native aluminium.

Crystallisation from melt

Native aluminium particles have been found in metalliferous sediments on the East Pacific Rise (Dekov et al. 1995). These sediments contain a high concentration of hydrothermally-generated metals and metal compounds along with clays, biogenic calcium carbonate and basalt clasts from nearby volcanism. The aluminium particles are comprised of thin, angular lamellae up to 900 µm in length on the longest axis. These usually occur as isolated particles, but in some cases the aluminium lamellae have been observed attached to or embedded within alumosilicate clasts. The largest particles and densest concentrations are found closest to the spreading axis, indicating that it is their point of origin. Particle size and density are also positively correlated with intensity of hydrothermal activity. The proposed method of native aluminium formation is crystallisation from basic or ultrabasic melts produced prior to the development of a magma chamber in areas of seafloor spreading (Dekov et al. 1995). The required conditions for native aluminium crystallisation in this setting are high pressure, high temperature and very low oxygen fugacity, which can result from high concentrations of H_2 and CH_4 in the melt. Following crystallisation, particles are transported upwards by hydrothermal fluid flow and vented onto the sea floor. Post-depositional oxidation of the aluminium is prevented by a surface coating of other minerals, including oxides, oxyhydroxides, silicates and chlorides.

Sediment cores taken from the base of seamounts in the Central Indian Basin have been found to contain native aluminium particles of similar shape and composition to those found on the East Pacific Rise (Iyer et al. 2007). Although the sampling area was not located directly on a spreading ridge, the area is prone to volcanic activity and contains a number of seamounts similar in composition to those on the East Pacific Rise (Mukhopadhyay et al. 1995). All particles were recovered from 8-26 cm depth in hydrothermally-generated

metalliferous sediments or volcaniclastic sediments containing glass shards and palagonite. The morphology of the particles correlates with the sediment type in which they were found, with hydrothermal sediment mostly containing spheroidal particles and the volcaniclastic sediments containing irregular or botryoidal particles with cracks thought to be formed by rapid chilling of molten material on contact with seawater. Unlike the examples from the East Pacific Rise, no intergrowth of native aluminium with alumosilicates has been observed.

Native aluminium has also been observed in crystalline rocks. A single flake 2 mm in length was found embedded in a pegmatite vein intruding biotite gneiss and serpentinized ultrabasic rocks in Bulgaria's Rila Mountain area (Dekov et al. 2009). The flake is coated with a thin layer containing carbon and oxygen, suggesting carbon may have been involved in its formation. Interaction between the low-silica ultrabasic rocks and the high-silica pegmatite is proposed as the key to formation of native aluminium. At the contact between the two rock types, silica is removed from the pegmatite by the ultrabasic rocks leaving behind an overabundance of aluminium that crystallises in metallic form. Serpentinization of the ultrabasic rocks may have been an important part of the process, as it results in the production of compounds such as hydrogen and methane that create reducing conditions where native metals are stable. Reducing compounds may also be produced via the Fischer-Tropsch process as mafic and ultramafic minerals react with water (Berndt et al. 1996).

Biogenic aluminium

Native aluminium has been found in settings with no known volcanic activity, such as surface and near-surface sediments in the South China Sea (Chen et al. 2010). The particles recovered here are similar in size and composition to those from the East Pacific Rise. In shape the particles also resemble examples found elsewhere, including lamellar plates similar to particles from the East Pacific Rise (Dekov et al. 1995) and cracked botryoidal globules almost identical to those reported by Iyer. et al (2007) in samples from the Central Indian Basin. Rather than a volcanogenic origin as is proposed for most occurrences of native aluminium, these particles are thought to be formed in situ by a microbe-facilitated reduction process above cold seeps. Cold seeps can emit high levels of reducing agents including H_2S, CH_4 and H_2, making the formation of a highly reducing microenvironment

possible. Reducing conditions are further encouraged by anaerobic oxidation of methane performed by microbes commonly found at cold seeps. Dissolution of aluminium hydroxides in pore water provides the source of Al^{3+}.

5.1.2 Terrestrial native iron

Most native iron on Earth is of meteoric origin, but it can also be produced by terrestrial processes. Similarly to native aluminium, formation of native iron in igneous rocks requires a strongly reducing environment with low oxygen fugacity. This section will cover two of the most well-known occurrences of terrestrial native iron, both of which are linked to the interaction between sediments and magma.

Disko Island

One of the most well-known occurrences of native iron-bearing rocks is Disko Island in western Greenland. Naturally-occurring boulders of cast iron up to 25 tons in weight have been reported since the 19th century (Nordenskiöld 1872). The host rock of this iron is a series of basaltic and andesitic lava flows fed by branching dikes. Prior to extrusion, the magma was contaminated by sediments during intrusion through Cretaceous-Tertiary fluvial sandstone, carbonaceous shale and coal approximately 3 kilometres below the surface (Ulff-Møller 1990). Sedimentary contamination of the magma is indicated by the presence of xenoliths of baked sedimentary rock up to 20cm long. Some xenoliths retain visible sedimentary bedding and have undergone intense but brief heating, while others have been partially melted (Pedersen 1979).

The resulting dikes and lava flows contain native iron in addition to pearlite, steadite (ferrite and iron phosphide) and rosette-shaped graphite (Ulff-Møller 1990). These are all features found in grey cast iron. The iron most commonly occurs as spherical grains 1-5mm in diameter, with occasional larger ellipsoids up to 10mm long and branching structures 20-30mm across. There is a positive correlation between the concentration of sedimentary xenoliths and native iron. Both are most abundant in the centre of the dikes. Some lava flows that lack native iron in the main body of the flow contain shale xenoliths with native iron that has formed from melt intruded into cracks. Unlike the iron grains found in the lava,

the iron that formed within xenoliths does not have a pearlitic texture. Pedersen (1979) interprets this as the result of slower cooling within the xenoliths.
The native iron is 84-98% pure and contains minor amounts of nickel, cobalt, copper and phosphorus (Ulff-Møller 1990). Individual grains are more pure in the centre and have increasing concentrations of cobalt, nickel and copper towards the outer edge. There is a positive correlation between the intensity of magma contamination and the concentration of cobalt and nickel in the iron, and a negative correlation with the concentration of phosphorus. The native iron grains are commonly associated with troilite, an iron sulfide mineral that occurs rarely in terrestrial rocks but is common in meteorites.

Ulff-Møller (1990) proposes that the native iron was produced by a low-oxygen, highly reducing environment resulting from contamination of the magma with carbonaceous shale rich in aluminium oxide. This is further supported by the examples of native iron-containing xenoliths in iron-free lava flows, indicating that the contact between sedimentary material and magma is an important step in the formation of native iron (Pedersen 1979). Isotope ratios of He, Ne, Ar and H_2 contained within the iron also point to its formation in the crust rather than the mantle (Poreda et al. 1990). When heated above 400°C, carbonaceous sediments release methane, carbon monoxide and hydrogen gases. Hydrogen is suggested as the main reductant by Pederson (1979) and Ulff-Møller (1990). Contamination of the magma is estimated to have taken place at depths greater than 3km.

Siberian Traps

The interaction between magmatic intrusions and carbon-rich sediment is a common feature of native iron-bearing regions. Another example can be found in the Siberian Traps flood basalt. The Siberian Traps is a large igneous province produced by voluminous eruptions of basalt at the end of the Permian (Renne & Basu 1991). Native iron is known from the Khungtukun, Khininda and Maimecha intrusions and the Dzhaltul complex, all of which are in the northern area of the Traps (Ryabov et al. 1985; Oleinikov et al. 1985). The country rocks through which the magma intruded consist of Carboniferous coal-bearing sediments and limestones. The igneous rocks in this area show evidence of contamination by carbon-rich sediments, including the presence of bitumen and graphite (Ryabov et al. 2006).

The host rock for the native iron is primarily doleritic dikes (Ryabov et al. 1985). The dikes have a brecciated texture, containing fragments of both igneous and sedimentary rocks. The metal occurs as small droplets 1-2mm in diameter and larger, irregular-shaped "blebs" that may be several cm in length. These can be disseminated throughout the dike or coalesced together to form lens-shaped deposits. The Dzhaltul complex and Khungtukun intrusion contain larger nodules of native iron that can weigh several kilograms (Ryabov & Lapkovsky 2010). The iron nodules are frequently associated with sulfide minerals. Within the nodules, iron occurs as α-ferrite (pure iron) associated with cohenite, troilite and wüstite. Anthraxolite, a type of bitumen, is also present (Okrugin et al. 1991).

The elemental composition of the native iron varies significantly between individual nodules (Ryabov & Lapkovsky 2010). Other metals found in the iron include platinum, palladium, rhodium, ruthenium, nickel, cobalt and copper. In general there is a 4:1 ratio between nickel and cobalt. The Siberian Traps native iron has a lower melting point than would be expected for its composition. Ryabov & Lapkovsky (2010) suggest the presence of micro-inclusions could act as a flux. Carbon, used as a flux in the industrial process of smelting iron ore to produce metallic iron, is suggested as the main fluxing agent by Kamenetsky et al. (2013) and would have been abundant in the magma due to contamination by coals and carbonaceous sediments.

Prior to the intrusion of basalt, the country rocks in the Siberian Traps region were subjected to fracturing and faulting Ryabov & Lapkovsky (2010). Zones of low pressure were produced along faults, leading to the movement of reservoir fluids (including hydrocarbons) and the formation of fluidised sediment. These faults also acted as conduits for magma once igneous activity began, resulting in the mixing of magma with the accumulated fluids and brecciated sedimentary rocks. Ryabov & Lapkovsky (2010) propose that hydrocarbons were the primary source of reducing compounds that produced the conditions required for the formation of native iron. These hydrocarbons were mainly produced from coals, but carbonate rocks heated by the intrusion may also have contributed hydrocarbons formed by catalytic reactions such as the Fischer–Tropsch process: a series of reactions in which CO and H_2 are converted into hydrocarbons (Szatmari 1989).

5.1.3 Copper and copper alloys

In comparison to aluminium and iron, native copper is relatively common and occurs in a variety of environments (Cornwall 1956). It is particularly common in basalts and is also found in intrusive volcanic rocks, oxidised copper sulfide deposits, sedimentary rocks and swamps. Native copper can be produced in both oxidising and reducing conditions, making it one of the most common native metals in nature.

Producing native copper directly from a basaltic melt requires high temperatures, reducing conditions and low concentrations of sulfur (Cornwall 1956; Zhang et al. 2006). Inclusions of native copper have been found inside serpentinized olivine phenocrysts in the Emishan Large Igneous Province (ELIP), a flood basalt in southwest China produced by continental rifting during the Late Permian (Zhang et al. 2006). These are interpreted to be derived from mantle material brought to the surface by a mantle plume. The copper is 98% pure with minor amounts of silicon and aluminium, which are not found in artificially manufactured copper. Other minerals present include native gold, native zinc and silicon carbide. Native copper is also present in native iron nodules and gabbro-dolerite in the Siberian Traps flood basalt (Ryabov & Lapkovsky 2010).

In addition to crystallising directly from the magma, native copper contained within basalts may have been precipitated by hydrothermal activity after the rock solidified. This is the suggested mechanism of formation for the native copper found in the Portage Lake Volcanics, a Precambrian tholeiitic flood basalt in Michigan, USA (Bornhorst & Paces 1988). Native copper occurs here in such high abundance that it is considered the primary ore mineral. It is concentrated in permeable areas of the flood basalt including fractures, volcanic conglomerates and the rubbly tops of individual lava flows. Where copper is abundant, there is also other evidence of hydrothermal alteration such as calcite, epidote and chlorite.

Native copper may be produced by weathering in the margins of ore deposits containing cuprite or chalcocite (Cornwall 1956). Pyrite, an extremely common mineral in copper ore

deposits, reacts with groundwater to produce sulfuric acid and iron sulfate, which may react with the copper minerals to produce native copper.

Precipitation of native copper has been observed to occur in swamps. Dissolved copper sulfates, derived from weathered ore deposits, enter the swamp via groundwater and react with organic matter to produce metallic copper (Cornwall 1956). The products of bacterial metabolism may also be involved in the reaction. This process is similar to the production of "bog iron", an iron hydroxide ore produced in swamps (Crerar et al. 1979).

5.2 Native metals in Clipper-1

5.2.1 Iron

The formation of native iron elsewhere in the world, such as in the Siberian Traps, have been compared to the processes that occur inside an industrial blast furnace (Ryabov & Lapkovsky 2010). The basic requirements for a blast furnace are a source of iron, a source of carbon and a flux to remove impurities such as silica. All of these components may be readily available in a mafic magma intruding sedimentary rocks. Carbonaceous sediments or coal act as the carbon source and produce a variety of reducing gases when heated, including H_2 and CO (Ryabov & Lapkovsky 2010). Mafic magma is a rich source of iron (Winter 2010). Calcium oxide is a common flux used in iron manufacturing, and is produced by burning limestone. If all the required components are present, the same chemical processes that are used to produce iron in an industrial furnace may occur naturally in the intrusion.

The most likely sources of carbon in this area of the Canterbury Basin are the coal measures and carbonaceous mudstones of the Clipper Formation, which lie directly above the basement contact. The high concentrations of native iron in the Katiki Formation suggests that the carbonaceous mudstones in this formation may also have contributed carbon to the melt (Fig. 38). The presence of pearlite and graphite in association with native iron is also an indicator that the melt that they crystallised from has assimilated carbon-rich sediments as it intruded through the sediments of the Clipper sub-basin. Examples of

naturally-occurring pearlite in other parts of the world have been suggested to have formed from mafic magmas that have assimilated sedimentary carbon (Ulff-Møller 1990; Ryabov & Lapkovsky 2010).

Where the native iron in Clipper-1 is particularly carbon-rich, it closely resembles an artificial iron alloy called grey cast iron (Fig. 104). Cast iron is produced from molten iron containing a minimum of 2% carbon (Davis 1996). The textures found in grey cast iron indicate that the melt had a high graphitization potential (Davis 1996). This is a measure of how readily the carbon separates from the iron during cooling to form graphite. The graphitization potential is primarily determined by the carbon content of the melt, but can also be increased by the presence of other impurities including Sn, Ph, Si, Al, Cu and Ni. The Clipper-1 iron contains substantial amounts of silicon, which increases the number of graphite particles and the ratio of ferrite (solid iron) to pearlite. This silicon content explains why the Clipper-1 iron often forms ferrite even when the carbon content is very high.

The similarity of the textures of the Clipper-1 iron to those found in cast iron show that it must have solidified from a melt rather than being precipitated by hydrothermal fluids (Chapter 3.2.3). This also further supports the possibility that the chemical processes that formed the iron are similar to those used in industrial iron smelting.

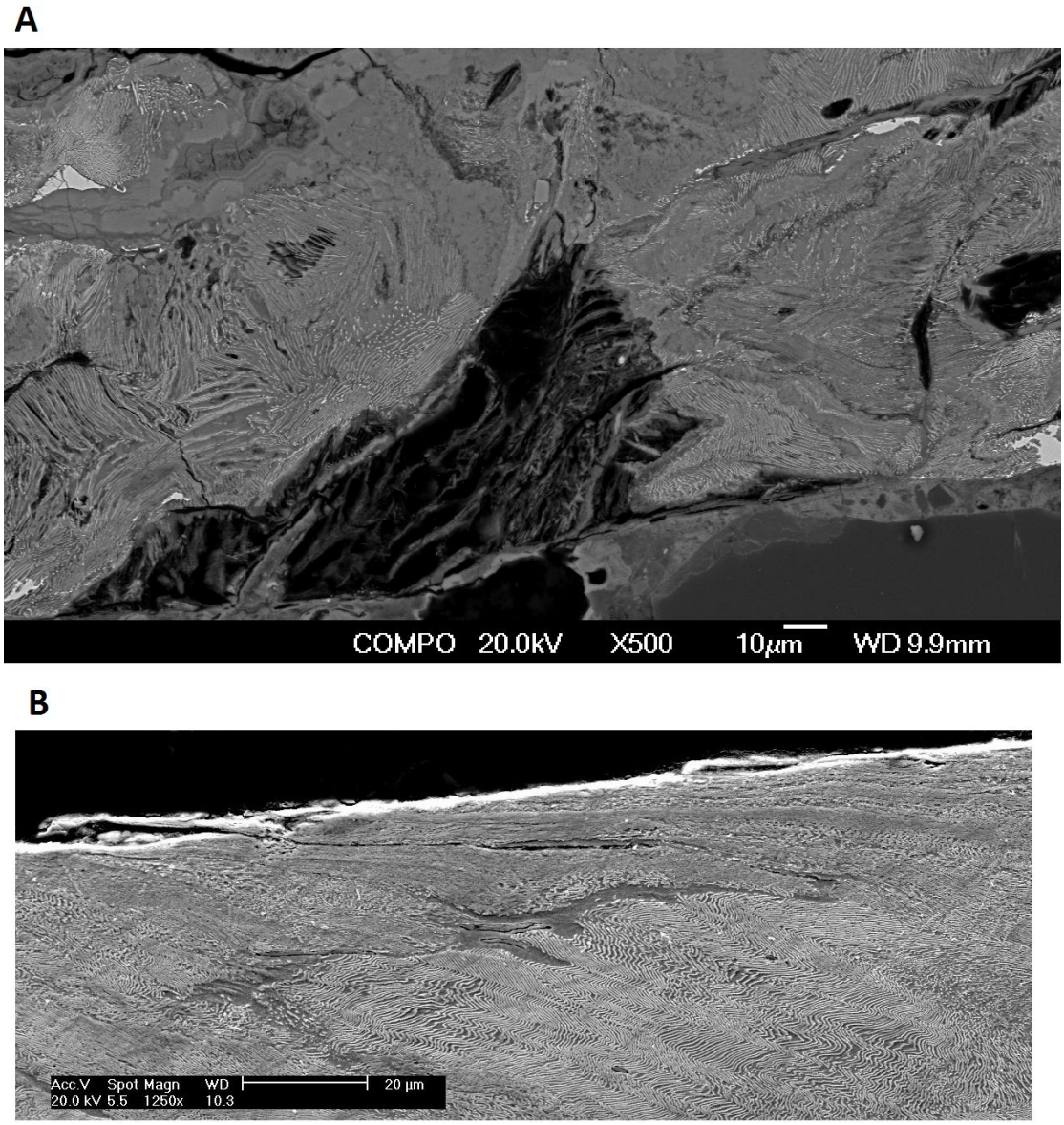

Fig. 104. SEM image of pearlite from Clipper-1 (A) compared to pearlite from industrially-produced rail steel (B). Rail steel image by John Garnham, University of Cambridge.

When iron is produced in a blast furnace using calcium oxide as a flux, silica is removed from the iron as molten slag, primarily consisting of calcium silicate ($CaSiO_3$) (Budinski & Budinski 1999). This material has not been identified in Clipper-1. One possibility is that it has separated from the iron and been incorporated into fluidised sediment, which in comparison to undisturbed sediment has reduced porosity resulting from the precipitation of secondary minerals. Alternatively, the concentrations of silica in the melt may have been very low, in which case little or no slag would have been produced. Low concentrations of

silica is a feature of most of the igneous mineral assemblages found in Clipper-1, suggesting that the source melt may have been silica-deficient.

A distinctive feature of the Clipper-1 native iron is that it is finely disseminated in sediment, rather than being contained within basalt as is the case with most examples of igneous native iron (Ulff-Møller 1990; Ryabov & Lapkovsky 2010). Examples of native iron in sedimentary xenoliths have been found in the iron-bearing lava flows of Disko Island, Greenland, but unlike the Clipper-1 iron these are also closely associated with basalt (Pedersen 1979). Another difference is that the Clipper-1 iron is not associated with iron sulfides, unlike the iron in Greenland (Ulff-Møller 1990).

5.2.2 Aluminium

The native aluminium in Clipper-1 is the first recorded occurrence of the metal being produced in-situ by igneous intrusion in marine sediments. It indicates an extremely unusual intrusive environment with low oxygen fugacity and an abundance of reducing compounds. The distribution of native aluminium in Clipper-1 may yield clues about how this environment was produced. In particular, the abundance of aluminium above the limestone beds suggests that the interaction between the melt and sedimentary carbonates was essential in its formation (Chapter 3.5, Fig. 38). The carbonates may have produced reducing compounds, as has been proposed for the formation of native iron in the Siberian Traps flood basalt (Ryabov & Lapkovsky 2010). The gases produced when carbonates are heated by igneous intrusion may also have helped produce a low-oxygen environment by driving off any gaseous oxygen present. Although the interaction of magma with carbonates has not been previously suggested as a mechanism for the formation of native aluminium as it has for native iron, the restriction of native aluminium in Clipper-1 to depths above the limestone beds strongly implies that carbonates are in some way required for the melt to begin crystallising native aluminium.

The variation in structure of the Clipper-1 native aluminium and the fragmentation of accessory minerals indicate that the material was deformed during or after cooling. The most intact accessory minerals are found in large, blob-shaped pieces of aluminium,

indicating that this is the form the aluminium takes when cooled with little or no deformation (Fig. 27, chapter 3.3). The highest degree of fragmentation in accessory minerals is found in association with thin, streaky lamellae of aluminium separated by glass (Fig. 29, chapter 3.3). The "streaky" shape of the aluminium lamellae indicates that this most likely occurred while the aluminium was still hot and highly ductile. This may represent flow of the material while the glassy component was still partially or entirely molten. Tectonic deformation is unlikely, as other materials such as native iron found at the same depth have not experienced similar deformation.

The inclusions found in association with the native aluminium are a wide range of metals and metal silicates with varying concentrations of aluminium. Their composition is extremely variable. The aluminium content ranges between 17% and 60% by mass. The other elements present are Si, Fe, Cu, Ni, Mn, Mg, and As, none of which occur in every example. The inclusions are most commonly present as small broken fragments distributed in the aluminium. Intact examples exhibit a wide variety of shapes, including euhedral hexagonal crystals, branching laths and irregular shaped blobs. The euhedral shapes and the fragmented nature of the inclusions indicates that they crystallised before the aluminium, allowing them to be broken up by the flow of the surrounding molten material. The inclusions most likely represent the components of the melt with a higher melting point than aluminium separating out and crystallising as the melt cooled.

The transparent or translucent material found between aluminium lamellae or intermingled with aluminium blobs is primarily composed of aluminium oxide with minor amounts of Na, Si, Cl, and Ca. The concentration of sodium may be as high as 12% by mass. Despite the very low concentrations of silica, it has the correct optical and physical properties to be defined as a glass. Naturally occurring aluminium oxides can be transparent in the form of corundum, but in thin section the material in Clipper-1 is isotropic and lacks the correct refractive index and crystal structure. The presence of shrinkage cracks and devitrification are also indicative of a glass. Although the term "glass" is almost always applied to silicate materials, it can be applied to any inorganic material in which the atoms are arranged randomly rather than in a crystal structure (Marshak 2001).

Where and how such an aluminium-rich melt originated remains uncertain. It may be a highly altered remnant of a more typical igneous intrusion, derived from melting of aluminium-rich sediments, or a mixture of both. The production of native iron in Greenland is thought to have involved the assimilation of Al_20_3-rich shale by the magma (Ulff-Møller 1990). Other remaining questions include why the assemblage is so low in silica, and whether it was produced by the same phase of intrusion that produced native iron. Native iron and native aluminium are rarely found intermingling in Clipper-1, and where it does occur brecciation of the iron minerals indicates that the aluminium was intruded after the iron minerals solidified. This seems to indicate a separate phase of intrusion. However, the scarcity of silica in both mineral assemblages may indicate a common origin.

5.2.3 Copper alloy, graphite and lead compounds

The very high concentration of graphite in this mineral assemblage suggests that a high abundance of carbon is required for its formation. This is also the case with native copper produced in swamps by the reaction of copper sulfate in groundwater with organic matter. Native copper is also present in the native iron-bearing igneous rocks of the Siberian Traps (Ryabov & Lapkovsky 2010).

The distinctive shape of some of the graphite fragments indicates that they are graphitized inertinite which may have originated in the Clipper coal measures at 4205-4260m depth (Fig. 37, chapter 3.4.). The rest of the graphite may be derived from vitrinite, the most common component of the Clipper coals. Vitrinite is softer and more volatile-rich than inertinite and so is less likely to retain its original structure when subjected to heating by an igneous intrusion.

The shape of the copper alloy pieces in this assemblage is unusual. In other examples of native copper or copper alloy, the metal is usually shaped into rounded blobs or nodules, or is found filling the available pore or fracture space (Cornwall 1956; Bornhorst & Paces 1988; Zhang et al. 2006). By contrast, the copper alloy in Clipper-1 occurs as loosely packed flakes, 1-2µm wide and up to 30µm long, interspersed with graphite (Chapter 3.4). The cause of this unusual shape is not clear.

The lead component of this mineral assemblage occurs as globular shapes up to 50µm in diameter. They contain up to 60% lead by atomic percentage, indicating that they are at least partially native lead. The second most abundant element is sulfur, suggesting the presence of galena (PbS). Oxygen is present at 15% by atomic percentage, which may be in the form of lead monoxide (PbO) or lead carbonate ($PbCO_3$). The native lead component could be produced by heating a mixture of galena and lead monoxide in the absence of oxygen.

Based on the extremely high abundance of graphite and the presence of inertinite structures, this mineral assemblage is interpreted to be highly altered fragments of coal that have been infiltrated by melt or mineral-rich fluids and transported from depth by the rising magma. This may be comparable to baked shale xenoliths containing native iron found in basalt flows on Disko Island, Greenland, where the organic components of the shale are considered to be a crucial component of native metal formation (Pedersen 1979). However, questions remain as to why the Clipper-1 copper and lead assemblage contains very little iron despite being found at the same depths as high concentrations of native iron.

5.2.4 Indicators of natural origin

When native metals are found in loose material such as drill cuttings, care must be taken to ensure the samples have not been contaminated with man-made metals. This is particularly important for the metals which occur very rarely in their native state, such as iron and aluminium.

One of the simplest ways to eliminate the possibility of contamination is to determine which metals the sample has come into contact with during sampling and processing. In this case this is not an option, as the samples were gathered decades before this study and the original sampling equipment is not available. However, contamination can be ruled out as the origin of the Clipper-1 native metals by a combination of other factors including elemental composition, texture, accessory minerals and distribution.

The texture of native metals observed in polished section, either with reflected light or SEM, are determined by their composition and the conditions during cooling. The textures in man-made alloys have been thoroughly documented in the literature as they affect the physical properties of the material, determining what they are useful for. Even if highly fragmented, metals will retain internal textures that may reveal their origin.

The elemental composition of man-made alloys is also a highly distinctive feature. Man-made alloys are manufactured with strictly controlled compositions in order to produce a homogeneous material with known physical properties. The copper alloys in Clipper-1 contain aluminium, which is not found in artificial copper or copper alloys (Zhang et al 2006).

The difference in composition between grains in the same sample also indicates that they are not contaminants. Contamination by an artificial alloy would produce grains of identical composition due to the homogeneity of the material. All of the metals in Clipper-1 show variation in composition between grains or even within a single grain.

The accessory minerals found in association with the metals can help distinguish between natural and artificial materials. Native aluminium in Clipper-1 is found with associated metal alloys, silicate minerals and glass that are not found in manufactured aluminium (Chapter 3.3). The interaction between native metal assemblages and sedimentary material can also indicate its intrusive origin. Although some of the native iron in Clipper-1 has textures that are extremely similar to artificial cast iron, the sediment grains cemented into the surrounding iron oxide and hydroxide minerals indicate that it must have formed in-situ and cannot be a contaminant that has recently been mixed with the sediments.

The distribution of metals through the Clipper-1 well also points to a natural origin (Chapter 3.5). If drilling or sample processing equipment was continuously shedding fragments of metal, the material would be expected to be evenly distributed throughout the cuttings. Alternatively, metal concentration might be expected to correlate with areas of hard rock that might chip fragments off equipment. The distribution of metals in the Clipper-1 cuttings do not match either of these scenarios. The concentration of metals ranges from below detection limits in some samples to being the most abundant material in others,

indicating that the equipment was not continuously shedding material. The most concentrated samples occur in relatively soft sedimentary rock, while the much harder schist basement rock has only small amounts of metals. This allows damage to drilling equipment from hard rock to be ruled out.

5.3 Microfacies VS

Due to the presence of vesicles and the fragmented nature of the material, Microfacies VS appears at first glance to be a vitric tuff that may have been produced by the intraplate volcanism that has occurred in Canterbury since the Cretaceous. However, a more detailed investigation of its textures, composition and distribution reveals features that do not fit with this explanation.

In particular, the consistency in appearance of the assemblage over several thousand metres of sedimentary strata is not consistent with it being an ashfall deposit, as this would require the production of visually identical tuffs from separate eruptions and separate magma sources over a span of approximately 50 million years (Fig. 105). In comparison to typical tuffs, Microfacies VS has a much finer texture. It also lacks the distinctive orange banding found in palagonite. These factors all suggest that despite its vesicular nature, Microfacies VS is an intrusive material.

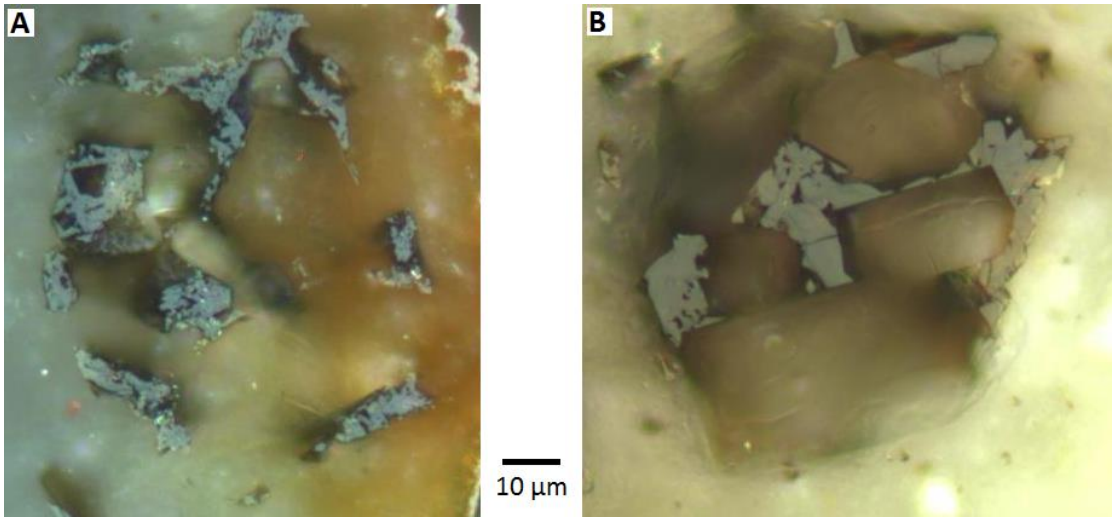

Fig. 105. Microfacies VS from Clipper-1 cuttings at (A) 3550m depth in late Cretaceous sediments and (B) 780m depth in late Pliocene sediments. Both display the same mix of phenocrysts, infilled vesicles and devitrified glass. Image in reflected light.

The highest concentration of Microfacies VS in Clipper-1 occurs in the uppermost recovered sample at 780m depth. Samples from shallower depths would normally have been collected, but mechanical problems prevented the recovery of cuttings (Shell BP Todd 1984). Although it may be purely coincidental, there is the possibility that the increased hardness of the rock caused by the high concentrations of Microfacies VS influenced the decision to begin collecting cuttings at this depth. The sudden spike in VS concentration at this depth may also indicate seafloor or near-seafloor volcanism, and so indicate that this is near the upper limit of the intrusion. Alternatively, it may represent a sill extending laterally from a larger intrusion some distance away. Biostratigraphic analysis indicates that this top sample is not contaminated by caved material (Crux et al. 1984). The sediments at this depth have been dated to the late Pliocene (Waipipian), making this the oldest possible age for any non-detrital material they contain. Microfacies VS has also been found in cuttings from 500m depth in Galleon-1, located 85km southwest of Clipper-1 (Chapter 3.7, Fig. 46). The sediments at this depth in Galleon-1 are of similar age to the 780m depth sample from Clipper-1.

A particularly unusual feature of Microfacies VS is the unusually low concentrations of silica in the glass and groundmass. An ultramafic rock would be expected to be at least 35% SiO_2 by weight, but using SEM with EDS the glass in VS was found to contain less than 5% silicon. The low silica content of the groundmass might be due to hydrothermal alteration following crystallisation altering silicate glass to clay that may be washed out by fluid flow, but this does not explain the similarly low levels of silica in the intact glass. This suggests that the material crystallised from an extremely low-silica melt.

The proportions of major elements in the glass component of Microfacies VS closely resembles that of a ferrocarbonatite (Chapter 3.7). Carbonatites are rare carbonate-based igneous rocks usually found in association with alkaline silicate rocks (Winter 2010). Long thought to be a highly altered form of limestone, they were accepted as igneous rocks following the observation of carbonatite lavas erupting from the Oldoinyo Lengai volcano in the East African rift system (Winter 2010). Similar to Microfacies VS, ferrocarbonatites are typically fine-grained and consist of calcite and iron minerals.

Although Microfacies VS has the correct proportion of major elements to be considered a carbonatite, XRF analysis of the material at 780m depth in Clipper-1 indicates that it lacks the distinctively high concentrations of trace elements including niobium, zirconium, lanthanum and cerium that are typical of this rock type (Winter 2010). If these results are representative of the material, they suggest that Microfacies VS is an igneous carbonate derived from the melting of crustal carbonate rocks rather than a true carbonatite. However, the similarity in major element composition means that the melt that produced Microfacies VS likely behaved in a similar way to a carbonatite melt.

In addition to the compositional similarities, the textures observed in Microfacies VS may be explained by some of the features of carbonate melts. High concentrations of CO_2 and water vapour are required for the melting of carbonates, and this may explain how vesicles were able to form several thousand metres below the surface (Winter 2010). The particular textures seen in Microfacies VS are significantly different to those seen in igneous carbonates or carbonatites, but this may be largely due to the difference in intrusive environment. The rapid chilling and high volatile content produced by the intrusion of carbonate melts into marine sediments with high concentrations of organic matter and water will have had a significant effect on the igneous textures of the rock. Later hydrothermal activity has also destroyed most of the original textures.

Late-stage carbonatite intrusions, in which ferrocarbonatites are a common feature, are often brecciated by hydrothermal fluids (Winter 2010). Microfacies VS shows evidence of substantial brecciation and secondary mineral precipitation, indicating the presence of hydrothermal fluids after the crystallisation of the melt. Intact vesicle fillings that have become separated from the glass indicate that the vesicles were infilled prior to the material becoming brecciated (Fig. 106). This suggests an early phase of hydrothermal activity that precipitated minerals in pore spaces without breaking apart the glass framework surrounding the vesicles. Microfacies VS is very finely brecciated and in some cases fluidised, with larger vesicles in the groundmass that are not contained within glass. These textural features may have been produced by a later phase of more intense hydrothermal activity.

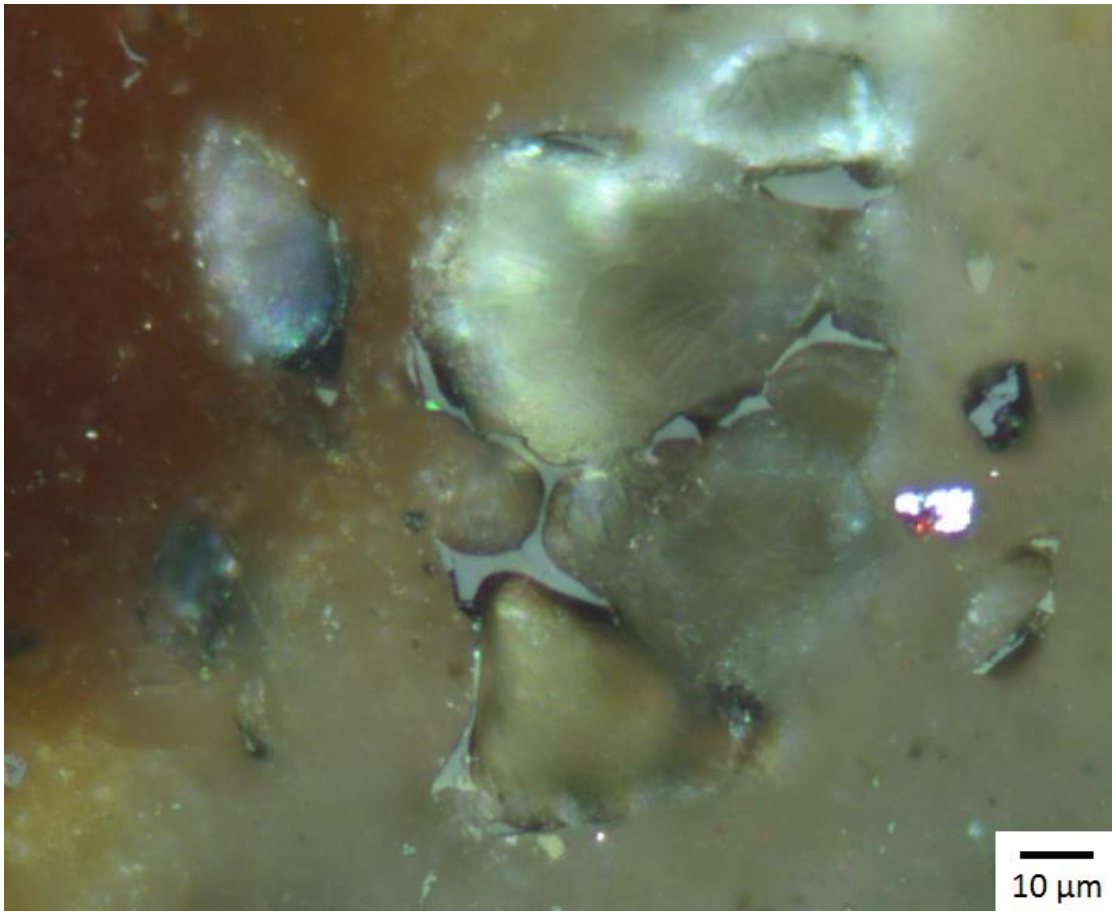

Fig. 106. Vesicle fillings in Microfacies VS retaining their rounded shape after their glassy margins have been partially broken away, showing that the vesicles were infilled prior to brecciation of the glass. Sample from Clipper-1 at 3550m depth. Image in reflected light.

Newman Energy Research Ltd has observed Microfacies VS in multiple locations around the world, including offshore basins in North America, South East Asia, the North Sea and all major New Zealand offshore basins (J. Newman 2015 pers. comm.). This suggests that it is the similar conditions found in sedimentary basins that encourage the formation of this material, rather than the specific chemistry of the Canterbury Basin magma source.

5.5 Basement rock features

The schist basement rock in the area of the Clipper-1 well shows evidence of brecciation and secondary mineral crystallisation (Chapter 3.9). The characteristics of these features indicate that they are post-metamorphic and may have been formed by hydrothermal activity associated with an igneous intrusion, including abundant undeformed carbonate

crystals cutting across the foliation of the schist. Microbrecciation of the schist may be an indicator of shearing or hydrothermal fluid flow. The schist is unusually rich in carbon in the form of finely dispersed graphite, particularly in the mica-rich layers. It is difficult to determine whether this is a primary or secondary feature.

Native iron-containing fissure fillings occur sparsely in the basement rock samples from Clipper-1 (Chapter 3.5). Unlike examples from higher up in the well, these do not have sediment grains cemented to their edges, suggesting that they formed within the schist rather than being caved material from higher up the drillhole. This indicates that highly reducing conditions were present in the basement rock. It remains uncertain whether these conditions were present in the melt during its initial intrusion of the basement rock, or whether recirculating fluids brought reducing compounds down from the carbon-rich sediments above the basement contact.

The continental rifting that occurred in this area during the Cretaceous produced numerous faults in the basement rock (Field & Browne 1989). These faults may have acted as conduits for hydrothermal fluids or igneous intrusions, controlling the distribution of secondary mineralisation in the Canterbury Basin. This has been observed on the Chatham Islands, where there is a correlation between the locations of volcanism and fractured areas of the basement rock (Gamble et al. 1986). As the Clipper sub-basin was one of the first areas to experience subsidence during the rifting phase, the basement rock in this area would be expected to be extensively faulted (Field & Browne 1989). This may explain why the mineralisation is particularly rich in Clipper-1 compared to other wells in the Canterbury Basin.

The similarity of the schist at the base of Clipper-1 to schist from gold-mining areas of Otago, such as the Intrashear schist in the Macraes goldmine (Craw 2002), also indicates that hydrothermal fluids have been present. Calcite, graphite, and euhedral pyrite are all common to both schists.

5.6 Outcrop sampling comparisons

Overall there is little similarity between the igneous materials or intrusion-affected sediments in Clipper-1 and the material sampled from outcrops in Otago and Lyttelton Harbour. This indicates that the intrusion in the offshore Canterbury Basin was substantially different to the other episodes of intraplate volcanism that have occurred in Canterbury and Otago since the Cretaceous. One of the most substantial differences is the lack of typical silicate igneous rocks in the offshore intrusion. In particular, the difference between the igneous rocks and minerals from Clipper-1 and those sampled from the Moeraki and Tokarahi sills strongly implies that the offshore intrusion was not a typical mafic intrusion that has been altered by contact with wet marine sediments, as the sills were intruded into a similar environment but have not produced the same type of extremely low silica igneous materials. One potentially important difference between the location of Clipper-1 and the outcrop sampling locations is the extremely thick layer of sedimentary rocks covering the basement in the Clipper sub-basin.

One feature that was found in both outcrop and well cuttings was a texture indicating fluidisation of sediment (Chapters 3.8 and 4.3). This was found in Clipper-1 at 1010m depth and in the sediment dikes of the Tokarahi Sill. This indicates that the sediments at that depth in Clipper-1 were similarly wet and unconsolidated at the time of intrusion and experienced a substantial amount of heating, as the sediment dikes in the Tokarahi Sill showing the same texture are in very close contact with the basalt. There is also a distinct similarity between parts of the sandstone adjacent to dikes at the Head of the Bay in Lyttelton Harbour and a grain of highly altered siltstone found at 780m depth in Clipper-1 (Chapter 4.4.3: Fig. 101, Chapter 3.8: Fig. 53). The sample at 780m depth in Clipper-1 is very rich in Microfacies VS, and the alteration of the siltstone may have occurred as the carbonate melt was intruded.

There are some limitations involved in using outcrops as a source of rock samples. For example, it is unavoidable that rock samples exposed in an outcrop will have experienced some degree of weathering, and so may not provide a perfect comparison to fresh rock from deep well cuttings. Native iron and aluminium are easily oxidised and so may not be

visible in an outcrop sample even if they are present in unweathered sections of the same rock unit. It is also unknown how well the distinctive textures of Microfacies VS survive when subjected to weathering. It is possible that the distinctive mineral assemblages observed in Clipper-1 may not occur in outcrop or even in near-surface drillholes where the rock is affected by oxygenated meteoric groundwater.

Although the outcrop sampling failed to reveal a comparable intrusion to the one found in the offshore Canterbury Basin, it has yielded useful insights. In particular, the outcrop at the Head of the Bay in Lyttelton Harbour is a useful example of how difficult it can be to distinguish igneous and sedimentary rocks in hand specimen if they have been affected by hydrothermal fluids (Chapter 4.4.3). Sedimentary rocks may recrystallise, becoming very well indurated and visually similar to an igneous rock, while igneous rocks may become oxidised and even disintegrate into separate grains, taking on the appearance of a fine-grained, poorly indurated sedimentary rock. In some cases a rock can only be identified as igneous by observation under a microscope, either in reflected or transmitted light. This may explain why intrusions intersected by petroleum exploration wells may not be recognised, particularly if the material is in the form of cuttings rather than core.

5.7 Hydrothermal activity

The fluidised and recrystallised sediments in Clipper-1 indicate that hydrothermal fluid flow has occurred in the Canterbury Basin (Chapter 3.8). The uppermost evidence of fluid flow is in the Tokama Siltstone between 780m and 1000m depth. This consists of sediments with reduced porosity, loss of original sedimentary texture and alignment of mica crystals with the direction of flow. This is visibly very similar to fluidised sediments injected into fissures in the Tokarahi Sill, indicating that the sediments in Clipper-1 may have been similarly wet and poorly indurated when affected by hydrothermal fluid flow.

Deformation of framboidal pyrite is another indicator of fluidised sediment. In parts of the Moeraki Formation, these normally spherical clusters of small pyrite crystals have been deformed into linear streaks. In the same sediment grain, framboids contained within fragments of harder, carbonate-mineralised sediments have retained their original shape.

The highly distinctive crenulated fabrics that occur in mineralised sediments deeper in Clipper-1 also indicate that they have been affected by fluid flow.

Carbonatite intrusions are commonly associated with a fenite aureole (Winter 2010). This metasomatic rock is produced when hot fluids generated by the magma infiltrate the surrounding rock. The mineralised sediments in Clipper-1 may be equivalent to a fenite. As carbonatites are most commonly found in continental rifts, fenites are usually produced in hard, igneous or metamorphic country rock. In the Canterbury Basin, magma has intruded into relatively young, wet, poorly-indurated sediments. This may account for the textural and possible chemical differences between typical fenites and the fluid-affected sediments in Clipper-1.

5.8 Intrusion history

The presence of Microfacies VS in Clipper-1 and Galleon-1 indicates the presence of crust-derived, carbonate-based intrusions in the Canterbury Basin extending from below the basement contact to a minimum depth of 780m at Clipper-1 and 500m at Galleon-1. The proposed source of the carbonate melt is the abundant secondary carbonates found in the schist basement rock of the Canterbury Basin. These carbonates may have been melted by a mafic intrusion in the basement rock, similar to those proposed based on thermal history modelling of the basin (Funnell 2005). Although the crustal origin of the carbonate melt means that it is not a true carbonatite, due to the similarity in major elemental composition it may have behaved in a similar way and so carbonatite intrusions may still provide a useful comparison. The large gaps between the depths in Clipper-1 where intrusive materials are found implies that the well is intersecting sills branching off the main body of the intrusion (Fig. 107).

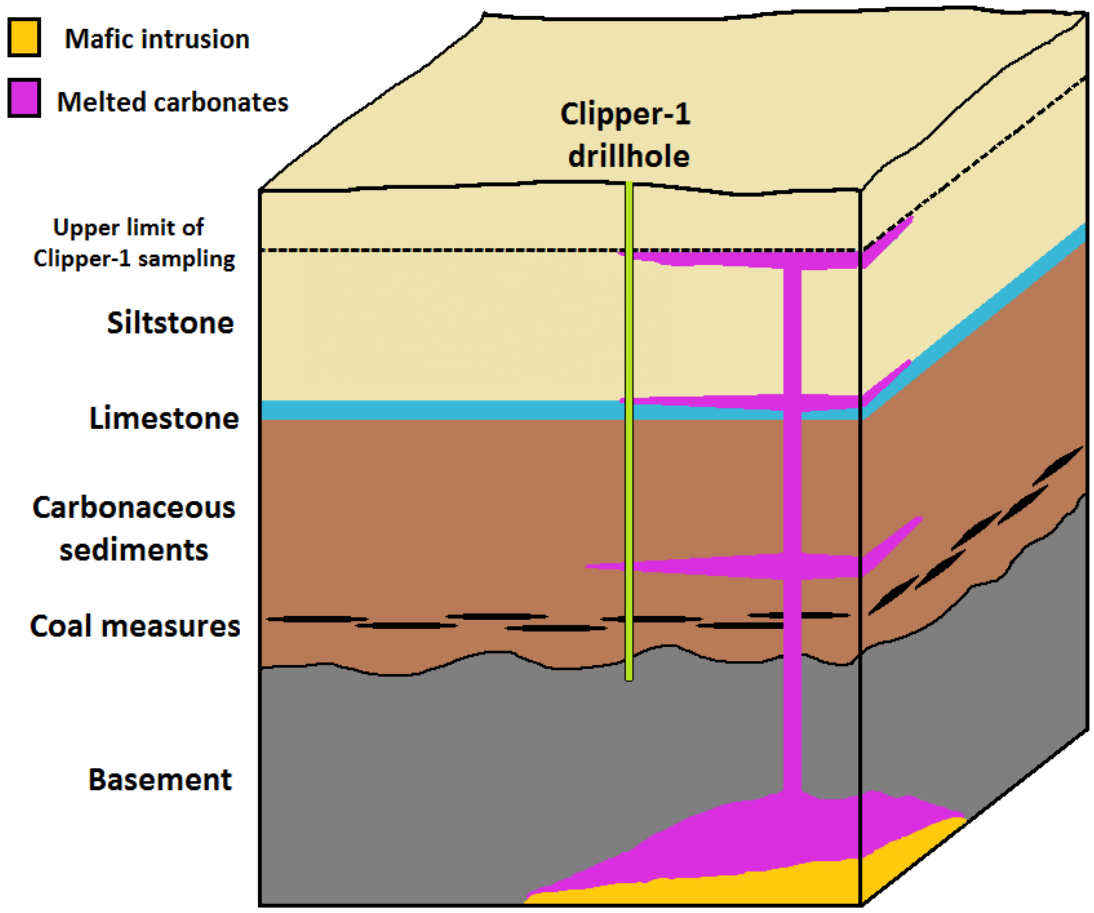

Fig. 107. Diagram of hypothetical intrusion in the area of Clipper-1 (not to scale). Melting of carbonates by a mafic intrusion below the basement contact produces a low-density, volatile rich melt that intrudes the overlying sediments to at least 780m below the surface, with sills extending laterally from the main intrusion.

In addition to the igneous carbonates, the intrusion also produced an unusual array of native metals including iron, aluminium and copper. There is a correlation between the presence of native metals and Microfacies VS up to 2000m depth in Clipper-1, which suggests that they were produced by the same intrusion. The high concentration of Microfacies VS at 780m depth is not associated with native metals, suggesting that the carbonate component of the intrusion reached shallower depths than the metals. This may be due to the low density and high volatile concentrations in carbonate melts.

The formation of the Canterbury Basin during the rifting of New Zealand from Antarctica involved extensive faulting of the schist basement rock (Field & Browne 1989). Although this

area is now seismically stable, these old faults are still present and may act as conduits for magma. The thinning of the continental crust in this region may also help to produce mafic intrusions, providing the heat source for melting basement carbonates. The high concentrations of igneous material in Clipper-1 compared to the other wells in the Canterbury Basin indicates that the igneous activity may have been more intense in the area of the Clipper sub-basin. This may be due to more extensive faulting of the basement rock in this area, due to it being the deepest part of the Canterbury Basin and one of the earliest depocentres to form during Cretaceous rifting (Field & Browne 1989). In addition, the greater thickness of sediments in the Clipper sub-basin suggest that this area has been subjected to more intense crustal thinning than the rest of the basin.

As the intrusion extends to the uppermost recovered samples from Clipper-1, the top of the intrusion cannot be defined and it remains unknown whether it reached the seabed. The high concentrations of igneous material in the top sample at 780m may indicate a change in the intrusive environment indicating shallow depths or looser sediments. This may be similar to the basaltic sill at Tokarahi, which formed in loose marine sediments at very shallow depths (Coombs et al. 1986).

Determining the finer structure of the intrusion is made difficult by the state of the material sampled from Clipper-1. Each sample consists of crushed, homogenised material representing three to ten metres of the drillhole. As no core is available from the depths where intrusive material is present, intrusive contacts and the structure of the intrusive bodies cannot be observed. As all the Clipper-1 samples analysed contain at least 50% sedimentary material, we can conclude that the intrusion in this area is fairly diffuse. Intrusive bodies substantially larger than the size of the sampling brackets would result in some samples being almost pure igneous material.

Native metals in Clipper-1 are not evenly distributed, but occur in high concentrations at particular depths (Chapter 3.5). This suggests that the Clipper-1 well does not intersect the main body of the intrusion, but is instead passing through sills or radial dikes extending laterally from the main intrusion. This conclusion is supported by the complete absence of native metals from the Clipper-1 cuttings between 2800m and 3500m depth. The high concentration of native metals, particularly native aluminium, at 2050m depth correlates

with a change in the sediments from limestones to sandstone. The relatively high permeability of the sandstone in comparison to the limestone may be the reason why the metals are concentrated here. The high concentrations of native iron at 3550m is difficult to explain as it does not correlate with a facies change.

Seismic surveys of the Canterbury Basin have not detected an igneous intrusion at the depths where Microfacies VS has been found in abundance. Carbonatite intrusive complexes are typically less than 25km^2 in cross section (Winter 2010), and if the Canterbury Basin carbonate intrusions are similar they may be too small to be reliably detected by seismic surveys. Alternatively, the intrusion may be very diffuse and produce a weak response as carbonate melts are low-density and low-viscosity (Winter 2010). However, some seismic reflectors in Clipper-1 that have formerly been attributed to facies changes or unconformities do occur at depths where there is intense mineralisation (Field & Browne 1989). In particular, seismic reflectors at 2044m and 3464m fall extremely close to the depths in Clipper-1 with the highest concentrations of native metals. These seismic reflectors are likely to have been produced by the high density of metals at these depths, but have been misidentified as facies changes or unconformities as it was not known that intrusive materials were present.

5.7.1 Intrusive phases

Despite the crushed state of the cuttings, scarce examples of contacts between the different mineral assemblages have been found. This allows the different phases of the intrusion to be placed in chronological order.

The earliest phases of the intrusion produced Microfacies VS and the solid oxide veins. When observed in contact with native iron and associated iron oxides, Microfacies VS is stained with iron oxides in a similar way to sediment (Fig. 108). This indicates that it is was emplaced earlier than the iron. The inclusion of broken fragments of solid oxide veins in the fissure fillings which contain native iron also indicates that the solid oxides were an earlier phase. The relative timing of the production of Microfacies VS and the other mineral

assemblages cannot be determined as no examples of contacts between them have been found.

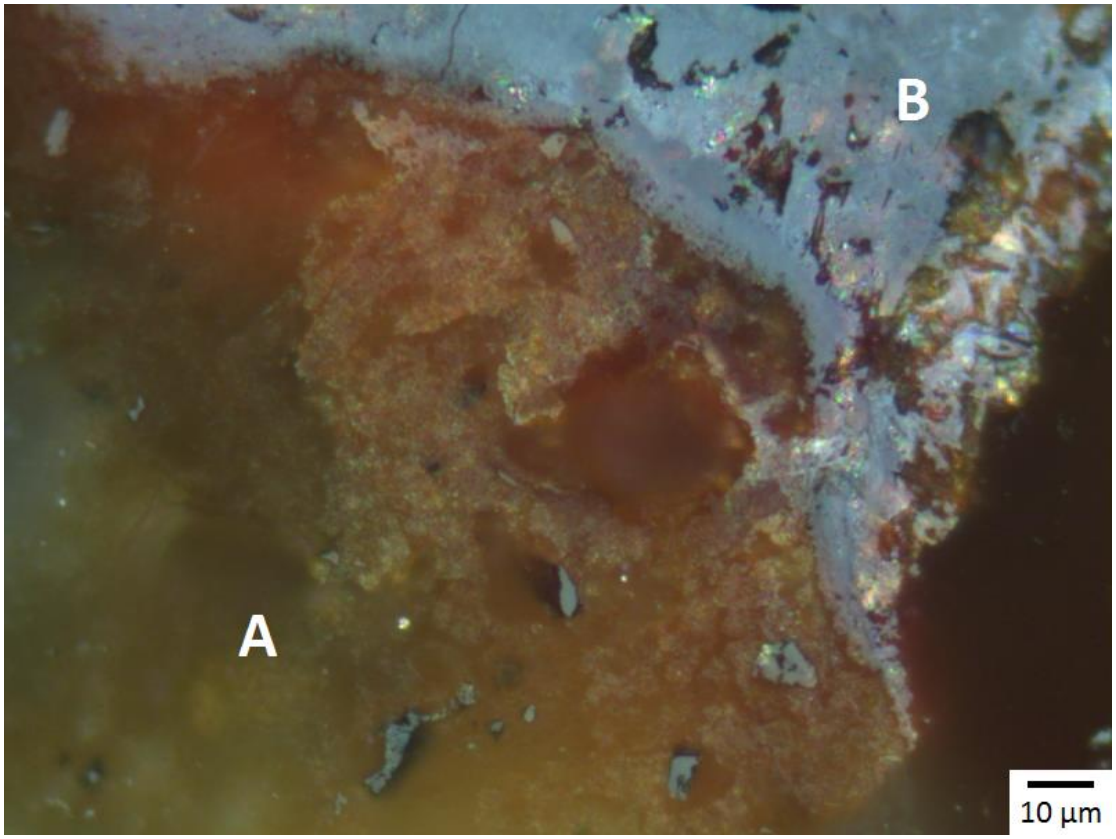

Fig. 108. Contact between highly brecciated Microfacies VS (A) and iron oxides at the edge of a fissure filling (B). The staining of the Microfacies VS with iron oxides indicates that it was emplaced before the fissure filling. From Clipper-1, 3550m depth. Image in reflected light.

5.7.2 Dating

A maximum age for the intrusion can be set based on the age of the youngest sediments in which it is found. In Clipper-1, the youngest recovered sediments have been dated to the late Pliocene (Field & Browne 1989). This is much more recent than the Cretaceous and Miocene intrusions that have been proposed based on thermal history modelling (Funnell 2005). The Timaru Basalt in onshore Canterbury has also been dated to the late Pliocene (Duggan & Reay 1986). It is possible that the Timaru Basalt and the intrusions in the offshore Canterbury Basin are part of the same episode of volcanism.

5.7.3 Effect of intrusion on hydrocarbon generation

The suggestion of a previously undiscovered intrusion in the Canterbury Basin has relevance to oil and gas exploration in the area. Funnell (2005) proposed a Cretaceous age intrusion into the basement rock and a late Miocene intrusion at approximately 4000m depth and these have been incorporated into thermal history models of the basin. However, the mineralisation in Clipper-1 indicates a much more recent and shallow intrusion. The effect of this on potential petroleum source rocks in the Canterbury Basin may require further investigation if oil and gas exploration in the area is to resume.

5.8 Comparison to previous work

One of the questions that arose during this study was how the intrusive materials present throughout Clipper-1 and more sparsely in other wells had been missed during the exploration of the offshore Canterbury Basin. Although the mineral assemblages described in this thesis have undoubtedly been seen before, this is the first time they have been properly identified and their significance recognised.

During the initial analysis of the well cuttings for the purposes of thermal history modelling, only the organic material was considered important. The mineral component of the samples was largely ignored. Any metallic minerals were assumed to be iron sulfides, a common component of sediments in petroleum basins. This is despite the substantial difference in colour and brightness between native metals and iron sulfides. Iron oxides and hydroxides associated with the native iron may be assumed to be the result of oxidation of iron sulfides. The cuttings from 3550m depth in Clipper-1 consist almost entirely of native iron and associated iron minerals, giving them a very distinctive "rusty" appearance, high density and strong paramagnetism. However, these features were not noticed during logging of the well cuttings, with material at this depth recorded as non-calcareous siltstone (Field & Browne 1989). During seismic surveys, this depth was marked as a seismic horizon with an increase in resistivity response and acoustic velocity, indicating denser material. This was interpreted as the equivalent of the top of the Shag Point coal measures which occur in the area of Endeavour-1, then later reinterpreted as an unconformity (Mound & Pratt 1984; Field &

Browne 1989). In fact, it is much more likely to have been produced by the high concentration of iron minerals at this depth.

The distinctive hard, grey flakes of native aluminium found in cuttings from the lower Tokama Siltstone were likewise not noticed as anything unusual despite appearing very different to the sediment at that depth. The high concentrations of native aluminium and iron at 2050m depth also correlates with a seismic horizon, which has previously been interpreted as a sediment wedge and as a calcareous sandstone unit (Mound & Pratt 1984; Field & Browne 1989). The high concentrations of native metals at this depth are also a more likely cause of this seismic anomaly.

The lack of attention given to Microfacies VS is more easily excused, as it is a very nondescript fine-grained grey rock in hand specimen and in polished section may be mistaken for ashfall-deposited vitric tuff. The unusual chemistry was not noticed as no chemical analysis was performed.

5.9 Unanswered questions and future work

As a side effect of revealing a substantial amount of information about igneous activity in the offshore Canterbury Basin, this thesis has also produced new questions that cannot be answered in the scope of the current study.

The vast majority of the material from the offshore wells in the Canterbury Basin is in the form of cuttings; crushed rock fragments usually less than 5mm in length. This places limitations on the information that can be gathered from the material. Any textures or structures of a larger scale than the size of the cuttings are lost. Minerals that are scarce or only occur in narrow bands may be missed, as each sample of cuttings represents 3-10m of the drillhole. Even a representative sample may be missing rare constituents when this much of the section is condensed down to a 10g sample. Core samples provide much better preservation of structures and a much more detailed view of the sedimentary section, but little core is available from the offshore Canterbury Basin wells and none from the depths where the native metals or Microfacies VS have been found. If further investigation of the

offshore Canterbury Basin for petroleum resources occurs, new opportunities for sample collection may become available. If sufficient quantities of native iron could be obtained with new sampling, it may be possible to test its melting point as has been done with the native iron from the Siberian Traps flood basalt (Ryabov & Lapkovsky 2010). The Siberian Traps iron has been found to melt at temperatures significantly below the normal melting point of iron, which has been interpreted as signifying the presence of a naturally-occurring flux. The results of a similar test on the Canterbury Basin iron could help in determining the temperature of the intrusion.

One of the most difficult to explain features of the intrusion is the extremely low levels of silica in the native metal assemblages, and the absence of typical silicate intrusive rocks. If the metals are derived from a mafic intrusion below the basement contact, they would be expected to contain substantial concentrations of silica. This is also the case if they were produced by the melting of metal-rich sedimentary rocks, as silica has a significantly lower melting point than iron. Alternatively, silica may have been removed from the metal melts prior to crystallisation, although how this could be achieved is unknown. Revealing the chemical processes involved in the production of native metals in the offshore Canterbury Basin would require a substantial amount of further study.

If Microfacies VS was produced by the melting of secondary carbonates in the schist basement, low levels of silica would not be as unexpected. However, the carbonate-based glass in Microfacies VS appears to contain euhedral quartz phenocrysts. How a melt could produce both quartz crystals and glass which is almost devoid of silica is unknown. The quartz may not have crystallised in the carbonate melt, but instead be pre-existing crystals that have been transported from depth by the melt. However, in this situation they would expect to be fragmented and eroded to some degree, rather than the very sharp-edged euhedral crystals that are observed in Microfacies VS. Another possibility is that they were precipitated from silica-rich hydrothermal fluids that have mixed with the carbonate melt.

Other remaining questions include the details of the inferred mafic intrusion below the basement contact, including depth, age, and whether it has any relation to the late Pliocene mafic volcanism that produced the Timaru Basalt. Details of the timing and mechanisms of

the carbonate and metal-based intrusions into the sediments are also in need of further study. Based on the lack of mixing between the different assemblages, it appears that the native iron, native aluminium and Microfacies VS each represent a distinct intrusive phase, but the relative timing and relationship between each phase is unclear.

6.0 Conclusions

1. An igneous carbonate, named here as "Microfacies VS", is found throughout Clipper-1 from the basement rock to the uppermost collected sample at 780m depth, a vertical span of almost 4km. This distribution indicates that it is an intrusive material rather than an ashfall deposit. The trace element concentrations of Microfacies VS indicate that it is not sourced from the mantle and so is not a carbonatite. The most likely origin for the carbonate melt that produced Microfacies VS is a mafic intrusion melting carbonates in the basement rock.

2. Secondary textures in sedimentary rocks throughout Clipper-1 have been produced by fluidisation and recrystallisation due to heating and hydrothermal fluid flow. Some examples are very similar to textures found in sedimentary rocks collected from outcrops adjacent to igneous dikes in inland Otago and Lyttelton Harbour.

3. Native metals are abundant in Clipper-1. These consist of iron and aluminium with rare occurrences of copper alloys and lead. The textures and associated minerals found in the native metals indicate that they formed from melt. The native metals were produced in highly reducing conditions derived from magma interactions with coals, carbonaceous mudstone and limestone. The presence of native aluminium is particularly unusual and its occurrence and stratigraphic distribution in Clipper-1, where it is found in abundance only above the Otekaike and Amuri limestones, provides important insights into the conditions under which this metal can form.

5. Native metal occurrence in Clipper-1 may be partially comparable to native iron found in basalt, such as the examples on Disko Island and in the Siberian Traps, which were also produced by reducing conditions due to interaction between magma and carbonaceous rocks. (Pedersen 1979; Ulff-Møller 1990; Ryabov et al. 2006; Ryabov & Lapkovsky 2010). However, there are substantial differences including the small size of the Clipper-1 intrusion, the lack of typical silicate igneous rocks, the presence of igneous carbonates, and the presence of other native metals in addition to iron including aluminium, copper and lead.

6. The igneous mineral assemblages described by this study appear to represent a previously unrecognised type of intrusive environment that has not been described in the scientific literature. The same distinctive assemblage of Microfacies VS and native metals has been observed in other basins in New Zealand and internationally during proprietary investigations of organic maturity (J Newman, pers comm. 2015). Consequently the Clipper-1 intrusive history is not expected to be a unique occurrence but is instead the first described example of a type of igneous intrusion that may be found globally.

7. This study demonstrates the benefits of a combination of optical and geochemical analysis techniques that are effective for identifying and interpreting mineral assemblages in sedimentary rocks. The virtual absence of relevant studies in the scientific literature on sedimentary basins that are analogous to the Canterbury Basin can be attributed at least partly to a widespread emphasis on organic petrology in petrographic investigations that are undertaken during petroleum exploration.

8. The proposed date of Microfacies VS intrusion in Clipper-1 is late Pliocene or younger based on the age of the youngest sediments in which the igneous carbonates have been found. Although this event may appear to be a recent manifestation of the intra-plate volcanism that has occurred sporadically throughout Canterbury and Otago since the Cretaceous, the mineralogy in Clipper-1 is distinctly different from any example of igneous intrusion found in outcrop in the Canterbury Basin. The presence of Microfacies VS in late Pliocene sediments in Galleon-1, 85km from Clipper-1, suggests that the intrusive activity was not restricted to the Clipper sub-basin and there may have been multiple small intrusions throughout the Canterbury Basin at this time.

9. Information on the intrusive history of petroleum basins is essential for accurate modelling of their thermal history and the potential effect of hydrothermal mineralisation on reservoir intervals. Identification of Microfacies VS and the native metal assemblages described by this study may help to define small and/or low-density intrusions that are not detectable by seismic or gravity surveys.

7.0 References

Bai, W., Yang, J., Fang, Q. (2004) Some native metals from ophiolitic chromitites in Tibet (in Chinese). *Earth Sci Front*, v. 11 p. 179-187.

Barley, M. E. (1987) Origin and evolution of mid-Cretaceous, garnet-bearing, intermediate and silicic volcanics from Canterbury, New Zealand. *Journal of Volcanology and Geothermal Research*, v. 32 p. 247-267.

Berndt, M. E., Allen, D. E., Seyfried, W. E. (1996) Reduction of CO2 during serpentinization of olivine at 300 °C and 500 bar. *Geology*, v. 24 p. 351-354.

Bornhorst, T. J., Paces, J. B. (1988) Age of Native Copper Mineralization, Keweenaw Peninsula, Michigan. *Economic Geology*, v. 83 p. 619-625.

Budinski, K. G., Budinski, M. K. (1999) *Engineering Materials: Properties and Selection (6th Ed.).* Prentice Hall, Upper Saddle River, N.J.

Butuzova, G. Y., Shterenberg, L. E., Voronin, B. I. (1987) Native metals in the ore-bearing sediments in the Red Sea. *Lith Ore Dep*, v. 2 p. 122-125.

Chen, Z., Huang, C.Y., Wu, B.H., Zhao, M.X., Yan, W. (2010) Discovery of native aluminum and its possible origin from prospective gas hydrate areas in the South China Sea. *Science China Earth Sciences*, v. 53 (3) p. 335-344.

Clark, A. M. (1993) *Hey's Mineral Index. Mineral species, varieties, and synonyms.* Chapman and Hall, London.

Coombs, D. S., Cas, R. A., Kawachi, Y., Landis, C. A., McDonough, W.F., Reay, A. (1986) Cenozoic volcanism in north, east and central Otago. *Late Cenozoic volcanism in New Zealand: The Royal Society of New Zealand Bulletin*, v. 23 p. 278-312.

Corcoran, P. L., Moore, L. N. (2008) Subaqueous eruption and shallow-water reworking of a small-volume Surtseyan edifice at Kakanui, New Zealand. *Canadian Journal of Earth Sciences*, v. 45 p. 1469-1485.

Cornwall, H. R. (1956) A summary of ideas on the origin of native copper deposits. *Economic Geology*, v. 51 p. 615-631.

Craw, D., Coombs, D.S., Kawachi, Y. (1982) Interlayered biotite-kaolin and other altered biotites, and their relevance to the biotite isograd in eastern Otago, New Zealand. *Mineralogical Magazine*, v. 45 (337) p. 79-85.

Craw, D. (2002) Geochemistry of late metamorphic hydrothermal alteration and graphitisation of host rock, Macraes gold mine, Otago Schist, New Zealand. *Chemical Geology*, v. 191 p. 257-275.

Crerar, D. A., Knox, G. W., Means, J. L. (1979) Biogeochemistry of bog iron in the New Jersey Pine Barrens. *Chemical Geology,* v. 24 (1-2) p. 111-135.

Crux, J. A., Eaton, G. L., Sturrock, S. J. (1984) Biostratigraphy of the Clipper-1 well, offshore New Zealand. Petroleum Report 1044. New Zealand Geological Survey Library.

Davis, J. R. (1996) *Cast Irons.* Materials Park, OH : ASM International.

Dekov. V. M., Mandova E. D., Dimitrov K., B., Rekkalov, K. N. (1995) Native aluminium in metalliferous sediments from the East Pacific Rise axial zone (21 °S). *Marine Geology,* v. 123 p. 87-103.

Dekov. V. M., Arnaudov, V., Munnik, F., Boycheva, T. B., Fiore, S. (2009) Native aluminum: Does it exist? *American Mineralogist*, v. 94 p. 1283-1286.

Devereux, I., Hendy, C. H., Vella, P. (1970) Pliocene and early Pleistocene sea temperature fluctuations. Mangaopari Stream, New Zealand. *Earth and planetary science letters,* v. 8 p. 163-168.

Duggan, M. B., Reay, A. (1986) The Timaru basalt. *Late Cenozoic volcanism in New Zealand: The Royal Society of New Zealand Bulletin*, v. 23 p. 264-277.

Field, B. D., Browne, G. H. and others (1989) Cretaceous and Cenozoic sedimentary basins and geological evolution of the Canterbury region, South Island, New Zealand. *New Zealand Geological Survey Basin Studies 2.*

Förster, A., Merriam, D.F., Hoth, P. (1998) Geohistory and thermal maturation in the Cherokee Basin (Mid-Continent, U.S.A.): results from modeling. *AMERICAN ASSOCIATION OF PETROLEUM GEOLOGISTS Bulletin*, v. 82 no. 9 p. 1673-1693.

Fulthorpe, C. S. (1991) Geological controls on seismic sequence resolution. *Geology*, v. 19 p. 61-65.

Fulthorpe, C. S., Carter, R. M. (1991) Continental-shelf progradation by sediment-drift accretion. *Geological Society of America Bulletin*, v. 103 p. 300-309.

Fulthorpe, C. S., Carter, R. M., Miller, K. G., Wilson, J. (1996) Marshall Paraconformity: a mid-Oligocene record of inception of the Antarctic Circumpolar Current and coeval glacio-eustatic lowstand? *Marine and Petroleum Geology*, v. 13 no. 1 p. 61-77.

Fulthorpe, C. S., Hoyanagi, K., Blum, P. (2011) IODP Expedition 317: Exploring the record of sea-level change off New Zealand. *Scientific Drilling*, v. 12 p. 4-14.

Funnell, R. H., Allis, R. G. (1996) Hydrocarbon maturation potential of offshore Canterbury and Great South Basins. *New Zealand Petroleum Conference Proceedings*, v. 1 p. 22-30.

Funnell, R. H. (2005) Petroleum Modelling in PEP38258 Offshore Canterbury Basin New Zealand. *Ministry of Economic Development New Zealand Unpublished Petroleum Report PR3504.*

Gamble, J. A., Morris, P. A., Adams, C. J. (1986) The geology, petrology and geochemistry of Cenozoic volcanic rocks from the Campbell Plateau and Chatham Rise. *Late Cenozoic volcanism in New Zealand: The Royal Society of New Zealand Bulletin*, v. 23 p. 344-365.

Gibbons, M. J., Fry, S. (1986) A geochemical study of the Galleon-1 well, Canterbury Basin, offshore New Zealand. B.P. Exploration internal report GCB/13/86. PR 1146 Institute of Geological and Nuclear Sciences, Lower Hutt.

Giggenbach, W. F., Sano, Y., Wakita, H. (1993) Isotopic composition of He, CO2 and CH4 contents in gases along the New Zealand part of a convergent plate boundary. *Geochimica et Cosmochimica Acta*, v. 57 (14) p. 3427-3455.

Haskell, T. H., Wylie, I. (1997) New Zealand's Canterbury Basin prospects reviewed in a continental Gondwana setting. *Oil and Gas Journal*, v. 95 (50) p. 57-62.
Hodell, D. A., Elmstrom, K. M., Kennett, J. P. (1986) Latest miocene benthic δ18O changes, global ice volume, sea level and the 'messinian salinity crisis'. *Nature*, v. 320 (6061) p. 411-414.

Iyer, S. D., Mascarenhas-Pereira, M. B. L., Nagender Nath, B. (2007) Native aluminium (spherules and particles) in the Central Indian Basin sediments: Implications on the occurrence of hydrothermal events. *Marine Geology,* v. 240 p. 177–184.

Kamenetsky, V. S., Charlier, B., Zhitova, L., Sharygin, V., Davidson, P., Feig, S. (2013) Magma chamber-scale liquid immiscibility in the Siberian Trapsrepresented by melt pools in native iron. *Geology*, v. 41 (10) p. 1091-1094.

Kennett, J. P., Watkins, N. D., Vella, P. (1971) Paleomagnetic chronology of Pliocene-early Pleistocene climates and the Plio-Pleistocene boundary in New Zealand. *Science*, v. 171 p. 276-279.

Kennett, J. P. (1986) Miocene to early Pliocene oxygen and carbon isotope stratigraphy in the southwest Pacific, Deep Sea Drilling Project 90. *Initial reports DSDP, Leg 90, Noumea, New Caledonia to Wellington, New Zealand. Part 2*, p. 1383-1411.

Kovalski, V. V., Oleynikov, O. B. (1985) Native metals and natural polymineral alloys of copper, zink, lead, tin and antimony in the rocks of the kimberlite pipe "Leningrad". *Doklady Acad Sci USSR*, v. 285 p. 203-208.

Lawver, L.A., Gahagan, L.M. (1994) Constraints on timing of extension in the Ross Sea: Tectonic evolution of the Southwest Pacific from 110 Ma to Present. *Terra Antarctica*, v. 1 p. 545–552.

Lewis, D.W., Belliss, S. E. (1984) Mid Tertiary unconformities in the Waitaki Subdivision, North Otago. *Journal of the Royal Society of New Zealand,* v. 14 (3) p. 251-276.

Lu, H., Fulthorpe, C. S., Mann, P. (2003) Three-dimensional architecture of shelf-building sediment drifts in the offshore Canterbury Basin, New Zealand. *Marine Geology*, v. 193 p. 19-47.

Lu, H., Fulthorpe, C. S., Mann, P., Kominz, M. A. (2005) Miocene-Recent tectonic and climatic controls on sediment supply and sequence stratigraphy: Canterbury basin, New Zealand. *Basin Research*, v. 17 p. 311-328.

Marshak, S. (2001) *Earth: Portrait of a Planet.* W. W. Norton & Company Ltd., 500 Fifth Avenue, New York.

Mound, D. G., Pratt, D. N. (1984) Interpretation and prospectivity of PPL 38202, Canterbury basin, New Zealand. Petroleum Report 1021. New Zealand Geological Survey Library.

Newman, J., Eckersley, K.M., Francis, D.A., Moore, N.A. (2000) Application of vitrinite-inertinite reflectance and fluorescence to maturity assessment in the East Coast and Canterbury Basins of New Zealand. *2000 New Zealand Petroleum Conference Proceedings,* p. 314-333.

New Zealand Petroleum & Minerals. (2013a) Great South-Canterbury Province. [ONLINE] Available at: http://www.nzpam.govt.nz/cms/pdf-library/petroleum-basins/great-south-canterbury.pdf/view. [Accessed 29 September 14].

New Zealand Petroleum & Minerals. (2013b) Canterbury Basin Fact File . [ONLINE] Available at: http://www.nzpam.govt.nz/cms/pdf-library/petroleum-basins/old-files/Canterbury%20Basin%20Fact%20File.pdf/view. [Accessed 17 September 14].

Nordenskiöld, A. E. (1872) Account of an expedition to Greenland in the year 1870. *Geological Magazine,* v. 9 (97) p. 289-306, 355-368, 409-427, 449-463, 516-524.

Novgorodova, M. I., Blokhina, N. A., Gorshkov, A. I. (1981) Structurally ordered native aluminum in skarns. *Doklady Acad Sci USSR*, v. 256 p. 445-447.

Novgorodova, M. I., Mamedov, Y. G. (1996) Native aluminium from mud volcano at the Bulla island, Caspian Sea. *Lith Min Res*, v. 31 p. 301-310.

Okrugin, A. V., Ievlev, A. A., Zueva, I. N. (1991) Anthraxolite in native iron in the Siberian Platform traps. In: Native ore formation in magmatic process: collected papers, pp. 17–28. Yakutian Scientific Center, Siberian Branch of the Russian Academy of Sciences. Yakutsk (in Russian).

Oleinikov, B. V., Okrugin, A. V., Tomshin, M. D., Levashov, V. K., Varganov, A. S., Kopylova, A. G., Pankov, V. Y. (1985) Native iron formation in platform basic rocks. Yakutian Scientific Center, Siberian Branch of the Russian Academy of Sciences. Yakutsk (in Russian).

Pedersen, A. K. (1979) A shale buehite xenolith with AI-armalcolite and native iron in a lava from Asuk, Disko, Central West Greenland. *Contributions to Mineralogy and Petrology*, v. 69 p. 83-94.

Poreda, R. J., Marti, K., Craig, H. (1990) Rare gases and hydrogen in native metals. *From mantle to meteorites: a garland of perspectives*, p. 153-172.

Renne, P. R., Basu, A. R. (1991) Rapid eruption of the Siberian Traps flood basalts at the Permo-Triassic boundary. *Science*, v. 253 (5016) p. 176-179.

Ryabov, V. V., Pavlov, A. L., Lopatin, G. G. (1985) Native iron of the Siberian traps. Nauka Publisher, Novosibirsk (in Russian).

Ryabov, V. V., Ponomarchuk, V. A., Talibova, A. G. (2006) Bitumen, graphite and carbonaceous matter in the rocks and ores of northwestern Siberian Platform: occurrence and isotope composition of carbon. *Topical problems of ore formation and metallogeny: theses of the International meeting devoted to the 100th anniversary of academician V. A. Kuznetsov*, pp. 189–190. GEO Publisher, Novosibirsk (in Russian).

Ryabov, V. V., Lapkovsky, A. A. (2010) Native iron (–platinum) ores from the Siberian Platform trap intrusions. *Australian Journal of Earth Sciences*, v. 57 pt 6, p. 707-736.

Sewell, R. J., Weaver, S. D., Thiele, B. W. (1988) Lyttelton. Geological map of New Zealand 1:50 000 sheet M36BD. *New Zealand Geological Survey: Department of Scientific and Industrial Research.*

Shell BP Todd (Canty) Services Ltd. (1984) Drilling Completion Report Clipper-1 PPL 38202 Offshore Canterbury, South Island NZ. *Ministry of Commerce New Zealand Unpublished Petroleum Report.*

Stipp, J. J., MacDougall, I. (1968) Geochronology of the Banks Peninsula volcanoes, New Zealand. *New Zealand Journal of Geology and Geophysics,* v. 11 p. 1239-1260.

Sykes, R., Funnell, R. H. (2002) Petroleum Source Rock Potential and Generation History in the Offshore Canterbury Basin. New Zealand Petroleum & Minerals, Petroleum Report Series PR2707.

Sykes, R. (2004) Peat biomass and early diagenetic controls on the paraffinic oil potential of humic coals, Canterbury Basin, New Zealand. *Petroleum Geoscience*, v. 10 p. 283-303.

Szatmari, P. (1989) Petroleum formation by Fischer-Tropsch synthesis in plate tectonics. *American Association of Petroleum Geologists Bulletin*, v. 73 (8) p. 989-998.

Taylor, G. H., Teichmüller, M., Davis, A., Diessel, C. F. K., Littke, R., Robert, P. (1998) *Organic Petrology.* Gebrüder Borntraeger, Berlin, Stuttgart.

Ulff-Møller, F. (1990) Formation of native iron in sediment-contaminated magma: I. A case study of the Hanekammen Complex on Disko Island, West Greenland. *Geochimica et Cosmochimica Acta*, v. 54 p. 57-70.

Vandeginste, V., John, C. M. (2013) Diagenetic implications of stylolitization in pelagic carbonates, Canterbury Basin, offshore New Zealand. *Journal of Sedimentary Research*, v. 83 (3) p. 226-240.

Weaver, S.D., Storey, B.C., Pankhurst, R.J., Mukasa, S.B., DiVenere, V.J., Bradshaw, J.D. (1994) Antarctica– New Zealand rifting and Marie Byrd Land lithospheric magnetism linked to ridge subduction and mantle plume activity. *Geology*, v. 22 p. 811–814.

Winter, J. D. (2010) *Principles of Igneous and Metamorphic Petrology.* 2nd edition, Pearson Prentice Hall, Upper Saddle River, New Jersey.

Wylie, I., Haskell, T. (1997) Recognition of a continental sequence beneath the Canterbury Basin, New Zealand and its effect on the region's prospectivity. *Petroleum Exploration in New Zealand News*, v. 49 p. 10-19.

Zhang, Z., Mao, J., Wang, F., Pirajno, F. (2006) Native gold and native copper grains enclosed by olivine phenocrysts in a picrite lava of the Emeishan large igneous province, SW China. *American Mineralogist*, v. 91 p. 1178-1183.

Appendix 1

Clipper-1 SEM data

2035m Pyrite

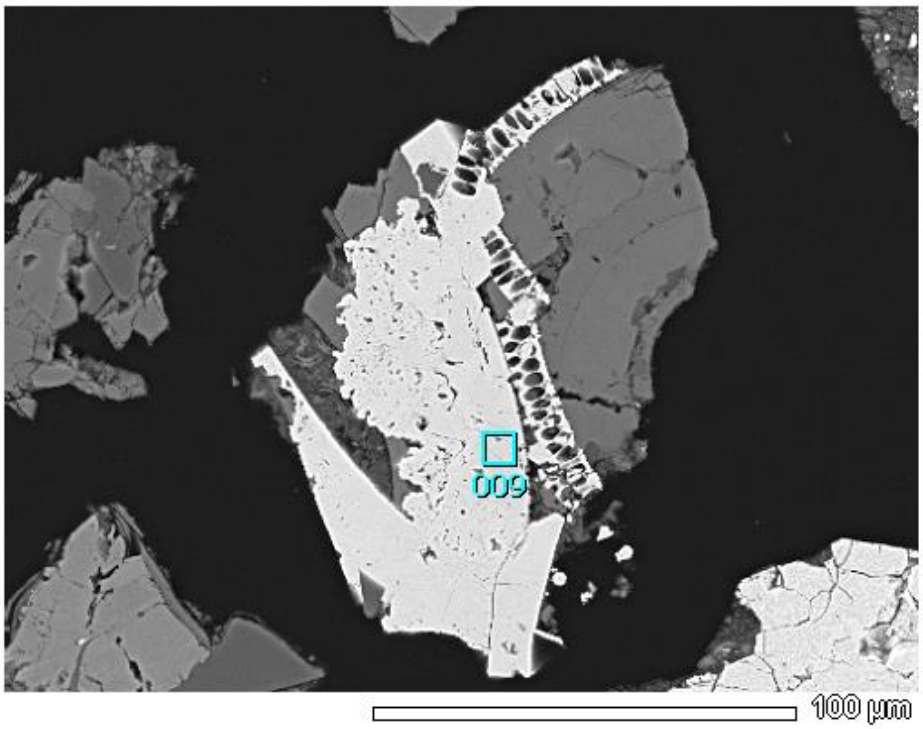


```
Title        : IMG1
--------------------------
Instrument   : 7000F
Volt         : 20.00 kV
Mag          : x 550
Date         : 2014/02/11
Pixel        : 512 x 384
```

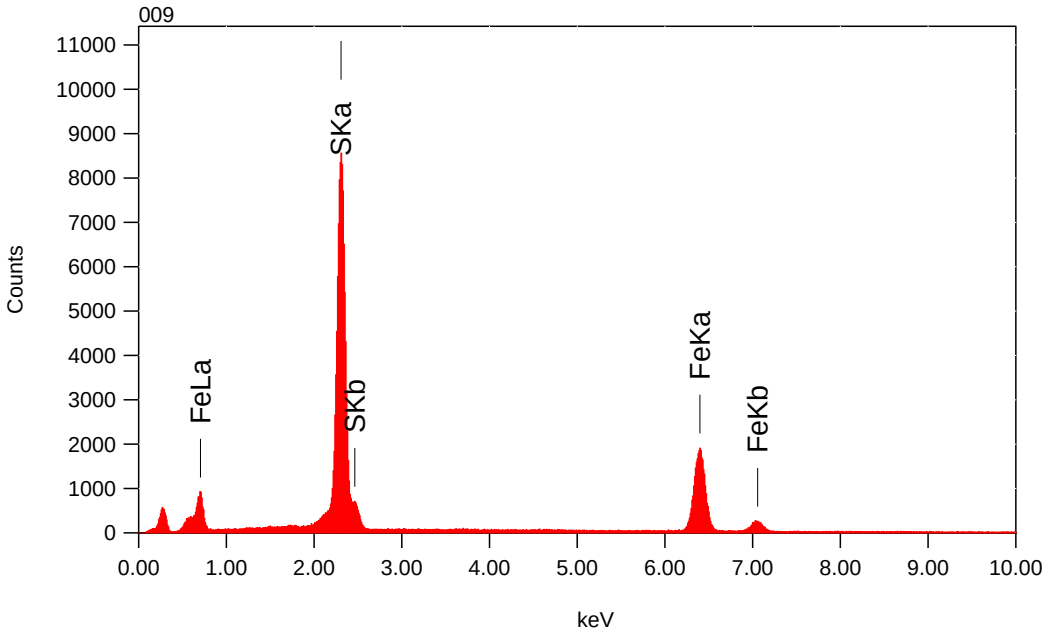


```
Acquisition Parameter
Instrument    : 7000F
Acc. Voltage  : 20.0 kV
Probe Current: 0.59000 nA
PHA mode      : T3
Real Time     : 45.28 sec
Live Time     : 30.00 sec
Dead Time     : 33 %
Counting Rate: 7467 cps
Energy Range :  0 - 20 keV
```

ZAF Method Standardless Quantitative Analysis
Fitting Coefficient : 0.1321

Element	(keV)	mass%	Error%	At%	Compound	mass%	Cation	K
S K	2.307	51.6	0.1	65.0				54.4103
Fe K	6.398	48.4	0.3	35.0				45.5897
Total		100.0		100.0				

2035m Pyrite

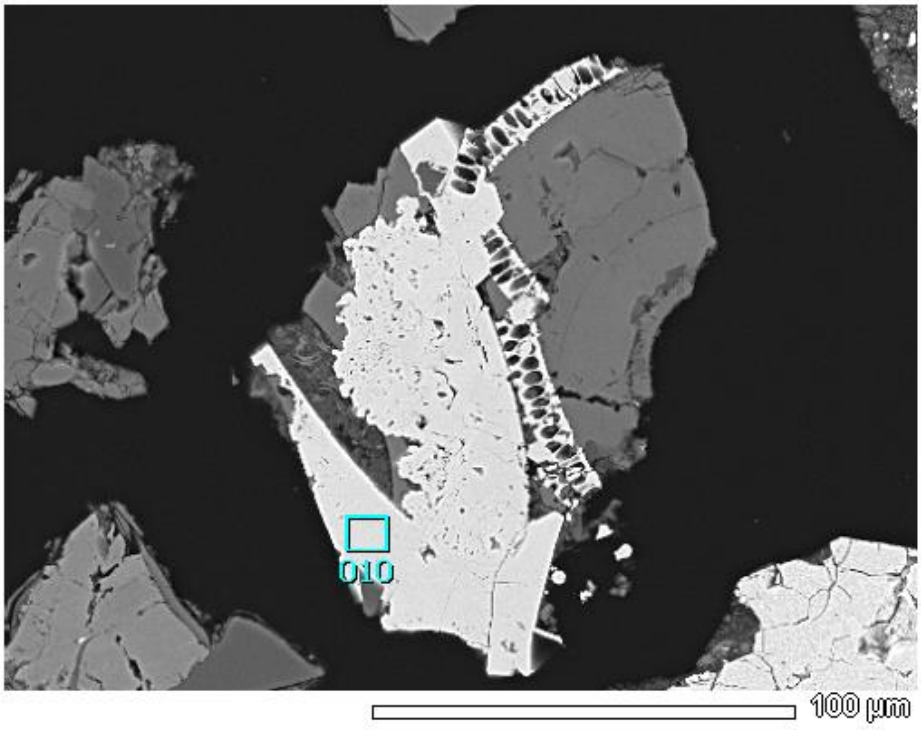


```
Title        : IMG1
--------------------------
Instrument   : 7000F
Volt         : 20.00 kV
Mag          : x 550
Date         : 2014/02/11
Pixel        : 512 x 384
```

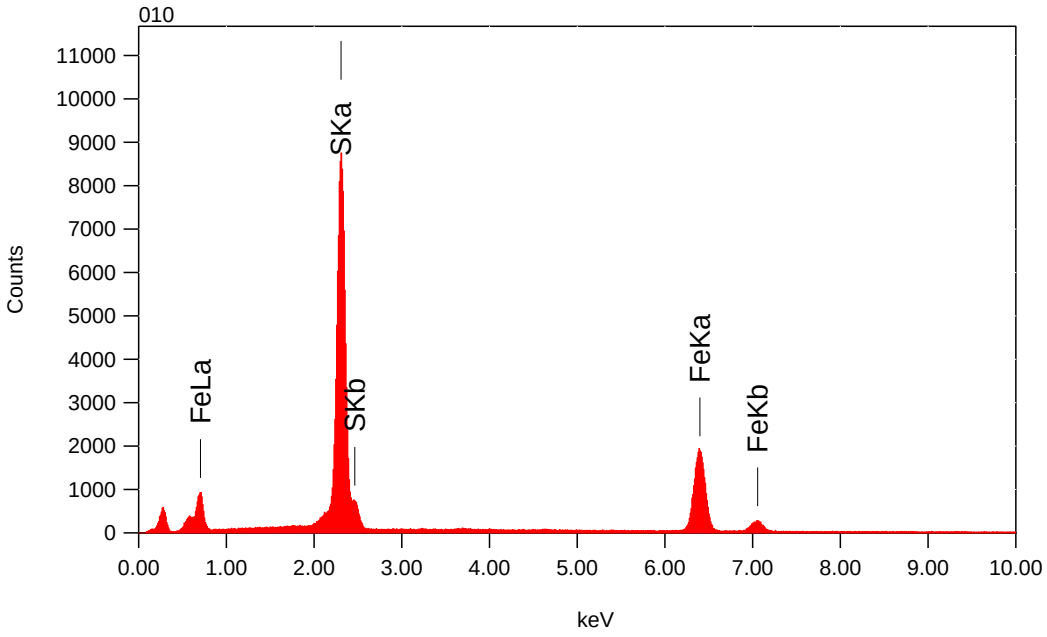


```
Acquisition Parameter
Instrument    : 7000F
Acc. Voltage  : 20.0 kV
Probe Current: 0.59000 nA
PHA mode      : T3
Real Time     : 45.66 sec
Live Time     : 30.00 sec
Dead Time     : 33 %
Counting Rate: 7512 cps
Energy Range :  0 - 20 keV
```

ZAF Method Standardless Quantitative Analysis
Fitting Coefficient : 0.1341

Element	(keV)	mass%	Error%	At%	Compound	mass%	Cation	K
S K	2.307	51.5	0.1	64.9				54.2801
Fe K	6.398	48.5	0.3	35.1				45.7199
Total		100.0		100.0				

2035m Pyrite

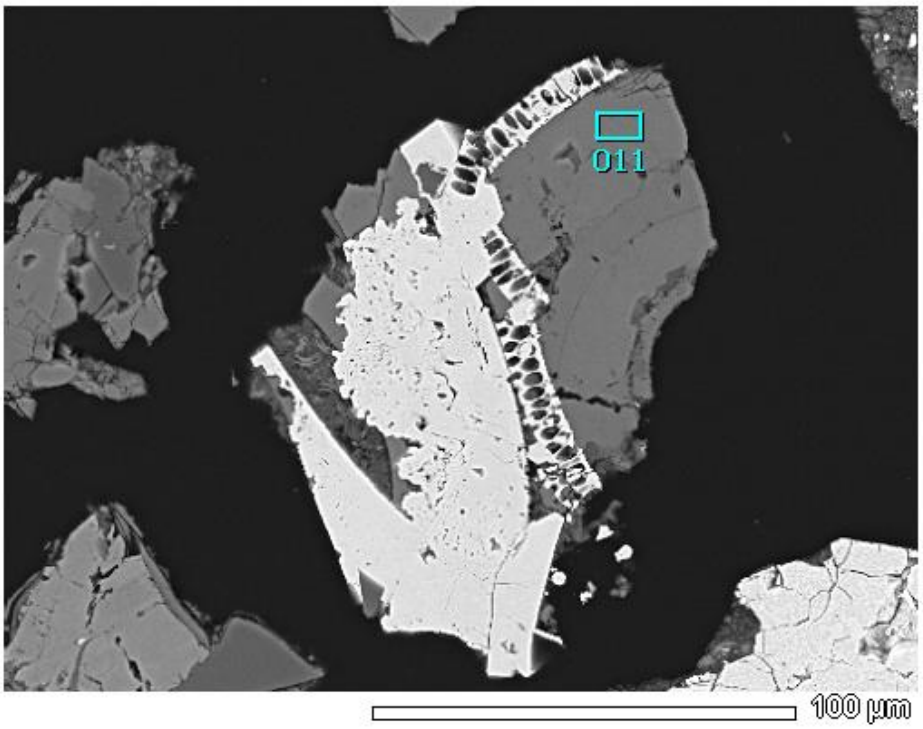


```
Title          : IMG1
---------------------------
Instrument     : 7000F
Volt           : 20.00 kV
Mag            : x 550
Date           : 2014/02/11
Pixel          : 512 x 384
```

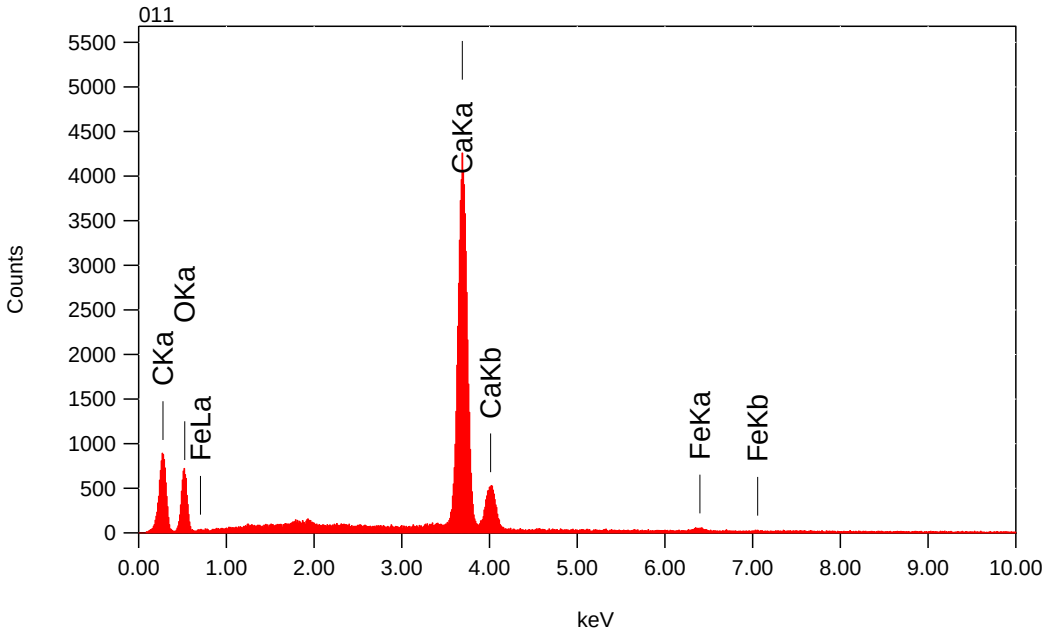


```
Acquisition Parameter
Instrument     : 7000F
Acc. Voltage   : 20.0 kV
Probe Current: 0.59000 nA
PHA mode       : T3
Real Time      : 37.13 sec
Live Time      : 30.00 sec
Dead Time      : 18 %
Counting Rate: 3891 cps
Energy Range :  0 - 20 keV
```

ZAF Method Standardless Quantitative Analysis
Fitting Coefficient : 0.1423

Element	(keV)	mass%	Error%	At%	Compound	mass%	Cation	K
C K*	0.277	19.3	0.0	31.3				13.7920
O K	0.525	40.8	0.2	49.5				17.5730
Ca K	3.690	39.0	0.1	18.9				67.4147
Fe K	6.398	0.9	0.1	0.3				1.2203
Total		100.0		100.0				

2035m Fissure filling

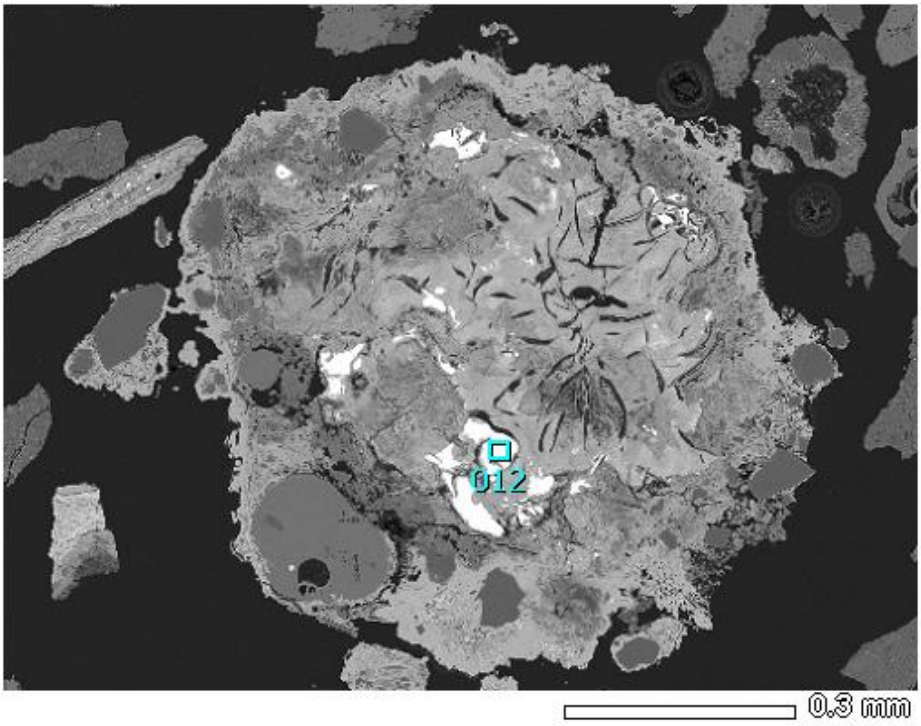


```
Title          : IMG1
---------------------------
Instrument     : 7000F
Volt           : 20.00 kV
Mag            : x 100
Date           : 2014/02/11
Pixel          : 512 x 384
```

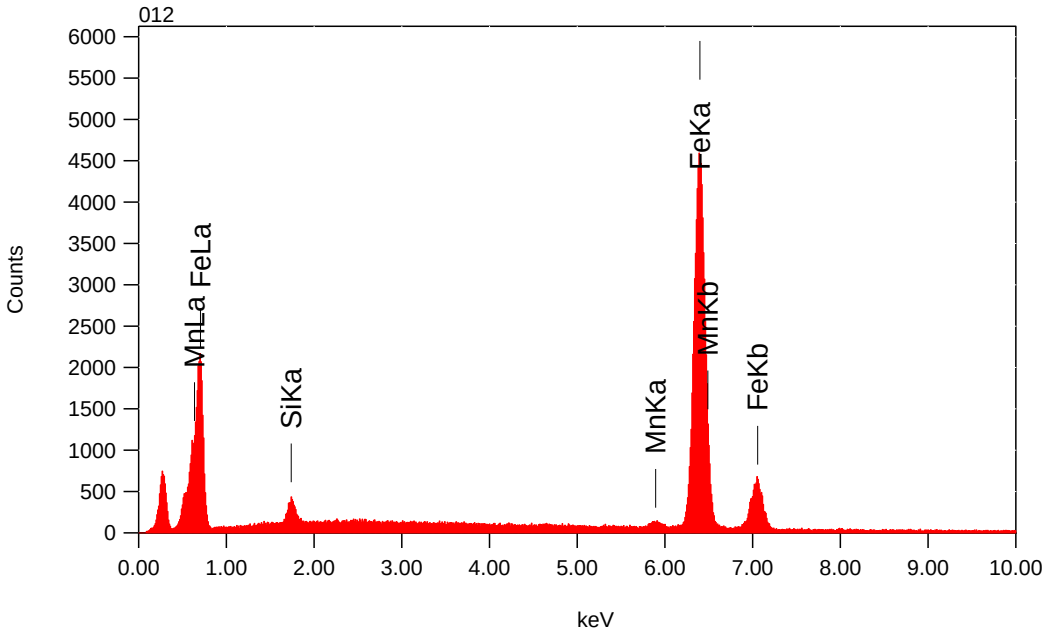


```
Acquisition Parameter
Instrument     : 7000F
Acc. Voltage   : 20.0 kV
Probe Current: 0.59000 nA
PHA mode       : T3
Real Time      : 44.38 sec
Live Time      : 30.00 sec
Dead Time      : 32 %
Counting Rate: 6974 cps
Energy Range :  0 - 20 keV
```

ZAF Method Standardless Quantitative Analysis
Fitting Coefficient : 0.1802

Element	(keV)	mass%	Error%	At%	Compound	mass%	Cation	K
Si K	1.739	1.8	0.1	3.6				1.0575
Mn K*	5.894	1.0	0.3	1.0				1.0035
Fe K	6.398	97.1	0.3	95.4				97.9391
Total		100.0		100.0				

2035m Fissure filling

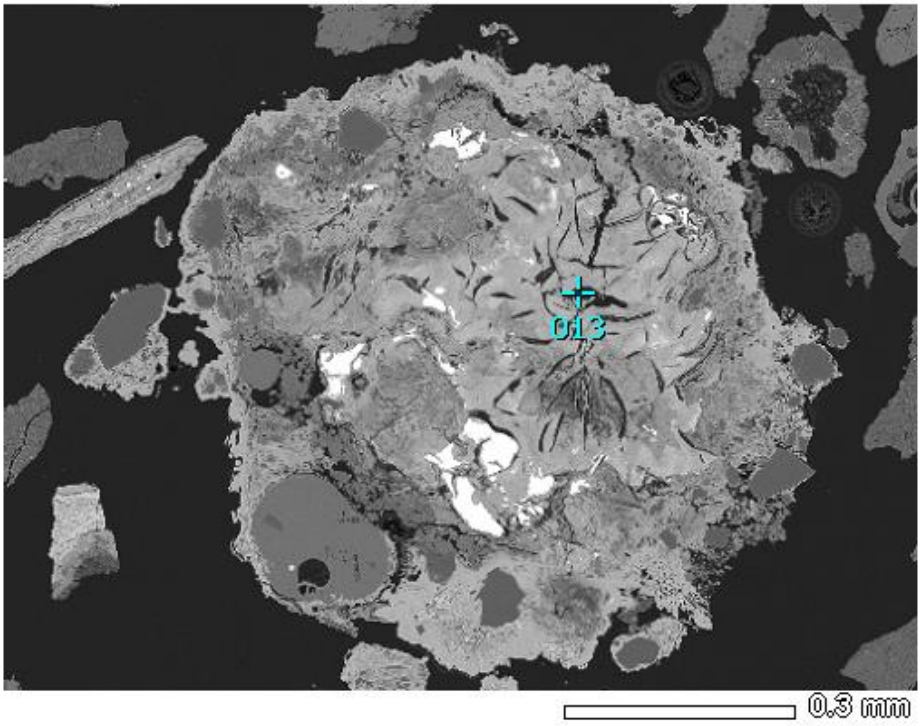


```
Title        : IMG1
--------------------------
Instrument   : 7000F
Volt         : 20.00 kV
Mag          : x 100
Date         : 2014/02/11
Pixel        : 512 x 384
```

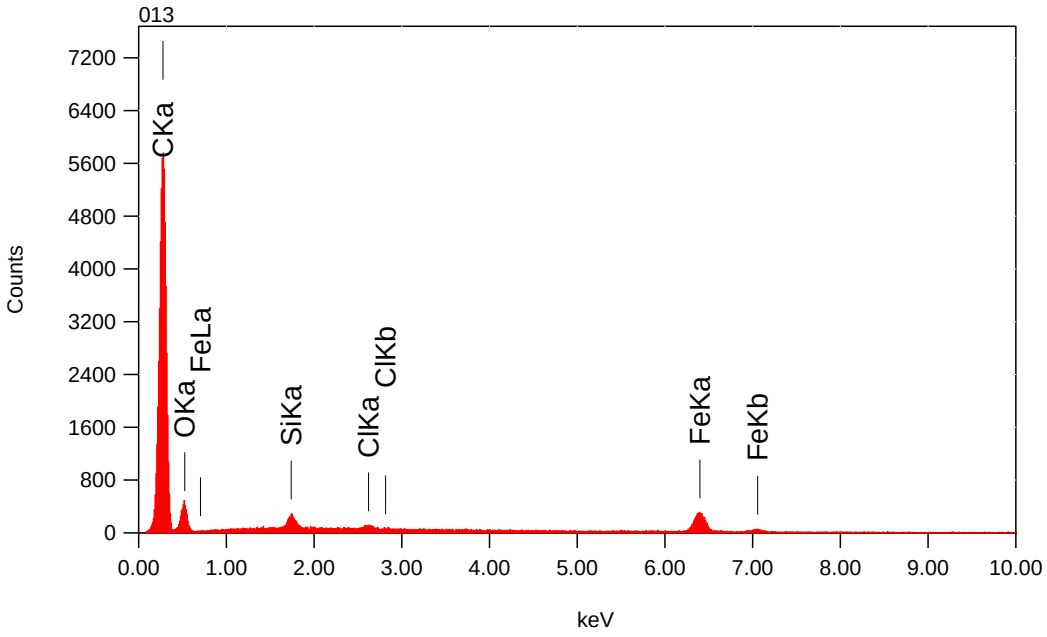


```
Acquisition Parameter
Instrument    : 7000F
Acc. Voltage  : 20.0 kV
Probe Current: 0.59000 nA
PHA mode      : T3
Real Time     : 34.93 sec
Live Time     : 30.00 sec
Dead Time     : 14 %
Counting Rate: 3140 cps
Energy Range :  0 - 20 keV
```

ZAF Method Standardless Quantitative Analysis
Fitting Coefficient : 0.2387

Element	(keV)	mass%	Error%	At%	Compound	mass%	Cation	K
C K	0.277	75.9	0.1	84.1				79.2187
O K	0.525	16.8	0.5	14.0				9.3400
Si K	1.739	0.8	0.1	0.4				1.1409
Cl K*	2.621	0.2	0.1	0.1				0.4512
Fe K	6.398	6.3	0.4	1.5				9.8493
Total		100.0		100.0				

2035m Fissure filling

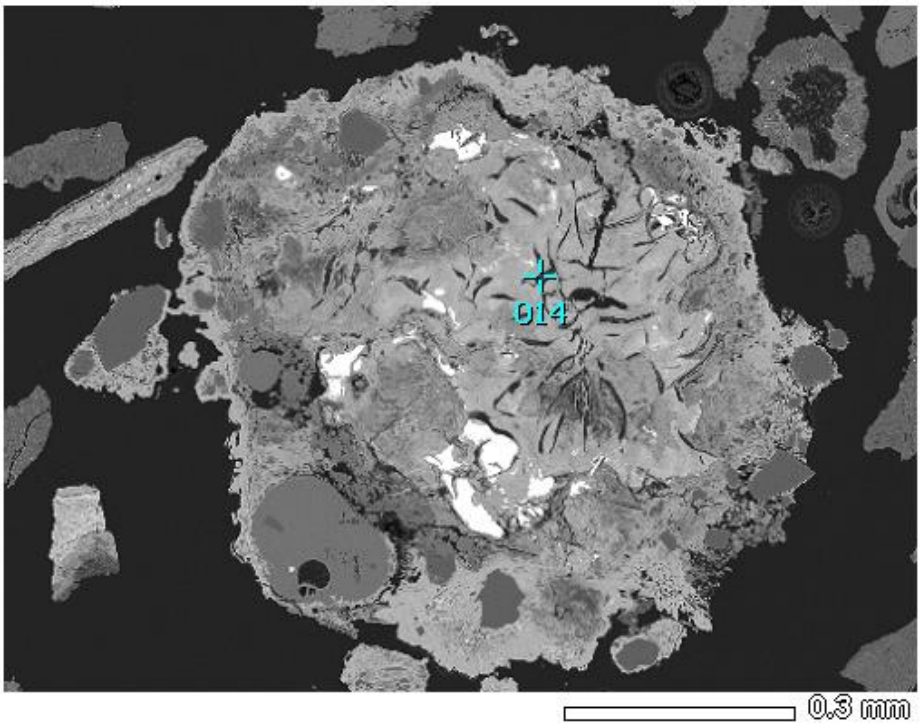


```
Title        : IMG1
-------------------------
Instrument   : 7000F
Volt         : 20.00 kV
Mag          : x 100
Date         : 2014/02/11
Pixel        : 512 x 384
```

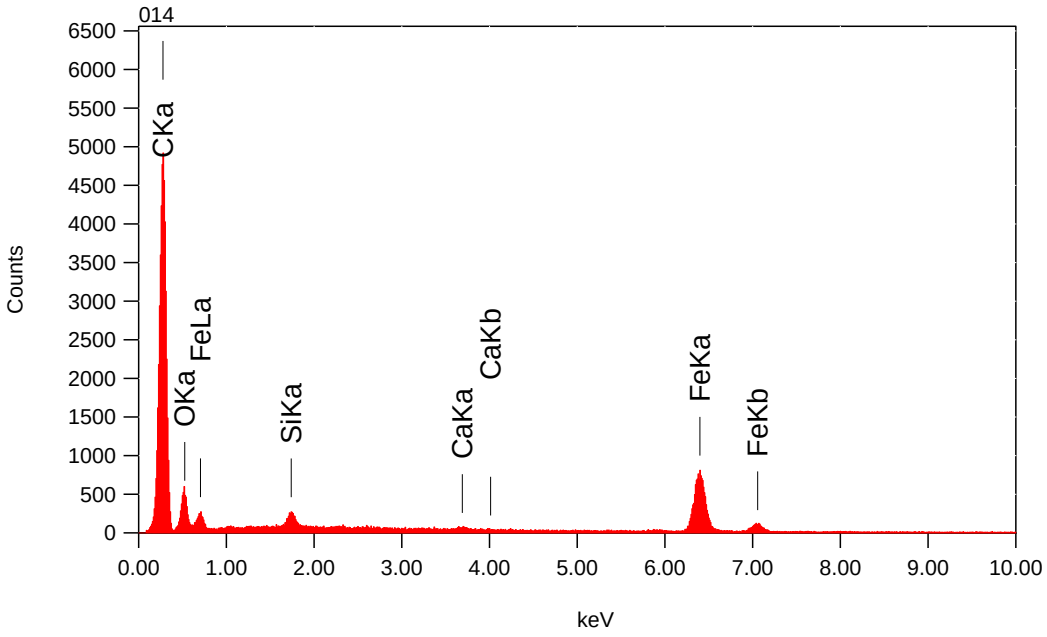


```
Acquisition Parameter
Instrument   : 7000F
Acc. Voltage : 20.0 kV
Probe Current: 0.59000 nA
PHA mode     : T3
Real Time    : 35.48 sec
Live Time    : 30.00 sec
Dead Time    : 15 %
Counting Rate: 3420 cps
Energy Range :  0 - 20 keV
```

ZAF Method Standardless Quantitative Analysis
Fitting Coefficient : 0.2161

Element	(keV)	mass%	Error%	At%	Compound	mass%	Cation	K
C K	0.277	67.9	0.1	81.0				62.9167
O K	0.525	16.6	0.3	14.9				11.2195
Si K	1.739	0.7	0.1	0.4				1.0496
Ca K*	3.690	0.2	0.1	0.1				0.3837
Fe K	6.398	14.6	0.3	3.7				24.4305
Total		100.0		100.0				

2035m Fissure filling

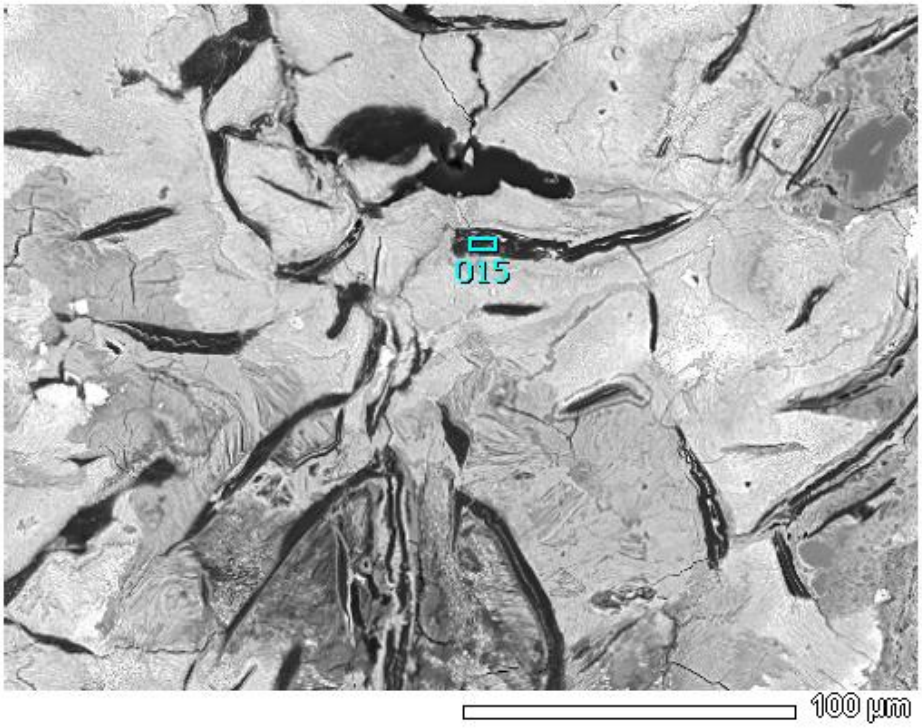


```
Title        : IMG1
--------------------------
Instrument   : 7000F
Volt         : 20.00 kV
Mag          : x 430
Date         : 2014/02/11
Pixel        : 512 x 384
```

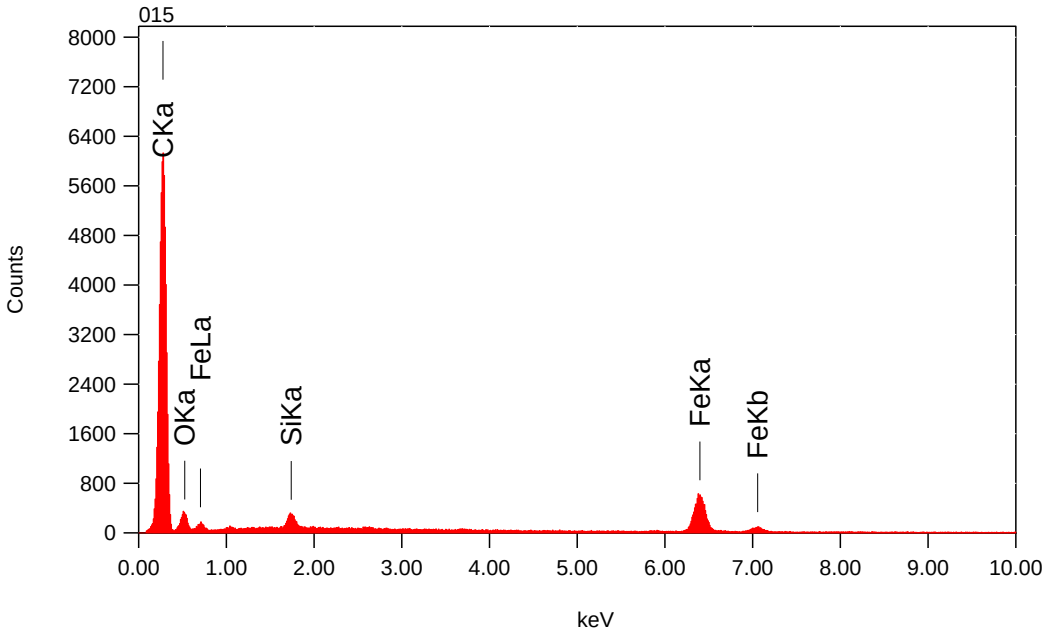


```
Acquisition Parameter
Instrument    : 7000F
Acc. Voltage  : 20.0 kV
Probe Current: 0.59000 nA
PHA mode      : T3
Real Time     : 35.65 sec
Live Time     : 30.00 sec
Dead Time     : 16 %
Counting Rate: 3609 cps
Energy Range :  0 - 20 keV
```

ZAF Method Standardless Quantitative Analysis
Fitting Coefficient : 0.2354

Element	(keV)	mass%	Error%	At%	Compound	mass%	Cation	K
C K	0.277	76.5	0.1	87.2				74.7194
O K	0.525	11.1	0.5	9.5				6.1235
Si K	1.739	0.9	0.1	0.4				1.2622
Fe K	6.398	11.4	0.3	2.8				17.8949
Total		100.0		100.0				

2035m Fissure filling

Title : IMG1

Instrument : 7000F
Volt : 20.00 kV
Mag : x 430
Date : 2014/02/11
Pixel : 512 x 384

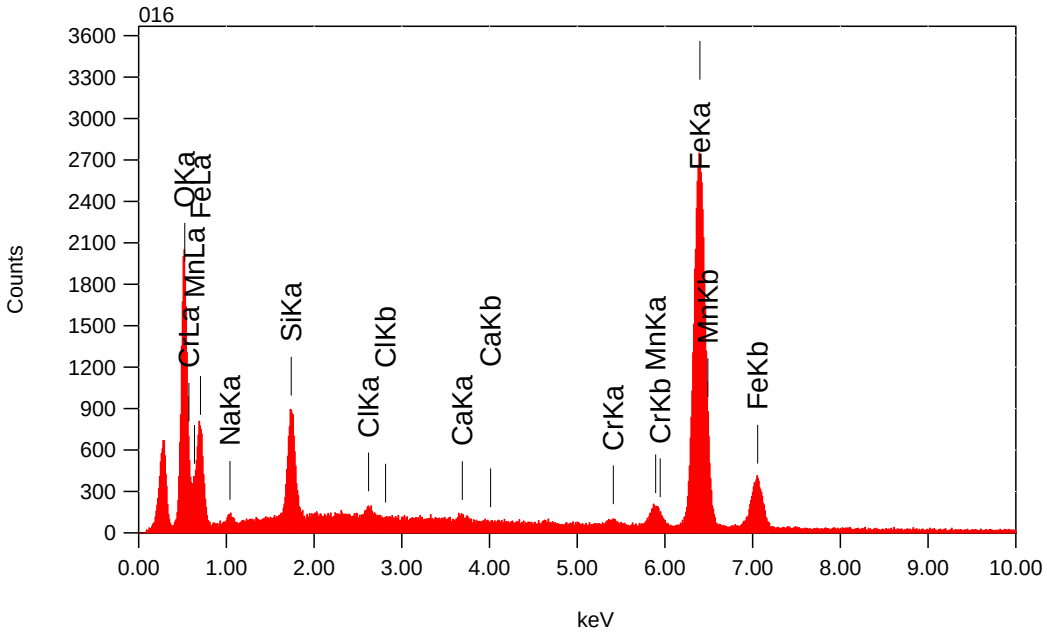

Acquisition Parameter
Instrument : 7000F
Acc. Voltage : 20.0 kV
Probe Current: 0.59000 nA
PHA mode : T3
Real Time : 40.75 sec
Live Time : 30.00 sec
Dead Time : 26 %
Counting Rate: 5588 cps
Energy Range : 0 - 20 keV

ZAF Method Standardless Quantitative Analysis
Fitting Coefficient : 0.1698

Element	(keV)	mass%	Error%	At%	Compound	mass%	Cation	K
O K	0.525	21.3	0.1	46.1				27.3155
Na K*	1.041	1.4	0.2	2.1				0.4702
Si K	1.739	5.7	0.1	7.0				3.3753
Cl K*	2.621	0.5	0.1	0.5				0.4766
Ca K*	3.690	0.4	0.1	0.3				0.4231
Cr K*	5.411	0.6	0.2	0.4				0.6201
Mn K*	5.894	2.9	0.2	1.8				2.7066
Fe K	6.398	67.3	0.3	41.8				64.6125
Total		100.0		100.0				

2035m Fissure filling

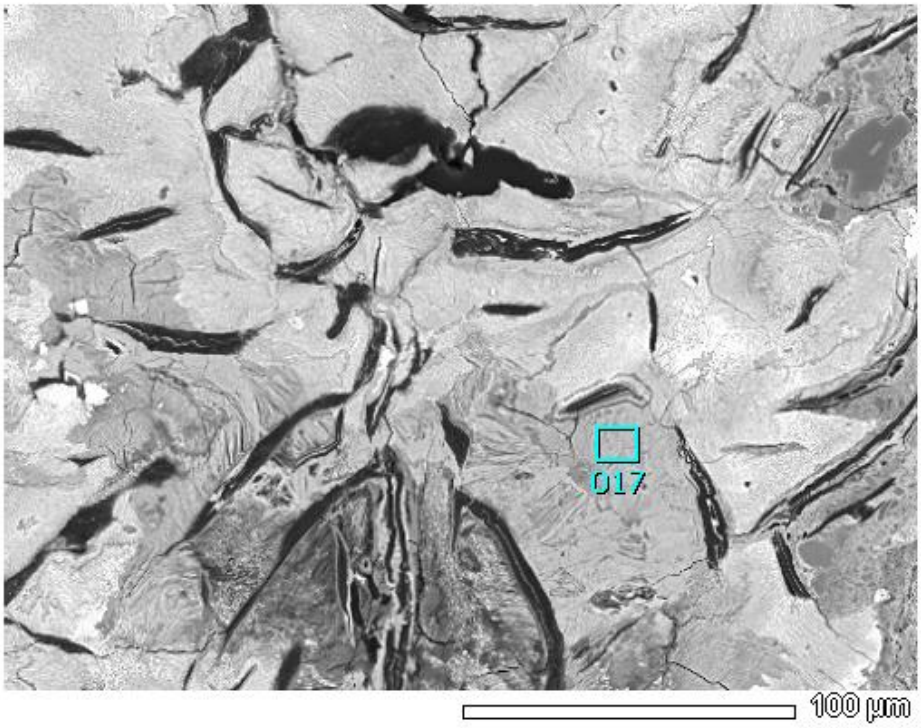


```
Title          : IMG1
---------------------------
Instrument     : 7000F
Volt           : 20.00 kV
Mag            : x 430
Date           : 2014/02/11
Pixel          : 512 x 384
```

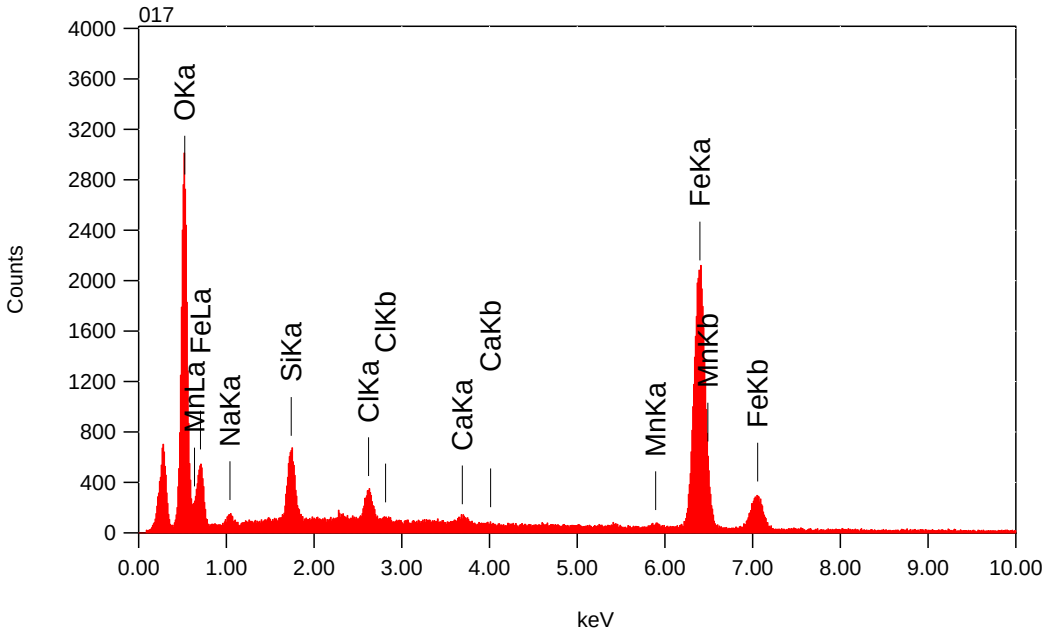


```
Acquisition Parameter
Instrument    : 7000F
Acc. Voltage  : 20.0 kV
Probe Current: 0.59000 nA
PHA mode      : T3
Real Time     : 39.39 sec
Live Time     : 30.00 sec
Dead Time     : 23 %
Counting Rate: 4930 cps
Energy Range :  0 - 20 keV
```

ZAF Method Standardless Quantitative Analysis
Fitting Coefficient : 0.2013

Element	(keV)	mass%	Error%	At%	Compound	mass%	Cation	K
O K	0.525	34.8	0.1	62.5				43.4133
Na K*	1.041	1.5	0.3	1.9				0.5205
Si K	1.739	4.3	0.1	4.4				2.4823
Cl K*	2.621	1.9	0.1	1.5				1.6984
Ca K*	3.690	0.4	0.1	0.3				0.4625
Mn K*	5.894	0.5	0.3	0.3				0.4824
Fe K	6.398	56.6	0.3	29.1				50.9406
Total		100.0		100.0				

2035m Fissure filling


```
Title          : IMG1
---------------------------
Instrument     : 7000F
Volt           : 20.00 kV
Mag            : x 430
Date           : 2014/02/11
Pixel          : 512 x 384
```

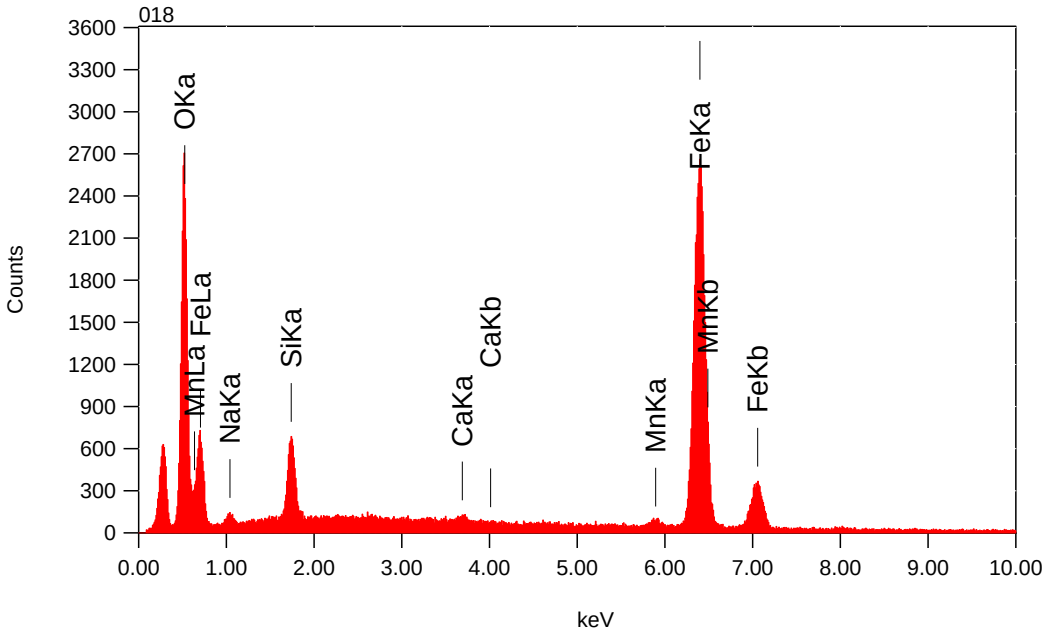


```
Acquisition Parameter
Instrument    : 7000F
Acc. Voltage  : 20.0 kV
Probe Current: 0.59000 nA
PHA mode      : T3
Real Time     : 40.06 sec
Live Time     : 30.00 sec
Dead Time     : 24 %
Counting Rate: 5244 cps
Energy Range :  0 - 20 keV
```

ZAF Method Standardless Quantitative Analysis
Fitting Coefficient : 0.1839

Element	(keV)	mass%	Error%	At%	Compound	mass%	Cation	K
O K	0.525	28.0	0.1	55.7				36.2292
Na K*	1.041	1.2	0.2	1.6				0.3782
Si K	1.739	4.2	0.1	4.8				2.4024
Ca K*	3.690	0.4	0.1	0.3				0.3964
Mn K*	5.894	0.8	0.3	0.5				0.7460
Fe K	6.398	65.4	0.3	37.2				59.8478
Total		100.0		100.0				

2035m Aluminium

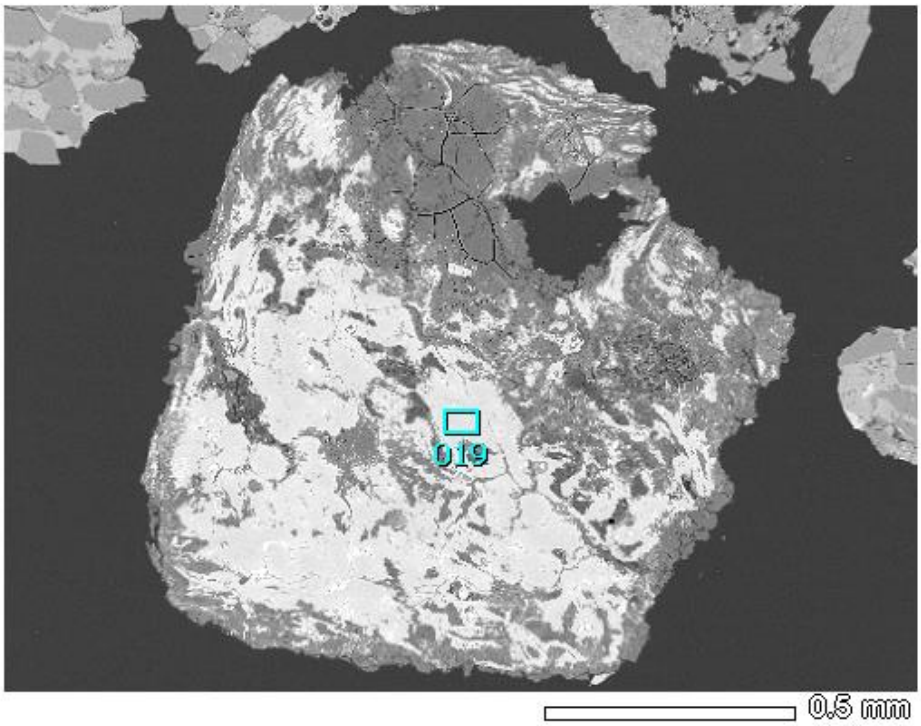


```
Title        : IMG1
--------------------------
Instrument   : 7000F
Volt         : 20.00 kV
Mag          : x 65
Date         : 2014/02/11
Pixel        : 512 x 384
```

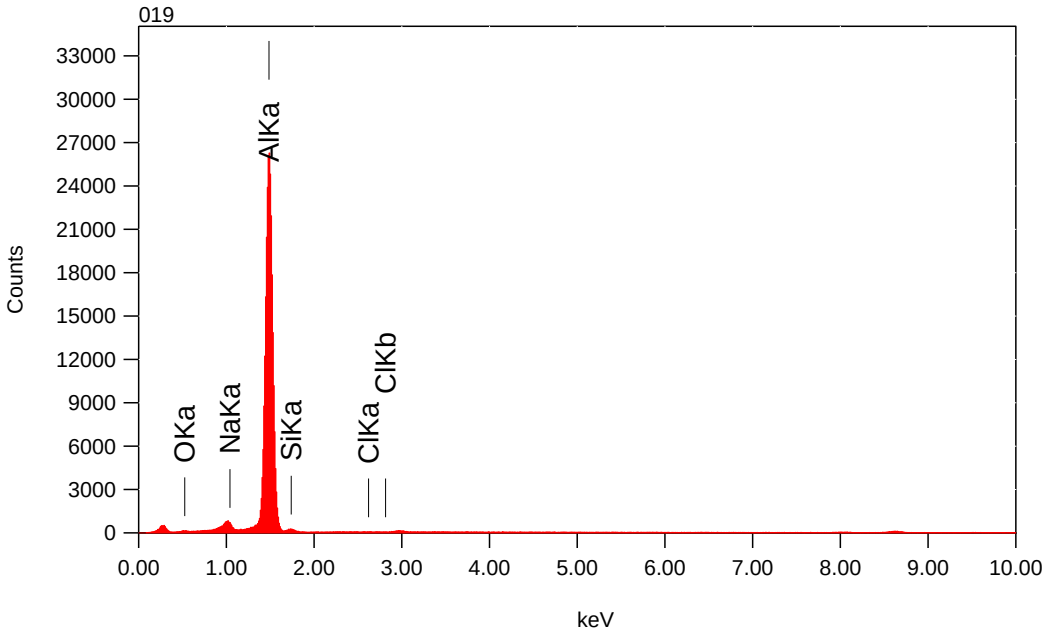


```
Acquisition Parameter
Instrument    : 7000F
Acc. Voltage  : 20.0 kV
Probe Current: 0.59000 nA
PHA mode      : T3
Real Time     : 56.26 sec
Live Time     : 30.00 sec
Dead Time     : 46 %
Counting Rate: 11204 cps
Energy Range :  0 - 20 keV
```

ZAF Method Standardless Quantitative Analysis
Fitting Coefficient : 0.1401

Element	(keV)	mass%	Error%	At%	Compound	mass%	Cation	K
O K	0.525	1.4	0.4	2.4				1.0022
Na K	1.041	1.4	0.2	1.7				1.9148
Al K	1.486	94.1	0.2	93.0				95.8916
Si K*	1.739	3.0	0.5	2.9				1.1728
Cl K	2.621	0.0	0.3	0.0				0.0185
Total		100.0		100.0				

2035m Aluminium

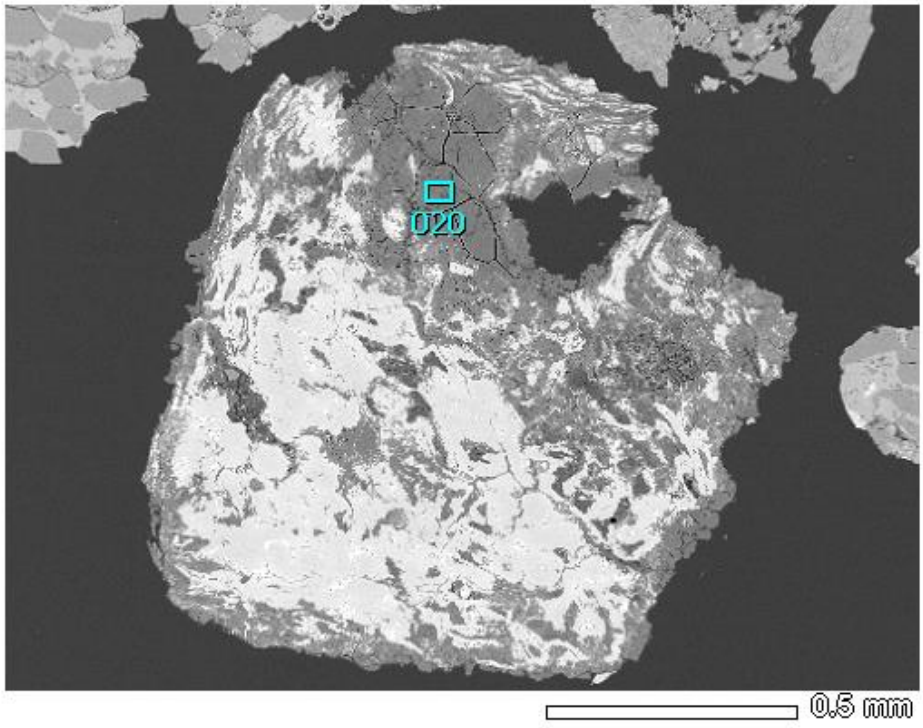


```
Title        : IMG1
--------------------------
Instrument   : 7000F
Volt         : 20.00 kV
Mag          : x 65
Date         : 2014/02/11
Pixel        : 512 x 384
```

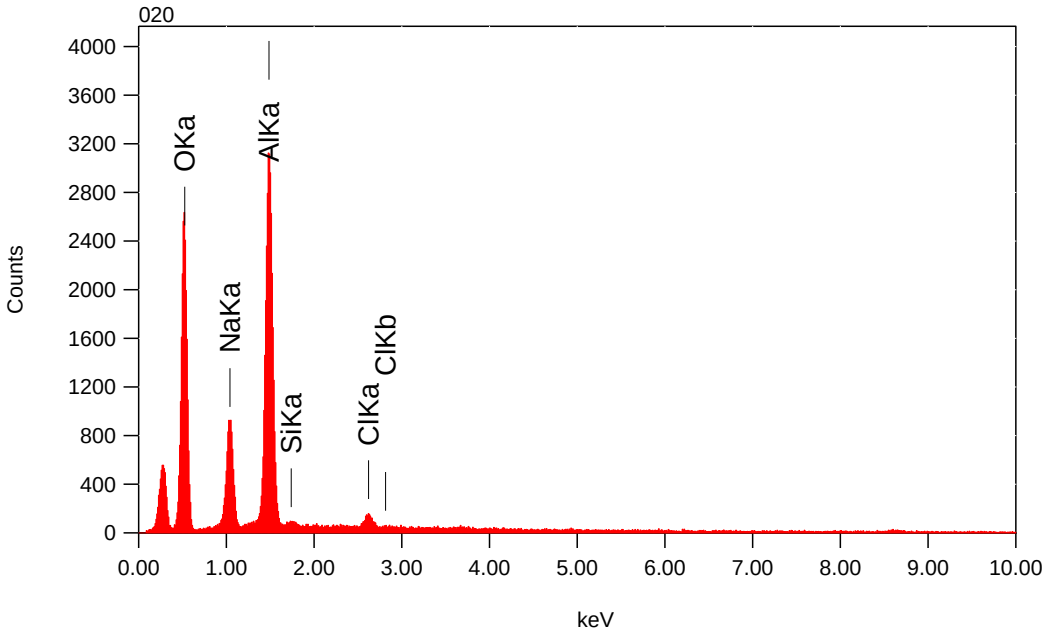


```
Acquisition Parameter
Instrument    : 7000F
Acc. Voltage  : 20.0 kV
Probe Current: 0.59000 nA
PHA mode      : T3
Real Time     : 35.96 sec
Live Time     : 30.00 sec
Dead Time     : 16 %
Counting Rate: 3262 cps
Energy Range :  0 - 20 keV
```

ZAF Method Standardless Quantitative Analysis
Fitting Coefficient : 0.2039

Element	(keV)	mass%	Error%	At%	Compound	mass%	Cation	K
O K	0.525	53.6	0.2	65.2				67.2502
Na K	1.041	12.4	0.2	10.5				9.4985
Al K	1.486	32.2	0.1	23.2				21.6760
Si K*	1.739	0.6	0.2	0.4				0.3125
Cl K	2.621	1.4	0.1	0.7				1.2628
Total		100.0		100.0				

2035m Aluminium

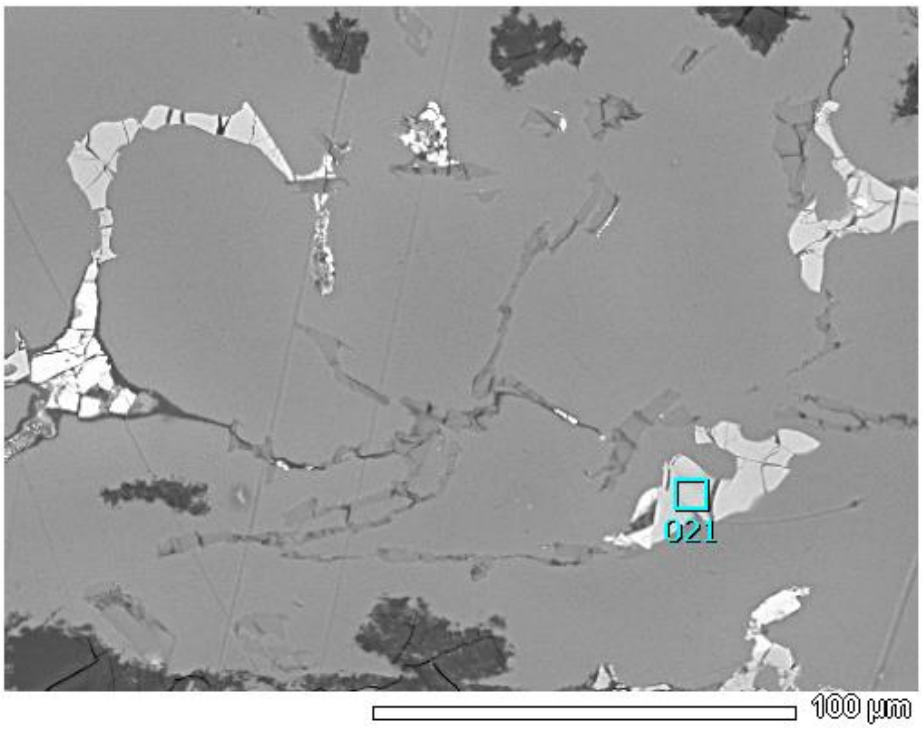


```
Title        : IMG1
--------------------------
Instrument   : 7000F
Volt         : 20.00 kV
Mag          : x 550
Date         : 2014/02/11
Pixel        : 512 x 384
```

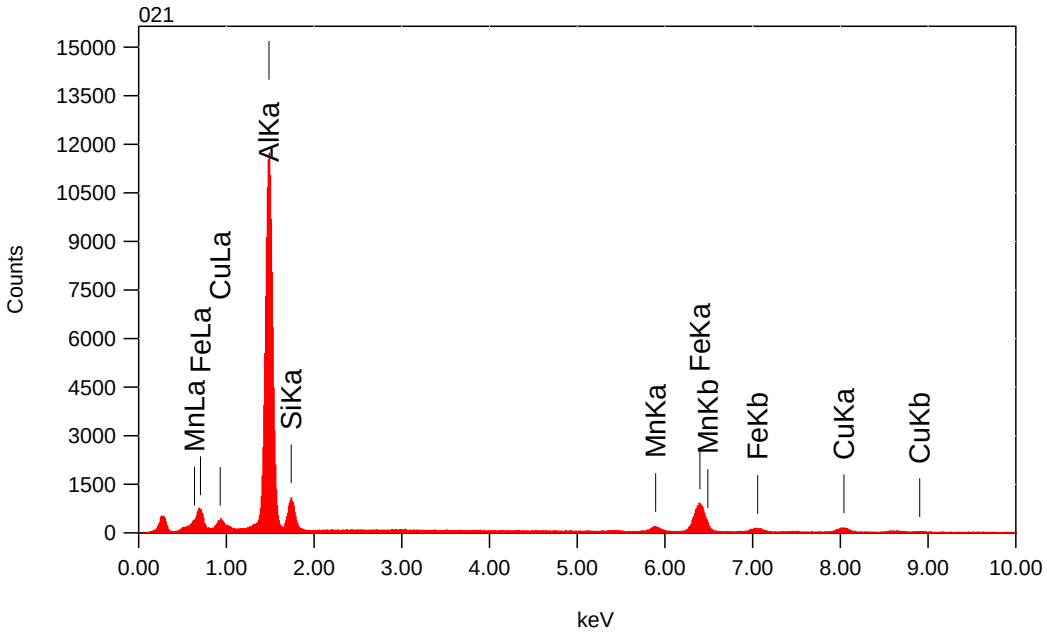


```
Acquisition Parameter
Instrument    : 7000F
Acc. Voltage  : 20.0 kV
Probe Current: 0.59000 nA
PHA mode      : T3
Real Time     : 45.58 sec
Live Time     : 30.00 sec
Dead Time     : 34 %
Counting Rate: 7550 cps
Energy Range :  0 - 20 keV
```

ZAF Method Standardless Quantitative Analysis
Fitting Coefficient : 0.1594

Element	(keV)	mass%	Error%	At%	Compound	mass%	Cation	K
Al K	1.486	60.8	0.1	72.6				57.4453
Si K	1.739	9.2	0.2	10.6				5.6428
Mn K	5.894	2.9	0.4	1.7				3.5437
Fe K	6.398	20.8	0.4	12.0				26.1244
Cu K	8.040	6.2	0.8	3.1				7.2438
Total		100.0		100.0				

2035m Aluminium

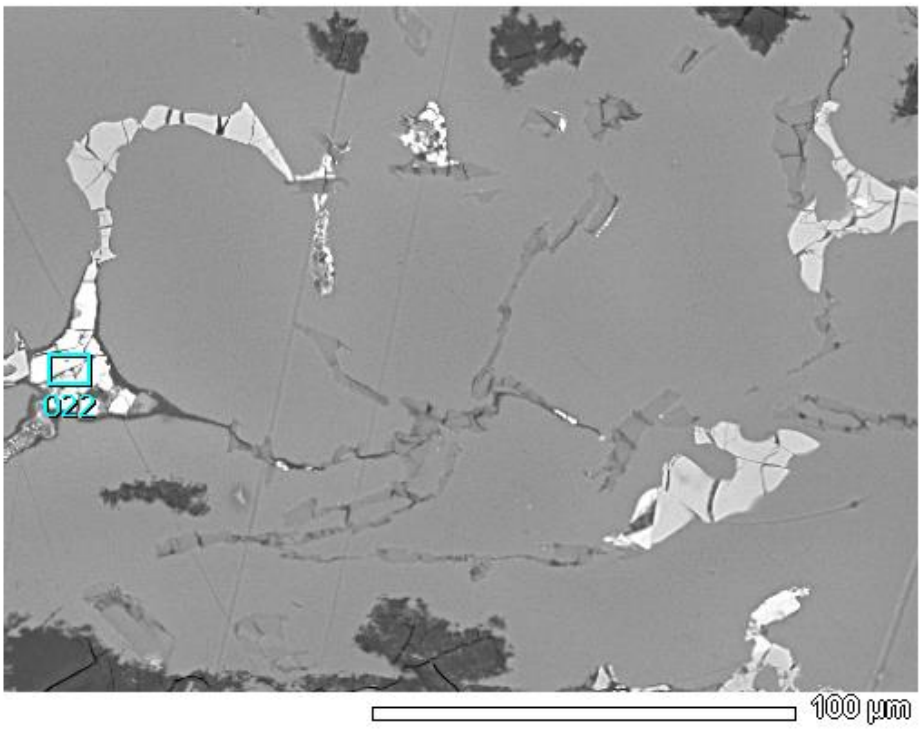


```
Title        : IMG1
--------------------------
Instrument   : 7000F
Volt         : 20.00 kV
Mag          : x 550
Date         : 2014/02/11
Pixel        : 512 x 384
```

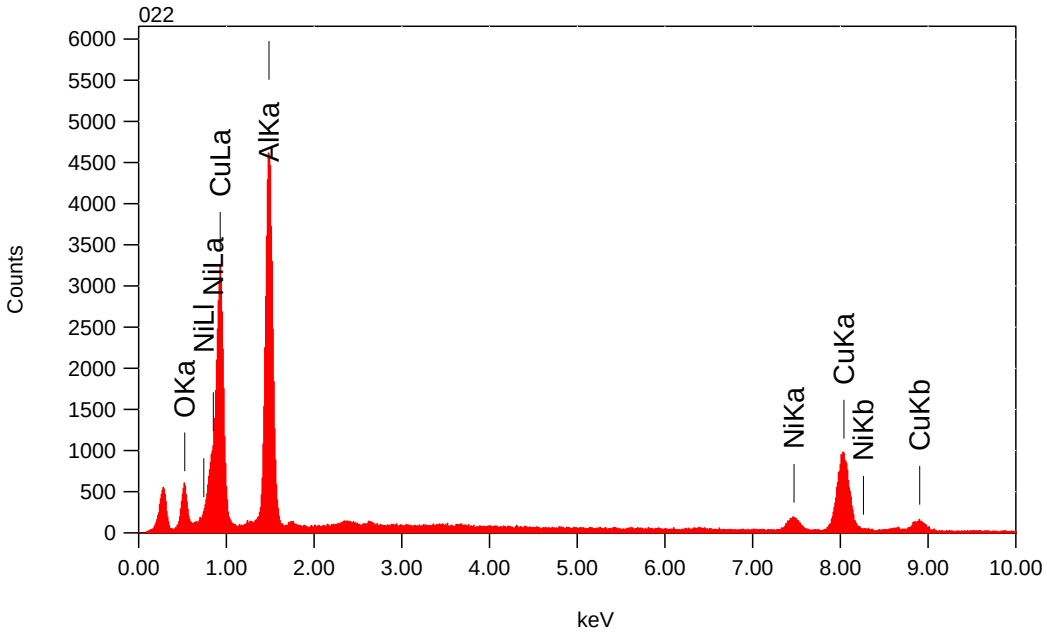


```
Acquisition Parameter
Instrument   : 7000F
Acc. Voltage : 20.0 kV
Probe Current: 0.59000 nA
PHA mode     : T3
Real Time    : 42.14 sec
Live Time    : 30.00 sec
Dead Time    : 28 %
Counting Rate: 6196 cps
Energy Range :  0 - 20 keV
```

ZAF Method Standardless Quantitative Analysis
Fitting Coefficient : 0.1942

Element	(keV)	mass%	Error%	At%	Compound	mass%	Cation	K
O K	0.525	8.3	0.1	18.6				10.1430
Al K	1.486	39.1	0.1	51.6				24.6739
Ni K	7.471	6.0	0.4	3.7				7.8080
Cu K	8.040	46.5	0.5	26.1				57.3751
Total		100.0		100.0				

2035m Aluminium

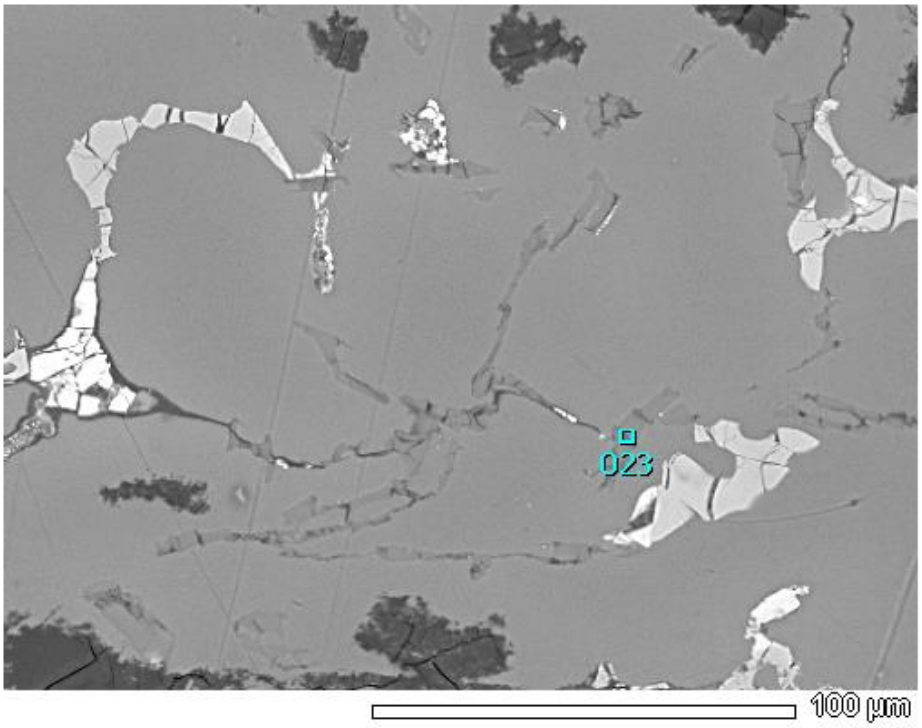


```
Title        : IMG1
--------------------------
Instrument   : 7000F
Volt         : 20.00 kV
Mag          : x 550
Date         : 2014/02/11
Pixel        : 512 x 384
```

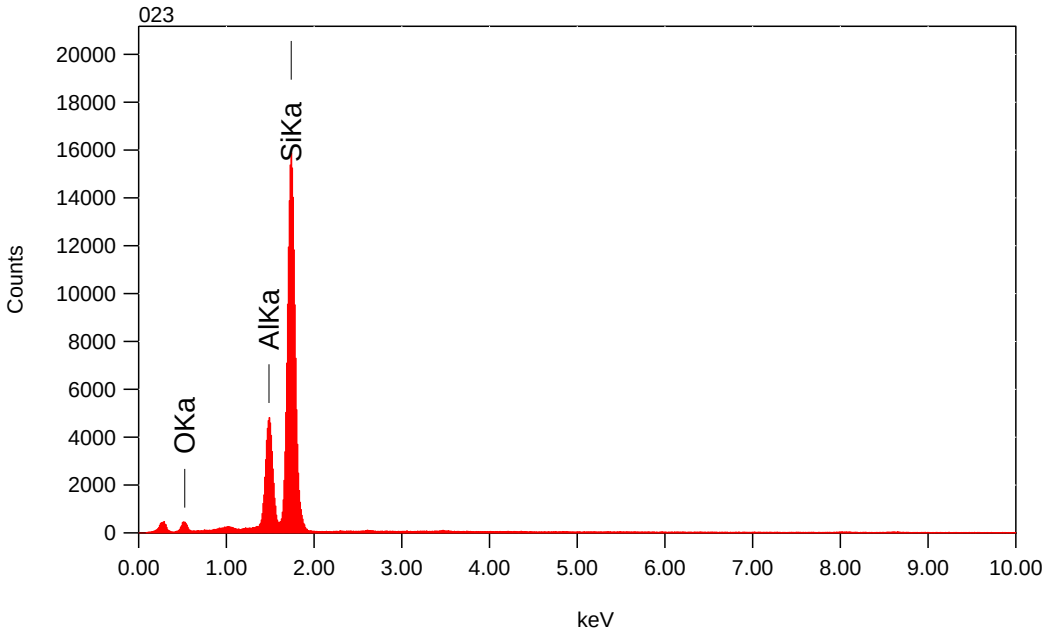


```
Acquisition Parameter
Instrument    : 7000F
Acc. Voltage  : 20.0 kV
Probe Current: 0.59000 nA
PHA mode      : T3
Real Time     : 50.43 sec
Live Time     : 30.00 sec
Dead Time     : 41 %
Counting Rate: 9699 cps
Energy Range :  0 - 20 keV
```

ZAF Method Standardless Quantitative Analysis
Fitting Coefficient : 0.1323

Element	(keV)	mass%	Error%	At%	Compound	mass%	Cation	K
O K	0.525	9.3	0.3	15.2				6.6449
Al K	1.486	16.8	0.1	16.3				19.7822
Si K	1.739	73.8	0.1	68.5				73.5729
Total		100.0		100.0				

2035m Iron oxide

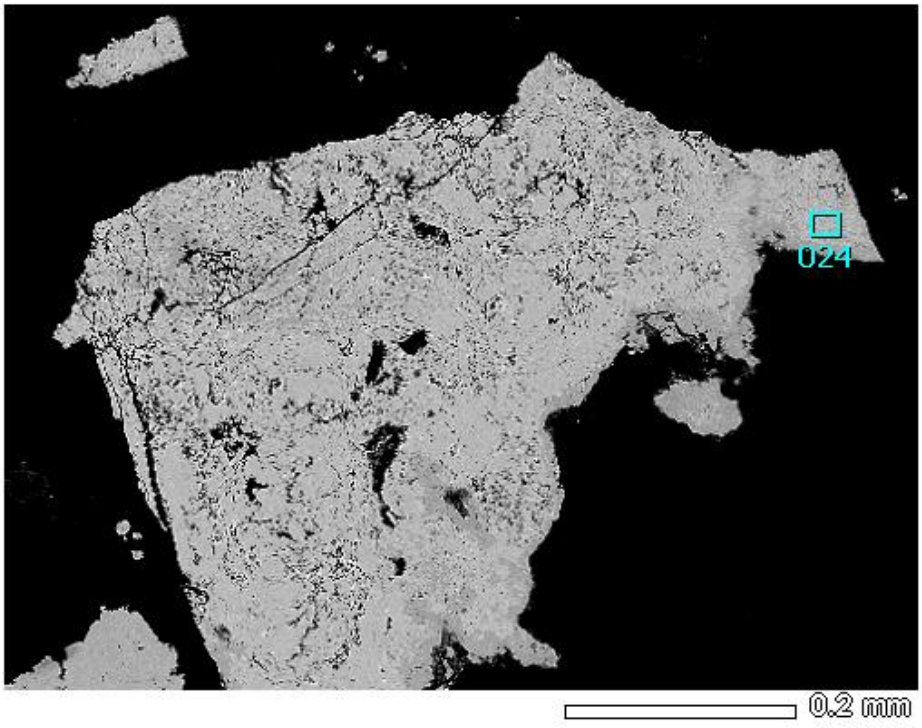


```
Title        : IMG1
--------------------------
Instrument   : 7000F
Volt         : 20.00 kV
Mag          : x 150
Date         : 2014/02/11
Pixel        : 512 x 384
```

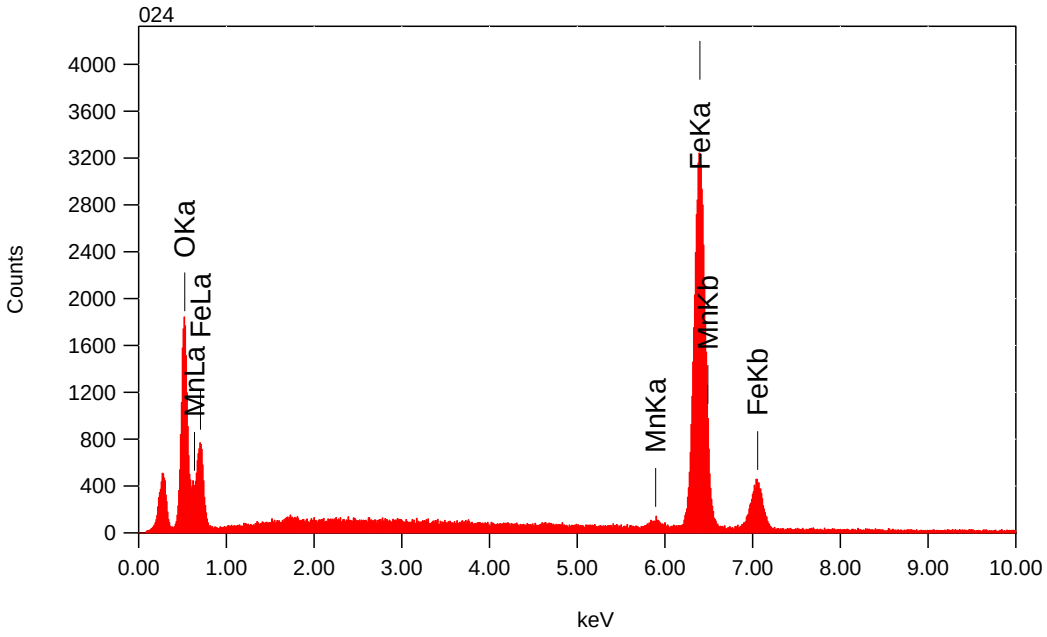


```
Acquisition Parameter
Instrument    : 7000F
Acc. Voltage  : 20.0 kV
Probe Current: 0.59000 nA
PHA mode      : T3
Real Time     : 39.93 sec
Live Time     : 30.00 sec
Dead Time     : 24 %
Counting Rate: 5161 cps
Energy Range :  0 - 20 keV
```

ZAF Method Standardless Quantitative Analysis
Fitting Coefficient : 0.1626

Element	(keV)	mass%	Error%	At%	Compound	mass%	Cation	K
O K	0.525	18.6	0.1	44.4				24.7028
Mn K*	5.894	1.0	0.2	0.7				0.8769
Fe K	6.398	80.4	0.2	55.0				74.4203
Total		100.0		100.0				

2035m Iron oxide

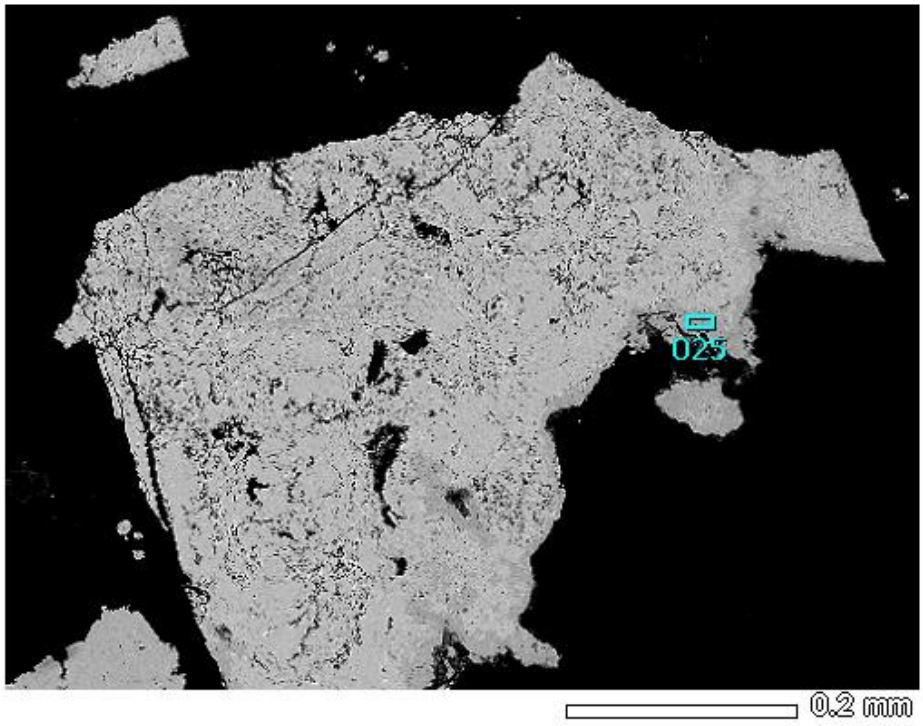


```
Title        : IMG1
--------------------------
Instrument   : 7000F
Volt         : 20.00 kV
Mag          : x 150
Date         : 2014/02/11
Pixel        : 512 x 384
```

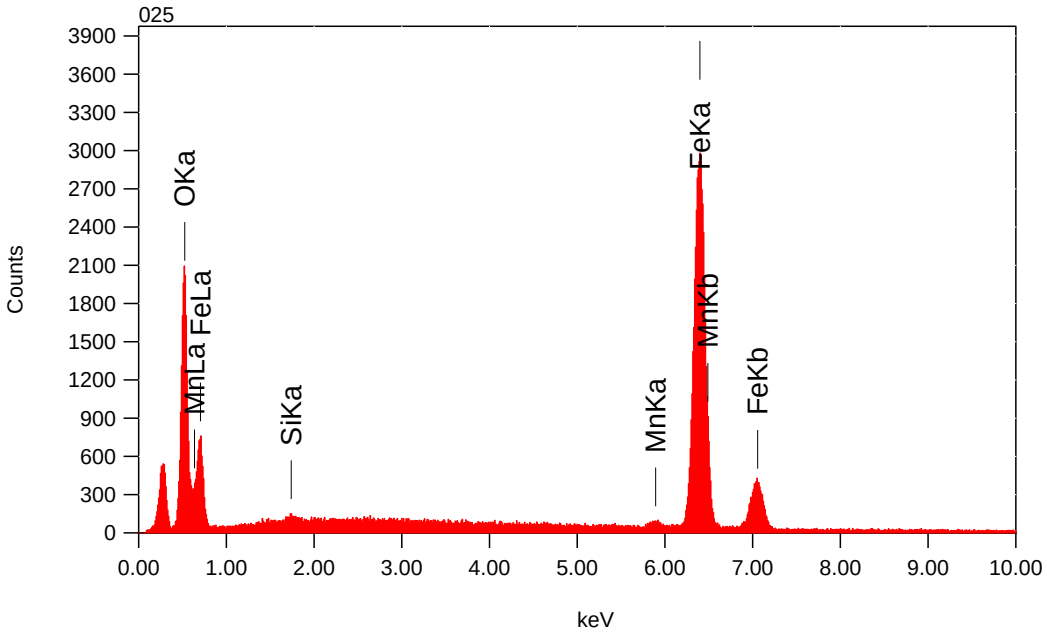


```
Acquisition Parameter
Instrument   : 7000F
Acc. Voltage : 20.0 kV
Probe Current: 0.59000 nA
PHA mode     : T3
Real Time    : 39.70 sec
Live Time    : 30.00 sec
Dead Time    : 24 %
Counting Rate: 5030 cps
Energy Range :  0 - 20 keV
```

ZAF Method Standardless Quantitative Analysis
Fitting Coefficient : 0.1716

Element	(keV)	mass%	Error%	At%	Compound	mass%	Cation	K
O K	0.525	22.0	0.1	49.5				29.0711
Si K*	1.739	0.2	0.1	0.3				0.1288
Mn K*	5.894	0.7	0.2	0.5				0.6333
Fe K	6.398	77.1	0.2	49.7				70.1668
Total		100.0		100.0				

2035m Iron oxide

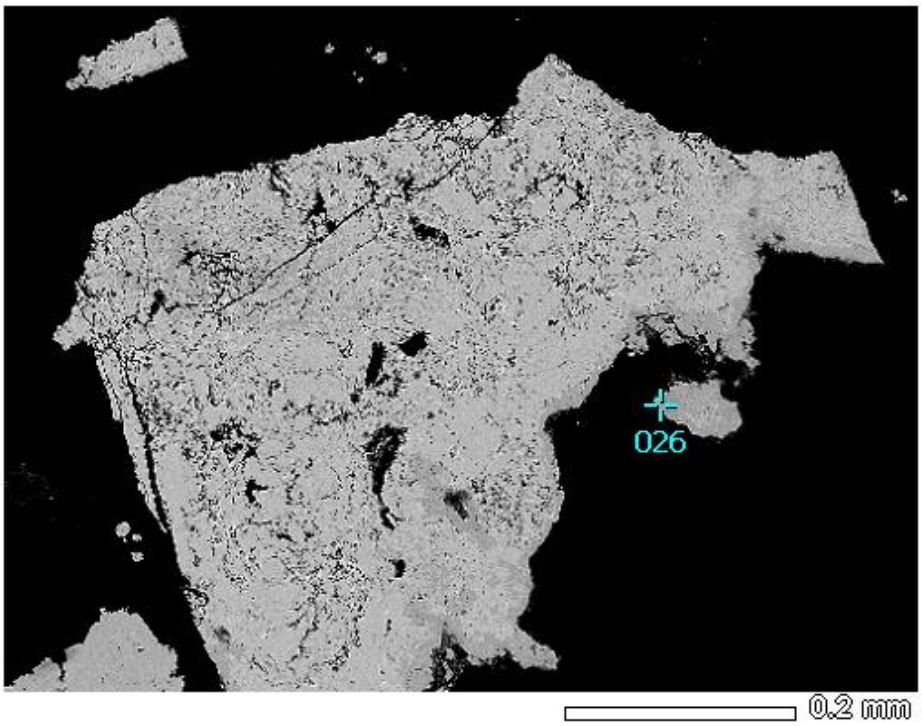


```
Title        : IMG1
--------------------------
Instrument   : 7000F
Volt         : 20.00 kV
Mag          : x 150
Date         : 2014/02/11
Pixel        : 512 x 384
```

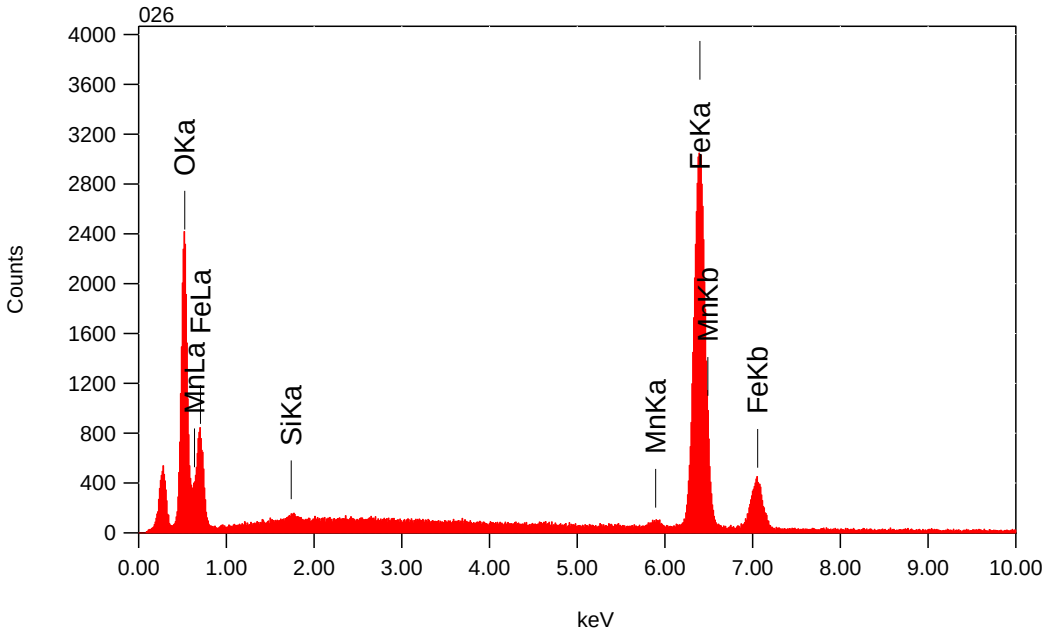


```
Acquisition Parameter
Instrument   : 7000F
Acc. Voltage : 20.0 kV
Probe Current: 0.59000 nA
PHA mode     : T3
Real Time    : 40.16 sec
Live Time    : 30.00 sec
Dead Time    : 24 %
Counting Rate: 5241 cps
Energy Range :  0 - 20 keV
```

ZAF Method Standardless Quantitative Analysis
Fitting Coefficient : 0.1712

Element	(keV)	mass%	Error%	At%	Compound	mass%	Cation	K
O K	0.525	24.1	0.1	52.5				31.8201
Si K*	1.739	0.2	0.1	0.3				0.1243
Mn K*	5.894	0.9	0.2	0.6				0.7678
Fe K	6.398	74.8	0.2	46.7				67.2878
Total		100.0		100.0				

2035m Iron oxide

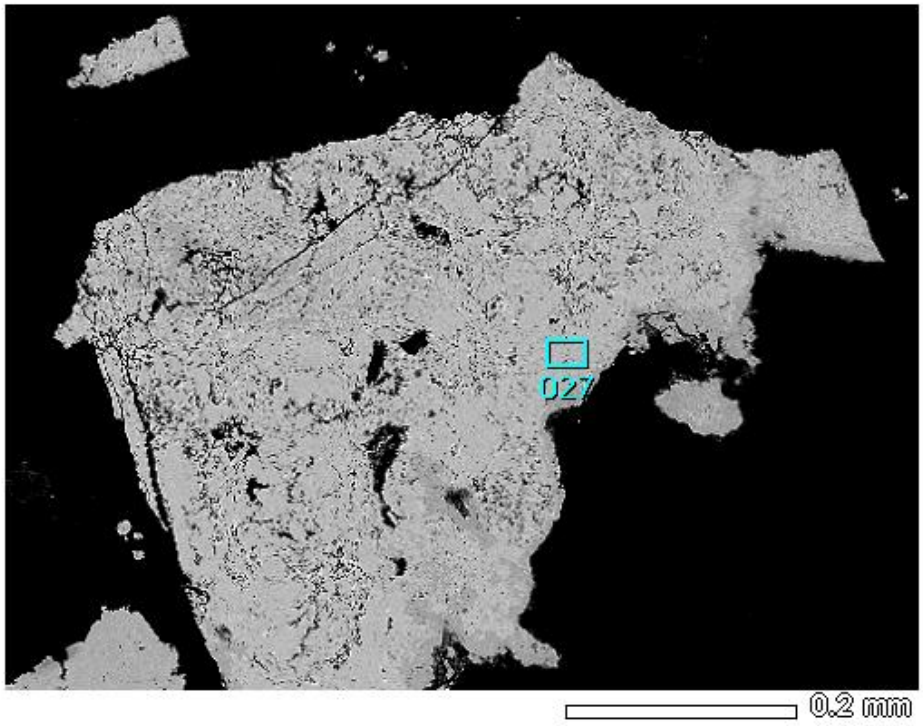


```
Title        : IMG1
--------------------------
Instrument   : 7000F
Volt         : 20.00 kV
Mag          : x 150
Date         : 2014/02/11
Pixel        : 512 x 384
```

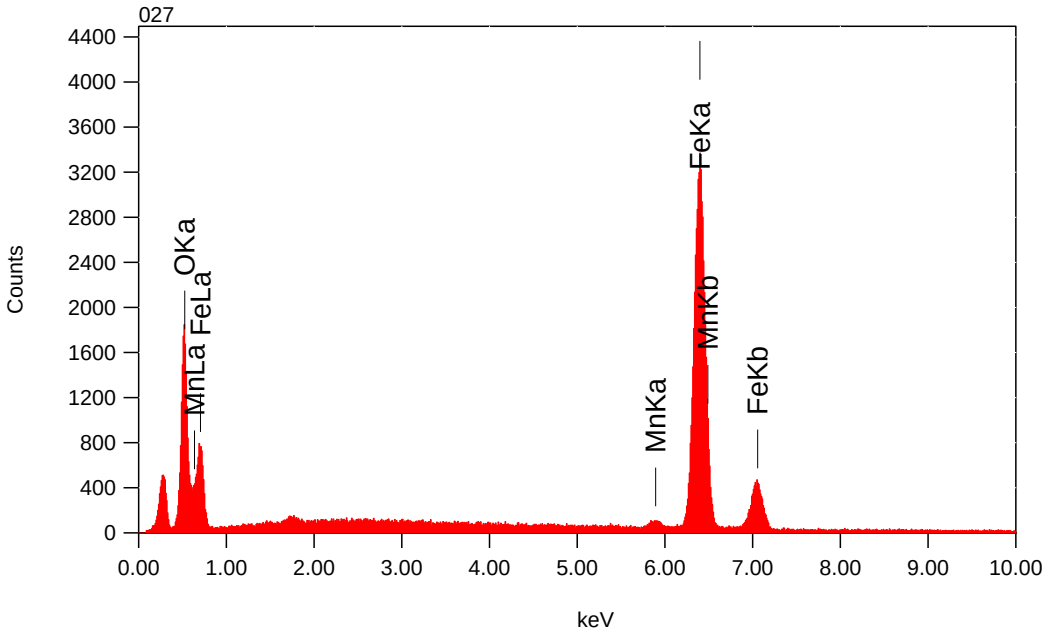


```
Acquisition Parameter
Instrument    : 7000F
Acc. Voltage  : 20.0 kV
Probe Current: 0.59000 nA
PHA mode      : T3
Real Time     : 40.01 sec
Live Time     : 30.00 sec
Dead Time     : 24 %
Counting Rate: 5182 cps
Energy Range :  0 - 20 keV
```

ZAF Method Standardless Quantitative Analysis
Fitting Coefficient : 0.1674

Element	(keV)	mass%	Error%	At%	Compound	mass%	Cation	K
O K	0.525	18.3	0.1	43.8				24.2641
Mn K	5.894	1.0	0.2	0.7				0.9094
Fe K	6.398	80.7	0.2	55.5				74.8264
Total		100.0		100.0				

2035m Fissure filling

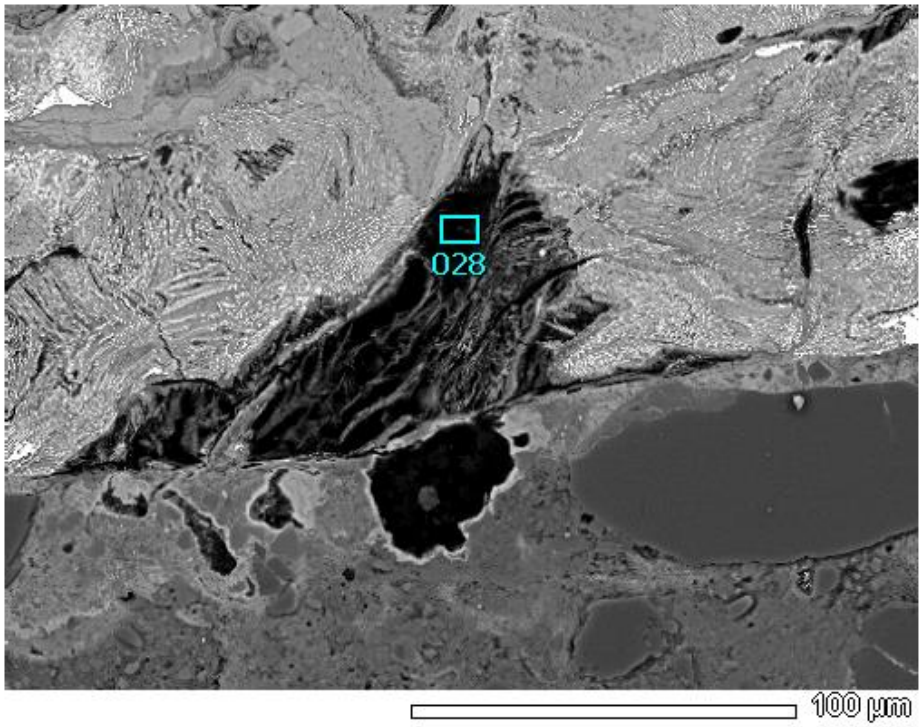


```
Title        : IMG1
-------------------------
Instrument   : 7000F
Volt         : 20.00 kV
Mag          : x 500
Date         : 2014/02/11
Pixel        : 512 x 384
```

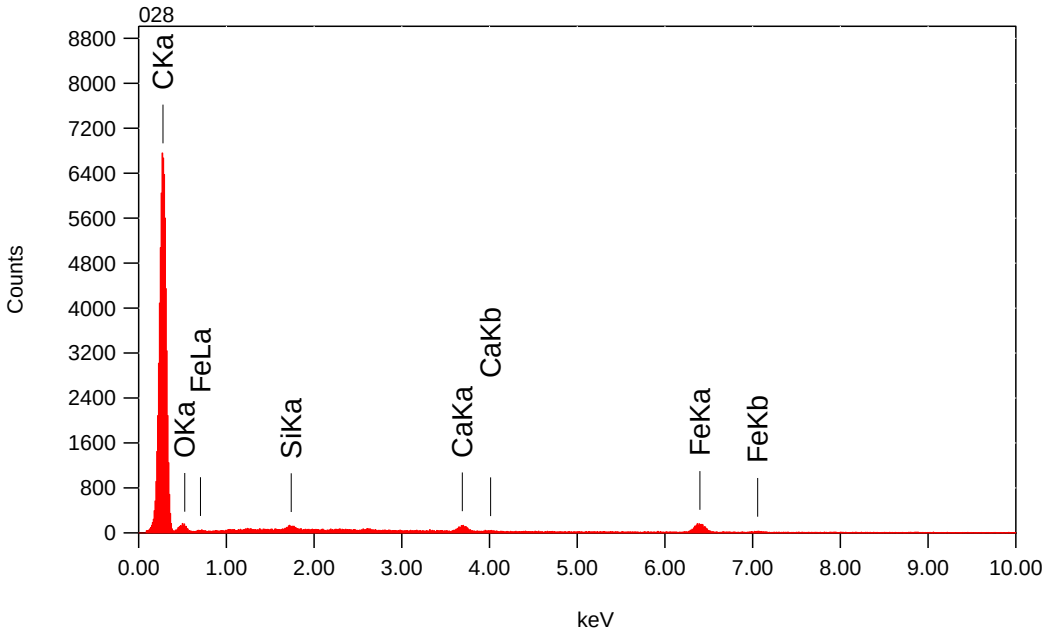


```
Acquisition Parameter
Instrument   : 7000F
Acc. Voltage : 20.0 kV
Probe Current: 0.59000 nA
PHA mode     : T3
Real Time    : 34.36 sec
Live Time    : 30.00 sec
Dead Time    : 12 %
Counting Rate: 2889 cps
Energy Range :  0 - 20 keV
```

ZAF Method Standardless Quantitative Analysis
Fitting Coefficient : 0.2420

Element	(keV)	mass%	Error%	At%	Compound	mass%	Cation	K
C K*	0.277	87.1	0.1	92.5				90.6590
O K	0.525	7.8	0.8	6.2				2.8216
Si K	1.739	0.3	0.1	0.1				0.3663
Ca K*	3.690	0.8	0.2	0.3				1.2896
Fe K	6.398	4.0	0.5	0.9				4.8636
Total		100.0		100.0				

2035m Fissure filling

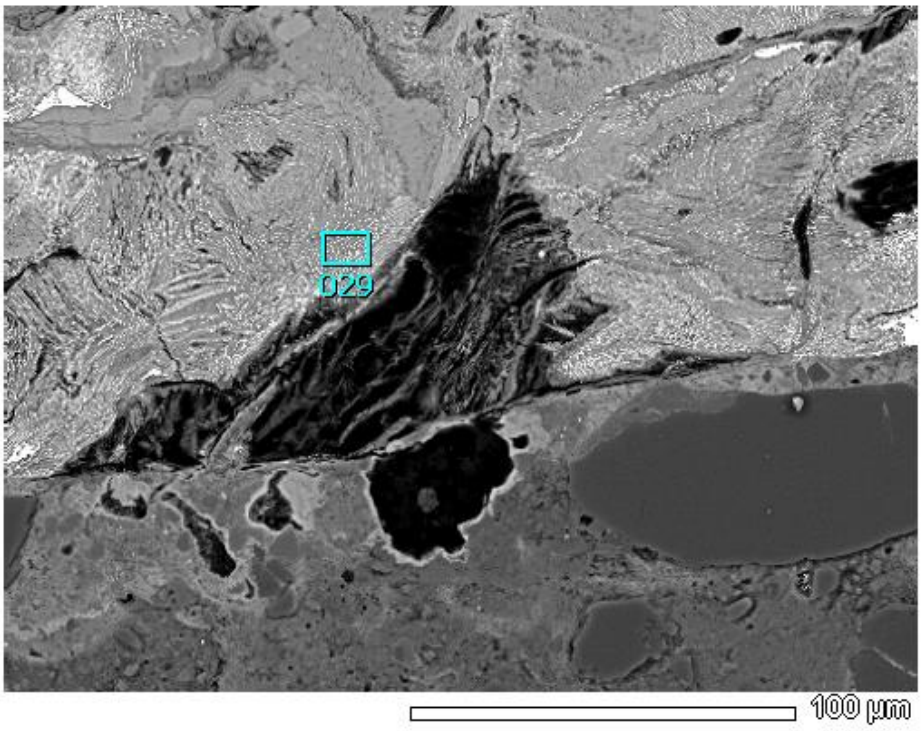


```
Title          : IMG1
---------------------------
Instrument     : 7000F
Volt           : 20.00 kV
Mag            : x 500
Date           : 2014/02/11
Pixel          : 512 x 384
```

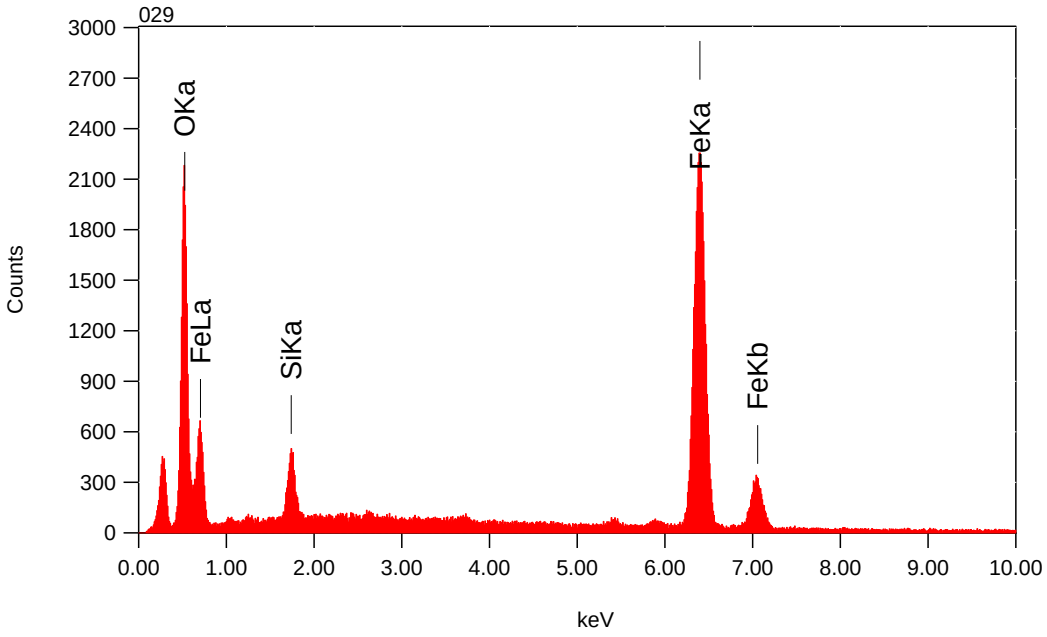


```
Acquisition Parameter
Instrument    : 7000F
Acc. Voltage  : 20.0 kV
Probe Current: 0.59000 nA
PHA mode      : T3
Real Time     : 38.27 sec
Live Time     : 30.00 sec
Dead Time     : 21 %
Counting Rate: 4445 cps
Energy Range :  0 - 20 keV
```

ZAF Method Standardless Quantitative Analysis
Fitting Coefficient : 0.2085

Element	(keV)	mass%	Error%	At%	Compound	mass%	Cation	K
O K	0.525	27.5	0.1	55.8				35.7008
Si K	1.739	3.5	0.1	4.1				1.9735
Fe K	6.398	69.0	0.3	40.1				62.3257
Total		100.0		100.0				

2035m Fissure filling

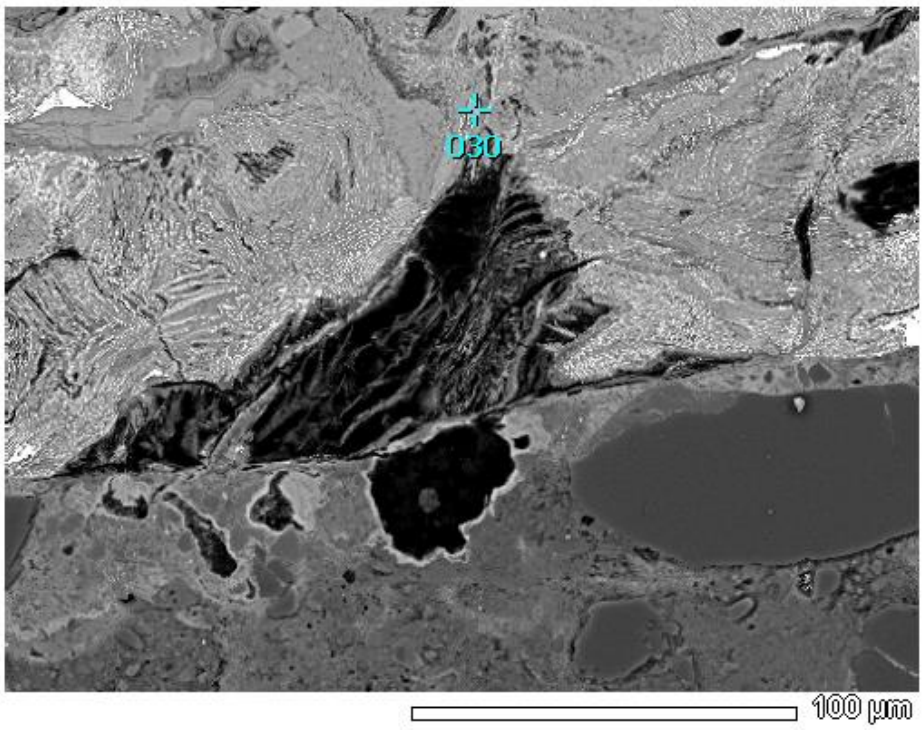


```
Title        : IMG1
--------------------------
Instrument   : 7000F
Volt         : 20.00 kV
Mag          : x 500
Date         : 2014/02/11
Pixel        : 512 x 384
```

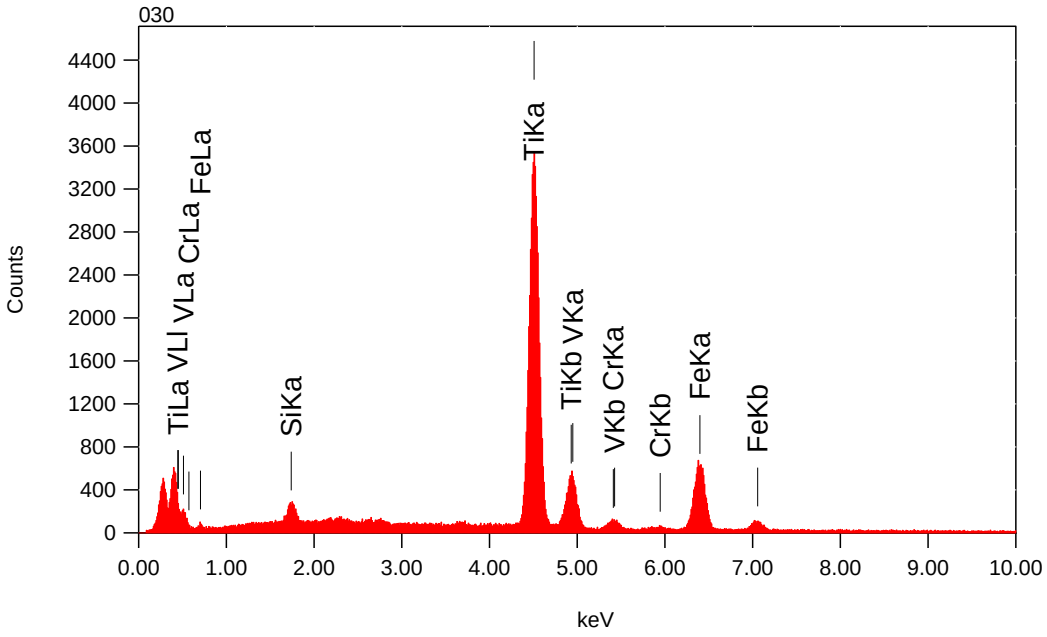


```
Acquisition Parameter
Instrument    : 7000F
Acc. Voltage  : 20.0 kV
Probe Current: 0.59000 nA
PHA mode      : T3
Real Time     : 38.80 sec
Live Time     : 30.00 sec
Dead Time     : 22 %
Counting Rate: 4639 cps
Energy Range :  0 - 20 keV
```

ZAF Method Standardless Quantitative Analysis
Fitting Coefficient : 0.1926

Element	(keV)	mass%	Error%	At%	Compound	mass%	Cation	K
Si K	1.739	1.7	0.1	3.1				1.2344
Ti K	4.508	67.0	0.2	69.0				69.6252
V K	4.949	2.0	0.2	1.9				2.0313
Cr K	5.411	2.1	0.3	2.0				1.8603
Fe K	6.398	27.2	0.4	24.0				25.2488
Total		100.0		100.0				

2055m Iron oxide

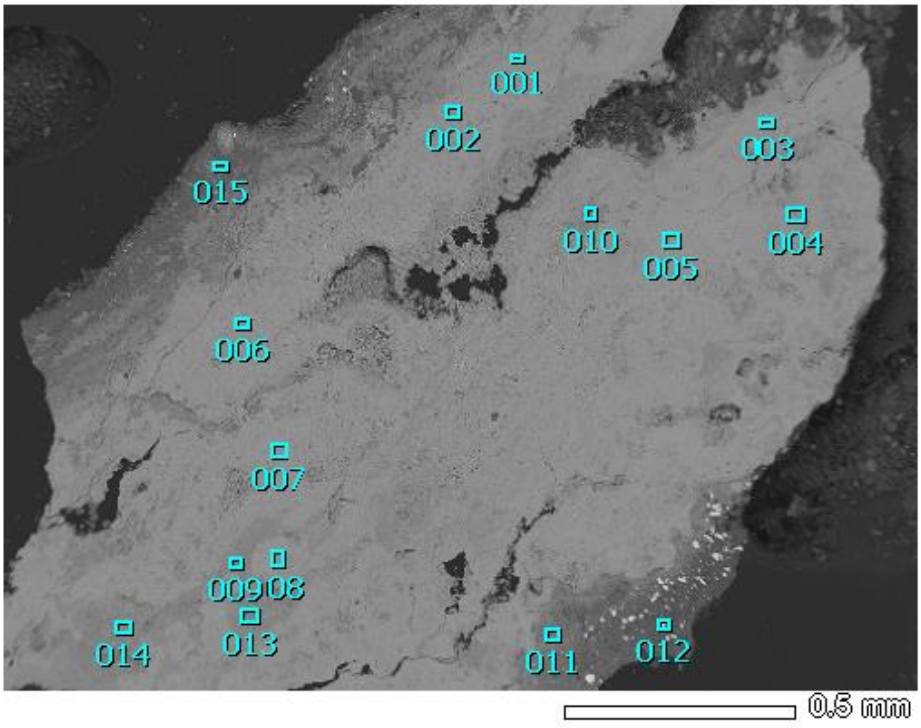


```
Title        : IMG1
---------------------------
Instrument   : 7000F
Volt         : 15.00 kV
Mag          : x 60
Date         : 2014/07/11
Pixel        : 512 x 384
```

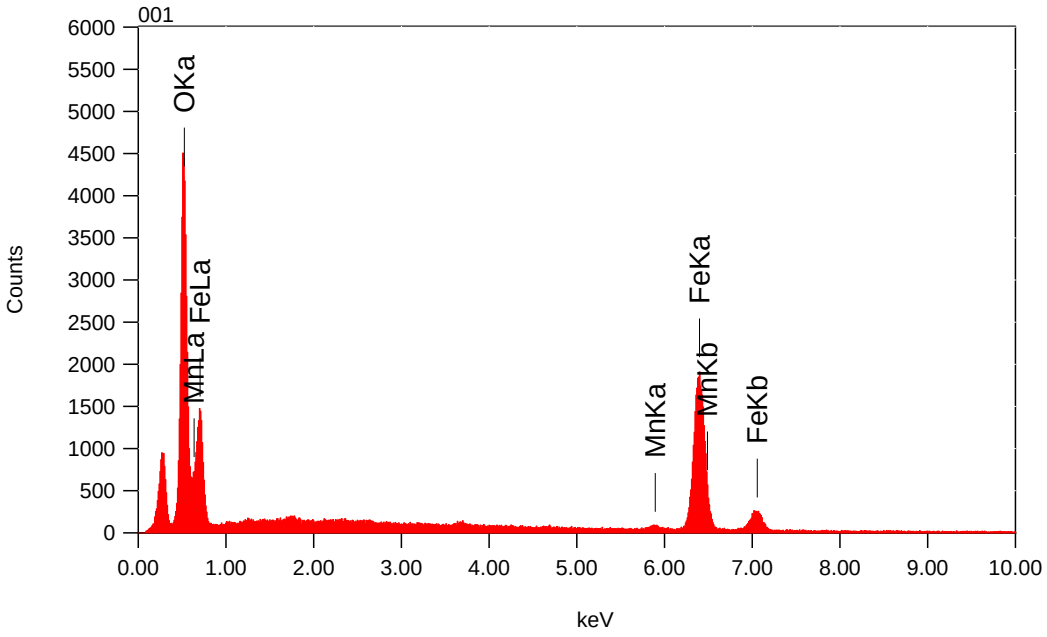


```
Acquisition Parameter
Instrument    : 7000F
Acc. Voltage  : 15.0 kV
Probe Current: 0.59000 nA
PHA mode      : T3
Real Time     : 40.87 sec
Live Time     : 30.00 sec
Dead Time     : 26 %
Counting Rate: 5645 cps
Energy Range :  0 - 20 keV
```

ZAF Method Standardless Quantitative Analysis
Fitting Coefficient : 0.2254

Element	(keV)	mass%	Error%	At%	Compound	mass%	Cation	K
O K	0.525	25.7	0.1	54.7				35.8438
Mn K*	5.894	1.4	0.6	0.9				1.1931
Fe K	6.398	72.9	0.7	44.5				62.9631
Total		100.0		100.0				

2055m Iron oxide

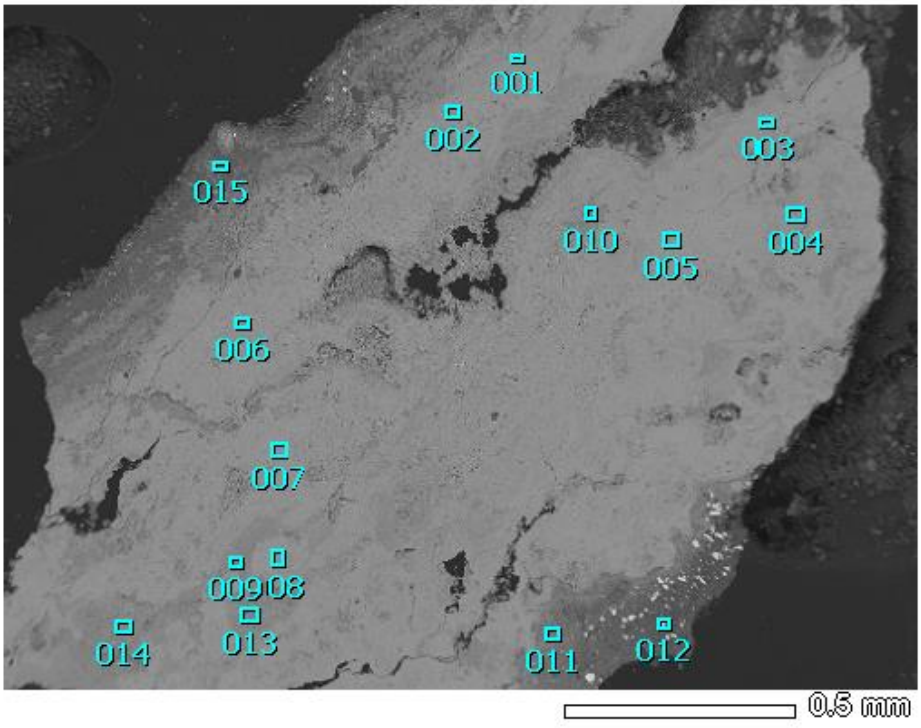


```
Title        : IMG1
---------------------------
Instrument   : 7000F
Volt         : 15.00 kV
Mag          : x 60
Date         : 2014/07/11
Pixel        : 512 x 384
```

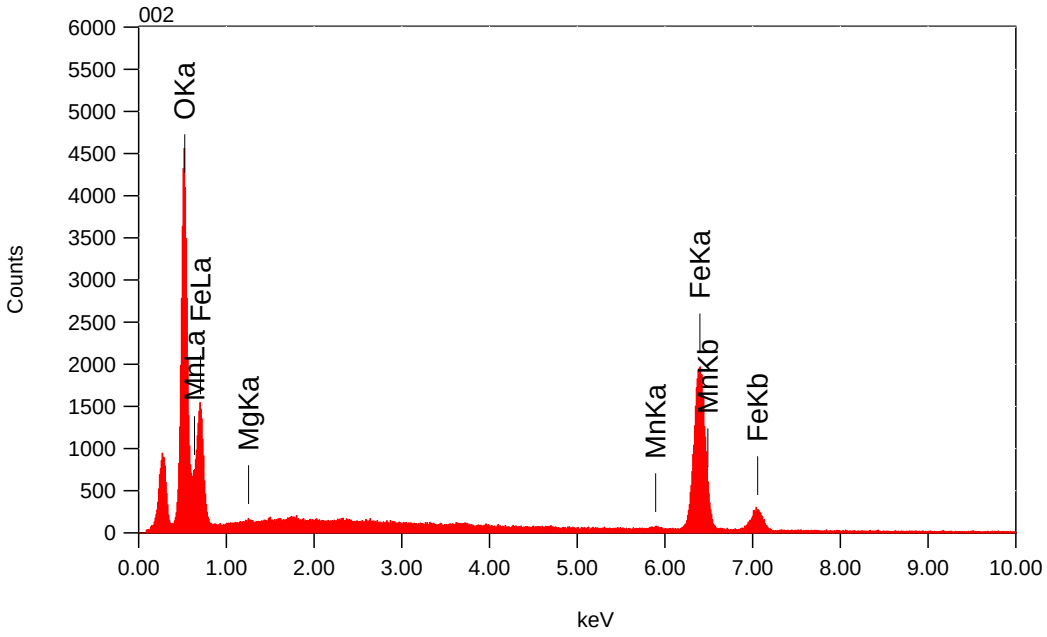


```
Acquisition Parameter
Instrument    : 7000F
Acc. Voltage  : 15.0 kV
Probe Current: 0.59000 nA
PHA mode      : T3
Real Time     : 41.00 sec
Live Time     : 30.00 sec
Dead Time     : 26 %
Counting Rate: 5701 cps
Energy Range :  0 - 20 keV
```

ZAF Method Standardless Quantitative Analysis
Fitting Coefficient : 0.2152

Element	(keV)	mass%	Error%	At%	Compound	mass%	Cation	K
O K	0.525	24.8	0.1	53.4				34.7180
Mg K*	1.253	0.2	0.2	0.3				0.1002
Mn K*	5.894	1.0	0.6	0.6				0.8145
Fe K	6.398	74.0	0.6	45.6				64.3673
Total		100.0		100.0				

2055m Iron oxide

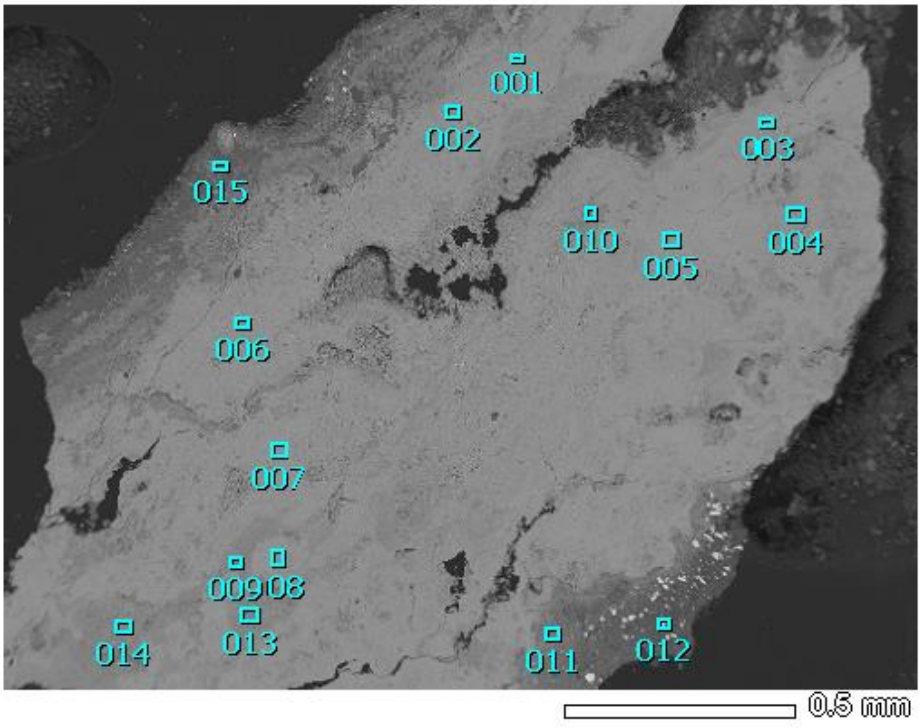


```
Title        : IMG1
---------------------------
Instrument   : 7000F
Volt         : 15.00 kV
Mag          : x 60
Date         : 2014/07/11
Pixel        : 512 x 384
```

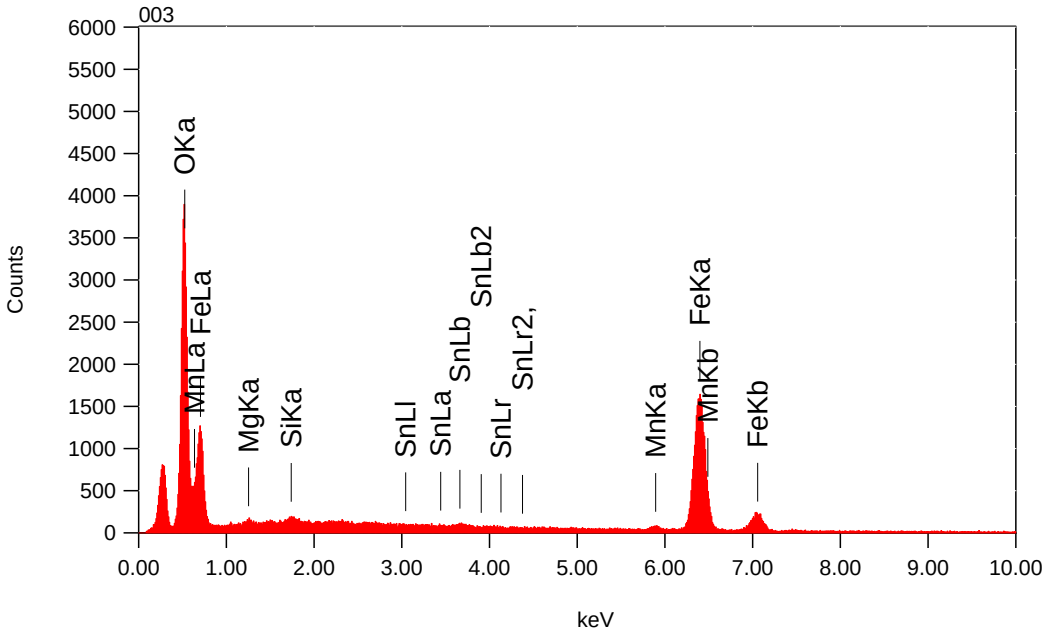


```
Acquisition Parameter
Instrument    : 7000F
Acc. Voltage  : 15.0 kV
Probe Current: 0.59000 nA
PHA mode      : T3
Real Time     : 39.18 sec
Live Time     : 30.00 sec
Dead Time     : 23 %
Counting Rate: 4872 cps
Energy Range :  0 - 20 keV
```

ZAF Method Standardless Quantitative Analysis
Fitting Coefficient : 0.2247

Element	(keV)	mass%	Error%	At%	Compound	mass%	Cation	K
O K	0.525	25.5	0.1	54.3				35.3924
Mg K*	1.253	0.4	0.2	0.6				0.1681
Si K*	1.739	0.3	0.1	0.3				0.1849
Mn K	5.894	1.7	0.6	1.1				1.4546
Fe K	6.398	71.6	0.6	43.6				62.4276
Sn L*	3.442	0.5	0.5	0.1				0.3724
Total		100.0		100.0				

2055m Iron oxide

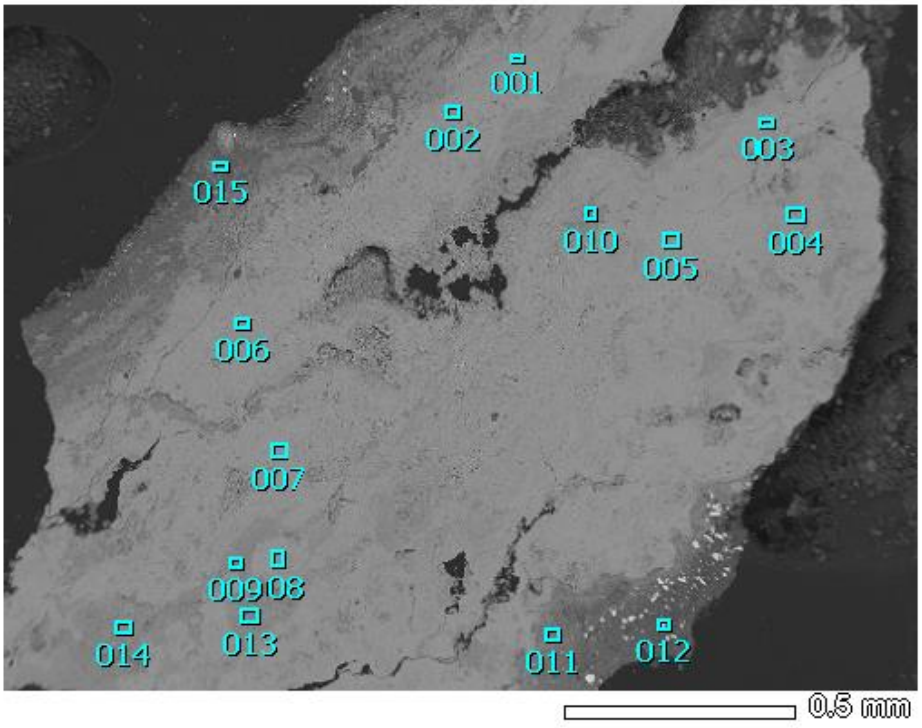


```
Title        : IMG1
---------------------------
Instrument   : 7000F
Volt         : 15.00 kV
Mag          : x 60
Date         : 2014/07/11
Pixel        : 512 x 384
```

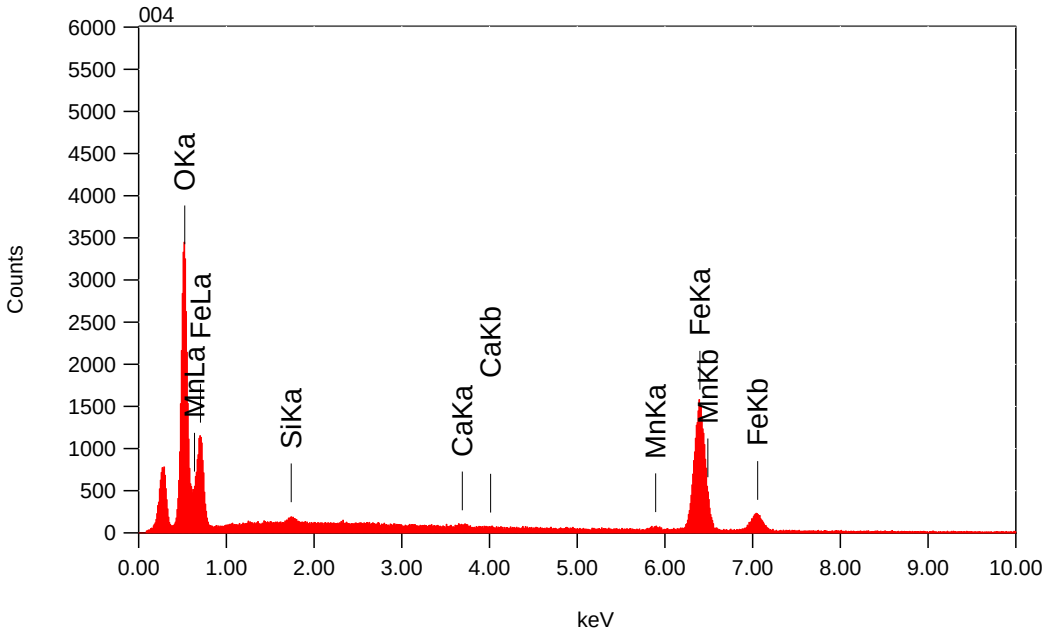


```
Acquisition Parameter
Instrument    : 7000F
Acc. Voltage  : 15.0 kV
Probe Current: 0.59000 nA
PHA mode      : T3
Real Time     : 38.41 sec
Live Time     : 30.00 sec
Dead Time     : 21 %
Counting Rate: 4531 cps
Energy Range :  0 - 20 keV
```

ZAF Method Standardless Quantitative Analysis
Fitting Coefficient : 0.2268

Element	(keV)	mass%	Error%	At%	Compound	mass%	Cation	K
O K	0.525	25.2	0.1	53.8				34.7836
Si K*	1.739	0.4	0.1	0.5				0.2589
Ca K*	3.690	0.4	0.2	0.4				0.4552
Mn K*	5.894	1.7	0.6	1.1				1.4788
Fe K	6.398	72.3	0.7	44.2				63.0235
Total		100.0		100.0				

2055m Iron oxide

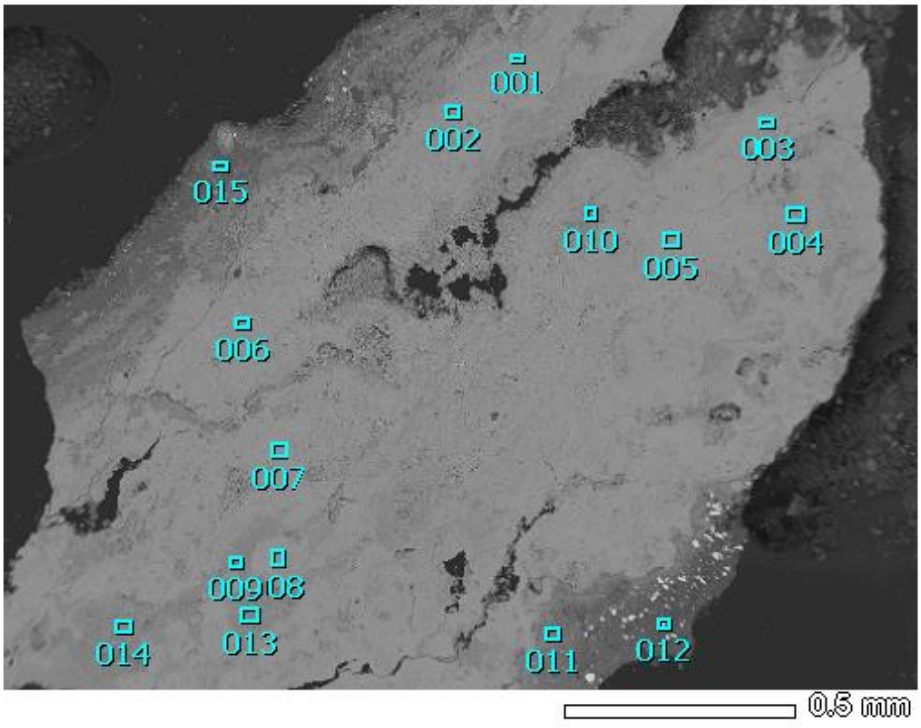


```
Title        : IMG1
--------------------------
Instrument   : 7000F
Volt         : 15.00 kV
Mag          : x 60
Date         : 2014/07/11
Pixel        : 512 x 384
```

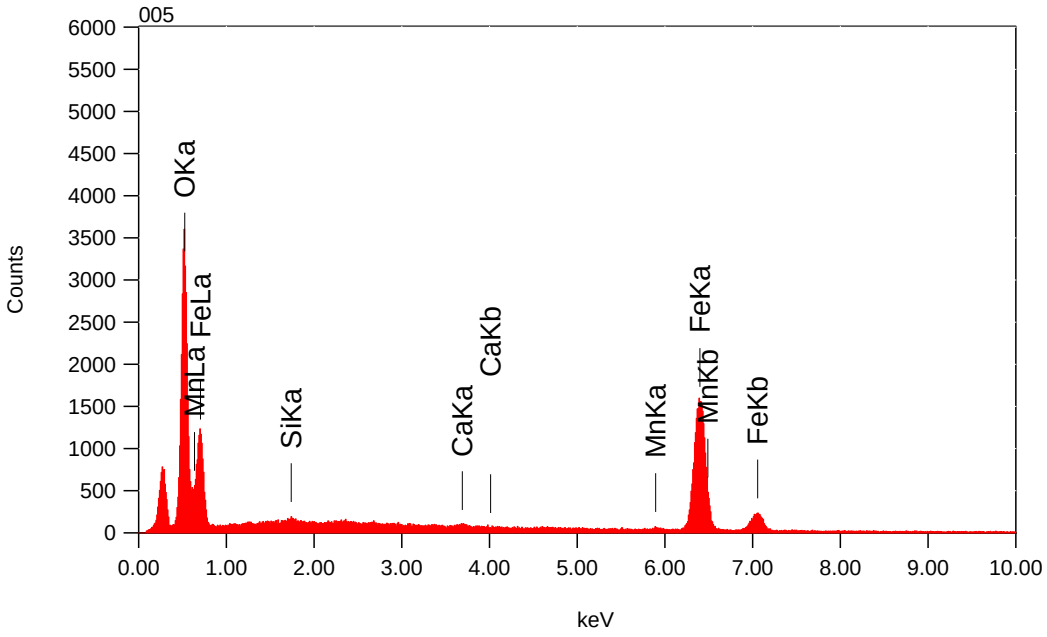


```
Acquisition Parameter
Instrument   : 7000F
Acc. Voltage : 15.0 kV
Probe Current: 0.59000 nA
PHA mode     : T3
Real Time    : 38.73 sec
Live Time    : 30.00 sec
Dead Time    : 22 %
Counting Rate: 4707 cps
Energy Range :  0 - 20 keV
```

ZAF Method Standardless Quantitative Analysis
Fitting Coefficient : 0.2413

Element	(keV)	mass%	Error%	At%	Compound	mass%	Cation	K
O K	0.525	24.4	0.1	52.8				33.7679
Si K*	1.739	0.3	0.1	0.3				0.1785
Ca K*	3.690	0.4	0.2	0.3				0.3784
Mn K*	5.894	1.0	0.6	0.7				0.9036
Fe K	6.398	74.0	0.7	45.9				64.7717
Total		100.0		100.0				

2055m Iron oxide

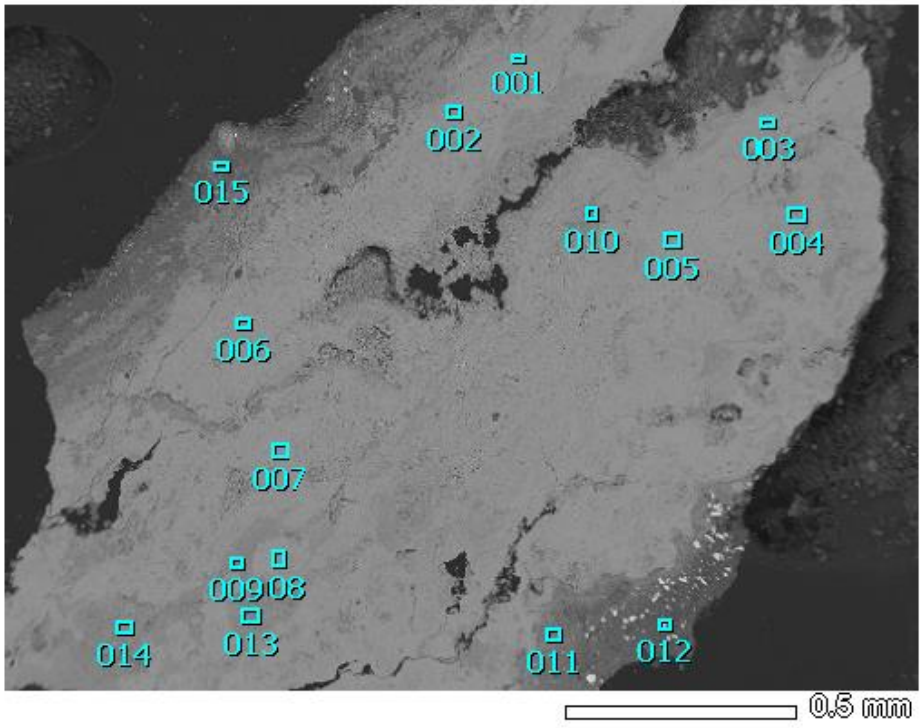


```
Title          : IMG1
---------------------------
Instrument     : 7000F
Volt           : 15.00 kV
Mag            : x 60
Date           : 2014/07/11
Pixel          : 512 x 384
```

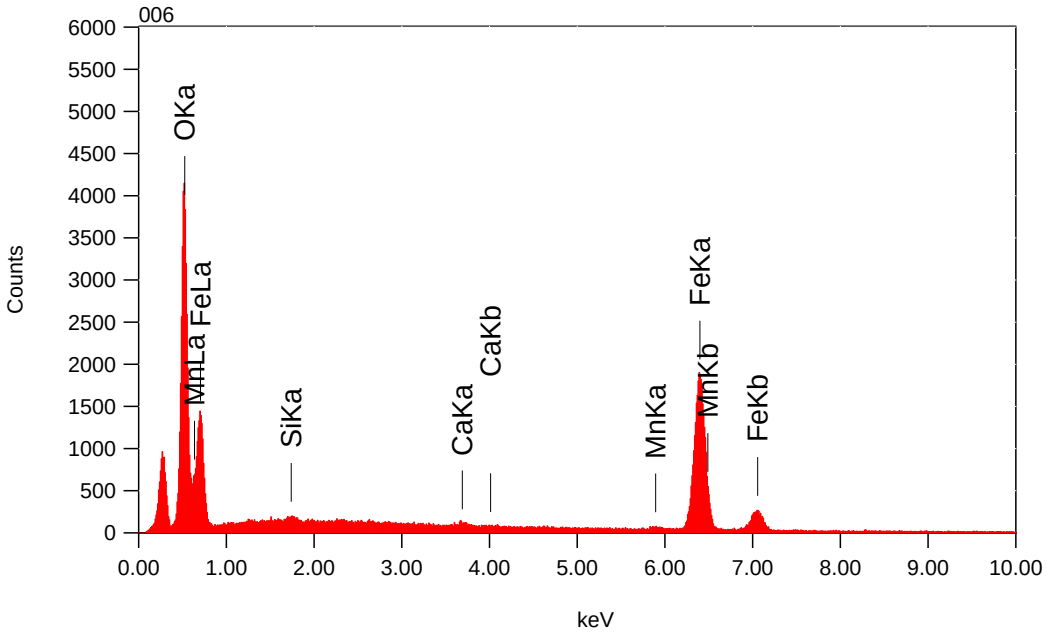


```
Acquisition Parameter
Instrument     : 7000F
Acc. Voltage   : 15.0 kV
Probe Current: 0.59000 nA
PHA mode       : T3
Real Time      : 40.29 sec
Live Time      : 30.00 sec
Dead Time      : 25 %
Counting Rate: 5383 cps
Energy Range :  0 - 20 keV
```

ZAF Method Standardless Quantitative Analysis
Fitting Coefficient : 0.2407

Element	(keV)	mass%	Error%	At%	Compound	mass%	Cation	K
O K	0.525	24.8	0.1	53.4				34.3681
Si K*	1.739	0.2	0.1	0.3				0.1404
Ca K*	3.690	0.4	0.2	0.4				0.4293
Mn K*	5.894	1.1	0.6	0.7				0.9514
Fe K	6.398	73.4	0.7	45.2				64.1109
Total		100.0		100.0				

2055m Iron oxide

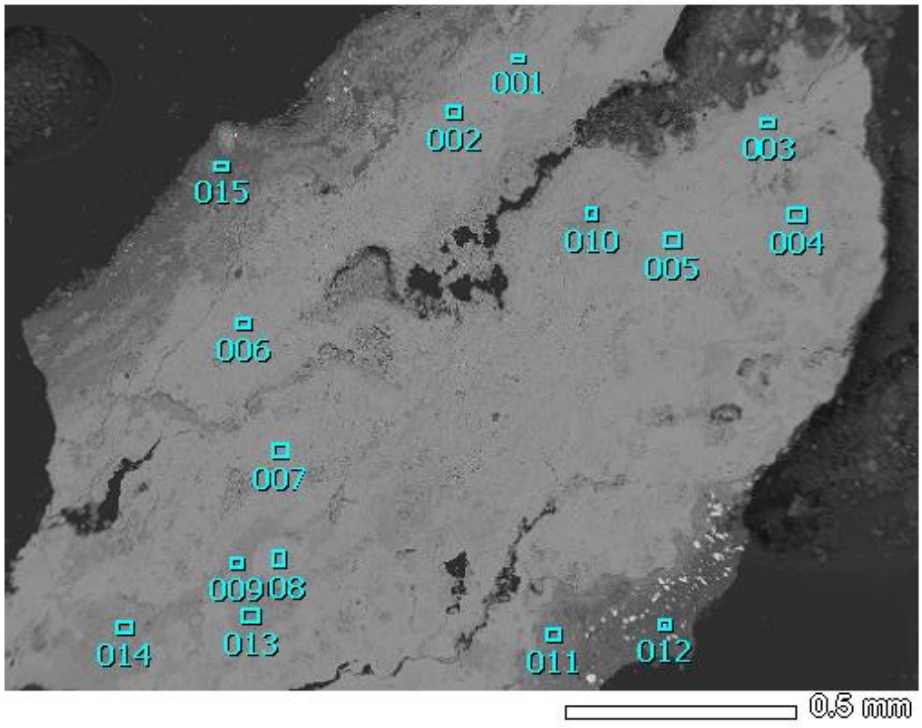


```
Title        : IMG1
---------------------------
Instrument   : 7000F
Volt         : 15.00 kV
Mag          : x 60
Date         : 2014/07/11
Pixel        : 512 x 384
```

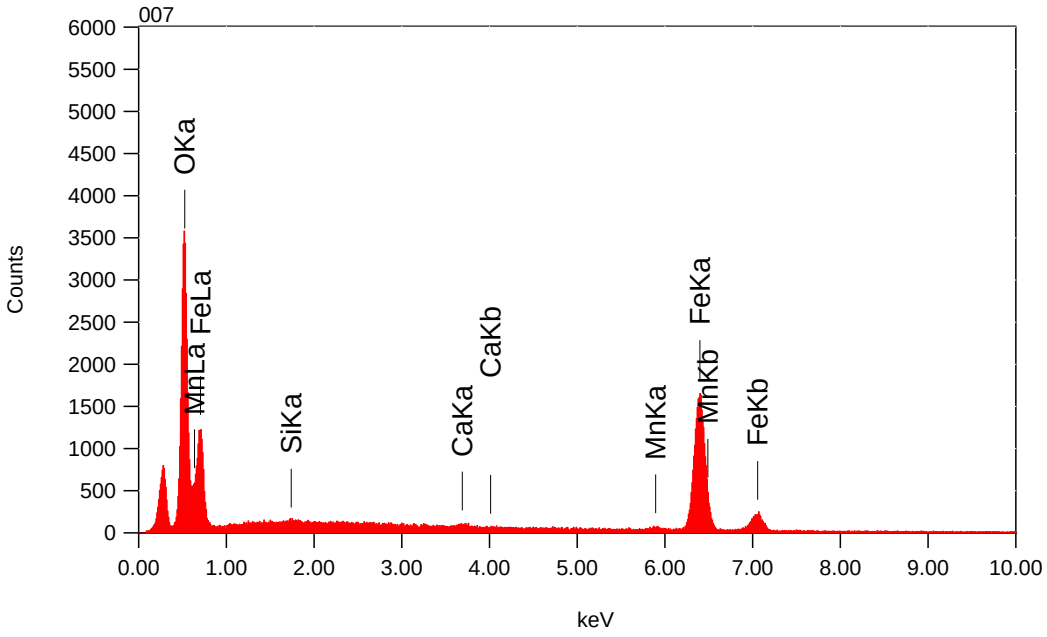


```
Acquisition Parameter
Instrument    : 7000F
Acc. Voltage  : 15.0 kV
Probe Current: 0.59000 nA
PHA mode      : T3
Real Time     : 38.77 sec
Live Time     : 30.00 sec
Dead Time     : 22 %
Counting Rate: 4718 cps
Energy Range :  0 - 20 keV
```

ZAF Method Standardless Quantitative Analysis
Fitting Coefficient : 0.2308

Element	(keV)	mass%	Error%	At%	Compound	mass%	Cation	K
O K	0.525	24.5	0.1	53.0				33.9592
Si K*	1.739	0.1	0.1	0.1				0.0435
Ca K*	3.690	0.3	0.2	0.3				0.3585
Mn K*	5.894	1.1	0.6	0.7				0.9679
Fe K	6.398	74.0	0.7	45.9				64.6708
Total		100.0		100.0				

2055m Iron oxide

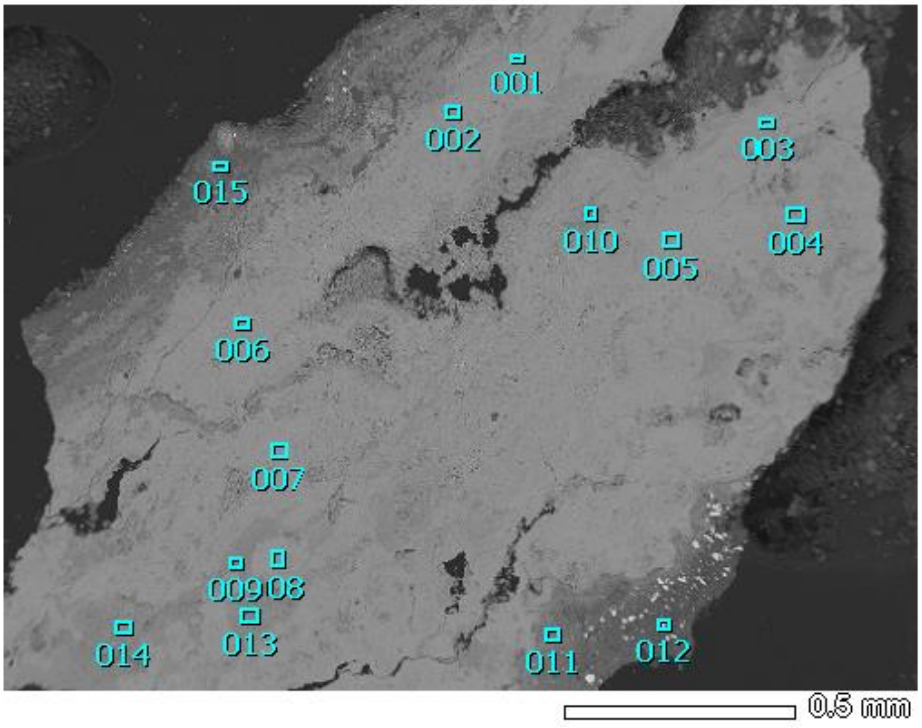


```
Title        : IMG1
---------------------------
Instrument   : 7000F
Volt         : 15.00 kV
Mag          : x 60
Date         : 2014/07/11
Pixel        : 512 x 384
```

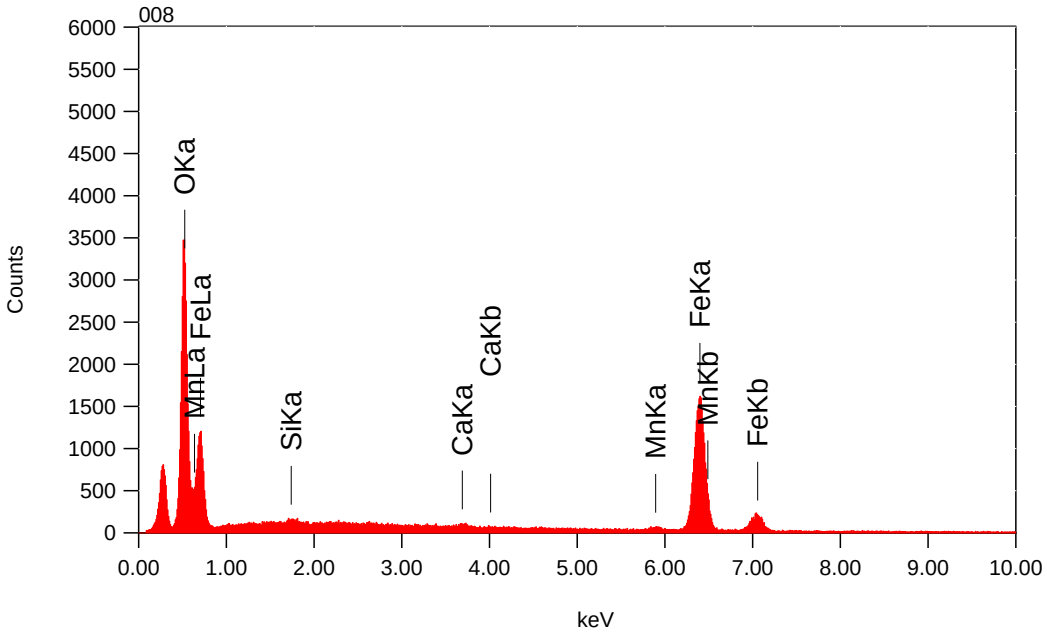


```
Acquisition Parameter
Instrument   : 7000F
Acc. Voltage : 15.0 kV
Probe Current: 0.59000 nA
PHA mode     : T3
Real Time    : 38.47 sec
Live Time    : 30.00 sec
Dead Time    : 22 %
Counting Rate: 4576 cps
Energy Range :  0 - 20 keV
```

ZAF Method Standardless Quantitative Analysis
Fitting Coefficient : 0.2243

Element	(keV)	mass%	Error%	At%	Compound	mass%	Cation	K
O K	0.525	24.2	0.1	52.5				33.4865
Si K*	1.739	0.2	0.1	0.3				0.1535
Ca K*	3.690	0.4	0.2	0.3				0.4124
Mn K*	5.894	1.2	0.6	0.7				0.9957
Fe K	6.398	74.1	0.7	46.1				64.9519
Total		100.0		100.0				

2055m Iron oxide

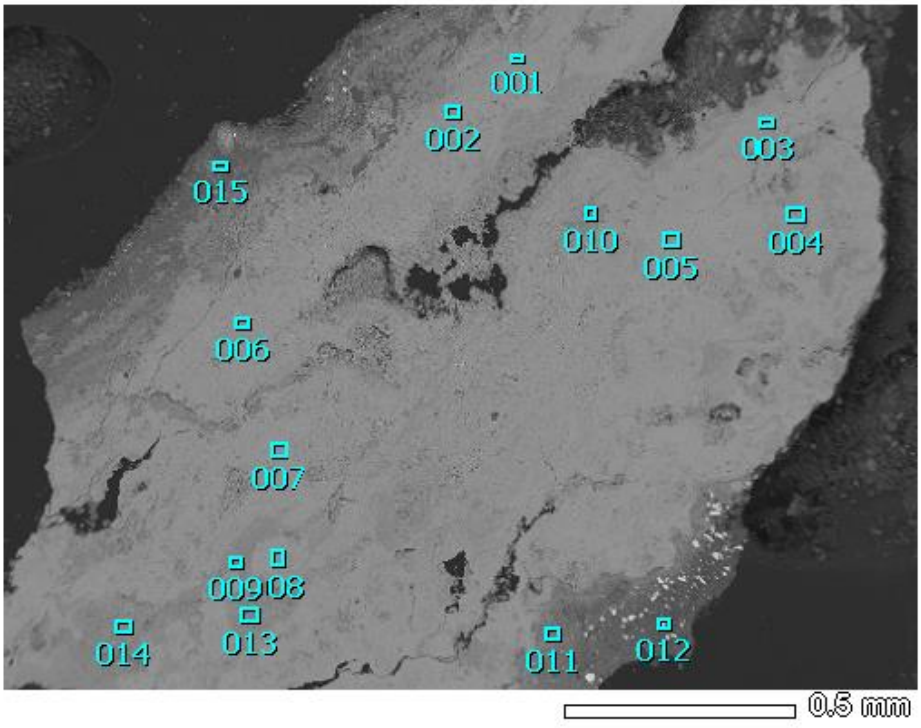


```
Title        : IMG1
---------------------------
Instrument   : 7000F
Volt         : 15.00 kV
Mag          : x 60
Date         : 2014/07/11
Pixel        : 512 x 384
```

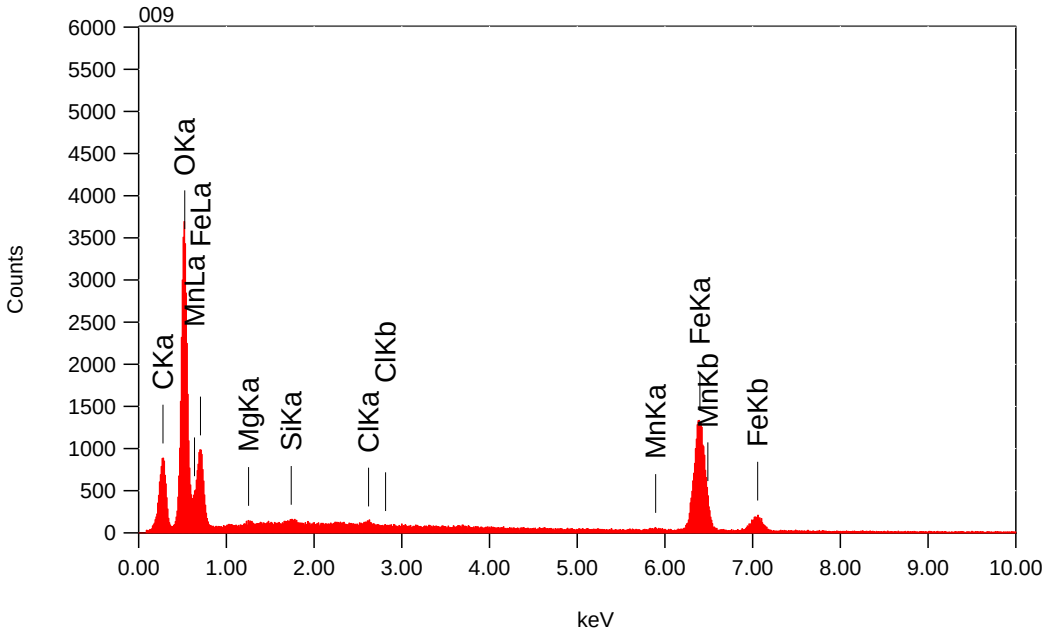


```
Acquisition Parameter
Instrument    : 7000F
Acc. Voltage  : 15.0 kV
Probe Current: 0.59000 nA
PHA mode      : T3
Real Time     : 37.86 sec
Live Time     : 30.00 sec
Dead Time     : 20 %
Counting Rate: 4292 cps
Energy Range :  0 - 20 keV
```

ZAF Method Standardless Quantitative Analysis
Fitting Coefficient : 0.2009

Element	(keV)	mass%	Error%	At%	Compound	mass%	Cation	K
C K	0.277	12.1	0.1	25.9				4.0253
O K	0.525	28.9	0.1	46.6				37.9339
Mg K*	1.253	0.3	0.1	0.3				0.1455
Si K*	1.739	0.2	0.1	0.2				0.1288
Cl K*	2.621	0.3	0.1	0.2				0.3635
Mn K*	5.894	0.7	0.4	0.3				0.7129
Fe K	6.398	57.5	0.5	26.5				56.6901
Total		100.0		100.0				

2055m Iron oxide

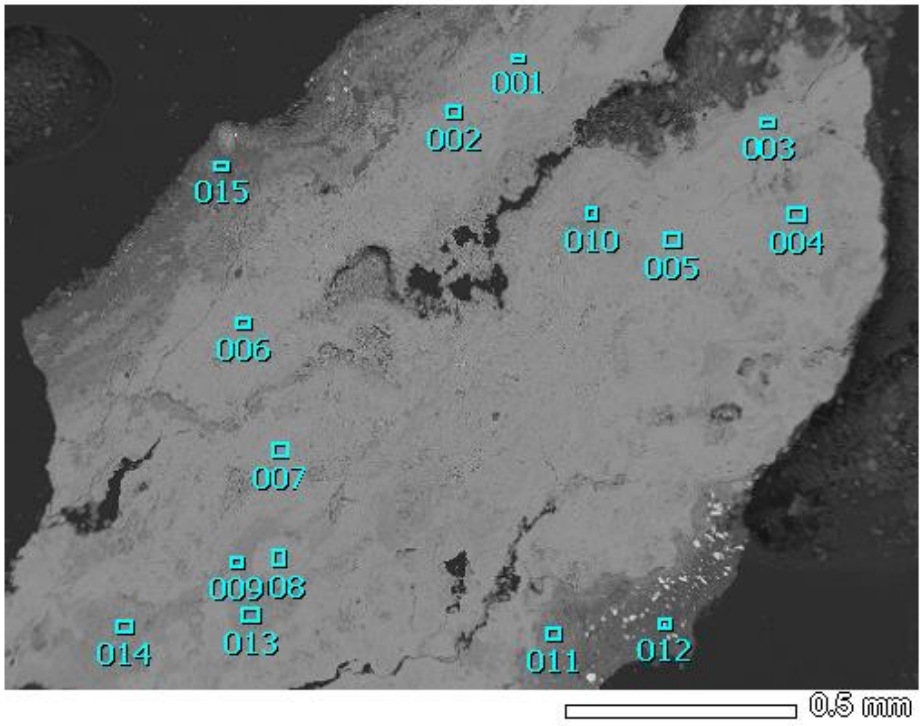


```
Title        : IMG1
---------------------------
Instrument   : 7000F
Volt         : 15.00 kV
Mag          : x 60
Date         : 2014/07/11
Pixel        : 512 x 384
```

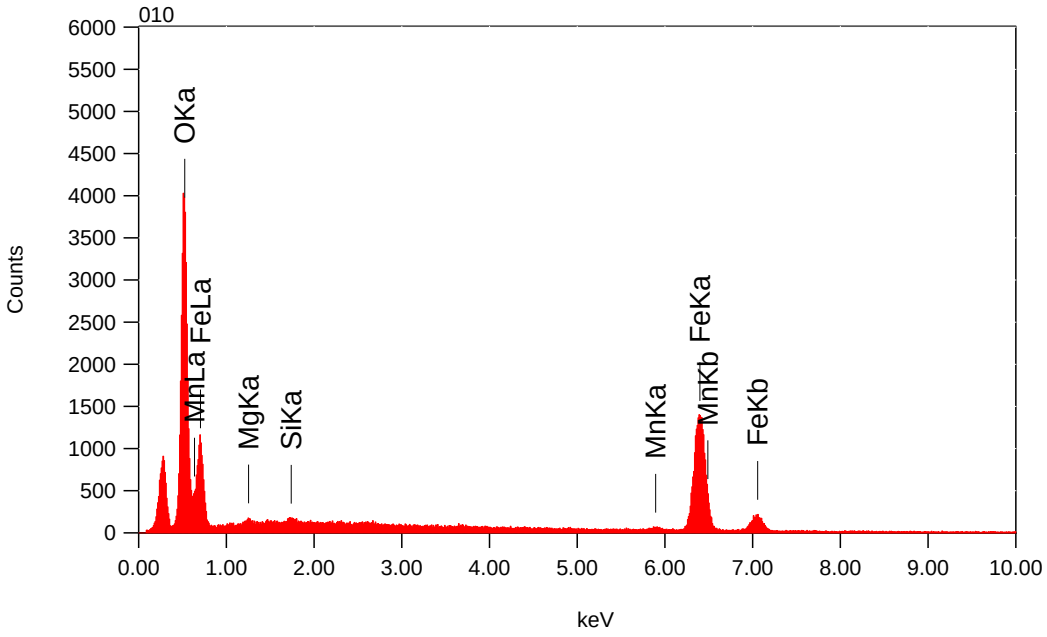


```
Acquisition Parameter
Instrument   : 7000F
Acc. Voltage : 15.0 kV
Probe Current: 0.59000 nA
PHA mode     : T3
Real Time    : 38.70 sec
Live Time    : 30.00 sec
Dead Time    : 22 %
Counting Rate: 4661 cps
Energy Range :  0 - 20 keV
```

ZAF Method Standardless Quantitative Analysis
Fitting Coefficient : 0.2370

Element	(keV)	mass%	Error%	At%	Compound	mass%	Cation	K
O K	0.525	29.1	0.1	58.5				40.2550
Mg K*	1.253	0.5	0.2	0.7				0.2123
Si K*	1.739	0.4	0.2	0.4				0.2488
Mn K*	5.894	1.3	0.7	0.8				1.0681
Fe K	6.398	68.7	0.8	39.6				58.2158
Total		100.0		100.0				

2055m Iron oxide

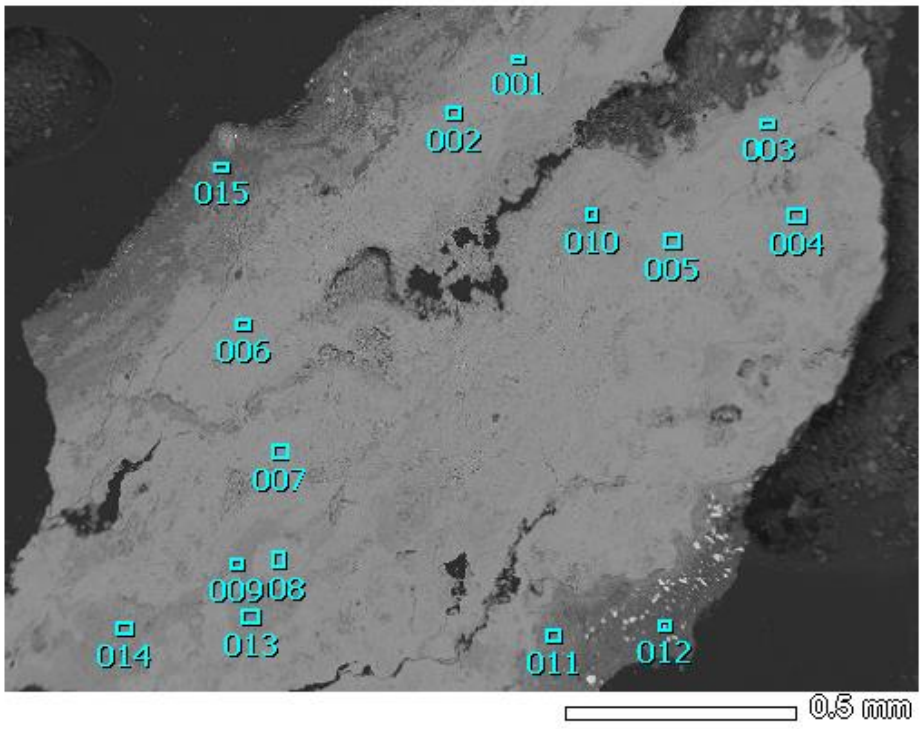


```
Title        : IMG1
---------------------------
Instrument   : 7000F
Volt         : 15.00 kV
Mag          : x 60
Date         : 2014/07/11
Pixel        : 512 x 384
```

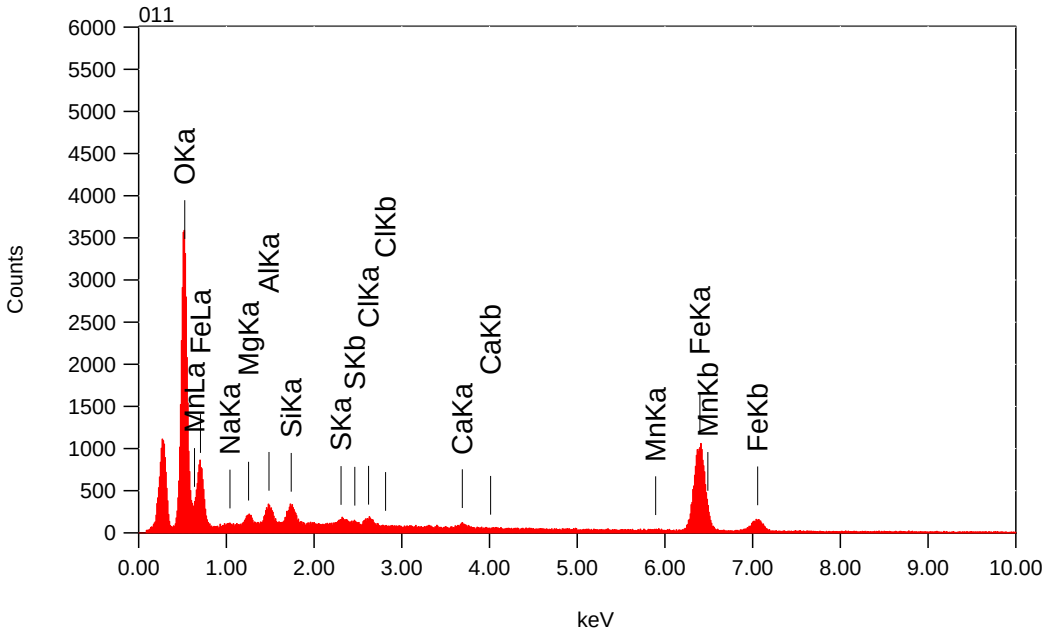


```
Acquisition Parameter
Instrument    : 7000F
Acc. Voltage  : 15.0 kV
Probe Current: 0.59000 nA
PHA mode      : T3
Real Time     : 37.71 sec
Live Time     : 30.00 sec
Dead Time     : 20 %
Counting Rate: 4236 cps
Energy Range :  0 - 20 keV
```

ZAF Method Standardless Quantitative Analysis
Fitting Coefficient : 0.2602

Element	(keV)	mass%	Error%	At%	Compound	mass%	Cation	K
O K	0.525	32.7	0.1	60.7				43.4084
Na K*	1.041	0.3	0.3	0.4				0.1334
Mg K	1.253	1.2	0.2	1.5				0.5325
Al K	1.486	1.8	0.2	2.0				0.9747
Si K	1.739	1.6	0.2	1.7				1.0546
S K*	2.307	0.4	0.2	0.4				0.3763
Cl K	2.621	0.9	0.2	0.8				0.8465
Ca K*	3.690	0.8	0.3	0.6				0.7969
Mn K*	5.894	0.5	0.9	0.3				0.4089
Fe K	6.398	59.8	1.0	31.8				51.4677
Total		100.0		100.0				

2055m Iron oxide

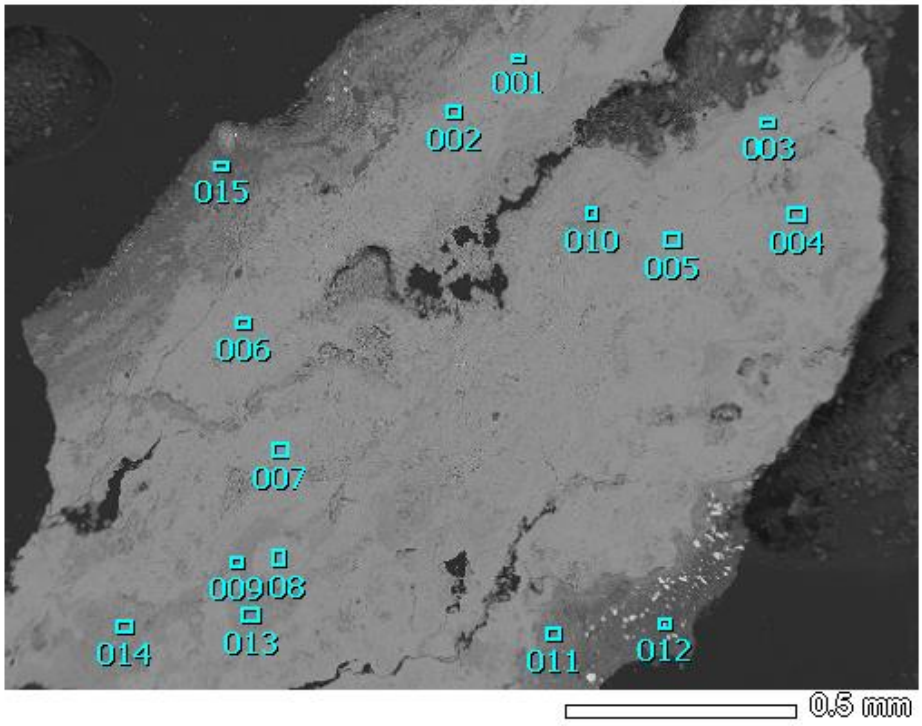


```
Title        : IMG1
---------------------------
Instrument   : 7000F
Volt         : 15.00 kV
Mag          : x 60
Date         : 2014/07/11
Pixel        : 512 x 384
```

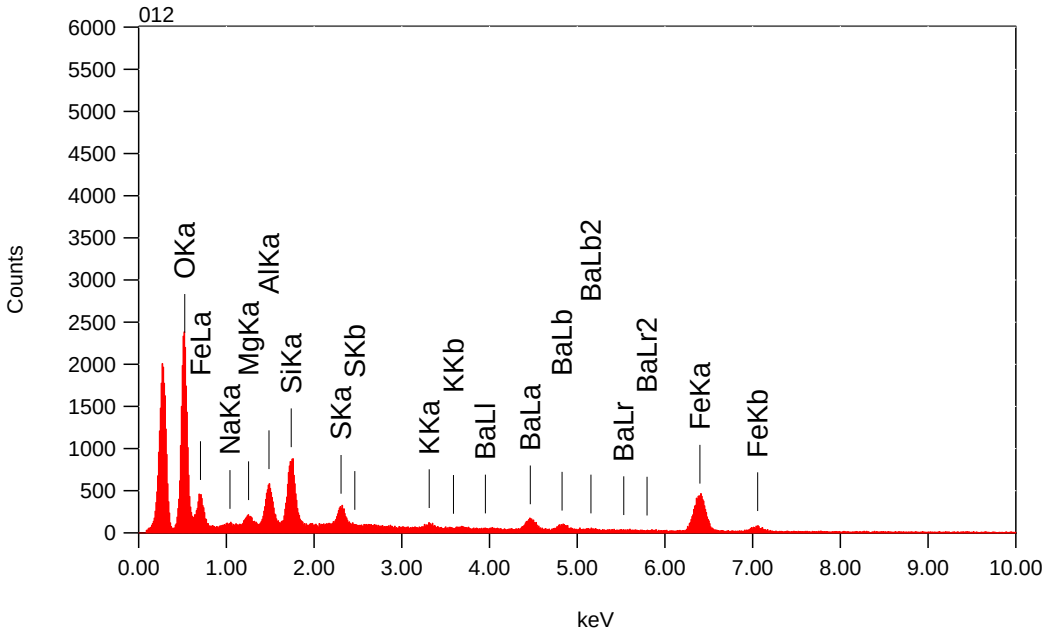


```
Acquisition Parameter
Instrument    : 7000F
Acc. Voltage  : 15.0 kV
Probe Current: 0.59000 nA
PHA mode      : T3
Real Time     : 36.72 sec
Live Time     : 30.00 sec
Dead Time     : 18 %
Counting Rate: 3801 cps
Energy Range :  0 - 20 keV
```

ZAF Method Standardless Quantitative Analysis
Fitting Coefficient : 0.3858

Element	(keV)	mass%	Error%	At%	Compound	mass%	Cation	K
O K	0.525	33.9	0.3	60.3				43.8051
Na K*	1.041	0.4	0.6	0.5				0.2148
Mg K	1.253	1.3	0.5	1.6				0.6909
Al K	1.486	5.1	0.5	5.4				3.1736
Si K	1.739	8.5	0.5	8.6				6.2236
S K	2.307	2.9	0.4	2.6				2.6618
K K	3.312	0.9	0.7	0.6				0.9147
Fe K	6.398	35.2	2.4	18.0				32.3136
Ba L	4.464	11.7	2.6	2.4				10.0018
Total		100.0		100.0				

2055m Iron oxide

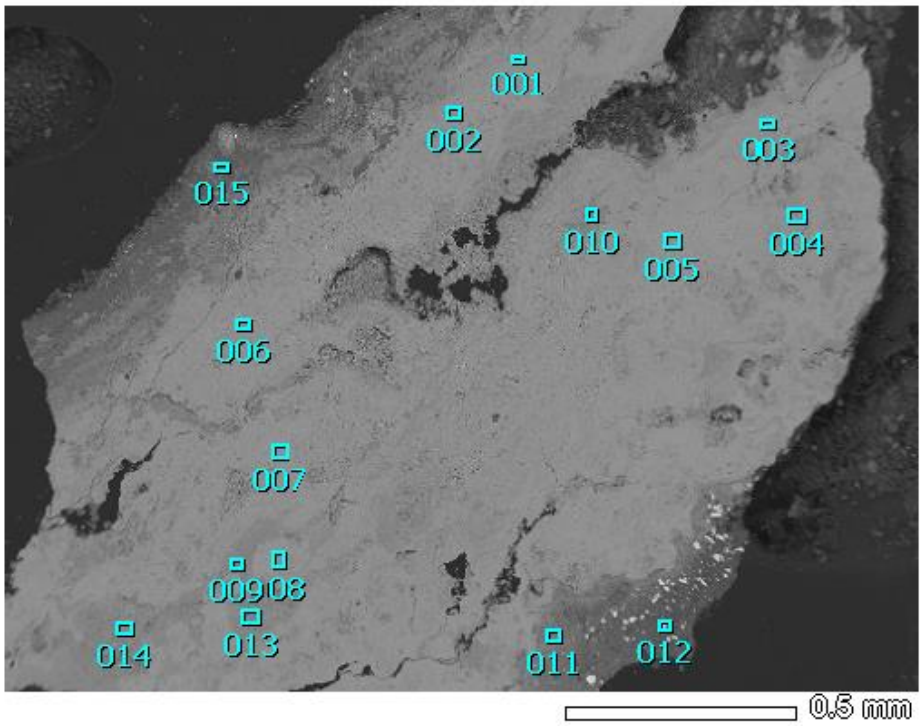


```
Title        : IMG1
---------------------------
Instrument   : 7000F
Volt         : 15.00 kV
Mag          : x 60
Date         : 2014/07/11
Pixel        : 512 x 384
```

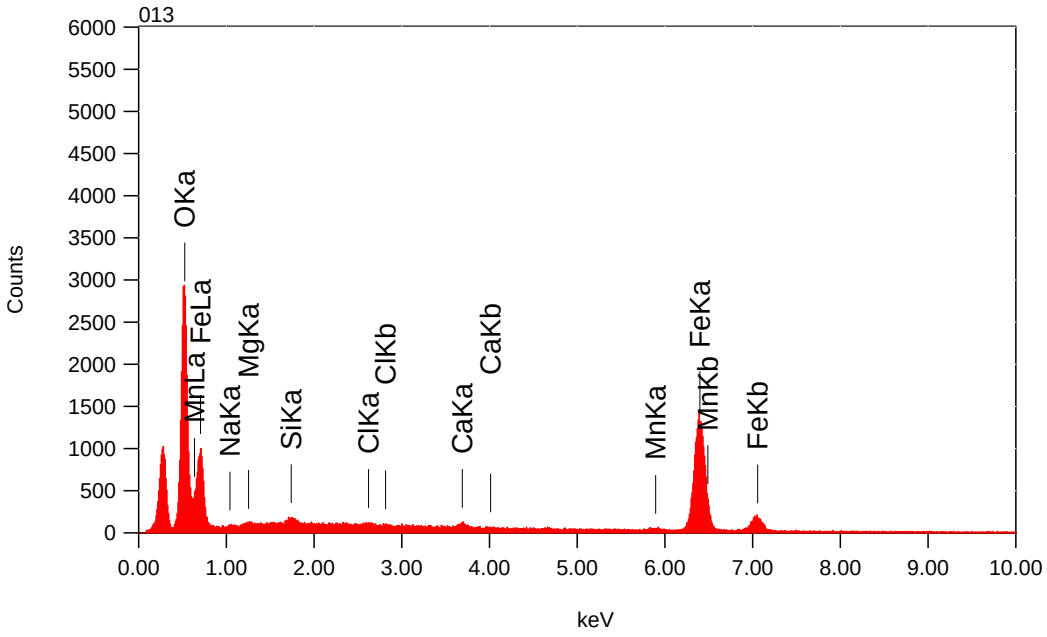


```
Acquisition Parameter
Instrument   : 7000F
Acc. Voltage : 15.0 kV
Probe Current: 0.59000 nA
PHA mode     : T3
Real Time    : 37.60 sec
Live Time    : 30.00 sec
Dead Time    : 20 %
Counting Rate: 4204 cps
Energy Range :  0 - 20 keV
```

ZAF Method Standardless Quantitative Analysis
Fitting Coefficient : 0.2593

Element	(keV)	mass%	Error%	At%	Compound	mass%	Cation	K
O K	0.525	24.4	0.1	52.4				33.3907
Na K*	1.041	0.3	0.3	0.4				0.1044
Mg K*	1.253	0.3	0.2	0.4				0.1166
Si K*	1.739	0.5	0.2	0.6				0.3006
Cl K*	2.621	0.3	0.2	0.3				0.2450
Ca K*	3.690	0.8	0.3	0.7				0.8485
Mn K	5.894	0.9	0.8	0.6				0.8009
Fe K	6.398	72.6	0.9	44.7				64.1935
Total		100.0		100.0				

2055m Iron oxide

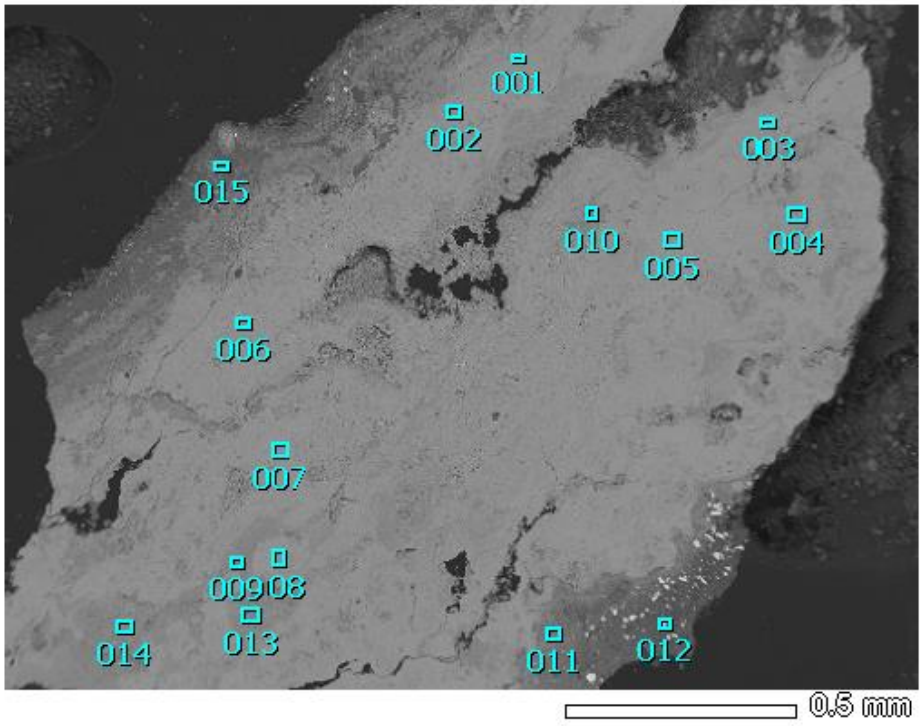


```
Title        : IMG1
---------------------------
Instrument   : 7000F
Volt         : 15.00 kV
Mag          : x 60
Date         : 2014/07/11
Pixel        : 512 x 384
```

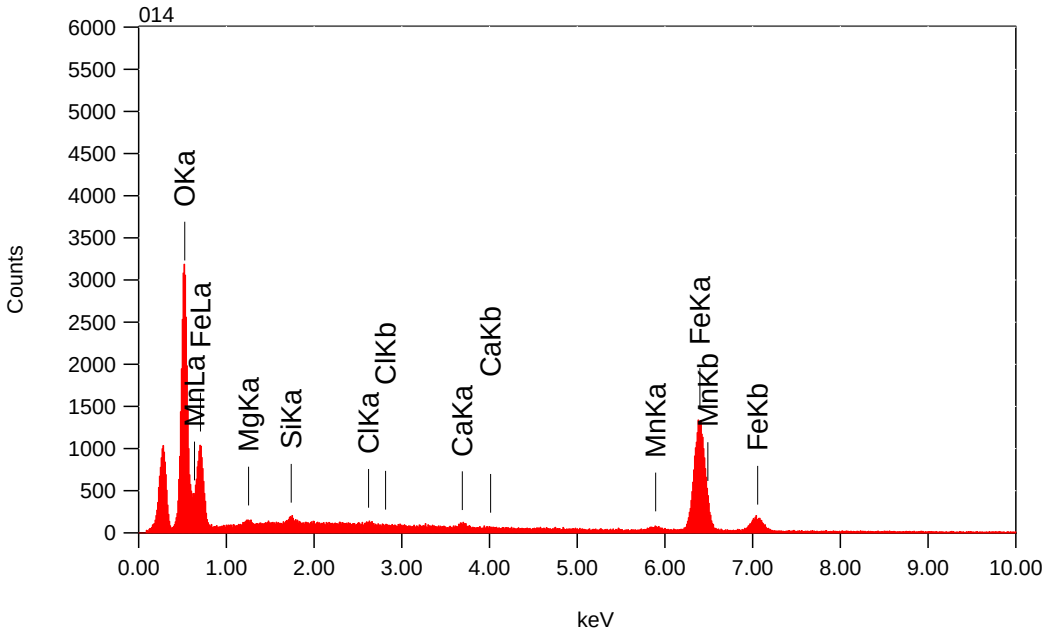


```
Acquisition Parameter
Instrument    : 7000F
Acc. Voltage  : 15.0 kV
Probe Current: 0.59000 nA
PHA mode      : T3
Real Time     : 37.76 sec
Live Time     : 30.00 sec
Dead Time     : 20 %
Counting Rate: 4272 cps
Energy Range :  0 - 20 keV
```

ZAF Method Standardless Quantitative Analysis
Fitting Coefficient : 0.2664

Element	(keV)	mass%	Error%	At%	Compound	mass%	Cation	K
O K	0.525	26.1	0.1	54.7				35.5377
Mg K*	1.253	0.5	0.2	0.7				0.2281
Si K*	1.739	0.6	0.2	0.7				0.3711
Cl K*	2.621	0.3	0.2	0.3				0.3100
Ca K*	3.690	0.8	0.3	0.7				0.8772
Mn K	5.894	1.6	0.8	1.0				1.4046
Fe K	6.398	70.0	0.9	41.9				61.2713
Total		100.0		100.0				

2055m Iron oxide

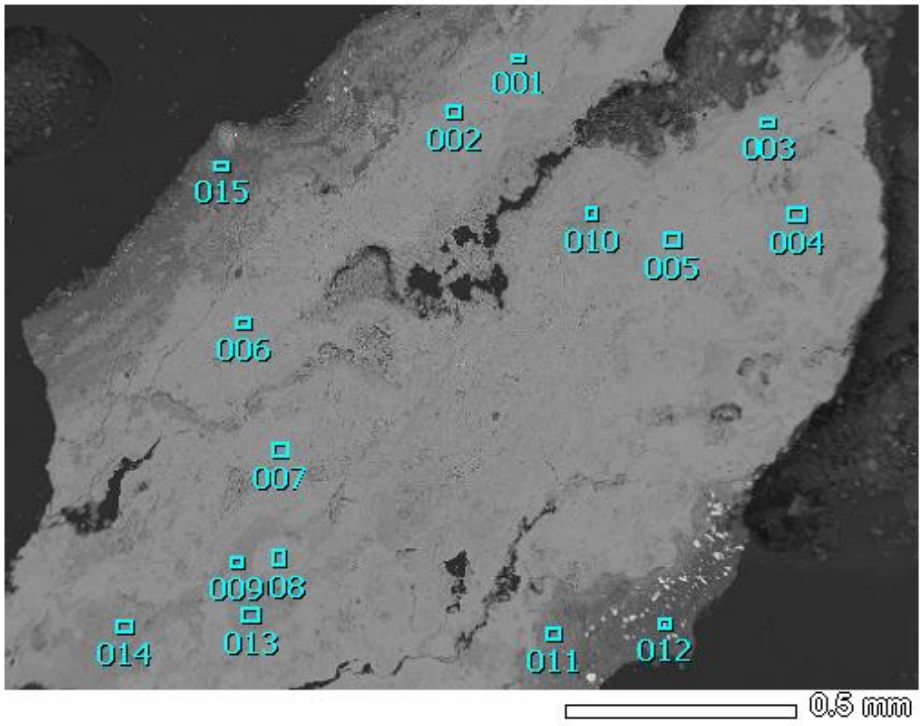


```
Title        : IMG1
---------------------------
Instrument   : 7000F
Volt         : 15.00 kV
Mag          : x 60
Date         : 2014/07/11
Pixel        : 512 x 384
```

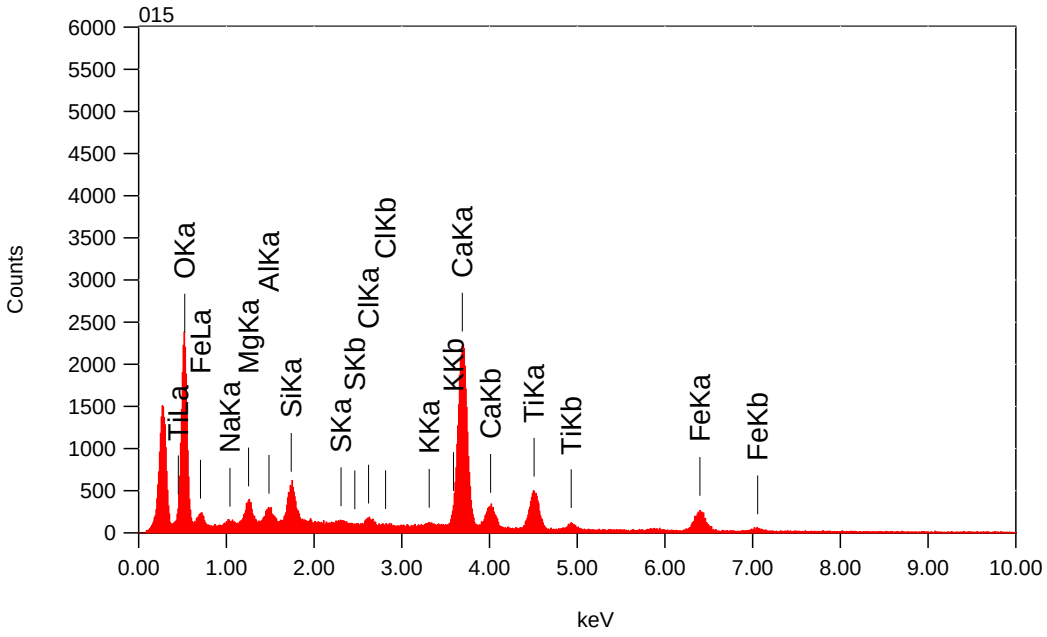


```
Acquisition Parameter
Instrument    : 7000F
Acc. Voltage  : 15.0 kV
Probe Current: 0.59000 nA
PHA mode      : T3
Real Time     : 38.79 sec
Live Time     : 30.00 sec
Dead Time     : 22 %
Counting Rate: 4729 cps
Energy Range :  0 - 20 keV
```

ZAF Method Standardless Quantitative Analysis
Fitting Coefficient : 0.2771

Element	(keV)	mass%	Error%	At%	Compound	mass%	Cation	K
O K	0.525	45.7	0.3	68.5				31.1987
Na K*	1.041	0.4	0.2	0.5				0.3235
Mg K*	1.253	1.7	0.2	1.6				1.2529
Al K	1.486	1.0	0.2	0.8				0.8477
Si K	1.739	2.3	0.2	2.0				2.4804
S K*	2.307	0.2	0.2	0.2				0.3083
Cl K	2.621	0.7	0.2	0.5				0.9911
K K*	3.312	0.3	0.3	0.2				0.4060
Ca K	3.690	27.1	0.4	16.2				38.8872
Ti K	4.508	9.5	0.5	4.8				10.6879
Fe K	6.398	11.1	1.1	4.8				12.6163
Total		100.0		100.0				

2055m Copper

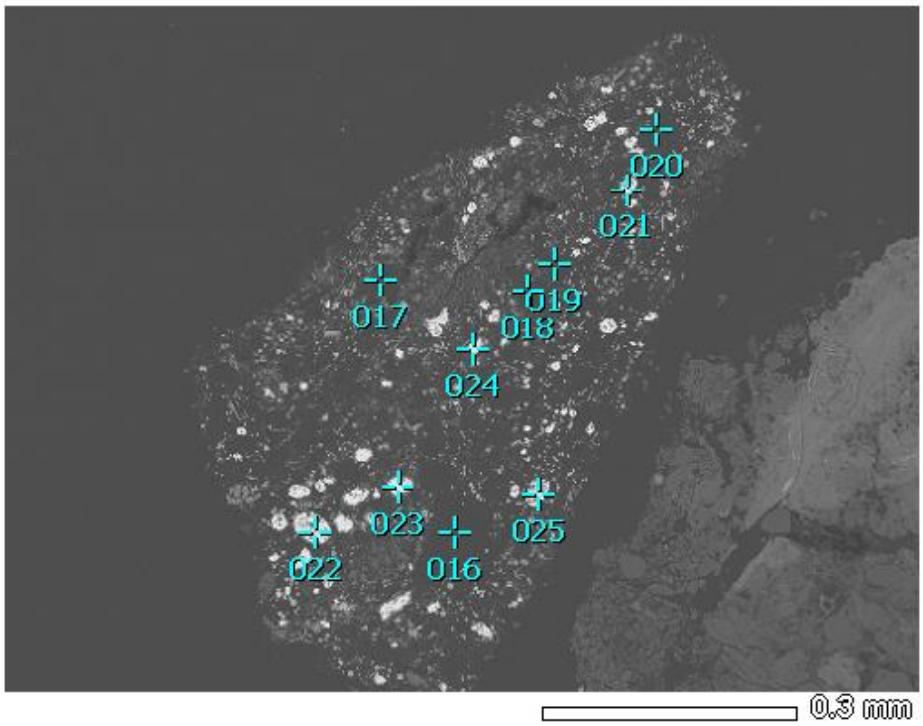


```
Title        : IMG1
--------------------------
Instrument   : 7000F
Volt         : 15.00 kV
Mag          : x 110
Date         : 2014/07/11
Pixel        : 512 x 384
```

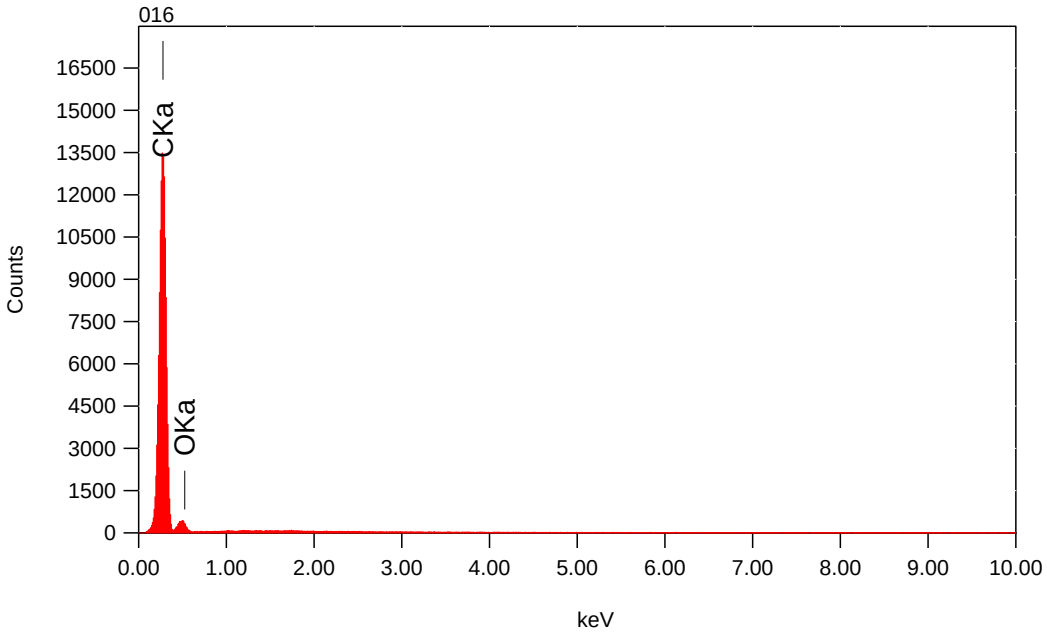


```
Acquisition Parameter
Instrument    : 7000F
Acc. Voltage  : 15.0 kV
Probe Current: 0.59000 nA
PHA mode      : T3
Real Time     : 36.84 sec
Live Time     : 30.00 sec
Dead Time     : 18 %
Counting Rate: 4415 cps
Energy Range :  0 - 20 keV
```

ZAF Method Standardless Quantitative Analysis
Fitting Coefficient : 0.4487

Element	(keV)	mass%	Error%	At%	Compound	mass%	Cation	K
C K	0.277	90.2	0.2	92.5				95.7893
O K	0.525	9.8	2.5	7.5				4.2107
Total		100.0		100.0				

2055m Copper

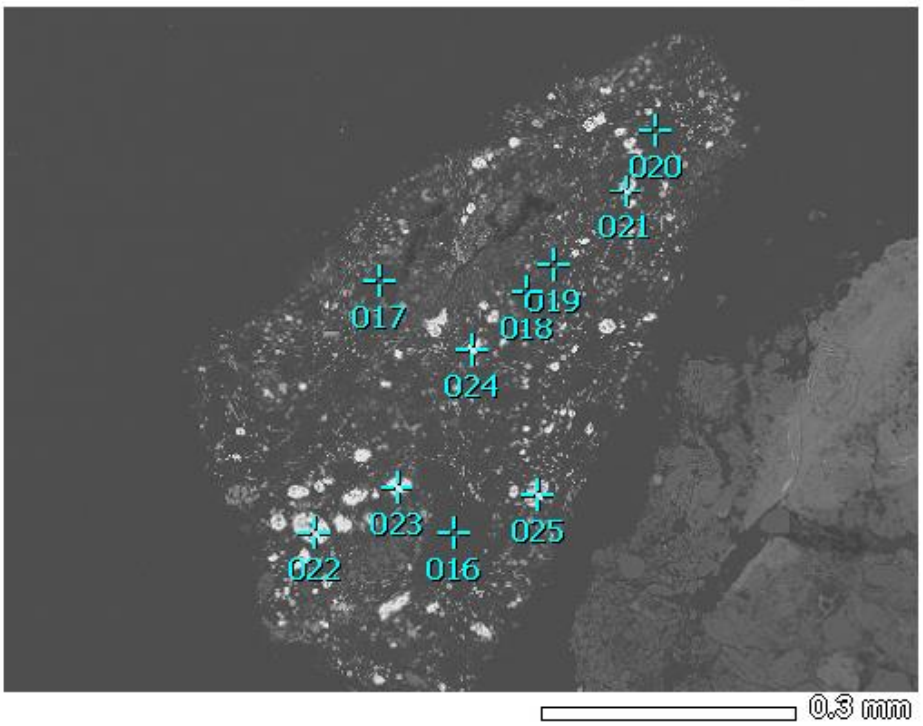


```
Title        : IMG1
--------------------------
Instrument   : 7000F
Volt         : 15.00 kV
Mag          : x 110
Date         : 2014/07/11
Pixel        : 512 x 384
```

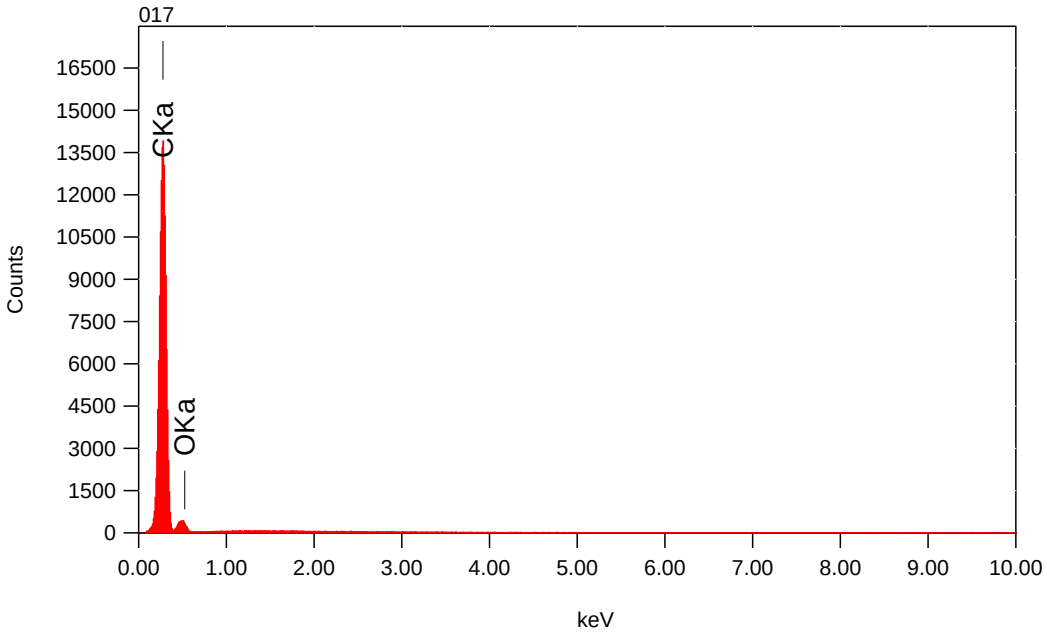


```
Acquisition Parameter
Instrument   : 7000F
Acc. Voltage : 15.0 kV
Probe Current: 0.59000 nA
PHA mode     : T3
Real Time    : 37.14 sec
Live Time    : 30.00 sec
Dead Time    : 19 %
Counting Rate: 4536 cps
Energy Range :  0 - 20 keV
```

ZAF Method Standardless Quantitative Analysis
Fitting Coefficient : 0.4934

Element	(keV)	mass%	Error%	At%	Compound	mass%	Cation	K
C K	0.277	89.7	0.2	92.0				95.4810
O K	0.525	10.3	2.9	8.0				4.5190
Total		100.0		100.0				

2055m Copper

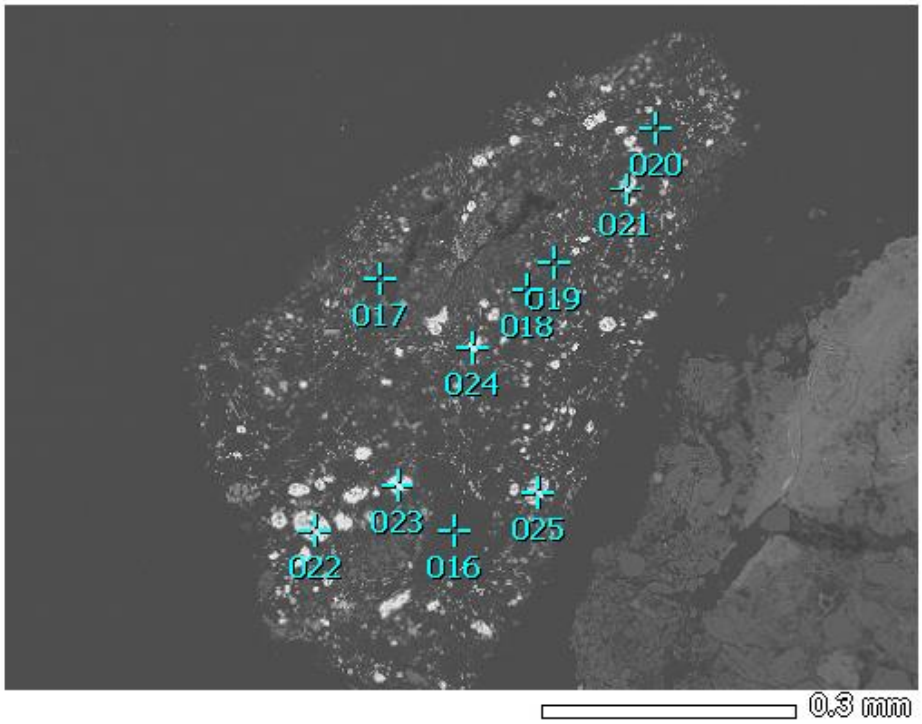


```
Title        : IMG1
---------------------------
Instrument   : 7000F
Volt         : 15.00 kV
Mag          : x 110
Date         : 2014/07/11
Pixel        : 512 x 384
```

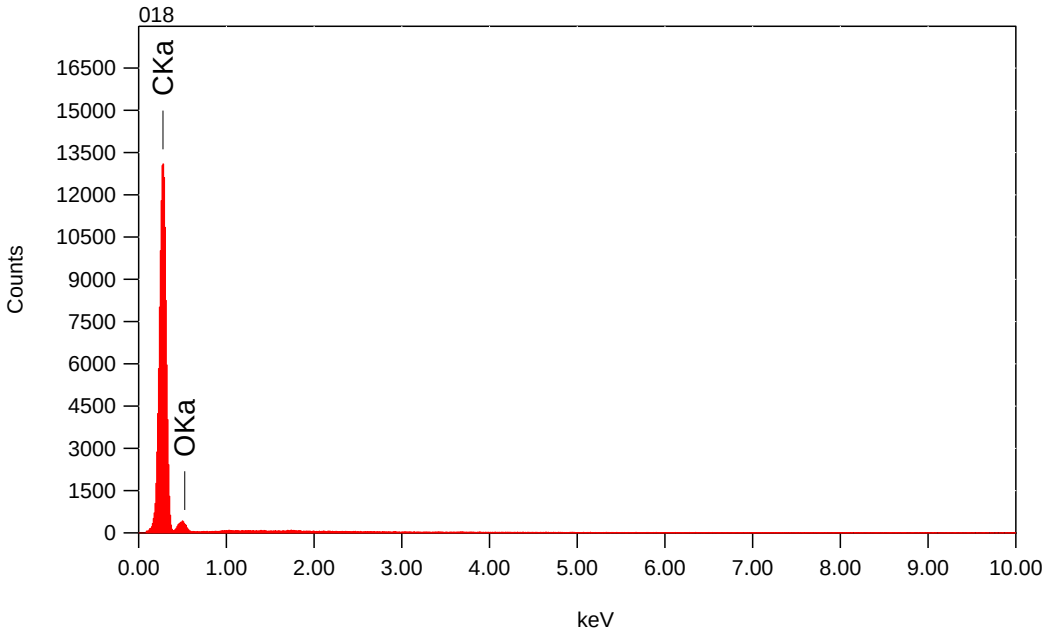


```
Acquisition Parameter
Instrument    : 7000F
Acc. Voltage  : 15.0 kV
Probe Current: 0.59000 nA
PHA mode      : T3
Real Time     : 36.71 sec
Live Time     : 30.00 sec
Dead Time     : 18 %
Counting Rate: 4329 cps
Energy Range :  0 - 20 keV
```

ZAF Method Standardless Quantitative Analysis
Fitting Coefficient : 0.4874

Element	(keV)	mass%	Error%	At%	Compound	mass%	Cation	K
C K	0.277	89.7	0.2	92.1				95.5234
O K	0.525	10.3	2.8	7.9				4.4766
Total		100.0		100.0				

2055m Copper

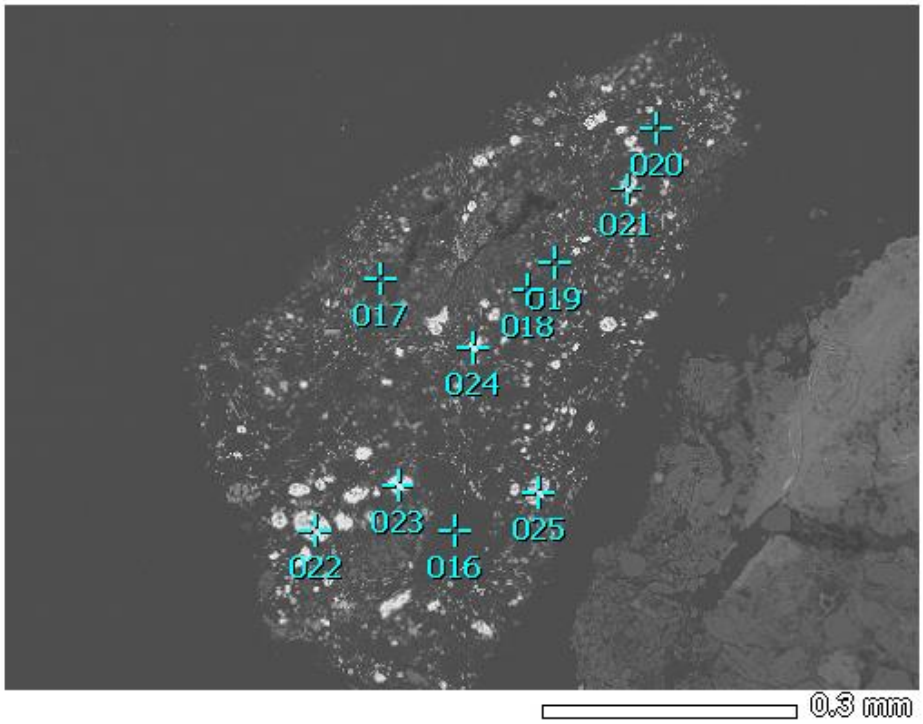


```
Title        : IMG1
--------------------------
Instrument   : 7000F
Volt         : 15.00 kV
Mag          : x 110
Date         : 2014/07/11
Pixel        : 512 x 384
```

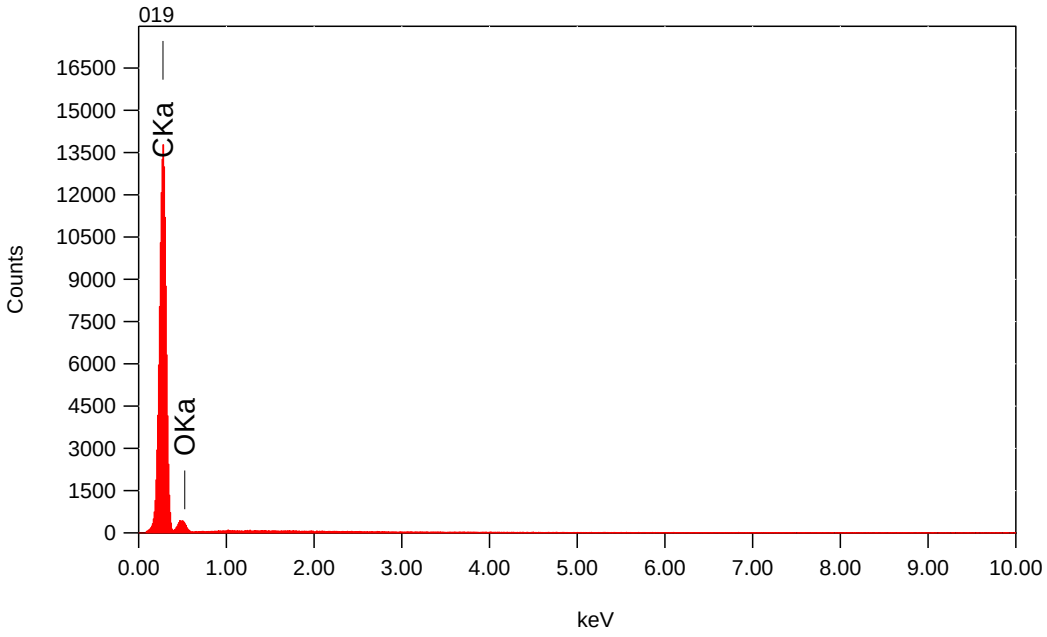


```
Acquisition Parameter
Instrument   : 7000F
Acc. Voltage : 15.0 kV
Probe Current: 0.59000 nA
PHA mode     : T3
Real Time    : 36.89 sec
Live Time    : 30.00 sec
Dead Time    : 18 %
Counting Rate: 4441 cps
Energy Range :  0 - 20 keV
```

ZAF Method Standardless Quantitative Analysis
Fitting Coefficient : 0.5047

Element	(keV)	mass%	Error%	At%	Compound	mass%	Cation	K
C K	0.277	89.8	0.2	92.1				95.5586
O K	0.525	10.2	3.0	7.9				4.4414
Total		100.0		100.0				

2055m Copper

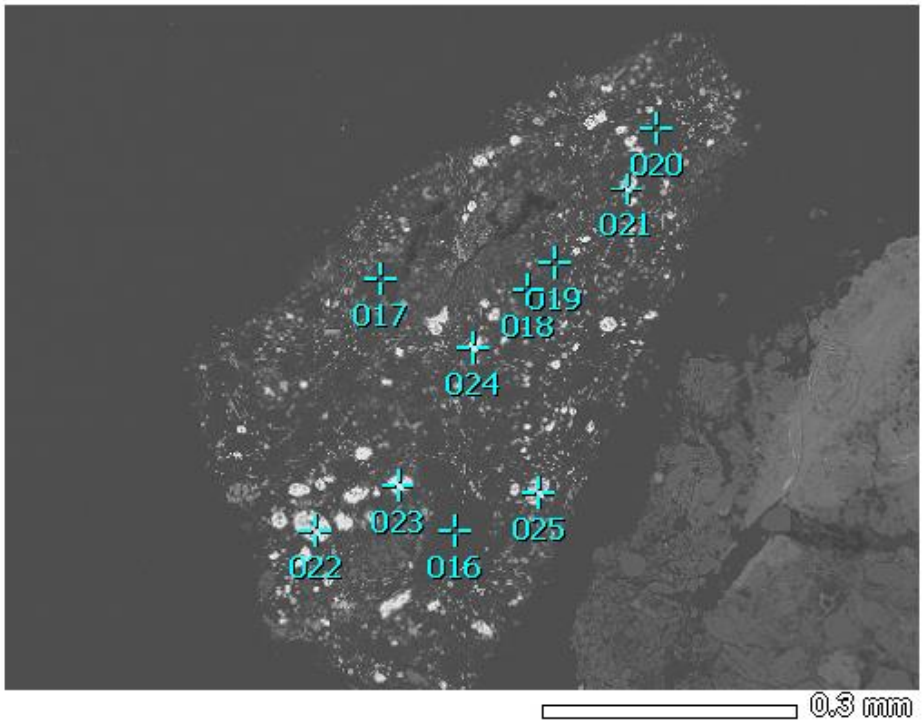


```
Title        : IMG1
--------------------------
Instrument   : 7000F
Volt         : 15.00 kV
Mag          : x 110
Date         : 2014/07/11
Pixel        : 512 x 384
```

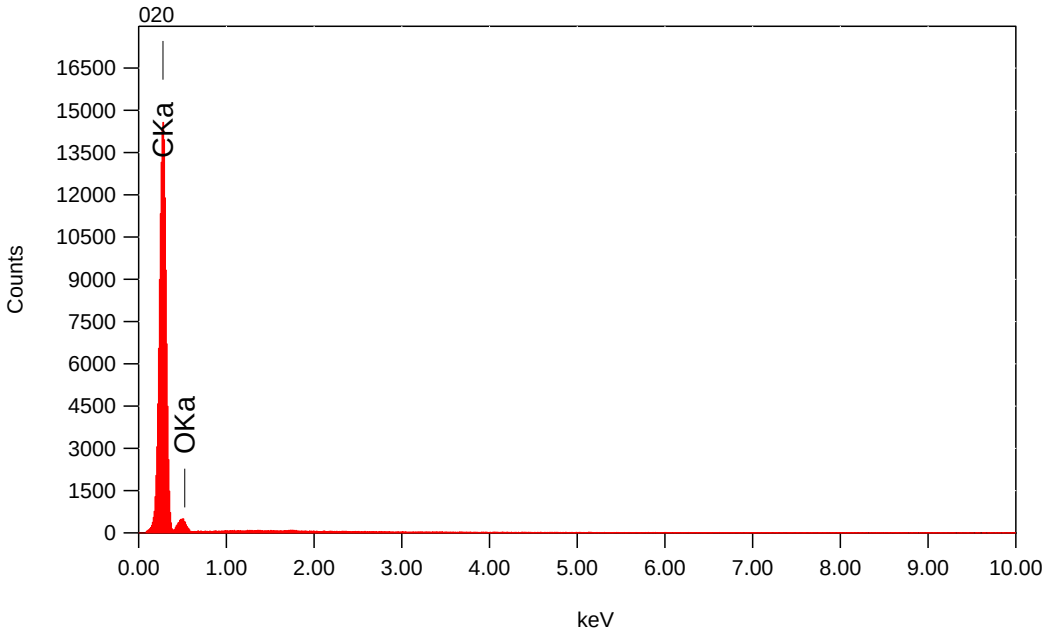


```
Acquisition Parameter
Instrument    : 7000F
Acc. Voltage  : 15.0 kV
Probe Current: 0.59000 nA
PHA mode      : T3
Real Time     : 37.55 sec
Live Time     : 30.00 sec
Dead Time     : 20 %
Counting Rate: 4778 cps
Energy Range :  0 - 20 keV
```

ZAF Method Standardless Quantitative Analysis
Fitting Coefficient : 0.4840

Element	(keV)	mass%	Error%	At%	Compound	mass%	Cation	K
C K	0.277	89.4	0.2	91.8				95.3414
O K	0.525	10.6	2.8	8.2				4.6586
Total		100.0		100.0				

2055m Copper

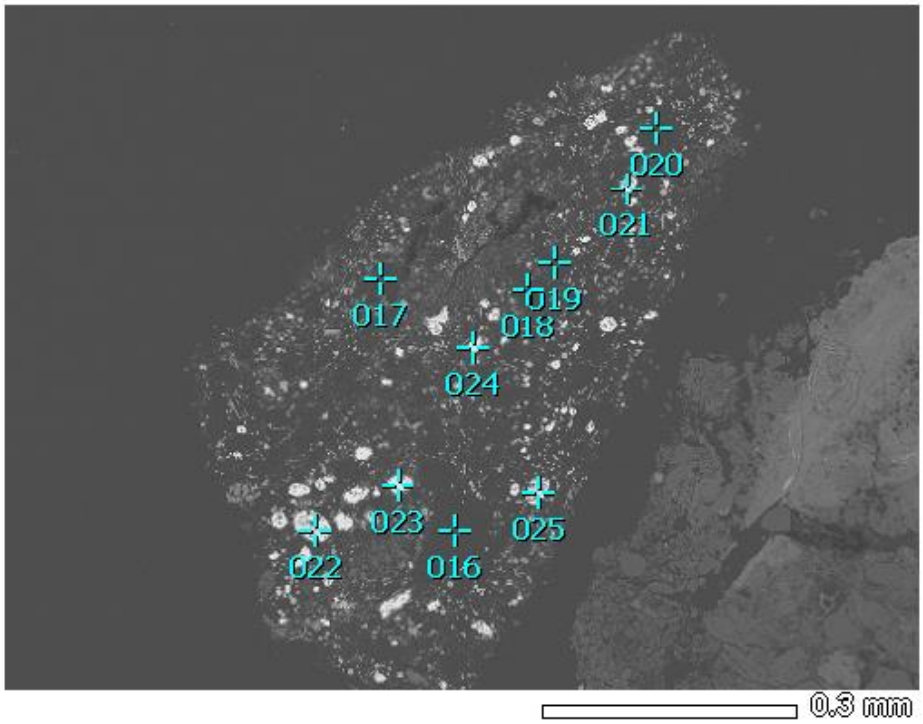


```
Title        : IMG1
---------------------------
Instrument   : 7000F
Volt         : 15.00 kV
Mag          : x 110
Date         : 2014/07/11
Pixel        : 512 x 384
```

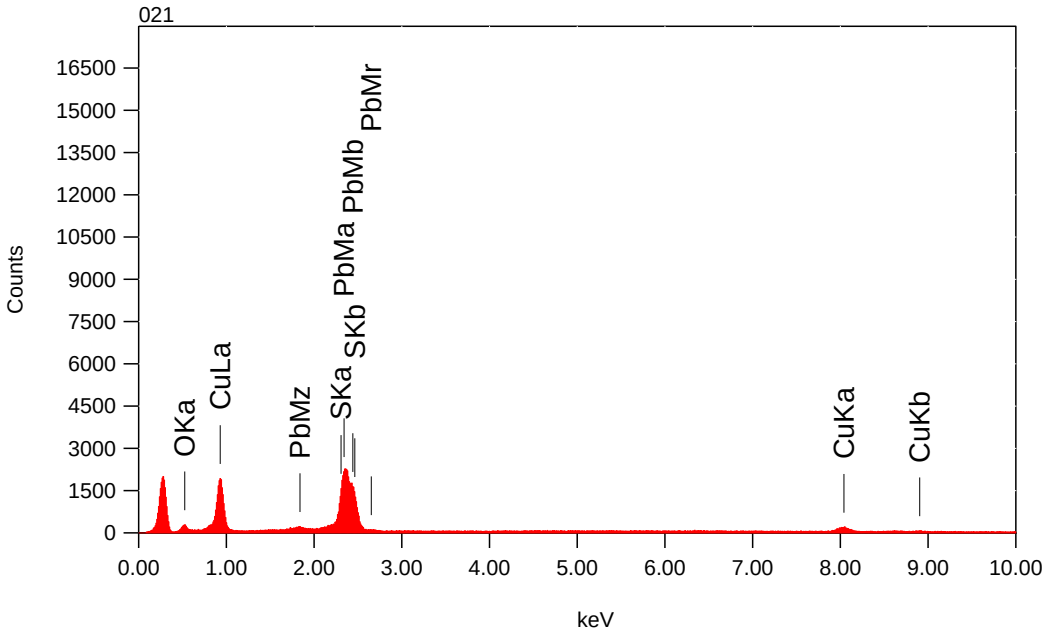


```
Acquisition Parameter
Instrument    : 7000F
Acc. Voltage  : 15.0 kV
Probe Current: 0.59000 nA
PHA mode      : T3
Real Time     : 39.90 sec
Live Time     : 30.00 sec
Dead Time     : 25 %
Counting Rate: 5367 cps
Energy Range :  0 - 20 keV
```

ZAF Method Standardless Quantitative Analysis
Fitting Coefficient : 0.4894

Element	(keV)	mass%	Error%	At%	Compound	mass%	Cation	K
O K	0.525	3.4	0.3	20.3				4.2342
S K	2.307	4.7	0.3	14.2				5.5841
Cu K	8.040	21.7	4.5	32.9				24.8429
Pb M	2.342	70.2	1.5	32.6				65.3388
Total		100.0		100.0				

2055m Copper

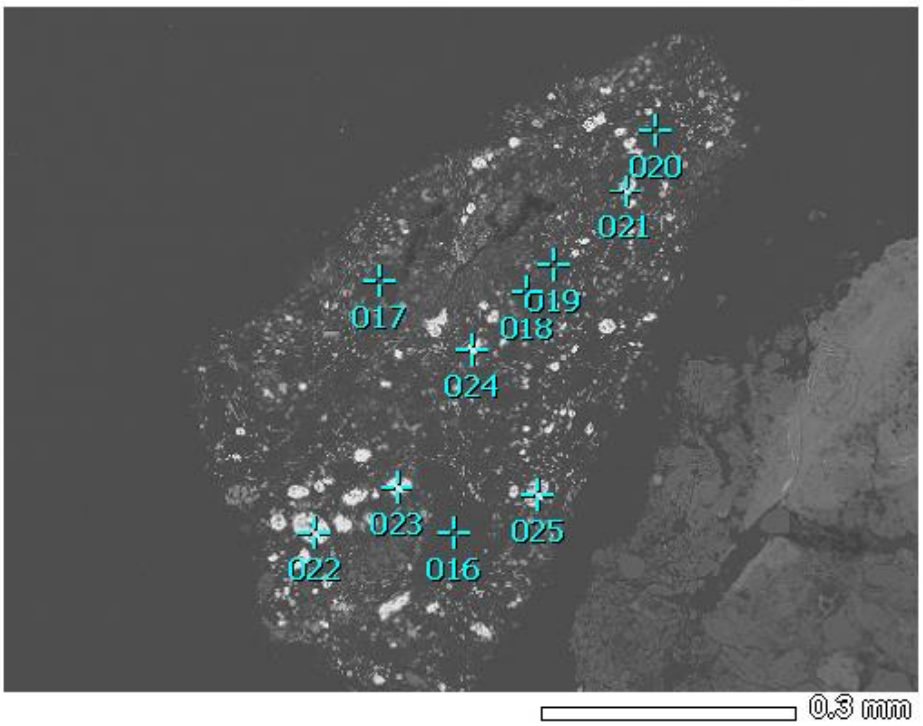


```
Title        : IMG1
---------------------------
Instrument   : 7000F
Volt         : 15.00 kV
Mag          : x 110
Date         : 2014/07/11
Pixel        : 512 x 384
```

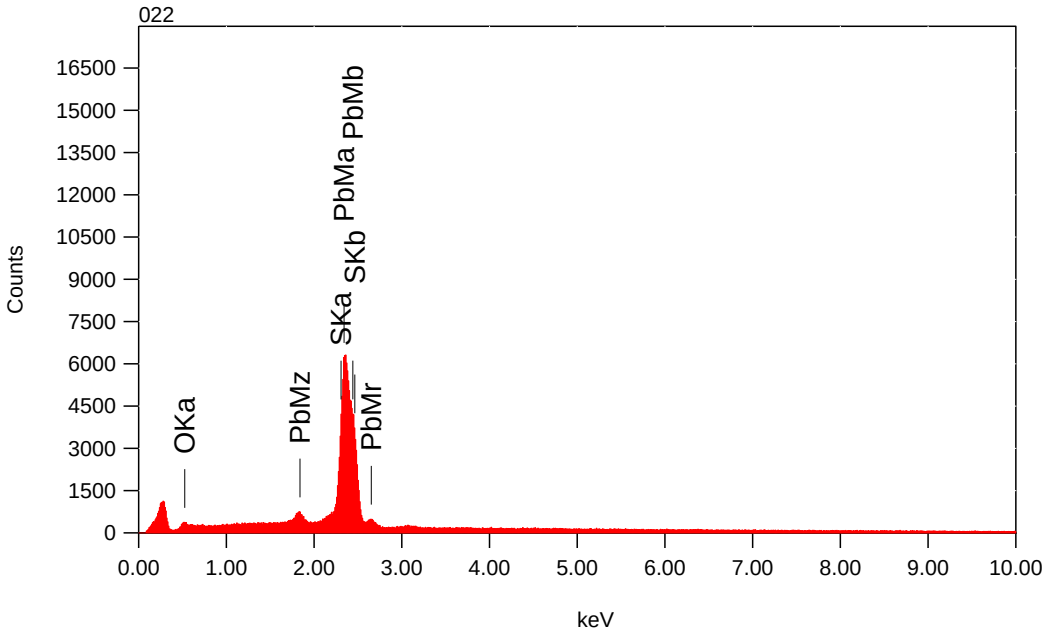


```
Acquisition Parameter
Instrument   : 7000F
Acc. Voltage : 15.0 kV
Probe Current: 0.59000 nA
PHA mode     : T3
Real Time    : 51.91 sec
Live Time    : 30.00 sec
Dead Time    : 41 %
Counting Rate: 9815 cps
Energy Range :  0 - 20 keV
```

ZAF Method Standardless Quantitative Analysis
Fitting Coefficient : 0.3817

Element	(keV)	mass%	Error%	At%	Compound	mass%	Cation	K
O K	0.525	1.6	0.1	13.7				1.9932
S K	2.307	6.1	0.1	25.9				7.6114
Pb M	2.342	92.3	0.5	60.4				90.3954
Total		100.0		100.0				

2055m Copper

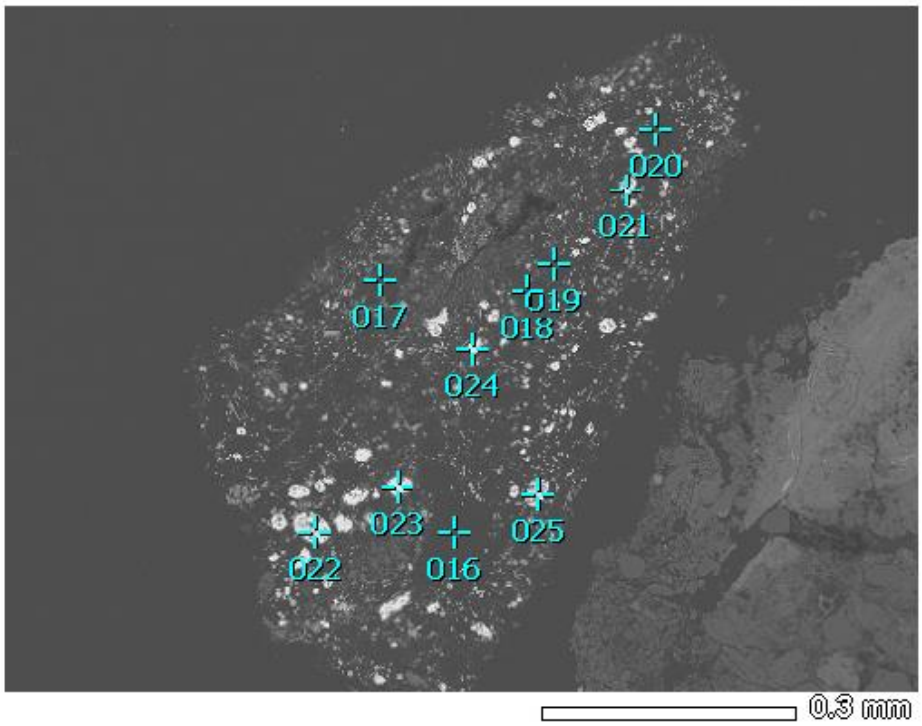


```
Title        : IMG1
--------------------------
Instrument   : 7000F
Volt         : 15.00 kV
Mag          : x 110
Date         : 2014/07/11
Pixel        : 512 x 384
```

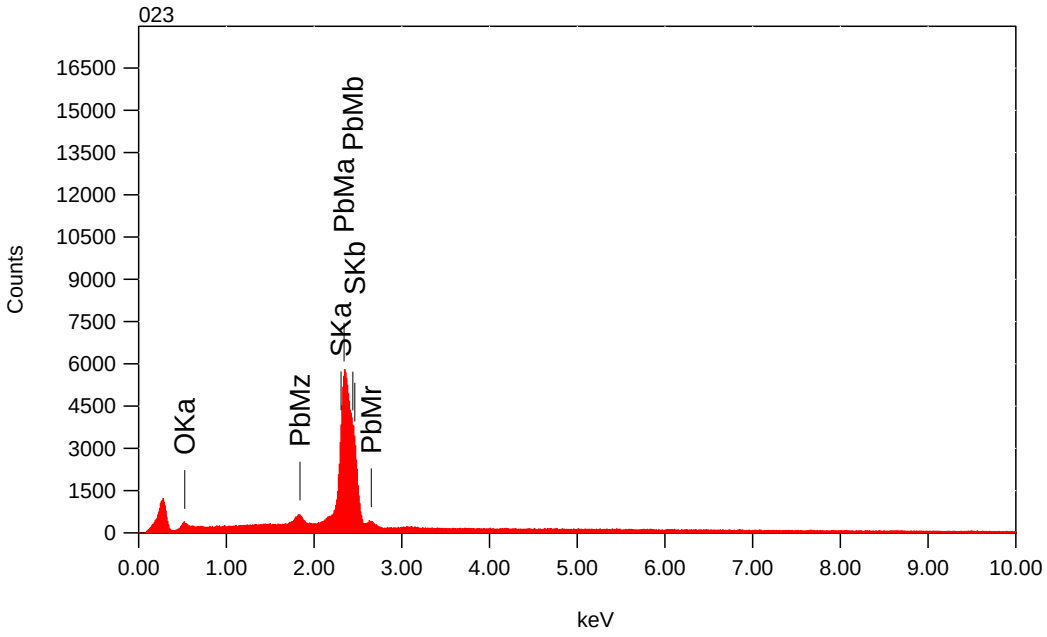


```
Acquisition Parameter
Instrument   : 7000F
Acc. Voltage : 15.0 kV
Probe Current: 0.59000 nA
PHA mode     : T3
Real Time    : 49.26 sec
Live Time    : 30.00 sec
Dead Time    : 38 %
Counting Rate: 8939 cps
Energy Range :  0 - 20 keV
```

ZAF Method Standardless Quantitative Analysis
Fitting Coefficient : 0.4048

Element	(keV)	mass%	Error%	At%	Compound	mass%	Cation	K
O K	0.525	1.9	0.1	15.9				2.3912
S K	2.307	6.3	0.1	25.9				7.8300
Pb M	2.342	91.7	0.5	58.2				89.7788
Total		100.0		100.0				

2055m Copper

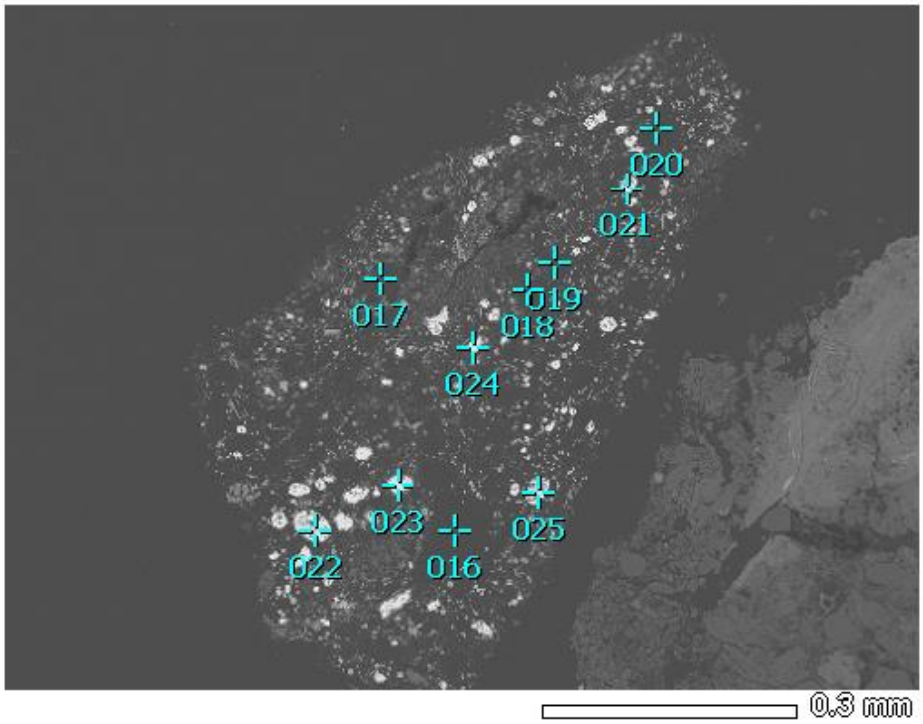


```
Title        : IMG1
---------------------------
Instrument   : 7000F
Volt         : 15.00 kV
Mag          : x 110
Date         : 2014/07/11
Pixel        : 512 x 384
```

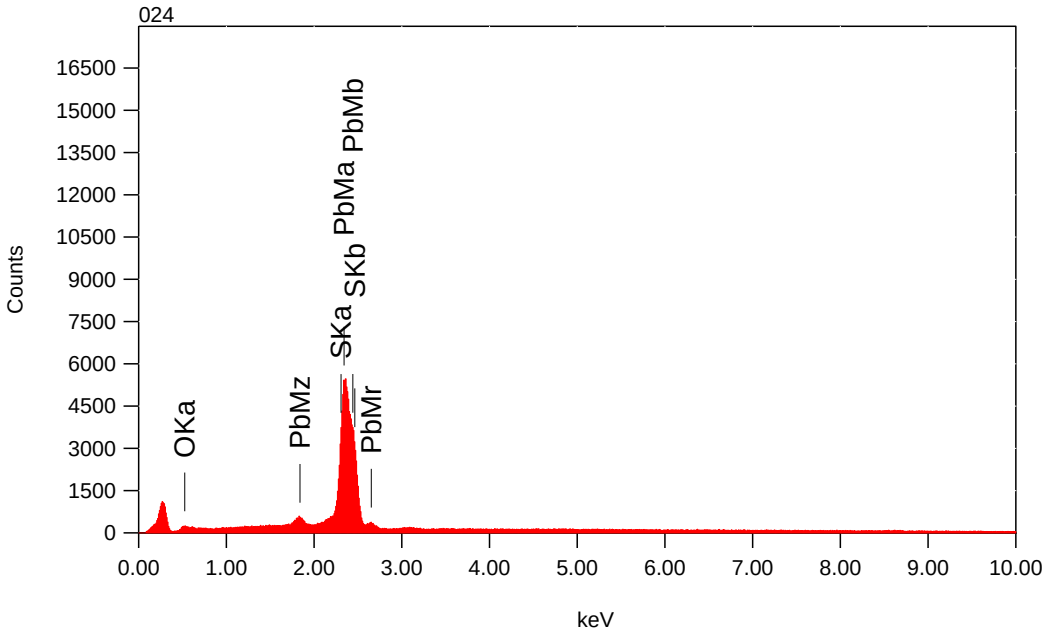


```
Acquisition Parameter
Instrument   : 7000F
Acc. Voltage : 15.0 kV
Probe Current: 0.59000 nA
PHA mode     : T3
Real Time    : 47.67 sec
Live Time    : 30.00 sec
Dead Time    : 36 %
Counting Rate: 8337 cps
Energy Range :  0 - 20 keV
```

ZAF Method Standardless Quantitative Analysis
Fitting Coefficient : 0.4040

Element	(keV)	mass%	Error%	At%	Compound	mass%	Cation	K
O K	0.525	1.2	0.1	10.4				1.5034
S K	2.307	6.9	0.1	29.2				8.5139
Pb M	2.342	91.9	0.5	60.4				89.9828
Total		100.0		100.0				

2055m Copper

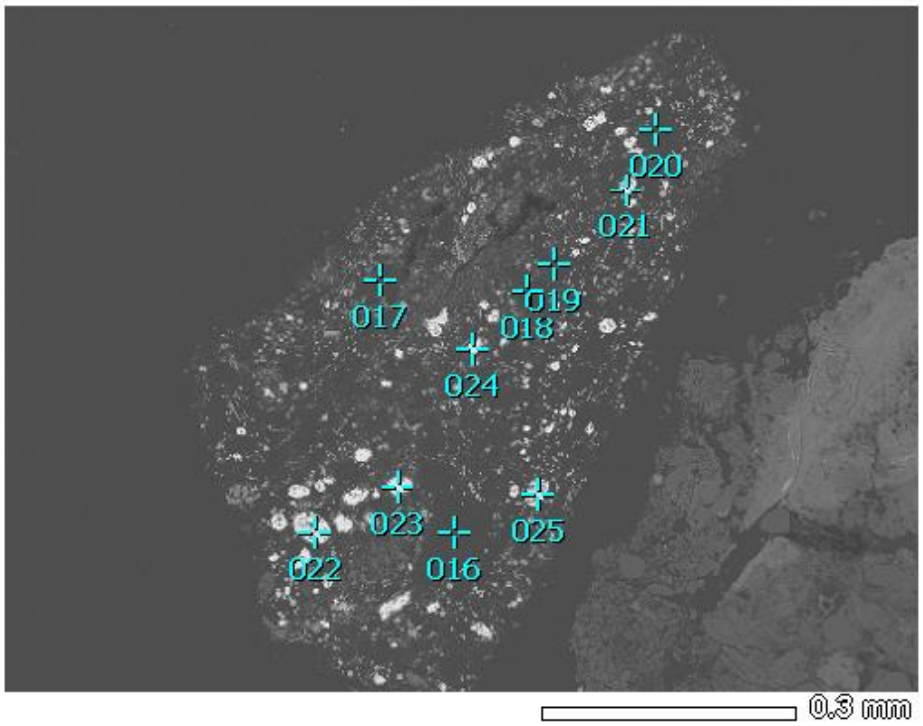


```
Title        : IMG1
---------------------------
Instrument   : 7000F
Volt         : 15.00 kV
Mag          : x 110
Date         : 2014/07/11
Pixel        : 512 x 384
```

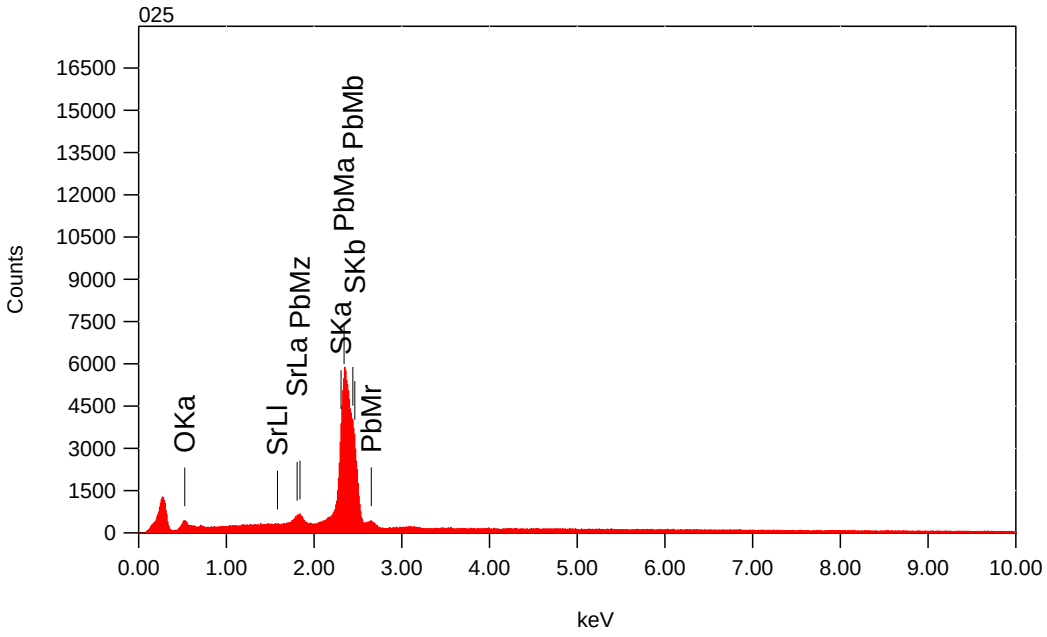


```
Acquisition Parameter
Instrument    : 7000F
Acc. Voltage  : 15.0 kV
Probe Current: 0.59000 nA
PHA mode      : T3
Real Time     : 49.41 sec
Live Time     : 30.00 sec
Dead Time     : 38 %
Counting Rate: 8856 cps
Energy Range :  0 - 20 keV
```

ZAF Method Standardless Quantitative Analysis
Fitting Coefficient : 0.3970

Element	(keV)	mass%	Error%	At%	Compound	mass%	Cation	K
O K	0.525	2.3	0.1	18.6				2.8480
S K	2.307	5.9	0.1	23.7				7.2996
Sr L	1.806	0.8	0.4	1.2				0.8591
Pb M	2.342	91.0	0.5	56.6				88.9933
Total		100.0		100.0				

2055m Copper

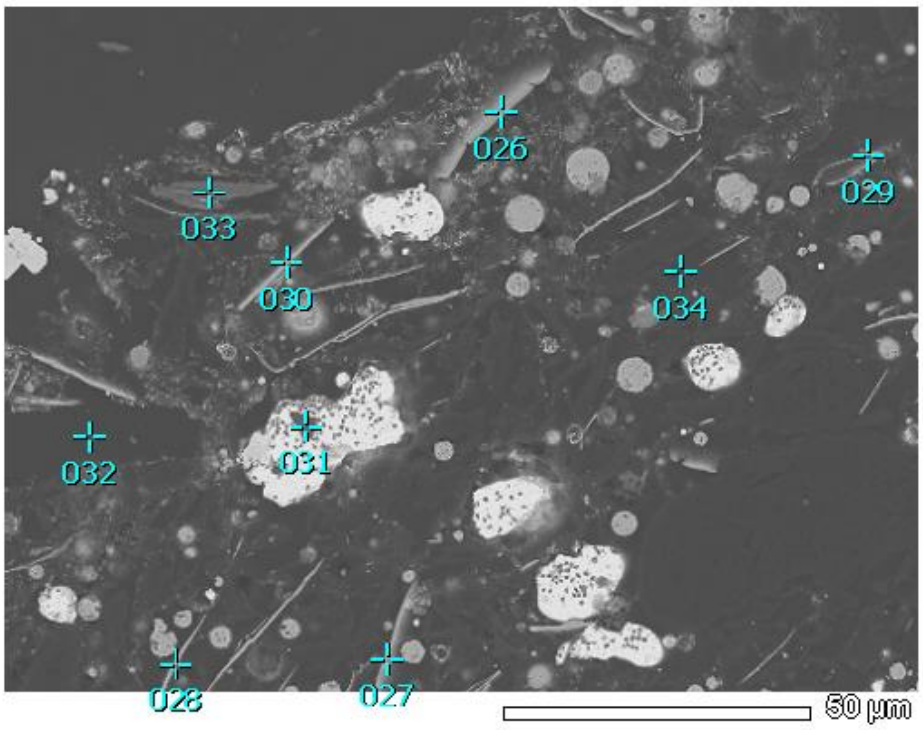


```
Title        : IMG1
--------------------------
Instrument   : 7000F
Volt         : 15.00 kV
Mag          : x 800
Date         : 2014/07/11
Pixel        : 512 x 384
```

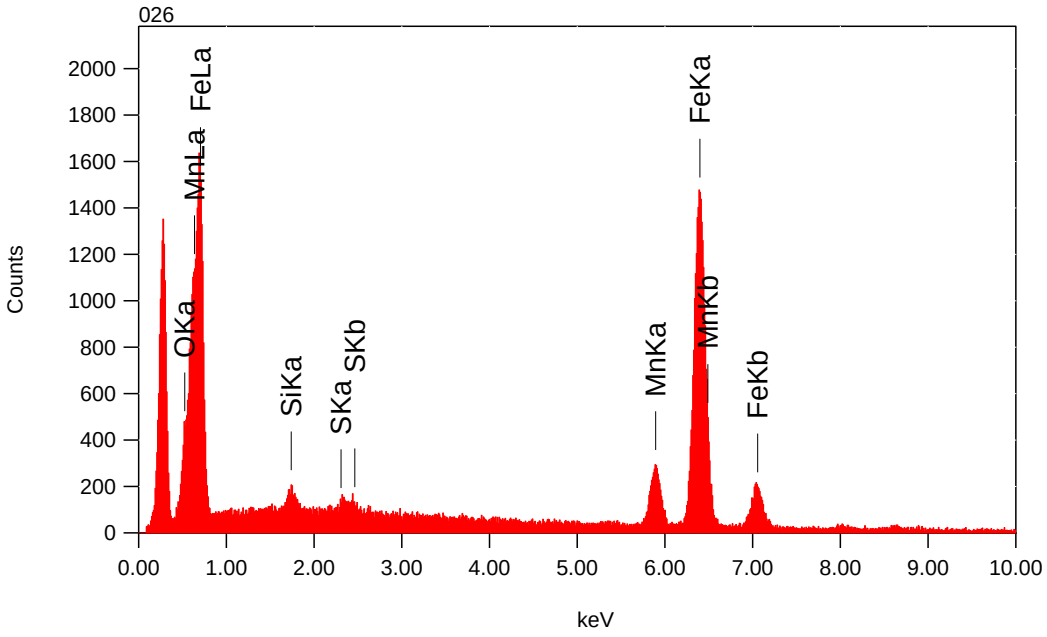


```
Acquisition Parameter
Instrument    : 7000F
Acc. Voltage  : 15.0 kV
Probe Current: 0.59000 nA
PHA mode      : T3
Real Time     : 37.37 sec
Live Time     : 30.00 sec
Dead Time     : 19 %
Counting Rate: 4075 cps
Energy Range :  0 - 20 keV
```

ZAF Method Standardless Quantitative Analysis
Fitting Coefficient : 0.3344

Element	(keV)	mass%	Error%	At%	Compound	mass%	Cation	K
O K*	0.525	1.4	0.1	4.6				2.0508
Si K	1.739	0.7	0.3	1.3				0.4715
S K*	2.307	0.2	0.2	0.3				0.1700
Mn K	5.894	12.3	1.0	12.0				12.0932
Fe K	6.398	85.4	1.1	81.8				85.2144
Total		100.0		100.0				

2055m Copper

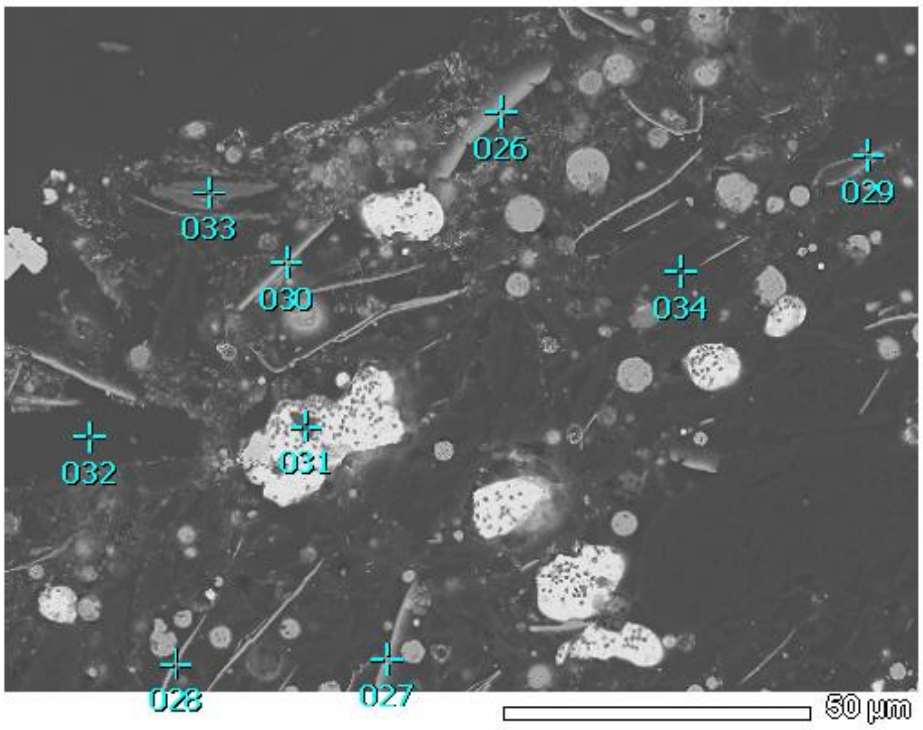


```
Title        : IMG1
---------------------------
Instrument   : 7000F
Volt         : 15.00 kV
Mag          : x 800
Date         : 2014/07/11
Pixel        : 512 x 384
```

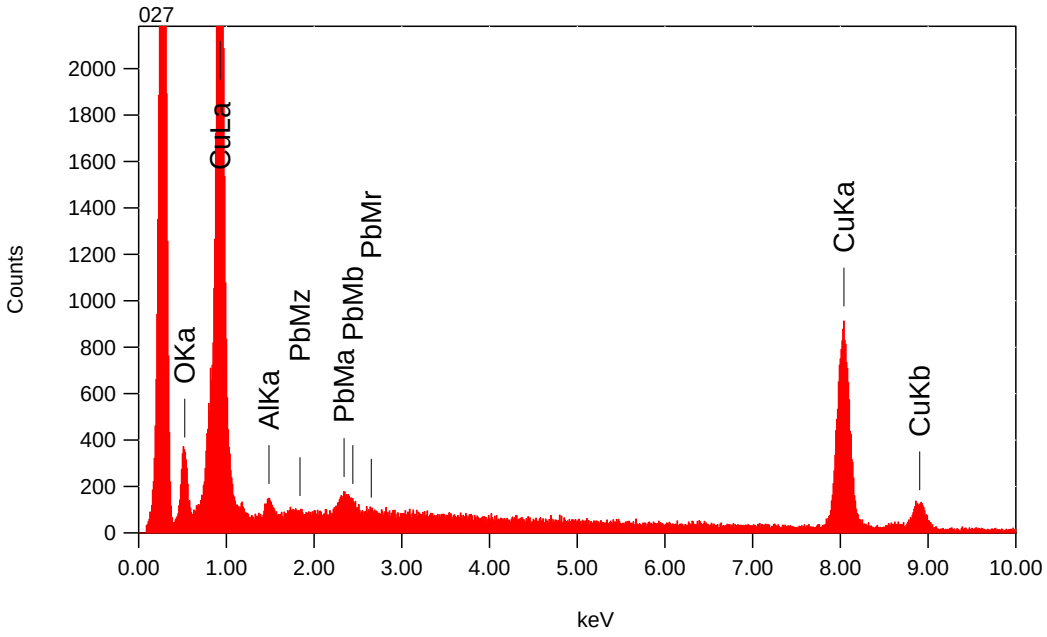


```
Acquisition Parameter
Instrument    : 7000F
Acc. Voltage  : 15.0 kV
Probe Current: 0.59000 nA
PHA mode      : T3
Real Time     : 39.03 sec
Live Time     : 30.00 sec
Dead Time     : 22 %
Counting Rate: 4971 cps
Energy Range :  0 - 20 keV
```

ZAF Method Standardless Quantitative Analysis
Fitting Coefficient : 0.4973

Element	(keV)	mass%	Error%	At%	Compound	mass%	Cation	K
O K	0.525	3.3	0.5	11.9				4.0439
Al K*	1.486	0.7	0.8	1.5				0.3505
Cu K	8.040	94.3	7.0	86.1				94.3928
Pb M*	2.342	1.7	2.6	0.5				1.2127
Total		100.0		100.0				

2055m Copper

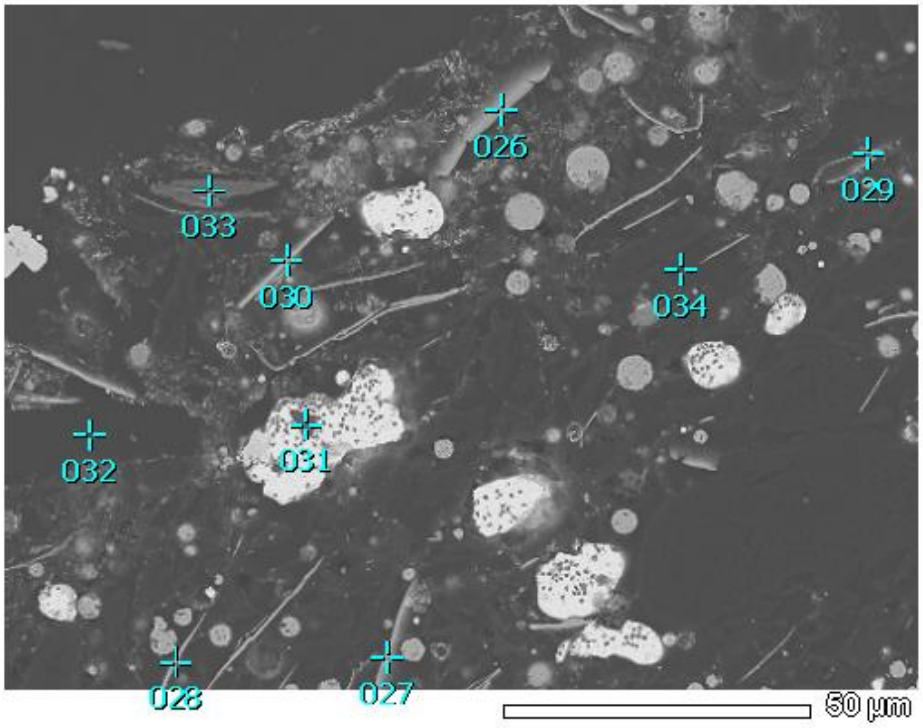


```
Title        : IMG1
--------------------------
Instrument   : 7000F
Volt         : 15.00 kV
Mag          : x 800
Date         : 2014/07/11
Pixel        : 512 x 384
```

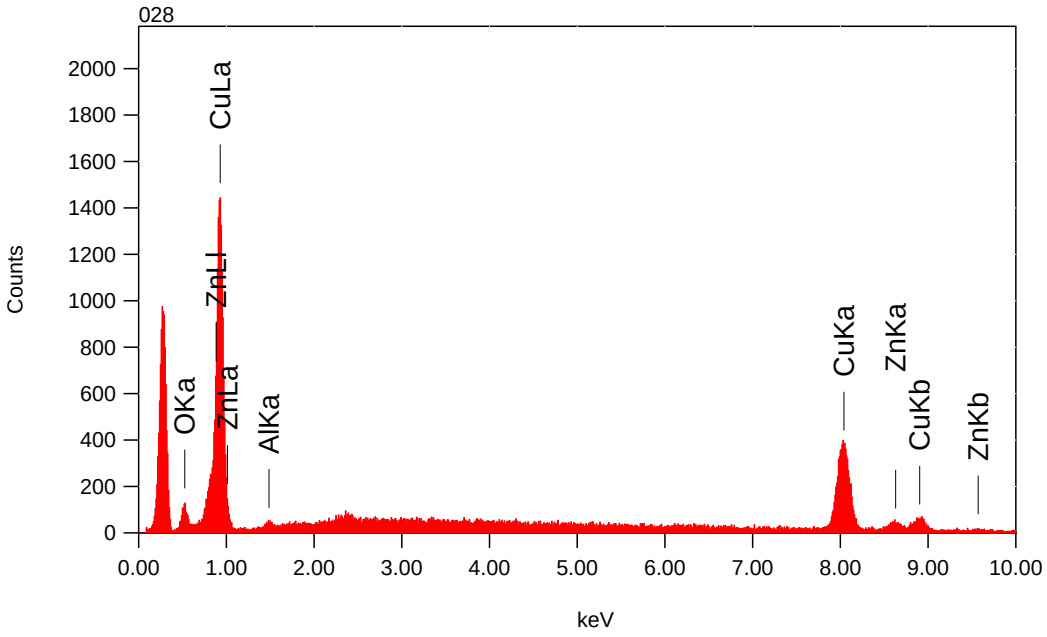


```
Acquisition Parameter
Instrument    : 7000F
Acc. Voltage  : 15.0 kV
Probe Current: 0.59000 nA
PHA mode      : T3
Real Time     : 33.76 sec
Live Time     : 30.00 sec
Dead Time     : 11 %
Counting Rate: 2331 cps
Energy Range :  0 - 20 keV
```

ZAF Method Standardless Quantitative Analysis
Fitting Coefficient : 0.4323

Element	(keV)	mass%	Error%	At%	Compound	mass%	Cation	K
O K	0.525	2.1	0.2	8.0				2.6005
Al K	1.486	0.6	0.4	1.2				0.2679
Cu K	8.040	86.3	3.5	80.8				86.1614
Zn K	8.630	11.0	4.9	10.0				10.9702
Total		100.0		100.0				

2055m Copper

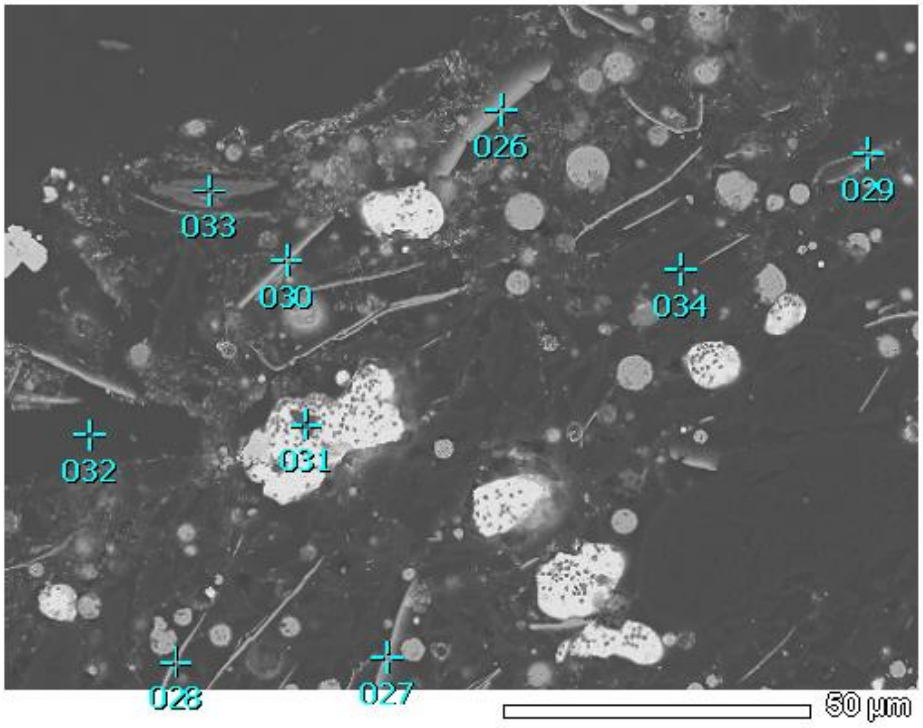


```
Title        : IMG1
---------------------------
Instrument   : 7000F
Volt         : 15.00 kV
Mag          : x 800
Date         : 2014/07/11
Pixel        : 512 x 384
```

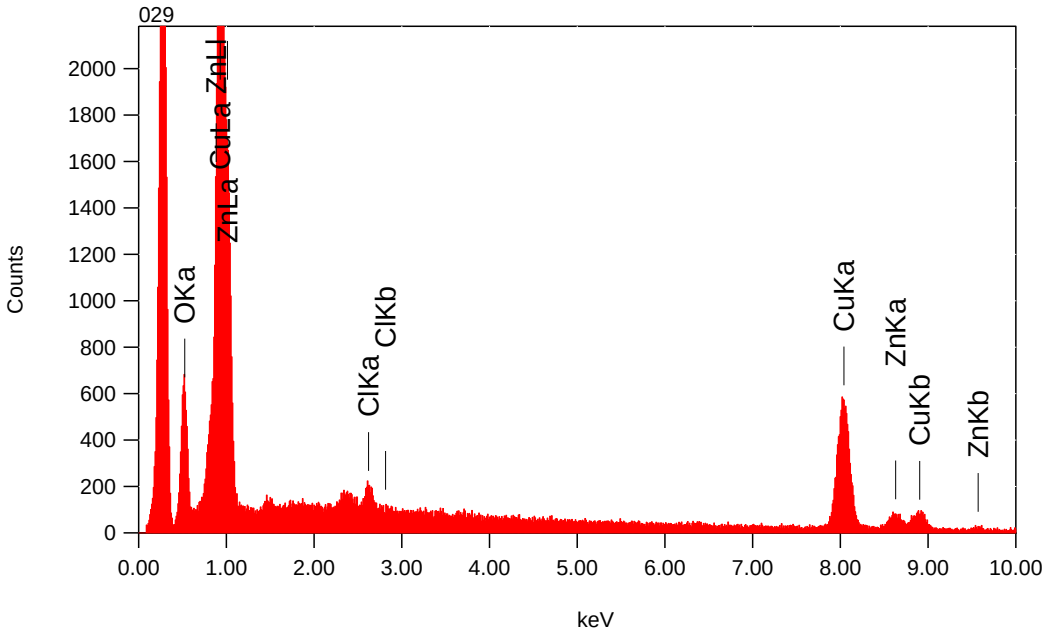


```
Acquisition Parameter
Instrument    : 7000F
Acc. Voltage  : 15.0 kV
Probe Current: 0.59000 nA
PHA mode      : T3
Real Time     : 39.14 sec
Live Time     : 30.00 sec
Dead Time     : 23 %
Counting Rate: 4982 cps
Energy Range :  0 - 20 keV
```

ZAF Method Standardless Quantitative Analysis
Fitting Coefficient : 0.5407

Element	(keV)	mass%	Error%	At%	Compound	mass%	Cation	K
O K	0.525	7.7	0.4	24.6				9.1996
Cl K	2.621	1.4	0.6	2.0				1.3360
Cu K	8.040	79.2	6.8	64.2				77.9098
Zn K	8.630	11.8	9.7	9.3				11.5546
Total		100.0		100.0				

2055m Copper

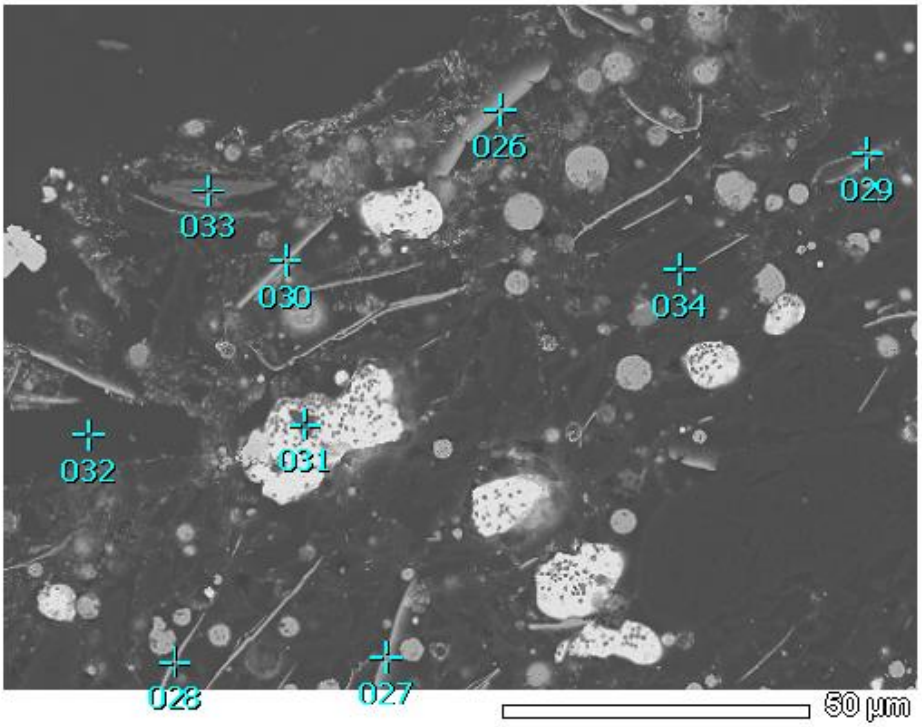


```
Title          : IMG1
---------------------------
Instrument     : 7000F
Volt           : 15.00 kV
Mag            : x 800
Date           : 2014/07/11
Pixel          : 512 x 384
```

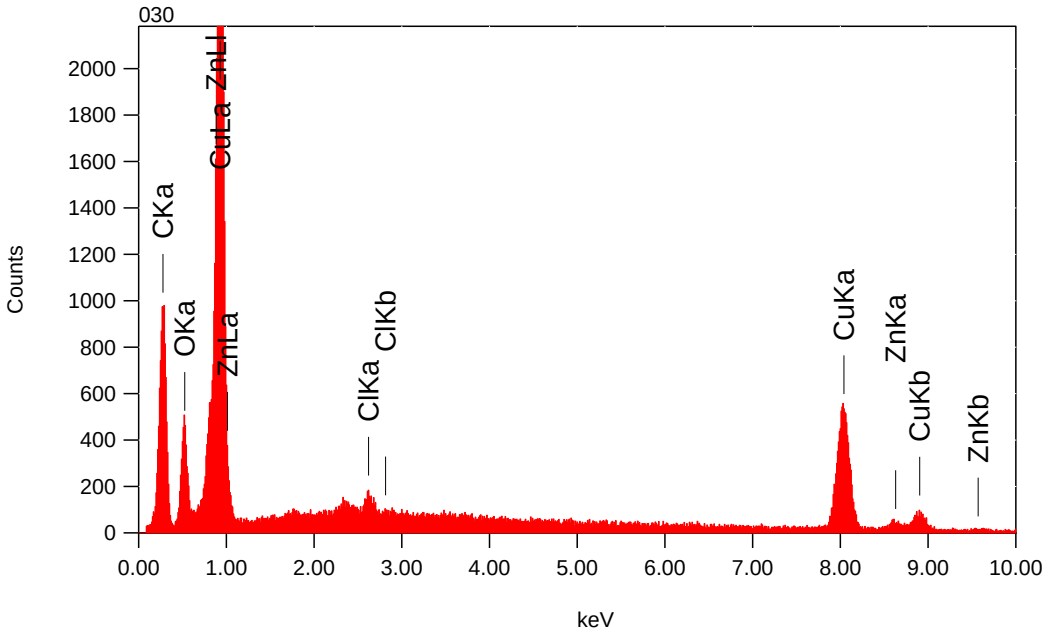


```
Acquisition Parameter
Instrument     : 7000F
Acc. Voltage   : 15.0 kV
Probe Current: 0.59000 nA
PHA mode       : T3
Real Time      : 36.78 sec
Live Time      : 30.00 sec
Dead Time      : 18 %
Counting Rate: 3820 cps
Energy Range :  0 - 20 keV
```

ZAF Method Standardless Quantitative Analysis
Fitting Coefficient : 0.2590

Element	(keV)	mass%	Error%	At%	Compound	mass%	Cation	K
C K	0.277	23.2	0.1	56.3				6.8126
O K	0.525	6.1	0.1	11.0				6.8727
Cl K	2.621	0.8	0.1	0.7				1.0617
Cu K	8.040	64.8	1.4	29.7				79.0037
Zn K	8.630	5.1	2.0	2.3				6.2493
Total		100.0		100.0				

2055m Copper

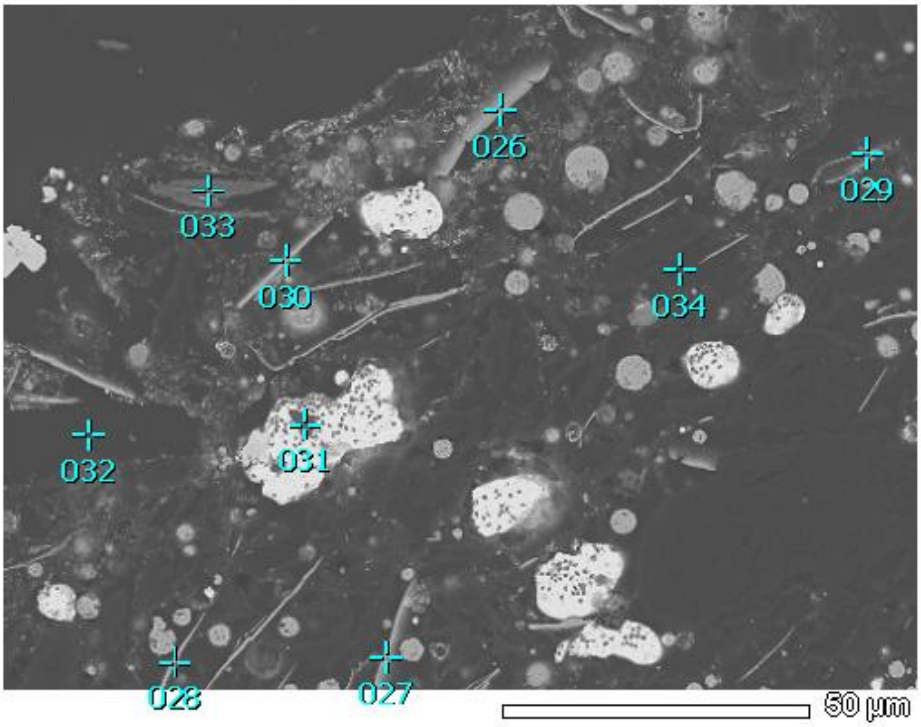


```
Title          : IMG1
---------------------------
Instrument     : 7000F
Volt           : 15.00 kV
Mag            : x 800
Date           : 2014/07/11
Pixel          : 512 x 384
```

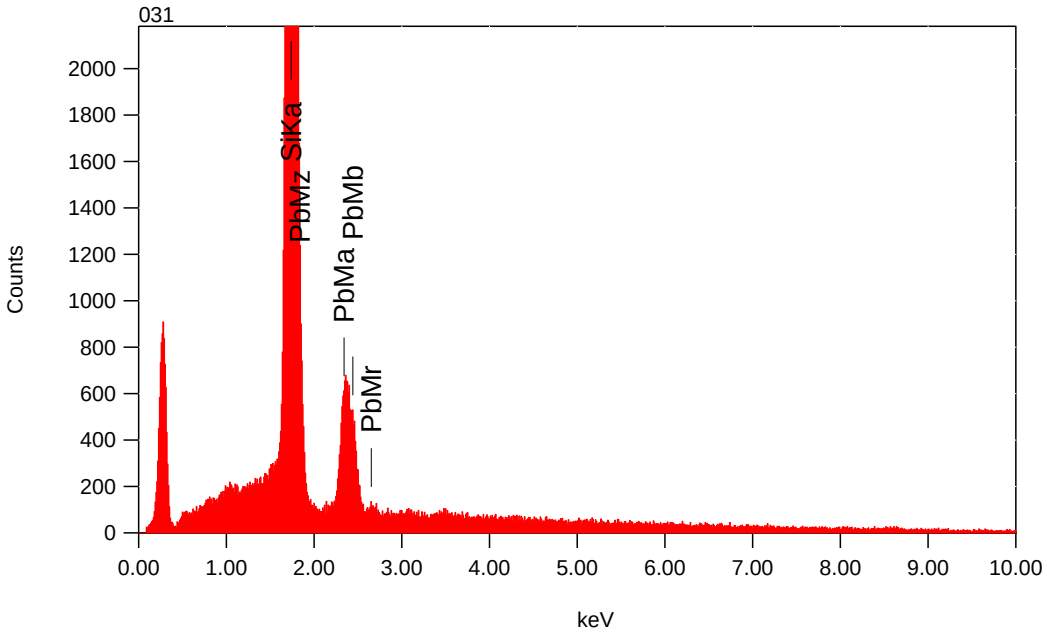


```
Acquisition Parameter
Instrument     : 7000F
Acc. Voltage   : 15.0 kV
Probe Current: 0.59000 nA
PHA mode       : T3
Real Time      : 45.13 sec
Live Time      : 30.00 sec
Dead Time      : 32 %
Counting Rate: 7262 cps
Energy Range :  0 - 20 keV
```

ZAF Method Standardless Quantitative Analysis
Fitting Coefficient : 0.2140

Element	(keV)	mass%	Error%	At%	Compound	mass%	Cation	K
Si K	1.739	79.9	0.2	96.7				87.0448
Pb M	2.342	20.1	1.7	3.3				12.9552
Total		100.0		100.0				

2055m Copper

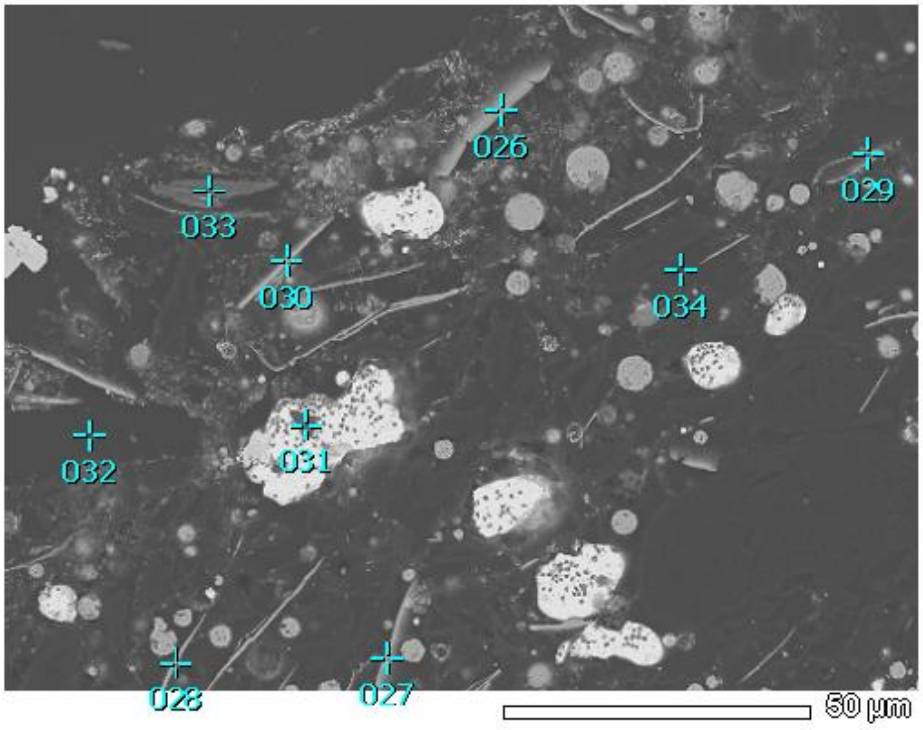


```
Title        : IMG1
--------------------------
Instrument   : 7000F
Volt         : 15.00 kV
Mag          : x 800
Date         : 2014/07/11
Pixel        : 512 x 384
```

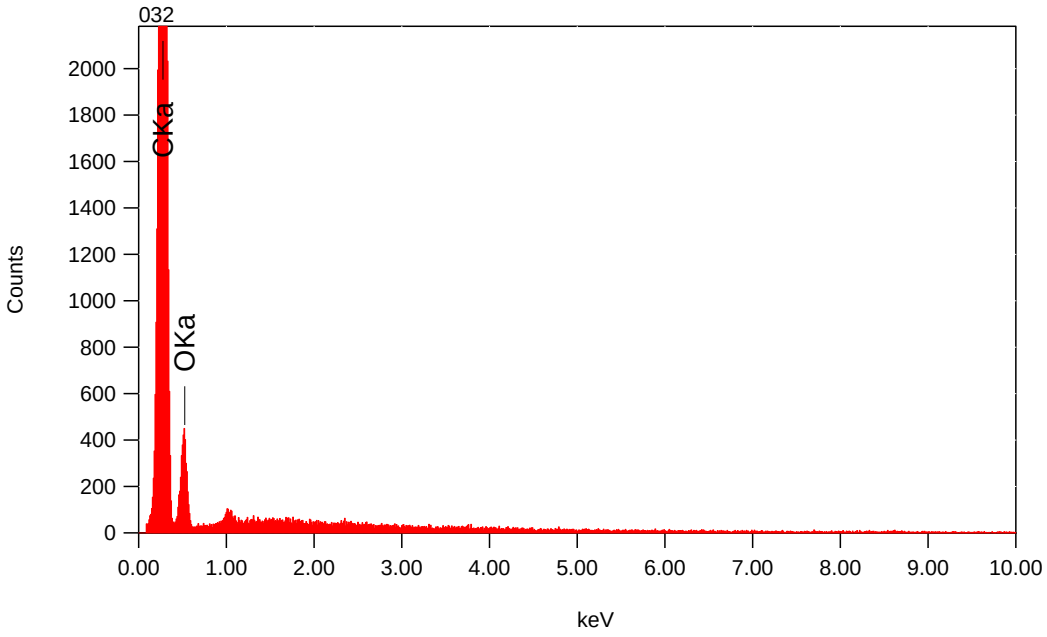


```
Acquisition Parameter
Instrument   : 7000F
Acc. Voltage : 15.0 kV
Probe Current: 0.59000 nA
PHA mode     : T3
Real Time    : 33.77 sec
Live Time    : 30.00 sec
Dead Time    : 11 %
Counting Rate: 2643 cps
Energy Range :  0 - 20 keV
```

ZAF Method Standardless Quantitative Analysis
Fitting Coefficient : 0.4879

Element	(keV)	mass%	Error%	At%	Compound	mass%	Cation	K
C K	0.277	78.3	0.2	82.8				87.0766
O K	0.525	21.7	2.0	17.2				12.9234
Total		100.0		100.0				

2055m Copper

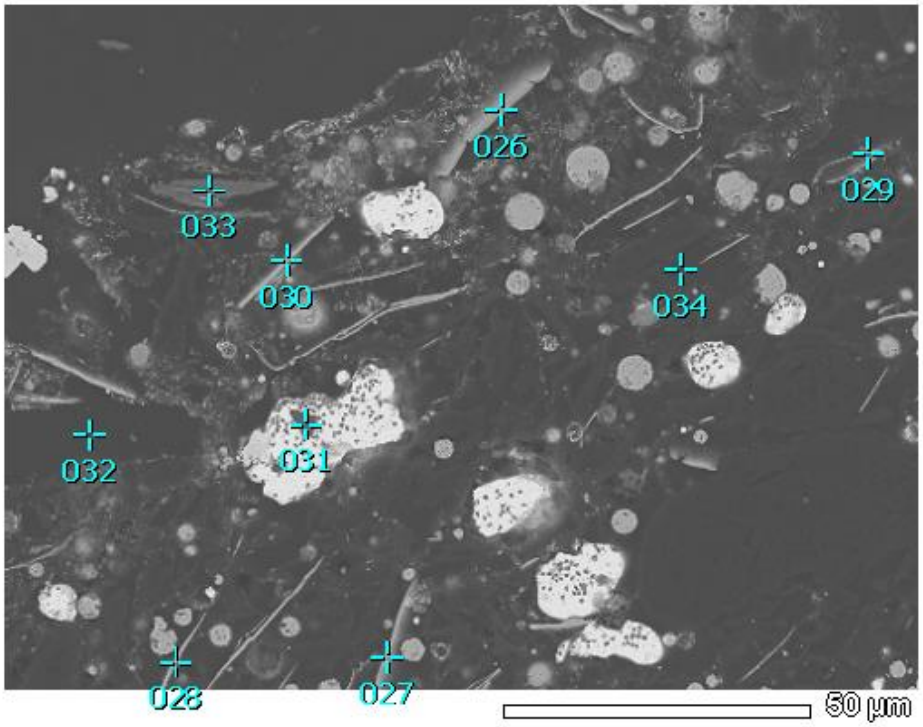


```
Title        : IMG1
---------------------------
Instrument   : 7000F
Volt         : 15.00 kV
Mag          : x 800
Date         : 2014/07/11
Pixel        : 512 x 384
```

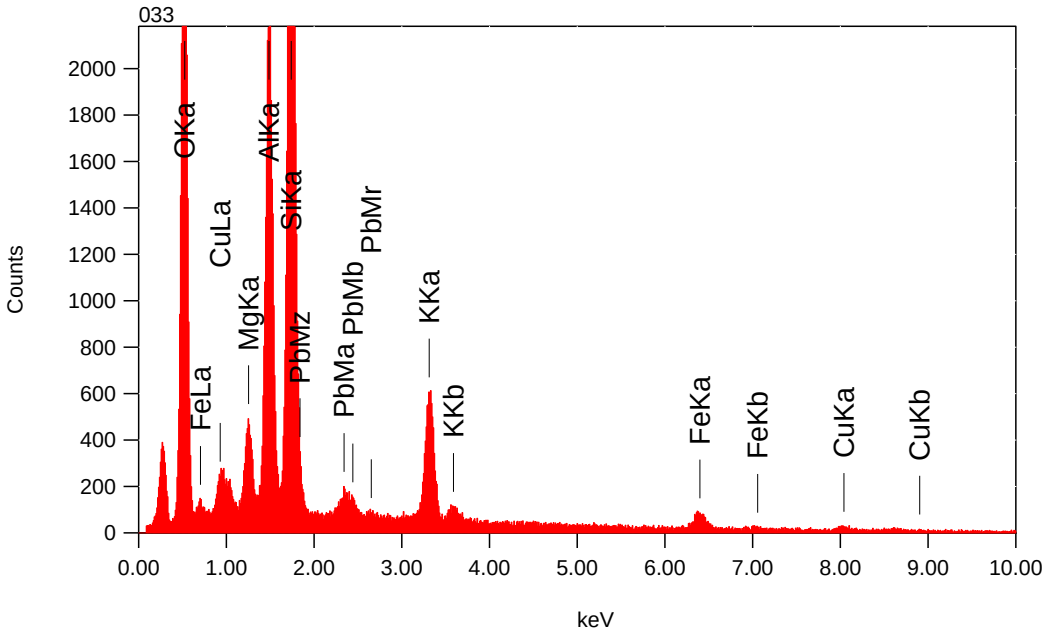


```
Acquisition Parameter
Instrument    : 7000F
Acc. Voltage  : 15.0 kV
Probe Current: 0.59000 nA
PHA mode      : T3
Real Time     : 39.58 sec
Live Time     : 30.00 sec
Dead Time     : 23 %
Counting Rate: 4967 cps
Energy Range :  0 - 20 keV
```

ZAF Method Standardless Quantitative Analysis
Fitting Coefficient : 0.2100

Element	(keV)	mass%	Error%	At%	Compound	mass%	Cation	K
O K	0.525	44.8	0.1	61.7				48.4998
Mg K	1.253	2.3	0.1	2.1				1.8384
Al K	1.486	12.9	0.1	10.6				11.4823
Si K	1.739	23.8	0.1	18.7				21.6875
K K	3.312	7.8	0.2	4.4				8.6544
Fe K	6.398	3.9	0.8	1.5				3.8795
Cu K	8.040	2.3	2.0	0.8				2.2305
Pb M	2.342	2.2	0.7	0.2				1.7276
Total		100.0		100.0				

2055m Copper

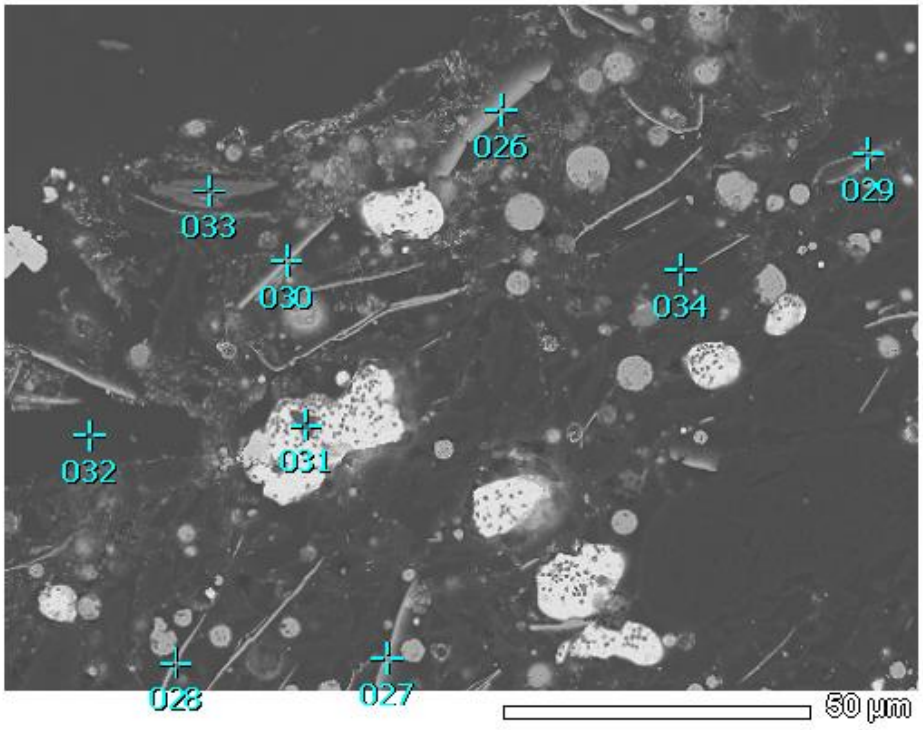


```
Title        : IMG1
--------------------------
Instrument   : 7000F
Volt         : 15.00 kV
Mag          : x 800
Date         : 2014/07/11
Pixel        : 512 x 384
```

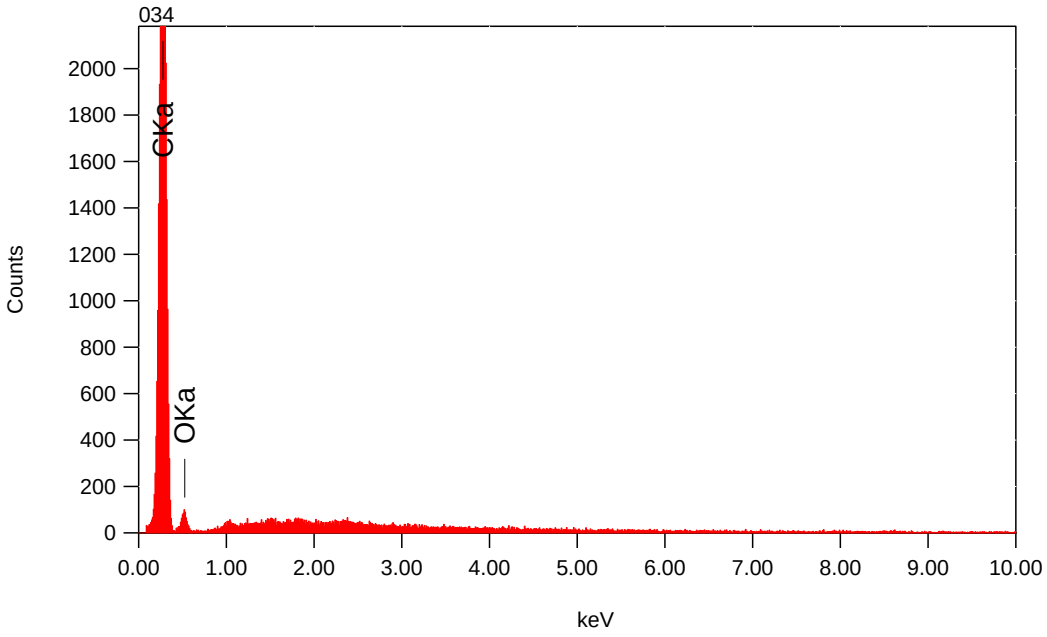


```
Acquisition Parameter
Instrument    : 7000F
Acc. Voltage  : 15.0 kV
Probe Current: 0.59000 nA
PHA mode      : T3
Real Time     : 32.22 sec
Live Time     : 30.00 sec
Dead Time     : 7 %
Counting Rate: 1741 cps
Energy Range :  0 - 20 keV
```

ZAF Method Standardless Quantitative Analysis
Fitting Coefficient : 0.4947

Element	(keV)	mass%	Error%	At%	Compound	mass%	Cation	K
C K	0.277	86.2	0.2	89.3				93.3715
O K	0.525	13.8	2.4	10.7				6.6285
Total		100.0		100.0				

2055m Microfacies VS

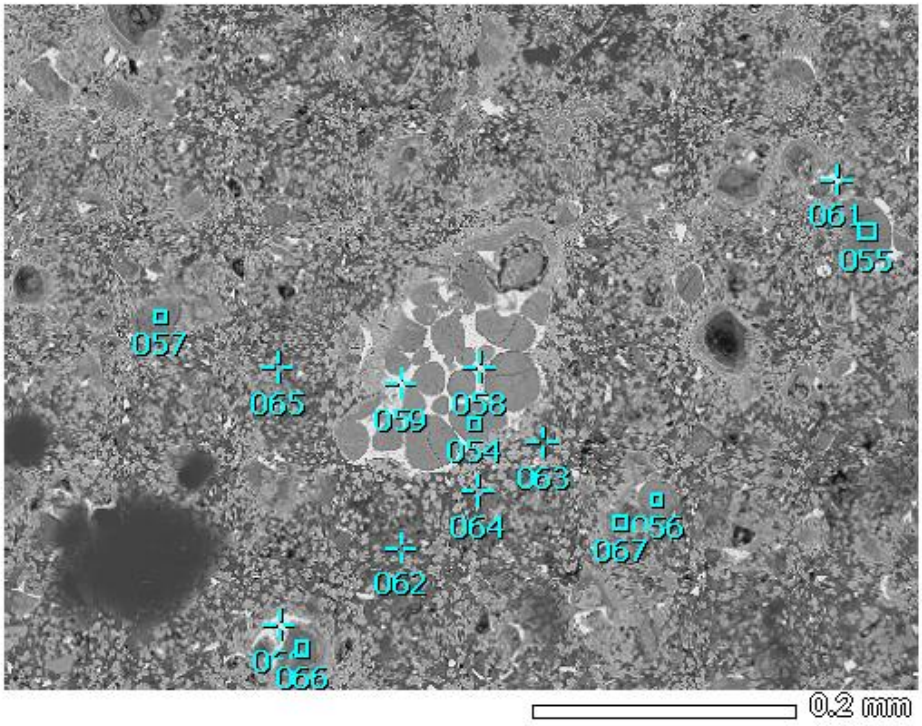


```
Title          : IMG1
---------------------------
Instrument     : 7000F
Volt           : 15.00 kV
Mag            : x 170
Date           : 2014/07/11
Pixel          : 512 x 384
```

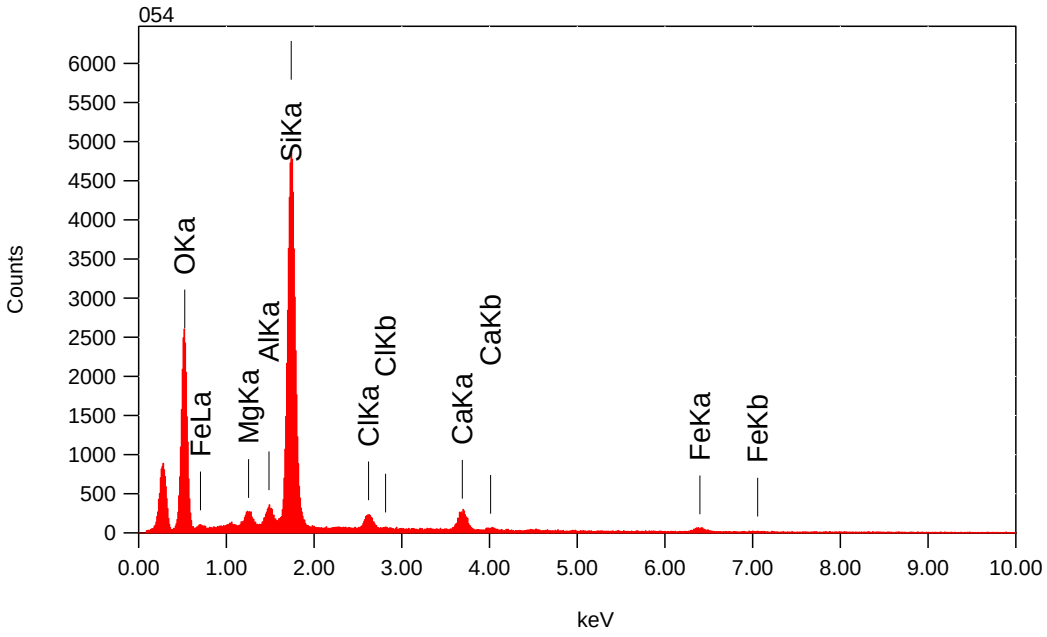


```
Acquisition Parameter
Instrument     : 7000F
Acc. Voltage   : 15.0 kV
Probe Current: 0.59000 nA
PHA mode       : T3
Real Time      : 37.76 sec
Live Time      : 30.00 sec
Dead Time      : 20 %
Counting Rate: 4178 cps
Energy Range :  0 - 20 keV
```

ZAF Method Standardless Quantitative Analysis
Fitting Coefficient : 0.2473

Element	(keV)	mass%	Error%	At%	Compound	mass%	Cation	K
O K	0.525	47.2	0.2	62.8				47.1361
Mg K	1.253	1.4	0.2	1.2				1.0718
Al K	1.486	1.8	0.2	1.4				1.5899
Si K	1.739	38.2	0.2	28.9				38.1368
Cl K	2.621	2.7	0.3	1.6				2.6831
Ca K	3.690	5.3	0.5	2.8				6.0065
Fe K	6.398	3.5	1.3	1.3				3.3759
Total		100.0		100.0				

2055m Microfacies VS

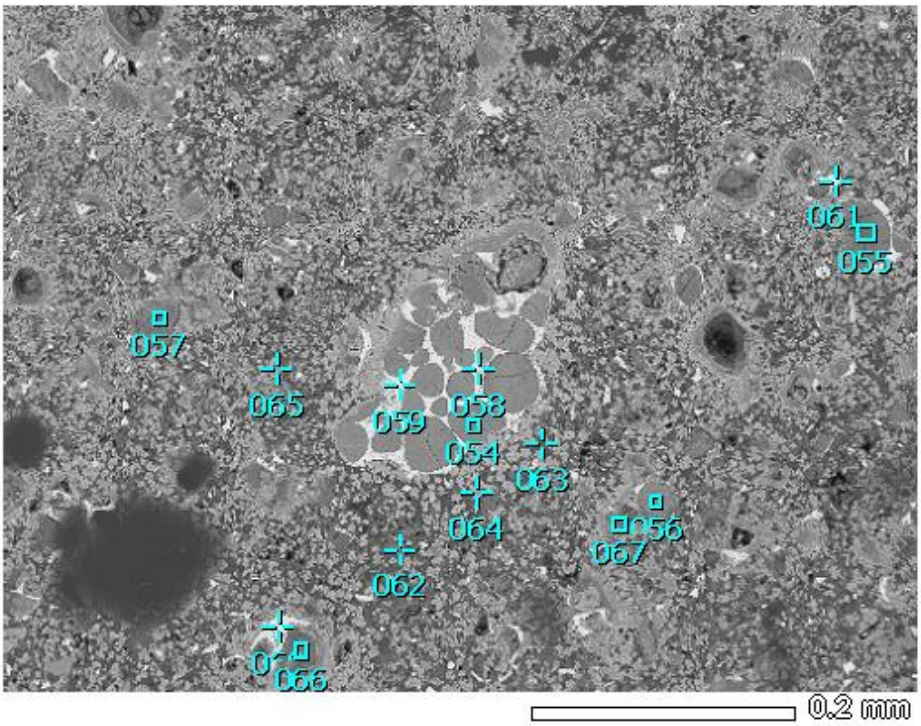


```
Title          : IMG1
---------------------------
Instrument     : 7000F
Volt           : 15.00 kV
Mag            : x 170
Date           : 2014/07/11
Pixel          : 512 x 384
```

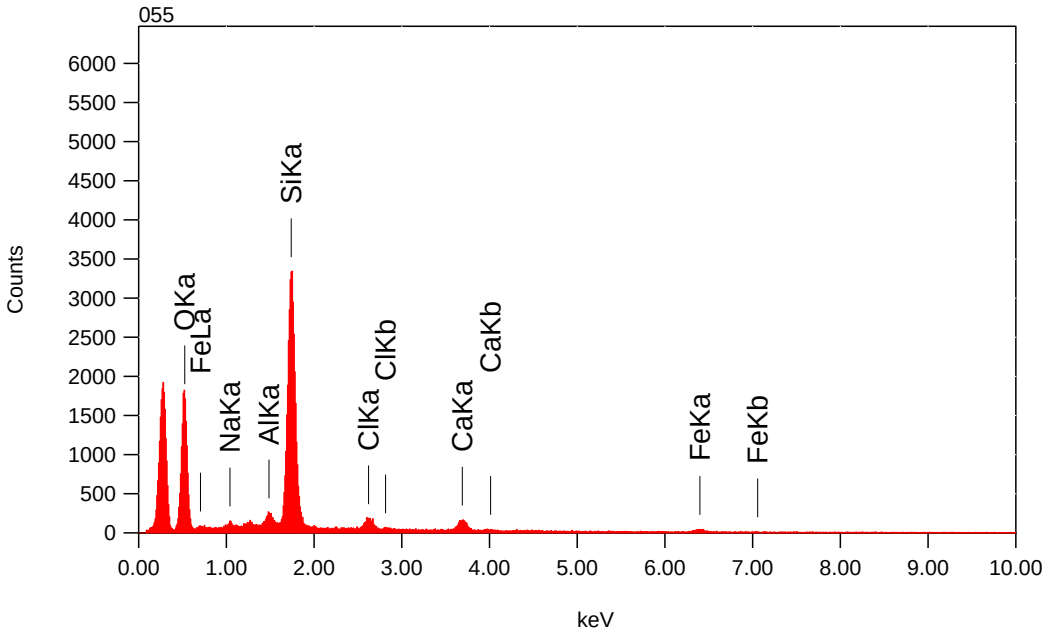


```
Acquisition Parameter
Instrument    : 7000F
Acc. Voltage  : 15.0 kV
Probe Current: 0.59000 nA
PHA mode      : T3
Real Time     : 36.01 sec
Live Time     : 30.00 sec
Dead Time     : 16 %
Counting Rate: 3442 cps
Energy Range :  0 - 20 keV
```

ZAF Method Standardless Quantitative Analysis
Fitting Coefficient : 0.3945

Element	(keV)	mass%	Error%	At%	Compound	mass%	Cation	K
O K	0.525	47.9	0.6	63.4				48.5114
Na K	1.041	0.9	0.6	0.9				0.7640
Al K	1.486	1.9	0.5	1.5				1.6708
Si K	1.739	38.1	0.5	28.7				37.6053
Cl K	2.621	3.1	0.7	1.8				3.0701
Ca K	3.690	4.3	1.2	2.3				4.8137
Fe K	6.398	3.7	3.3	1.4				3.5648
Total		100.0		100.0				

2055m Microfacies VS

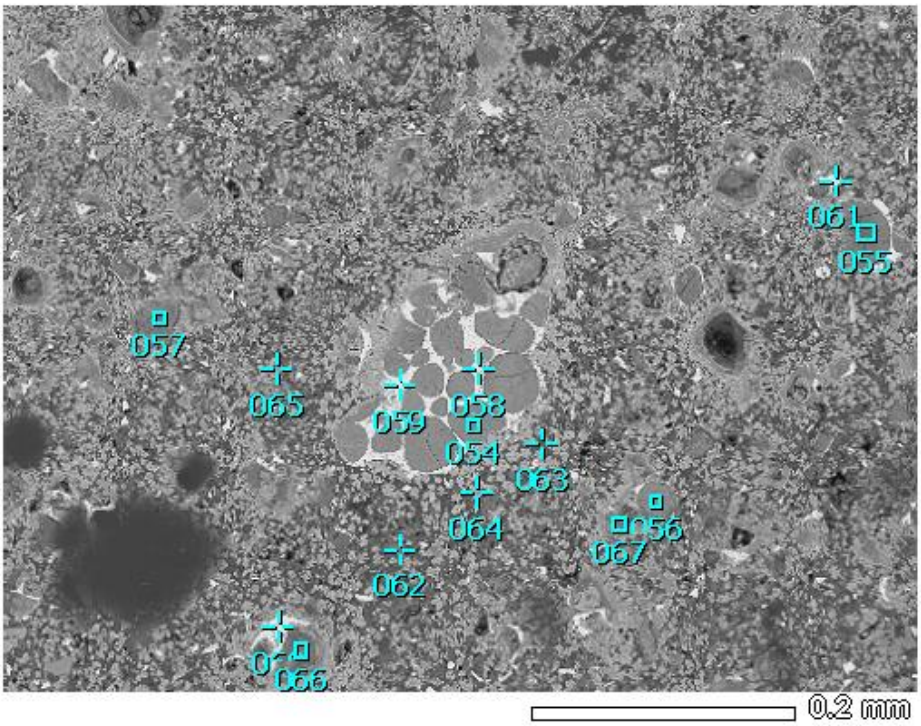


```
Title          : IMG1
---------------------------
Instrument     : 7000F
Volt           : 15.00 kV
Mag            : x 170
Date           : 2014/07/11
Pixel          : 512 x 384
```

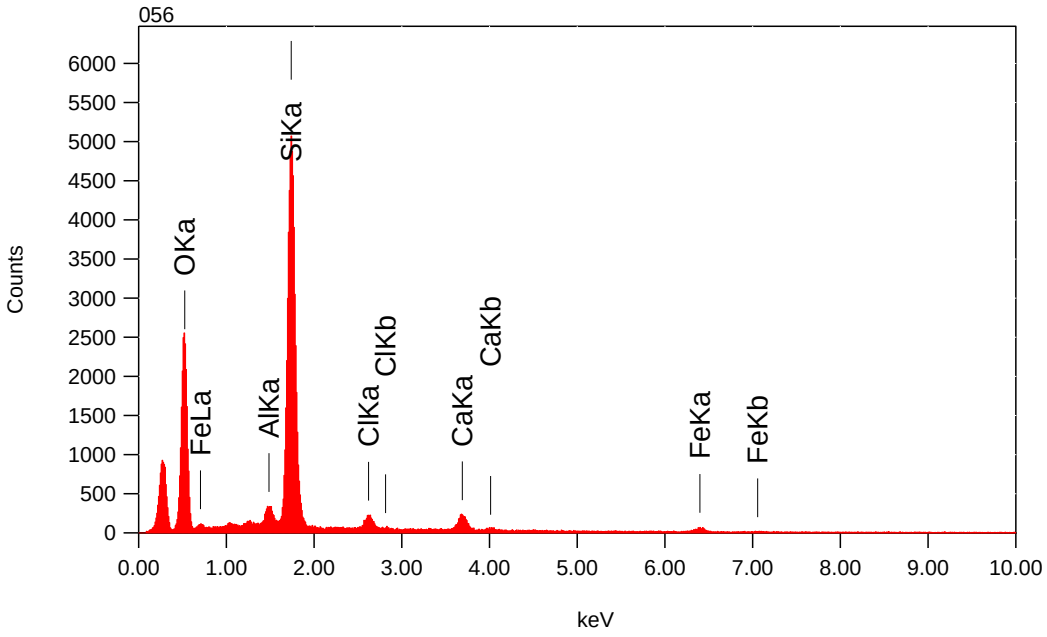


```
Acquisition Parameter
Instrument     : 7000F
Acc. Voltage   : 15.0 kV
Probe Current: 0.59000 nA
PHA mode       : T3
Real Time      : 37.66 sec
Live Time      : 30.00 sec
Dead Time      : 20 %
Counting Rate: 4195 cps
Energy Range :  0 - 20 keV
```

ZAF Method Standardless Quantitative Analysis
Fitting Coefficient : 0.2567

Element	(keV)	mass%	Error%	At%	Compound	mass%	Cation	K
O K	0.525	47.2	0.3	62.7				47.2870
Al K	1.486	1.9	0.2	1.5				1.7421
Si K	1.739	40.3	0.2	30.5				40.0539
Cl K	2.621	2.5	0.3	1.5				2.4843
Ca K	3.690	4.4	0.5	2.3				4.8679
Fe K	6.398	3.7	1.4	1.4				3.5648
Total		100.0		100.0				

2055m Microfacies VS

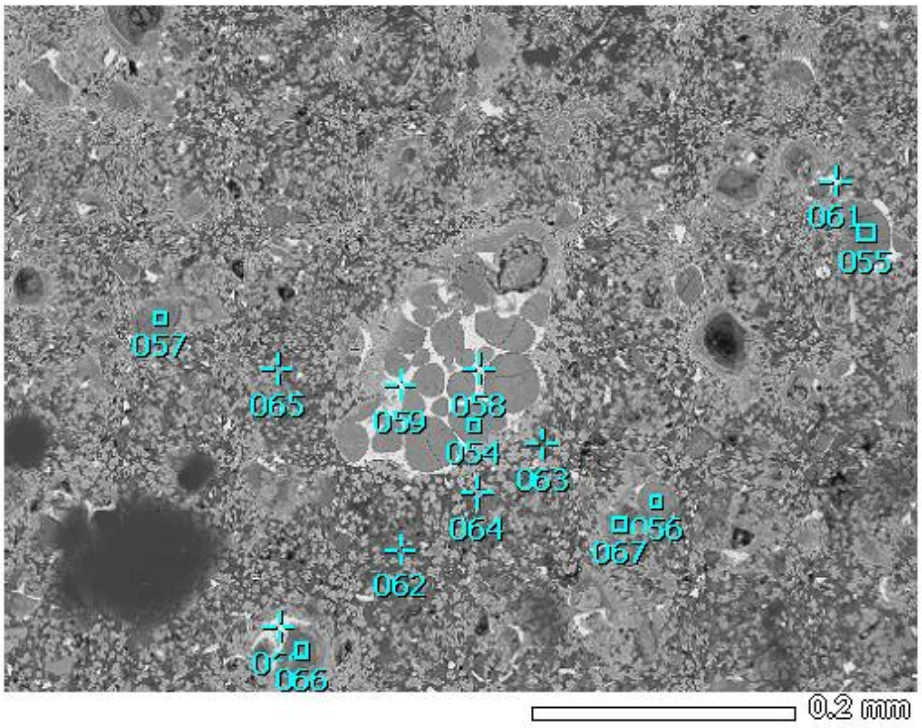


```
Title          : IMG1
---------------------------
Instrument     : 7000F
Volt           : 15.00 kV
Mag            : x 170
Date           : 2014/07/11
Pixel          : 512 x 384
```

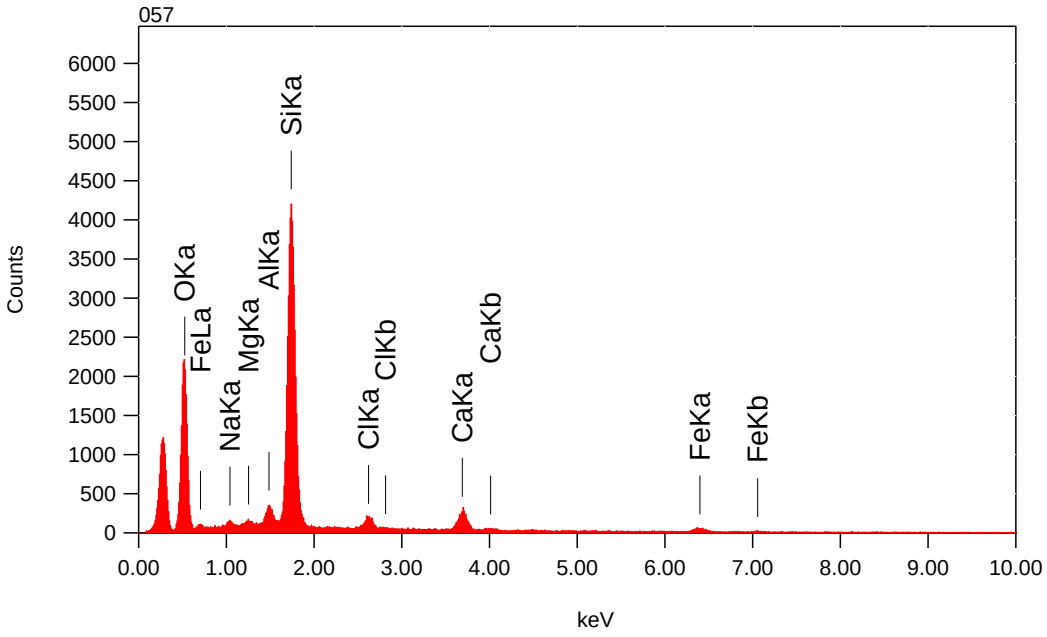


```
Acquisition Parameter
Instrument    : 7000F
Acc. Voltage  : 15.0 kV
Probe Current: 0.59000 nA
PHA mode      : T3
Real Time     : 36.91 sec
Live Time     : 30.00 sec
Dead Time     : 18 %
Counting Rate: 3877 cps
Energy Range :  0 - 20 keV
```

ZAF Method Standardless Quantitative Analysis
Fitting Coefficient : 0.2956

Element	(keV)	mass%	Error%	At%	Compound	mass%	Cation	K
O K	0.525	47.1	0.3	62.8				47.0254
Na K	1.041	0.9	0.3	0.8				0.7449
Mg K*	1.253	0.5	0.3	0.4				0.3914
Al K	1.486	2.2	0.3	1.7				1.9481
Si K	1.739	37.1	0.3	28.2				36.9798
Cl K	2.621	2.5	0.4	1.5				2.5167
Ca K	3.690	5.8	0.6	3.1				6.6215
Fe K	6.398	3.9	1.8	1.5				3.7722
Total		100.0		100.0				

2055m Microfacies VS

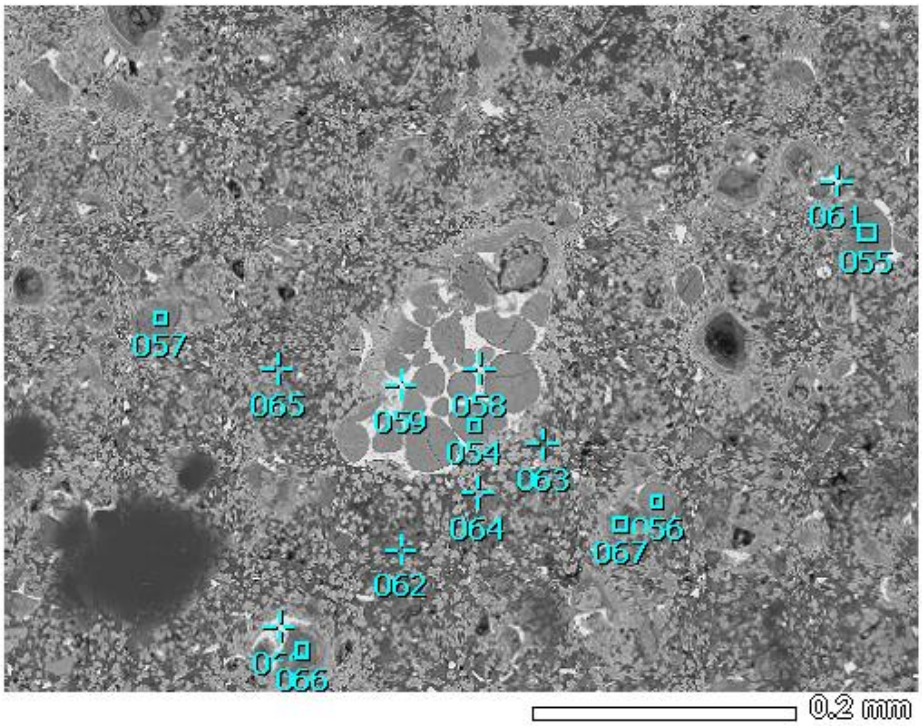


```
Title          : IMG1
---------------------------
Instrument     : 7000F
Volt           : 15.00 kV
Mag            : x 170
Date           : 2014/07/11
Pixel          : 512 x 384
```

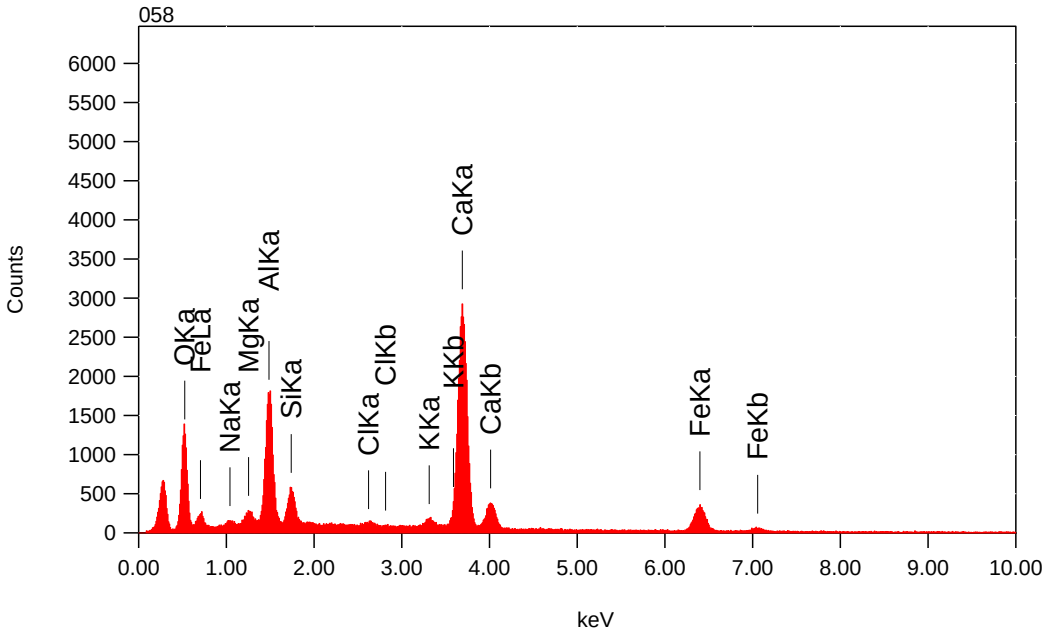


```
Acquisition Parameter
Instrument    : 7000F
Acc. Voltage  : 15.0 kV
Probe Current: 0.59000 nA
PHA mode      : T3
Real Time     : 38.91 sec
Live Time     : 30.00 sec
Dead Time     : 22 %
Counting Rate: 4757 cps
Energy Range :  0 - 20 keV
```

ZAF Method Standardless Quantitative Analysis
Fitting Coefficient : 0.2071

Element	(keV)	mass%	Error%	At%	Compound	mass%	Cation	K
O K	0.525	30.2	0.2	51.0				18.2074
Na K*	1.041	0.6	0.1	0.7				0.4174
Mg K	1.253	1.0	0.1	1.1				0.7071
Al K	1.486	10.1	0.1	10.1				8.6353
Si K	1.739	3.0	0.1	2.8				2.7782
Cl K*	2.621	0.4	0.1	0.3				0.4780
K K	3.312	1.1	0.2	0.7				1.3971
Ca K	3.690	37.6	0.2	25.4				50.0337
Fe K	6.398	16.2	0.6	7.8				17.3458
Total		100.0		100.0				

2055m Microfacies VS

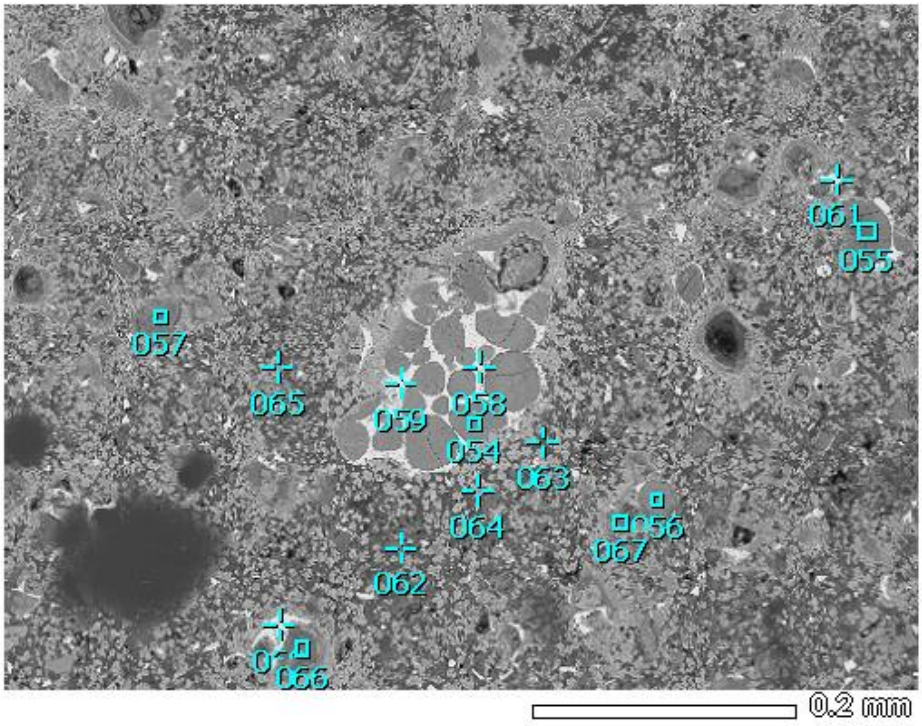


```
Title        : IMG1
--------------------------
Instrument   : 7000F
Volt         : 15.00 kV
Mag          : x 170
Date         : 2014/07/11
Pixel        : 512 x 384
```

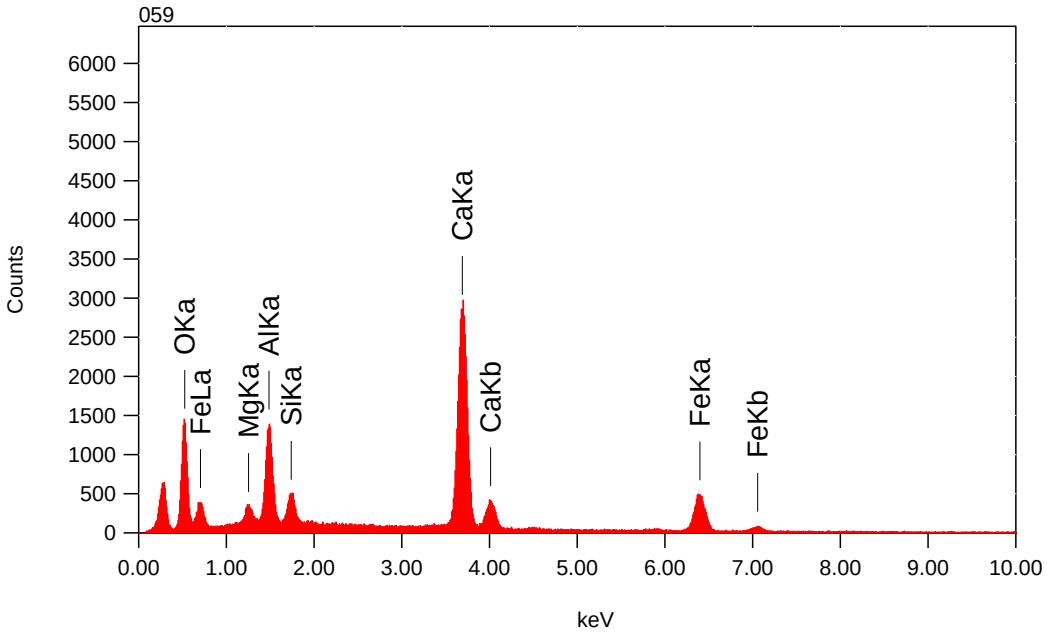


```
Acquisition Parameter
Instrument    : 7000F
Acc. Voltage  : 15.0 kV
Probe Current: 0.59000 nA
PHA mode      : T3
Real Time     : 39.10 sec
Live Time     : 30.00 sec
Dead Time     : 23 %
Counting Rate: 4829 cps
Energy Range :  0 - 20 keV
```

ZAF Method Standardless Quantitative Analysis
Fitting Coefficient : 0.1997

Element	(keV)	mass%	Error%	At%	Compound	mass%	Cation	K
O K	0.525	28.6	0.2	50.5				18.0039
Mg K	1.253	1.4	0.1	1.6				0.9605
Al K	1.486	7.5	0.1	7.8				6.0425
Si K	1.739	2.4	0.1	2.4				2.1838
Ca K	3.690	36.5	0.2	25.7				47.9066
Fe K	6.398	23.6	0.5	11.9				24.9027
Total		100.0		100.0				

2055m Microfacies VS

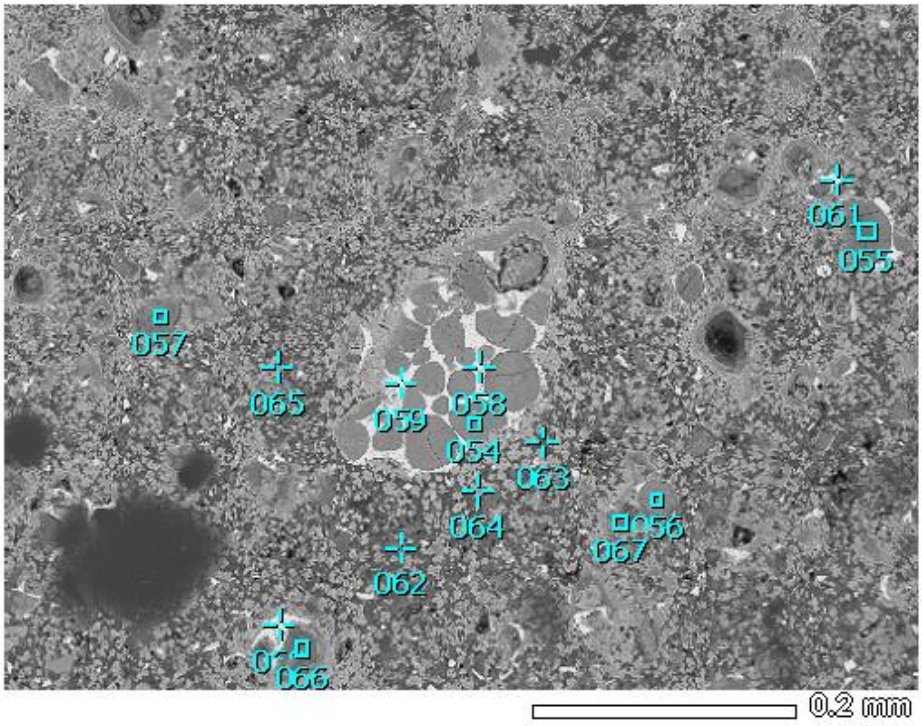


```
Title          : IMG1
---------------------------
Instrument     : 7000F
Volt           : 15.00 kV
Mag            : x 170
Date           : 2014/07/11
Pixel          : 512 x 384
```

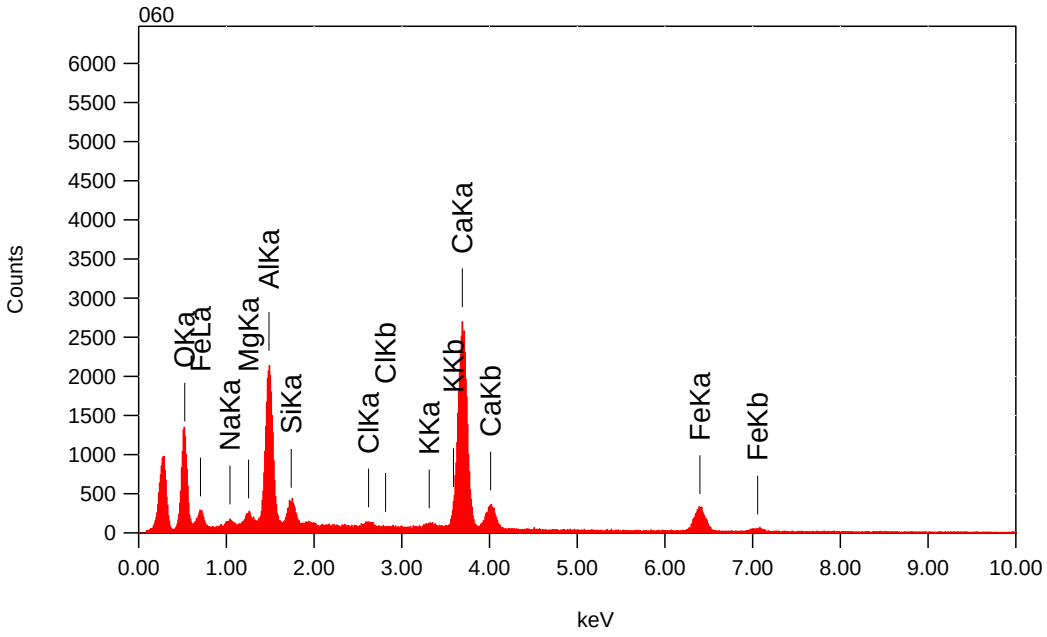


```
Acquisition Parameter
Instrument    : 7000F
Acc. Voltage  : 15.0 kV
Probe Current: 0.59000 nA
PHA mode      : T3
Real Time     : 38.66 sec
Live Time     : 30.00 sec
Dead Time     : 22 %
Counting Rate: 4627 cps
Energy Range :  0 - 20 keV
```

ZAF Method Standardless Quantitative Analysis
Fitting Coefficient : 0.2323

Element	(keV)	mass%	Error%	At%	Compound	mass%	Cation	K
O K	0.525	30.0	0.3	50.6				18.7430
Na K*	1.041	0.7	0.2	0.8				0.5135
Mg K	1.253	1.0	0.1	1.1				0.7134
Al K	1.486	12.3	0.1	12.3				10.6172
Si K	1.739	2.1	0.2	2.1				1.9905
Cl K	2.621	0.5	0.2	0.4				0.6448
K K*	3.312	0.5	0.2	0.3				0.6095
Ca K	3.690	36.3	0.3	24.4				48.3502
Fe K	6.398	16.6	0.8	8.0				17.8177
Total		100.0		100.0				

2055m Microfacies VS

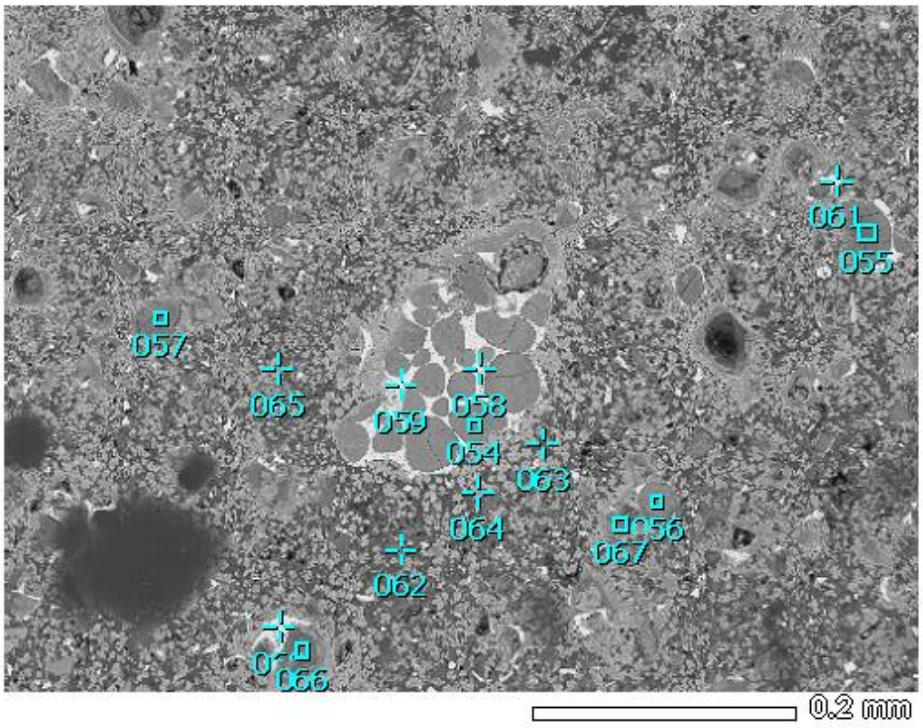


```
Title          : IMG1
---------------------------
Instrument     : 7000F
Volt           : 15.00 kV
Mag            : x 170
Date           : 2014/07/11
Pixel          : 512 x 384
```

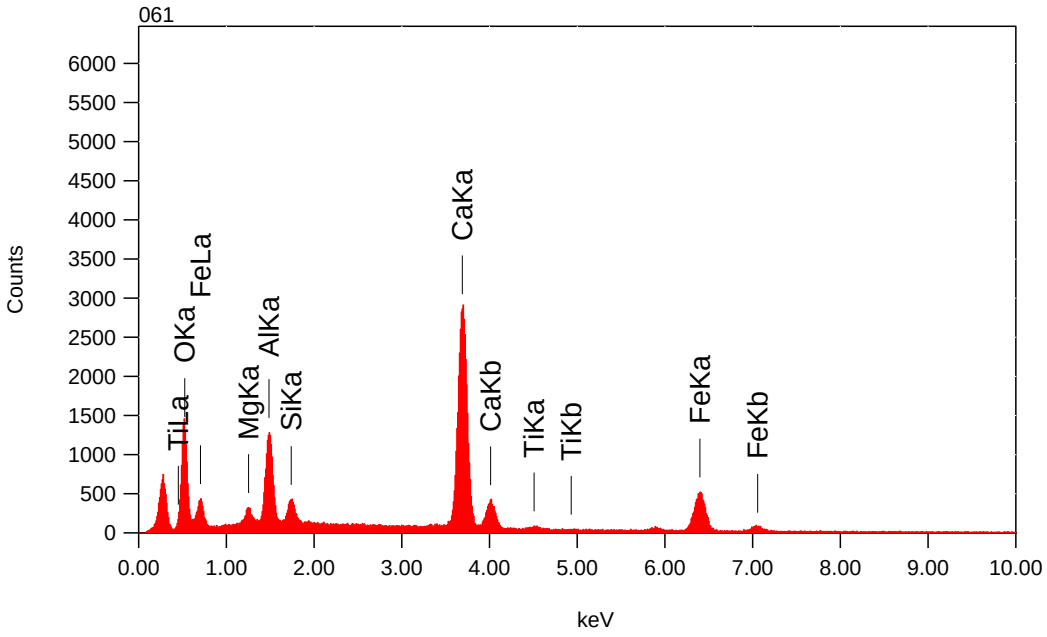


```
Acquisition Parameter
Instrument    : 7000F
Acc. Voltage : 15.0 kV
Probe Current: 0.59000 nA
PHA mode      : T3
Real Time     : 38.97 sec
Live Time     : 30.00 sec
Dead Time     : 22 %
Counting Rate: 4717 cps
Energy Range :  0 - 20 keV
```

ZAF Method Standardless Quantitative Analysis
Fitting Coefficient : 0.2073

Element	(keV)	mass%	Error%	At%	Compound	mass%	Cation	K
O K	0.525	28.6	0.2	50.8				17.7925
Mg K	1.253	1.3	0.1	1.5				0.8809
Al K	1.486	6.9	0.1	7.3				5.5265
Si K	1.739	1.9	0.1	1.9				1.7392
Ca K	3.690	36.5	0.2	25.9				47.9368
Ti K*	4.508	0.7	0.3	0.4				0.7017
Fe K	6.398	24.1	0.5	12.3				25.4224
Total		100.0		100.0				

2055m Microfacies VS

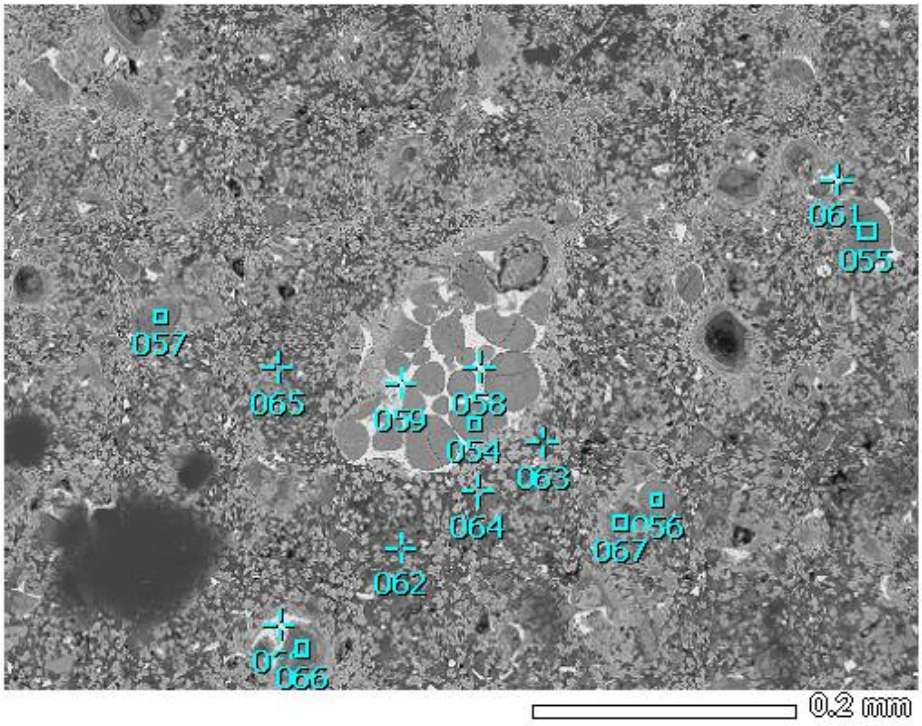


```
Title          : IMG1
---------------------------
Instrument     : 7000F
Volt           : 15.00 kV
Mag            : x 170
Date           : 2014/07/11
Pixel          : 512 x 384
```

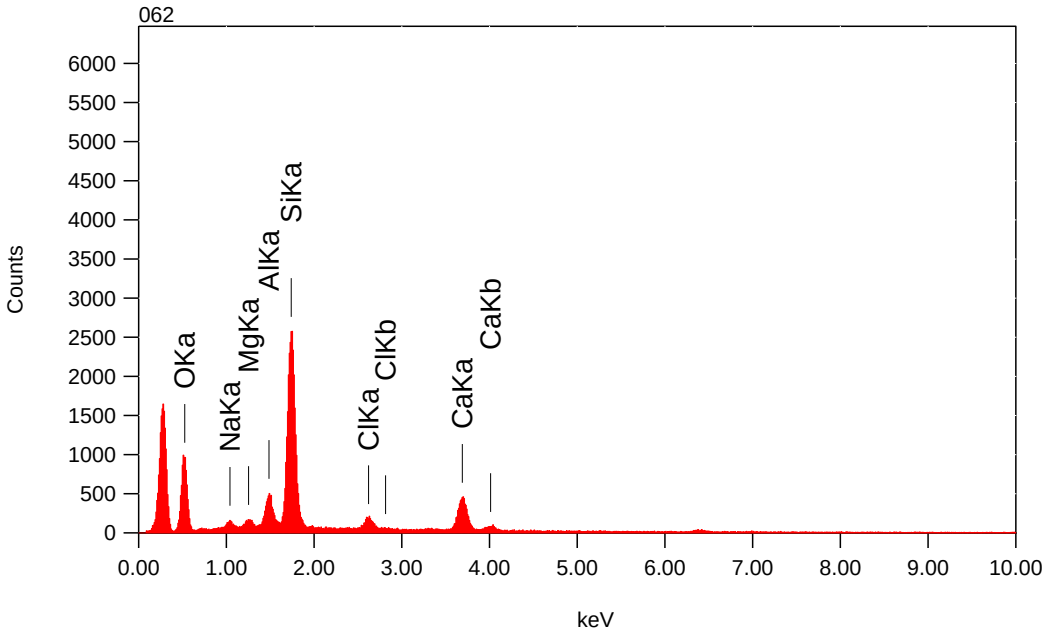


```
Acquisition Parameter
Instrument     : 7000F
Acc. Voltage   : 15.0 kV
Probe Current: 0.59000 nA
PHA mode       : T3
Real Time      : 35.38 sec
Live Time      : 30.00 sec
Dead Time      : 15 %
Counting Rate: 3078 cps
Energy Range :  0 - 20 keV
```

ZAF Method Standardless Quantitative Analysis
Fitting Coefficient : 0.3819

Element	(keV)	mass%	Error%	At%	Compound	mass%	Cation	K
O K	0.525	40.4	0.8	56.2				33.8226
Na K	1.041	1.5	0.5	1.5				1.4110
Mg K	1.253	1.2	0.5	1.1				1.1066
Al K	1.486	5.0	0.5	4.1				4.9792
Si K	1.739	33.8	0.5	26.8				36.4172
Cl K	2.621	3.4	0.7	2.1				3.7863
Ca K	3.690	14.7	1.1	8.2				18.4771
Total		100.0		100.0				

2055m Microfacies VS

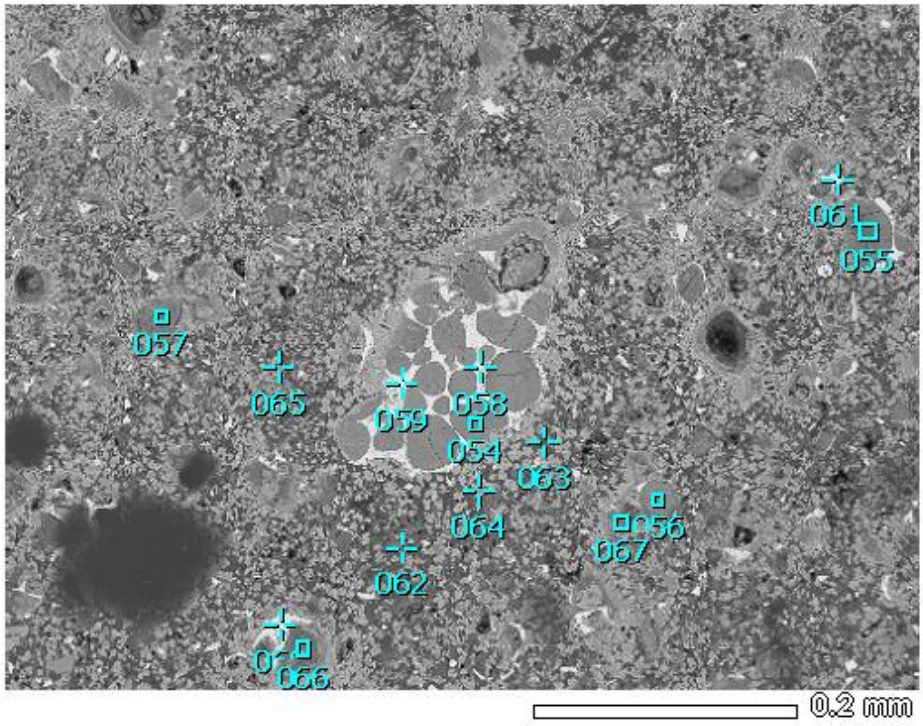


```
Title          : IMG1
---------------------------
Instrument     : 7000F
Volt           : 15.00 kV
Mag            : x 170
Date           : 2014/07/11
Pixel          : 512 x 384
```

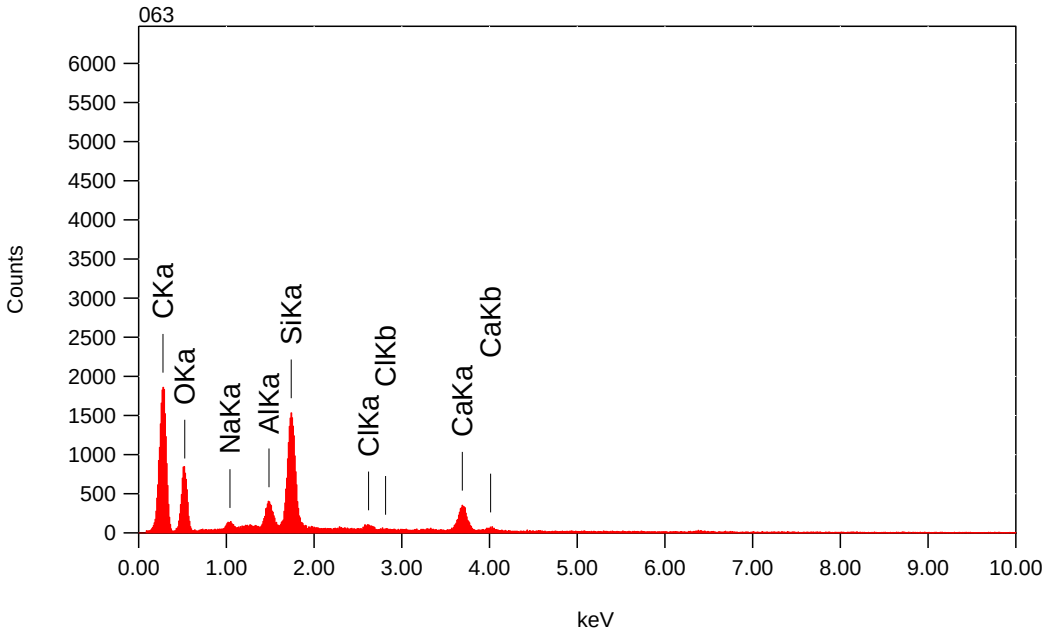


```
Acquisition Parameter
Instrument     : 7000F
Acc. Voltage : 15.0 kV
Probe Current: 0.59000 nA
PHA mode       : T3
Real Time      : 34.12 sec
Live Time      : 30.00 sec
Dead Time      : 12 %
Counting Rate: 2510 cps
Energy Range :  0 - 20 keV
```

ZAF Method Standardless Quantitative Analysis
Fitting Coefficient : 0.3240

Element	(keV)	mass%	Error%	At%	Compound	mass%	Cation	K
C K	0.277	46.9	0.1	59.9				28.0727
O K	0.525	29.5	0.4	28.3				29.1405
Na K	1.041	1.0	0.2	0.7				1.4953
Al K	1.486	2.6	0.2	1.5				4.1516
Si K	1.739	12.1	0.2	6.6				21.1904
Cl K	2.621	0.9	0.2	0.4				1.6692
Ca K	3.690	7.0	0.4	2.7				14.2803
Total		100.0		100.0				

2055m Microfacies VS

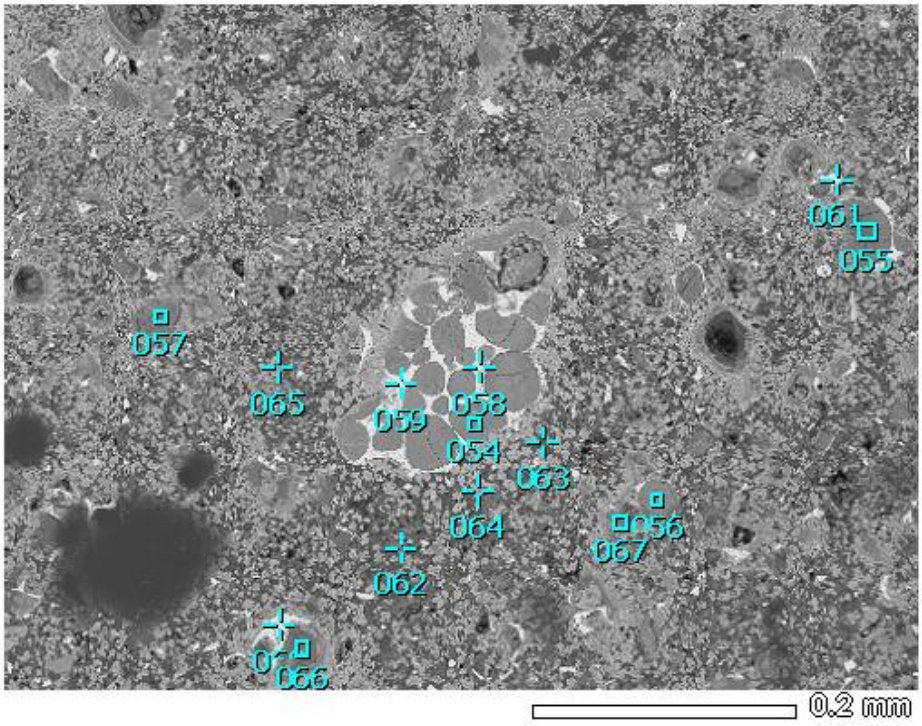


```
Title        : IMG1
---------------------------
Instrument   : 7000F
Volt         : 15.00 kV
Mag          : x 170
Date         : 2014/07/11
Pixel        : 512 x 384
```

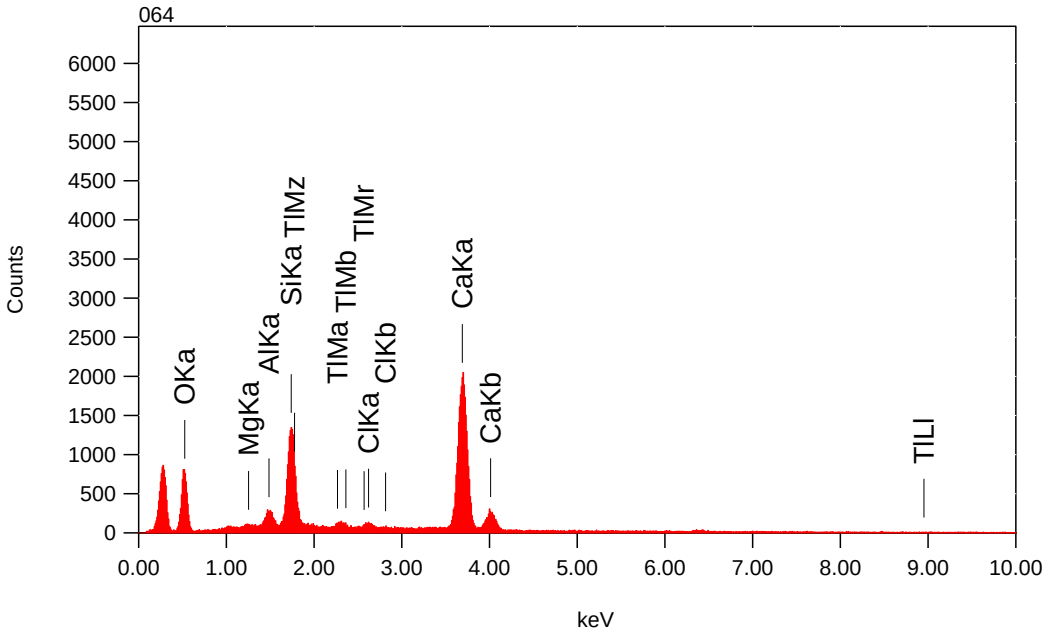


```
Acquisition Parameter
Instrument    : 7000F
Acc. Voltage  : 15.0 kV
Probe Current: 0.59000 nA
PHA mode      : T3
Real Time     : 35.66 sec
Live Time     : 30.00 sec
Dead Time     : 15 %
Counting Rate: 3219 cps
Energy Range :  0 - 20 keV
```

ZAF Method Standardless Quantitative Analysis
Fitting Coefficient : 0.2947

Element	(keV)	mass%	Error%	At%	Compound	mass%	Cation	K
O K	0.525	37.2	0.5	58.3				19.4719
Mg K*	1.253	0.3	0.2	0.3				0.2552
Al K	1.486	1.8	0.2	1.7				1.7348
Si K	1.739	11.8	0.2	10.5				12.9097
Cl K	2.621	0.9	0.2	0.7				1.1667
Ca K	3.690	44.9	0.4	28.1				60.9466
Tl M	2.267	3.1	0.8	0.4				3.5150
Total		100.0		100.0				

2055m Microfacies VS

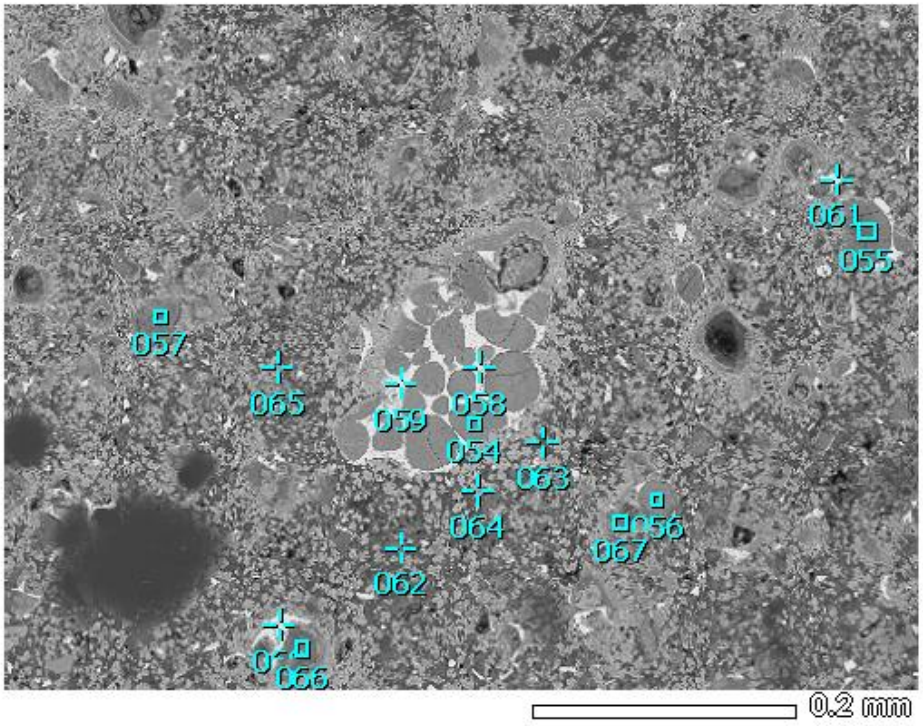


```
Title        : IMG1
---------------------------
Instrument   : 7000F
Volt         : 15.00 kV
Mag          : x 170
Date         : 2014/07/11
Pixel        : 512 x 384
```

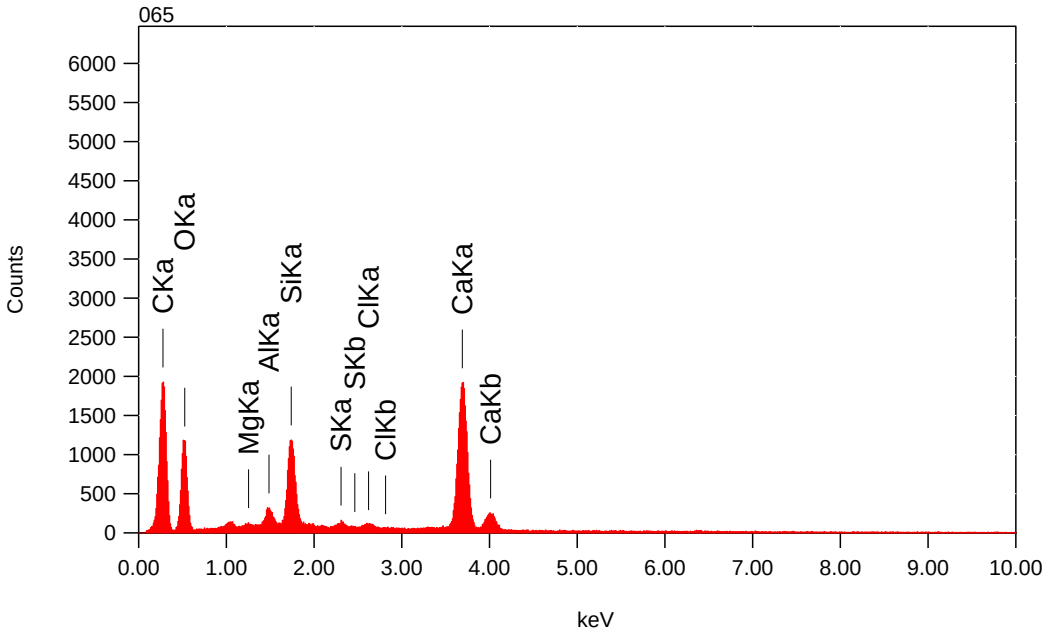


```
Acquisition Parameter
Instrument    : 7000F
Acc. Voltage  : 15.0 kV
Probe Current: 0.59000 nA
PHA mode      : T3
Real Time     : 36.24 sec
Live Time     : 30.00 sec
Dead Time     : 17 %
Counting Rate: 3559 cps
Energy Range :  0 - 20 keV
```

ZAF Method Standardless Quantitative Analysis
Fitting Coefficient : 0.2503

Element	(keV)	mass%	Error%	At%	Compound	mass%	Cation	K
C K	0.277	27.1	0.1	41.1				16.0235
O K	0.525	35.3	0.4	40.1				23.4231
Mg K	1.253	0.2	0.1	0.2				0.2504
Al K	1.486	1.3	0.1	0.9				1.5644
Si K	1.739	6.8	0.1	4.4				9.3623
S K*	2.307	0.5	0.1	0.3				0.8160
Cl K	2.621	0.4	0.2	0.2				0.7191
Ca K	3.690	28.4	0.3	12.9				47.8413
Total		100.0		100.0				

2055m Microfacies VS

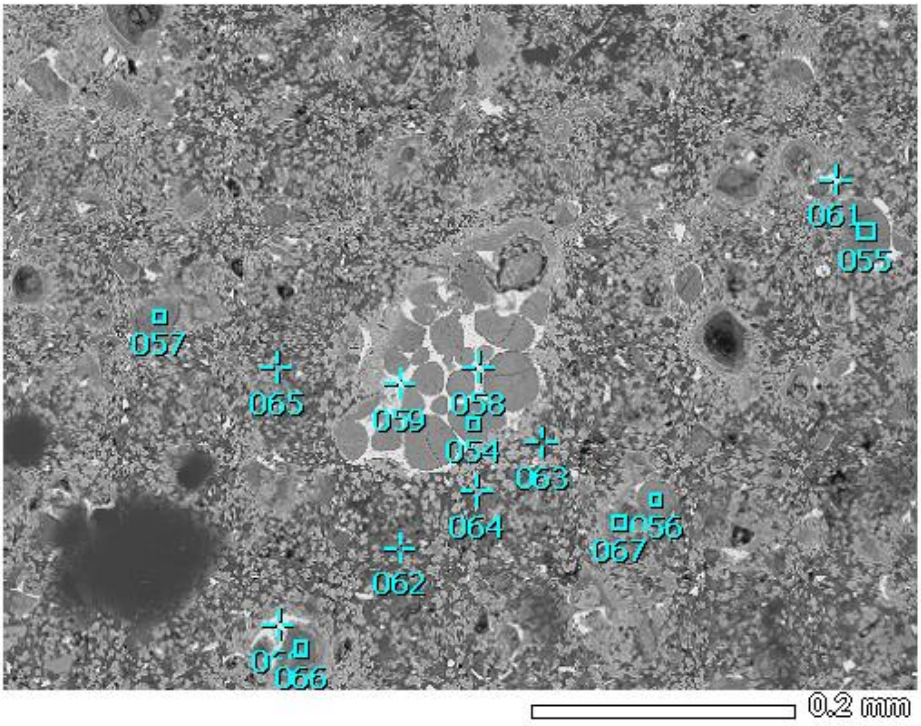


```
Title        : IMG1
---------------------------
Instrument   : 7000F
Volt         : 15.00 kV
Mag          : x 170
Date         : 2014/07/11
Pixel        : 512 x 384
```

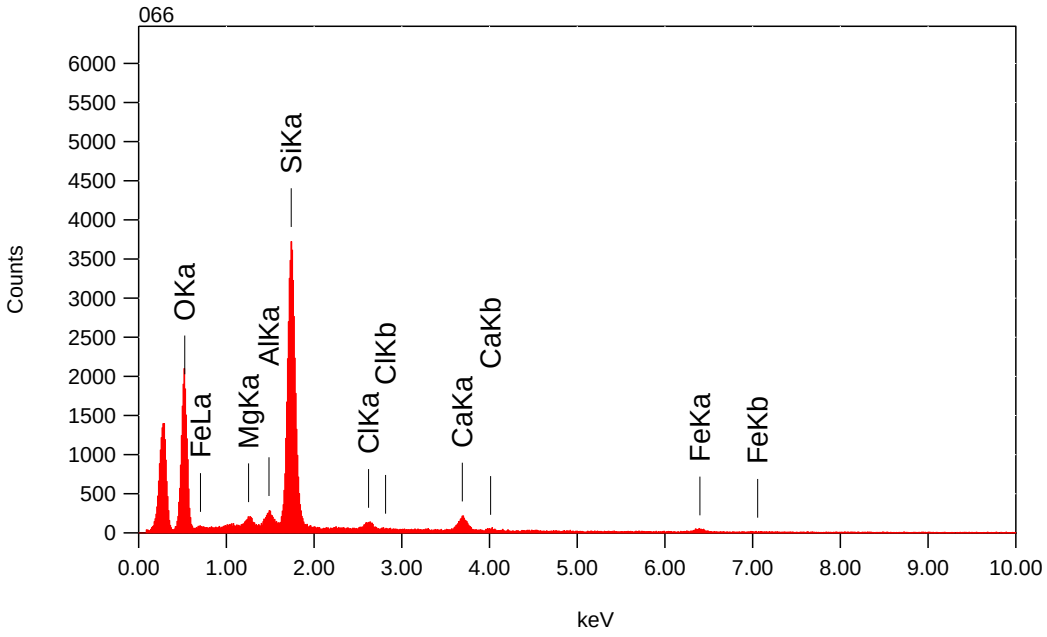


```
Acquisition Parameter
Instrument    : 7000F
Acc. Voltage  : 15.0 kV
Probe Current: 0.59000 nA
PHA mode      : T3
Real Time     : 36.16 sec
Live Time     : 30.00 sec
Dead Time     : 16 %
Counting Rate: 3497 cps
Energy Range :  0 - 20 keV
```

ZAF Method Standardless Quantitative Analysis
Fitting Coefficient : 0.3349

Element	(keV)	mass%	Error%	At%	Compound	mass%	Cation	K
O K	0.525	48.1	0.4	63.5				48.8188
Mg K	1.253	1.2	0.3	1.0				0.9070
Al K	1.486	1.8	0.3	1.4				1.5954
Si K	1.739	38.6	0.4	29.1				37.9602
Cl K	2.621	1.7	0.5	1.0				1.6776
Ca K	3.690	4.8	0.8	2.5				5.3526
Fe K	6.398	3.9	2.3	1.5				3.6884
Total		100.0		100.0				

2055m Microfacies VS

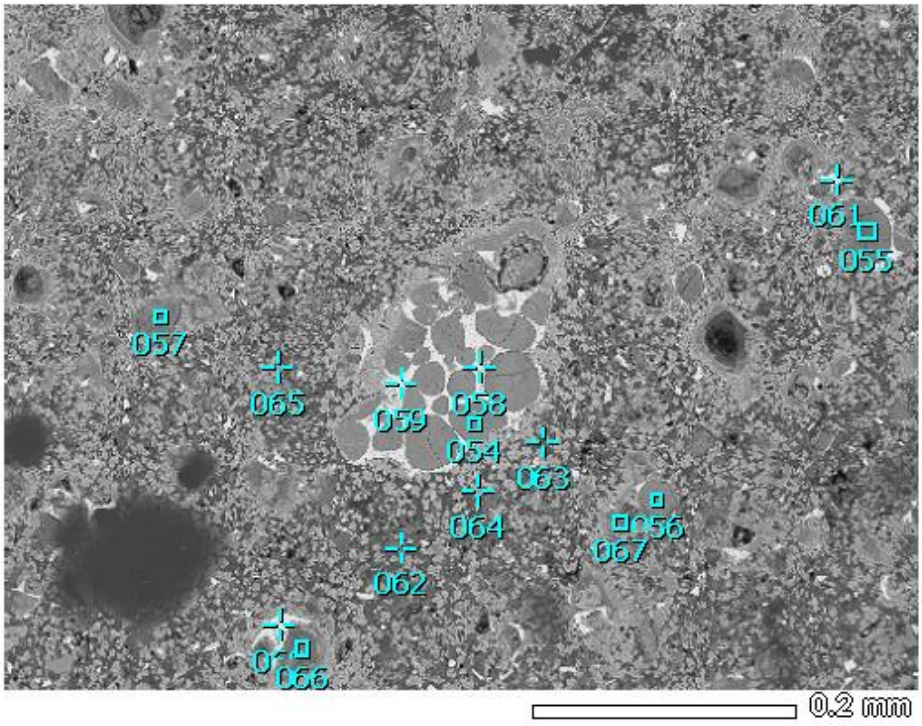


```
Title        : IMG1
---------------------------
Instrument   : 7000F
Volt         : 15.00 kV
Mag          : x 170
Date         : 2014/07/11
Pixel        : 512 x 384
```

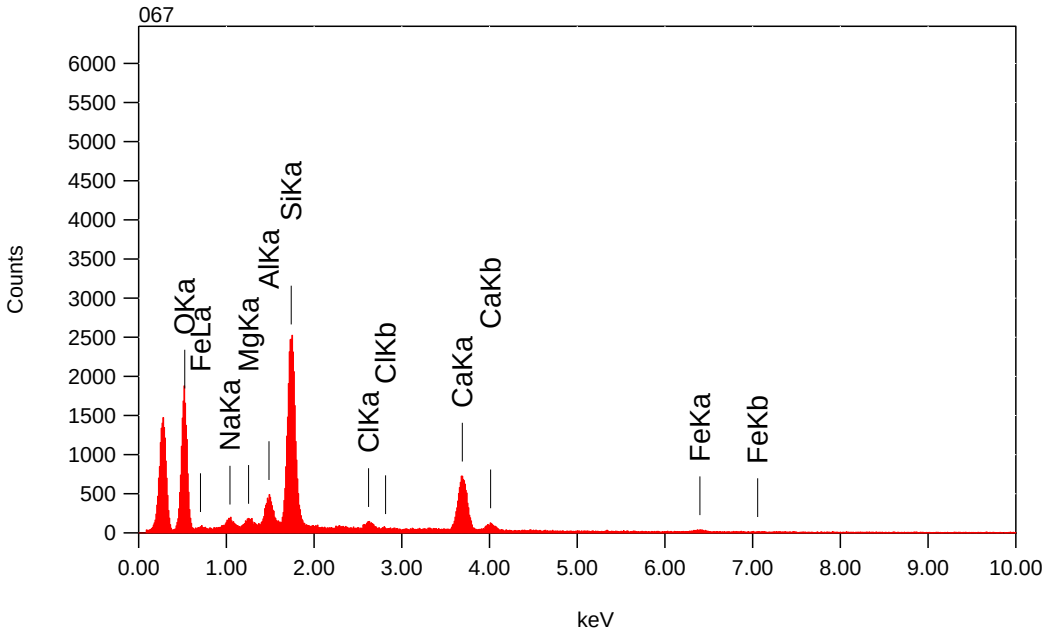


```
Acquisition Parameter
Instrument    : 7000F
Acc. Voltage  : 15.0 kV
Probe Current: 0.59000 nA
PHA mode      : T3
Real Time     : 36.11 sec
Live Time     : 30.00 sec
Dead Time     : 16 %
Counting Rate: 3476 cps
Energy Range :  0 - 20 keV
```

ZAF Method Standardless Quantitative Analysis
Fitting Coefficient : 0.3389

Element	(keV)	mass%	Error%	At%	Compound	mass%	Cation	K
O K	0.525	49.1	0.5	65.7				43.1436
Na K	1.041	1.3	0.4	1.2				1.1332
Mg K	1.253	1.0	0.3	0.9				0.8206
Al K	1.486	3.4	0.3	2.7				3.2271
Si K	1.739	24.6	0.3	18.7				25.9602
Cl K	2.621	1.5	0.4	0.9				1.7286
Ca K	3.690	17.0	0.7	9.1				21.8214
Fe K*	6.398	2.0	2.1	0.8				2.1653
Total		100.0		100.0				

2055m Microfacies VS

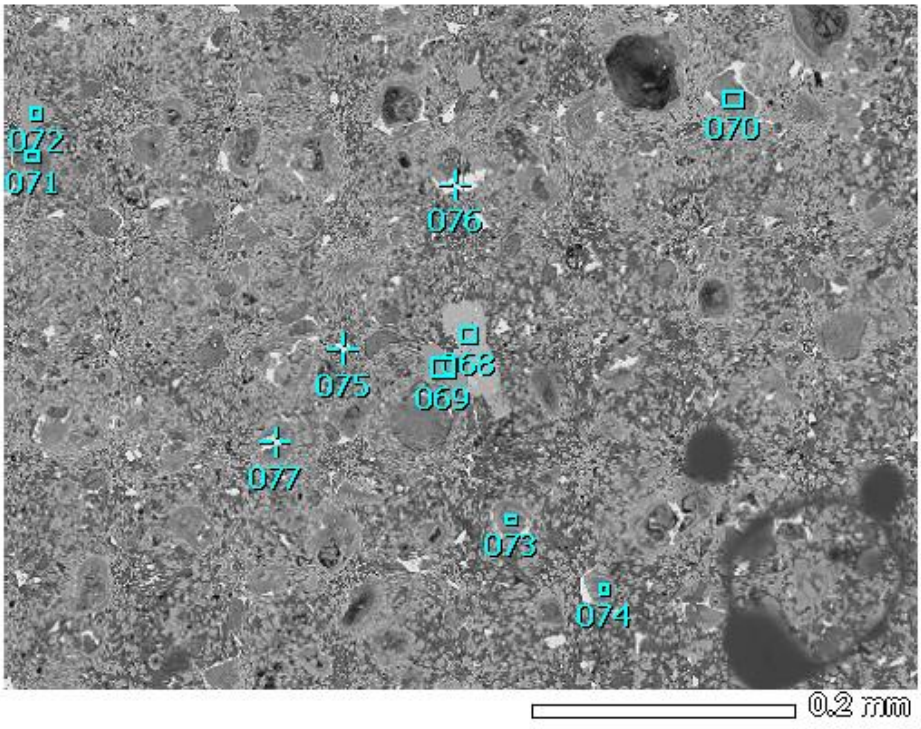


```
Title        : IMG1
--------------------------
Instrument   : 7000F
Volt         : 15.00 kV
Mag          : x 170
Date         : 2014/07/11
Pixel        : 512 x 384
```

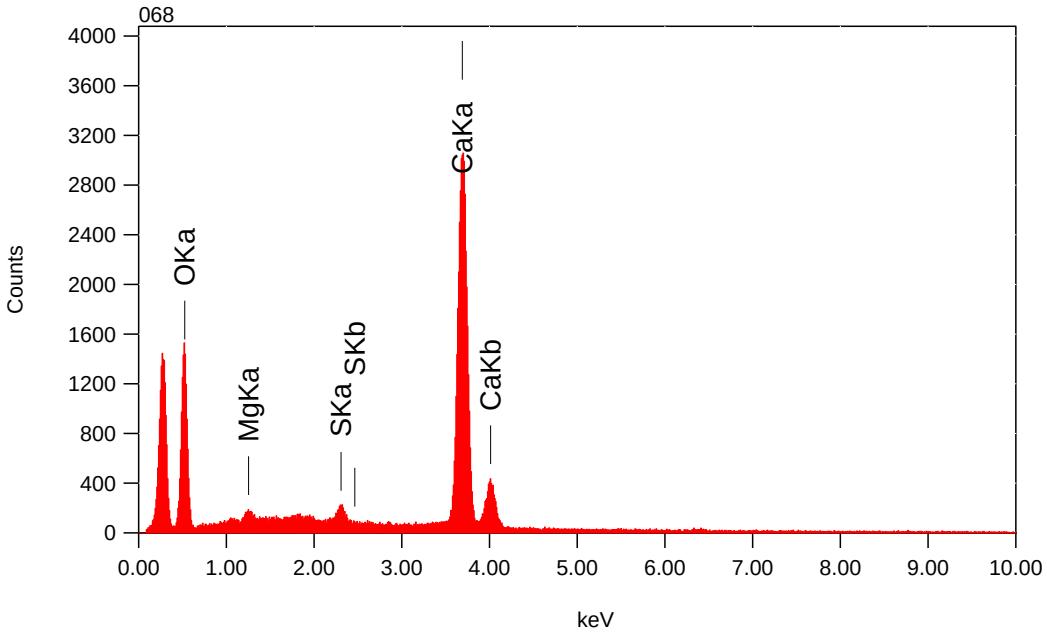


```
Acquisition Parameter
Instrument    : 7000F
Acc. Voltage  : 15.0 kV
Probe Current: 0.59000 nA
PHA mode      : T3
Real Time     : 36.88 sec
Live Time     : 30.00 sec
Dead Time     : 18 %
Counting Rate: 3880 cps
Energy Range :  0 - 20 keV
```

ZAF Method Standardless Quantitative Analysis
Fitting Coefficient : 0.3032

Element	(keV)	mass%	Error%	At%	Compound	mass%	Cation	K
O K	0.525	48.9	0.6	70.3				26.3837
Mg K	1.253	0.6	0.2	0.6				0.4876
S K	2.307	1.1	0.2	0.8				1.5071
Ca K	3.690	49.4	0.4	28.4				71.6215
Total		100.0		100.0				

2055m Microfacies VS

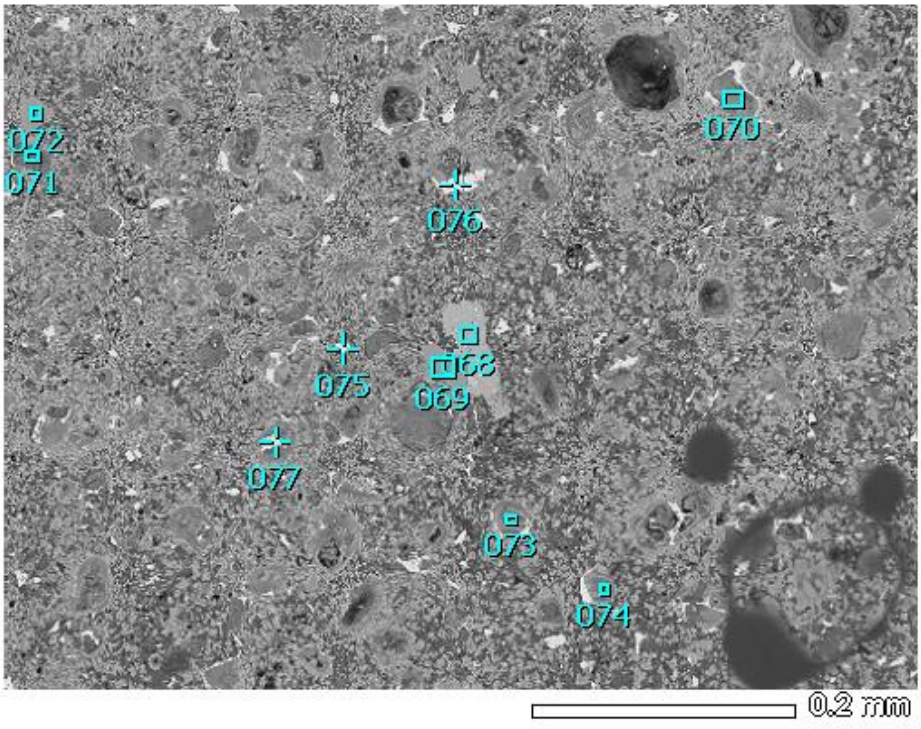


```
Title        : IMG1
--------------------------
Instrument   : 7000F
Volt         : 15.00 kV
Mag          : x 170
Date         : 2014/07/11
Pixel        : 512 x 384
```

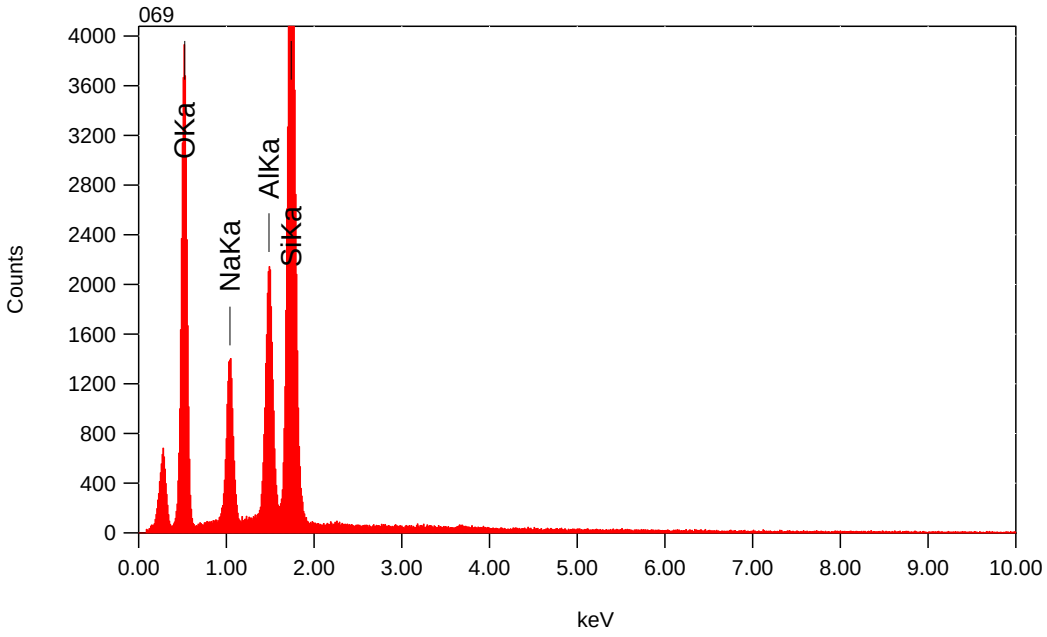


```
Acquisition Parameter
Instrument    : 7000F
Acc. Voltage  : 15.0 kV
Probe Current: 0.59000 nA
PHA mode      : T3
Real Time     : 40.71 sec
Live Time     : 30.00 sec
Dead Time     : 26 %
Counting Rate: 5508 cps
Energy Range :  0 - 20 keV
```

ZAF Method Standardless Quantitative Analysis
Fitting Coefficient : 0.2225

Element	(keV)	mass%	Error%	At%	Compound	mass%	Cation	K
O K	0.525	44.2	0.2	57.1				51.0891
Na K	1.041	9.1	0.2	8.2				8.1825
Al K	1.486	11.5	0.2	8.8				9.8414
Si K	1.739	35.2	0.2	25.9				30.8870
Total		100.0		100.0				

2055m Microfacies VS

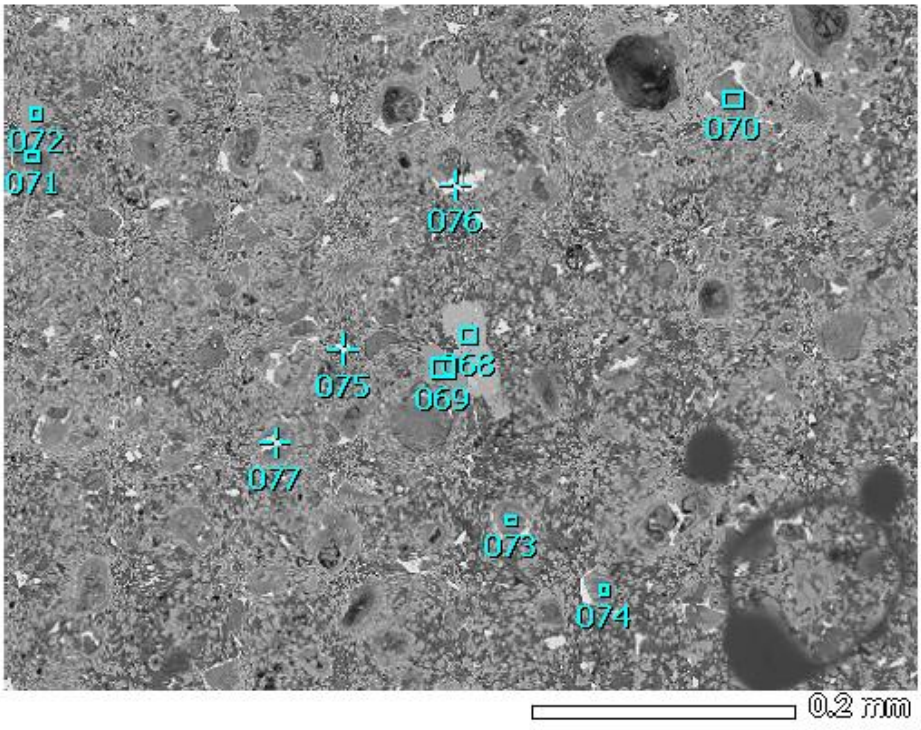


```
Title        : IMG1
--------------------------
Instrument   : 7000F
Volt         : 15.00 kV
Mag          : x 170
Date         : 2014/07/11
Pixel        : 512 x 384
```

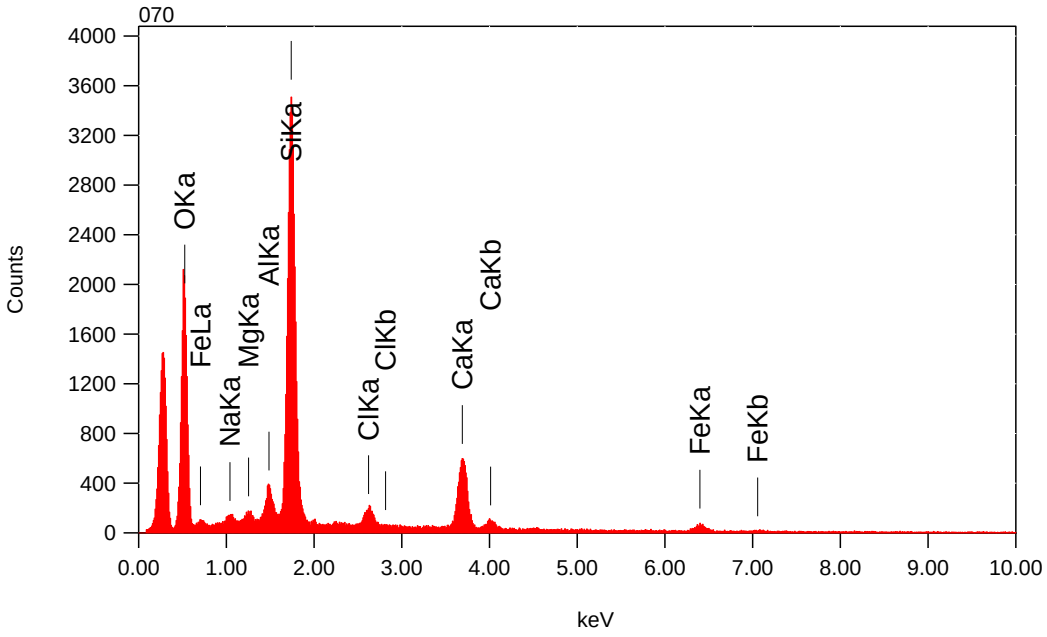


```
Acquisition Parameter
Instrument    : 7000F
Acc. Voltage  : 15.0 kV
Probe Current: 0.59000 nA
PHA mode      : T3
Real Time     : 36.88 sec
Live Time     : 30.00 sec
Dead Time     : 18 %
Counting Rate: 3864 cps
Energy Range :  0 - 20 keV
```

ZAF Method Standardless Quantitative Analysis
Fitting Coefficient : 0.3142

Element	(keV)	mass%	Error%	At%	Compound	mass%	Cation	K
O K	0.525	47.2	0.4	63.8				43.2083
Na K	1.041	0.8	0.3	0.8				0.6995
Mg K	1.253	0.7	0.3	0.6				0.5702
Al K	1.486	2.3	0.3	1.9				2.1538
Si K	1.739	29.9	0.3	23.1				31.0868
Cl K	2.621	2.0	0.4	1.2				2.2463
Ca K	3.690	12.8	0.7	6.9				15.7249
Fe K	6.398	4.2	1.9	1.6				4.3102
Total		100.0		100.0				

2055m Microfacies VS

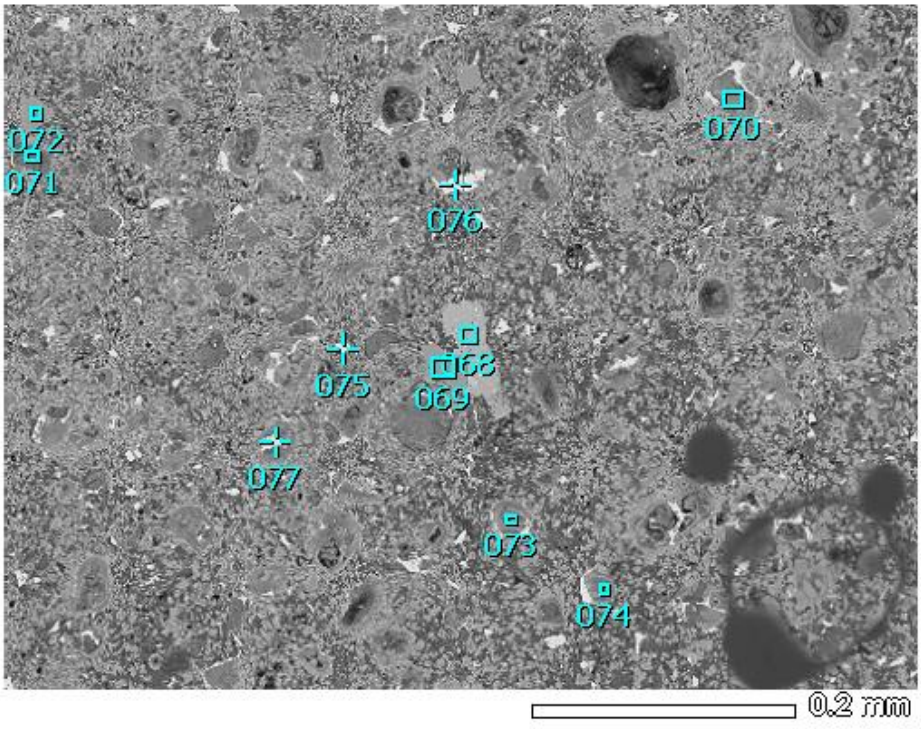


```
Title          : IMG1
---------------------------
Instrument     : 7000F
Volt           : 15.00 kV
Mag            : x 170
Date           : 2014/07/11
Pixel          : 512 x 384
```

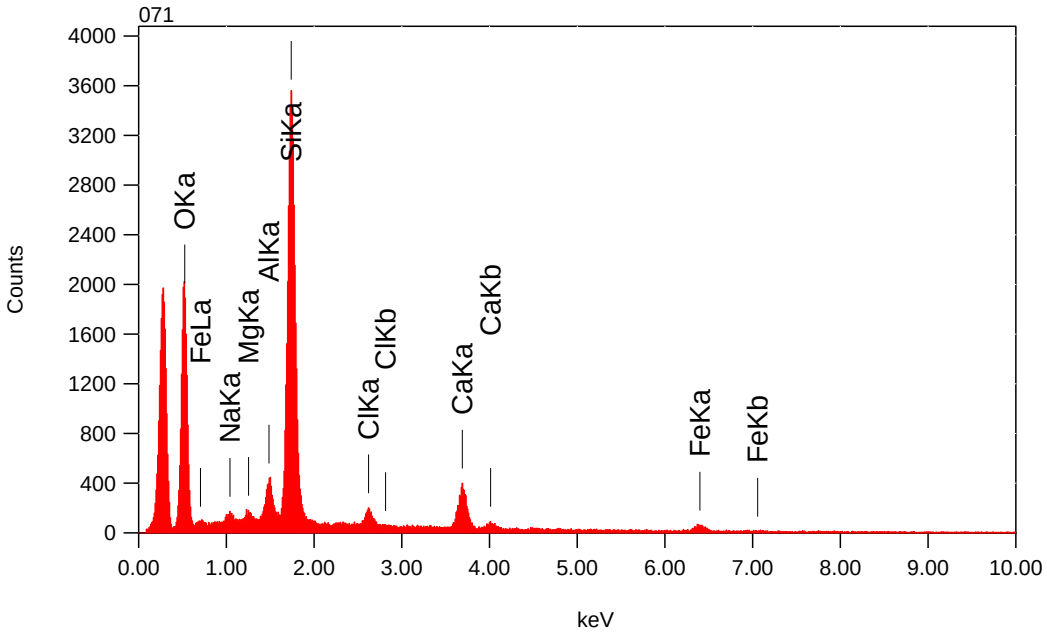


```
Acquisition Parameter
Instrument     : 7000F
Acc. Voltage   : 15.0 kV
Probe Current: 0.59000 nA
PHA mode       : T3
Real Time      : 36.78 sec
Live Time      : 30.00 sec
Dead Time      : 18 %
Counting Rate: 3901 cps
Energy Range :  0 - 20 keV
```

ZAF Method Standardless Quantitative Analysis
Fitting Coefficient : 0.3621

Element	(keV)	mass%	Error%	At%	Compound	mass%	Cation	K
O K	0.525	47.0	0.5	63.1				45.8487
Na K*	1.041	0.9	0.5	0.8				0.7083
Mg K	1.253	0.8	0.4	0.7				0.6156
Al K	1.486	3.1	0.4	2.5				2.7861
Si K	1.739	33.2	0.4	25.4				33.3068
Cl K	2.621	2.2	0.6	1.3				2.3228
Ca K	3.690	8.4	1.0	4.5				9.9238
Fe K	6.398	4.5	2.7	1.7				4.4879
Total		100.0		100.0				

2055m Microfacies VS

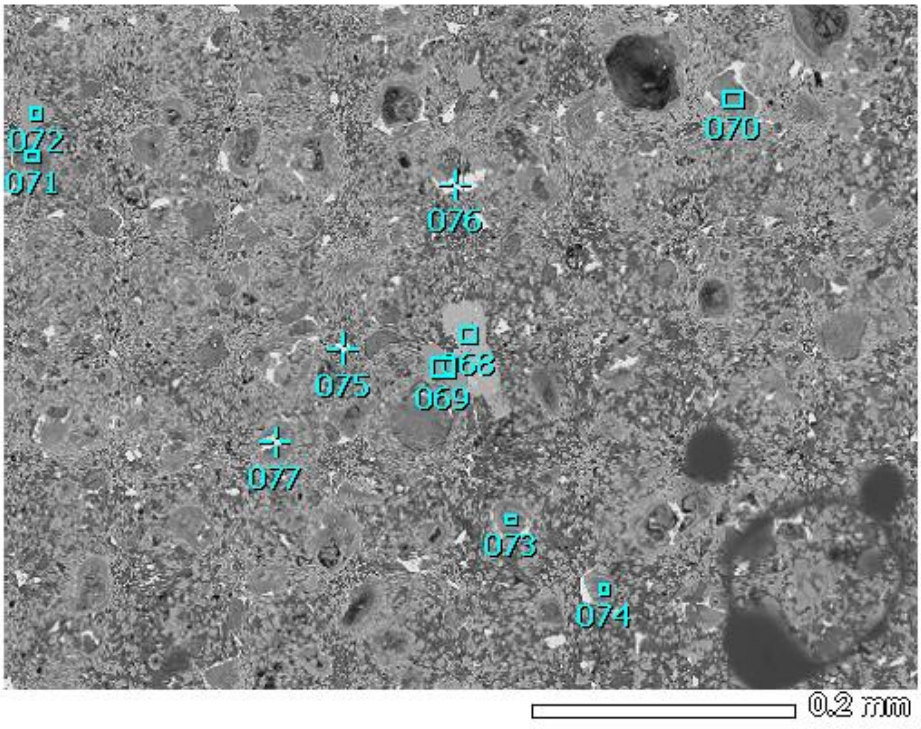


```
Title          : IMG1
---------------------------
Instrument     : 7000F
Volt           : 15.00 kV
Mag            : x 170
Date           : 2014/07/11
Pixel          : 512 x 384
```

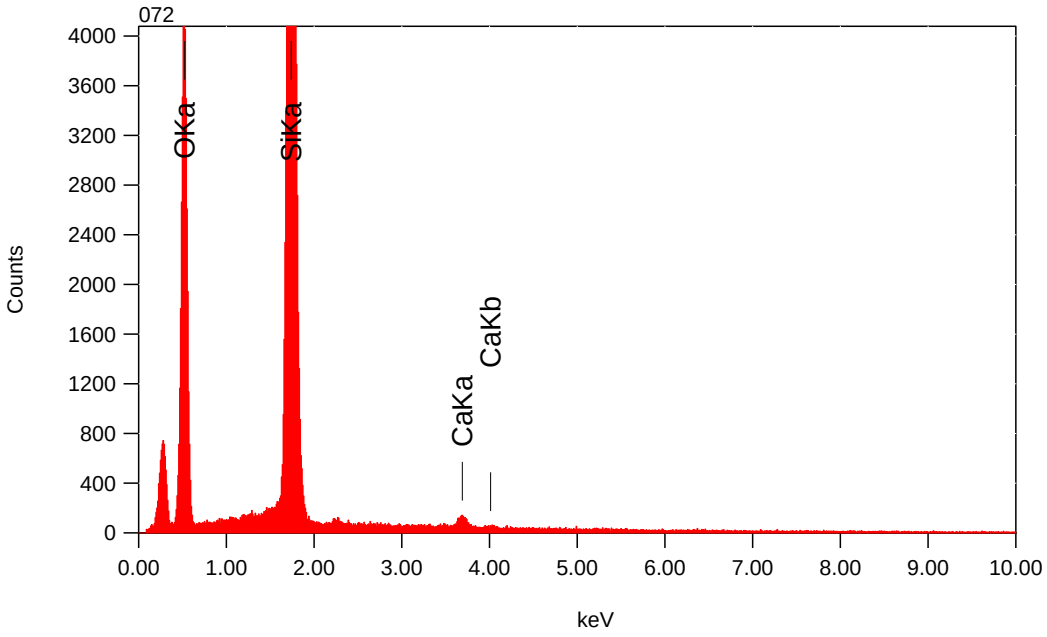


```
Acquisition Parameter
Instrument     : 7000F
Acc. Voltage   : 15.0 kV
Probe Current: 0.59000 nA
PHA mode       : T3
Real Time      : 43.52 sec
Live Time      : 30.00 sec
Dead Time      : 30 %
Counting Rate: 6479 cps
Energy Range :  0 - 20 keV
```

ZAF Method Standardless Quantitative Analysis
Fitting Coefficient : 0.2150

Element	(keV)	mass%	Error%	At%	Compound	mass%	Cation	K
O K	0.525	47.4	0.2	61.5				47.9979
Si K	1.739	51.3	0.2	37.9				50.7089
Ca K	3.690	1.2	0.5	0.6				1.2932
Total		100.0		100.0				

2055m Microfacies VS

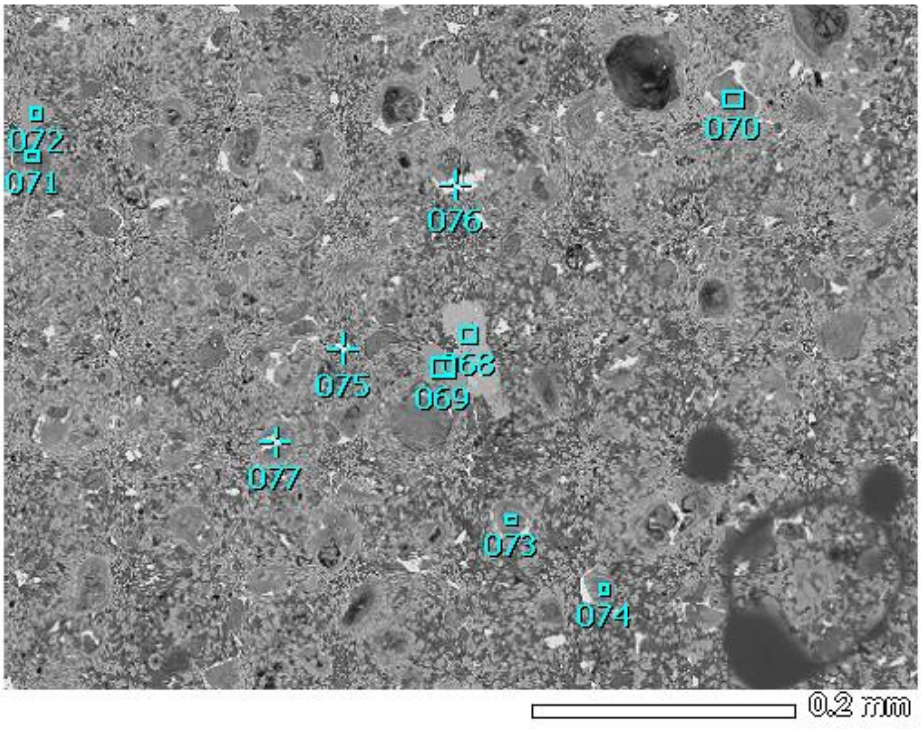


```
Title        : IMG1
---------------------------
Instrument   : 7000F
Volt         : 15.00 kV
Mag          : x 170
Date         : 2014/07/11
Pixel        : 512 x 384
```

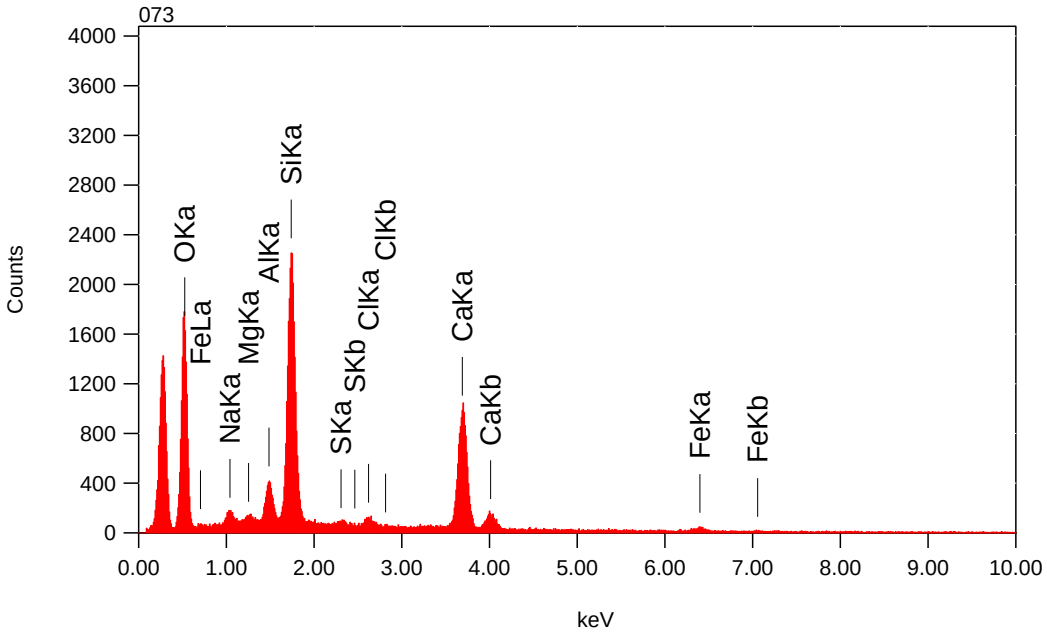


```
Acquisition Parameter
Instrument    : 7000F
Acc. Voltage  : 15.0 kV
Probe Current: 0.59000 nA
PHA mode      : T3
Real Time     : 36.13 sec
Live Time     : 30.00 sec
Dead Time     : 17 %
Counting Rate: 3517 cps
Energy Range :  0 - 20 keV
```

ZAF Method Standardless Quantitative Analysis
Fitting Coefficient : 0.3315

Element	(keV)	mass%	Error%	At%	Compound	mass%	Cation	K
O K	0.525	49.5	0.5	67.0				40.3666
Na K	1.041	1.3	0.4	1.2				1.0958
Mg K*	1.253	0.4	0.3	0.4				0.3611
Al K	1.486	3.0	0.3	2.4				2.8325
Si K	1.739	19.6	0.3	15.1				21.1855
S K*	2.307	0.4	0.3	0.3				0.4415
Cl K	2.621	0.9	0.4	0.6				1.1426
Ca K	3.690	22.5	0.6	12.2				29.9544
Fe K	6.398	2.4	1.9	0.9				2.6199
Total		100.0		100.0				

2055m Microfacies VS

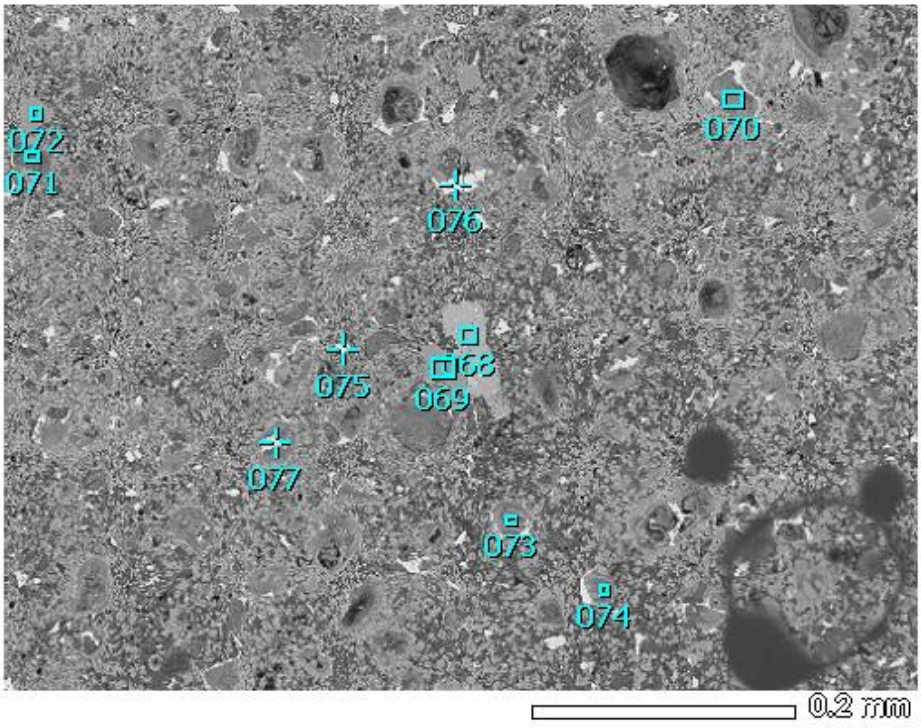


```
Title          : IMG1
---------------------------
Instrument     : 7000F
Volt           : 15.00 kV
Mag            : x 170
Date           : 2014/07/11
Pixel          : 512 x 384
```

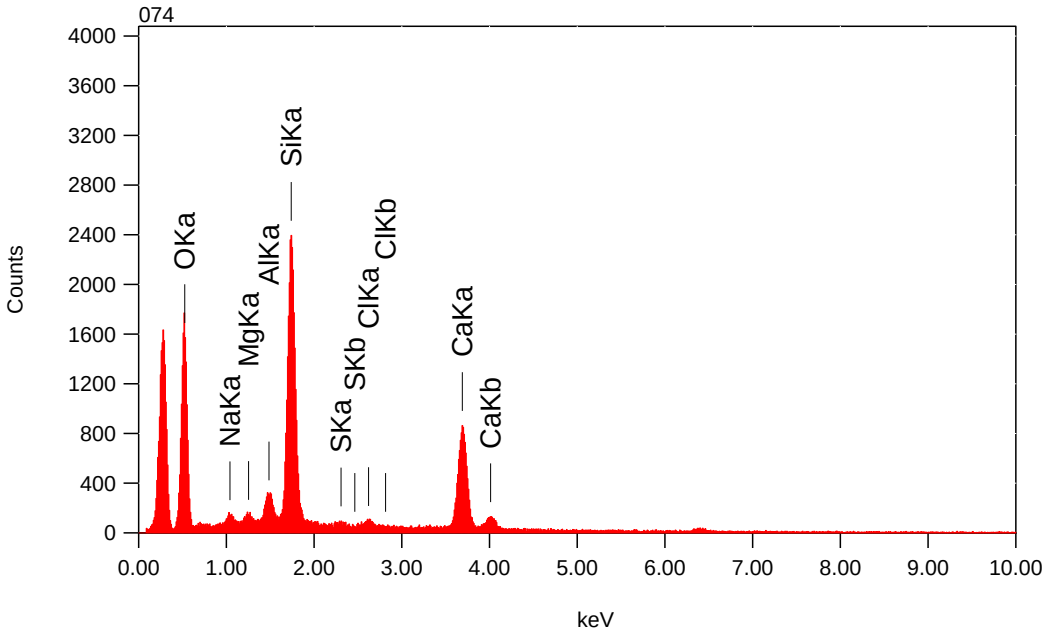


```
Acquisition Parameter
Instrument     : 7000F
Acc. Voltage   : 15.0 kV
Probe Current: 0.59000 nA
PHA mode       : T3
Real Time      : 35.93 sec
Live Time      : 30.00 sec
Dead Time      : 16 %
Counting Rate: 3388 cps
Energy Range :  0 - 20 keV
```

ZAF Method Standardless Quantitative Analysis
Fitting Coefficient : 0.3577

Element	(keV)	mass%	Error%	At%	Compound	mass%	Cation	K
O K	0.525	51.2	0.6	67.7				42.6823
Na K	1.041	1.1	0.4	1.0				0.9480
Mg K	1.253	0.8	0.4	0.7				0.6488
Al K	1.486	2.2	0.4	1.8				2.1684
Si K	1.739	22.8	0.4	17.2				24.8546
S K*	2.307	0.4	0.4	0.3				0.4510
Cl K	2.621	0.8	0.5	0.4				0.9010
Ca K	3.690	20.8	0.8	11.0				27.3459
Total		100.0		100.0				

2055m Microfacies VS

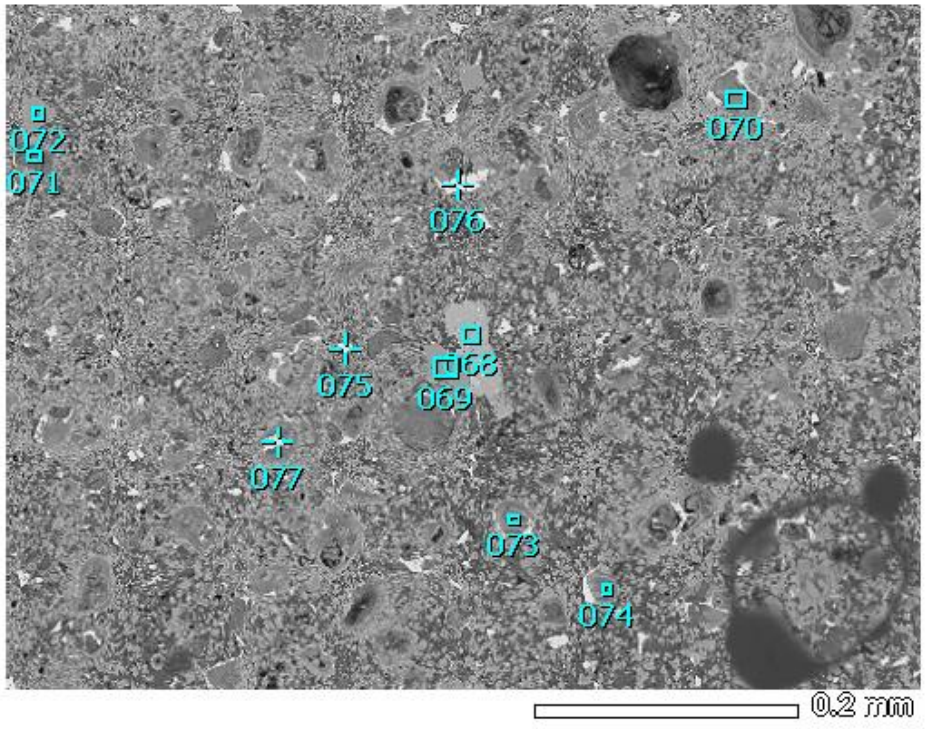


```
Title          : IMG1
---------------------------
Instrument     : 7000F
Volt           : 15.00 kV
Mag            : x 170
Date           : 2014/07/11
Pixel          : 512 x 384
```

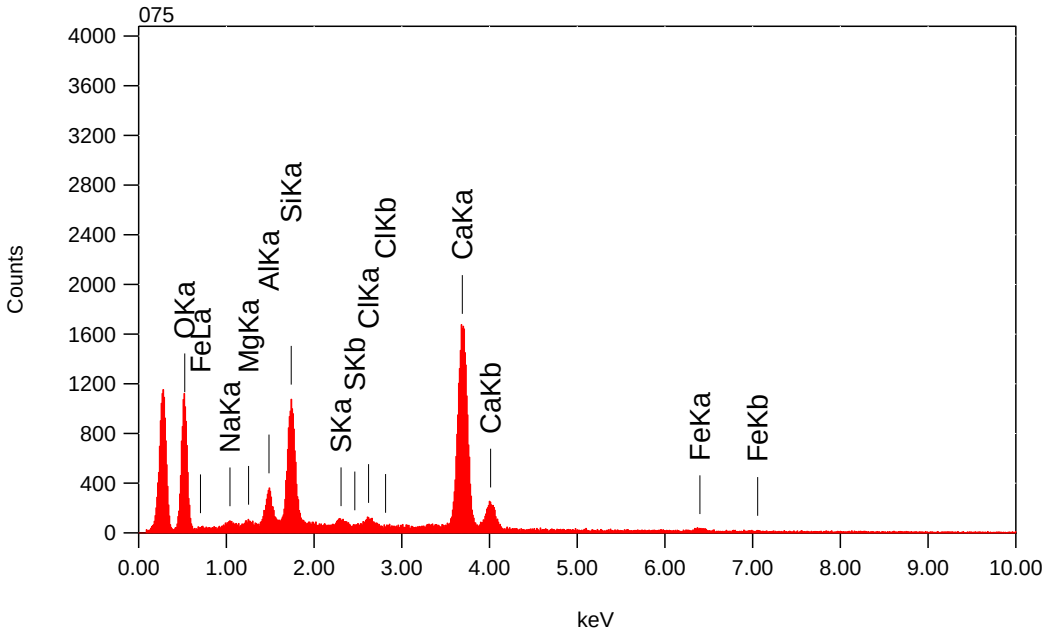


```
Acquisition Parameter
Instrument     : 7000F
Acc. Voltage   : 15.0 kV
Probe Current: 0.59000 nA
PHA mode       : T3
Real Time      : 35.31 sec
Live Time      : 30.00 sec
Dead Time      : 15 %
Counting Rate: 3077 cps
Energy Range :  0 - 20 keV
```

ZAF Method Standardless Quantitative Analysis
Fitting Coefficient : 0.3199

Element	(keV)	mass%	Error%	At%	Compound	mass%	Cation	K
O K	0.525	44.7	0.6	64.8				27.7030
Na K*	1.041	0.4	0.3	0.4				0.3498
Mg K*	1.253	0.4	0.3	0.4				0.3452
Al K	1.486	2.7	0.3	2.3				2.6054
Si K	1.739	9.6	0.3	7.9				10.5420
S K	2.307	0.6	0.2	0.5				0.8210
Cl K	2.621	0.8	0.3	0.5				1.0528
Ca K	3.690	38.7	0.5	22.4				54.3272
Fe K*	6.398	2.0	1.6	0.8				2.2537
Total		100.0		100.0				

2055m Microfacies VS

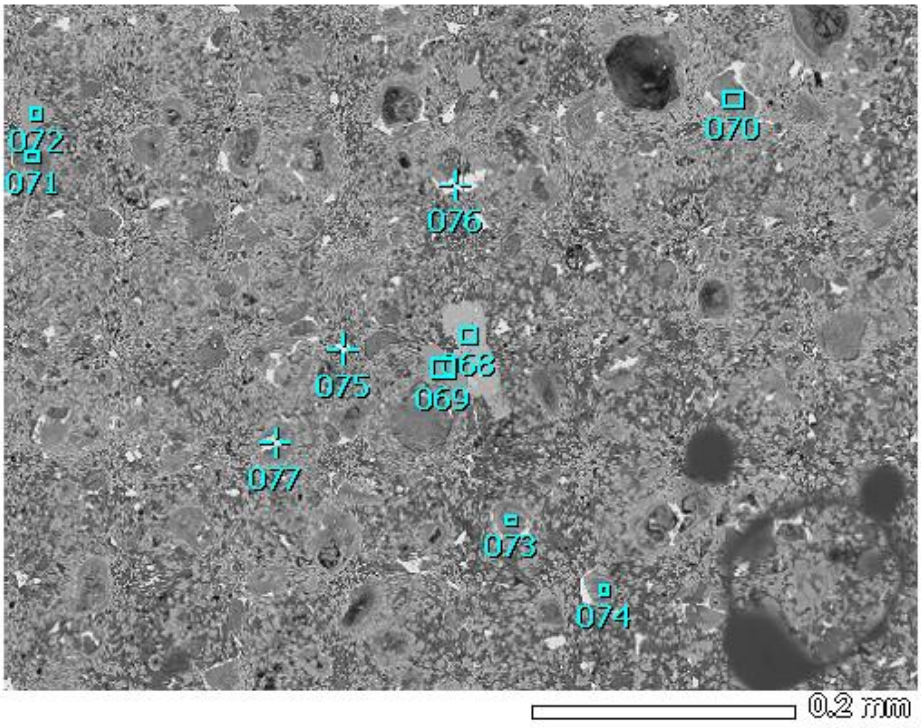


```
Title          : IMG1
---------------------------
Instrument     : 7000F
Volt           : 15.00 kV
Mag            : x 170
Date           : 2014/07/11
Pixel          : 512 x 384
```

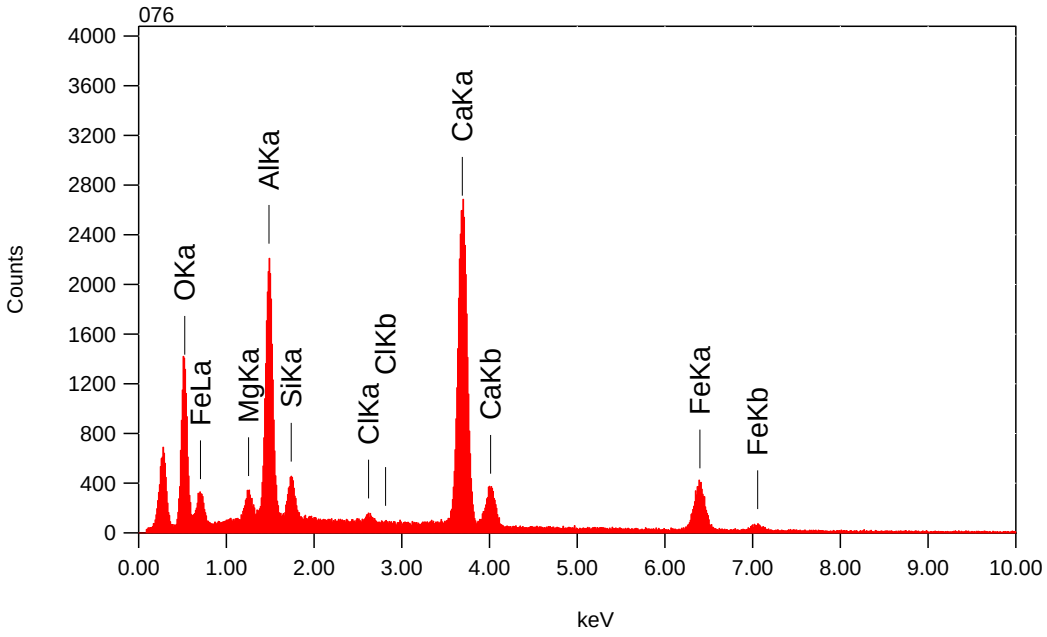


```
Acquisition Parameter
Instrument     : 7000F
Acc. Voltage   : 15.0 kV
Probe Current: 0.59000 nA
PHA mode       : T3
Real Time      : 38.96 sec
Live Time      : 30.00 sec
Dead Time      : 22 %
Counting Rate: 4748 cps
Energy Range :  0 - 20 keV
```

ZAF Method Standardless Quantitative Analysis
Fitting Coefficient : 0.1932

Element	(keV)	mass%	Error%	At%	Compound	mass%	Cation	K
O K	0.525	29.2	0.2	50.0				18.7145
Mg K	1.253	1.4	0.1	1.5				0.9842
Al K	1.486	12.2	0.1	12.4				10.3201
Si K	1.739	2.3	0.1	2.2				2.0610
Cl K	2.621	0.6	0.1	0.4				0.6815
Ca K	3.690	35.0	0.2	23.9				46.4531
Fe K	6.398	19.4	0.6	9.5				20.7857
Total		100.0		100.0				

2055m Microfacies VS

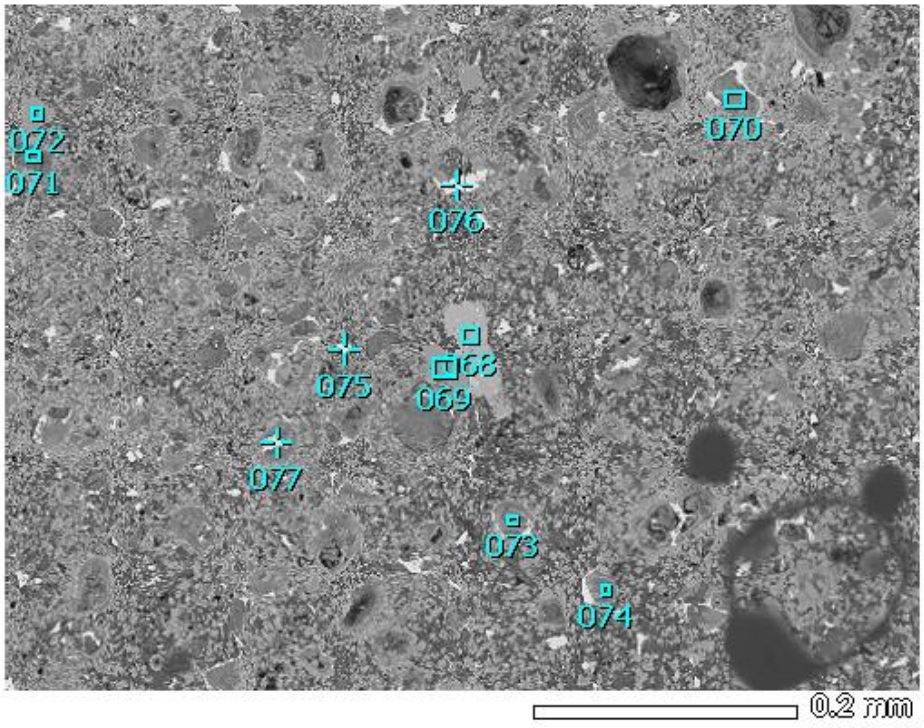


```
Title          : IMG1
---------------------------
Instrument     : 7000F
Volt           : 15.00 kV
Mag            : x 170
Date           : 2014/07/11
Pixel          : 512 x 384
```

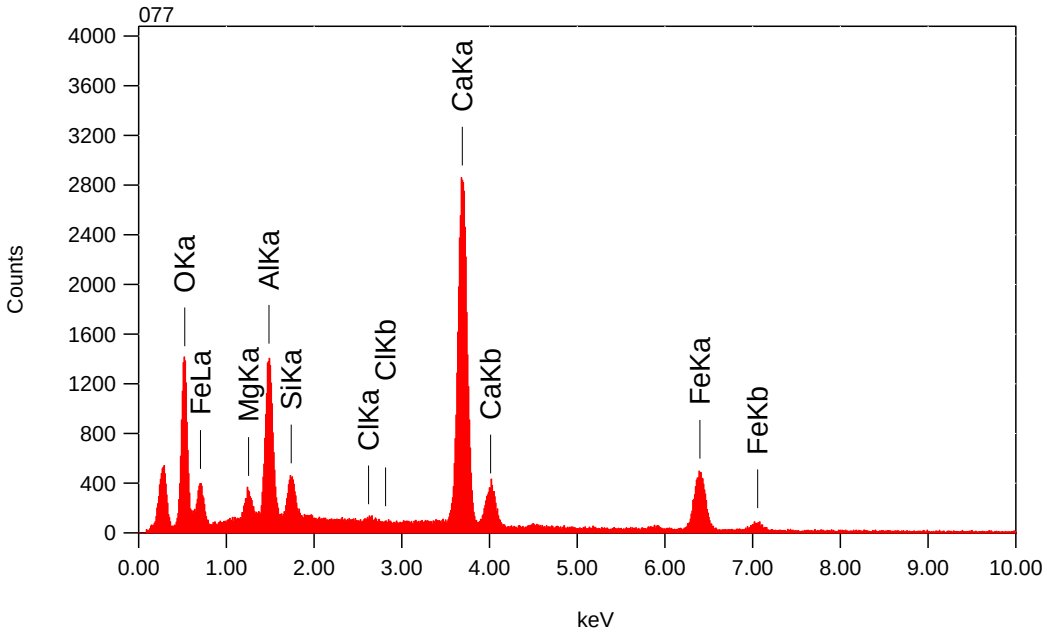


```
Acquisition Parameter
Instrument    : 7000F
Acc. Voltage  : 15.0 kV
Probe Current: 0.59000 nA
PHA mode      : T3
Real Time     : 38.94 sec
Live Time     : 30.00 sec
Dead Time     : 22 %
Counting Rate: 4690 cps
Energy Range :  0 - 20 keV
```

ZAF Method Standardless Quantitative Analysis
Fitting Coefficient : 0.1914

Element	(keV)	mass%	Error%	At%	Compound	mass%	Cation	K
O K	0.525	28.7	0.1	50.6				18.0488
Mg K	1.253	1.4	0.1	1.7				0.9706
Al K	1.486	7.6	0.1	7.9				6.1000
Si K	1.739	2.1	0.1	2.2				1.9576
Cl K*	2.621	0.2	0.1	0.2				0.2855
Ca K	3.690	36.4	0.2	25.6				47.7632
Fe K	6.398	23.5	0.5	11.9				24.8743
Total		100.0		100.0				

2055m Aluminium

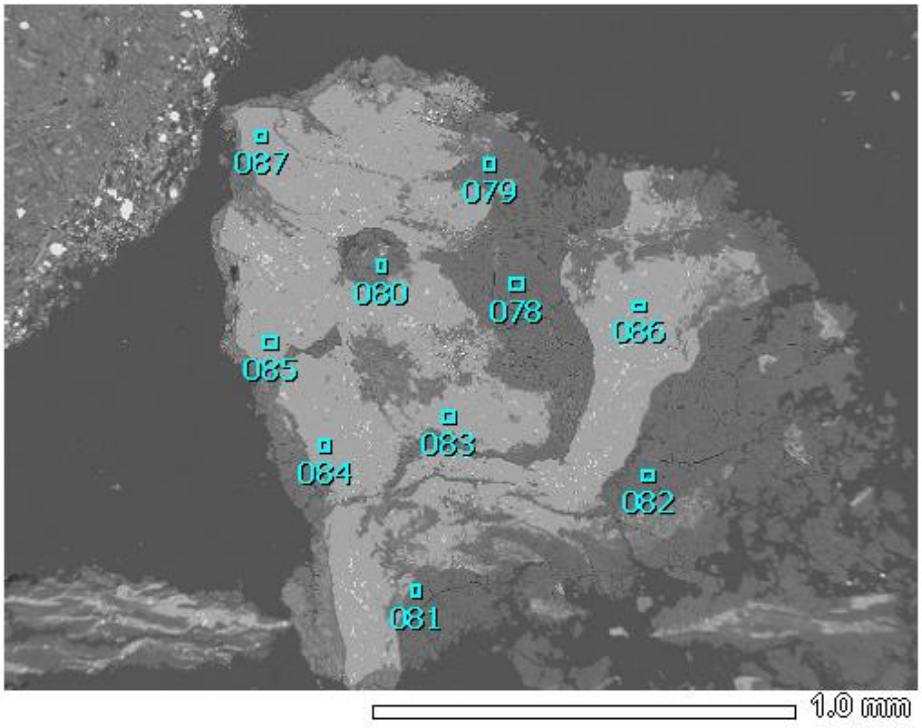


```
Title        : IMG1
---------------------------
Instrument   : 7000F
Volt         : 15.00 kV
Mag          : x 55
Date         : 2014/07/11
Pixel        : 512 x 384
```

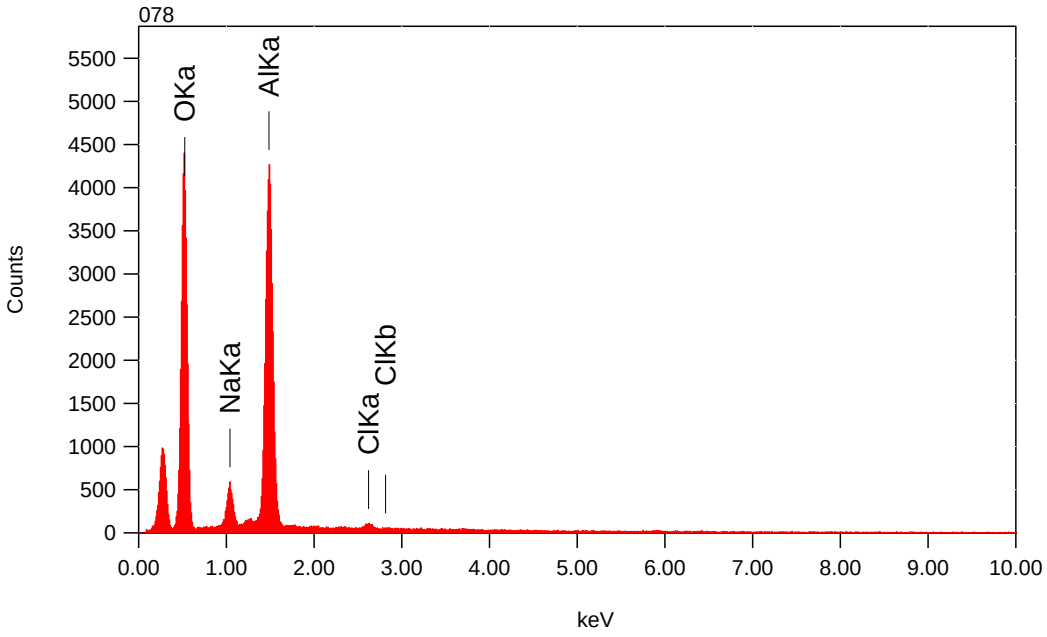


```
Acquisition Parameter
Instrument    : 7000F
Acc. Voltage  : 15.0 kV
Probe Current: 0.59000 nA
PHA mode      : T3
Real Time     : 37.53 sec
Live Time     : 30.00 sec
Dead Time     : 20 %
Counting Rate: 4165 cps
Energy Range :  0 - 20 keV
```

ZAF Method Standardless Quantitative Analysis
Fitting Coefficient : 0.2561

Element	(keV)	mass%	Error%	At%	Compound	mass%	Cation	K
O K	0.525	58.1	0.2	69.7				70.3575
Na K	1.041	5.3	0.3	4.4				3.6588
Al K	1.486	35.6	0.3	25.4				25.1606
Cl K	2.621	1.0	0.3	0.5				0.8230
Total		100.0		100.0				

2055m Aluminium

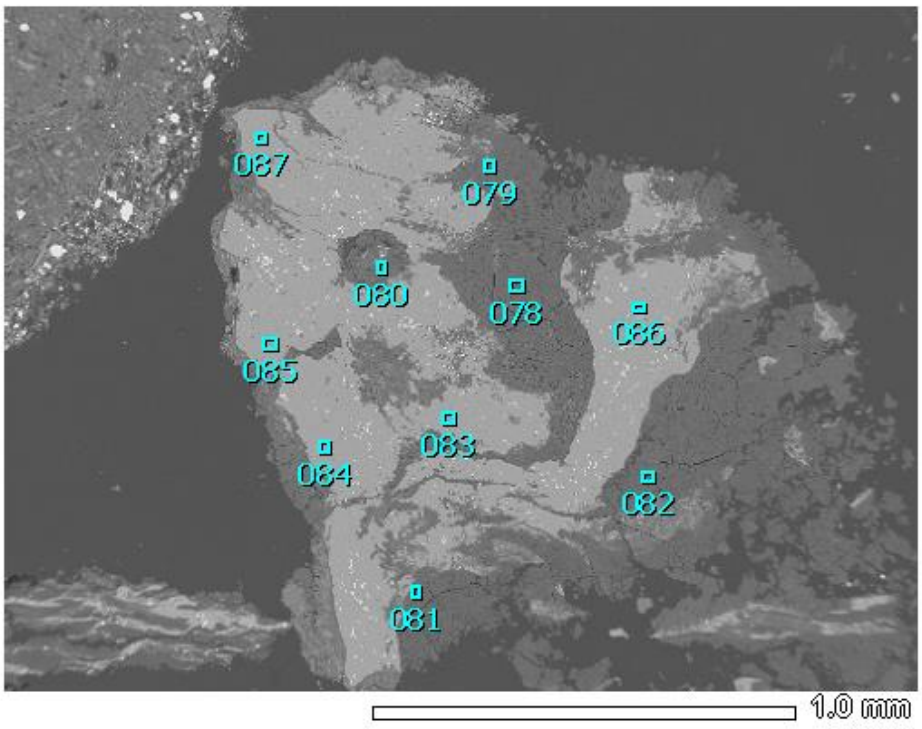


```
Title        : IMG1
---------------------------
Instrument   : 7000F
Volt         : 15.00 kV
Mag          : x 55
Date         : 2014/07/11
Pixel        : 512 x 384
```

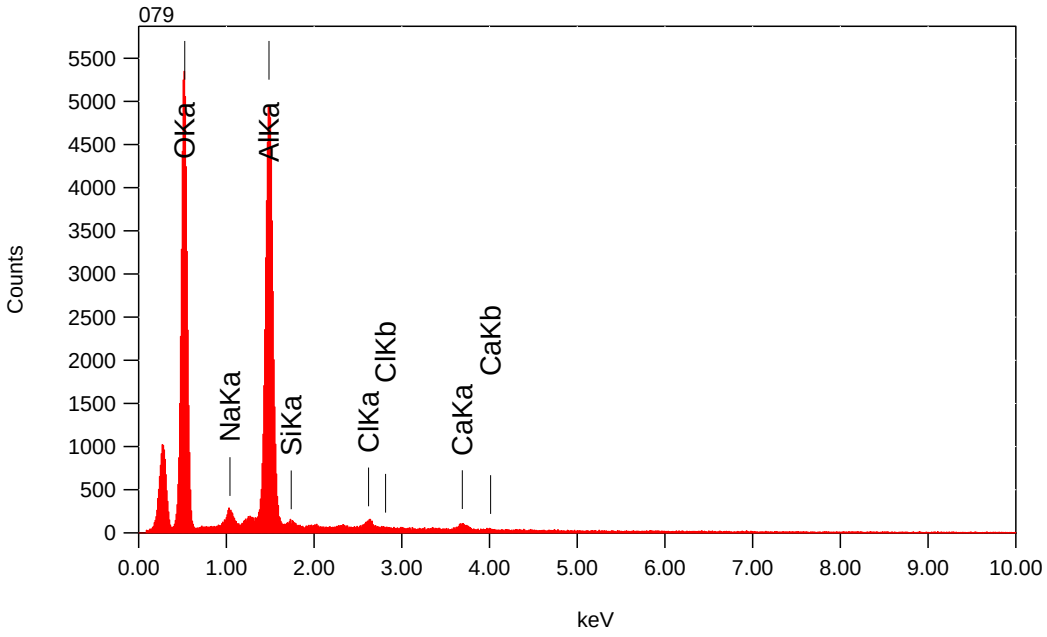


```
Acquisition Parameter
Instrument    : 7000F
Acc. Voltage  : 15.0 kV
Probe Current: 0.59000 nA
PHA mode      : T3
Real Time     : 39.05 sec
Live Time     : 30.00 sec
Dead Time     : 23 %
Counting Rate: 4933 cps
Energy Range :  0 - 20 keV
```

ZAF Method Standardless Quantitative Analysis
Fitting Coefficient : 0.2551

Element	(keV)	mass%	Error%	At%	Compound	mass%	Cation	K
O K	0.525	61.1	0.2	72.8				71.8139
Na K	1.041	1.7	0.3	1.4				1.1167
Al K	1.486	34.0	0.2	24.0				24.4907
Si K*	1.739	0.9	0.3	0.6				0.5631
Cl K	2.621	1.1	0.3	0.6				0.9240
Ca K	3.690	1.2	0.6	0.6				1.0916
Total		100.0		100.0				

2055m Aluminium

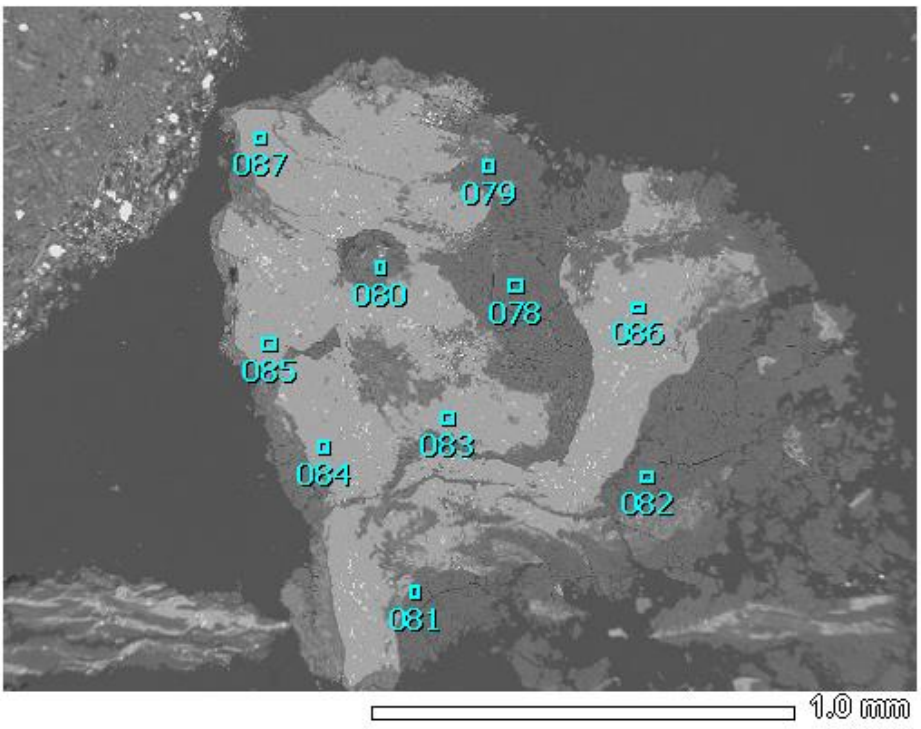


```
Title        : IMG1
--------------------------
Instrument   : 7000F
Volt         : 15.00 kV
Mag          : x 55
Date         : 2014/07/11
Pixel        : 512 x 384
```

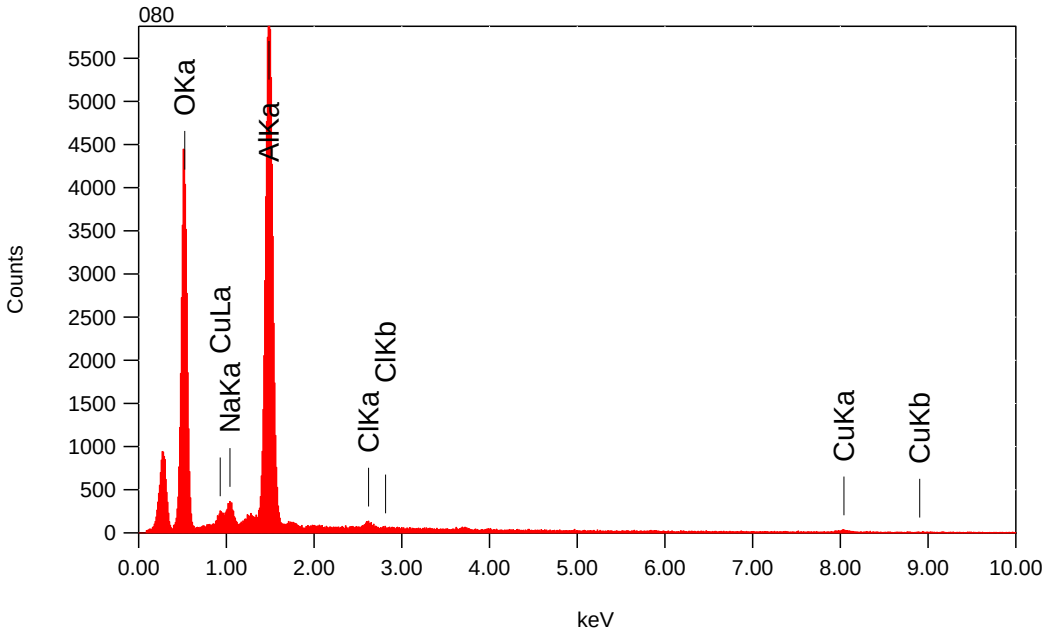


```
Acquisition Parameter
Instrument    : 7000F
Acc. Voltage  : 15.0 kV
Probe Current: 0.59000 nA
PHA mode      : T3
Real Time     : 39.37 sec
Live Time     : 30.00 sec
Dead Time     : 23 %
Counting Rate: 5008 cps
Energy Range :  0 - 20 keV
```

ZAF Method Standardless Quantitative Analysis
Fitting Coefficient : 0.2409

Element	(keV)	mass%	Error%	At%	Compound	mass%	Cation	K
O K	0.525	51.3	0.2	64.9				62.4364
Na K	1.041	2.2	0.3	1.9				1.6026
Al K	1.486	41.9	0.2	31.5				32.2427
Cl K	2.621	0.9	0.3	0.5				0.7635
Cu K	8.040	3.7	3.7	1.2				2.9548
Total		100.0		100.0				

2055m Aluminium

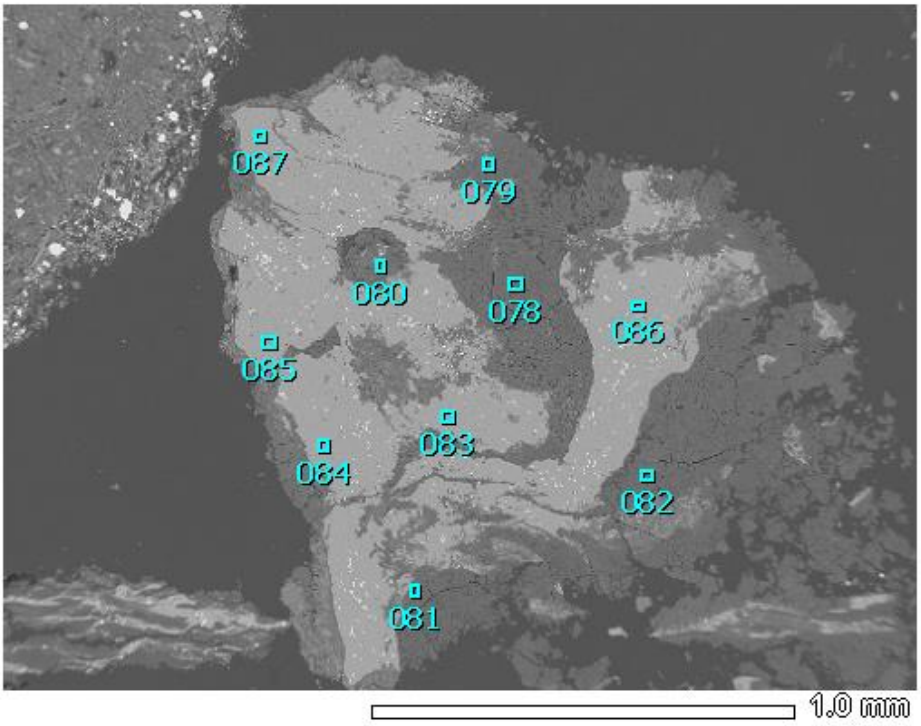


```
Title        : IMG1
---------------------------
Instrument   : 7000F
Volt         : 15.00 kV
Mag          : x 55
Date         : 2014/07/11
Pixel        : 512 x 384
```

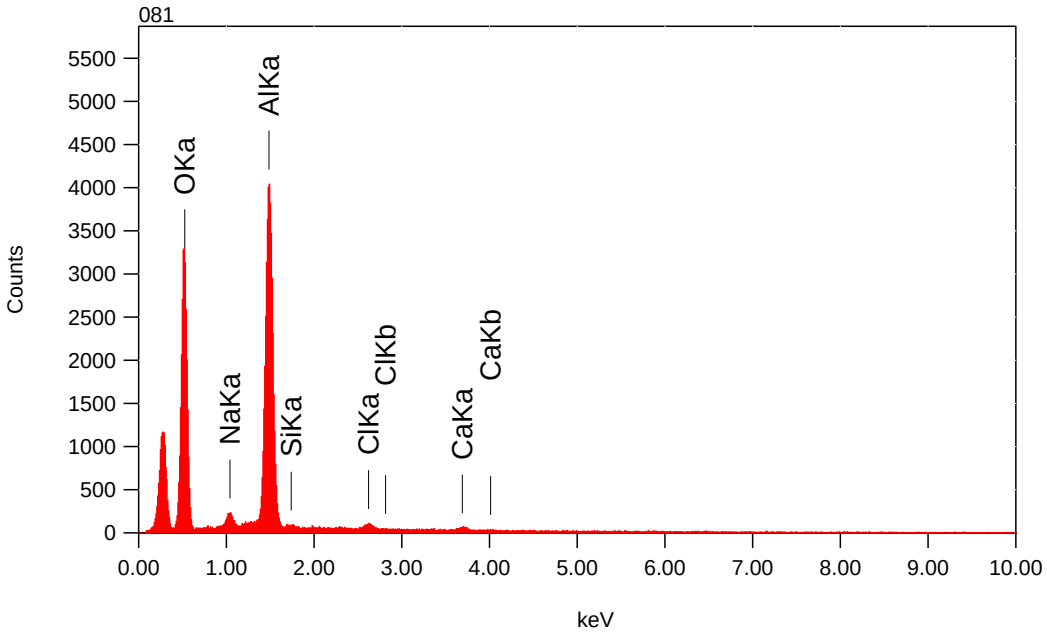


```
Acquisition Parameter
Instrument   : 7000F
Acc. Voltage : 15.0 kV
Probe Current: 0.59000 nA
PHA mode     : T3
Real Time    : 36.62 sec
Live Time    : 30.00 sec
Dead Time    : 18 %
Counting Rate: 3767 cps
Energy Range :  0 - 20 keV
```

ZAF Method Standardless Quantitative Analysis
Fitting Coefficient : 0.2927

Element	(keV)	mass%	Error%	At%	Compound	mass%	Cation	K
O K	0.525	56.5	0.3	68.8				66.7180
Na K	1.041	2.1	0.4	1.8				1.5300
Al K	1.486	38.5	0.3	27.8				29.3355
Si K*	1.739	0.9	0.5	0.6				0.5545
Cl K	2.621	1.0	0.4	0.6				0.9075
Ca K*	3.690	1.0	0.7	0.5				0.9546
Total		100.0		100.0				

2055m Aluminium

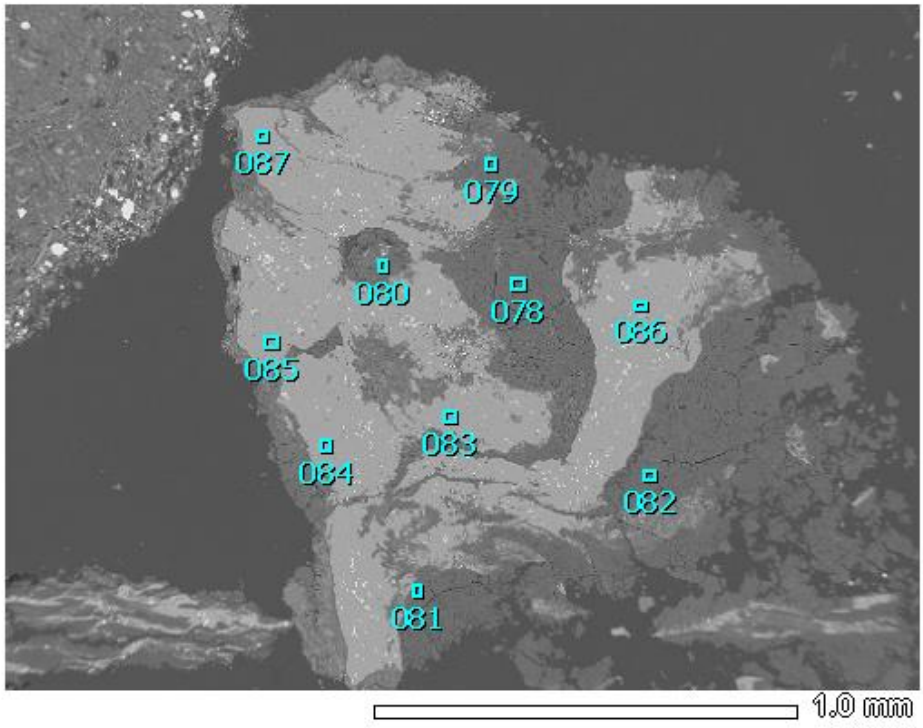


```
Title        : IMG1
---------------------------
Instrument   : 7000F
Volt         : 15.00 kV
Mag          : x 55
Date         : 2014/07/11
Pixel        : 512 x 384
```

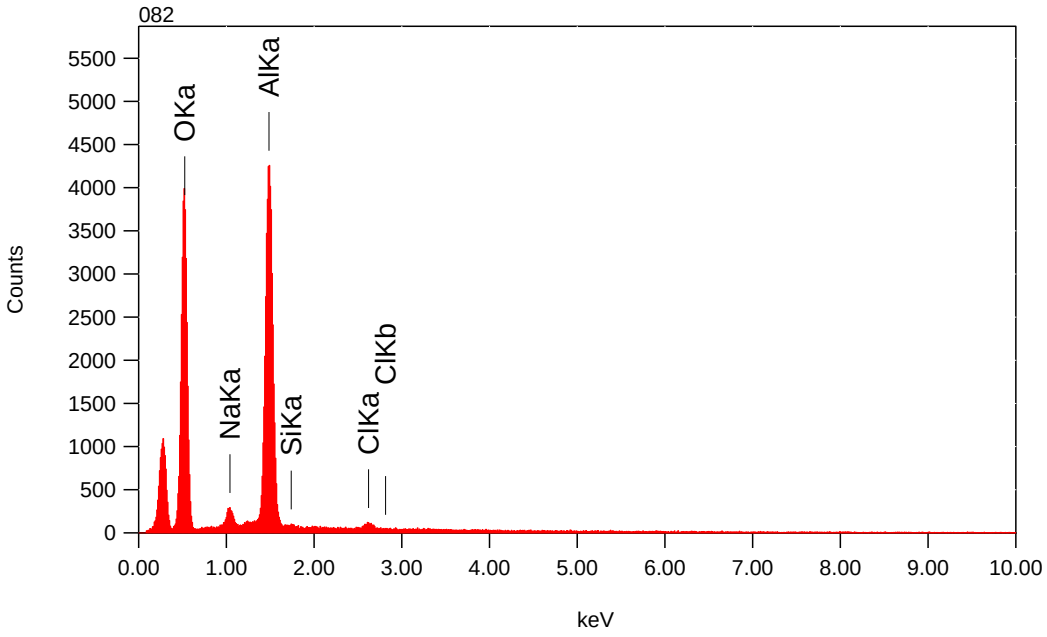


```
Acquisition Parameter
Instrument    : 7000F
Acc. Voltage  : 15.0 kV
Probe Current: 0.59000 nA
PHA mode      : T3
Real Time     : 37.24 sec
Live Time     : 30.00 sec
Dead Time     : 19 %
Counting Rate: 4117 cps
Energy Range :  0 - 20 keV
```

ZAF Method Standardless Quantitative Analysis
Fitting Coefficient : 0.2681

Element	(keV)	mass%	Error%	At%	Compound	mass%	Cation	K
O K	0.525	58.0	0.2	69.9				69.4067
Na K	1.041	2.5	0.3	2.1				1.7483
Al K	1.486	37.7	0.3	26.9				27.5169
Si K*	1.739	0.7	0.4	0.5				0.4438
Cl K	2.621	1.0	0.4	0.6				0.8843
Total		100.0		100.0				

2055m Aluminium

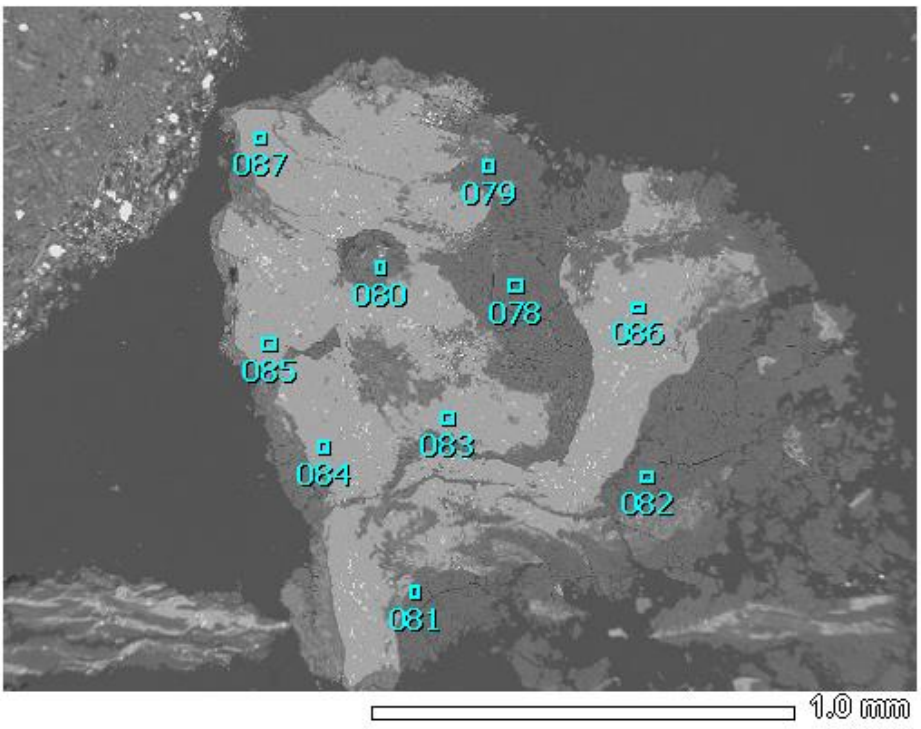


```
Title        : IMG1
---------------------------
Instrument   : 7000F
Volt         : 15.00 kV
Mag          : x 55
Date         : 2014/07/11
Pixel        : 512 x 384
```

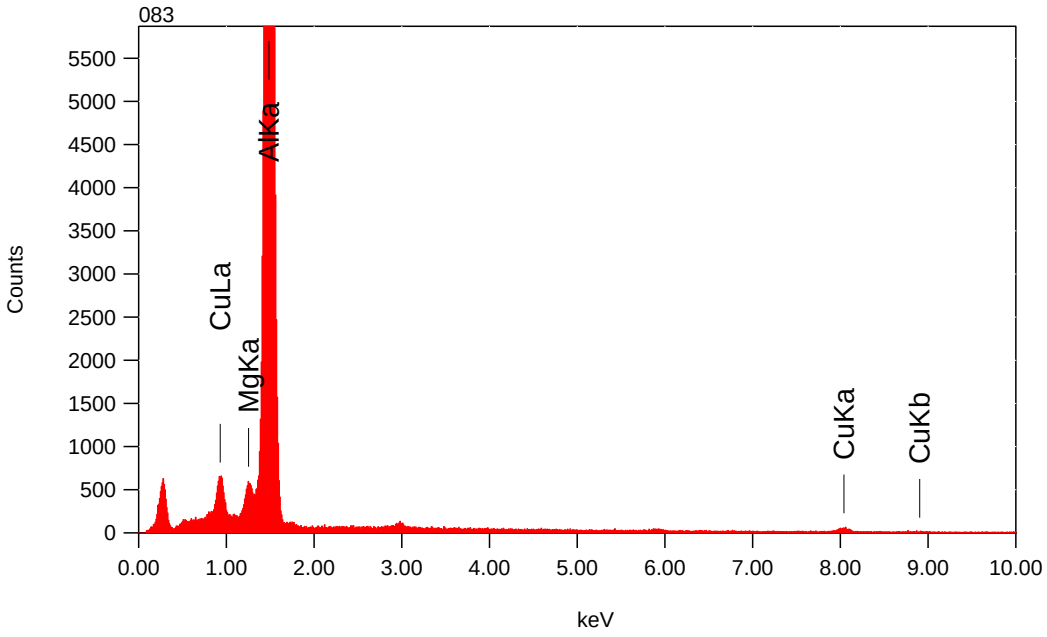


```
Acquisition Parameter
Instrument   : 7000F
Acc. Voltage : 15.0 kV
Probe Current: 0.59000 nA
PHA mode     : T3
Real Time    : 50.50 sec
Live Time    : 30.00 sec
Dead Time    : 40 %
Counting Rate: 9432 cps
Energy Range :  0 - 20 keV
```

ZAF Method Standardless Quantitative Analysis
Fitting Coefficient : 0.1707

Element	(keV)	mass%	Error%	At%	Compound	mass%	Cation	K
Mg K	1.253	1.5	0.2	1.7				1.5135
Al K	1.486	93.2	0.3	95.9				93.7962
Cu K	8.040	5.3	5.3	2.3				4.6903
Total		100.0		100.0				

2055m Aluminium

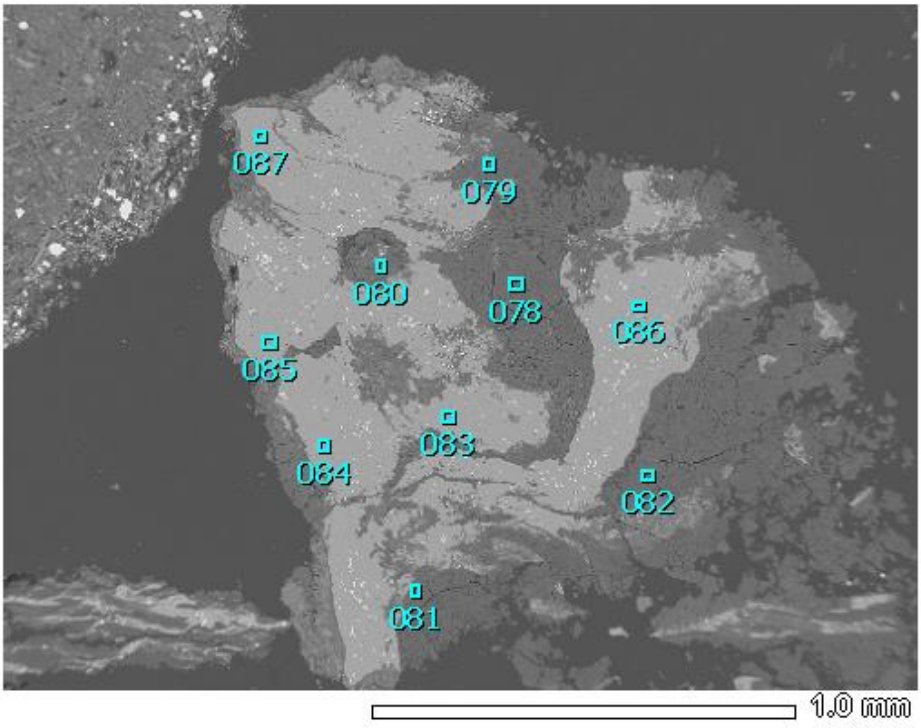


```
Title        : IMG1
---------------------------
Instrument   : 7000F
Volt         : 15.00 kV
Mag          : x 55
Date         : 2014/07/11
Pixel        : 512 x 384
```

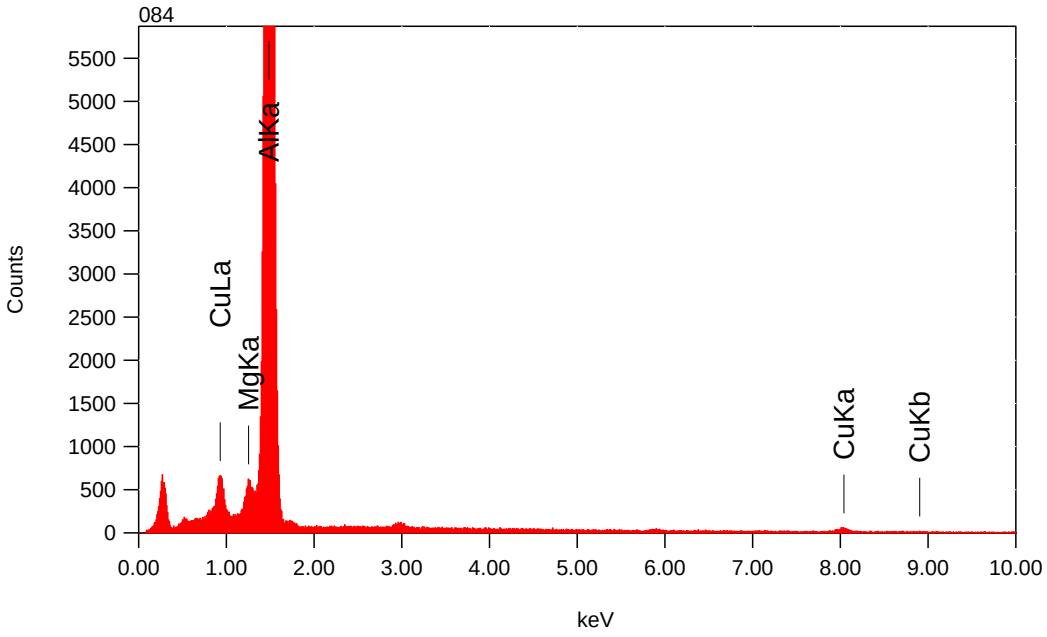


```
Acquisition Parameter
Instrument    : 7000F
Acc. Voltage  : 15.0 kV
Probe Current: 0.59000 nA
PHA mode      : T3
Real Time     : 51.18 sec
Live Time     : 30.00 sec
Dead Time     : 41 %
Counting Rate: 9644 cps
Energy Range :  0 - 20 keV
```

ZAF Method Standardless Quantitative Analysis
Fitting Coefficient : 0.1657

Element	(keV)	mass%	Error%	At%	Compound	mass%	Cation	K
Mg K	1.253	1.4	0.2	1.6				1.4534
Al K	1.486	93.7	0.2	96.3				94.3611
Cu K	8.040	4.8	5.0	2.1				4.1855
Total		100.0		100.0				

2055m Aluminium

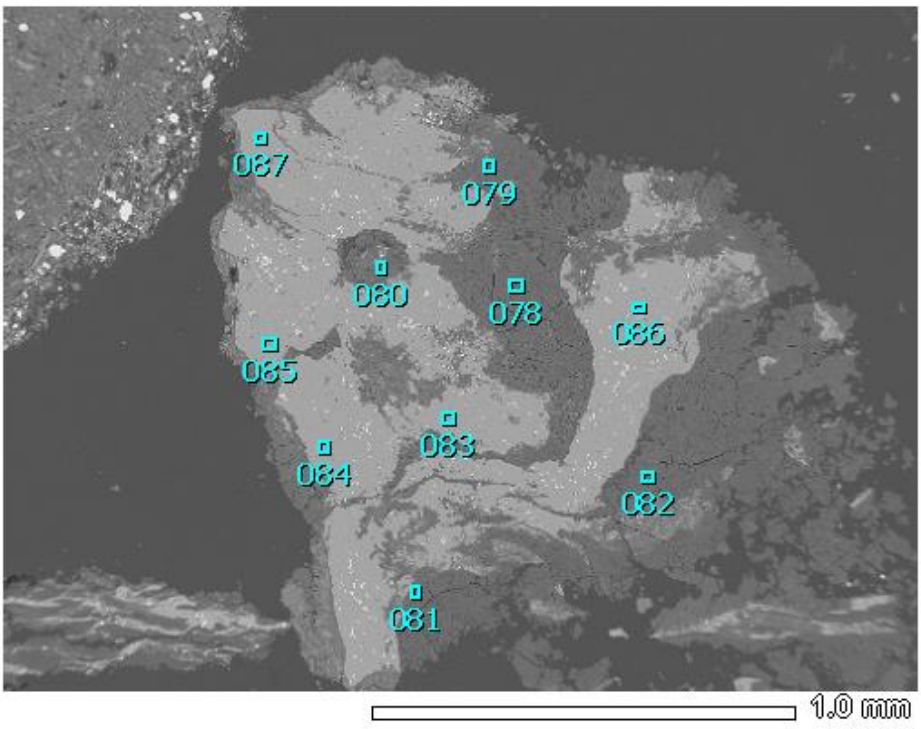


```
Title          : IMG1
---------------------------
Instrument     : 7000F
Volt           : 15.00 kV
Mag            : x 55
Date           : 2014/07/11
Pixel          : 512 x 384
```

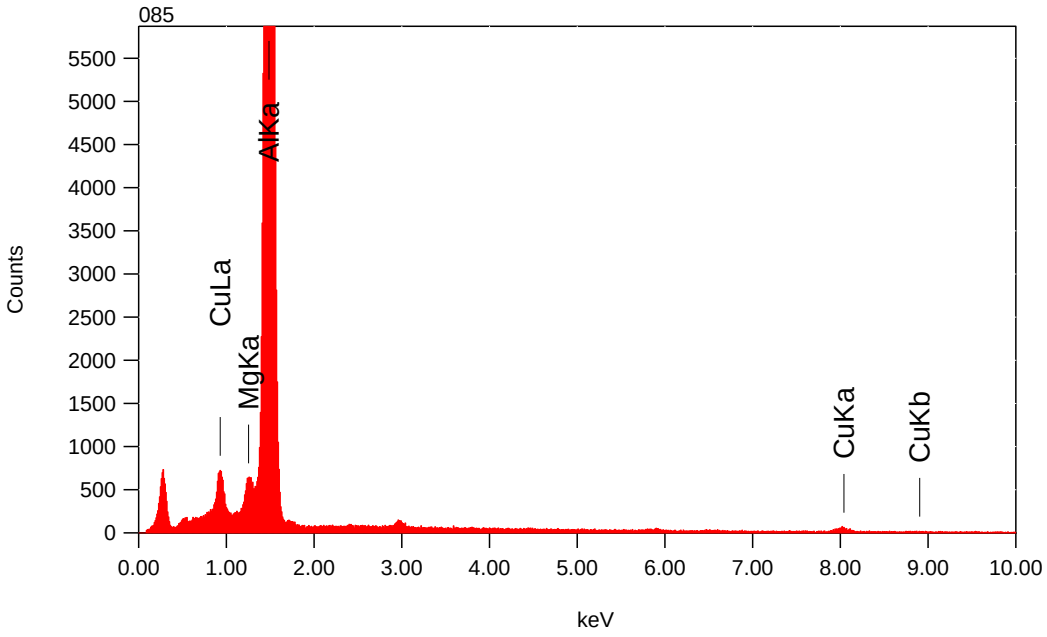


```
Acquisition Parameter
Instrument     : 7000F
Acc. Voltage   : 15.0 kV
Probe Current: 0.59000 nA
PHA mode       : T3
Real Time      : 54.04 sec
Live Time      : 30.00 sec
Dead Time      : 44 %
Counting Rate: 10566 cps
Energy Range :  0 - 20 keV
```

ZAF Method Standardless Quantitative Analysis
Fitting Coefficient : 0.1799

Element	(keV)	mass%	Error%	At%	Compound	mass%	Cation	K
Mg K	1.253	1.4	0.2	1.6				1.4011
Al K	1.486	93.9	0.3	96.4				94.5193
Cu K	8.040	4.7	5.8	2.0				4.0796
Total		100.0		100.0				

2055m Aluminium

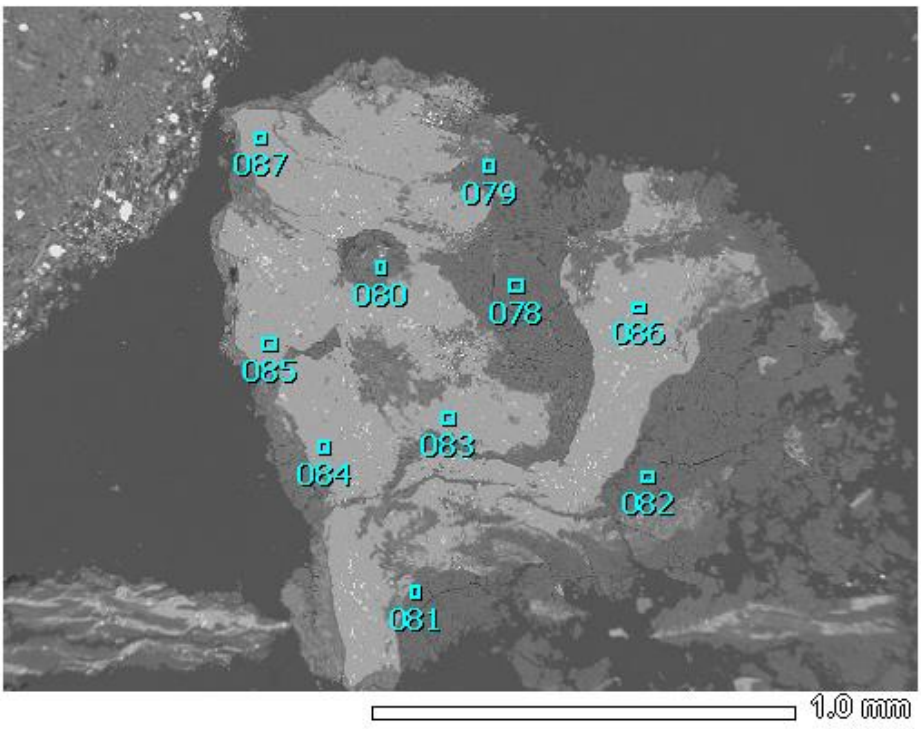


```
Title        : IMG1
---------------------------
Instrument   : 7000F
Volt         : 15.00 kV
Mag          : x 55
Date         : 2014/07/11
Pixel        : 512 x 384
```

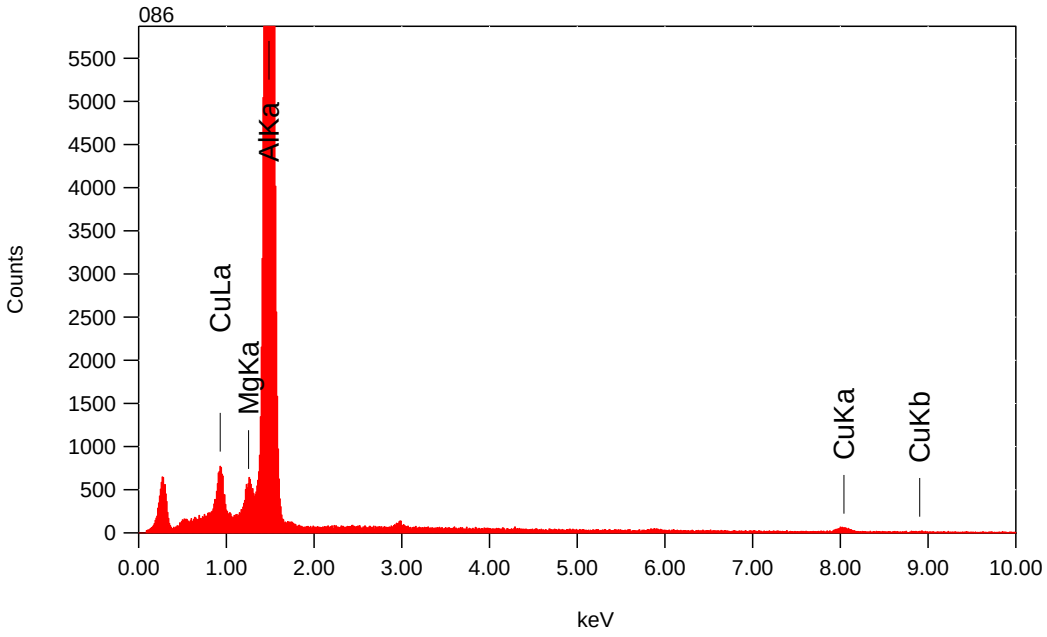


```
Acquisition Parameter
Instrument    : 7000F
Acc. Voltage  : 15.0 kV
Probe Current: 0.59000 nA
PHA mode      : T3
Real Time     : 51.09 sec
Live Time     : 30.00 sec
Dead Time     : 41 %
Counting Rate: 9618 cps
Energy Range :  0 - 20 keV
```

ZAF Method Standardless Quantitative Analysis
Fitting Coefficient : 0.1747

Element	(keV)	mass%	Error%	At%	Compound	mass%	Cation	K
Mg K	1.253	1.5	0.2	1.8				1.5546
Al K	1.486	92.8	0.3	95.7				93.4132
Cu K	8.040	5.7	5.3	2.5				5.0322
Total		100.0		100.0				

2055m Aluminium

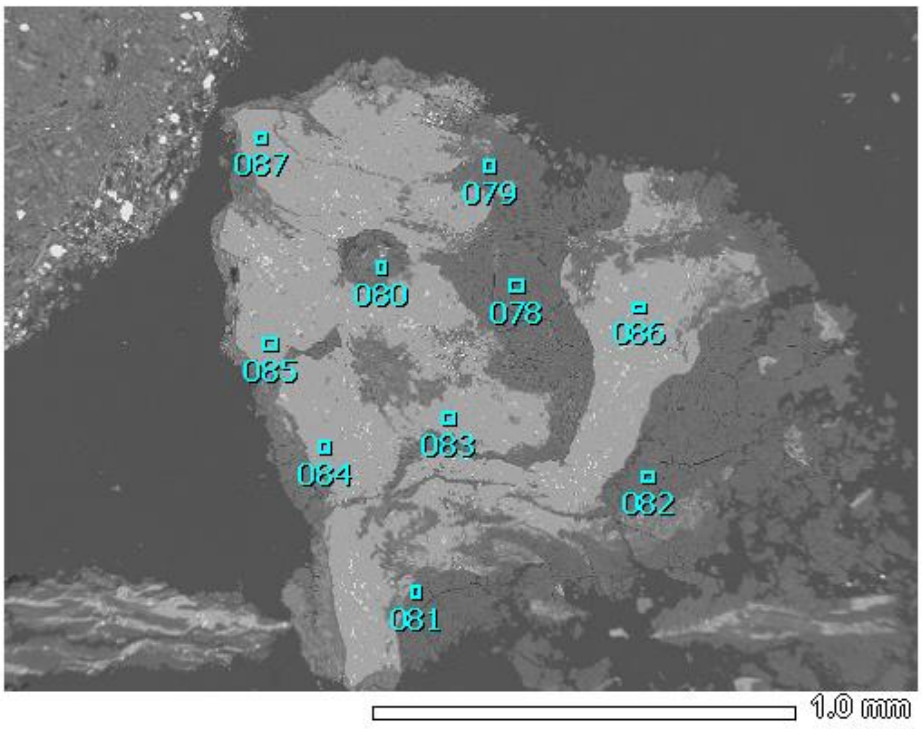


```
Title        : IMG1
---------------------------
Instrument   : 7000F
Volt         : 15.00 kV
Mag          : x 55
Date         : 2014/07/11
Pixel        : 512 x 384
```

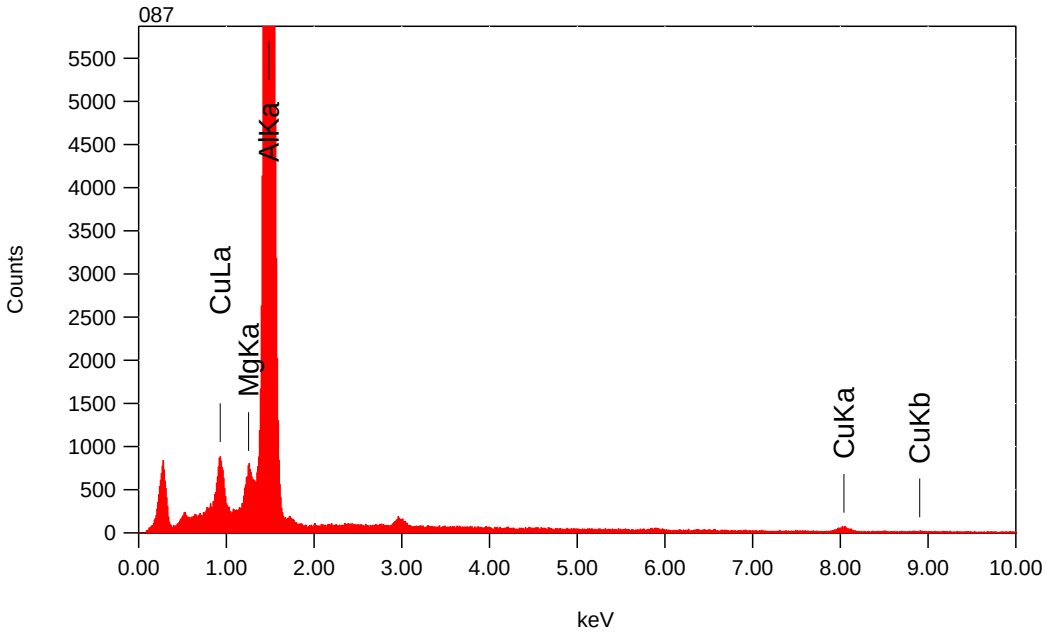


```
Acquisition Parameter
Instrument    : 7000F
Acc. Voltage  : 15.0 kV
Probe Current: 0.59000 nA
PHA mode      : T3
Real Time     : 59.25 sec
Live Time     : 30.00 sec
Dead Time     : 48 %
Counting Rate: 12102 cps
Energy Range :  0 - 20 keV
```

ZAF Method Standardless Quantitative Analysis
Fitting Coefficient : 0.1718

Element	(keV)	mass%	Error%	At%	Compound	mass%	Cation	K
Mg K	1.253	1.5	0.2	1.7				1.4932
Al K	1.486	93.9	0.3	96.3				94.4778
Cu K	8.040	4.6	5.4	2.0				4.0290
Total		100.0		100.0				

2055m Aluminium

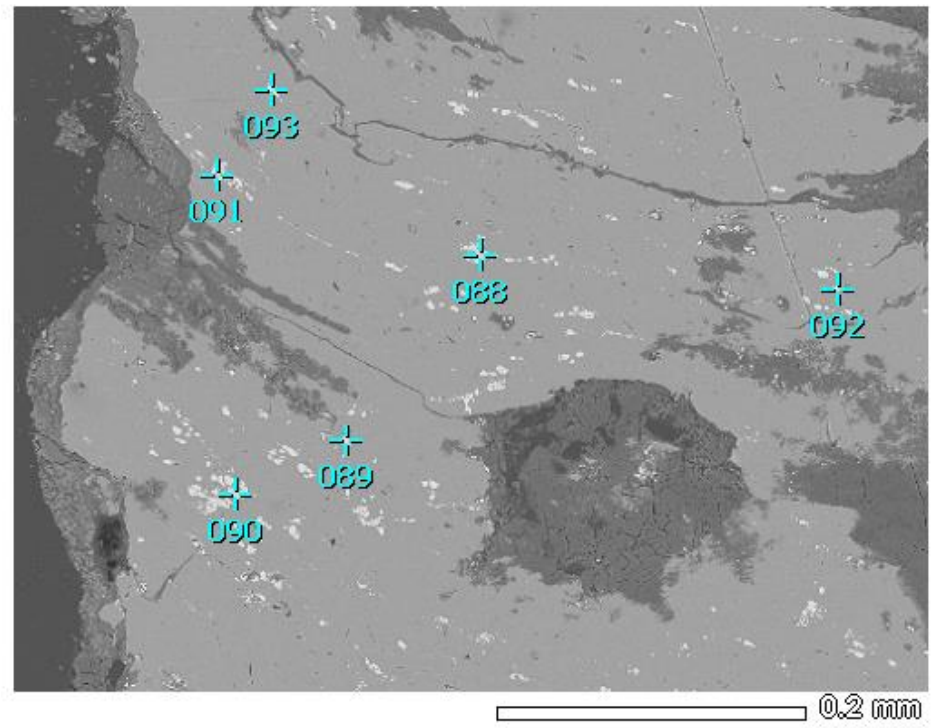


```
Title        : IMG1
---------------------------
Instrument   : 7000F
Volt         : 15.00 kV
Mag          : x 200
Date         : 2014/07/11
Pixel        : 512 x 384
```

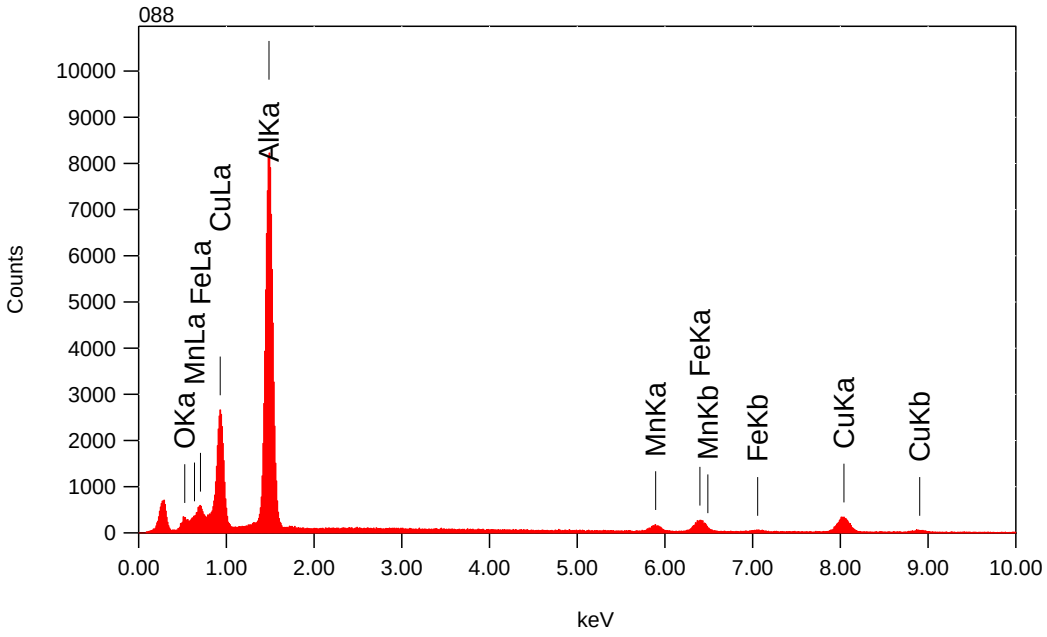


```
Acquisition Parameter
Instrument    : 7000F
Acc. Voltage  : 15.0 kV
Probe Current: 0.59000 nA
PHA mode      : T3
Real Time     : 42.65 sec
Live Time     : 30.00 sec
Dead Time     : 29 %
Counting Rate: 6464 cps
Energy Range :  0 - 20 keV
```

ZAF Method Standardless Quantitative Analysis
Fitting Coefficient : 0.2144

Element	(keV)	mass%	Error%	At%	Compound	mass%	Cation	K
O K	0.525	2.3	0.2	5.2				3.0194
Al K	1.486	48.1	0.2	65.1				39.7784
Mn K	5.894	4.6	0.8	3.0				5.4138
Fe K	6.398	10.3	0.9	6.7				12.6664
Cu K	8.040	34.7	2.3	19.9				39.1221
Total		100.0		100.0				

2055m Aluminium

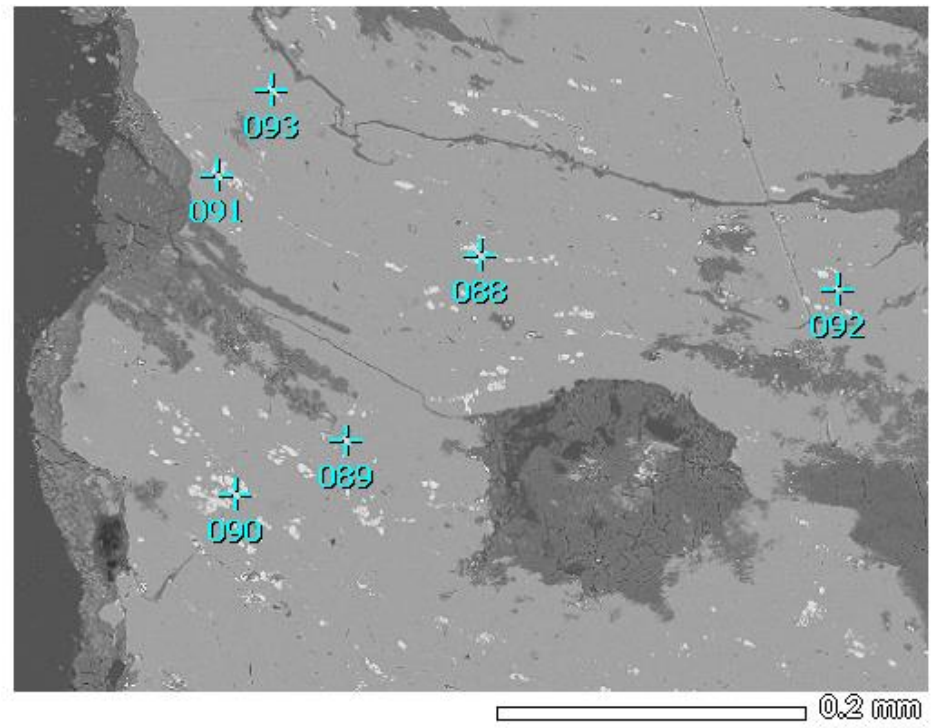


```
Title        : IMG1
--------------------------
Instrument   : 7000F
Volt         : 15.00 kV
Mag          : x 200
Date         : 2014/07/11
Pixel        : 512 x 384
```

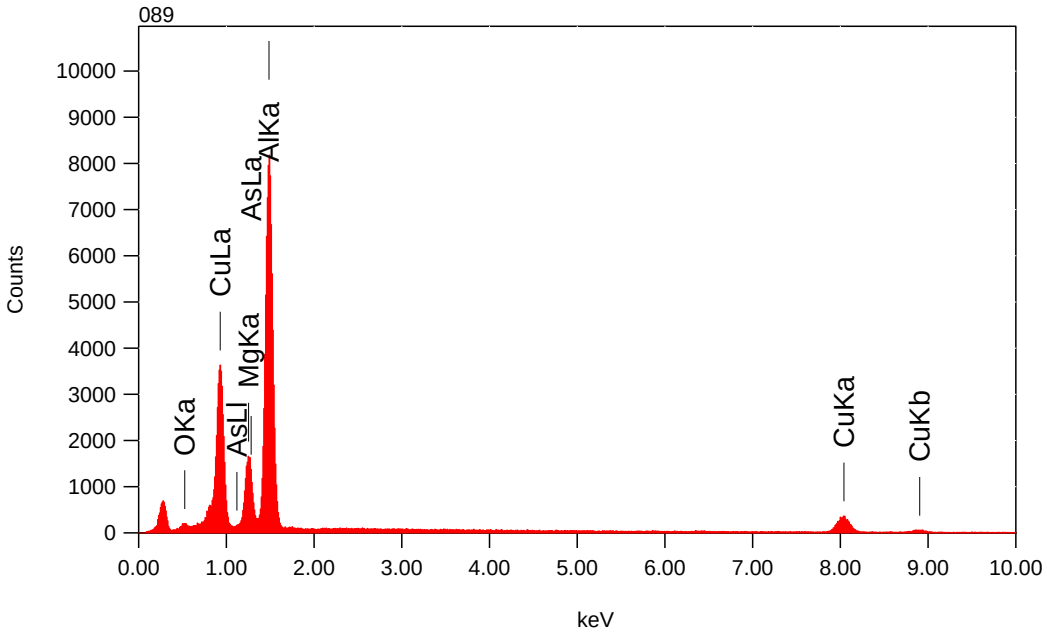


```
Acquisition Parameter
Instrument   : 7000F
Acc. Voltage : 15.0 kV
Probe Current: 0.59000 nA
PHA mode     : T3
Real Time    : 43.21 sec
Live Time    : 30.00 sec
Dead Time    : 30 %
Counting Rate: 6688 cps
Energy Range :  0 - 20 keV
```

ZAF Method Standardless Quantitative Analysis
Fitting Coefficient : 0.1973

Element	(keV)	mass%	Error%	At%	Compound	mass%	Cation	K
O K	0.525	1.2	0.2	2.5				1.5395
Mg K	1.253	9.4	0.2	13.1				7.7156
Al K	1.486	50.5	0.2	63.8				43.5316
Cu K	8.040	36.0	2.3	19.3				43.8540
As L	1.282	3.0	0.4	1.3				3.3592
Total		100.0		100.0				

2055m Aluminium

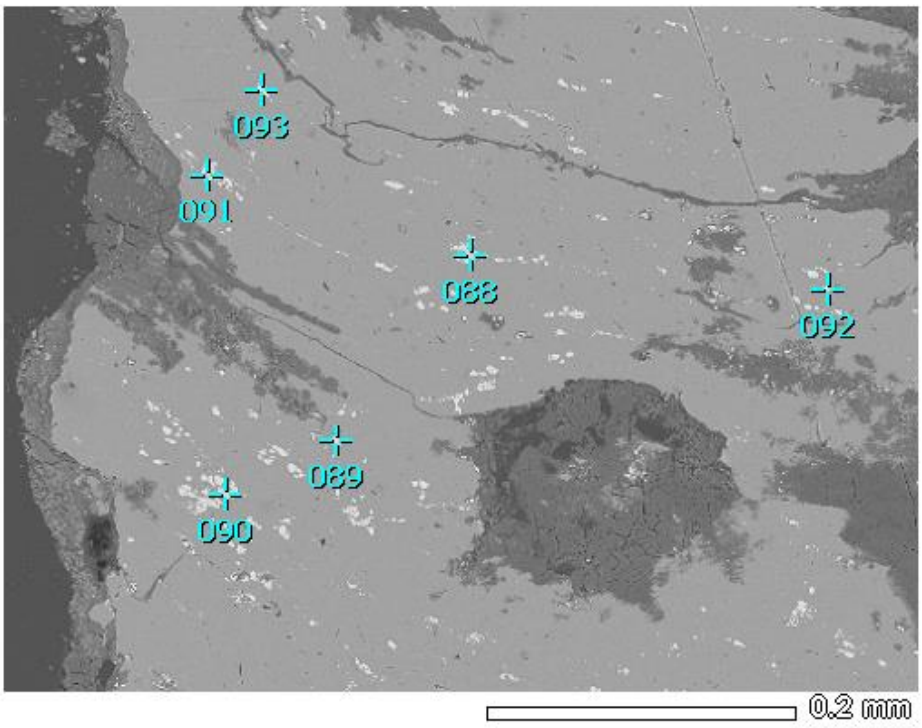


```
Title        : IMG1
---------------------------
Instrument   : 7000F
Volt         : 15.00 kV
Mag          : x 200
Date         : 2014/07/11
Pixel        : 512 x 384
```

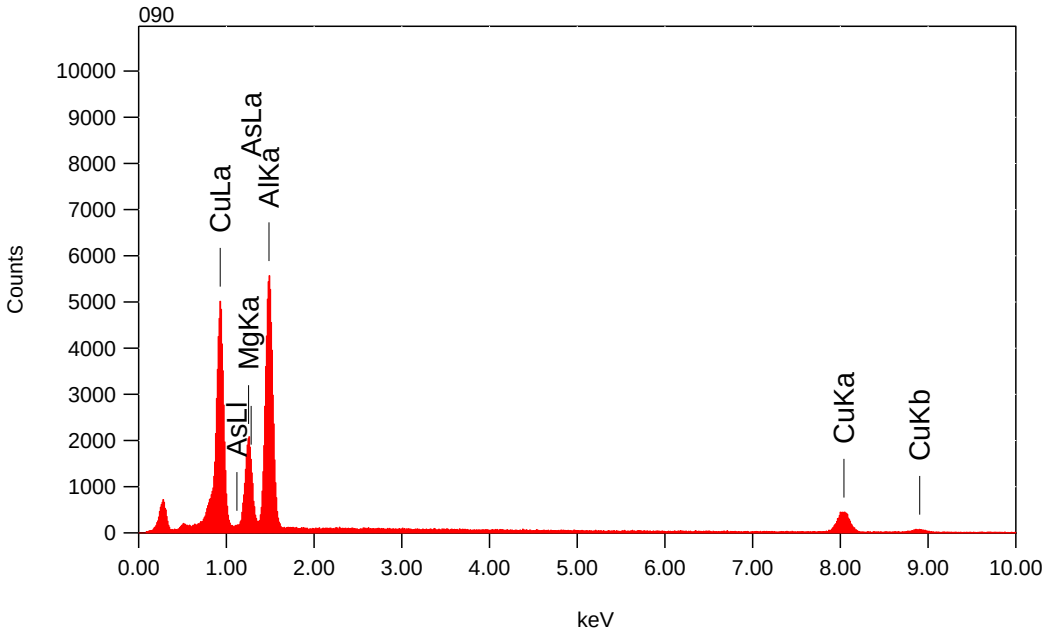


```
Acquisition Parameter
Instrument    : 7000F
Acc. Voltage  : 15.0 kV
Probe Current: 0.59000 nA
PHA mode      : T3
Real Time     : 43.03 sec
Live Time     : 30.00 sec
Dead Time     : 30 %
Counting Rate: 6587 cps
Energy Range :  0 - 20 keV
```

ZAF Method Standardless Quantitative Analysis
Fitting Coefficient : 0.2179

Element	(keV)	mass%	Error%	At%	Compound	mass%	Cation	K
Mg K	1.253	12.4	0.2	19.2				9.1176
Al K	1.486	36.5	0.2	50.9				28.2192
Cu K	8.040	47.4	2.1	28.1				58.9426
As L	1.282	3.7	0.4	1.8				3.7206
Total		100.0		100.0				

2055m Aluminium

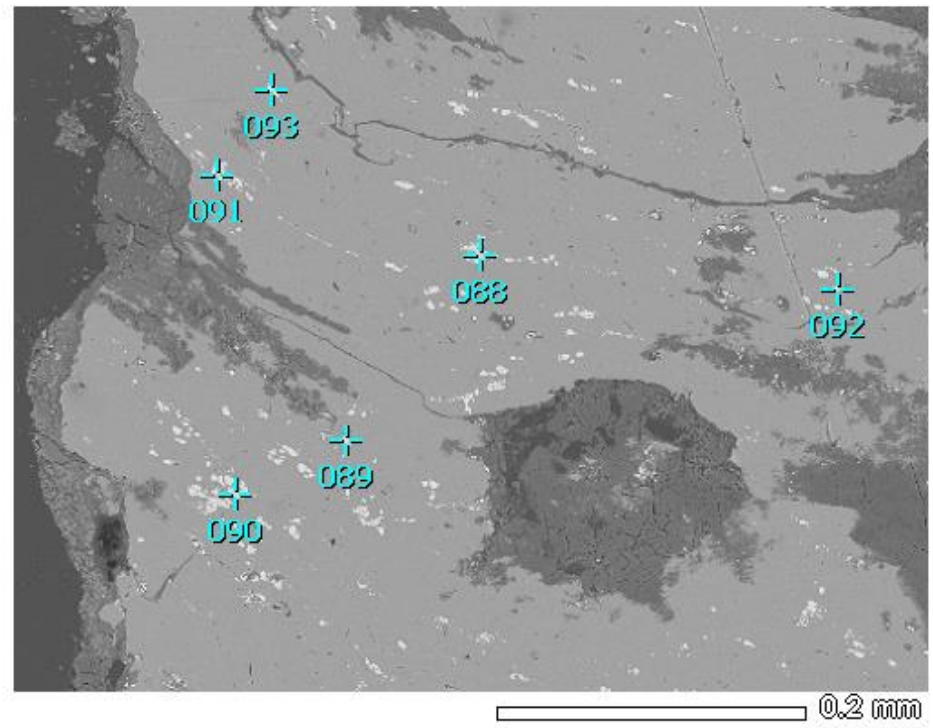


```
Title        : IMG1
---------------------------
Instrument   : 7000F
Volt         : 15.00 kV
Mag          : x 200
Date         : 2014/07/11
Pixel        : 512 x 384
```

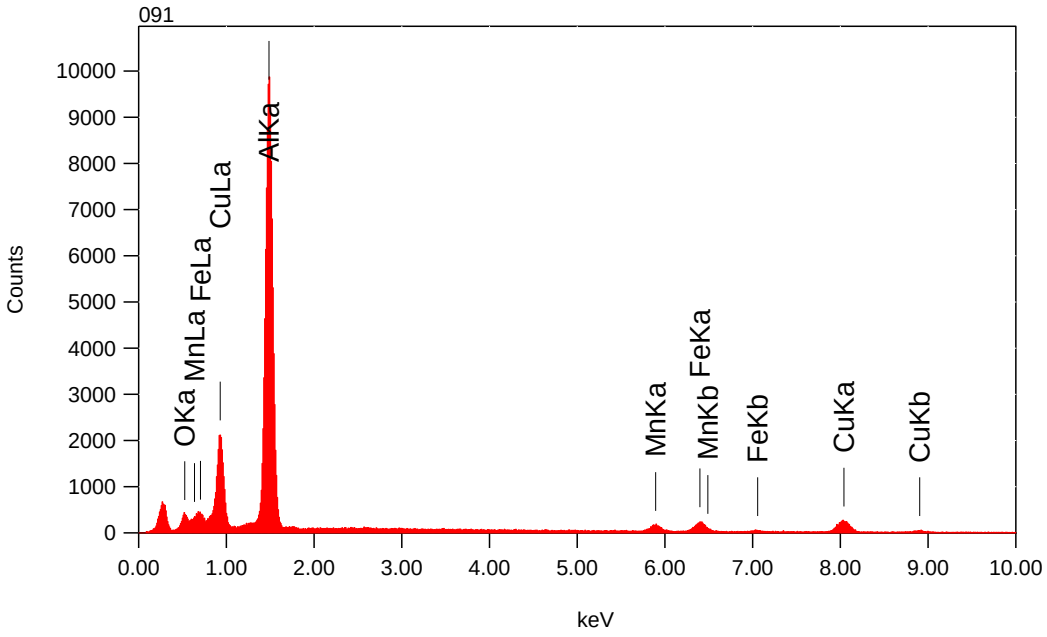


```
Acquisition Parameter
Instrument    : 7000F
Acc. Voltage  : 15.0 kV
Probe Current: 0.59000 nA
PHA mode      : T3
Real Time     : 43.16 sec
Live Time     : 30.00 sec
Dead Time     : 30 %
Counting Rate: 6636 cps
Energy Range :  0 - 20 keV
```

ZAF Method Standardless Quantitative Analysis
Fitting Coefficient : 0.2158

Element	(keV)	mass%	Error%	At%	Compound	mass%	Cation	K
O K	0.525	3.2	0.2	6.8				4.1054
Al K	1.486	55.3	0.2	69.8				48.5709
Mn K	5.894	5.1	0.9	3.2				6.0123
Fe K	6.398	9.0	1.0	5.5				10.8095
Cu K	8.040	27.4	2.6	14.7				30.5018
Total		100.0		100.0				

2055m Aluminium

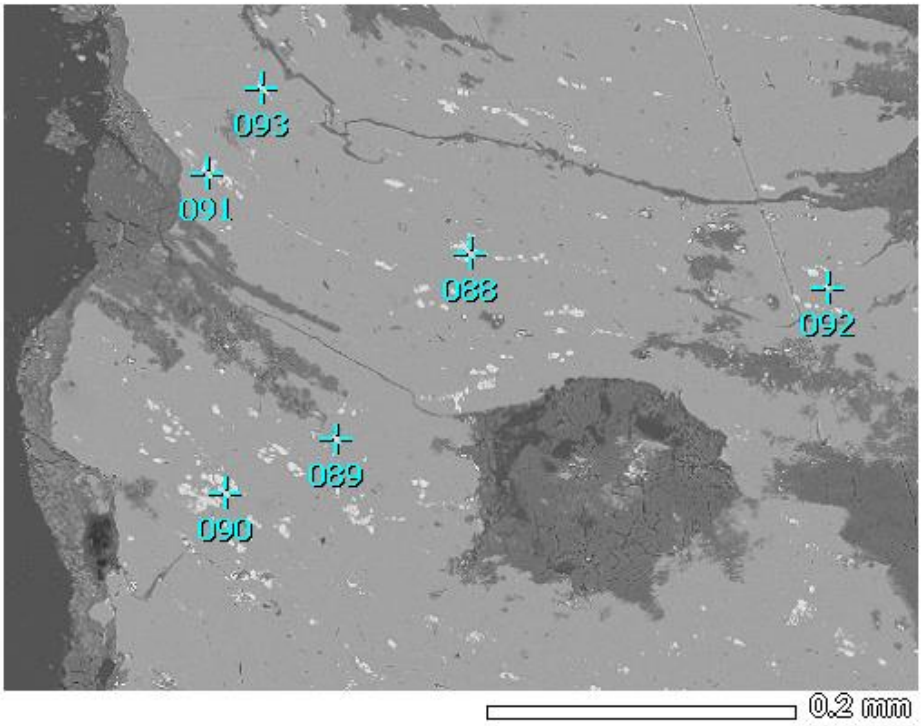


```
Title          : IMG1
---------------------------
Instrument     : 7000F
Volt           : 15.00 kV
Mag            : x 200
Date           : 2014/07/11
Pixel          : 512 x 384
```

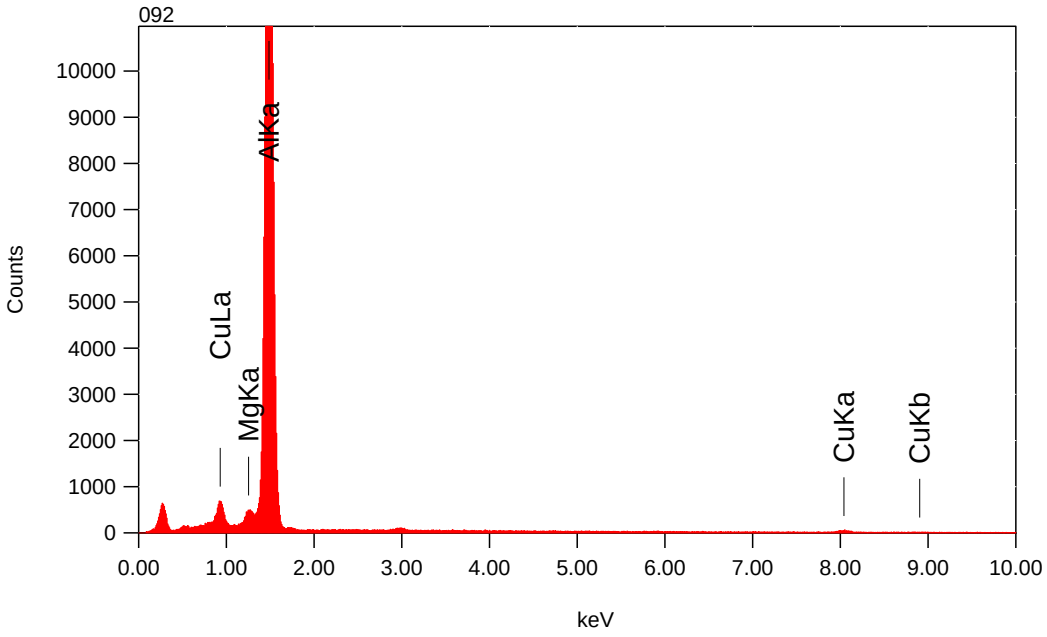


```
Acquisition Parameter
Instrument     : 7000F
Acc. Voltage   : 15.0 kV
Probe Current: 0.59000 nA
PHA mode       : T3
Real Time      : 47.47 sec
Live Time      : 30.00 sec
Dead Time      : 36 %
Counting Rate: 8335 cps
Energy Range :  0 - 20 keV
```

ZAF Method Standardless Quantitative Analysis
Fitting Coefficient : 0.1790

Element	(keV)	mass%	Error%	At%	Compound	mass%	Cation	K
Mg K	1.253	1.4	0.2	1.6				1.4277
Al K	1.486	93.2	0.3	96.0				93.8747
Cu K	8.040	5.4	5.5	2.3				4.6976
Total		100.0		100.0				

2055m Aluminium

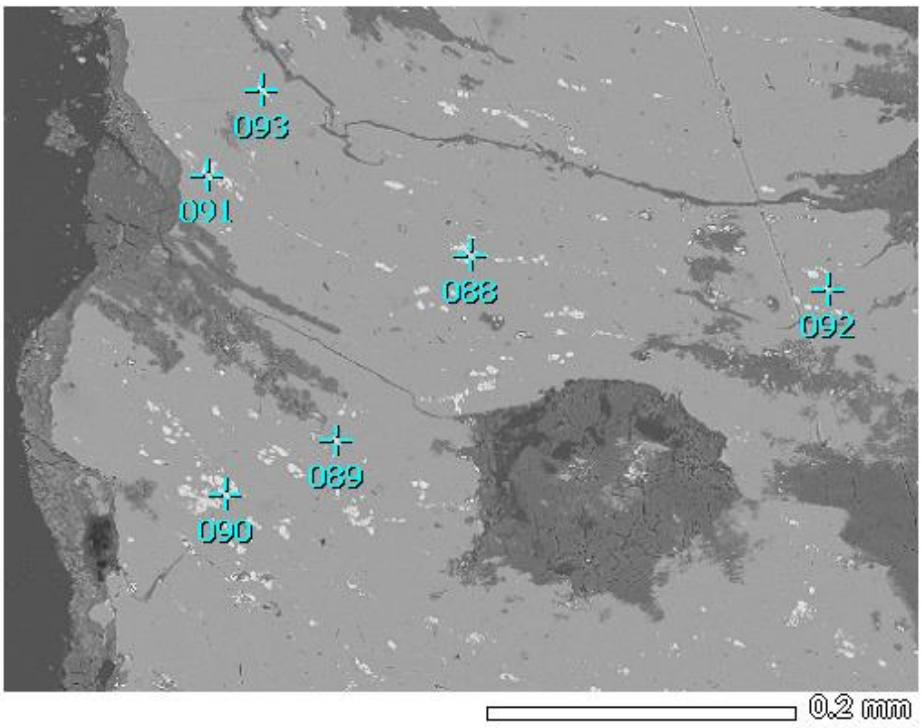


```
Title        : IMG1
---------------------------
Instrument   : 7000F
Volt         : 15.00 kV
Mag          : x 200
Date         : 2014/07/11
Pixel        : 512 x 384
```

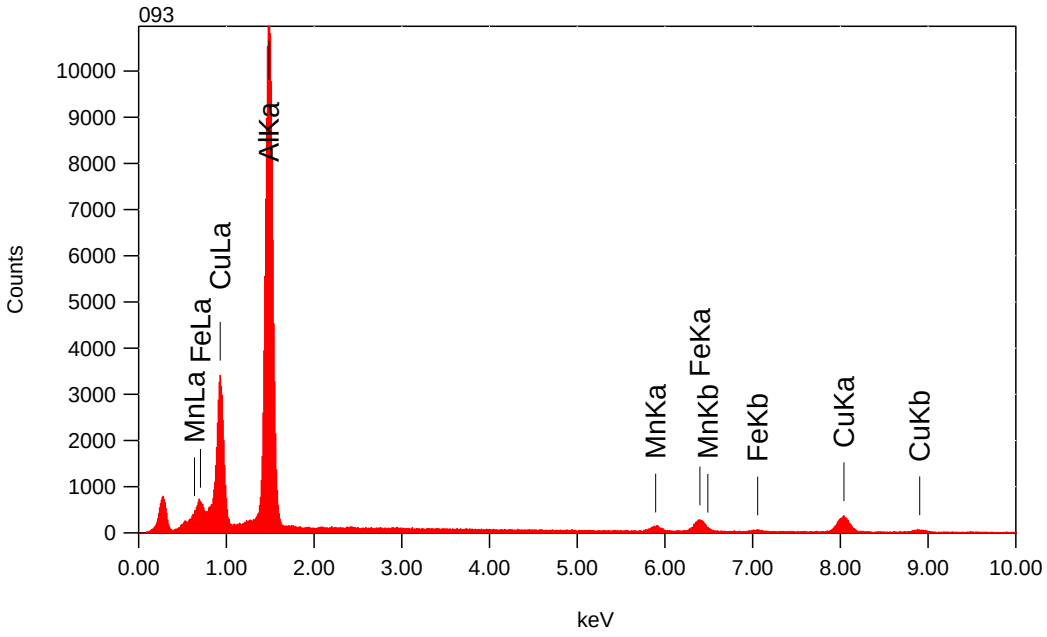


```
Acquisition Parameter
Instrument   : 7000F
Acc. Voltage : 15.0 kV
Probe Current: 0.59000 nA
PHA mode     : T3
Real Time    : 46.76 sec
Live Time    : 30.00 sec
Dead Time    : 35 %
Counting Rate: 8072 cps
Energy Range :  0 - 20 keV
```

ZAF Method Standardless Quantitative Analysis
Fitting Coefficient : 0.2172

Element	(keV)	mass%	Error%	At%	Compound	mass%	Cation	K
Al K	1.486	55.8	0.2	74.1				48.8804
Mn K	5.894	3.4	0.9	2.2				4.0789
Fe K	6.398	9.5	1.0	6.1				11.6918
Cu K	8.040	31.2	2.7	17.6				35.3490
Total		100.0		100.0				

2055m Fissure filling

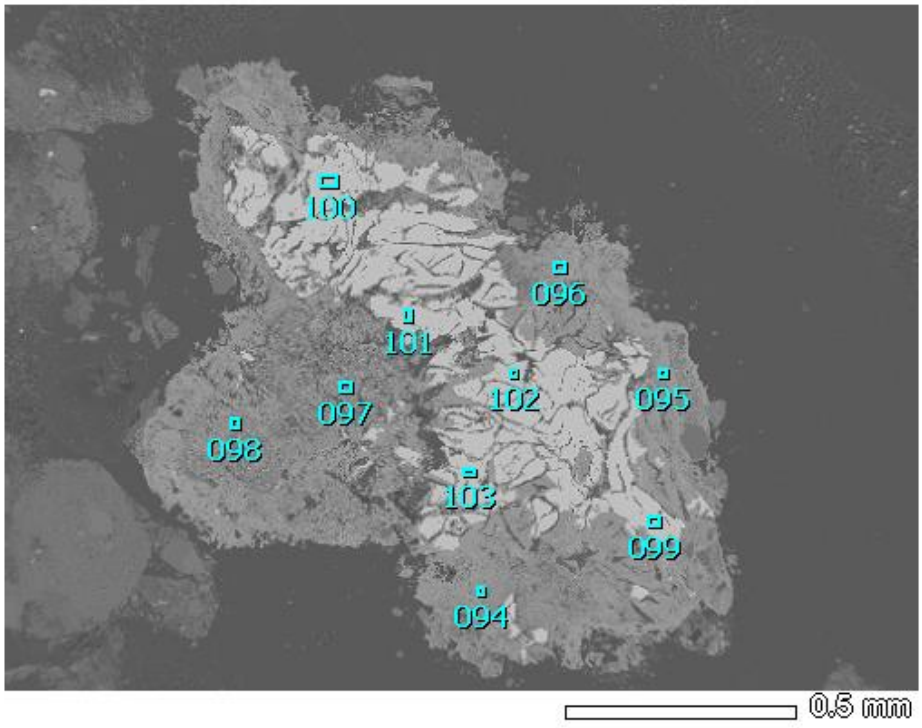


```
Title        : IMG1
---------------------------
Instrument   : 7000F
Volt         : 15.00 kV
Mag          : x 60
Date         : 2014/07/11
Pixel        : 512 x 384
```

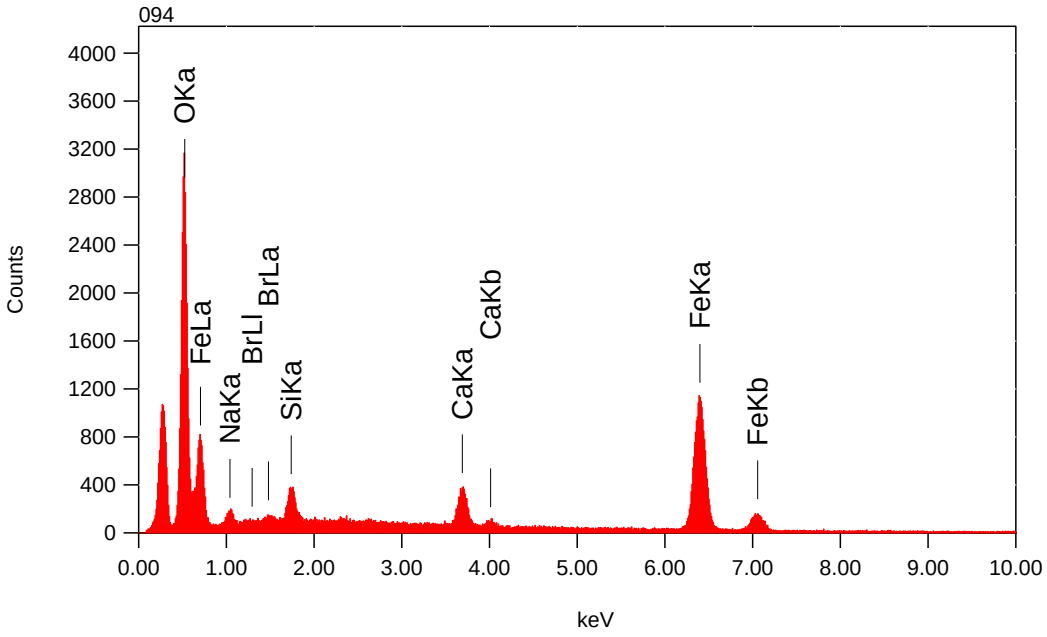


```
Acquisition Parameter
Instrument   : 7000F
Acc. Voltage : 15.0 kV
Probe Current: 0.59000 nA
PHA mode     : T3
Real Time    : 37.60 sec
Live Time    : 30.00 sec
Dead Time    : 20 %
Counting Rate: 4221 cps
Energy Range :  0 - 20 keV
```

ZAF Method Standardless Quantitative Analysis
Fitting Coefficient : 0.2772

Element	(keV)	mass%	Error%	At%	Compound	mass%	Cation	K
O K	0.525	30.2	0.1	58.3				37.3933
Na K	1.041	1.6	0.3	2.1				0.6647
Si K	1.739	2.0	0.2	2.2				1.4061
Ca K	3.690	4.6	0.3	3.6				5.0475
Fe K	6.398	60.9	1.0	33.6				55.1091
Br L*	1.480	0.7	0.4	0.3				0.3794
Total		100.0		100.0				

2055m Fissure filling

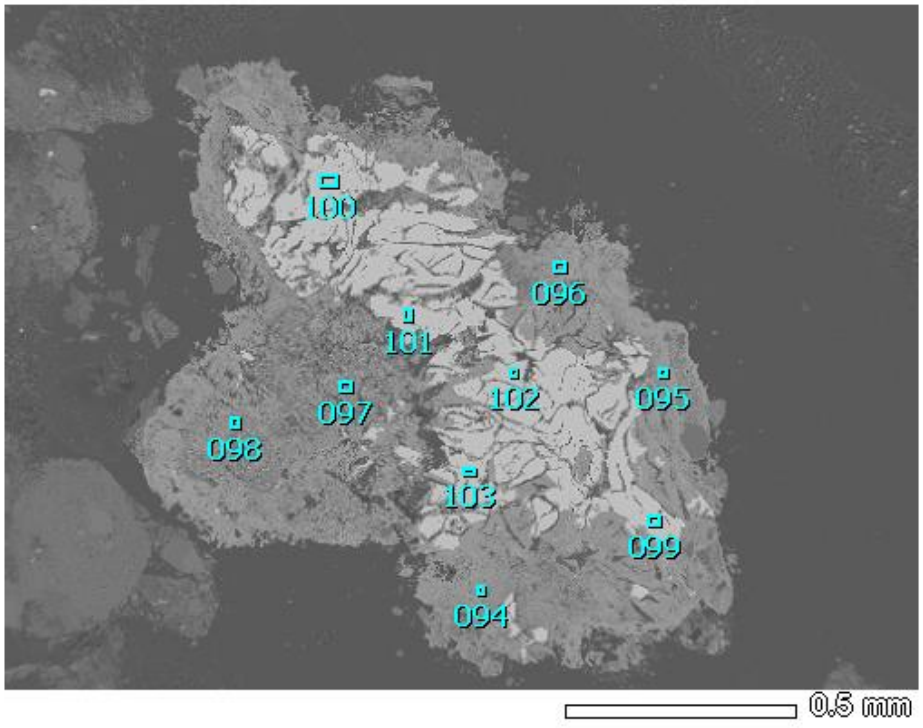


```
Title        : IMG1
---------------------------
Instrument   : 7000F
Volt         : 15.00 kV
Mag          : x 60
Date         : 2014/07/11
Pixel        : 512 x 384
```

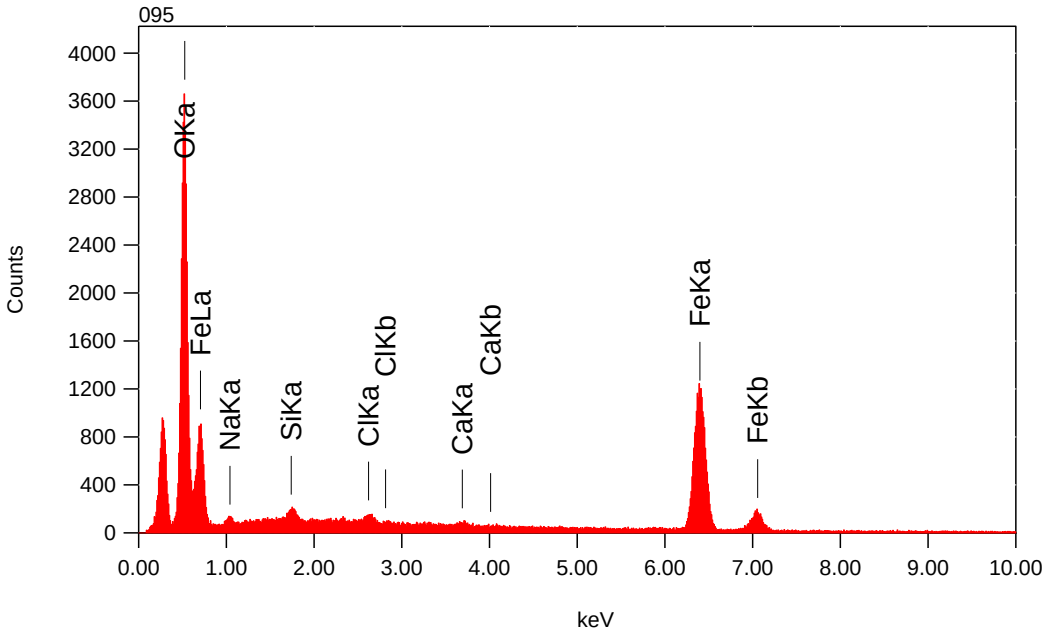


```
Acquisition Parameter
Instrument   : 7000F
Acc. Voltage : 15.0 kV
Probe Current: 0.59000 nA
PHA mode     : T3
Real Time    : 37.61 sec
Live Time    : 30.00 sec
Dead Time    : 20 %
Counting Rate: 4160 cps
Energy Range :  0 - 20 keV
```

ZAF Method Standardless Quantitative Analysis
Fitting Coefficient : 0.2753

Element	(keV)	mass%	Error%	At%	Compound	mass%	Cation	K
O K	0.525	30.3	0.1	59.4				41.1113
Na K	1.041	0.9	0.3	1.2				0.3486
Si K*	1.739	0.6	0.2	0.6				0.3774
Cl K	2.621	0.6	0.2	0.5				0.5563
Ca K*	3.690	0.4	0.3	0.3				0.4242
Fe K	6.398	67.2	0.9	37.8				57.1821
Total		100.0		100.0				

2055m Fissure filling

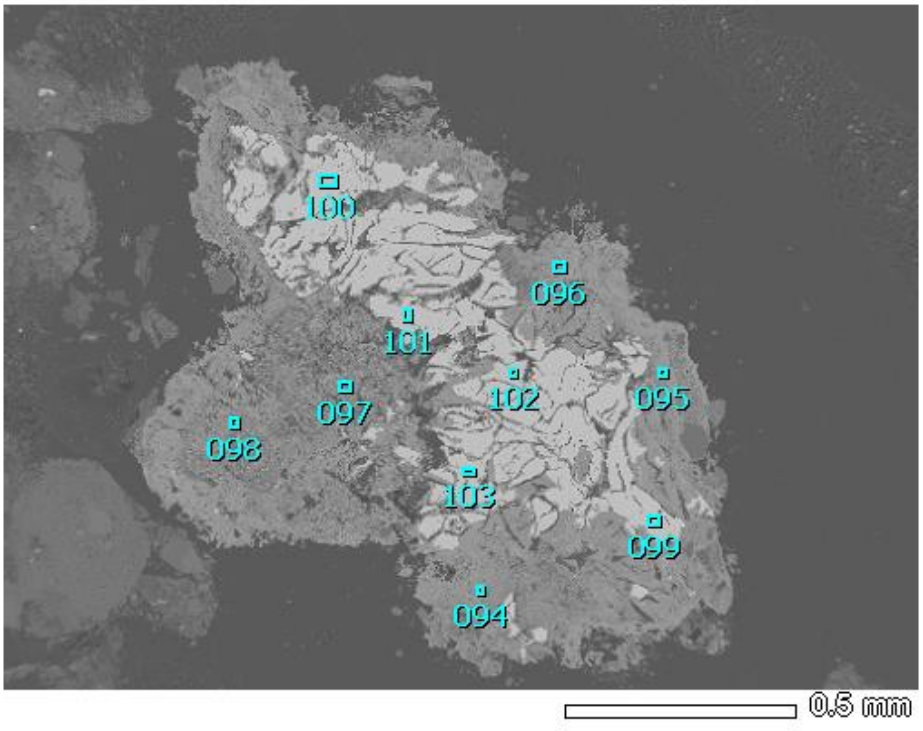


```
Title        : IMG1
---------------------------
Instrument   : 7000F
Volt         : 15.00 kV
Mag          : x 60
Date         : 2014/07/11
Pixel        : 512 x 384
```

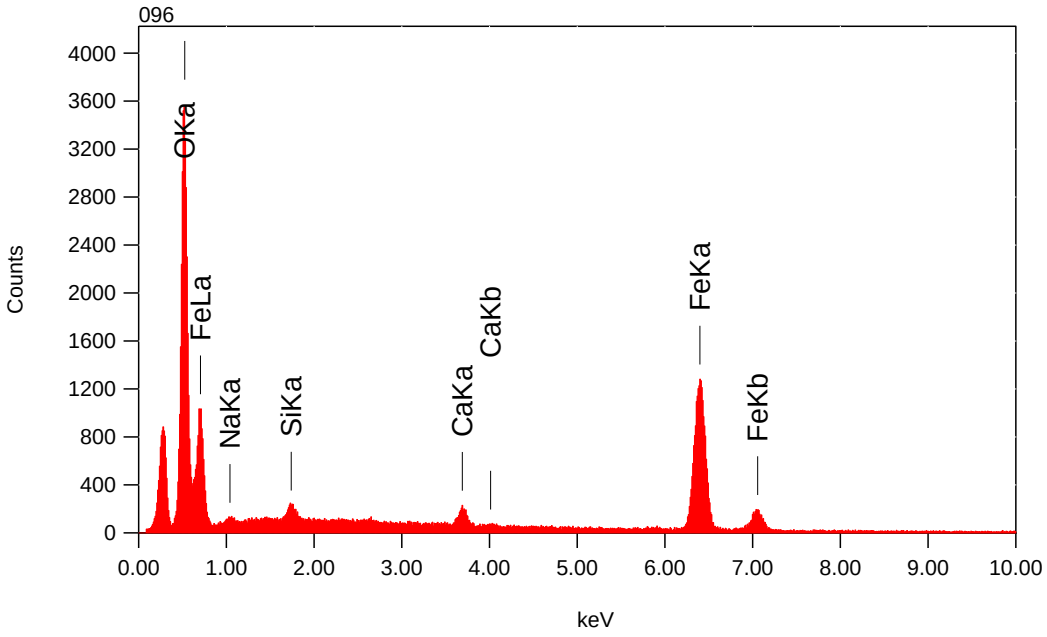


```
Acquisition Parameter
Instrument    : 7000F
Acc. Voltage  : 15.0 kV
Probe Current: 0.59000 nA
PHA mode      : T3
Real Time     : 37.99 sec
Live Time     : 30.00 sec
Dead Time     : 21 %
Counting Rate: 4321 cps
Energy Range :  0 - 20 keV
```

ZAF Method Standardless Quantitative Analysis
Fitting Coefficient : 0.2618

Element	(keV)	mass%	Error%	At%	Compound	mass%	Cation	K
O K	0.525	29.8	0.1	58.8				39.1501
Na K*	1.041	0.6	0.3	0.8				0.2328
Si K	1.739	0.8	0.2	0.9				0.5490
Ca K	3.690	2.1	0.3	1.6				2.1516
Fe K	6.398	66.8	0.9	37.8				57.9165
Total		100.0		100.0				

2055m Fissure filling

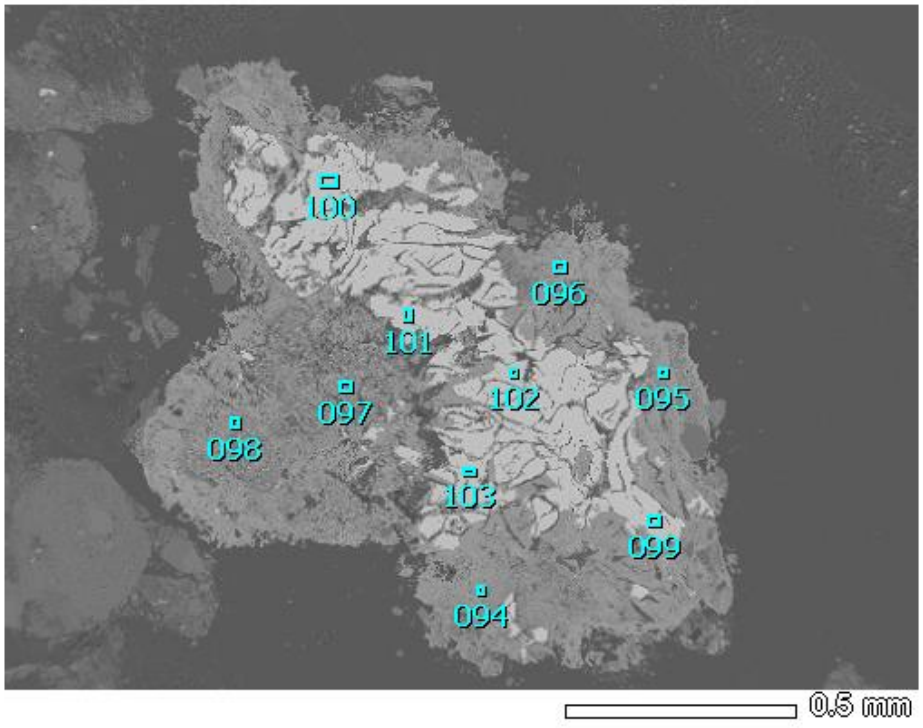


```
Title        : IMG1
---------------------------
Instrument   : 7000F
Volt         : 15.00 kV
Mag          : x 60
Date         : 2014/07/11
Pixel        : 512 x 384
```

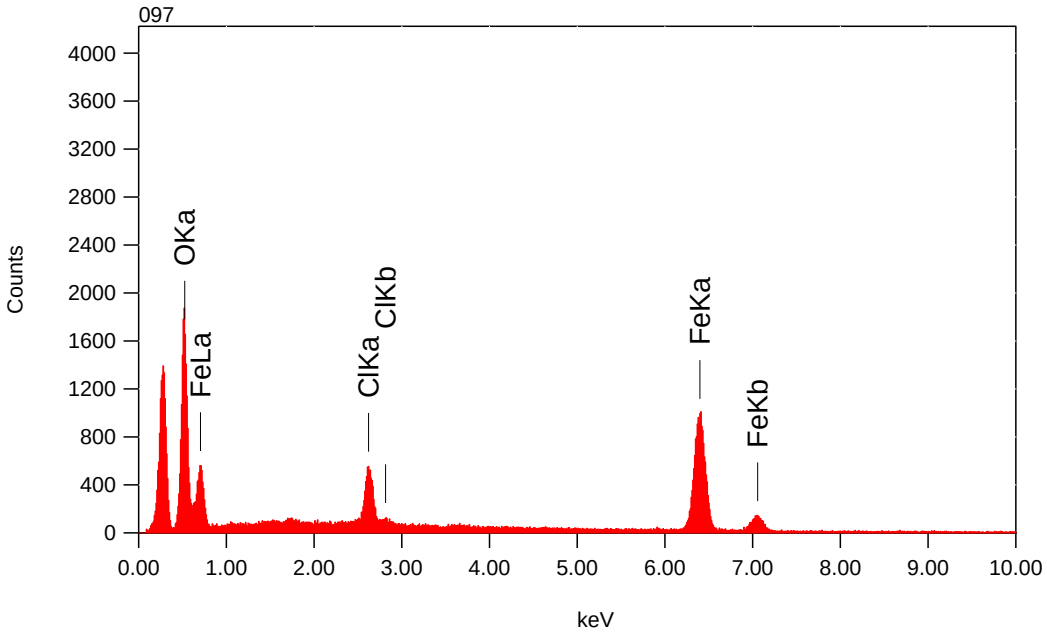


```
Acquisition Parameter
Instrument   : 7000F
Acc. Voltage : 15.0 kV
Probe Current: 0.59000 nA
PHA mode     : T3
Real Time    : 35.77 sec
Live Time    : 30.00 sec
Dead Time    : 16 %
Counting Rate: 3319 cps
Energy Range :  0 - 20 keV
```

ZAF Method Standardless Quantitative Analysis
Fitting Coefficient : 0.3504

Element	(keV)	mass%	Error%	At%	Compound	mass%	Cation	K
O K	0.525	22.5	0.2	49.2				29.0561
Cl K	2.621	6.3	0.3	6.2				6.1476
Fe K	6.398	71.2	1.5	44.6				64.7963
Total		100.0		100.0				

2055m Fissure filling

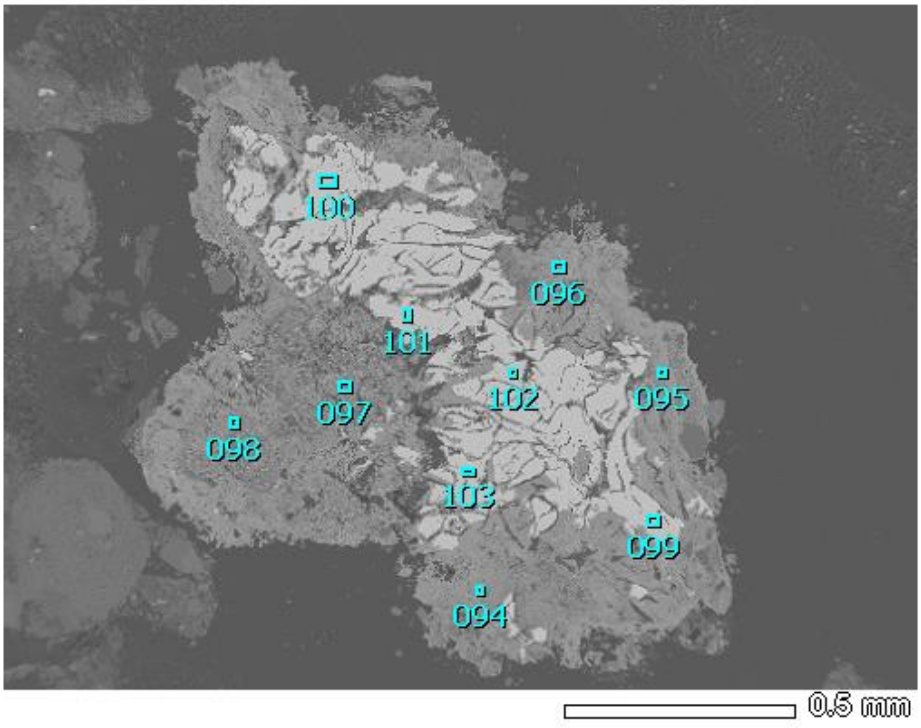


```
Title        : IMG1
---------------------------
Instrument   : 7000F
Volt         : 15.00 kV
Mag          : x 60
Date         : 2014/07/11
Pixel        : 512 x 384
```

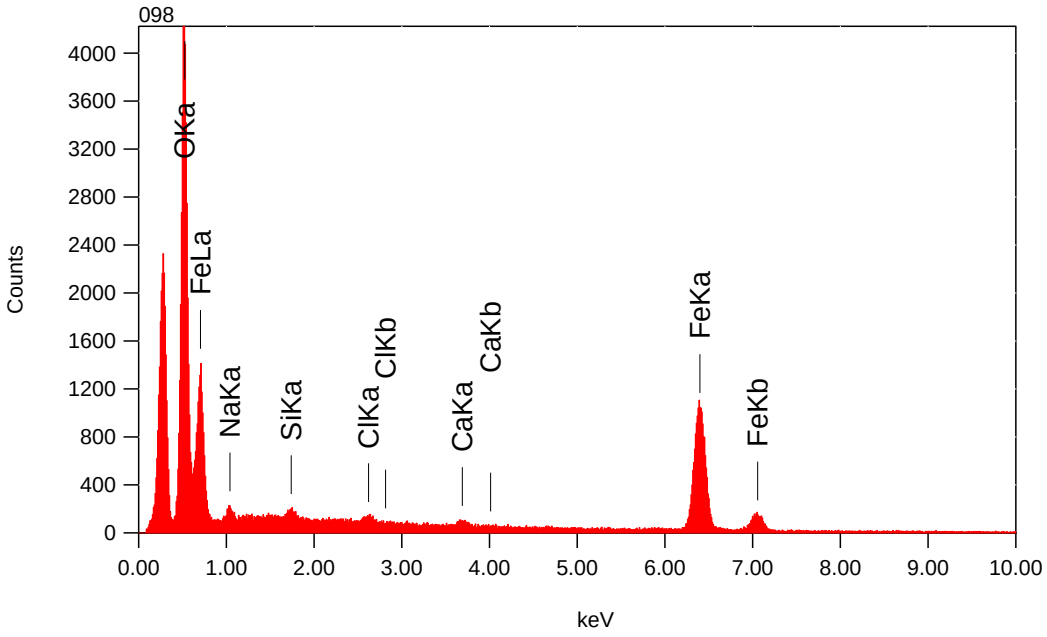


```
Acquisition Parameter
Instrument    : 7000F
Acc. Voltage  : 15.0 kV
Probe Current: 0.59000 nA
PHA mode      : T3
Real Time     : 38.99 sec
Live Time     : 30.00 sec
Dead Time     : 22 %
Counting Rate: 4835 cps
Energy Range :  0 - 20 keV
```

ZAF Method Standardless Quantitative Analysis
Fitting Coefficient : 0.3539

Element	(keV)	mass%	Error%	At%	Compound	mass%	Cation	K
O K	0.525	36.1	0.2	65.1				48.2197
Na K	1.041	1.7	0.6	2.1				0.6488
Si K*	1.739	0.5	0.4	0.6				0.3499
Cl K*	2.621	0.5	0.4	0.4				0.4299
Ca K*	3.690	0.6	0.7	0.5				0.6385
Fe K	6.398	60.6	1.9	31.3				49.7132
Total		100.0		100.0				

2055m Fissure filling

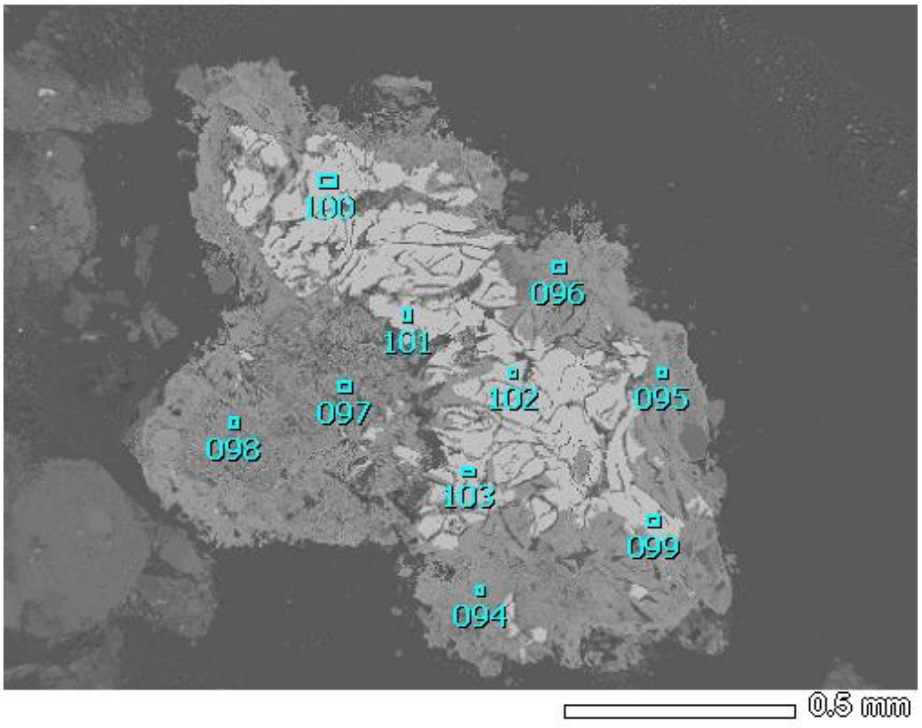


```
Title          : IMG1
---------------------------
Instrument     : 7000F
Volt           : 15.00 kV
Mag            : x 60
Date           : 2014/07/11
Pixel          : 512 x 384
```

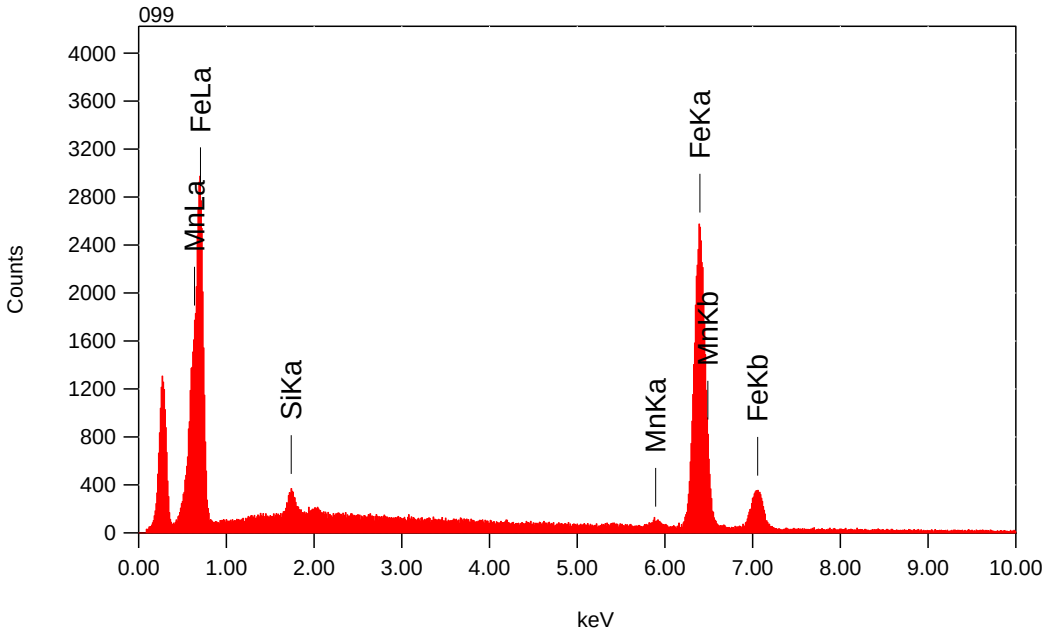


```
Acquisition Parameter
Instrument     : 7000F
Acc. Voltage   : 15.0 kV
Probe Current: 0.59000 nA
PHA mode       : T3
Real Time      : 41.26 sec
Live Time      : 30.00 sec
Dead Time      : 27 %
Counting Rate: 5880 cps
Energy Range :  0 - 20 keV
```

ZAF Method Standardless Quantitative Analysis
Fitting Coefficient : 0.2622

Element	(keV)	mass%	Error%	At%	Compound	mass%	Cation	K
Si K	1.739	1.1	0.2	2.2				0.8048
Mn K	5.894	1.8	0.7	1.8				1.7978
Fe K	6.398	97.0	0.8	96.0				97.3975
Total		100.0		100.0				

2055m Fissure filling

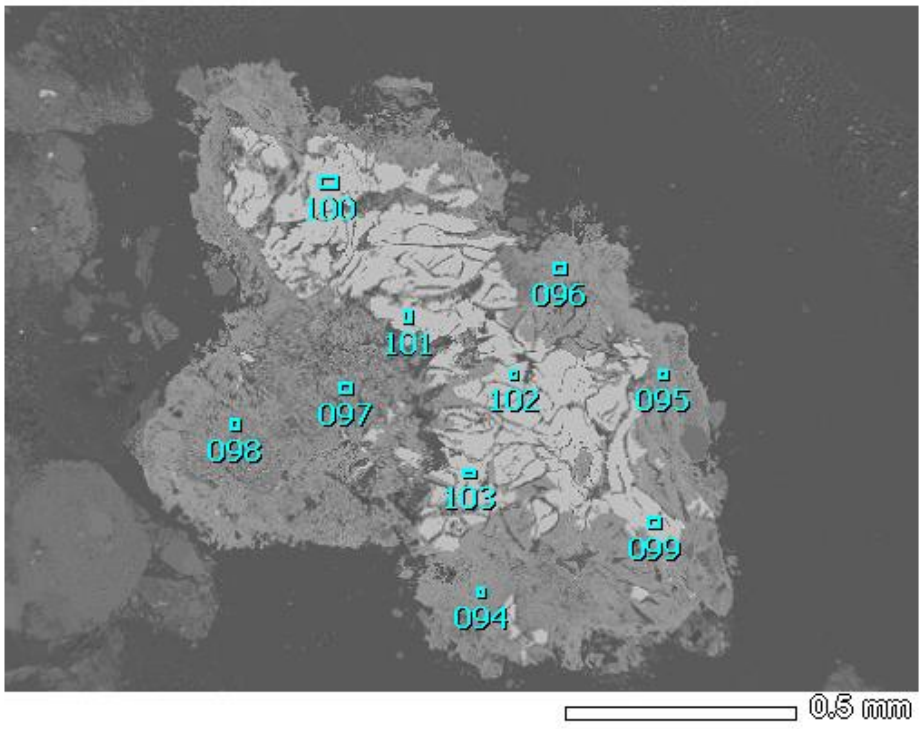


```
Title          : IMG1
---------------------------
Instrument     : 7000F
Volt           : 15.00 kV
Mag            : x 60
Date           : 2014/07/11
Pixel          : 512 x 384
```

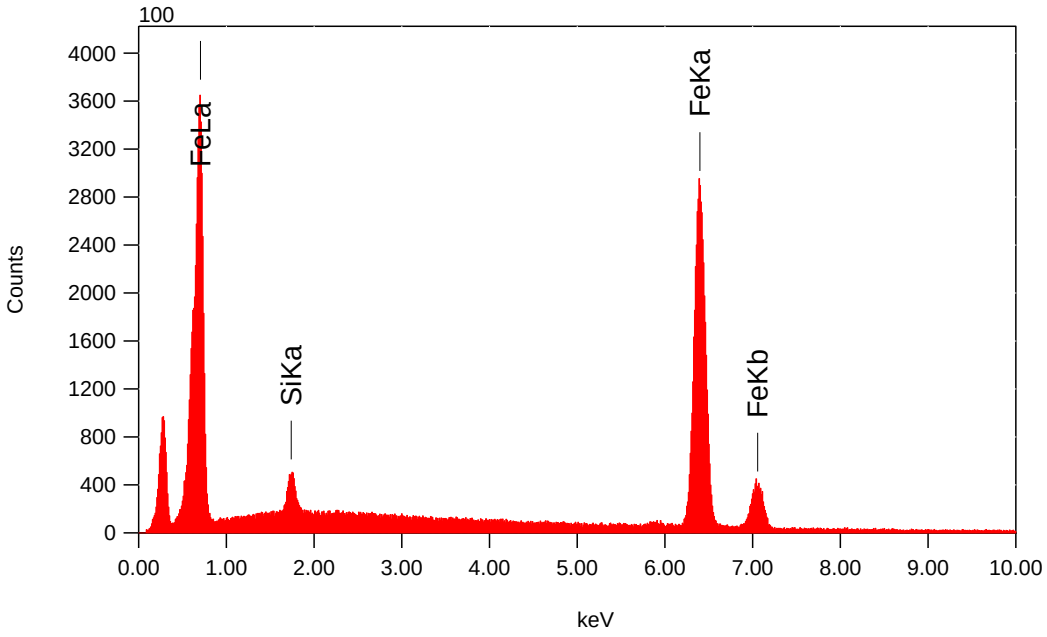


```
Acquisition Parameter
Instrument     : 7000F
Acc. Voltage   : 15.0 kV
Probe Current: 0.59000 nA
PHA mode       : T3
Real Time      : 42.90 sec
Live Time      : 30.00 sec
Dead Time      : 29 %
Counting Rate: 6488 cps
Energy Range :  0 - 20 keV
```

ZAF Method Standardless Quantitative Analysis
Fitting Coefficient : 0.2300

Element	(keV)	mass%	Error%	At%	Compound	mass%	Cation	K
Si K	1.739	1.6	0.1	3.2				1.1603
Fe K	6.398	98.4	0.5	96.8				98.8397
Total		100.0		100.0				

2055m Fissure filling

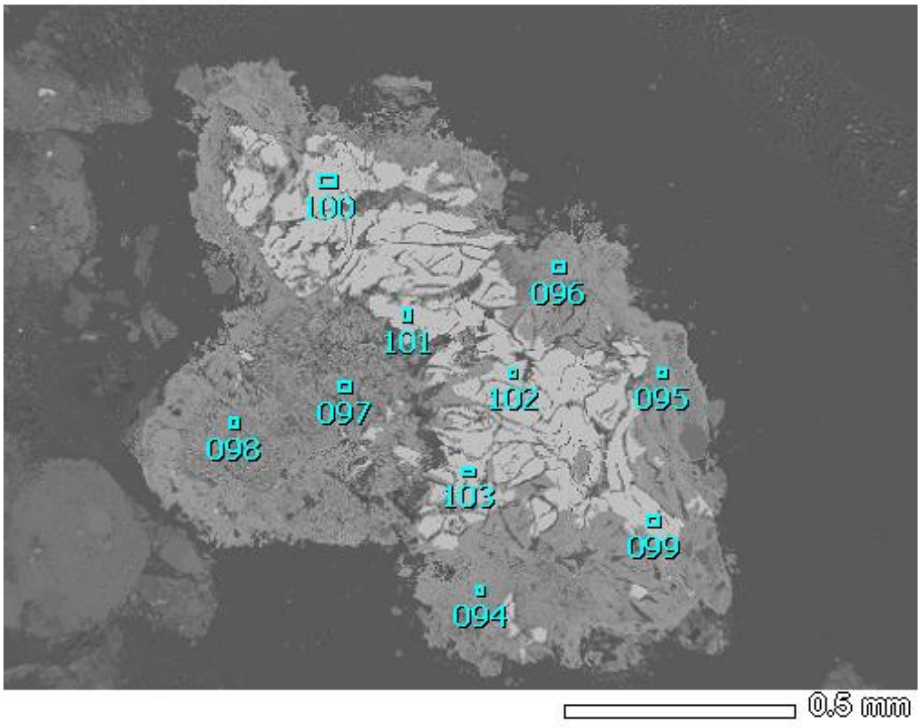


```
Title        : IMG1
--------------------------
Instrument   : 7000F
Volt         : 15.00 kV
Mag          : x 60
Date         : 2014/07/11
Pixel        : 512 x 384
```

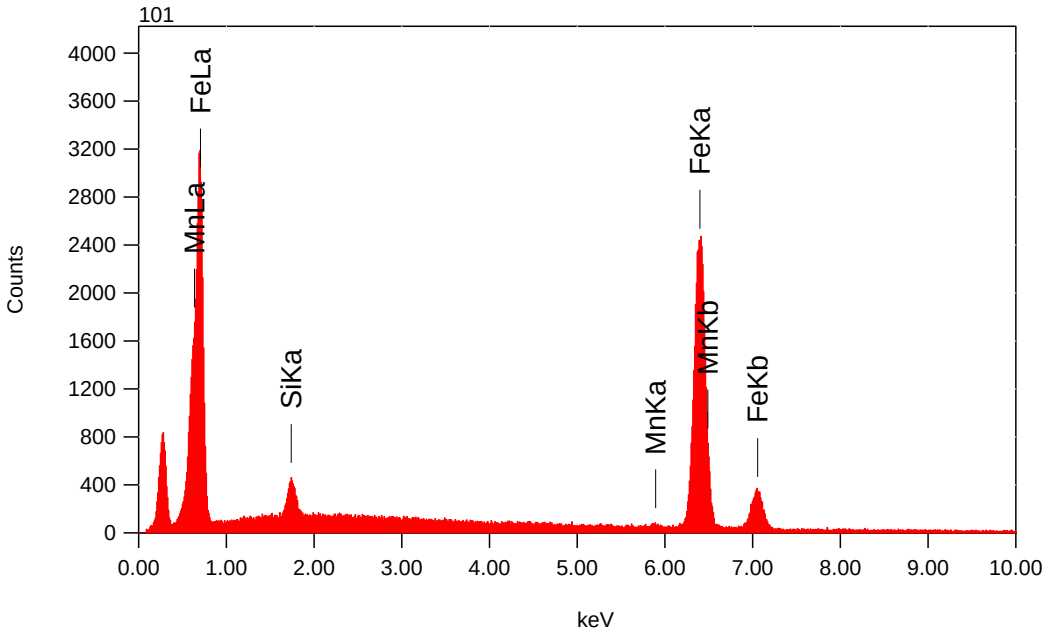


```
Acquisition Parameter
Instrument   : 7000F
Acc. Voltage : 15.0 kV
Probe Current: 0.59000 nA
PHA mode     : T3
Real Time    : 40.89 sec
Live Time    : 30.00 sec
Dead Time    : 26 %
Counting Rate: 5588 cps
Energy Range :  0 - 20 keV
```

ZAF Method Standardless Quantitative Analysis
Fitting Coefficient : 0.2207

Element	(keV)	mass%	Error%	At%	Compound	mass%	Cation	K
Si K	1.739	1.5	0.1	2.9				1.0594
Mn K	5.894	1.2	0.5	1.2				1.1700
Fe K	6.398	97.3	0.5	95.9				97.7705
Total		100.0		100.0				

2055m Fissure filling

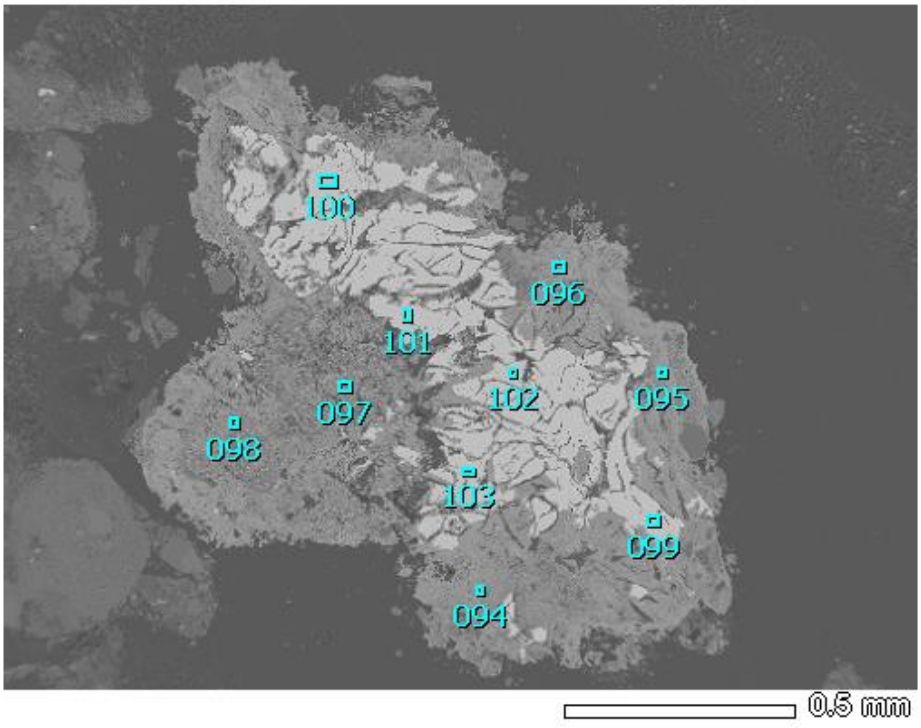


```
Title          : IMG1
---------------------------
Instrument     : 7000F
Volt           : 15.00 kV
Mag            : x 60
Date           : 2014/07/11
Pixel          : 512 x 384
```

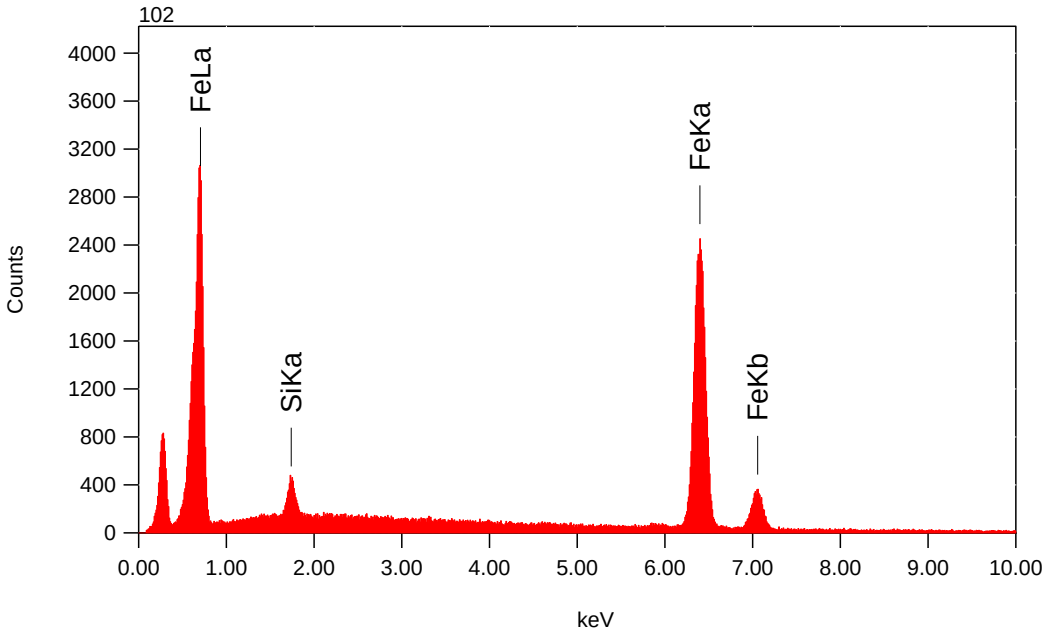


```
Acquisition Parameter
Instrument     : 7000F
Acc. Voltage   : 15.0 kV
Probe Current: 0.59000 nA
PHA mode       : T3
Real Time      : 40.59 sec
Live Time      : 30.00 sec
Dead Time      : 25 %
Counting Rate: 5487 cps
Energy Range :  0 - 20 keV
```

ZAF Method Standardless Quantitative Analysis
Fitting Coefficient : 0.2353

Element	(keV)	mass%	Error%	At%	Compound	mass%	Cation	K
Si K	1.739	1.7	0.1	3.3				1.2276
Fe K	6.398	98.3	0.5	96.7				98.7724
Total		100.0		100.0				

2055m Fissure filling

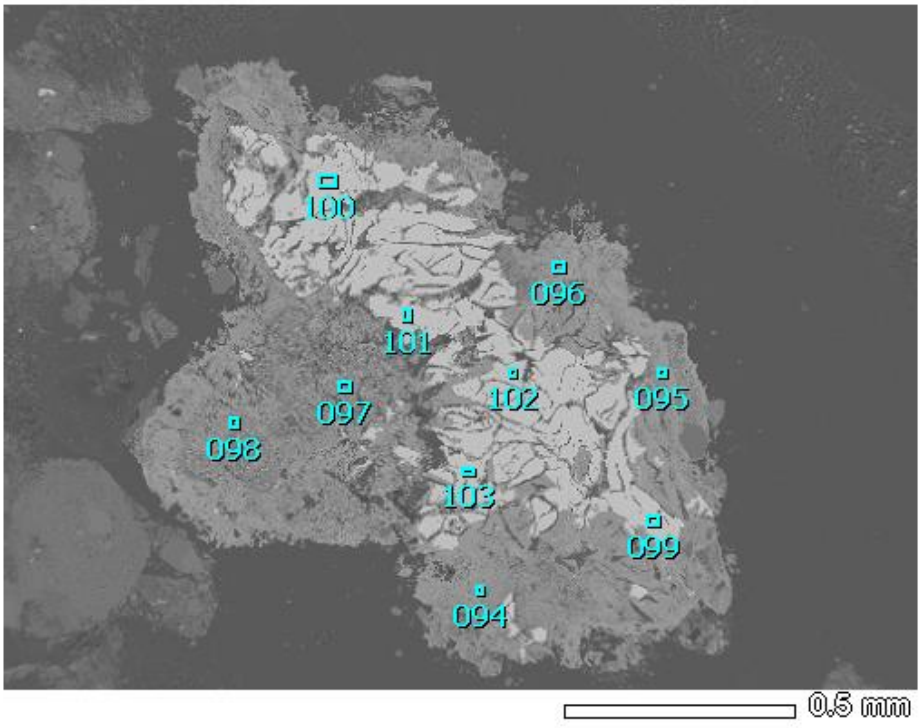

Title : IMG1

Instrument : 7000F
Volt : 15.00 kV
Mag : x 60
Date : 2014/07/11
Pixel : 512 x 384

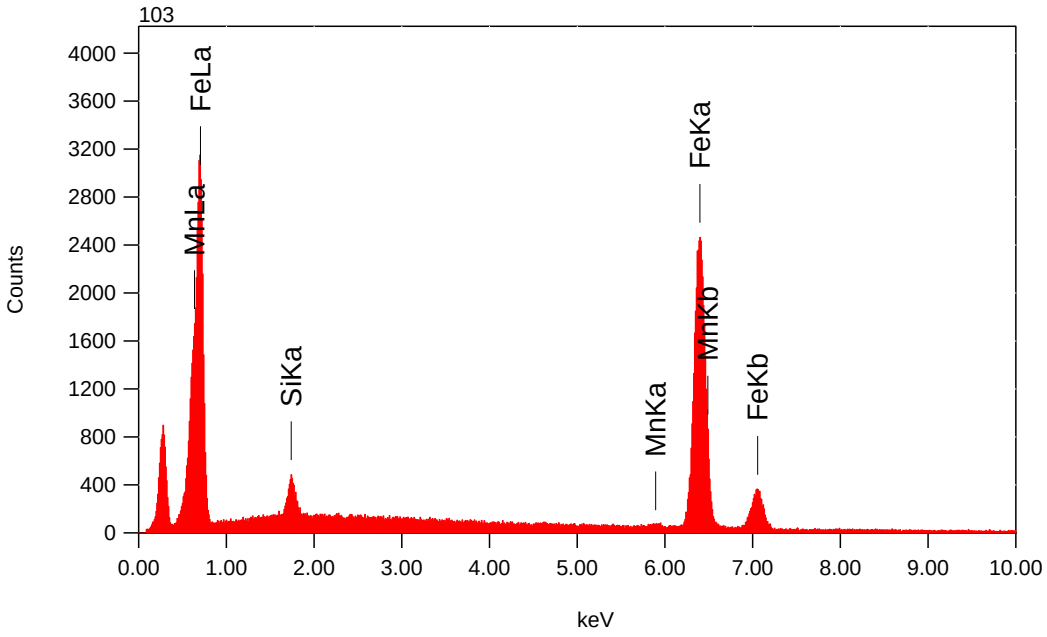

Acquisition Parameter
Instrument : 7000F
Acc. Voltage : 15.0 kV
Probe Current: 0.59000 nA
PHA mode : T3
Real Time : 40.68 sec
Live Time : 30.00 sec
Dead Time : 25 %
Counting Rate: 5471 cps
Energy Range : 0 - 20 keV

ZAF Method Standardless Quantitative Analysis
Fitting Coefficient : 0.2290

Element	(keV)	mass%	Error%	At%	Compound	mass%	Cation	K
Si K	1.739	1.7	0.1	3.3				1.2010
Mn K	5.894	1.2	0.5	1.2				1.2022
Fe K	6.398	97.1	0.5	95.5				97.5969
Total		100.0		100.0				

2055m Fissure filling

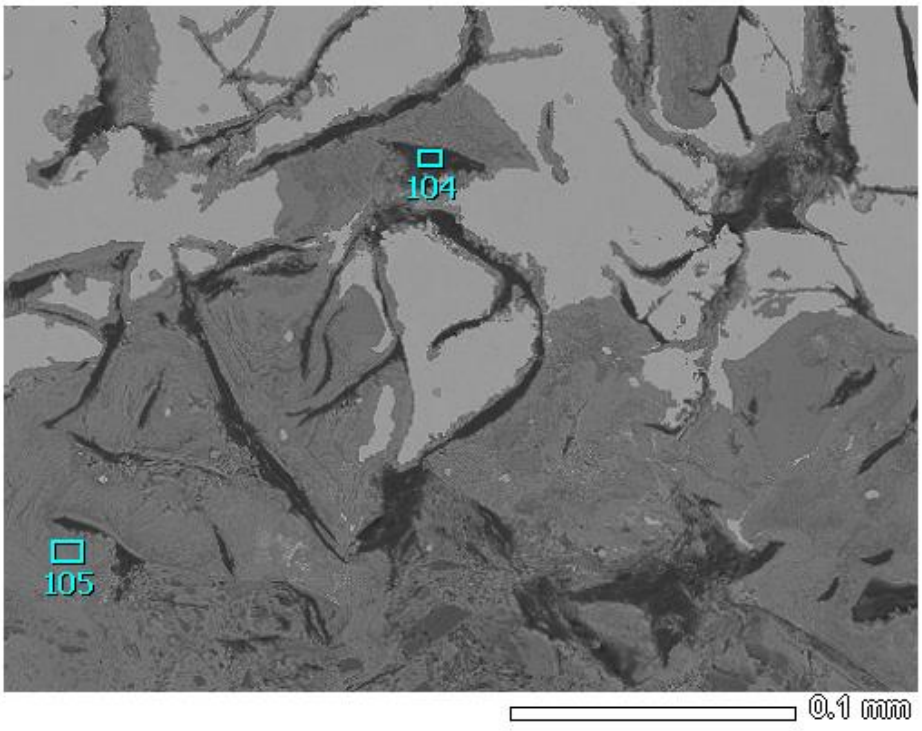


```
Title        : IMG1
--------------------------
Instrument   : 7000F
Volt         : 15.00 kV
Mag          : x 370
Date         : 2014/07/11
Pixel        : 512 x 384
```

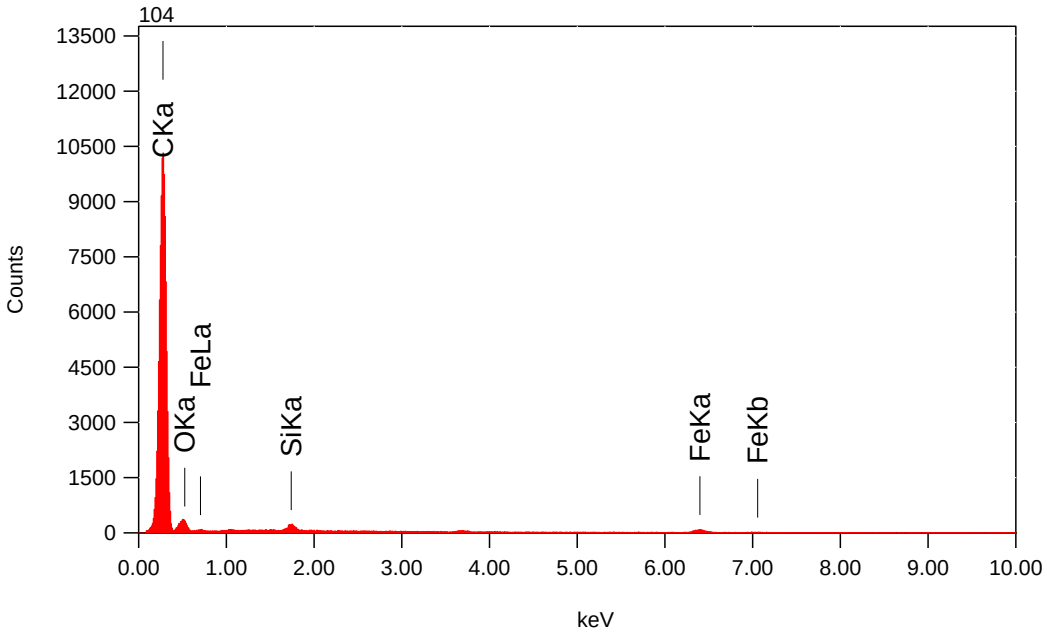


```
Acquisition Parameter
Instrument    : 7000F
Acc. Voltage  : 15.0 kV
Probe Current: 0.59000 nA
PHA mode      : T3
Real Time     : 35.94 sec
Live Time     : 30.00 sec
Dead Time     : 16 %
Counting Rate: 3789 cps
Energy Range :  0 - 20 keV
```

ZAF Method Standardless Quantitative Analysis
Fitting Coefficient : 0.4999

Element	(keV)	mass%	Error%	At%	Compound	mass%	Cation	K
C K	0.277	83.8	0.2	90.0				87.1187
O K	0.525	10.5	2.2	8.5				5.9170
Si K	1.739	1.0	0.8	0.5				1.3072
Fe K	6.398	4.7	5.3	1.1				5.6571
Total		100.0		100.0				

2055m Fissure filling

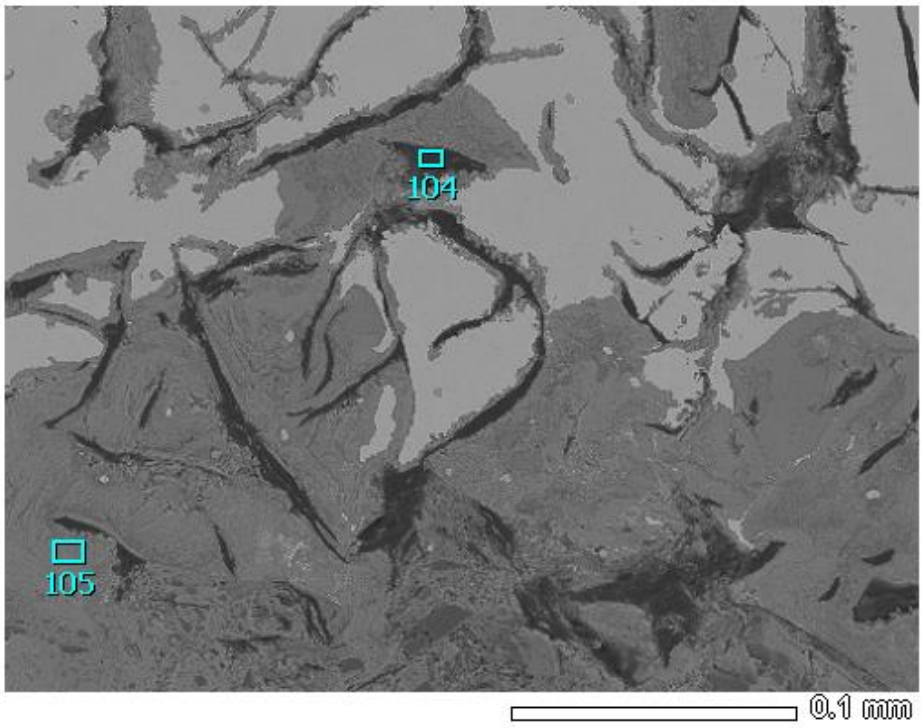


```
Title        : IMG1
--------------------------
Instrument   : 7000F
Volt         : 15.00 kV
Mag          : x 370
Date         : 2014/07/11
Pixel        : 512 x 384
```

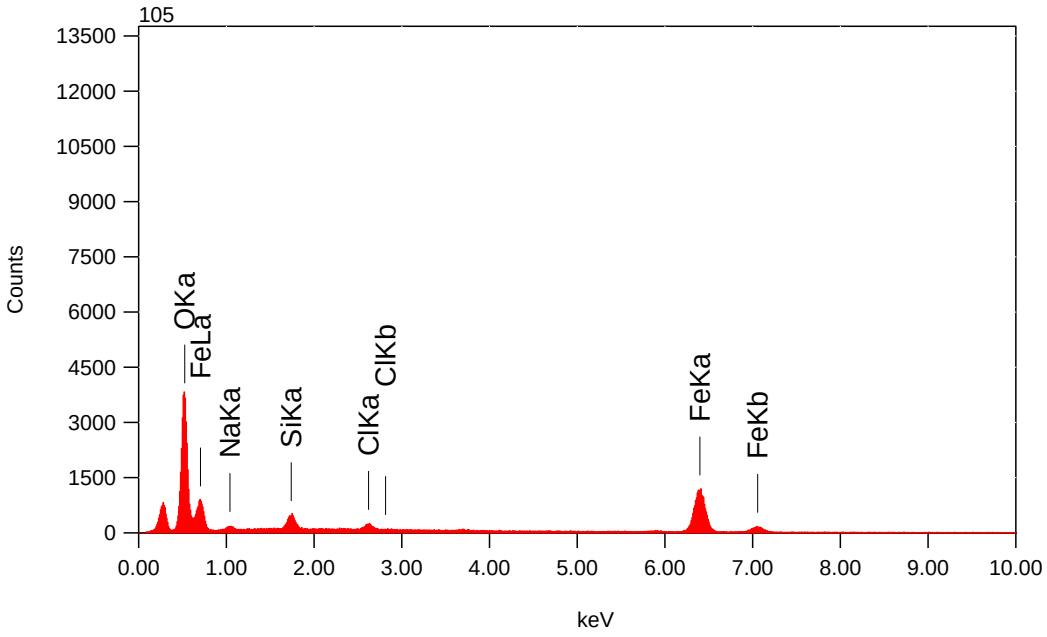


```
Acquisition Parameter
Instrument   : 7000F
Acc. Voltage : 15.0 kV
Probe Current: 0.59000 nA
PHA mode     : T3
Real Time    : 37.94 sec
Live Time    : 30.00 sec
Dead Time    : 20 %
Counting Rate: 4326 cps
Energy Range :  0 - 20 keV
```

ZAF Method Standardless Quantitative Analysis
Fitting Coefficient : 0.2526

Element	(keV)	mass%	Error%	At%	Compound	mass%	Cation	K
O K	0.525	31.4	0.1	59.8				42.3512
Na K	1.041	1.3	0.3	1.7				0.5019
Si K	1.739	2.7	0.2	2.9				1.8051
Cl K	2.621	1.4	0.2	1.2				1.3216
Fe K	6.398	63.1	0.8	34.4				54.0202
Total		100.0		100.0				

2055m Breccia

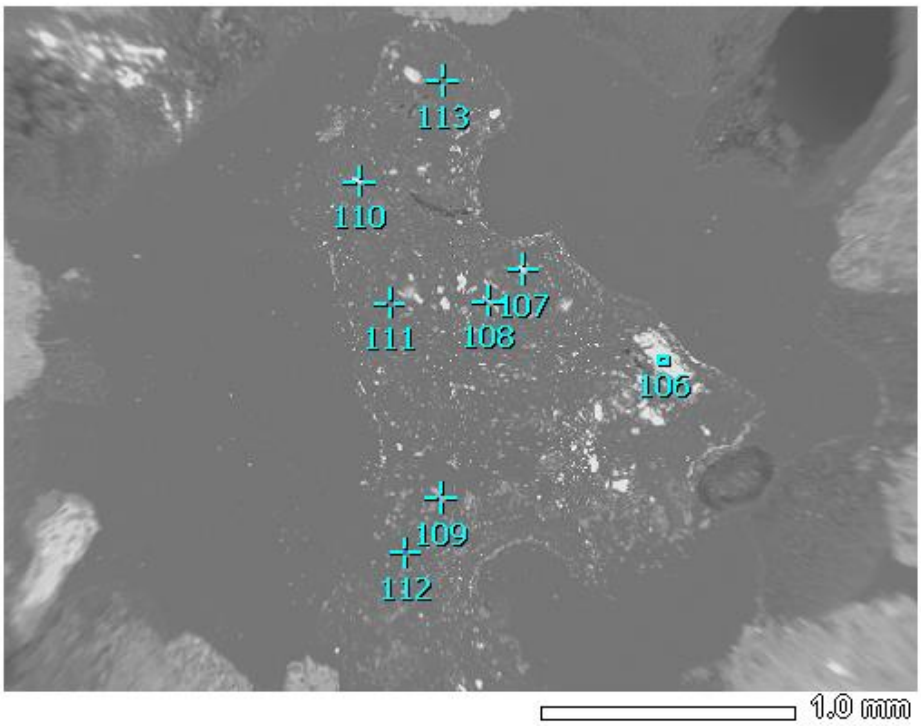


```
Title        : IMG1
-------------------------
Instrument   : 7000F
Volt         : 15.00 kV
Mag          : x 33
Date         : 2014/07/11
Pixel        : 512 x 384
```

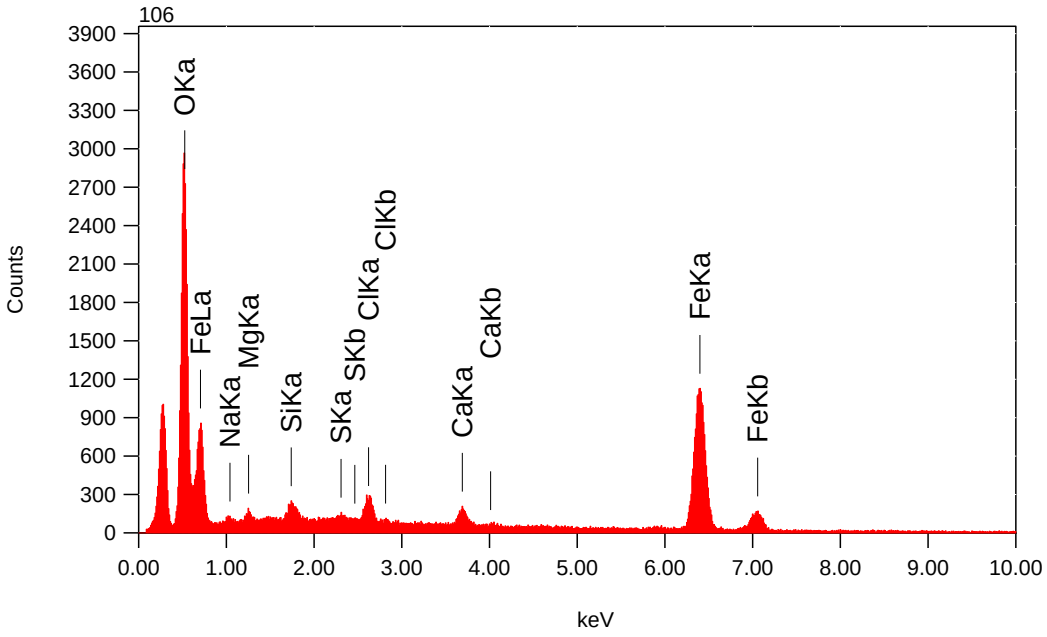


```
Acquisition Parameter
Instrument   : 7000F
Acc. Voltage : 15.0 kV
Probe Current: 0.59000 nA
PHA mode     : T3
Real Time    : 37.39 sec
Live Time    : 30.00 sec
Dead Time    : 19 %
Counting Rate: 4068 cps
Energy Range :  0 - 20 keV
```

ZAF Method Standardless Quantitative Analysis
Fitting Coefficient : 0.2677

Element	(keV)	mass%	Error%	At%	Compound	mass%	Cation	K
O K	0.525	28.3	0.1	56.4				36.4202
Na K*	1.041	0.6	0.3	0.8				0.2331
Mg K	1.253	0.8	0.2	1.1				0.3705
Si K	1.739	0.8	0.2	0.9				0.5586
S K*	2.307	0.3	0.2	0.3				0.2674
Cl K	2.621	2.2	0.2	2.0				2.1124
Ca K	3.690	2.0	0.3	1.6				2.1177
Fe K	6.398	65.0	0.9	37.0				57.9202
Total		100.0		100.0				

2055m Breccia

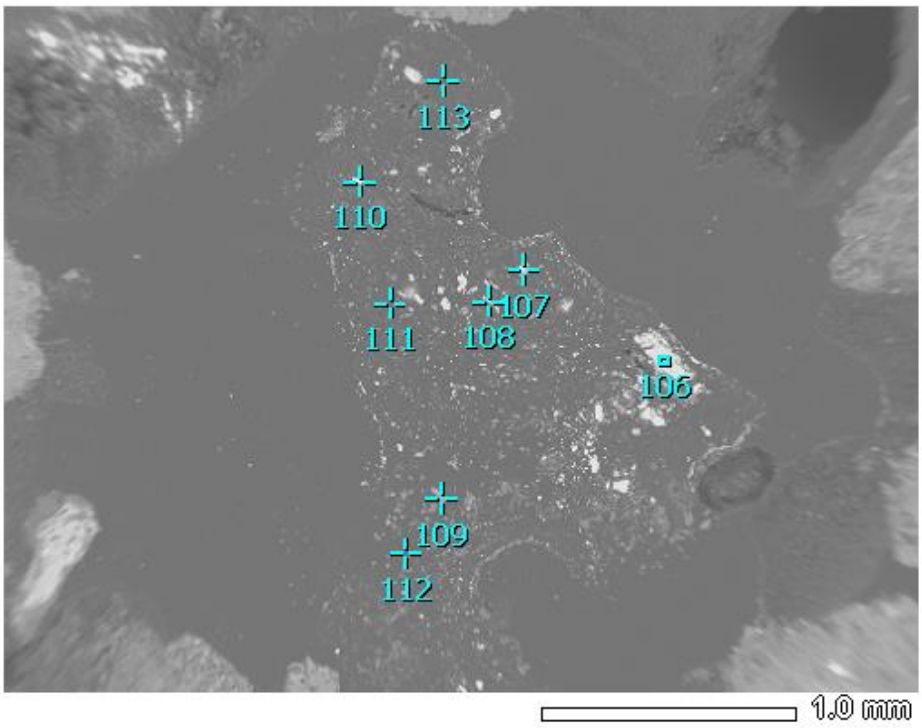


```
Title        : IMG1
--------------------------
Instrument   : 7000F
Volt         : 15.00 kV
Mag          : x 33
Date         : 2014/07/11
Pixel        : 512 x 384
```

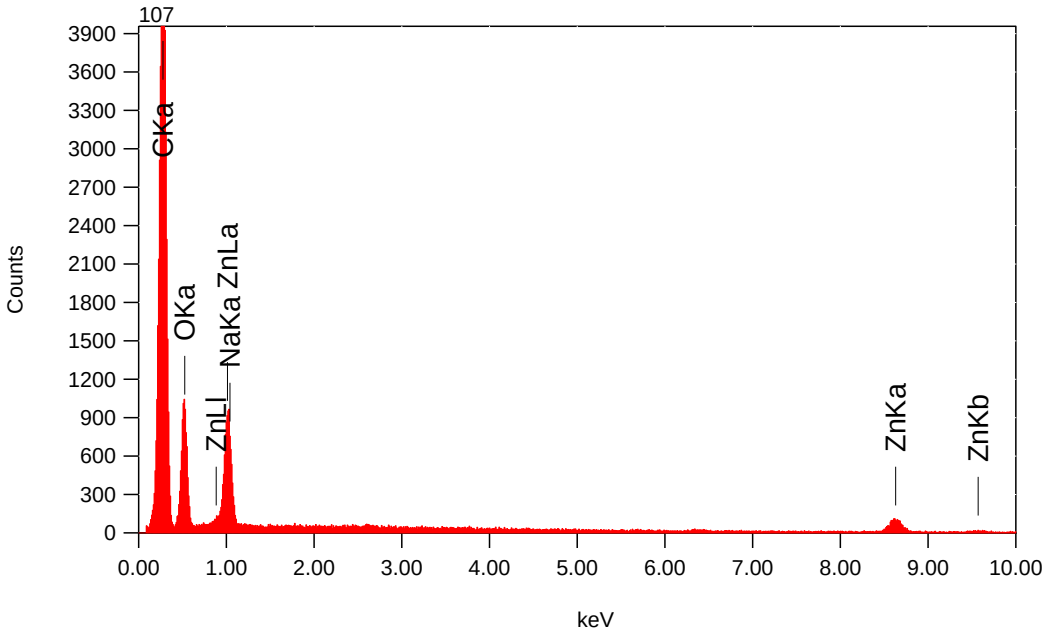


```
Acquisition Parameter
Instrument   : 7000F
Acc. Voltage : 15.0 kV
Probe Current: 0.59000 nA
PHA mode     : T3
Real Time    : 34.61 sec
Live Time    : 30.00 sec
Dead Time    : 13 %
Counting Rate: 2976 cps
Energy Range :  0 - 20 keV
```

ZAF Method Standardless Quantitative Analysis
Fitting Coefficient : 0.4027

Element	(keV)	mass%	Error%	At%	Compound	mass%	Cation	K
C K	0.277	58.0	0.1	73.7				46.2947
O K	0.525	21.6	0.6	20.6				22.7816
Na K	1.041	2.2	0.5	1.5				2.6627
Zn K	8.630	18.1	7.2	4.2				28.2611
Total		100.0		100.0				

2055m Breccia

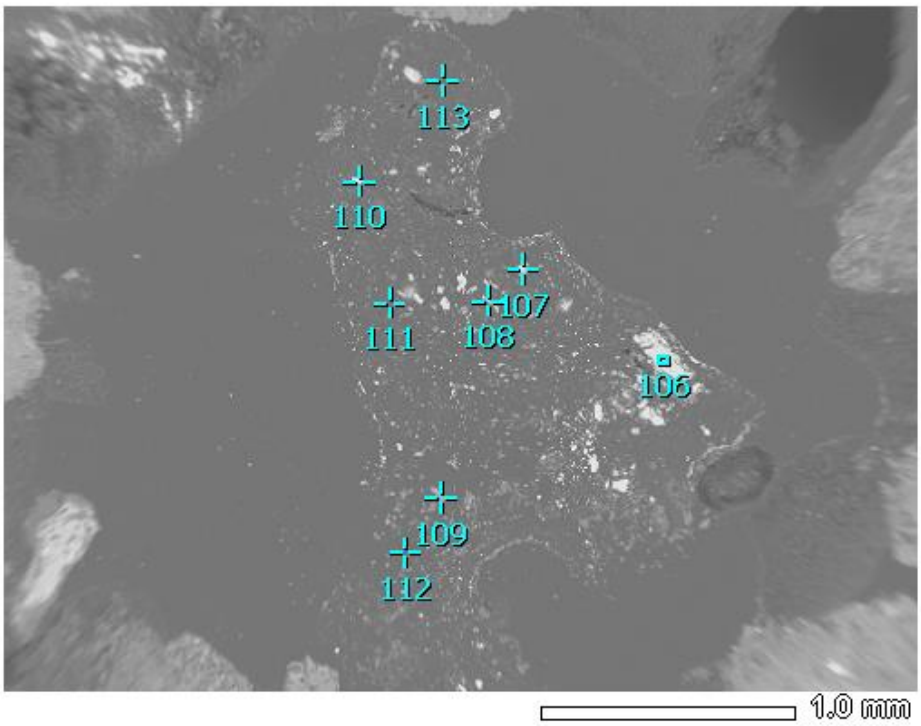


```
Title        : IMG1
--------------------------
Instrument   : 7000F
Volt         : 15.00 kV
Mag          : x 33
Date         : 2014/07/11
Pixel        : 512 x 384
```

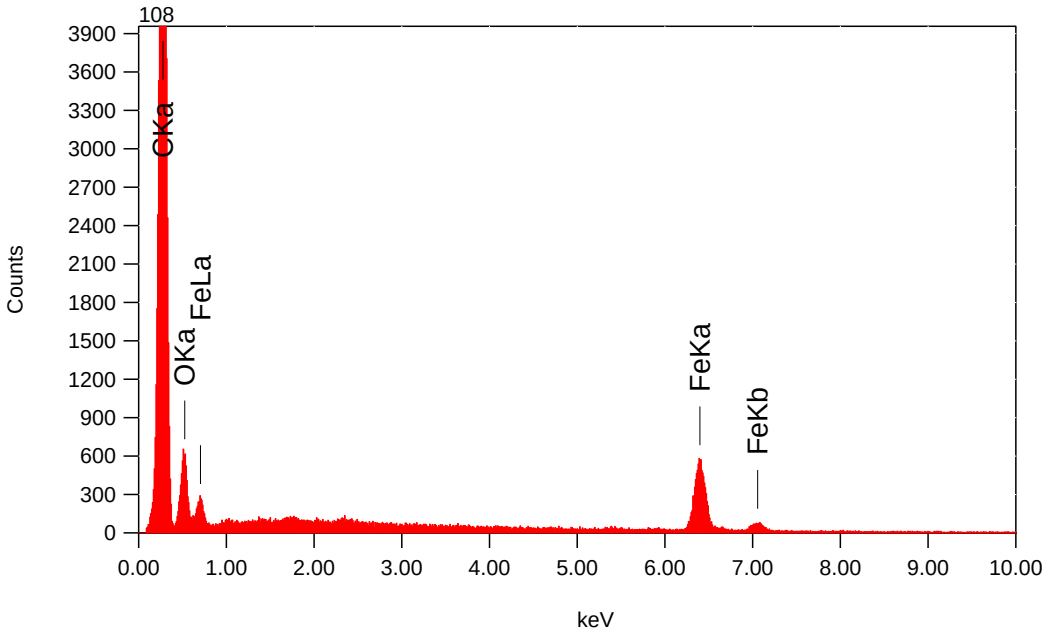


```
Acquisition Parameter
Instrument   : 7000F
Acc. Voltage : 15.0 kV
Probe Current: 0.59000 nA
PHA mode     : T3
Real Time    : 36.45 sec
Live Time    : 30.00 sec
Dead Time    : 17 %
Counting Rate: 4006 cps
Energy Range :  0 - 20 keV
```

ZAF Method Standardless Quantitative Analysis
Fitting Coefficient : 0.4338

Element	(keV)	mass%	Error%	At%	Compound	mass%	Cation	K
C K	0.277	63.9	0.2	82.2				54.3144
O K	0.525	11.3	0.8	10.9				9.8895
Fe K	6.398	24.8	2.6	6.9				35.7961
Total		100.0		100.0				

2055m Breccia

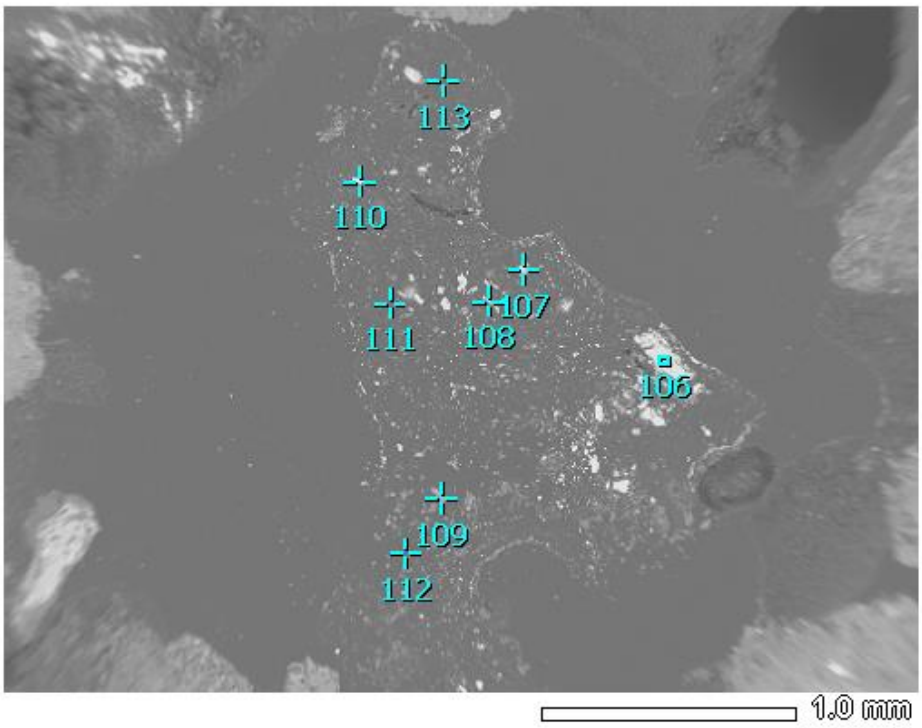


```
Title        : IMG1
--------------------------
Instrument   : 7000F
Volt         : 15.00 kV
Mag          : x 33
Date         : 2014/07/11
Pixel        : 512 x 384
```

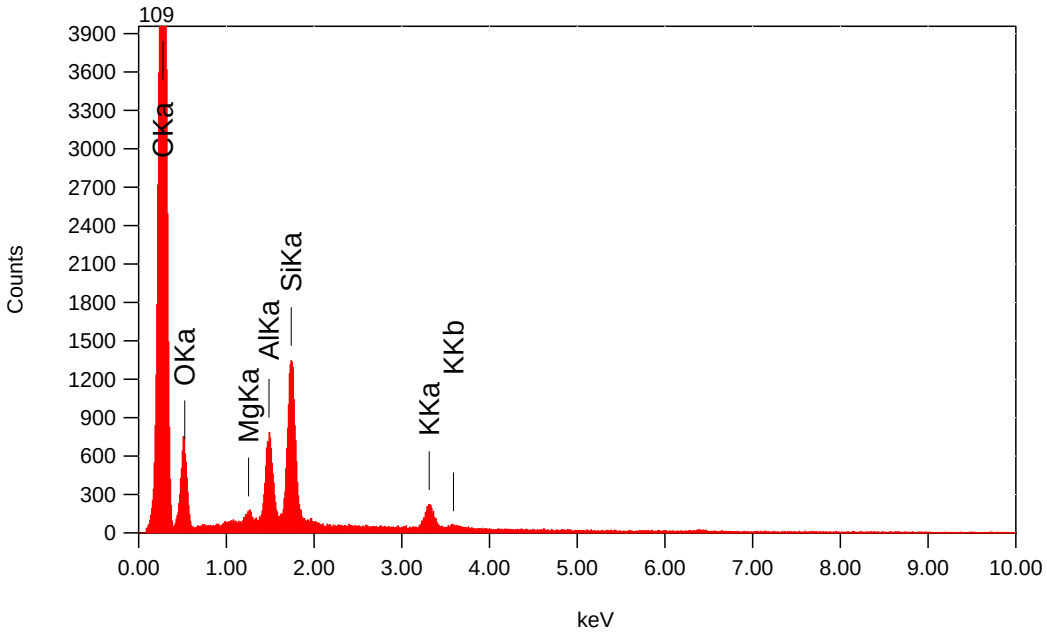


```
Acquisition Parameter
Instrument    : 7000F
Acc. Voltage  : 15.0 kV
Probe Current: 0.59000 nA
PHA mode      : T3
Real Time     : 36.49 sec
Live Time     : 30.00 sec
Dead Time     : 17 %
Counting Rate: 3990 cps
Energy Range :  0 - 20 keV
```

ZAF Method Standardless Quantitative Analysis
Fitting Coefficient : 0.4090

Element	(keV)	mass%	Error%	At%	Compound	mass%	Cation	K
C K	0.277	72.5	0.2	81.1				67.1369
O K	0.525	16.5	1.1	13.8				13.4698
Mg K	1.253	0.4	0.4	0.2				0.5595
Al K	1.486	2.9	0.4	1.5				4.7998
Si K	1.739	5.9	0.4	2.8				10.5097
K K	3.312	1.8	0.8	0.6				3.5243
Total		100.0		100.0				

2055m Breccia

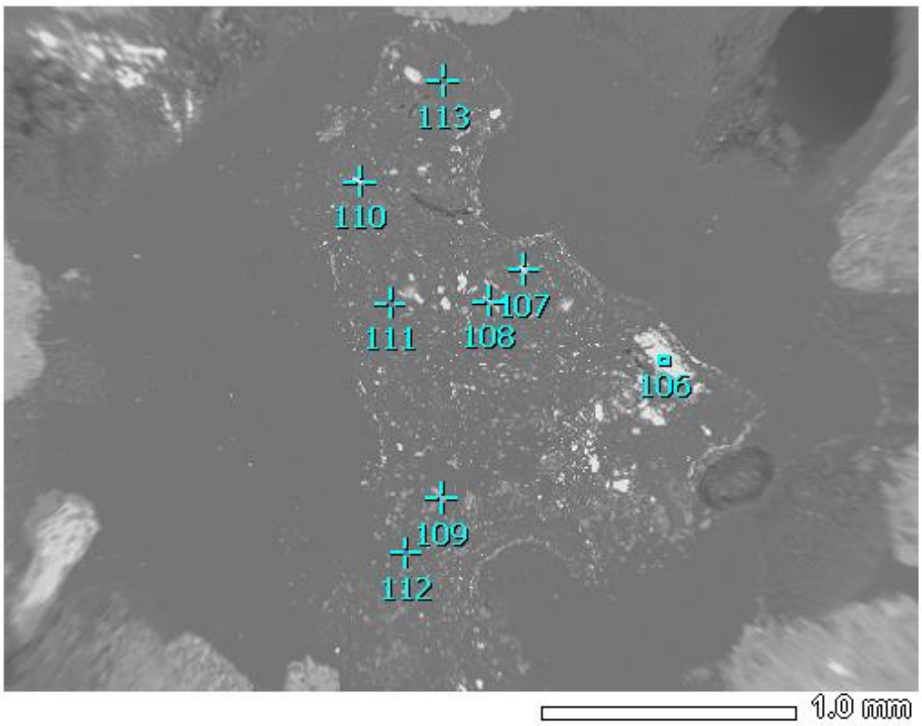


```
Title        : IMG1
--------------------------
Instrument   : 7000F
Volt         : 15.00 kV
Mag          : x 33
Date         : 2014/07/11
Pixel        : 512 x 384
```

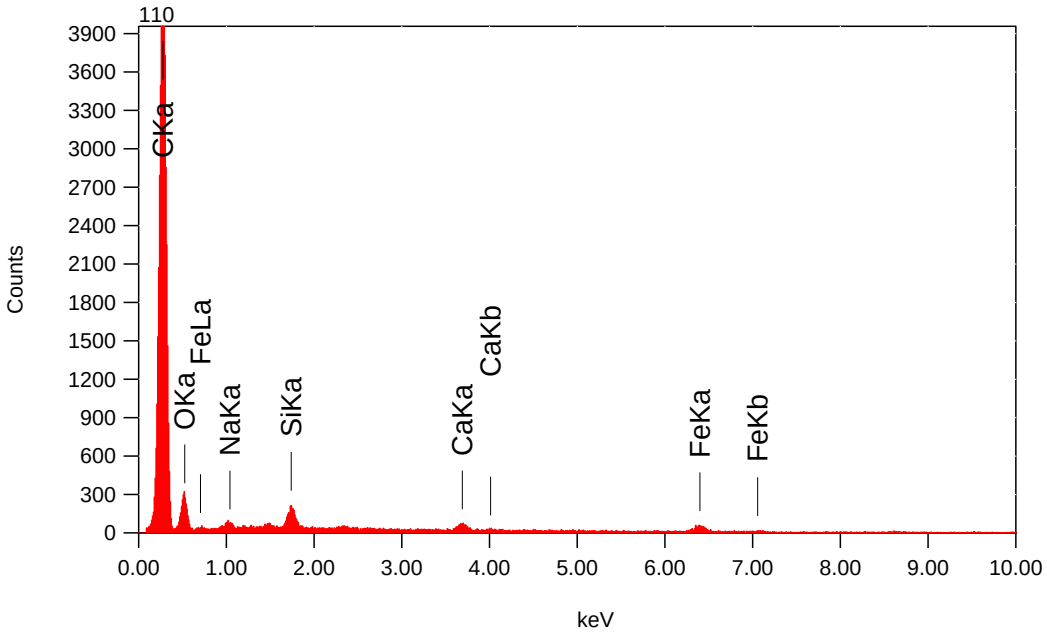


```
Acquisition Parameter
Instrument   : 7000F
Acc. Voltage : 15.0 kV
Probe Current: 0.59000 nA
PHA mode     : T3
Real Time    : 33.22 sec
Live Time    : 30.00 sec
Dead Time    : 10 %
Counting Rate: 2173 cps
Energy Range :  0 - 20 keV
```

ZAF Method Standardless Quantitative Analysis
Fitting Coefficient : 0.4674

Element	(keV)	mass%	Error%	At%	Compound	mass%	Cation	K
C K	0.277	74.3	0.2	83.1				75.7439
O K	0.525	16.7	1.4	14.0				11.5387
Na K*	1.041	0.6	0.7	0.4				0.7614
Si K	1.739	1.7	0.6	0.8				2.4860
Ca K	3.690	1.5	1.3	0.5				2.5037
Fe K	6.398	5.2	3.9	1.2				6.9663
Total		100.0		100.0				

2055m Breccia

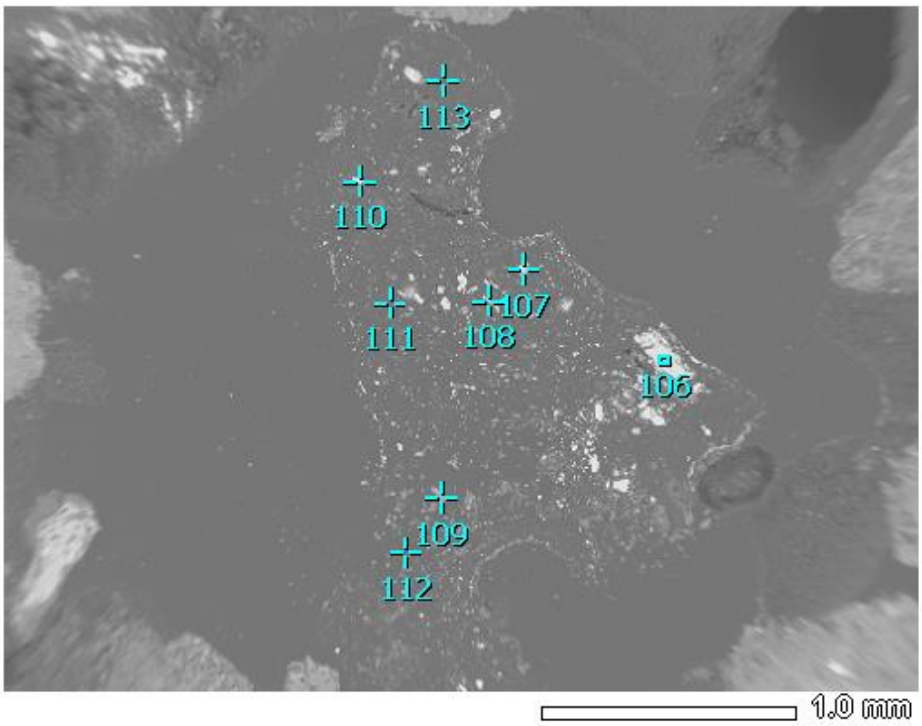


```
Title        : IMG1
--------------------------
Instrument   : 7000F
Volt         : 15.00 kV
Mag          : x 33
Date         : 2014/07/11
Pixel        : 512 x 384
```

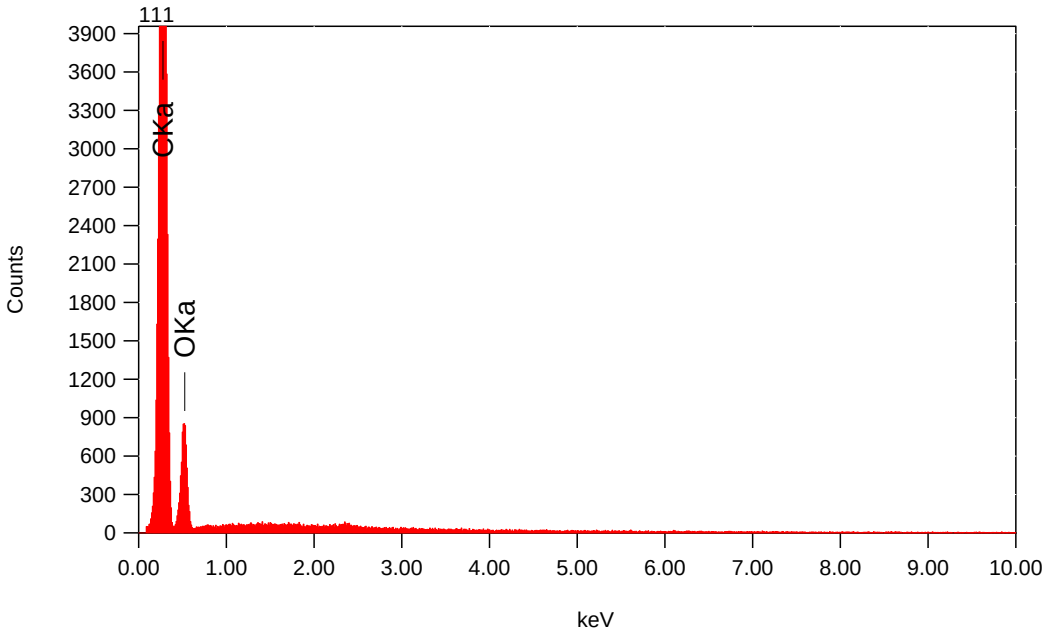


```
Acquisition Parameter
Instrument   : 7000F
Acc. Voltage : 15.0 kV
Probe Current: 0.59000 nA
PHA mode     : T3
Real Time    : 34.59 sec
Live Time    : 30.00 sec
Dead Time    : 13 %
Counting Rate: 3028 cps
Energy Range :  0 - 20 keV
```

ZAF Method Standardless Quantitative Analysis
Fitting Coefficient : 0.4656

Element	(keV)	mass%	Error%	At%	Compound	mass%	Cation	K
C K	0.277	70.7	0.2	76.3				79.0763
O K	0.525	29.3	1.5	23.7				20.9237
Total		100.0		100.0				

2055m Breccia

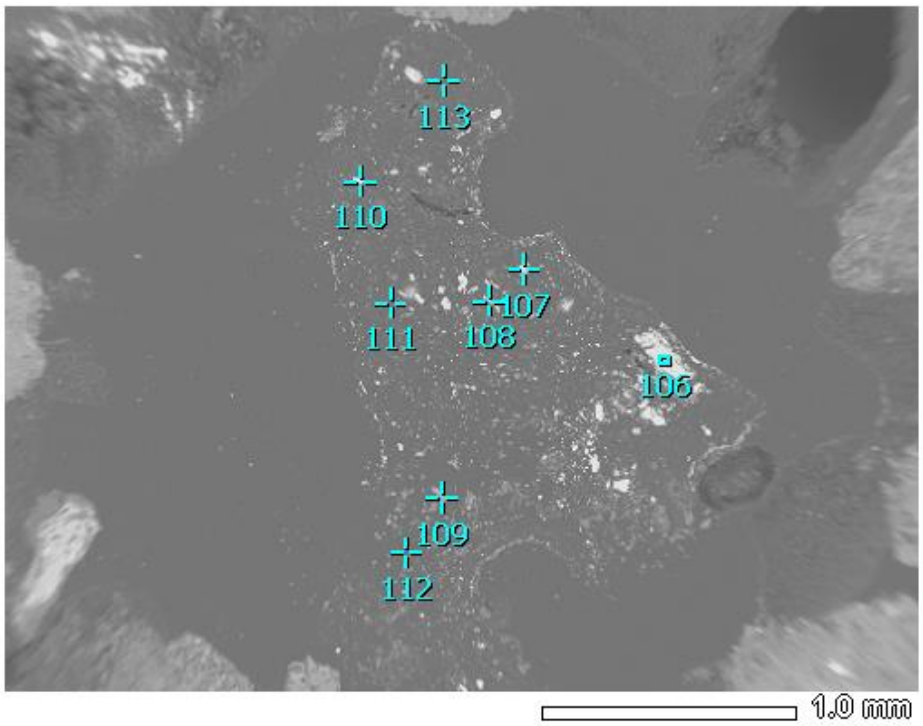


```
Title        : IMG1
--------------------------
Instrument   : 7000F
Volt         : 15.00 kV
Mag          : x 33
Date         : 2014/07/11
Pixel        : 512 x 384
```

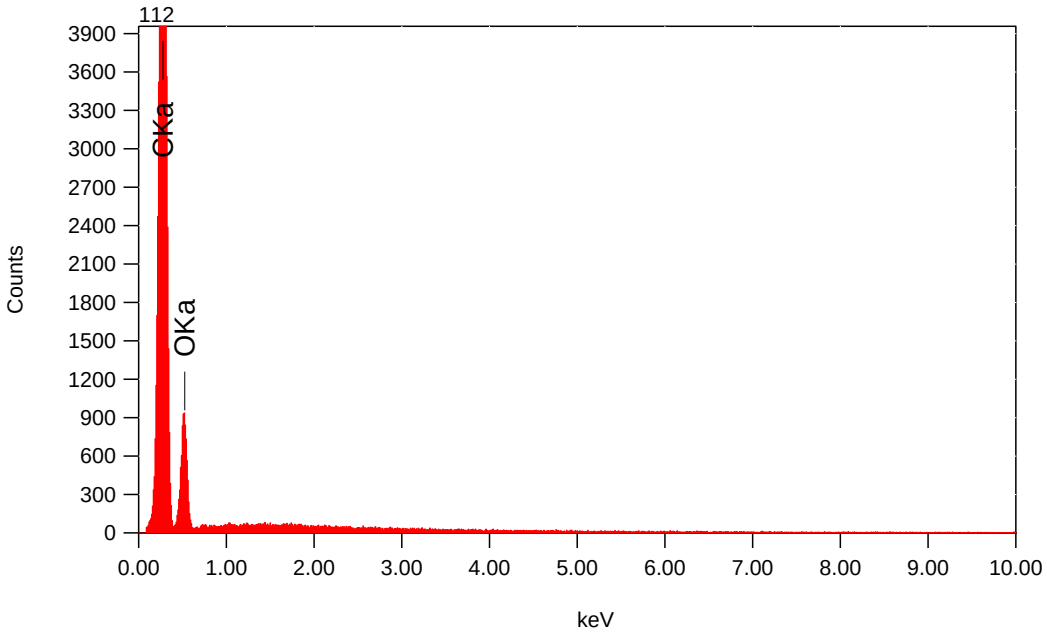


```
Acquisition Parameter
Instrument   : 7000F
Acc. Voltage : 15.0 kV
Probe Current: 0.59000 nA
PHA mode     : T3
Real Time    : 34.59 sec
Live Time    : 30.00 sec
Dead Time    : 13 %
Counting Rate: 3064 cps
Energy Range :  0 - 20 keV
```

ZAF Method Standardless Quantitative Analysis
Fitting Coefficient : 0.4545

Element	(keV)	mass%	Error%	At%	Compound	mass%	Cation	K
C K	0.277	70.2	0.2	75.8				78.4836
O K	0.525	29.8	1.4	24.2				21.5164
Total		100.0		100.0				

2055m Breccia

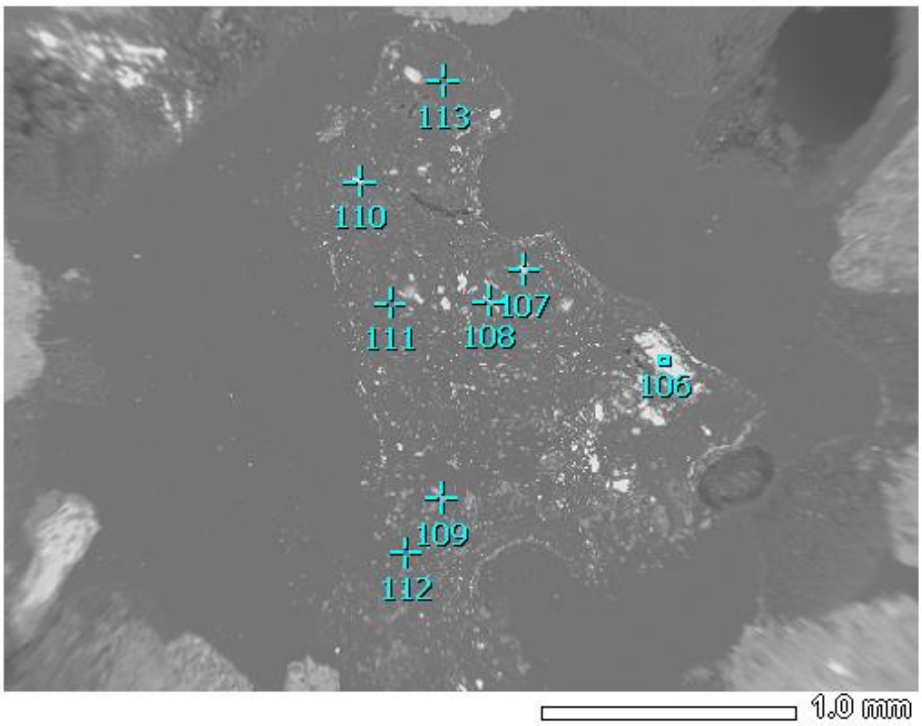


```
Title        : IMG1
--------------------------
Instrument   : 7000F
Volt         : 15.00 kV
Mag          : x 33
Date         : 2014/07/11
Pixel        : 512 x 384
```

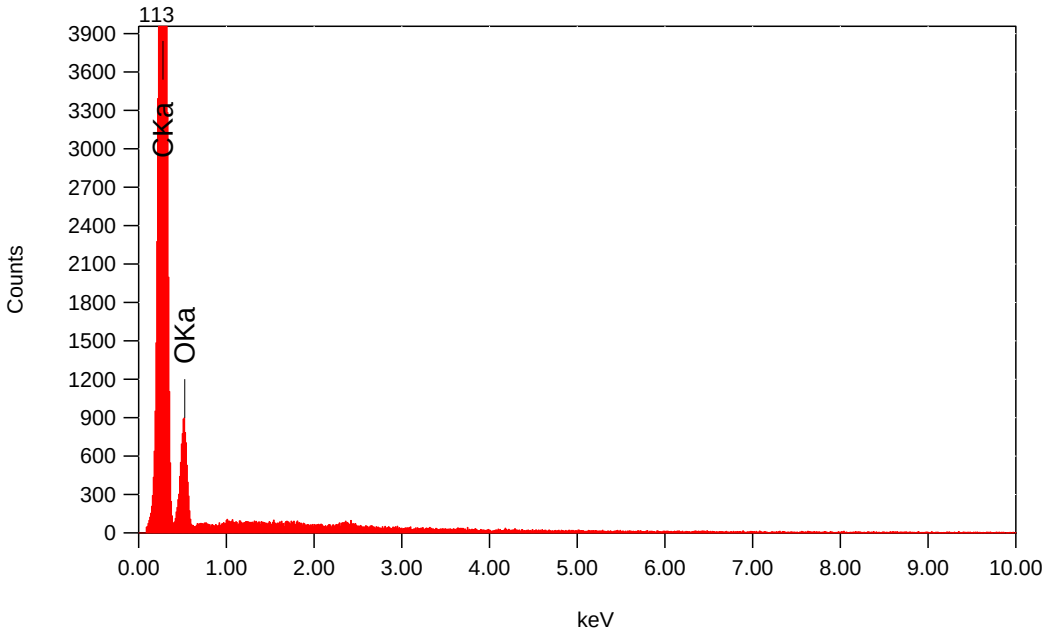


```
Acquisition Parameter
Instrument   : 7000F
Acc. Voltage : 15.0 kV
Probe Current: 0.59000 nA
PHA mode     : T3
Real Time    : 36.06 sec
Live Time    : 30.00 sec
Dead Time    : 16 %
Counting Rate: 3904 cps
Energy Range :  0 - 20 keV
```

ZAF Method Standardless Quantitative Analysis
Fitting Coefficient : 0.4704

Element	(keV)	mass%	Error%	At%	Compound	mass%	Cation	K
C K	0.277	75.9	0.2	80.7				84.7560
O K	0.525	24.1	1.8	19.3				15.2440
Total		100.0		100.0				

2125m Microfacies VS

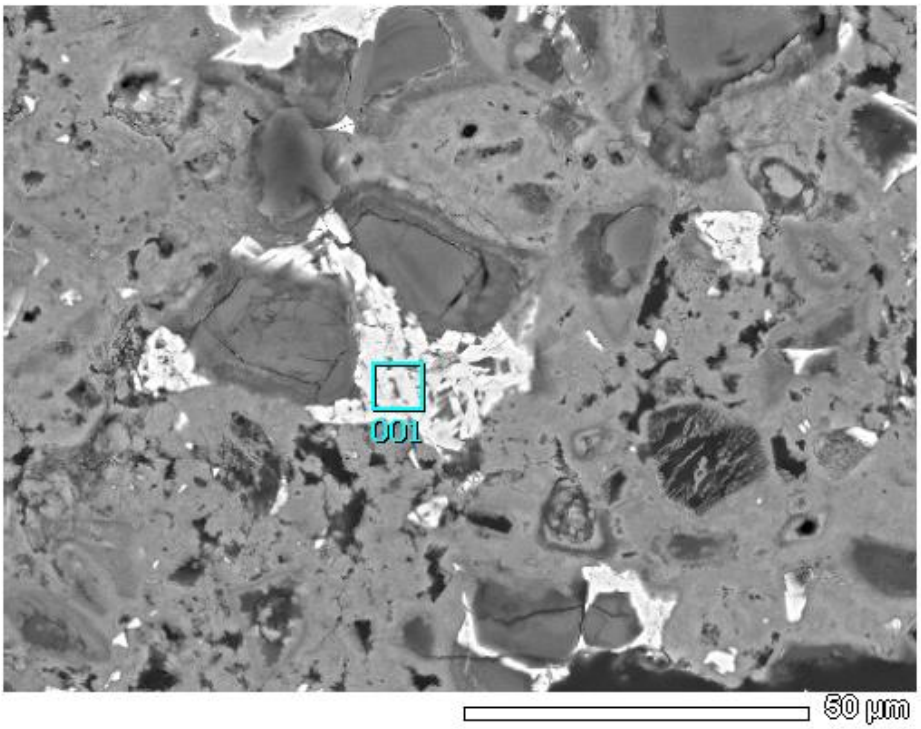


```
Title        : IMG1
--------------------------
Instrument   : 7000F
Volt         : 20.00 kV
Mag          : x 900
Date         : 2014/02/11
Pixel        : 512 x 384
```

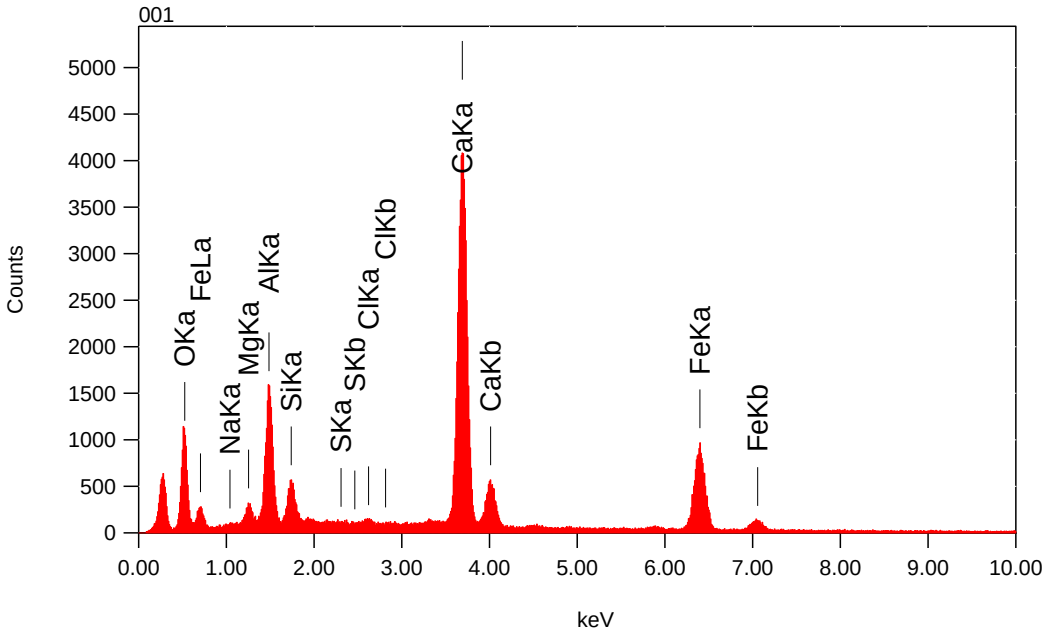


```
Acquisition Parameter
Instrument    : 7000F
Acc. Voltage  : 20.0 kV
Probe Current: 0.59000 nA
PHA mode      : T3
Real Time     : 41.59 sec
Live Time     : 30.00 sec
Dead Time     : 27 %
Counting Rate: 5925 cps
Energy Range :  0 - 20 keV
```

ZAF Method Standardless Quantitative Analysis
Fitting Coefficient : 0.1668

Element	(keV)	mass%	Error%	At%	Compound	mass%	Cation	K
O K	0.525	33.6	0.2	55.6				19.1374
Na K*	1.041	0.2	0.1	0.2				0.1085
Mg K*	1.253	1.6	0.1	1.7				0.9519
Al K	1.486	8.9	0.1	8.8				6.5927
Si K	1.739	2.6	0.1	2.5				2.2130
S K	2.307	0.1	0.1	0.1				0.0894
Cl K	2.621	0.3	0.1	0.2				0.3837
Ca K	3.690	31.9	0.1	21.1				46.1921
Fe K	6.398	20.8	0.2	9.9				24.3314
Total		100.0		100.0				

2125m Microfacies VS

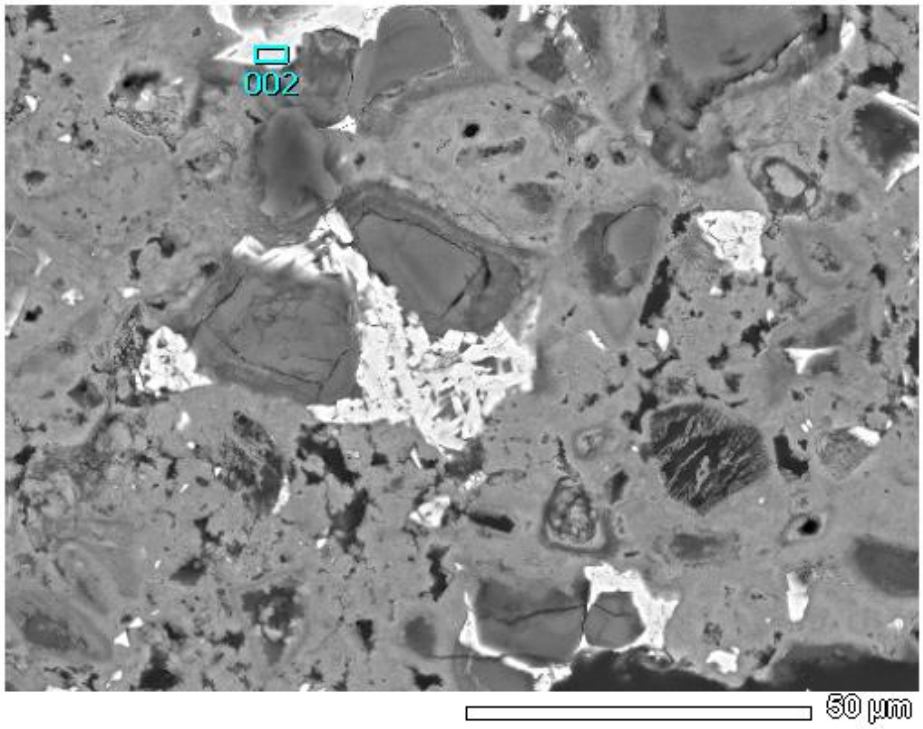

Title : IMG1

Instrument	: 7000F
Volt	: 20.00 kV
Mag	: x 900
Date	: 2014/02/11
Pixel	: 512 x 384

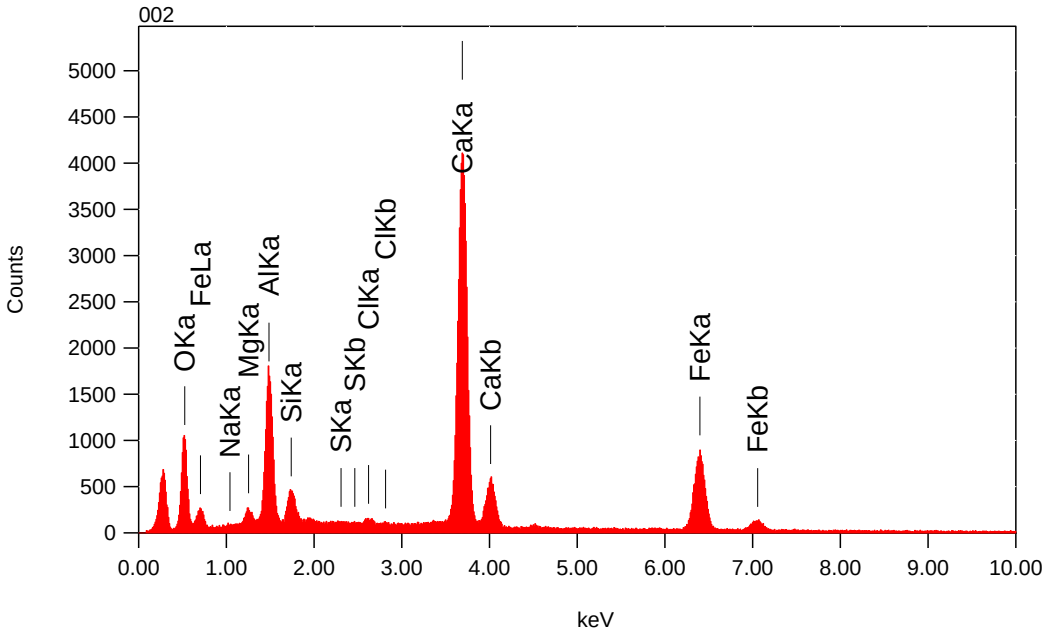

Acquisition Parameter

Instrument	: 7000F
Acc. Voltage	: 20.0 kV
Probe Current	: 0.59000 nA
PHA mode	: T3
Real Time	: 41.55 sec
Live Time	: 30.00 sec
Dead Time	: 27 %
Counting Rate	: 5805 cps
Energy Range	: 0 - 20 keV

ZAF Method Standardless Quantitative Analysis
Fitting Coefficient : 0.1557

Element	(keV)	mass%	Error%	At%	Compound	mass%	Cation	K
O K	0.525	32.9	0.2	54.7				18.2723
Na K*	1.041	0.1	0.1	0.1				0.0531
Mg K*	1.253	1.3	0.1	1.4				0.7594
Al K	1.486	10.2	0.1	10.1				7.6402
Si K	1.739	2.1	0.1	2.0				1.7813
S K	2.307	0.0	0.1	0.0				0.0605
Cl K	2.621	0.4	0.1	0.3				0.5076
Ca K	3.690	32.7	0.1	21.7				47.3063
Fe K	6.398	20.3	0.2	9.7				23.6194
Total		100.0		100.0				

2125m Microfacies VS

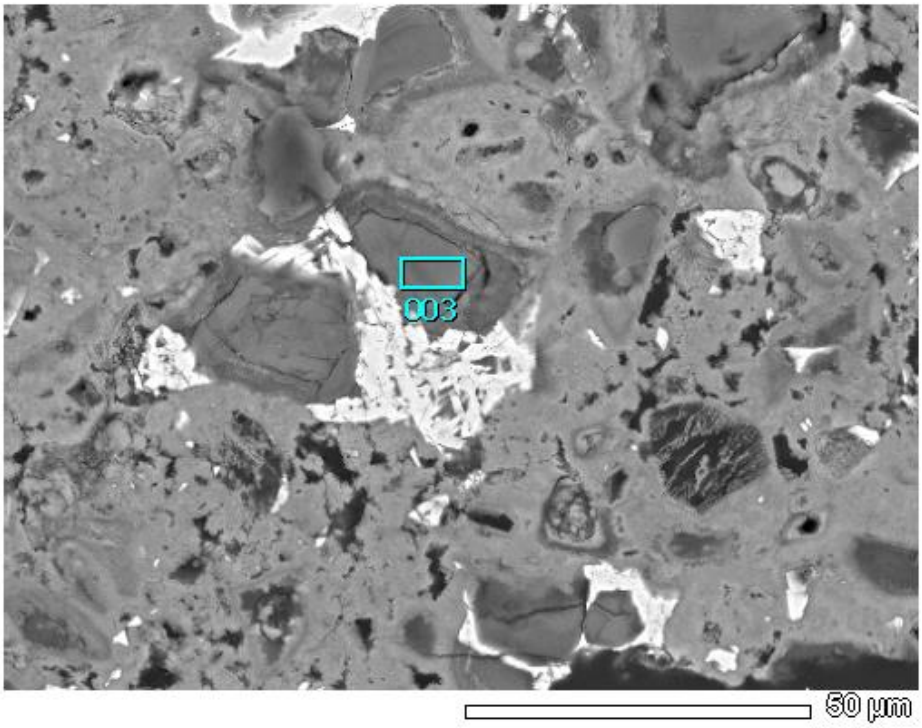


```
Title        : IMG1
--------------------------
Instrument   : 7000F
Volt         : 20.00 kV
Mag          : x 900
Date         : 2014/02/11
Pixel        : 512 x 384
```

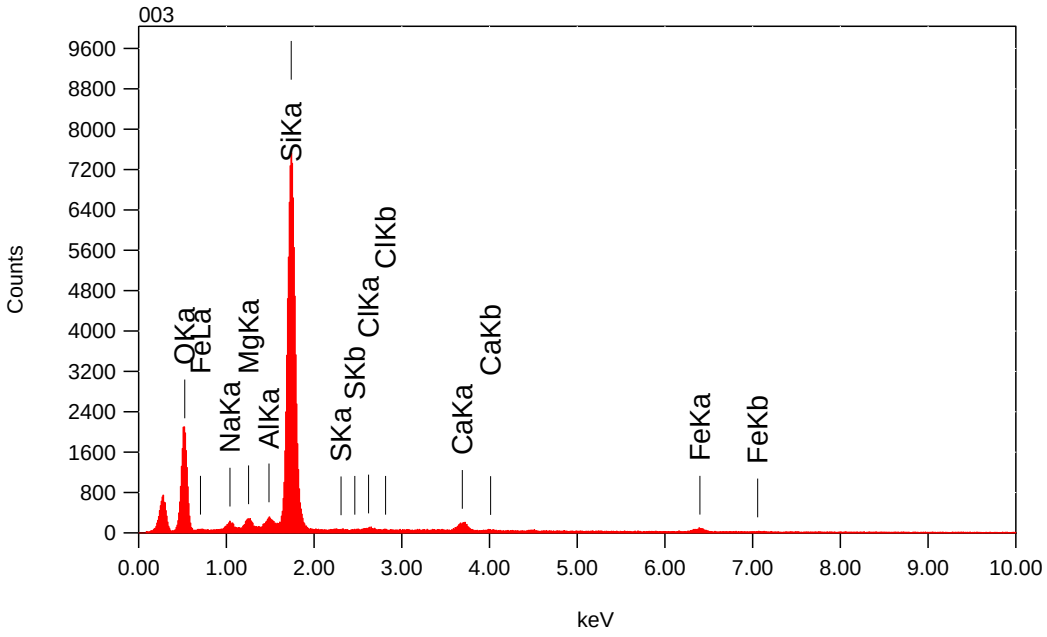


```
Acquisition Parameter
Instrument    : 7000F
Acc. Voltage  : 20.0 kV
Probe Current: 0.59000 nA
PHA mode      : T3
Real Time     : 39.65 sec
Live Time     : 30.00 sec
Dead Time     : 23 %
Counting Rate: 5007 cps
Energy Range :  0 - 20 keV
```

ZAF Method Standardless Quantitative Analysis
Fitting Coefficient : 0.1947

Element	(keV)	mass%	Error%	At%	Compound	mass%	Cation	K
O K	0.525	45.2	0.2	59.6				44.6113
Na K*	1.041	1.4	0.2	1.3				1.2166
Mg K*	1.253	1.6	0.2	1.3				1.1642
Al K	1.486	1.2	0.1	0.9				1.0636
Si K	1.739	46.4	0.1	34.8				47.1935
S K	2.307	0.1	0.2	0.0				0.0680
Cl K	2.621	0.3	0.2	0.2				0.3391
Ca K	3.690	1.8	0.2	0.9				2.1101
Fe K	6.398	2.1	0.5	0.8				2.2338
Total		100.0		100.0				

2125m Microfacies VS

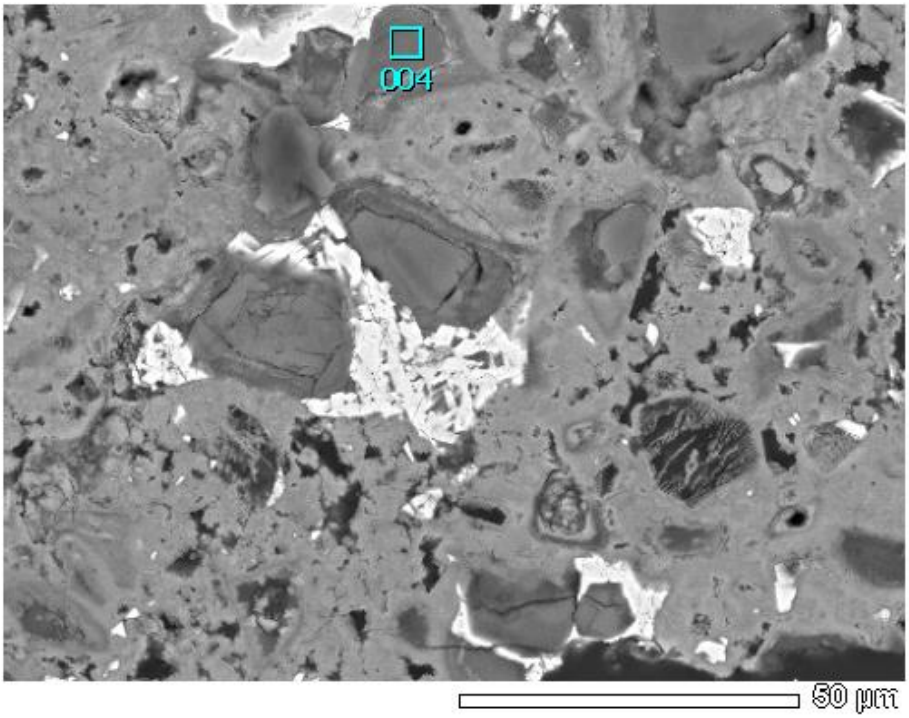


```
Title        : IMG1
--------------------------
Instrument   : 7000F
Volt         : 20.00 kV
Mag          : x 900
Date         : 2014/02/11
Pixel        : 512 x 384
```

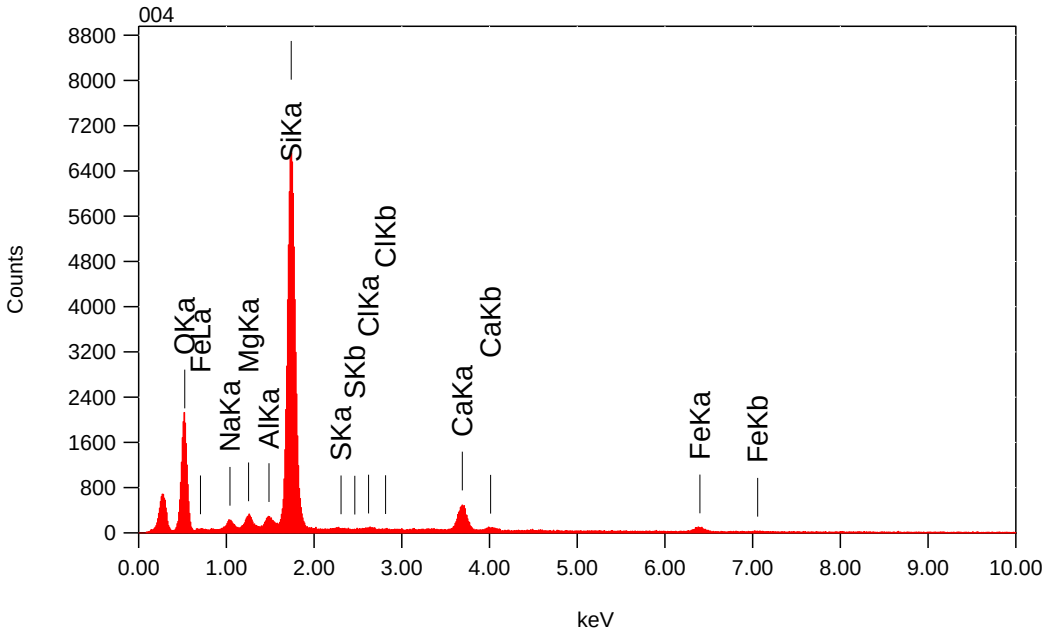


```
Acquisition Parameter
Instrument    : 7000F
Acc. Voltage  : 20.0 kV
Probe Current: 0.59000 nA
PHA mode      : T3
Real Time     : 39.38 sec
Live Time     : 30.00 sec
Dead Time     : 23 %
Counting Rate: 5021 cps
Energy Range :  0 - 20 keV
```

ZAF Method Standardless Quantitative Analysis
Fitting Coefficient : 0.1846

Element	(keV)	mass%	Error%	At%	Compound	mass%	Cation	K
O K	0.525	46.4	0.2	61.3				44.2411
Na K*	1.041	1.6	0.2	1.5				1.3676
Mg K*	1.253	1.7	0.1	1.5				1.2853
Al K	1.486	1.3	0.1	1.0				1.1687
Si K	1.739	41.2	0.1	31.0				42.5522
S K	2.307	0.1	0.1	0.0				0.0654
Cl K	2.621	0.3	0.1	0.2				0.2677
Ca K	3.690	5.0	0.2	2.7				6.3445
Fe K	6.398	2.4	0.4	0.9				2.7076
Total		100.0		100.0				

2125m Microfacies VS

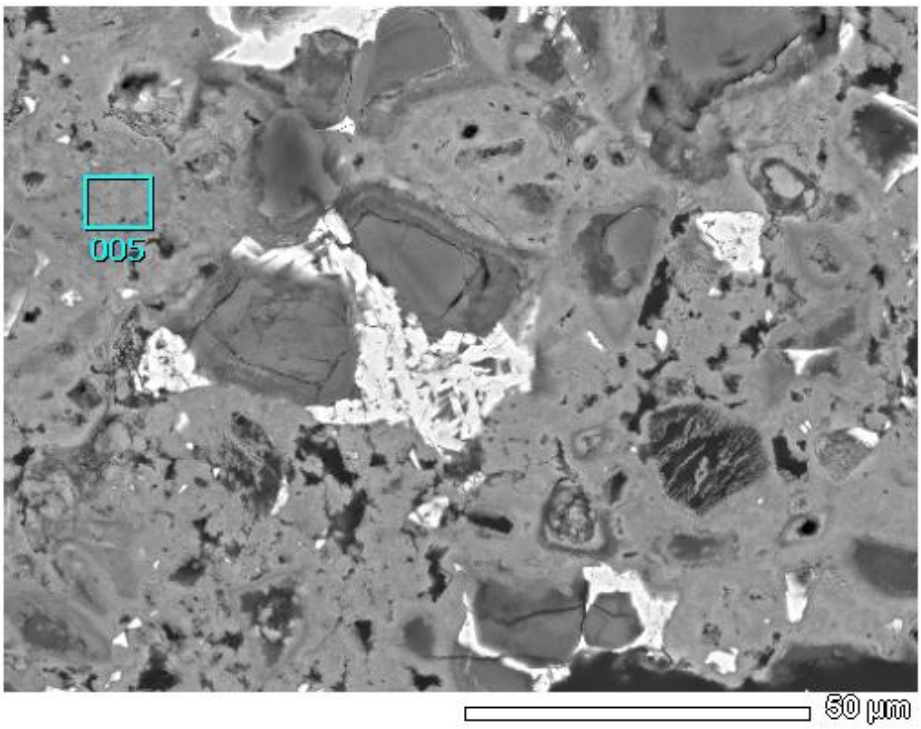


```
Title        : IMG1
--------------------------
Instrument   : 7000F
Volt         : 20.00 kV
Mag          : x 900
Date         : 2014/02/11
Pixel        : 512 x 384
```

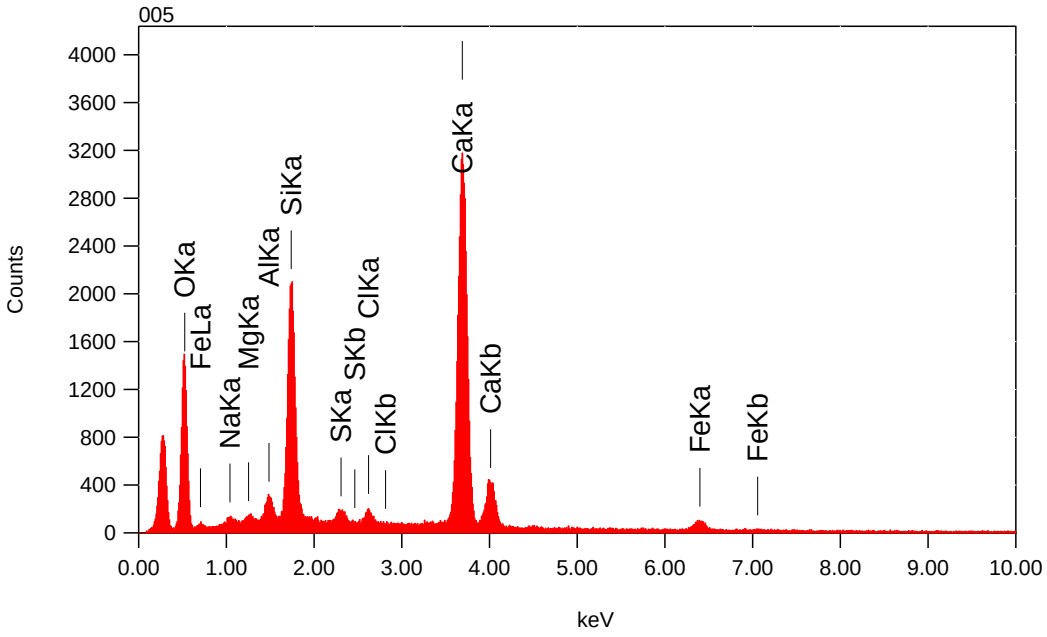


```
Acquisition Parameter
Instrument    : 7000F
Acc. Voltage  : 20.0 kV
Probe Current: 0.59000 nA
PHA mode      : T3
Real Time     : 38.86 sec
Live Time     : 30.00 sec
Dead Time     : 22 %
Counting Rate: 4761 cps
Energy Range :  0 - 20 keV
```

ZAF Method Standardless Quantitative Analysis
Fitting Coefficient : 0.1968

Element	(keV)	mass%	Error%	At%	Compound	mass%	Cation	K
O K	0.525	52.2	0.4	70.8				32.9546
Na K*	1.041	0.6	0.2	0.5				0.4613
Mg K*	1.253	0.4	0.1	0.4				0.3158
Al K	1.486	1.4	0.1	1.1				1.2441
Si K	1.739	12.1	0.1	9.3				13.4089
S K	2.307	0.7	0.1	0.5				0.9498
Cl K	2.621	0.8	0.1	0.5				1.1421
Ca K	3.690	29.7	0.2	16.1				46.7959
Fe K	6.398	2.2	0.4	0.8				2.7275
Total		100.0		100.0				